GROUND-BASED RADIO WAVE PROPAGATION STUDIES OF THE LOWER IONOSPHERE

CONFERENCE PROCEEDINGS

11-15 APRIL, 1966

OTTAWA, CANADA

VOLUME 2

DECEMBER 1967

CONFERENCE ON GROUND-BASED RADIO WAVE PROPAGATION STUDIES OF THE LOWER IONOSPHERE

First Row: Mr. T.J. Elkins, AFCRL – Dr. W. Elling, Max-Planck Inst. Germany – Mr. L.W. Hewitt, DRTE – Dr. R.C. Whitten, SRI – Dr. William Swider, Jr., AFCRL – Dr. W. Pfister, AFCRL – Mr. Samuel Horowitz, AFCRL – Dr. J.S. Belrose, DRTE – Dr. Klaus Bibl, Lowell Tech., – Dr. H. Volland, U. of Bonn, Germany – Dr. R.A. Smith, U. of New England, Australia – Mr. Glenn Falcon, ITSA – Mr. L.R. Megill, ITSA.

Second Row: Mr. D.P. Hayes, Lowell Tech. – Dr. A.C. Aikin, NASA/GSFC – Dr. T.M. Georges, ITSA – Mr. Richard S. Allen, AFCRL – Dr. E.V. Thrane, NDRE, Norway – Dr. Ben Segal, DRTE – Frank T. Davies, CS/DRTE – Lt. Col. J.D. Brown, DASA – Mr. V.E. Hildebrand, U.S. Naval Ord. Lab. – Dr. Gary S. Sales, AFCRL – Dr. E.S. Owen Jones, Bedford College, England – Dr. H.A. von Biel, Cornell Aero Labs. – Mr. B.R. May, RSRS, Slough, England.

Third Row: Dr. J.S. Shirke, U. of Illinois – Mr. D.B. Ross, DRTE – Miss Doris H. Jelly, DRTE – Dr. J.A. Kane, NASA/GSFC – Dr. R.I. Fenwick, Stanford U. – Mr. K. Olson, Lowell Tech. – Mr. B.W. Reinisch, Lowell Tech. – Dr. A.K. Paul, Max-Planck Inst. Germany – Dr. J.W. Wright, ITSA – Dr. G. Lanza, Northeastern U. – Mr. D. Reitz, GE/TEMPO – Mr. Jerry T. Jones, IIT Research Inst.

Fourth Row: Mr. G.W. Adams, Douglas MSSD – Dr. A.H. Manson, Chicago U. – Dr. J.B. Gregory, U. of Saskatchewan – Dr. I. Bourne, DRTE – Mr. W.T. Roberts, NASA/MSFC – Mr. Arne Haug, NDRE, Norway – Dr. M.L.V. Pitteway, Nottingham U. England – Dr. L.M. La Londe, Cornell U. – Mr. Arne Pedersen, NASA/GSFC – Mr. Noboru Wakai, ITSA – Lt. J.E. Barety, USAF Weapons Lab. – Dr. E. Gossard, U.S. Navy Electronics Lab.

VOLUME 2

PROCEEDINGS OF A CONFERENCE HELD 11 TO 15 APRIL, 1966

AT

DEFENCE RESEARCH TELECOMMUNICATIONS ESTABLISHMENT
RADIO PHYSICS LABORATORY
Shirley Bay, Ottawa, Ontario, Canada

GROUND-BASED RADIO WAVE PROPAGATION STUDIES OF THE LOWER IONOSPHERE

Compiled by

J.S. Belrose, I.A. Bourne and L.W. Hewitt

SPONSORED BY

Defence Research Telecommunications Establishment
Ottawa, Ontario

and

Air Force Cambridge Research Laboratories
Hanscom Field, Massachusetts, U.S.A.

December 1967

Defence Research Board
Department of National Defence
Canada

66-571

96414—1½

CONFERENCE PLANNING AND DRTE MANAGEMENT STAFF

Conference General Chairman

Dr. J.S. Belrose

Secretary

Mrs. Edna Robertson

Program Planning

Dr. J.S. Belrose	–	Defence Research Telecommunications Establishment Ottawa 4
Dr. W. Pfister	–	Geophysics Research Directorate Air Force Cambridge Research Laboratories Bedford, Massachusetts

Local Arrangements

Dr. I.A. Bourne	–	Publications
Mr. L.W. Hewitt	–	Chief Reporter
Mr. H.E. Checkley	–	Facilities
Mrs. Judy Mulvihill	–	Conference Secretarial Assistance

DRTE Management

Mr. Frank T. Davies	–	Chief Superintendent
Dr. John H. Chapman	–	Deputy Chief Superintendent
Dr. Irvine Paghis	–	Superintendent, Radio Physics Laboratory
Dr. J.H. Meek	–	Superintendent, Communications Laboratory
Dr. R.C. Langille	–	Superintendent, Electronics Laboratory

PREFACE

The lower ionosphere, consisting of the D region and part of the E region below about 120 km. in height, is perhaps the most imperfectly understood part of the ionosphere at the present time. This is partly because of observational limitations and partly because of difficulties in interpreting the observational data that have been obtained. Under normal conditions the electron number densities are so low that low frequencies are needed for reflection in this height range. Despite an abundance of experimental data, few results have, until recently, emerged from these studies. Under abnormal conditions (SID, PCA, and auroral disturbances) the attenuation of radio waves propagating within the region can become so great that radio reflections, other than from the base of the ionosphere, are not obtained. The dynamic range of variation is large: under normal conditions the electron density and collision frequency values change by up to five orders of magnitude in the height range 30 to 120 km.; and under disturbance conditions electron density increases by several orders of magnitude can occur at low heights.

Thus, while ground-based studies of the lower ionosphere are both scarce and difficult to interpret, the situation is not much improved in the case of experiments conducted "in situ". The relative high gas densities make environmental measurements with sounding rockets difficult, and most experiments have been designed to provide information about the ionosphere at heights above about 90 km. A few results have been obtained for the normal D region, but in general these are less reliable than those obtained at times when radio wave absorption was great.

The magnitude of the electron density and its variation with height in the lower ionosphere is roughly known, at least at middle latitudes, but superimposed on a general increase with height are important structural features, the dynamic changes of which cannot be studied by means of rockets. For example it is becoming increasingly evident that meteorology plays an important part in the variability of the undisturbed D region. There is therefore a need for a reliable means of studying the lower ionosphere by ground-based experiments capable of synoptic application. In recent years, several new techniques have been developed for studying the lower ionosphere, e.g., partial reflections and pulse cross modulation, and new progress is being made in the numerical interpretation of low frequency propagation data. Since an increasing number of research laboratories and organizations are exploiting one or more of these techniques, it is important at this time to evaluate the reliability of the data, so that the best experiments can be undertaken in a synoptic application. It is important at this epoch of the solar cycle to increase the latitude coverage of D-region observations before solar activity increases.

With this aim in mind, a working conference was planned to bring together specialists concerned with the various ground-based experiments. The various experimental techniques were reviewed, emphasizing the state of the art and the problems to be resolved, and new and stimulating results not yet appearing in the literature were presented. When soliciting papers for the conference, it was made clear that a Conference Proceedings would be published, and that an edited discussion following each paper would be included. Even so, it was our intention to keep the atmosphere of the conference as informal as possible so as to promote discussion (or debate), even to the extent of intentionally forcing an argument. This procedure sometimes worked so well, it later proved difficult to obtain final manuscripts from some of the speakers, and the task of preparing an edited version of the discussions was a difficult one.

Unfortunately, the three main experiments (partial reflections, pulse cross modulation, and LF propagation) have little in common, apart from the fact that they are concerned with the reflection and propagation of radio waves in the ionosphere, and workers in the three fields do not necessarily have a good understanding of all the experiments or, for that matter, of the D region.

The purpose of Session 1 was therefore to give a general background of D-region properties, insofar as they are currently known, and to show the difficulties that are encountered because of limited knowledge concerning the existence of minor constituents and the uncertainties of dominant production and loss rates. The majority of the work in Session 1 is a summary of previously published work, of which a knowledge is necessary if the merits (and defects) of the partial reflection, wave interaction, and LF propagation experiments, which are discussed in the main sessions of the conference, are to be appreciated.

The partial reflection and the pulse cross modulation experiments and observational results obtained by these techniques, and the long wave propagation interpretive results, are the subjects of Sessions 2, 3, and 4 respectively. Other experiments, e.g., ionosondes and radio wave absorption, and observational results obtained from an analysis of these data, are the subjects of Sessions 5 and 6.

The concluding discussion is intended to compare the various data, to update the present knowledge summaries given in Session 1 in the light of the new observational results presented at this conference, and to define the areas where new observational data or new interpretations are needed.

In setting up this conference, we were guided by the concept that its prime purpose should be the dissemination of viewpoints, technical information, and scientific results among a relatively small number of active researchers, following a pre-arranged program of subject material. Accordingly, the meeting was not open to all who might have desired to attend. We hope that this record will be of some value to them, and that it will serve as a basic text to be used by future investigators of the lower ionosphere.

John S. Belrose
Conference Chairman

ACKNOWLEDGMENTS

Any success achieved by the Conference or its Proceedings is undoubtedly due to the authors of the various papers and to the speakers and session chairmen. All participants are to be congratulated for the quality of the material brought to the conference and for the willingness with which they responded to the critical spirit of the meetings.

We have wielded a heavy and sometimes arbitrary editorial hand in preparing the papers, especially the discussions, in a coherent form for printing. Accordingly, we take full responsibility for any misquotation or misrepresentation of a participant's remarks which may appear.

The help freely given by the many members of the Defence Research Board staff in the organization of the conference and the production of this volume is gratefully acknowledged. The whole hearted co-operation of Dr. L.W. Billingsley and the DRB/DSIS staff who organized the technical production of this Proceedings, and of Mr. E.A. Atkins of the DRTE Publications Section, deserves particular mention. Mr. A.F. Adams and Mr. J.E. Colbert of the DRTE Illustration and Photography Sections also gave able assistance.

Special mention should be made of the DRTE technical staff who operated projection and recording facilities during the conference, and of the secretarial staff, especially Mrs. Edna Robertson, who prepared typed copy of the many discussions.

J.S. Belrose
I.A. Bourne
L.W. Hewitt
Editorial Committee

LIST OF ATTENDEES AT CONFERENCE

Mr. Gene Adams
Douglas MSSD.,
Santa Monica, California, U.S.A.

Dr. A.C. Aikin
NASA/GSFC,
Greenbelt, Maryland, U.S.A.

Dr. Richard Allen
Air Force Cambridge Research Laboratories,
Bedford, Massachusetts, U.S.A.

Dr. Ian Axford
Cornell University,
Astronomy Department,
Ithaca, New York, U.S.A.

Lt. J.E. Barety
Kirtland Air Force Base,
Air Force Weapons Laboratory,
Albuquerque, New Mexico, U.S.A.

Dr. R.E. Barrington
Defence Research Telecommunications Establishment,
Ottawa, Canada.

Mr. C.D. Bell
Pennsylvania State University,
University Park,
Pennsylvania, U.S.A.

Dr. J.S. Belrose
Defence Research Telecommunications Establishment,
Ottawa, Canada.

Dr. K. Bibl
Lowell Technological Institute Research Foundation,
Lowell, Massachusetts, U.S.A.

Dr. I.A. Bourne
Defence Research Telecommunications Establishment,
Ottawa, Canada.

Lt.-Col. J.D. Brown
Department of Defence,
Defence Atomic Support Agency,
Washington, D.C., U.S.A.

Mr. J.W. Cox
Defence Research Telecommunications Establishment,
Ottawa, Canada.

Dr. C.M. Crain
The Rand Corporation,
1700 Main Street,
Santa Monica, California, U.S.A.

Dr. A. Dalgarno
Department of Applied Mathematics,
Queens University of Belfast
Belfast, Northern Ireland.

Mr. Frank T. Davies
Chief Superintendent
Defence Research Telecommunications Establishment,
Ottawa, Canada

Mr. Terence J. Elkins
Wentworth Institute,
550 Huntington Avenue,
Boston, Massachusetts, U.S.A.

Dr. W. Elling
Max-Planck Institut Fur Aeronomie,
Lindau UB. North /Han., Germany.

Mr. G. Falcon
Institute for Telecommunication Sciences and Aeronomy,
Environmental Science Services Administration,
Boulder, Colorado, U.S.A.

Dr. R.B. Fenwick
Radioscience Laboratory,
Stanford University,
Stanford, California, U.S.A.

Dr. A.J. Ferraro
Ionospheric Research Laboratory,
Pennsylvania State University,
University Park,
Pennsylvania, U.S.A.

Dr. P.A. Forsyth
Department of Physics,
University of Western Ontario,
London, Ontario, Canada.

Mr. T.M. Georges
Institute for Telecommunication Sciences and Aeronomy,
Environmental Science Services Administration,
Boulder, Colorado, U.S.A.

Dr. E.E. Gossard
US Navy Electronics Laboratory,
San Diego, California, U.S.A.

Dr. J.B. Gregory
University of Saskatchewan,
Saskatoon, Saskatchewan, Canada.

Dr. T.R. Hartz
Defence Research Telecommunications Establishment,
Ottawa, Canada.

Mr. A. Haug
Norwegian Defence Research Establishment,
P.O. Box 25,
Kjeller/Lillistrom, Norway.

Mr. Daniel P. Hayes
Lowell Technological Institute Research Foundation,
450 Aiken Street,
Lowell, Massachusetts, U.S.A.

Dr. R.J.W. Henry
NASA/GSFC,
Greenbelt, Maryland, U.S.A.

Mr. L.W. Hewitt
Defence Research Telecommunications Establishment,
Ottawa, Canada.

Mr. Verne E. Hildebrand
Naval Ordnance Laboratory,
Corona, California, U.S.A.

Mr. S. Horowitz
Air Force Cambridge Research Laboratories,
Bedford, Massachusetts, U.S.A.

Miss Doris Jelly
Defence Research Telecommunications Establishment,
Ottawa, Ontario, Canada.

Dr. J.R. Johler
Institute for Telecommunication Sciences and Aeronomy,
Environmental Science Services Administration,
Boulder, Colorado, U.S.A.

Dr. E.S.O. Jones
Bedford College, Physics Department,
Regents Park, London N.W. 1, England.

Mr. Jerry Jones
IIT Research Institute,
10 West 35th Street,
Chicago, Illinois, U.S.A.

Dr. J.A. Kane
NASA/GSFC,
Greenbelt, Maryland, U.S.A.

Dr. Arthur J. Kantor
Air Force Cambridge Research Laboratories,
Bedford, Massachusetts, U.S.A.

Mr. J. Kert
Space Information Systems,
North American Aviation Incorporated,
Downey, California, U.S.A.

Dr. L.M. Lalonde
Clark Hall, Cornell University,
Ithaca, New York, U.S.A.

Dr. G. Lanza
Physics Department,
Northeastern University,
Boston, Massachusetts, U.S.A.

Dr. H.S. Lee,
Pennsylvania State University,
University Park,
Pennsylvania, U.S.A.

Dr. Alan Henry Manson
University of Chicago,
Chicago 37, Illinois, U.S.A.

Mr. B.R. May
Radio and Space Research Station,
Ditton Park,
Slough, Bucks, England.

Mr. L.R. Megill
Institute for Telecommunication Sciences and Aeronomy,
Environmental Science Services Administration,
Boulder, Colorado, U.S.A.

Mr. K.V. Narasinga Rao
Air Force Cambridge Research Laboratories,
Bedford, Massachusetts, U.S.A.

Dr. G.L. Nelms
Defence Research Telecommunications Establishment,
Ottawa, Canada.

Mr. Kirtland Olson
Lowell Technological Institute Research Foundation,
450 Aiken Street,
Lowell, Massachusetts, U.S.A.

Dr. I. Paghis
Defence Research Telecommunications Establishment,
Ottawa, Canada.

Dr. A.K. Paul
Max-Planck Institut Fur Aeronomie,
Lindau UB. North/Han., Germany.

Mr. Arne Pedersen
NASA/GSFC,
Greenbelt, Maryland, U.S.A.

Mr. L. Petrie
Defence Research Telecommunications Establishment,
Ottawa, Ontario, Canada.

Dr. W. Pfister
Geophysics Research Directorate,
Air Force Cambridge Research Laboratories,
Bedford, Massachusetts, U.S.A.

Mr. T.P. Pinkerton
Pennsylvania State University,
University Park,
Pennsylvania, U.S.A.

Dr. M.L.V. Pitteway
Cripps Computing Centre,
Nottingham University,
Nottingham, England.

Lt. R.M. Price
Institute for Exploratory Research, Division C,
Department of Army, US Army Electronics Command,
Fort Monmouth, New Jersey, U.S.A.

Mr. Bodo Reinisch
Lowell Technological Institute, Research Foundation,
450 Aiken Street,
Lowell, Massachusetts, U.S.A.

Mr. David Reitz
DASA Information + Analysis Center, GE. Tempo,
816 State Street,
Santa Barbara, California, U.S.A.

Dr. D. Rice
Defence Research Telecommunications Establishment,
Ottawa, Canada.

Mr. W.T. Roberts
NASA,
Marshall Space Flight Center,
Huntsville, Alabama, U.S.A.

Mr. D.B. Ross
Defence Research Telecommunications Establishment,
Ottawa, Canada.

Dr. Gary S. Sales
Upper Atmosphere Physics Laboratory,
Air Force Cambridge Research Laboratories,
Bedford, Massachusetts, U.S.A.

Dr. B. Segal
Defence Research Telecommunications Establishment,
Ottawa, Canada.

Dr. J.S. Shirke
Department of Electrical Engineering,
University of Illinois,
Urbana, Illinois,
U.S.A.

Dr. R.A. Smith
University of New England,
Armidale, N.S.W., Australia.

Dr. Wm. Swider, Jr.
Air Force Cambridge Research Laboratories,
Bedford, Massachusetts, U.S.A.

Dr. E. Thrane
Norwegian Defence Research Establishment,
P.O. Box 25,
Kjeller/Lillistrom, Norway.

Dr. H. Volland
Mitteilungen Der Astromischen Institute,
Der Universitat Bonn,
Bonn, Germany.

Dr. A. von Biel
Cornell Aeronautical Laboratory Incorporated,
Buffalo 21, New York, U.S.A.

Dr. E.S. Warren
Defence Research Telecommunications Establishment,
Ottawa, Canada.

Mr. Noboru Wakai
Institute for Telecommunication Sciences and Aeronomy,
Environmental Science Services Administration,
Boulder, Colorado, U.S.A.

Dr. A.H. Waynick
Ionosphere Research Laboratory,
Pennsylvania State University,
University Park,
Pennsylvania, U.S.A.

Dr. R.C. Whitten
Department of Atmospherics Sciences,
Stanford Research Institute,
Menlo Park, California, U.S.A.

Dr. J.W. Wright
Institute for Telecommunication Sciences and Aeronomy,
Environmental Science Services Administration,
Boulder, Colorado, U.S.A.

Dr. S.P. Zimmerman
Air Force Cambridge Research Laboratories,
Bedford, Massachusetts, U.S.A.

TABLE OF CONTENTS

SECTION 5 – Ionospheric Sounding
Chairman – Dr. G.L. Nelms,
DRTE, Ottawa

SECTION 6 – Ionospheric Absorption
Chairman – Dr. W. Pfister,
AFCRL, Bedford

SECTION 7 – Discussion

SECTION 8 – Epilogue

SECTION 4

REFLECTION OF LONG RADIO WAVES

4.1.1 SOME COMMENTS ON THE DETERMINATION OF D-REGION ELECTRON DENSITY DISTRIBUTIONS FROM THE REFLECTION OF LONG RADIO WAVES

by

J.S. Belrose and B. Segal

Radio Physics Laboratory
Defence Research Telecommunications Establishment
Ottawa, Ontario, Canada

Presented by B. Segal

1. Introduction

Large amounts of data pertaining to the propagation of long and very-long radio waves for a multitude of paths have been accumulated over the past two decades. Despite the fact that these waves are reflected near the base of the ionosphere and therefore contain information about the electron number densities and collision frequencies in this region, few quantitative results have thus far emerged from these data. Experimentally, difficulties arise because of the long wavelengths involved. The ground-wave for these frequencies propagates easily to great distances, so that measurements of the sky-reflected signals are often contaminated by unwanted components. Theoretically, also, the long wavelengths result in difficulties. At 30 kHz., the free-space wavelength is 10 km. Over such intervals, the lower portions of the ionosphere may drastically alter their properties. Hence, it is essential that a full-wave theory be used to study the propagation and reflection of low-frequency radio waves. Until the widespread introduction of high-speed digital computers, full-wave calculations were impractical except for limited cases. Recently, progress has been made in overcoming these limitations, and a number of programs exist for the solution of the differential equations that govern the propagation and reflection of long radio waves, such as those of Krasnushkin (1961), Johler and Harper (1962), Pitteway (1965) and others. The two methods most widely used in the study of long-wave propagation have been those of Pitteway and Johler.

2. Numerical Methods

The Pitteway program is based on the method described by Budden (1955) and considers two linearly independent solutions of the wave equation. Horizontally stratified electron density and collision frequency profiles are assumed and the wave integration is started at high heights subject to the boundary condition that all the energy in the wave must be upgoing. The solutions are then followed downward through the ionosphere until free space is encountered. Here the solutions are identified with the upgoing and downcoming components, and the reflection coefficients and polarization are obtained. Since the solutions of the wave equation are orthogonal, suitable linear combinations of these solutions may be formed to allow for any desired incident polarization.

Gossard (1964) has used a similar technique based on the method of Barron and Budden (1959), to compare the polarization of sky-reflected signals in the VLF band steeply incident on the ionosphere with predictions based on a number of different electron density models for the D region. Since Gossard did not calculate the ionospheric reflection coefficients either as functions of frequency or angle of incidence, the results are of limited value to other workers concerned with different VLF circuits.

Inoue and Horowitz (1966) have recently reported on a new numerical technique for solving the wave equation in a horizontally stratified, inhomogeneous, anisotropic ionosphere. In this technique, four solutions are obtained for the equations within the ionosphere, giving a complete description of both the upgoing and downcoming waves.

The method of Johler and Harper (1962) assumes a field incident on the base of the ionosphere. As in the previous cases, arbitrary vertical profiles of electron density and collision frequency are assumed. The program, however, proceeds differently. In Johler's method, the ionosphere is divided into a large number of thin, homogeneous slabs; the incident wave proceeds upward through the ionosphere and the transmission and reflection coefficients are evaluated at each interface, due regard being taken of the partial reflection at all other interfaces. After traversing the entire ionosphere, downgoing fields are integrated and the four reflection coefficients are computed. The number of uniform slabs is automatically increased until a stationary solution is obtained. A copy of this program has been borrowed from the National Bureau of Standards and is being used at DRTE to compare the results of long-wave propagation with results obtained by other experimenters. Some of the results thus far obtained will be discussed later.

Quite a different technique has been outlined by Krasnushkin (1961), who assumes that the collision frequency profile as a function of height, and the variation of the reflection and conversion coefficients as functions of angle of incidence, are known. It is claimed that the electron density profile can be determined uniquely from this data, and accuracies of about ± 1 km. in height or about ± 25 per cent in electron density are indicated. Computational details are few; however, using the reflection coefficients of Bracewell, Budden et al. (1951), some interesting N(h) profiles were published by Krasnushkin and Kolesnikov (1962). Some of these profiles will be discussed shortly.

3. Collision Frequencies

Unfortunately, most of the full-wave methods of studying propagation in the ionosphere make use of Appleton-Hartree theory, which treats the collision frequency as a real constant. The work of Molmud (1959), Sen and Wyller (1960) and others (Shkarofsky 1960, Budden 1965) leads to the use of an 'effective' collision frequency in the Appleton-Hartree equation, which usually varies from $3/2\ \nu_m$ at low heights where $\omega_H << \nu_m$, to $5/2\nu_m$ at higher heights where $\omega_H >> \nu_m$. Budden (1965) has considered long-wave propagation of 16 and 200 kHz. waves at steep incidence and has found that the use of generalized theory gives results in agreement with Appleton-Hartree theory if $\nu_{eff} = 5/2\nu_m$ is used. Significant differences in the wave polarization, however, occurred at low heights. Deeks (1966) has indicated that the differences between the reflection coefficients calculated by generalized theory and Appleton-Hartree theory are small at steep incidence in middle latitudes, the generalized theory predicting slightly less absorption at all heights. Budden (1965) has suggested that significant errors might be involved in the propagation of very-low-frequency waves at grazing incidence, or near the magnetic equator.

Deeks (1965) and the authors have both started with the asymptotic approximations $\nu_{eff} = 3/2\nu_m$ and $5/2\nu_m$, and have varied ν_{eff} smoothly from one asymptote to the other. There is no good justification for this; in fact, work done by Burke (1961) at DRTE and by Seliga (1965) have indicated that such approximations are not valid since the collision frequency enters differently into the real and imaginary parts of the Appleton-Hartree equations, and different curves should be used for each. Futhermore, a slightly different collision frequency relation should be used for each different wave frequency.

Fig. 1 shows the collision frequency profiles used in this work. The two asymptotic curves $\nu_{eff}=3/2\nu_m$ and $\nu_{eff} = 5/2\nu_m$ are shown as well as the transition curves, which were used for the bulk of the work to be discussed. The profile used by Deeks (1965) and May (1965) for their winter and equinox calculations resembled the curve $\nu_{eff} = 3/2\nu_m$, while for their summer calculations they used a profile close to the $5/2\nu_m$ curve. Krasnushkin and Kolesnikov (1962) used "effective" collision frequencies that were close to the $5/2\nu_m$ curve.

4. Experimental Measurements of Reflection Coefficients

Low-frequency reflection coefficients experimentally determined by Belrose (1963) are shown in Fig. 2. Data for different seasons and for different times of day for quiet sun years are presented. Note that the data are plotted with frequency times the cosine of the angle of incidence as abscissa. The use of an "effective" frequency in this manner has been suggested by Allcock (1955) as a method of comparing steep and oblique incidence data for different frequencies. In summer there is a sharp drop in the reflection coefficient observed in the 20 to 35 kHz. range. The steep incidence observations of Bracewell et al. (1953) made in sunspot maximum years, more clearly illustrate that in summer there is a sharp change in the field in the 30 to 35 kHz. frequency range, which is more restricted in frequency than the oblique incidence sunspot minimum results (for "effective" frequency) of Belrose (1963) would suggest. Unfortunately, no steep incidence data for these frequencies were available in sunspot minimum years. Data points labelled by letters in Fig. 2 are steep incidence measurements of conversion coefficient (which approximately equal the reflection coefficient in this distance range) and the data points labelled by numerals are oblique incidence measurements of reflection coefficient. If the points in this frequency band could be ignored, one might draw a totally different curve through the remaining points— more in keeping with those for other seasons. Deeks adopted the dashed line as being representative of the average summer ionosphere during periods of minimum solar activity. For winter and equinox he chose values that agree closely with the curves shown in the figure. Using these relations, he sought and ultimately arrived at N(h) profiles that gave these variations when the frequency was varied between 16 and 70 kHz. for steep incidence.

5. The Deeks and Krasnushkin Profiles

Some of the results obtained by Deeks using Pitteway's program, and by Krasnushkin and Kolesnikov, are shown in Fig. 3. Curves 5, 6 and 7 are Deeks' winter, equinox, and summer profiles, while curves 2 and 3 are Krasnushkin's winter and summer profiles. Notice that Deeks was compelled to have a well-defined minimum between the C and D layers for all seasons, while Krasnushkin indicates only an inflection in the N(h) curves. Notice also in comparing the winter and summer curves that Krasnushkin found virtually the same N(h) profile below 65 or 70 km., but an order of magnitude difference above 75 km. Deeks' curves are nearly the same above 75 km. for all seasons. In comparing these results it should be borne in mind that they refer to different epochs of the solar cycle, the Deeks curves shown here being for SS minimum and the Krasnushkin curves for SS maximum.

6. Some Calculations of Conversion Coefficient

In Fig. 4, the Deeks summer N(h) curve is shown in greater detail. The peak in electron density that occurs between 60 and 65 km. is followed by a reduction to nearly half the density at 68 km. The profile then rises more or less smoothly to 10^5 electrons/c.c. at 100 km. In order to compare the National Bureau of Standards program with the Pitteway program, the conversion coefficients $_{\parallel}R_{\perp}$ were computed using the Deeks summer profile with the NBS program. The results, for an angle of incidence of 30°, are indicated in Fig. 5 along with the data used by Deeks in deducing his N(h) profile. Note the excellent agreement between the two sets of data for frequencies up to 60 or 70 kHz. In view of the fact that the scaling of the Deeks profile was done from a poor copy of the original curve (local departures of 10 per cent might reasonably be expected), as well as the slightly different collision frequency profiles used, it is felt that the agreement obtained was good and this has provided confidence in the numerical results. Since this work was first reported, a more detailed check was performed using a set of electron density and collision frequency profiles obtained from Dr. Pitteway. Agreement to within 1 per cent in the magnitudes and 2.5 per cent in the phases of the four reflection coefficients was obtained for a frequency of 16 kHz. and angle of incidence of 80°.

Fig. 6 compares the Deeks summer profiles with two other summer profiles measured at Ottawa. It is seen that the two most significant differences between the "average" summer profile and the Deeks profile are that the Deeks curve is deficient in electron density in the 65 to 72 km. height range, and that beyond 10^3 electrons/c.c. the "average" curve is lower by some 2 or 3 km. than the Deeks profile. One would expect qualitatively that at very low frequencies the "average" profile would provide greater attenuation and thus reduced reflection coefficients, while at higher frequencies the effect of lowering the height of reflection would play a more significant role and that the total absorption would be reduced. These qualitative conclusions are borne out by the results shown in Fig. 7.

The 26 June, Ottawa profile would be expected to show enhanced absorption at all frequencies in the 10 to 100 kHz. range, compared with the "average" profile. The results shown in Fig. 7 again bear this out. The increase in conversion coefficient at frequencies greater than 40 kHz. compared with the Deeks profile is again due to the fact that the enhanced ionization results in a lowering of the reflection height and a reduction in the total absorption.

The outstanding feature of the 26 June profile lies in the behavior of the conversion coefficient in the vicinity of 30 kHz. In Fig. 7 the value of $_{\parallel}R_{\perp}$ for 30 kHz. is seen to be precisely a factor of 10 below an otherwise smooth curve. The possibility of an interference effect acting is suggested by the fact that for this profile the classical "ray theory" reflection height for a 30-kHz. wave occurs exactly one free-space wavelength above the C-region peak in electron density near 70 km. This sharp reduction in conversion coefficient near 30 kHz. is probably related to the previously mentioned experimental observation of Belrose that conversion coefficients in summer are significantly less, in the 30 to 35 kHz. range, than would be expected from observations at other seasons.

In order to investigate the interference hypothesis more fully, conversion coefficients for the 26 June profile were computed for a number of closely spaced frequencies from 20 to 50 kHz. Fig. 8 shows clearly the positive nature of this interference. Three complete oscillations are observed above 30 kHz. and the pattern would certainly continue to higher frequencies if more points had been calculated. A similar but less dramatic oscillation has been observed by Deeks (1965) commencing at about 40 kHz. This profile, as with the 26 June profile under consideration, showed a well-developed C-layer peak in electron density with a sharp "ledge" some 10 km. above the peak.

Various modifications of the "average" summer profile are indicated in Fig. 9. In modification 'A', the gradient of electron density has been reduced above 90 km. The effect of this change (see Fig. 10) is small indeed and is just noticeable at 80 and 100 kHz., in agreement with the fact that the modification commences at the level where ray theory predicts 80-kHz. reflection. The result is what one would expect from the slight increase in reflection height. The change in gradient does not appear to be important. Modification 'B' is more extensive, starting at about 400 electrons/c.c. One would thus expect an increase in the conversion coefficients for all frequencies greater than about 20 kHz. This is what is observed. The slight increase at 10 kHz. was unexpected, but the amount is small and is due to penetration of the wave beyond the height where $X = 1 + Y$. Change 'C' in the profile should reduce the attenuation for waves of all frequencies that penetrate this region, and in agreement with previous observations this is observed.

The increase in ionization between 55 and 63 km. indicated as modification 'D' did not produce a significant change in reflection coefficient, even for 10-kHz. waves which are reflected just a short distance above. Another modification, not shown here, in which the electron density gradient at the base of the profile was markedly reduced, affected the entire curve only slightly.

The influence of ionization in the 60 to 75 km. height range, as exemplified by modification 'C' is carried one step further in Fig. 11, where the summer profile "bulge" in electron density has gone through a linear variation to a minimum in the "average" slightly disturbed winter profile. The remaining portions of the profiles are similar. Note that the reflection coefficients have again been increased at all frequencies. The dashed line in Fig. 12 is the winter observation of Belrose (1963). From the observations made in the course of this paper, if one sought a better agreement between the winter N(h) profile and the observational results of Belrose, the entire winter profile would be raised by about 2 or 3 km., with the upper portion of the profile raised an additional 1 or 2 km. If this were done, then one would in fact arrive at precisely that profile deduced by Deeks (1965) from this observational data.

Until this point, we have considered the effects of various electron density profiles on the ionospheric reflection of low-frequency waves. Fig. 13 shows the results obtained when the reflection coefficients were calculated using the "average" summer profile and the three different collision frequency curves shown in Fig. 1. All previous results have been obtained using the transition curve going from $\nu_{eff} = 3/2\nu_m$ to $5/2\nu_m$ with increasing height. The results obtained with the two asymptotic limits $\nu_{eff} = 3/2\,\nu_m$ and $\nu_{eff} = 5/2\nu_m$ were somewhat unexpected. The increased reflection coefficients computed with the $3/2\nu_m$ curve are a direct consequence of the reduced attenuation at all heights; however, the results obtained with the profile that varied from $3/2\nu_m$ to $5/2\nu_m$ are close to those for the $\nu_{eff} = 5/2\nu_m$ curve. This fact, and the fact that the results lie entirely outside the bounds formed by the two asymptotic limits, must be connected in some way with the gradient of collision frequency with height near the reflection level.

7. Discussion of Results

A computer program, developed at the National Bureau of Standards, has been employed successfully at DRTE to compute the ionospheric reflection coefficients for long radio waves using various electron density profiles including a number measured at Ottawa by the partial reflection technique. The results of this program, for both steep and oblique incidence, have been compared with those predicted by a different method and were found to be in good agreement.

Variations in reflection coefficient as a function of frequency, in general, agreed qualitatively with what one would expect from the electron density profile. The sensitivity of the results to profile changes suggests that the experimental measurement of steep incidence conversion coefficients at a number of frequencies might provide a useful technique for corroborating N(h) profiles deduced by other experimental methods, particularly in the height range above 65 km. This might help settle an important question in the partial reflection experiment, namely, whether the reflection mechanism is due to fluctuations in the ambient electron density or in the collision frequency (Belrose et al.).

The electron density profile for a particular summer day, measured at Ottawa, was found to predict a sharply reduced ionospheric return at 30 kHz., with an oscillatory behavior at higher frequencies in a manner suggesting the destructive interference of two or more reflected components. A similar observation made by Deeks suggests that this may be a more or less regular feature of N(h) profiles that possess a deep minimum between the C and D layers. This behavior may have some bearing on the experimental observations of Belrose and Krasnushkin that reflection coefficients in summer in the 30 to 40 kHz. range are less than one would expect from observations at other frequencies or at different times of year. It also points out clearly the serious errors that may be incurred by the use of reflection coefficient data interpolated from observations at a few widely spaced frequencies.

There is evidence to suggest that ionospheric reflection coefficients calculated using the Appleton-Hartree equations with a value of $\nu_{eff} = 5/2\nu_m$ agree with calculations using the generalized theory (Budden). Other work (Deeks) suggests that a profile which varies from 3/2 to $5/2\nu_m$ should be used. For at least one N(h) profile – an average summer curve for Ottawa – similar results were obtained using both these approximations. The results for $\nu_{eff} = 3/2\nu_m$ differed from these by a significant amount suggesting that the gradient of collision frequency with height is an important parameter in the reflection process.

REFERENCES

Allcock, G. McK. Ionospheric absorption at low and medium frequencies. Proceedings of the Conference, "The Physics of the Ionosphere", 1954, 14-19. Phys. Soc., London, 1955.

Barron, D.W. and K.G. Budden. The numerical solution of differential equations governing reflexion of long radio waves, part III. Proc. Roy. Soc., A249, 387-401, 1959.

Belrose, J.S. The oblique reflection of low-frequency radio waves from the ionosphere. AGARDOgraph 74, 149-165, Pergamon Press, London, 1963.

Belrose, J.A. and M.J. Burke. Study of the lower ionosphere using partial reflection, part I. Experimental technique and methods of analysis. J.G.R., 69, 2799-2818, 1964.

Belrose, J.S., Bourne, I.A. and L.W. Hewitt. A critical review of the partial reflection experiment, paper 2.1, these proceedings, 1966.

Bracewell, R.N., Budden, K.G., Ratcliffe, J.A., Straker, T.W., and K. Weeks. The ionospheric propagation of low- and very-low-frequency radio waves over distances less than 1000 km. Proc. Inst. Elect. Eng., III, 98, 221-236, 1951.

Bracewell, R.N., Harwood, J., and T.W. Straker. The ionospheric propagation of radio waves of frequency 30 to 65 kc/s. over short distances. Proc. Inst. Elect. Eng., Monograph No. 84, December 1953.

Budden, K.G. The numerical solution of differential equations governing reflexion of long radio waves from the ionosphere, part I. Proc. Roy. Soc. A227, 516-537, 1955.

Budden, K.G. Effect of electron collisions on the formulas of magneto-ionic theory. Radio Science, 69D, 191-211, 1965.

Burke, M.J. Private communication, 1961.

Deeks, D.G. D-region electron distributions in middle latitudes deduced from the reflexion of long radio waves. Internal memorandum No. 219, Radio and Space Research Station, Slough, (Privately circulated) 1965. Also published in Proc. Roy. Soc., A291, 413-437, 1966.

Deeks, D.G. Generalized full-wave theory for energy-dependent collision frequencies. Internal memorandum No. 244. Radio and Space Research Station, Slough, (Privately circulated) 1966. Also published in J.A.T.P., 28, 839-846, 1966.

Gossard, E.E. Model studies of the nighttime ionospheric D-region from polarization measurements made at the ground. Report No. 1249, U.S. Navy Electronics Laboratory, 1964.

Ionoue, Y. and S. Horowitz. Numerical solution of full-wave equation with mode coupling, Research paper No. 196. U.S. Air Force Cambridge Research Laboratories, 1966. Also published in Radio Science 1, 957-970, 1966.

Johler, J.R. and J.D. Harper. Reflection and transmission of radio waves at a continuously stratified plasma with arbitrary magnetic induction. J. Res. 66D, 81-99, 1962.

Krasnushkin, P.Y. The propagation of long and ultra-long radio waves about the earth in the lower layers of the ionosphere in the light of information theory. Doklady Alkademiya Nauk SSSR 139, 67-70, 1961. Translated in Soviet Physics-Doklady 6, 576-579, 1962.

Krasnushkin, P.Y. and N.L. Kolesnikov. Investigation of the lower ionosphere by means of long radio waves and low-frequency probes installed on a rocket, detection of a new ionospheric layer. Doklady Akademiya Nauk SSSR, 146, 596-599, 1962, Translated in report AID 62-207. Aerospace Information Division, Library of Congress, Washington, 1962.

May, B.R. The investigation of experimentally determined distributions of D-region electron density using full-wave techniques. Internal memorandum No. 208, Radio and Space Research Station, Slough, (Privately circulated) 1965.

Molmud, P. Langevin equation and the AC conductivity of non-Maxwellian plasmas. Phys. Rev. 114, 29-32, 1959.

Pitteway, M.L.V. The numerical calculation of wave-fields, reflexion coefficients and polarizations for long radio waves in the lower ionosphere, part I. Phil. Trans. Roy. Soc. A257, 219-241, 1965.

Seliga, T.A. Electron densities in the D-region of the ionosphere from low-frequency signal strength measurements in rockets. Scientific Report No. 254, Ionosphere Research Laboratory, Penn. State Univ., 1965.

Sen, H.K. and A.A. Wyller. On the generalization of the Appleton-Hartree magnetoionic formulas. J.G.R. 65, 3931-3950, 1960.

Shkarofsky, I.P. Values of the transport coefficients in a plasma for any degree of ionization based on a Maxwellian distribution. Research report 7-801, R.C.A. Victor, Ltd., Research Laboratories, Montreal, 1960.

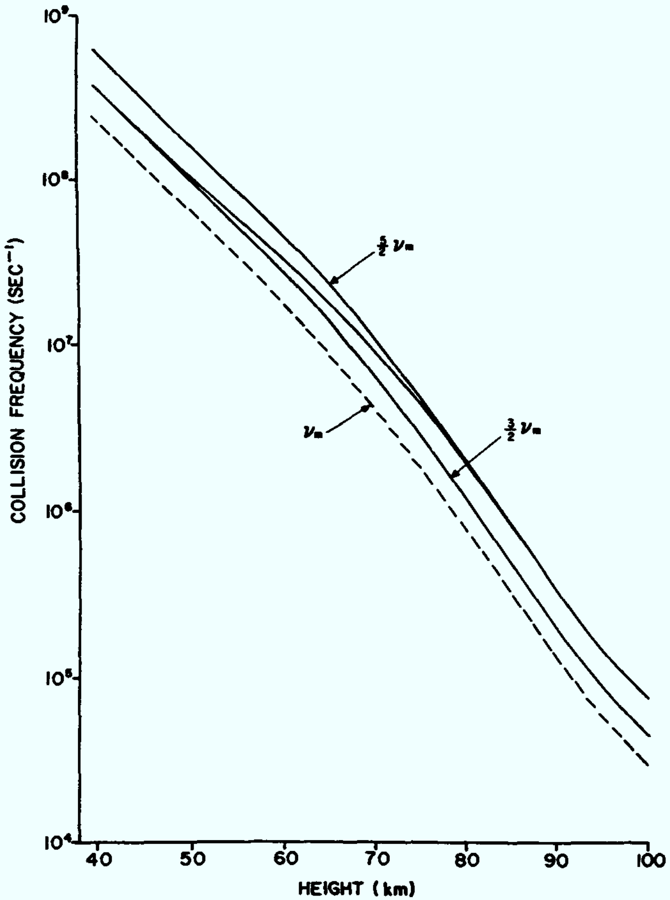

Fig. 1. Collision frequency versus height profiles. The dashed curve, ν_m, gives the collision frequency for monoenergetic electrons of energy kT (Belrose and Burke). The curves $3/2\nu_m$ and $5/2\ \nu_m$ are the asymptotic approximations for ν_{eff} in Appleton-Hartree theory valid at low heights and high heights respectively.

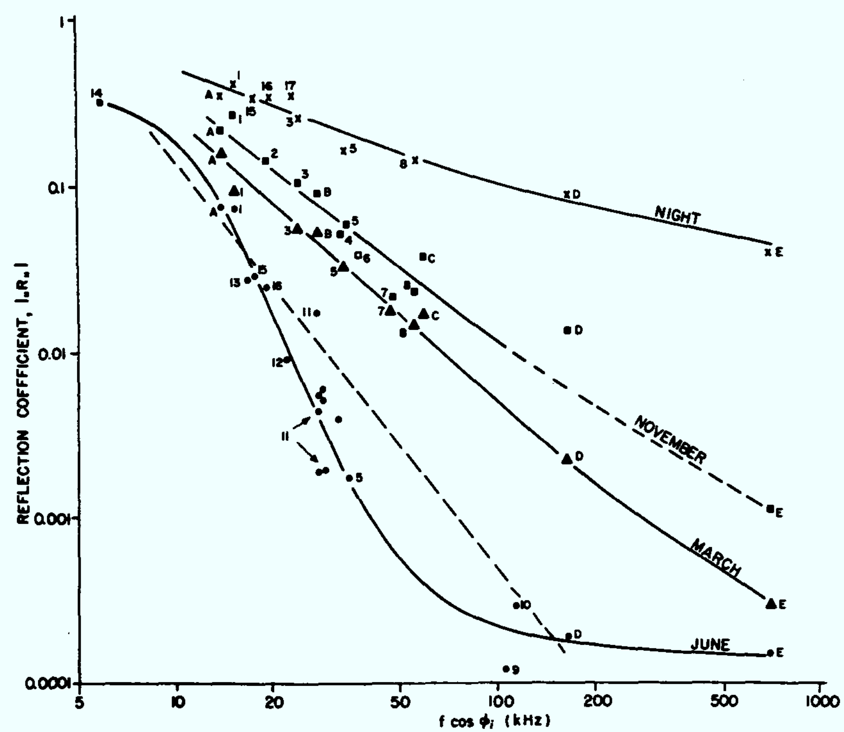

Fig. 2. Reflection coefficients experimentally determined by Belrose for various LF and VLF circuits during quiet sun years. An "effective" frequency, equal to the wave frequency multiplied by the cosine of the ionospheric angle of incidence, is used as abscissa (after Allcock).

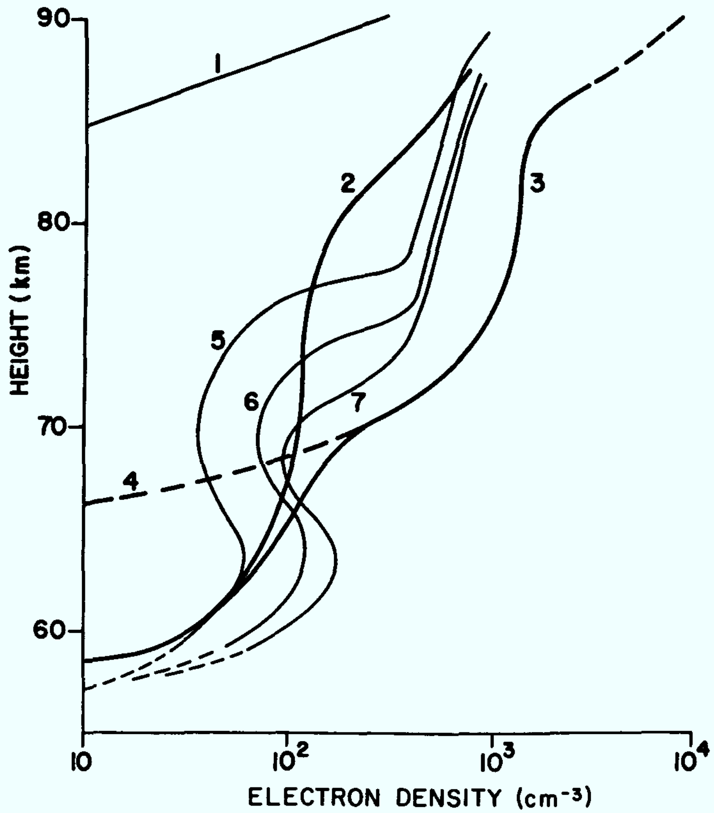

Fig. 3. N(h) profiles deduced from analysis of long-wave propagation data. Curves 1, 2, 3 and 4 are from Krasnushkin and Kolesnikov and refer to night, midday winter and midday summer at middle latitudes, and midday at equatorial latitudes respectively. These data refer to periods of maximum solar activity. Curves 5, 6 and 7 are from Deeks and refer to midday for winter, equinox, and summer at middle latitudes during sunspot minimum years.

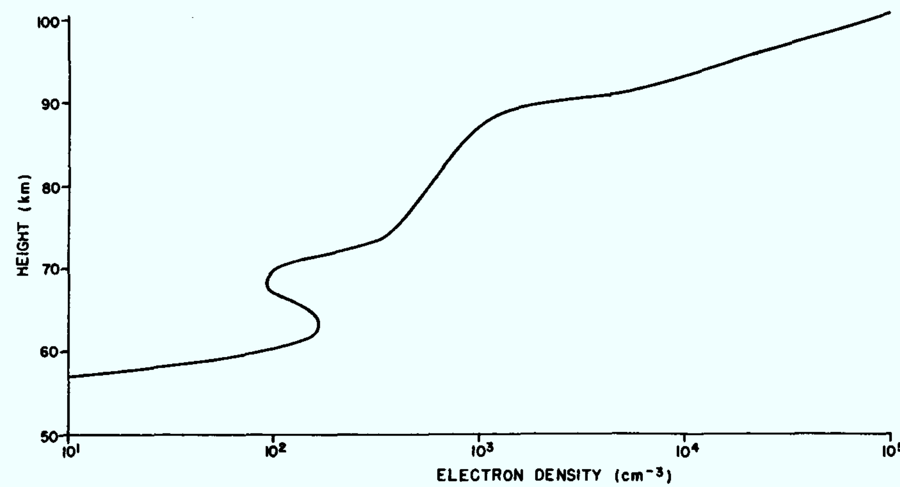

Fig. 4. Electron density profile deduced by Deeks for midday summer, sunspot minimum.

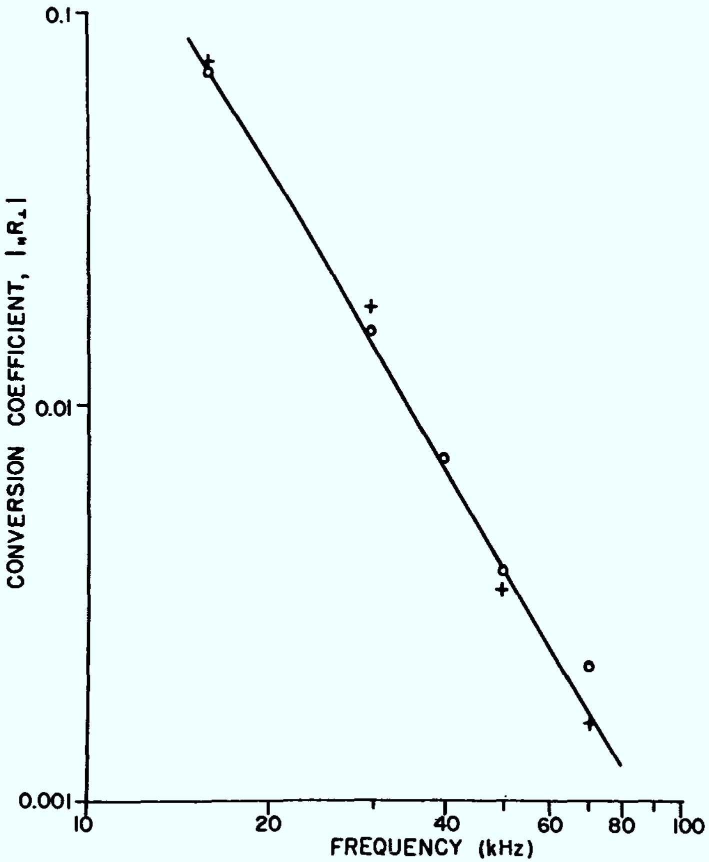

Fig. 5. Conversion coefficient, $_{\parallel}R_{\perp}$, as a function of frequency assumed by Deeks to represent summer conditions for quiet sun years. The crosses represent the points re-calculated by Deeks – the open circles the points computed as described in the text.

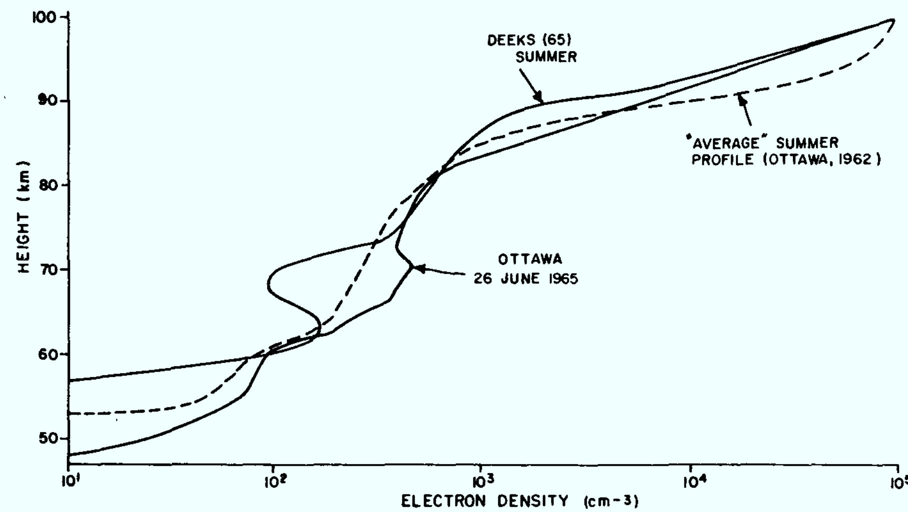

Fig. 6. The Deeks electron density profile for summer compared with two other summer N(h) profiles measured at Ottawa.

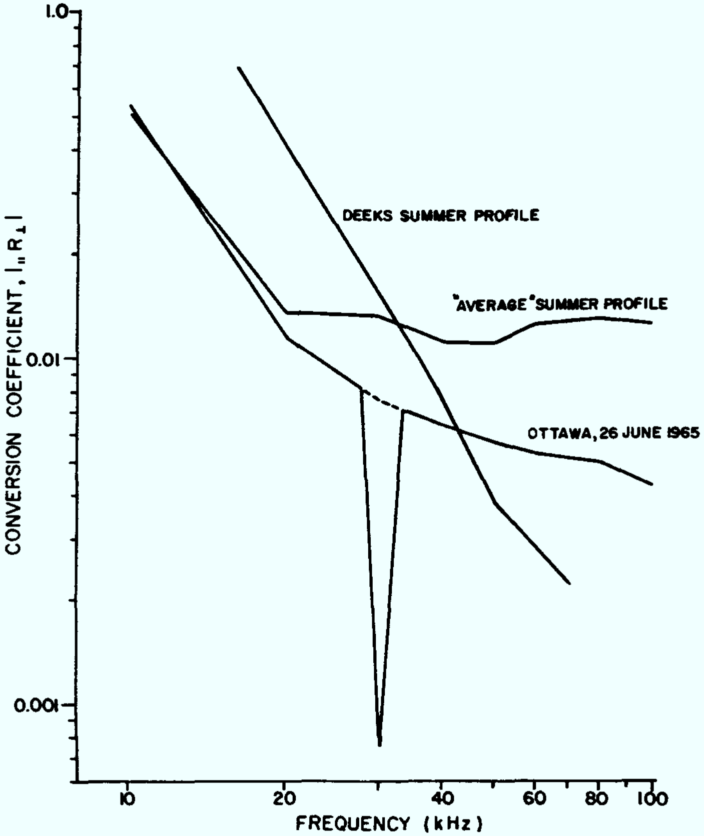

Fig. 7. The conversion coefficients as functions of frequency for the N(h) profiles of Fig. 6. The angle of incidence of the wave on the base of the ionosphere is 30° in the case of the Deeks profile and 20° for the other profiles.

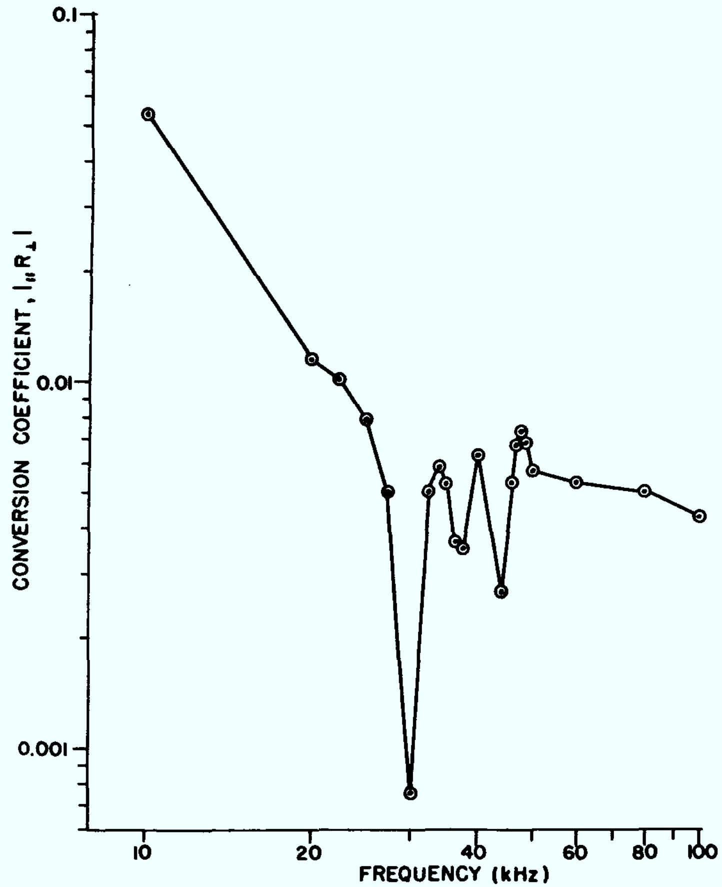

Fig. 8. The conversion coefficient as a function of frequency for the Ottawa, 26 June 1965 profile of Fig. 6. The conversion coefficients have been calculated for more closely-spaced frequencies in the range 20 to 50 kHz. and indicate more clearly the nature of the interference commencing at about 30 kHz.

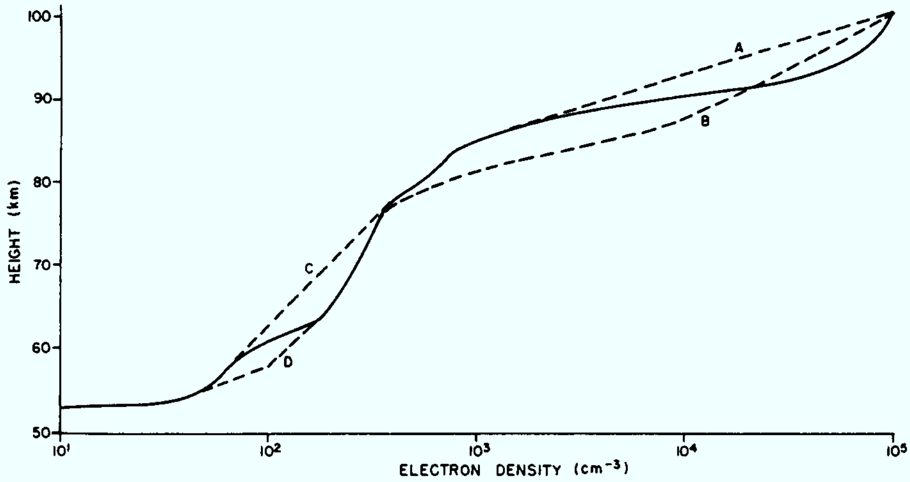

Fig. 9. The "average" summer profile of Fig. 6 with several modifications indicated.

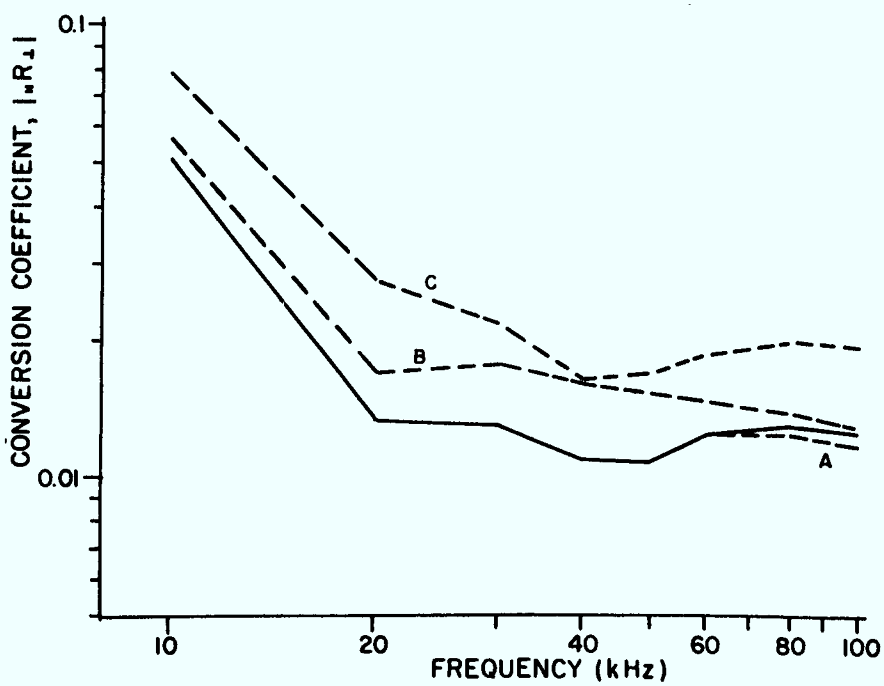

Fig. 10. The conversion coefficients, $_{\parallel}R_{\perp}$, computed for the profiles of Fig. 9 as functions of frequency. The waves were assumed incident on the ionosphere at an angle of 20°.

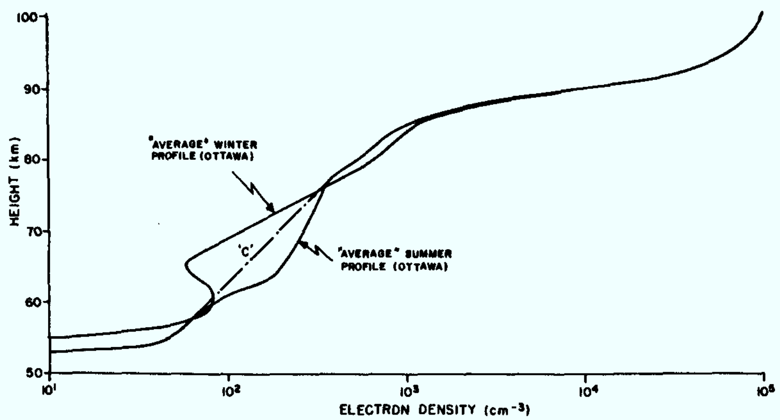

Fig. 11. Average summer and winter N(h) profiles measured at Ottawa having enhanced and diminished electron density respectively in the 60 to 75 km. height range, relative to modification 'C' of the "average" summer profile.

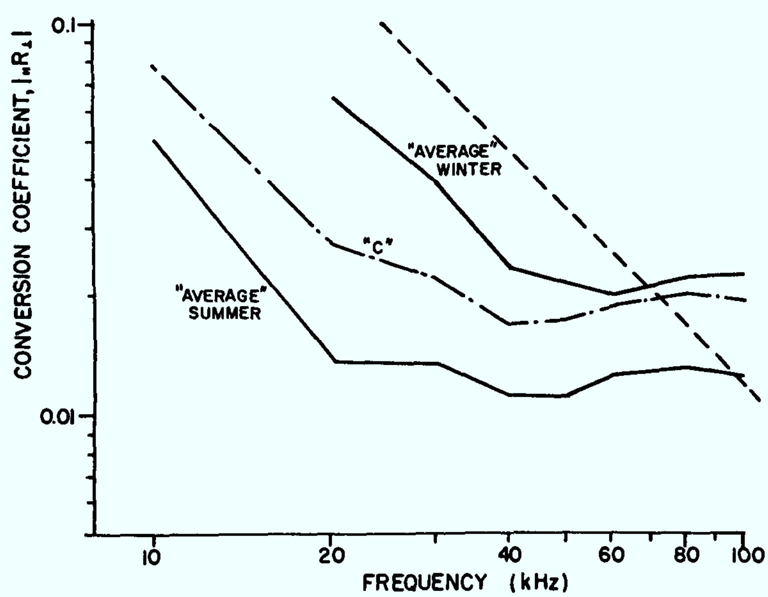

Fig. 12. Conversion coefficients as functions of frequency for the electron density profiles of Fig. 11 and an angle of incidence of 20°. The dashed curve is the winter curve of Belrose.

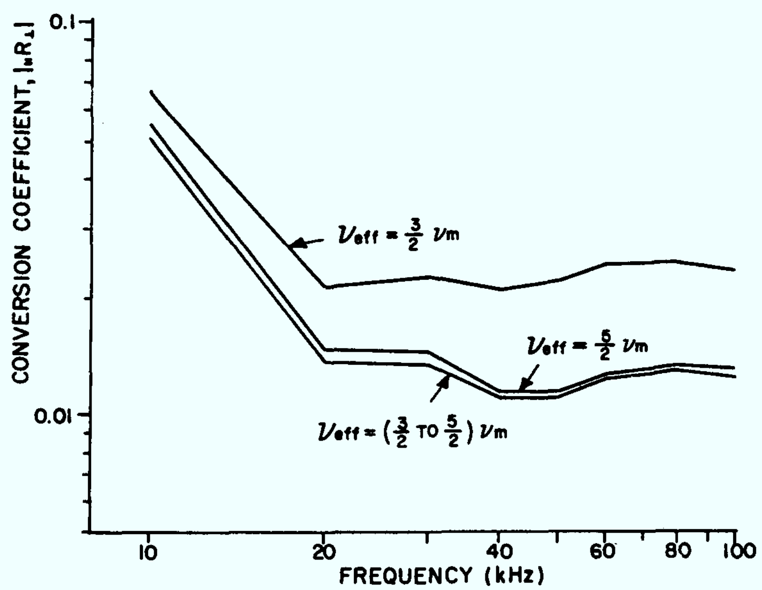

Fig. 13. Results obtained using the three collision frequency profiles of Fig. 1 and the "average" summer N(h) curve.

Discussion on Paper 4.1.1 presented by B. Segal

Bibl: Did I understand correctly that the effect of increasing the electron density below 85 km. has the inverse effect of an increase above 85 km. in the frequency dependence of the reflection coefficient?

Segal: Yes, this was so for the profiles discussed here. The nature of the profiles was such that at most of the frequencies considered the waves were reflected from the rapidly increasing portion above about 80 km.; thus, increasing the density at low heights increased the wave absorption. Above this height, increasing the electron density served to lower the reflection height and thus reduce the integrated attenuation. A similar behavior was noted by Piggott et al. (1965) for 16 kHz. waves with the "crossover" occurring at 70 km.

Bibl: Is it actually the changes in electron density, or the gradient of electron density, that produced these effects? It would be helpful if you could obtain an approximate formula relating how the density and the changes in gradient get into the picture.

Segal: It would indeed be helpful, but I doubt that such a formula could be much simpler than the actual full-wave equations for computing the reflection coefficients themselves.

Belrose: The astonishing thing is that small changes in profiles make a marked difference in the slope of the curves for conversion coefficient. The major difference between the Deeks summer profile and the "average" summer profile is in the 60- to 70-km. range, and yet it produced a marked difference. With these two curves ("average" summer profile and June 26 profile, Fig. 6) we don't get as much absorption as Deeks at the higher frequencies.

Sales: For the higher frequencies you have increased the gradient at the high levels – possibly by a fair amount – and this may play a more important role than filling the "hole" in the 60- to 70-km. range. It would be nice to play with artificial models and test such things quantitatively when making the changes – one change independent of the other. In this figure you have two changes, and so you cannot say which is more important.

Segal: Related work that we have done has led us to believe that the actual gradient at high heights is not significant.

Bibl: Would it be an idea to have as parameters the electron density and the gradient of electron density?

Segal: It is not possible to alter the slope of the profile without simultaneously changing the electron densities.

Volland: I think Dr. Bibl's question can be answered if you calculate the reflection coefficients in such a form that you build up the layer from top to bottom and calculate the reflection coefficients step by step. Then plot reflection coefficients against height to see where the largest change occurs; then you can decide whether this comes from a gradient or from something else.

Belrose: The only way in which you can obtain answers that look, for example, like the Deeks answers is to use the Deeks profile. There appears to be something unique about each profile.

Waynick: You have mentioned that unique profiles could be obtained. It struck me that perhaps some people have either forgotten or not heard of the beautiful piece of work by Kay several years ago (Kay 1959), in which he shows that to obtain a unique profile from data such as these, one must obtain the reflection coefficient and the height of reflection as a function of frequency from zero to infinity, as you might expect. But an additional fact from this report is that you could get estimates of the accuracy and uniqueness of your profiles. I believe this is useful.

Piggott, W.R., Pitteway, M.L.V. and E.V. Thrane. *The Numerical Calculation of Wave-Fields, Reflexion Coefficients and Polarizations for Long Radio Waves in the Lower Ionosphere, Part II.* Phil. Trans. Roy. Soc. **A257**, pp. 243 – 271, 1965.

Kay, I. *Remarks Concerning the Determination of Electron Distribution in the Ionosphere by Means of Radio Soundings.* Research Report EM-149, Inst. Math. Sci., New York Univ., 1959.

4.1.2 THEORY OF PROPAGATION OF LOW FREQUENCY TERRESTRIAL RADIO WAVES– MATHEMATICAL TECHNIQUES FOR THE INTERPRETATION OF D-REGION PROPAGATION STUDIES

by

J.R. Johler

Institute for Telecommunication Sciences and Aeronomy, Environmental Science Services Administration, Boulder, Colorado, U.S.A. *

Abstract

The various forms of the solution of Maxwell's equations for propagation of low frequencies in the waveguide between a spherical earth and a concentric ionosphere are given. A tutorial discussion gives various solutions to acquaint experimenters with the practical techniques available. A feature of these solutions is the accommodation of the effect of variation with height of the electrical properties of the upper boundary (ionosphere). Forms of the waveguide solution include the zonal harmonics series for total field, mode sum, and geometric (wavehop) series. Connections between various forms are shown. The discussion is enhanced by sample calculations of the geometric series type solution for normal day and night.

1. Introduction

Imagine the terrestrial waveguide for low frequency radio wave propagation between the ionosphere and the ground as a finitely conducting sphere and a concentric reflecting shell. This model is mathematically tractable for wave propagation, since solutions of Maxwell's equations, $\vec{E}$, volts/meter, and $\vec{H}$, amperes/meter, can be found for an electrical point source in the waveguide. The boundary conditions are of course imposed at the boundaries of the waveguide. In fact, further simplification of this model to a two-dimensional circular cross section, $a < r < g$, (Fig. 1) where r is the radial distance from the center of the terrestrial sphere and a is the radius at the surface of the ground, is a suitable model for a variety of practical applications. At low frequencies a comparatively definite surface (or in two dimensions a line), $g = a + h$, can usually be regarded as the upper boundary of the waveguide. This boundary is located in the D region of the ionosphere in the real world. Mathematically, however, the reflection process at or near this boundary is complicated by the physical fact that the reflector is a magneto-plasma into which waves penetrate a considerable distance before reflecting. This latter phenomenon requires the introduction of mathematical techniques for treating profiles of electron density, collision frequency, and possibly ion densities.

---

* Formerly the Central Radio Propagation Laboratory of the National Bureau of Standards, Boulder, Colorado, CRPL was transferred to ESSA in October, 1965.

Further consideration of the reflection process at the ionosphere, r = g = a + h, (Fig. 1), (Johler and Berry 1964, and Budden 1961) leads to a characterization of the reflection process as a matrix, T,

$$T = \begin{bmatrix} T_{ee} & T_{em} \\ T_{me} & T_{mm} \end{bmatrix} \tag{1.1}$$

where T_{ee} is the Fresnel type reflection coefficient (which can be corrected for sphericity) described by Johler and Harper (1962) for TM (transverse magnetic) mode of propagation in the waveguide (the ratio of vertical electric reflected to vertical electric incident fields). Here, T_{em} is the abnormal component (the ratio of vertical magnetic reflected to vertical electric incident fields) giving rise to the TE propagation modes in the waveguide. Similarly, T_{mm} refers to the TE-mode and T_{me} is the corresponding abnormal component. Thus, notwithstanding a pure TM-mode waveguide excitation (vertical electric dipole), the TE-mode exists as a consequence of the anisotropic boundary, r = g. Under such conditions the ground reflection process at r = a, is represented by the matrix,

$$R = p\begin{bmatrix} R_e & 0 \\ 0 & R_m \end{bmatrix}. \tag{1.2}$$

Here R_e and R_m are spherical reflection coefficients, while p is a spherical wave propagation factor.

2. The Wave Propagation Formulas

Define $P_n(z)$ to be a Legendre function (for mathematical details see Abramowitz and Stegen 1964). Also, let the spherical wave functions $\zeta_n^{(1,2)}$, $\psi_n(z)$ be determined by

$$\zeta^{(1,2)}(z) = \sqrt{\frac{\pi z}{2}}\ H_{n+\frac{1}{2}}^{(1,2)}(z). \tag{2.1}$$

$$\psi_n(z) = \sqrt{\frac{\pi z}{2}}\ J_{n+\frac{1}{2}}(z) \tag{2.2}$$

where $J_{n+\frac{1}{2}}(z)$ and $H_{n+\frac{1}{2}}^{(1,2)}(z)$ are Bessel and Hankel functions, respectively, or order n + ½, and argument z and $H_n^{(1,2)}$ may be of the first or second kind (Watson 1958). The classical zonal harmonic series solution of the propagated field in the terrestrial waveguide model for the particular case of the vertical electric field, E_r, on the surface r = a placed a distance d = aθ (the length of the geodetic) from the vertical electric dipole point source of moment $I_0\ell$, ampere-meters is (Johler and Berry 1964)

$$E_r = \frac{I_0\ell}{k_1^2 a^4}\ \frac{\mu_0 c}{8\pi} \sum_{n=0}^{\infty} F(n)\ \zeta_{1\,a}^{(2)}\ \zeta_{1\,a}^{(1)}\ (1 + R_{e,n})\ \frac{|1 + \rho_n T_n|}{|1 - \rho_n R_{e,\,n} T_n|}\ , \tag{2.3}$$

where $F(n) = n(n+1)(2n+1)\ P_n(\cos\theta)$, $k_1 = \frac{\omega}{c}\eta_1$, for a frequency $f = \omega/2\pi$, where c is the speed of light, η_1 = 1.0001 to 1.0003 for air or η_1 = 1 in a vacuum, and $\mu_0 = 4\pi(10^{-7})$ is the permeability. The abbreviation, $\zeta_{1\,a}^{(1,2)} = \zeta_n^{(1,2)}(k_1 a)$ has been employed. The unit matrix, 1, is here defined

$$\mathit{1} = \begin{bmatrix} 1 & 0 \\ 0 & 1 \end{bmatrix} \tag{2.4}$$

and

$$R_e = \begin{bmatrix} R_e & 0 \\ 0 & -1 \end{bmatrix}, \tag{2.5}$$

$$\rho = p\begin{bmatrix} 1 & 0 \\ 0 - & R_m \end{bmatrix}, \tag{2.6}$$

$$p = \left(\frac{\zeta^{(1)}_{1\,a}}{\zeta^{(2)}_{1\,a}} \cdot \frac{\zeta^{(2)}_{1\,g}}{\zeta^{(1)}_{1\,g}} \right). \tag{2.7}$$

Finally, it is noted that the relation,

$$\psi_n(z) = \tfrac{1}{2} \left[\zeta_n^{(1)}(z) + \zeta_n^{(2)}(z) \right], \tag{2.8}$$

has been introduced.

The series (2.3) is slowly convergent but nonetheless useful at frequencies below approximately 10 kc/s. Each mode n is a solution of Maxwell's equations for the terrestrial waveguide, as is the sum. Watson (1918, 1919) proposed a representation of the zonal harmonic series as a contour integral, which can be written after introduction of the modern reflection coefficient matrices (2.4), (2.5), and (2.6)

$$\mathbf{E}_r = \frac{i}{k_1^2 a^4} \frac{\mu_0 c}{8\pi} \int_c \frac{F(\nu-\frac{1}{2})}{\cos \nu\pi} \zeta^{(2)}_{\nu-\frac{1}{2}}(k_1 a)\, \zeta^{(1)}_{\nu-\frac{1}{2}}(k_1 a) \frac{|\mathit{1} + \rho_{\nu-\frac{1}{2}} T_{\nu-\frac{1}{2}}|}{|\mathit{1} - \rho_{\nu-\frac{1}{2}} R_{e,\,\nu-\frac{1}{2}} T_{\nu-\frac{1}{2}}|} d\nu, \tag{2.9}$$

where

$$F(\nu-\tfrac{1}{2}) = 2\nu(\nu^2 - \tfrac{1}{4})\, P_{\nu-\frac{1}{2}}(-\cos\theta). \tag{2.10}$$

Stretching the contour, C, in a semicircle on the infinity of the right half of the complex ν-plane, it can be concluded that the field can be represented as a series of residues or waveguide modes, $s = 0, 1, 2, 3 \ldots,$

$$\mathbf{E}_r = \left[\frac{\mu_0 c}{4\pi} I_0 \ell\right]\left[\frac{-2\pi}{k_1^2 a^4}\right] \sum_{s=0}^{\infty} \frac{F(\nu_s - \frac{1}{2})}{\cos \nu_s \pi} \zeta^{(2)}_{\nu_s-\frac{1}{2}}(k_1 a)\, \zeta^{(1)}_{\nu_s-\frac{1}{2}}(k_1 a)$$

$$\times \frac{|\mathit{1} + \rho_{\nu_s-\frac{1}{2}} T_{\nu_s-\frac{1}{2}}|}{\left\{ \frac{\partial}{\partial \nu} |\mathit{1} - \rho_{\nu-\frac{1}{2}} R_{e,\,\nu-\frac{1}{2}} T_{\nu-\frac{1}{2}}| \right\}_{\nu=\nu_s}}. \tag{2.11}$$

It is, of course, now necessary to locate the poles, $\nu = \nu_s$, in the complex ν-plane with the well-known mode equation,

$$|I - \rho_{\nu-\frac{1}{2}} R_{e,\nu-\frac{1}{2}} T_{\nu-\frac{1}{2}}| = 0. \quad (\nu = \nu_s) \tag{2.12}$$

This solution (2.11) and (2.12) is the basic waveguide mode solution, and has been found to be especially useful at VLF and ELF. For details, see Wait's (1962) treatise. Johler and Berry (1964) have presented some computation techniques for the anisotropic case especially oriented toward use of electronic computers.

Another approach to the problem (Johler 1964, 1966, Berry 1964), utilizes the expansion of the determinant ratio in (2.8) in a geometric series,

$$\frac{|I + \rho_n T_n|}{|I - \rho_n R_{e,n} T_n|} = \left| I + (I + R_{e,n}) \sum_{j=1}^{\infty} (\rho_n R_{e,n} T_n)^{j-1} \rho_n T_n \right|. \tag{2.13}$$

This leads to the zonal harmonic-geometric series solution,

$$E_r = E_{r,0} + \sum_{j=1}^{\infty} E_{r,j}, \tag{2.14}$$

where, $j = 0$ is the ground wave. $j = 1, 2, 3 \ldots$ are the ionosphere waves, reflecting to and fro between the ionosphere and the ground.

$$E_{r,0} = \frac{\mu_0 c}{8\pi} \frac{I_0 \ell}{k_1^2 a^4} \sum_{n=0}^{\infty} F(n)\, \zeta_{1n}^{(2)} \zeta_{1n}^{(1)} (1 + R_n). \tag{2.15}$$

$$E_{r,j} = \frac{\mu_0 c}{8\pi} \frac{I_0 \ell}{k_1^2 a^4} \sum_{n=0}^{\infty} F(n)\, \zeta_{1n}^{(2)} \zeta_{1n}^{(1)} (1 + R_n)^2,\ p^j C_j \tag{2.16}$$

where

$$(\rho_n T_n R_{e,n})^{j-1} \rho_n T_n = p^j \begin{bmatrix} C_j & x_j \\ y_j & z_j \end{bmatrix}. \tag{2.17}$$

Then it can be readily shown that (Johler 1961)

$$\begin{aligned} C_1 &= T_{ee} \\ C_2 &= R_e T_{ee}^2 + R_m T_{em} T_{me} \\ C_3 &= 2 R_e R_m T_{ee} T_{em} T_{me} + R_e^2 T_{ee}^3 + R_{em}^2 T_{mm} T_{em} T_{me} \\ &\ldots \end{aligned} \tag{2.18}$$

The geometric series representation permits the introduction of local reflection coefficients. This is depicted in Fig. 1 with the aid of rays j = 1, 2, 3. It should be noted that (2.15) and (2.16) are not geometric-optical rays but rather a wave solution. In the geometric optical ray limit (Johler 1964), these rays represent an approximate solution valid at short distances. A study of these rays leads to the interesting conclusion that the local reflection points at the ionosphere can be considered. Thus the first ionospheric wave, j = 1, has a reflection (see Fig. 1) in the region of the point (1,1) located in the middle of the propagation path. The reflection coefficient matrix $T(1,1)$ is ascribed to this reflection region. The third ionospheric wave, j = 3, also shares this reflection region in addition to the regions $T(3,1)$, $T(3,3)$. The second ionospheric reflection would employ reflection matrices $T(2,1)$, $T(2,2)$. It is therefore possible within limits not well defined as yet to introduce different electrical properties of the ionosphere along the propagation path. Thus, a different profile of electron density can be ascribed to each point (1,1), (2,1), (2,2).... Furthermore, the reflection height can be altered along the path as p(1,1), p(2,1), .. where g = a + h, h is determined from the profile and p is given by (2.7). The harmonic series (2.16) is useful in demonstrating the local nature of the reflection, since the angle of incidence on the ionosphere for each spherical wave, n, can be ascertained from,

$$\cos \phi_i = \mathrm{Re}\left(i\,\frac{\zeta_{1\,g}^{(2)\prime}}{\zeta_{1\,g}^{(2)}}\right) \sim \mathrm{Re}\left(\sqrt{1-\frac{n(n+1)}{(k_1 g)^2}}\right)$$

$$\sin \phi_i \sim \frac{\sqrt{n(n+1)}}{k_1 g}\,. \tag{2.19}$$

For $\phi_i \sim 0$, or vertical incidence, or n small, the contribution of the terms of the harmonic series is small relative to the total field. As $\sin \phi_i$ approaches unity, the field is determined. Thereafter, the series converges rapidly. Therefore, at great distance ($d = a\theta$, $d > 500$ km.) with a small range of values near $n \sim k_1 g$ the field is primarily determined (Johler 1966).

Finally, (2.15) and (2.16) can be written as a contour integral,

$$E_{r,0} = \frac{i}{k_1^2 a^4}\,\frac{\mu_0 c}{8\pi}\int_c \frac{F(\nu-\frac{1}{2})}{\cos \nu\pi}\,\zeta^{(2)}_{\nu-\frac{1}{2}}(k_1 a)\,\zeta^{(1)}_{\nu-\frac{1}{2}}(k_1 a)(1+R_e)\,d\nu \tag{2.20}$$

$$E_{r,j} = \frac{i}{k_1^2 a^4}\,\frac{\mu_0 c}{8\pi}\int_c \frac{F(\nu-\frac{1}{2})}{\cos \nu\pi}\,\zeta^{(2)}_{\nu-\frac{1}{2}}(k_1 a)\,\zeta^{(1)}_{\nu-\frac{1}{2}}(k_1 a)\,(1+R_e)^2 C_j\,d\nu \tag{2.21}$$

where $R_e = R_e(\nu-\frac{1}{2})$

$C_j = C_j(\nu-\frac{1}{2})$.

This approach and formula was originally proposed by Wait (1961) as a rigorous geometric optics. Berry (1964) and Berry and Chrisman (1965) have developed computation techniques for this formula, and field calculations are facilitated by a computer program that has received comparatively wide usage. The integrals in (2.20) and (2.21) are evaluated by numerical integration, summation of a residue series, and by the saddle-point approximation. The direct method for evaluating (2.20) and (2.21) consists of using Gaussian quadrature on the contour integral. The integration is usually performed along the real axis from $\nu = k_1 a$ to $\nu \gg k_1 g$ and into the complex ν-plane from $\nu = k_1 a$ to some value Re $\nu \ll k_1 a$ such that convergence is obtained. The slope of the straight line contour in the complex ν-plane can be increased to speed up convergence, but care must be taken to avoid crossing the non-analytic points with the contour (Berry 1964). The solutions (2.20), (2.21) and (2.15), (2.16) are exact and indeed yield identical answers.

At a distance of approximately 2000 km. or less, the classical geometric-optics with diffractive corrections is a useful technique, and in fact exhibits considerable computation advantages for the experimentalist, because computations are comparatively simple. In this form (Johler 1961, 1962, 1964), (2.16) becomes,

$$E_{r,j} = C\, D_j^{-1} \exp(i\omega t_j') \sin^2 \tau_j (1+R_e)^2 p^j C_j, \tag{2.22}$$

where,

$$C = i\omega(10^{-7})\, I_0 \ell/d,$$

$$D_j = 2j\,[(a+h)\cos\varphi_{i,j} - a\cos\tau_j],$$

$$\cos\varphi_{i,j} = [a(1-\cos\frac{\theta}{2j}) + h]\,\Delta_j^{-1},$$

$$\cos\tau_j = [a(\cos\frac{\theta}{2j} - 1) + h\cos\frac{\theta}{2j}]\,\Delta_j^{-1},$$

$$\Delta_j = [2a(a+h)(1-\cos\frac{\theta}{2j}) + h^2]^{\frac{1}{2}},$$

$$p^j \sim \left\{1 + \frac{h}{a}\left[(2j\sin\frac{\theta}{2j})/\sin\theta\right]\right\}^{\frac{1}{2}},$$

$$\times \left\{\left[a(1-\cos\frac{\theta}{2j}) + h\right] / \left[(a+h)\cos\frac{\theta}{2j} - a\right]\right\}^2 A_j,$$

where $A_j \sim 1,\ j > 1$, or

$$A_j \sim \left[\frac{\pi}{2} z_j\right]^{\frac{1}{2}} H_{\frac{1}{3}}^{(2)}(z_j) \exp\{-i[5\pi/12 - z_j]\},$$

and

$$z_j = k_1 a \cos^3 \tau_j / 3 \sin^2 \tau_j,$$

and, $t_j' = \eta_1 D_j/c$. Here, $\phi_{i,j}$ and τ_j are angles of incidence on the ionosphere and ground, respectively, of the ionospheric ray of order j.

3. Reflection Coefficients for the Ground

The ground reflection coefficient for the TM-wave is,

$$R_{e,n} = \frac{\dfrac{\zeta_{1a}^{(1)\prime}}{\zeta_{1a}^{(1)}} - \dfrac{k_1}{k_2}\dfrac{\zeta_{2a}^{(1)\prime}}{\zeta_{2a}^{(1)}}}{\dfrac{-\zeta_{1a}^{(2)\prime}}{\zeta_{1a}^{(2)}} + \dfrac{k_1}{k_2}\dfrac{\zeta_{2a}^{(1)\prime}}{\zeta_{2a}^{(1)}}}, \tag{3.1}$$

or

$$R_{e,n} \sim \frac{\cos\tau_j - \dfrac{k_1}{k_2}\sqrt{1 - \left(\dfrac{k_1}{k_2}\sin\tau_j\right)^2}}{\cos\tau_j + \dfrac{k_1}{k_2}\sqrt{1 - \left(\dfrac{k_1}{k_2}\sin\tau_j\right)^2}} \tag{3.2}$$

if

$$\sin\tau_j \sim \frac{\sqrt{n(n+1)}}{k_1 a}. \tag{3.3}$$

In (3.1),

$$\zeta_{1a}^{(1,2)\prime}(z) = \frac{d}{dz}\,\zeta_{1a}^{(1,2)}(z). \tag{3.4}$$

Here (3.2) is the well-known Fresnel approximation valid only at short distances from the source. The coefficient of reflection for TE waves is,

$$R_{m,n} = \frac{\dfrac{\zeta_{1a}^{(1)\prime}}{\zeta_{1a}^{(1)}} - \dfrac{k_2}{k_1}\dfrac{\zeta_{2a}^{(1)\prime}}{\zeta_{2a}^{(1)}}}{\dfrac{-\zeta_{1a}^{(2)\prime}}{\zeta_{1a}^{(2)}} + \dfrac{k_2}{k_1}\dfrac{\zeta_{2a}^{(1)\prime}}{\zeta_{2a}^{(1)}}}. \tag{3.5}$$

Also,

$$R_{m,n} \sim \frac{\cos\tau_j - \dfrac{k_2}{k_1}\sqrt{1 - \left(\dfrac{k_1}{k_2}\sin\tau_j\right)^2}}{\cos\tau_j + \dfrac{k_2}{k_1}\sqrt{1 - \left(\dfrac{k_1}{k_2}\sin\tau_j\right)^2}}. \tag{3.6}$$

In (2.9), (2.11), (2.12), (2.20), and (2.21), n is a complex number, $n = \nu - \frac{1}{2}$. In all formulas except the geometric-optical formula (2.22) at short distances the spherical ground reflection coefficients (3.1) and (3.5) are preferable if not necessary for precise calculations.

4. Concept of Continuous Stratification of an Electron Density Profile

The detailed description of the ionosphere boundary $r = g = a + h$, (Fig. 1) requires the introduction of the notion of a profile of electron density. Thus, instead of a sharp boundary, consisting of a single slab of plasma emplaced at an altitude h, a variation in electron (and possibly ion) density is taken into account in the general analysis. Since the ionosphere is anisotropic, the use of spherical geometry leads to intractable equations with conventional techniques. However, plane wave, plane ionosphere solutions are found which are exact and can indeed take account of a profile of electron density, ion density, and collision frequency. In fact, a variation of the magnetic field with altitude can also be introduced.

The reflection coefficients (1.1) can be derived under these conditions in an exact manner. Byproducts of this analysis are the transmission through the ionosphere and the effective reflection height of the waveguide. The method for introducing plane reflection coefficients into the waveguide propagation is built into the propagation formulas discussed in section 2 (Johler and Berry 1964). The reflection coefficient calculation from profiles has been discussed at length in the literature (Johler and Walters 1960 , Johler and Harper 1962, 1963, Johler 1961, 1962, 1963, and Price 1964). These references in essence describe the continuous stratification method. Wait and Walters (1963) have also derived reflection coefficients for the waveguide boundary. Finally, another interesting approach to this problem which employs numerical integration of the differential equations has been described by Budden (1955), Barron (1961), and Pitteway (1965). Swift (1962) discusses the transition from a stratified ionosphere profile to a continuous profile using the quasi-longitudinal approximation.

Price (1964) presents techniques for solving the general matrix equation for the stratified model originally presented by Johler and Harper (1962). Johler and Berry (1962, 1965) have introduced a hydrodynamic equation for a four-species gas mixture, positive ions, negative ions, electrons, and neutrals with the corresponding 12 collision frequencies. This type of analysis is important in the nuclear environment. Thus, the presence of nuclear debris in the ionosphere produces a large number density of ions relative to electrons in the D region and in the atmosphere, such that an electron gas (with neutral collisions) is no longer an adequate model to describe low frequency propagation. This method also has been introduced into the continuously stratified method, using a profile for each species number density. It was also necessary to introduce the corresponding profiles of collision frequency.

Consider a right-handed local co-ordinate system x, y, z at each point (1,1), (2,1), (2,2)..., in Fig. 1, oriented such that the co-ordinate z points in the direction of increasing altitude, h. Thus, a profile N(h) of electron density is also a profile N(z), and a collision frequency $\nu(h)$ is also a collision frequency $\nu(z)$.

Fig. 2 illustrates a theoretical daytime electrification profile for the D region of the ionosphere and the atmosphere used by Johler and Berry (1965). Electron density, N_e, positive ion density, N_+, and negative ion density, N_-, are illustrated as a function of altitude, h, above the ground. As a consequence of the high collision frequency in the denser atmosphere, the electrification below 40 km. in this model is insignificant to the low frequency propagation problem. At frequencies above approximately 1 kc/s. the electrons only are important. The model can then be regarded as an electron gas with neutral collisions. This assumption is not necessarily true, however, for the disturbed or nuclear environment. Nevertheless, in this normal profile, the curve, N_e, is of prime interest.

Maxwell's equations, for $\frac{\partial}{\partial t} = i\omega$,

$$\begin{aligned} \nabla \times \vec{E} + \mu_0 i\omega\vec{H} &= 0 \\ \nabla \times \vec{H} - \varepsilon_0 i\omega\vec{E} &= -Ne\vec{V} \end{aligned} \tag{4.1}$$

and the hydrodynamic for an electron gas,

$$m_e i\omega\vec{V} + m\nu\vec{V} + \mu_0 e(\vec{V} \times \vec{H}) + e\vec{E} = 0 \tag{4.2}$$

are satisfied by the plane wave

$$E = A \exp \left(i\omega t - i \frac{\omega}{c} \eta D\right) \tag{4.3}$$

where

$$\eta D = x \sin \phi_i \sin \phi_a + y \sin \phi_i \cos \phi_a + z\zeta. \tag{4.4}$$

In the ionosphere, ϕ_i is the angle of incidence of the plane wave and ϕ_a is the direction of propagation relative to magnetic north. $\vec{H}$ is the earth's static magnetic field vector oriented in the y-z plane with a dip angle I measured from the horizontal. Equations (4.1), (4.2), and (4.3) can be written

$$\begin{bmatrix} a_{11} & a_{12} & a_{13} \\ a_{21} & a_{22} & a_{23} \\ a_{31} & a_{32} & a_{33} \end{bmatrix} \begin{bmatrix} E_x \\ E_y \\ E_z \end{bmatrix} = 0. \tag{4.5}$$

If the field $\vec{E}$ exists, it can be concluded that the determinant of (4.5) vanishes, or,

$$a_4\zeta^4 + a_3\zeta^3 + a_2\zeta^2 + a_1\zeta + a_0 = 0 \tag{4.6}$$

and,

$$\eta^2 = \zeta^2 + \sin^2 \phi_i. \tag{4.7}$$

In the case of a gas mixture $N_i = N_i(h)$, i = e, +, -, o corresponding to electrons, positive ions, negative ions, and neutrals, respectively, it is possible to find an analogous solution of Maxwell's equations and the hydrodynamic equations by writing instead of (4.1), (4.2),

$$\begin{aligned} &\nabla \times \vec{E} + \mu_0 i\omega\vec{H} = 0 \\ &\nabla \times \vec{H} - \varepsilon_0 i\omega\vec{E} = \sum_i q_i N_i \vec{V}_i \end{aligned} \tag{4.8}$$

and

$$i\omega\vec{V}_i + \frac{q_i}{m_i}\vec{E} + \frac{\mu_0 q_i}{m_i}(\vec{V}_i \times \vec{H}) + \sum_i \frac{m_j}{m_i + m_j}(\vec{V}_i - \vec{V}_j), \tag{4.9}$$

where

$$q_i = \begin{bmatrix} -e \\ e \\ e \\ 0 \end{bmatrix} \quad \text{if} \quad i = \begin{bmatrix} + \\ e \\ - \\ o \end{bmatrix} \tag{4.10}$$

and,

$$j = \begin{bmatrix} o - e \\ o - + \\ o + e \\ - + e \end{bmatrix} \quad \text{if} \quad i = \begin{bmatrix} + \\ e \\ - \\ o \end{bmatrix} \tag{4.11}$$

In this case also, it can be concluded that the quartic (4.6) is to be solved for $\zeta = \zeta^{i,r}_{o,e}$ corresponding to four roots: ordinary (o) and extraordinary (3), upgoing (i) and down-going (r) wave components in the ionosphere (Johler and Berry 1965).

Considering again the detailed structure of a typical daytime-noon ionosphere model, which is illustrated in Fig. 2 as an electron-ion number density profile N(h), it can be noted that the solution of the quartic (4.6) can be accomplished for each altitude on this curve. Collision frequency-altitude profiles previously published (Johler 1962) must also be considered. These vertical structures can be represented by plasma consisting of a flexible stack of slabs as illustrated in Fig. 3, of arbitrary thickness (except for the topmost slab of thickness $z_p = \infty$). Both the number of such slabs, p, and the thickness are quite flexible, since the notion of continuous stratification means that the measured electron density-altitude and collision frequency-altitude ($N(z)$ and $\nu(z)$, respectively) profiles can be approximated to any desired accuracy by decreasing z_n and increasing p simultaneously until a stable reflection process is obtained.

A constant electron density, collision frequency, and static magnetic field with respect to altitude, z, are, of course, assumed within each slab, and associated with each such slab the set of four roots, ζ, is identified. Two of the roots will exhibit a negative imaginary part (Im ζ negative), corresponding to an upgoing propagation component (+ z direction, Fig. 3). Also, two of these roots will exhibit a positive imaginary part (Im ζ positive), corresponding to a downgoing propagation component (- z direction). Except for the topmost slab, it is necessary to consider both upgoing and downgoing components in this analysis.

It is necessary to equate the tangential $\vec{E}$ and $\vec{H}$ fields at each boundary (top and bottom of each slab), whereupon it can be concluded that a 4p×4p matrix equation defines the propagation:

$$
\begin{bmatrix}
a_{1,1}\,a_{1,2}\,a_{1,3}\,a_{1,4}\,a_{1,5}\,a_{1,6} & & & \\
b_{1,1}\,b_{1,2}\,b_{1,3}\,b_{1,4}\,b_{1,5}\,b_{1,6} & & & \\
c_{1,1}\,c_{1,2}\,c_{1,3}\,c_{1,4}\,c_{1,5}\,c_{1,6} & & & \\
d_{1,1}\,d_{1,2}\,d_{1,3}\,d_{1,4}\,d_{1,5}\,d_{1,6} & & & \\
 & a_{2,3}\,a_{2,4}\,a_{2,5}\,a_{2,6}\,a_{2,7}\,a_{2,8}\,a_{2,9}\,a_{2,10} & & \\
 & b_{2,3}\,b_{2,4}\,b_{2,5}\,b_{2,6}\,b_{2,7}\,b_{2,8}\,b_{2,9}\,b_{2,10} & & \\
 & c_{2,3}\,c_{2,4}\,c_{2,5}\,c_{2,6}\,c_{2,7}\,c_{2,8}\,c_{2,9}\,c_{2,10} & & \\
 & d_{2,3}\,d_{2,4}\,d_{2,5}\,d_{2,6}\,d_{2,7}\,d_{2,8}\,d_{2,9}\,d_{2,10} & & \\
 & & a_{3,7}\,a_{3,8}\,a_{3,9}\,a_{3,10}\,a_{3,11}\,a_{3,12}\,a_{3,13}\,a_{3,14} & \\
 & & b_{3,7}\,b_{3,8}\,b_{3,9}\,b_{3,10}\,b_{3,11}\,b_{3,12}\,b_{3,13}\,b_{3,14} & \\
 & & c_{3,7}\,c_{3,8}\,c_{3,9}\,c_{3,10}\,c_{3,11}\,c_{3,12}\,c_{3,13}\,c_{3,14} & \\
 & & d_{3,7}\,d_{3,8}\,d_{3,9}\,d_{3,10}\,d_{3,11}\,d_{3,12}\,d_{3,13}\,d_{3,14} & \\
 & & & \cdots\cdots\cdots\cdots \\
 & & & \cdots\cdots\cdots\cdots \\
 & & & \cdots\cdots\cdots\cdots \\
 & & & \cdots\cdots\cdots\cdots \\
 & & & a_{p,4p-5}\cdots\cdots a_{p,4p} \\
 & & & b_{p,4p-5}\cdots\cdots b_{p,4p} \\
 & & & c_{p,4p-5}\cdots\cdots c_{p,4p} \\
 & & & d_{p,4p-5}\cdots\cdots d_{p,4p}
\end{bmatrix}
\begin{bmatrix}
T_{em}, & T_{mm} \\
T_{ee}, & T_{me} \\
U^{(1)}_{eio}, & U^{(1)}_{mio} \\
U^{(1)}_{eie}, & U^{(1)}_{mie} \\
U^{(1)}_{ero}, & U^{(1)}_{mre} \\
U^{(1)}_{ere}, & U^{(1)}_{mre} \\
U^{(2)}_{eio}, & U^{(2)}_{mio} \\
U^{(2)}_{eie}, & U^{(2)}_{mie} \\
U^{(2)}_{ero}, & U^{(2)}_{mro} \\
U^{(2)}_{ere}, & U^{(2)}_{mre} \\
\cdot & \cdot \\
\cdot & \cdot \\
\cdot & \cdot \\
\cdot & \cdot \\
U^{(p-1)}_{eio}, & U^{(p-1)}_{mio} \\
U^{(p-1)}_{cie}, & U^{(p-1)}_{mie} \\
U^{(p-1)}_{ero}, & U^{(p-1)}_{mro} \\
U^{(p-1)}_{ere}, & U^{(p-1)}_{mre} \\
U^{(p)}_{eio}, & U^{(p)}_{mio} \\
U^{(p)}_{eie}, & U^{(p)}_{mie}
\end{bmatrix}
+
\begin{bmatrix}
a_{oe}, & a_{om} \\
b_{oe}, & b_{om} \\
c_{oe}, & c_{om} \\
d_{oe}, & d_{om} \\
 & \\
\end{bmatrix}
= 0,
\tag{4.12}
$$

where the elements a_{11}... can be deduced as a consequence of these boundary conditions, provided the reflection coefficients, T, and the transmission coefficients, U, are defined,

$$
\begin{array}{lll}
T_{ee} = \dfrac{E_{y'r}}{E_{y't}} & U^{(n)}_{eio} = \dfrac{E^{(n)}_{yio}}{E_{y't}} & U^{(n)}_{ero} = \dfrac{E^{(n)}_{yro}}{E_{y't}} \\
T_{em} = \dfrac{E_{z'r}}{E_{y't}} & U^{(n)}_{mio} = \dfrac{E^{(n)}_{yio}}{E_{z't}} & U^{(n)}_{mro} = \dfrac{E^{(n)}_{yro}}{E_{z't}} \\
T_{me} = \dfrac{E_{y'r}}{E_{z't}} & U^{(n)}_{eie} = \dfrac{E^{(n)}_{yie}}{E_{y't}} & U^{(n)}_{ere} = \dfrac{E^{(n)}_{yre}}{E_{y't}} \\
T_{mm} = \dfrac{E_{z'r}}{E_{z't}} & U^{(n)}_{mie} = \dfrac{E^{(n)}_{yie}}{E_{z't}} & U^{(n)}_{mre} = \dfrac{E^{(n)}_{yre}}{E_{z't}}
\end{array}
\tag{4.13}
$$

where, in Fig. 3, $n = 1, 2, 3 \cdots, p - 1, p$.

The distinction between the four propagation components, upgoing (i) and downgoing (r), ordinary (o) and extraordinary (e), becomes obscure when the ionosphere is considered to be nonuniform in the vertical z-direction. This is a consequence of the coupling at each boundary. Thus, the boundary conditions at each slab are introduced as an expression for the continuity of the tangential $\vec{E}$ and $\vec{H}$ fields and possibly the normal $\vec{H}$ at each boundary of the model plasmas. This is accomplished by equating the field immediately above and immediately below each boundary, which, after considerable ado, results in the complex matrix equation.

The matrix equation (4.12) can be subjected to a recursive reduction[1]. Instead of solving (4.12) directly, divide it into 4 × 4 block submatrices and 4 × 2 vectors:

$$
\begin{bmatrix}
A_{11} & A_{12} & & & \cdot & & & & & & \\
A_{21} & A_{22} & A_{23} & & \cdot & & & & & & \\
 & A_{32} & A_{33} & A_{34} & \cdot & & & & & & \\
0 & 0 & \cdot & \cdot & \cdot & 0 & 0 & \cdot & \cdot & \cdot & \cdot \\
 & & & & & A_{p-1,p-2} & & A_{p-1,p-1} & & A_{p-1,p} & \\
 & & & & & 0 & & A_{p,p-1} & & A_{pp} &
\end{bmatrix}
\begin{bmatrix} U_1 \\ U_2 \\ U_3 \\ \cdot \\ \cdot \\ U_p \end{bmatrix}
=
\begin{bmatrix} K \\ 0 \\ 0 \\ \cdot \\ \cdot \\ 0 \end{bmatrix}
\tag{4.14}
$$

Consider the rows as separate equations and solve the last one for U_p:

$$U_p = A^{-1}_{pp} A_{p,p-1} U_{p-1}. \tag{4.15}$$

Substitute this value into the next-to-last equation, such that it contains only two unknowns, and solve for U_{p-1}. Let $B_p = A_{pp}$, and let

$$B_k = A_{kk} - A_{k,k+1} B^{-1}_{k+1,k}. \quad (1 \le k < p) \tag{4.16}$$

Then $B_1 U_1 = K$ or $U_1 = B_1^{-1} K$. (4.17)

---

[1] This reduction was employed in a computer program for (4.12) developed by Berry (1965).

The first two rows of U_1 are the reflection coefficients. The transmission coefficients are then found from

$$U_k = - B_k^{-1} A_{k,k-1} U_{k-1}. \tag{4.18}$$

The process described is equivalent to applying the appropriate boundary conditions consecutively to each boundary, as was accomplished by Price (1964) for anisotropic layers.

The electron density profile is defined by stating the height at which $z = 0$, and giving the electron density (in electrons/c.c.) at a number of heights. The density between these heights is found by linear interpolation. The collision frequency used is (Johler and Berry 1965)

$$\nu(h) = 1.6(10^{11}) \frac{P(h)}{P_o} \tag{4.19}$$

where $P(h)$ is the pressure at height h as given by the standard model atmosphere (U.S. Standard Atmosphere, 1962) and P_o is the pressure at sea level.

5. Discussion Concerning Some Theoretical Low Frequency Field Calculations Based on the Normal Environment

Figs. 5, 6, 7, 8, and 9 illustrate field calculations (amplitude as a function of distance) at frequencies of 10, 20, 50, 100, and 200 kc/s. The ionosphere was modeled with the electron density profile, $N_e(h)$ illustrated in Fig. 2. Each calculation was accomplished by considering the model to be an electron plasma with neutral collisions. Thus, in the normal environment the ions N_+ and N_- can be neglected at frequencies above 1 kc/s. If, however, the ion density reached 10^5 at altitudes above 20 km., for example, it would be necessary to include the effect of ions in the calculation. Such an enhancement can be found in the disturbed environment and the nuclear environment.

The effective height of the upper boundary of the waveguide can be estimated from the transmission coefficient curve depicted in Fig. 4. Note that ϕ_a is the angle between the vertical plane containing the earth's magnetic field vector and the direction of propagation of the incident plane wave, and that ϕ_i is the angle of incidence on the ionosphere. Let $E_{y,i}$ be the normal component of the incident electric field in the plane of incidence (vertical polarization) and let $E_{x,i}$ be the component perpendicular to the plane of incidence (horizontal polarization). Let $E_{y,u}$ and $E_{x,u}$ be the corresponding upgoing waves inside the ionosphere and $E_{y,d}$ and $E_{x,d}$ be the downgoing waves. Then the ratios

$\frac{E_{\hat{x},u}}{E_{\hat{x},i}}$ and $\frac{E_{\hat{y},u}}{E_{\hat{x},i}}$ describe the propagation of waves into the ionosphere. Here $\hat{x}$ and $\hat{y}$ are transformed co-ordinates given by Johler and Harper (1962). In this formulation the transmission coefficient U_e, for vertical polarized waves, is given by the quantity

$$U_e = \frac{E_{y,u}}{E_{\hat{y},i}},$$

or, (Johler and Berry 1965),

$$U_e \sim \frac{E_{\hat{y},u}}{E_{\hat{y},i}} \cos \phi_i \cos \phi_a.$$

The latter of these equations becomes precisely an equality only in an isotropic plasma, but in an anisotropic plasma there are small additional terms caused by the anisotropy. The transmission coefficient U_m, for the horizontally polarized incident wave, can be written

$$U_m = \frac{E_{y,u}}{E_{\hat{x},i}}$$

$$U_m \sim \frac{E_{\hat{x},u}}{E_{\hat{x},i}} \sin \phi_a .$$

Thus, the transmission of the vertical electric polarization of the wave into the ionosphere can be conveniently studied when $\phi_a = 0, 180^o$, while $\phi_a = 270^o, 90^o$ is simplest for the horizontal electric polarization. Fig. 4, for 100 kc/s. shows $|U_e|$ and $|U_m|$ for both upgoing and downgoing waves as a function of distance, z, into the ionosphere. The profile illustrated in Fig. 2 is the assumed model for the electron density variation with altitude. It is further assumed that the propagation is into the west (ϕ_a is 270^o), and that the angle of incidence of the wave on the ionosphere, ϕ_i is 82^o (grazing incidence). The magnetic dip, I, is 60^o. Fig. 4 shows that $|U_{m,u}| \sim 1$ just inside the ionosphere, $z \sim 0$, where $z = 0$ corresponds to $h = 40$ km. in Fig. 2. Here, virtually no energy has as yet reflected. This situation continues with only a slight decrease in $|U_{m,u}|$ until the wave penetrates approximately 25 km. into the ionosphere. There is then a sharp decrease in the next few kilometers. This sharp decrease in the field indicates a decrease in the upgoing energy. Hence, as far as the reflection coefficient is concerned, the greatest contribution occurs before the upgoing wave has diminished to negligible amplitude. At this point the transmission coefficient, $|U_{e,m}|$, has decreased slightly from unity. A few kilometers beyond this point, $|U_{e,m}|$ diminished rapidly. It is apparent, in Fig. 4, that the effective height of reflection lies between approximately $z \sim 20$ and $z \sim 30$ km. and depends on the precise ratio $|U|$ used to define such a point. The uncertainty of resolution of the point follows, of course, since some energy, however small, is reflected at all heights, z. It can be concluded, therefore, that the approximate value for the waveguide height, $h \sim 65$ km. This value was employed to calculate Figs. 5, 6, 7, and 8 since only a weak frequency dependence of the reflection height exists.

The propagation curves for normal day profile in Fig. 2 at a frequency of 10 kc/s. are illustrated in Fig. 5. The complete field Σ_j together with the geometrical components $j = 0, 1, 2, 3, 4$, and 5 are shown. The field Σ_j is identical to results obtained with the zonal harmonics formula (2.4) or the mode solution (2.12). The decomposition of Σ_j into the terms of the geometric series, however, appeals to the geometric intuition such as is depicted in Fig. 1. Figs. 6, 7, 8, and 9 illustrate the propagation at frequencies of 20, 50, 100, and 200 kc/s., respectively.

Another typical daytime noon model ionosphere, appropriate to temperate latitudes according to Knapp (1965), is illustrated in Fig. 10. The typical nighttime curve is given in Fig. 12. These curves can be compared with Belrose (1964) and Barrington and Thrane (1964), for example. Whereas the theoretical curves given in these figures are much smoother than the experimentally derived curves, the agreement is quite satisfactory. The corresponding field calculations are presented in Figs. 11 and 13. Apparently, the Knapp (1965) model gives considerably less attenuation with distance at 100 kc/s. when compared with the Johler and Berry (1965) model field calculations of Fig. 8. The field calculation for nighttime conditions illustrated in Fig. 13 demonstrates the fact that a large number of terms in the geometric series are required to obtain Σ_j. Since the terms j = 0, 1, 2, 3, 4, 5 were considered to be an insufficient number to obtain Σ_j, the latter curves were not included. It is also of interest to note that the reflection height is 100 km.

It is of interest to note that the first ionospheric wave, j = 1, is the dominant propagation component at 10 kc/s. to a distance of approximately 3000 km. in the normal day example, Fig. 5. Of course, at distances less than 1000 km., the ground wave, j = 0, becomes an important component of the total field. This is also true of 20 kc/s., Fig. 6, 50 kc/s., Fig. 7, 100 kc/s., Fig. 8, and 200 kc/s. In fact, at 200 kc/s., the first ionospheric wave is the dominant wave to a distance of 4000 km. At this frequency, however, Fig. 9, the ionospheric wave to ground wave ratio is considerably less, since the ionospheric reflection coefficient, T, decreases rapidly in value as frequency is increased.

The ionospheric waves exhibit a pseudo-Brewster angle in the reflection coefficients of the ionosphere and the ground. This phenomenon occurs when the angle of incidence on the medium reaches a certain critical value that can be translated into a critical distance from the transmitter (see Johler (1963) for a discussion of the ionospheric reflection coefficient as a function of angle of incidence). For the normal day model the pseudo-Brewster angle for the ionosphere occurs at a distance less than 100 km. for j = 1, j = 2 at f = 100 kc/s., Fig. 8, for example. In this region the angle of incidence on the ionosphere has not, as yet, reached grazing incidence. A similar phenomenon occurs in the second and higher order terms, j = 2, 3, 4, 5··· when the waves approach grazing incidence on the ground (3000 km. for j = 2). Beyond this point the field recovers and approaches a ground wave type diffraction curve.

6. Conclusions

Research that uses low frequencies to study the D region of the ionosphere with ground-based techniques can use a theory of propagation based on Maxwell's equations to considerable advantage. Thus, based on measurements of profile of electron and ion density along the propagation path, the propagated field can be predicted. In the absence of such measurements, theoretical profiles can be introduced into the analysis. An interesting possibility of this analysis is the introduction of different profiles at various points along the propagation path and different reflection heights for each such profile. This, in essence, permits the introduction of an inhomogeneous, anisotropic model ionosphere by reference to the geometric-optics. Thus, the mathematics at the present state of the art appears to be approximating nature more precisely as a consequence of recently developed, computer oriented techniques.

This paper was written as part of the work performed under Defense Atomic Support Agency interagency cost reimbursement orders 807-64, 804-65.

REFERENCES

Abramowitz, M. and I.A. Stegun. Handbook of mathematical functions, NBS Appl. Math. Ser. 55. 1964.

Barrington, R.L. and E.V. Thrane. Electron density profile in the quiet D-region derived from observations of cross modulation, Propagation of Radio Waves at Frequencies Below 300 kc/s., Agardograph 74, 25-33 (Pergamon Press). 1964.

Barron, D.W. The numerical solution of differential equations governing the reflection of long radio waves from the ionosphere, IV. Proc. Roy. Soc. A-260, p. 393. 1961.

Belrose, J.S. Present knowledge of the lowest ionosphere, Propagation of Radio Waves at Frequencies Below 300 kc/s., Agardograph 74, 3-23 (Pergamon Press). 1964.

Berry, L.A. Wave hop theory of long distance propagation of LF radio waves, Radio Sci. NBS/USNC-URSI 68D, No. 12, 1275-1282. Dec. 1964.

Berry, L.A. Computer program "TUIK", Private communication. 1965.

Berry, L.A. and M.E. Chrisman. The path integrals of LF/VLF wave hop theory, Radio Sci. J. Res. NBS 64D, 1469-1480. Nov. 1965.

Budden, K.G. The numerical solution of the differential equations governing the reflection of long radio waves from the ionosphere, II, Phil. Trans. Roy. Soc. of London, Ser. A-248, 45-72 (1955-56). 1955.

Budden, K.G. Radio waves in the ionosphere (Cambridge Univ. Press). 1961.

Cole, R.K., Jr. and E.T. Pierce. Electrification in the earth's atmosphere for altitudes between 0 and 100 km, J. Geophys. Res. 70, No. 12, 2735-2749. June 15, 1965.

Johler, J.R. On the analysis of LF ionospheric radio propagation phenomena, J. Res. NBS 65D, No. 5, 517-529. Sept.-Oct. 1961.

Johler, J.R. Propagation of the low frequency radio signal, Proc. IRE 50, No. 4, 404-427. Apr. 1962.

Johler, J.R. Radio wave reflections at a continuously stratified plasma with collisions proportional to energy and arbitrary magnetic induction, International Conference on the Ionosphere, London, July 1962 (Inst. Phys. Physical Soc., London), 436-445. 1963.

Johler, J.R. Concerning limitations and further corrections to geometric-optical theory for LF, VLF propagation between the ionosphere and the ground, Radio Sci. J. Res. NBS/USNC-URSI 68D, No. 1, 67-78. Jan. 1964.

Johler, J.R. Zonal harmonics in low frequency terrestrial radio wave propagation, NBS Technical Note 335. Apr. 13, 1966.

Johler, J.R. and L.A. Berry. Propagation of terrestrial radio waves of long wavelength — theory of zonal harmonics with improved summation technique, J. Res. NBS 66D (Radio Prop.), No. 6, 737-773. Nov.-Dec. 1962.

Johler, J.R. and L.A. Berry. A complete mode sum for LF, VLF, ELF terrestrial radio wave fields, NBS Monograph 78. Oct. 1964.

Johler, J.R. and L.A. Berry. On the effect of heavy ions on LF propagation, with special reference to a nuclear environment, NBS Technical Note No. 313. June 1965.

Johler, J.R. and J.D. Harper, Jr. Reflection and transmission of radio waves at a continuously stratified plasma with arbitrary magnetic induction, J. Res. NBS 66D (Radio Prop.), No. 1, 81-99. Jan.-Feb. 1962.

Johler, J.R. and J.D. Harper, Jr. On plasma collision frequencies proportional to energy in the radio wave reflection and transmission process, NBS Technical Note No. 164. Mar. 1963.

Johler, J.R. and L.C. Walters. On the theory of reflection of low- and very low-radiofrequency waves from the ionosphere, J. Res. NBS 64D (Radio Prop.), No. 3, 169-285. May-June 1960.

Knapp, W.S. G.E. Tempo (private communication). 1965.

Pitteway, M.L.V. The numerical calculation of wave fields reflexion coefficients and polarizations for long radio waves in the lower ionosphere, Part 1, Phil. Trans. Roy. Soc. A-257, 219-241. 1965.

Price, G.H. Propagation of EM waves through a continuously varying stratified anisotropic medium, Radio Sci. J. Res. NBS 68D, No. 4, 407-418. Apr. 1965.

Swift, D.W. VLF radio propagation in the ionosphere, J. Res. NBS 66D (Radio Prop.), No. 6, 663-680. Nov.-Dec. 1962.

U.S. Standard Atmosphere, Superintendent of Documents, U.S. Govt. Printing Office, Washington, D.C. Dec. 1962.

Wait, J.R. A diffraction theory of LF sky wave propagation, J. Geophys. Res. 66, No. 6, 1713-1724. June 1961.

Wait, J.R. Electromagnetic waves in stratified media. (Pergamon Press). 1962.

Wait, J.R. and L.C. Walters. Reflection of VLF radio waves from an inhomogeneous ionosphere, J. Res. NBS 63D (Radio Prop.), No. 5, 519-523. Sept.-Oct. 1963.

Watson, G.N. The transmission of electric waves by the earth, Proc. Roy. Soc. London AXCV, 83. 1918.

Watson, G.N. The transmission of electric waves round the earth, Proc. Roy. Soc. London, ACXV, 546. 1919.

Watson, G.N. Theory of Bessel functions, 2nd ed. (Cambridge Univ. Press). 1958.

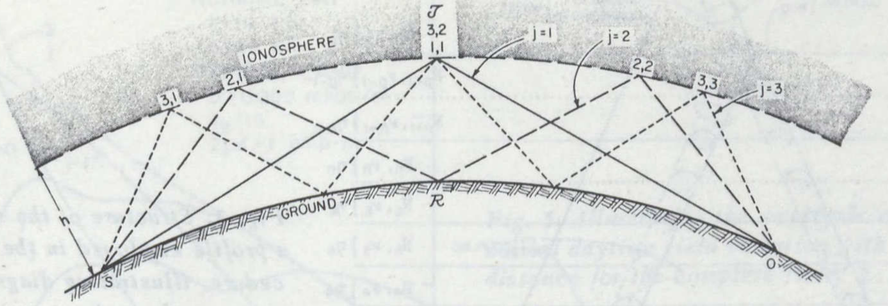

Fig. 1. Illustrating geometric-optical rays between the ionosphere and the ground with corresponding regions of reflection for each ray (j, k). j = order of term of the geometric series, j = 1, 2, 3.. and k is the order of the reflection region.

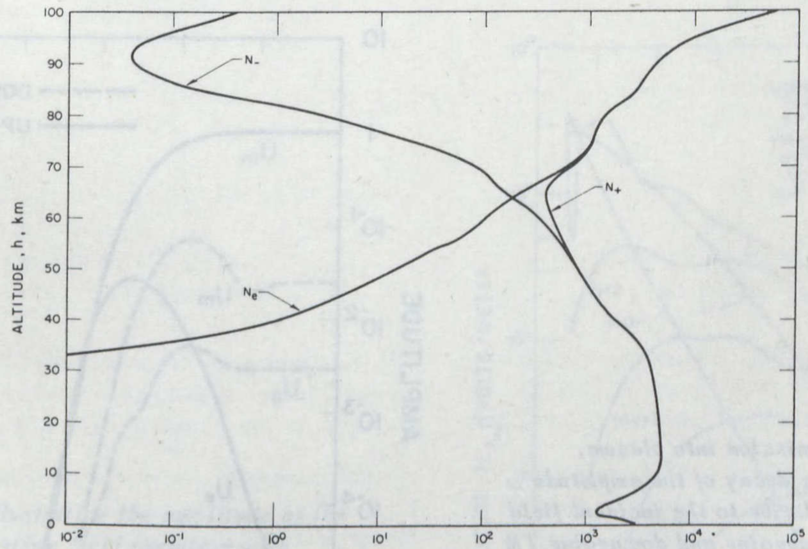

Fig. 2. Theoretical profiles of electron and ion densities, illustrating state of electrification of the ionosphere and atmosphere. h > 40 km. after Jobler and Berry (1965), h < 40 km. after Cole and Pierce (1965).

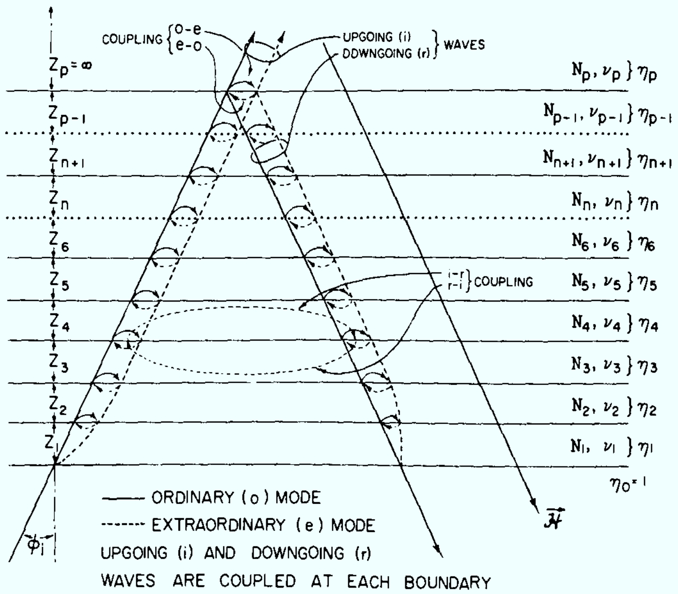

Fig. 3. Structure of the stratification of a profile employed in the analysis procedure, illustrating diagrammatically the concept of continuous stratification.

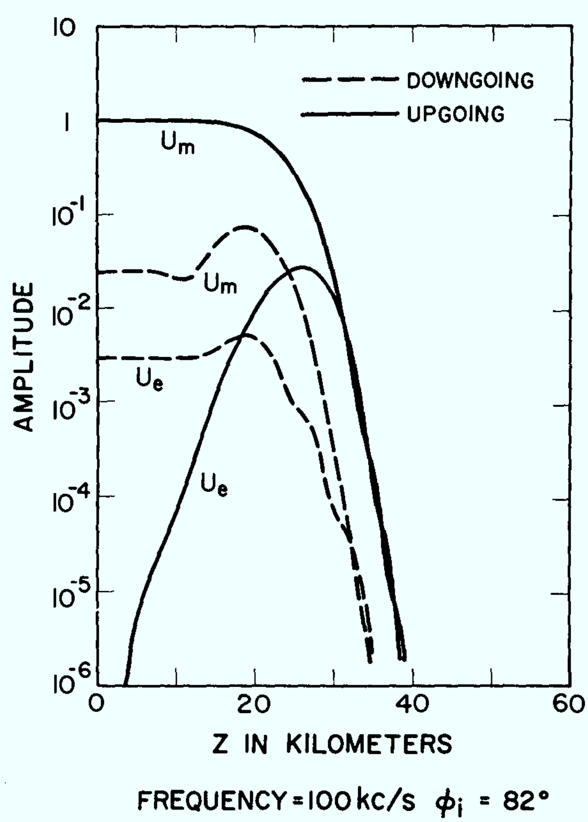

Fig. 4. Transmission into plasma, illustrating the decay of the amplitude of the field relative to the incident field amplitude for upgoing and downgoing TM and TE waves in the ionosphere. The effective reflection height z ~ 25 km. or h ~ 65 km.

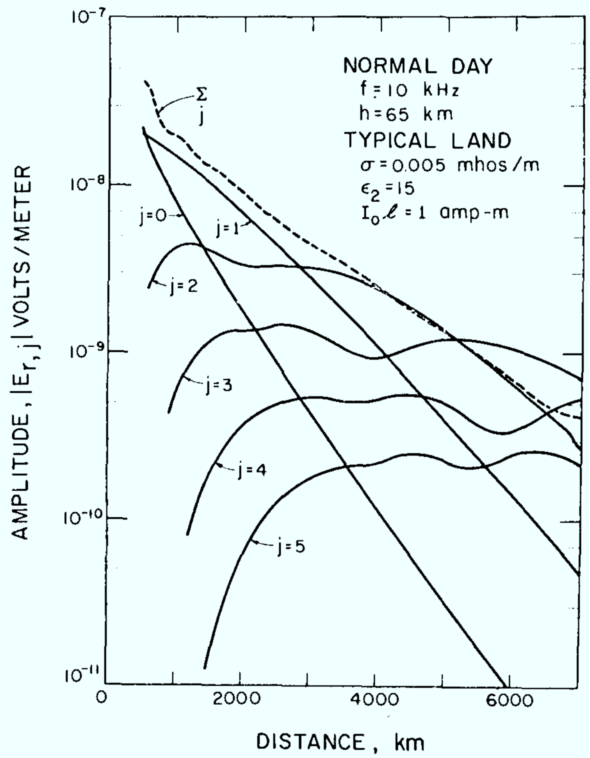

Fig. 5. Illustrating the amplitude of the normal daytime field variation with distance for the complete field, $\sum_j$, and the various geometric series components, $j = 0, 1, 2, 3\ldots$, at a frequency of 10 kc/s. Magnetic dip $I = 60°$, magnetic azimuth $\phi_a = 270°$, magnetic intensity $|\vec{H}| = 40$ amp./m.

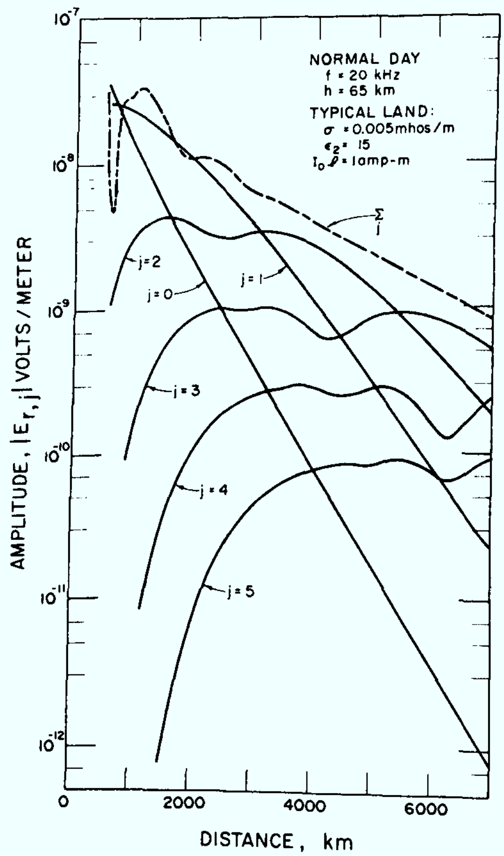

Fig. 6. Illustrating the amplitude of the normal daytime field variation with distance for the complete field, $\sum_j$, and the various geometric series components, $j = 0, 1, 2, 3\ldots$, at a frequency of 20 kc/s. Magnetic dip $I = 60°$, magnetic azimuth $\phi_a = 270°$, magnetic intensity $|\vec{H}| = 40$ amp./m.

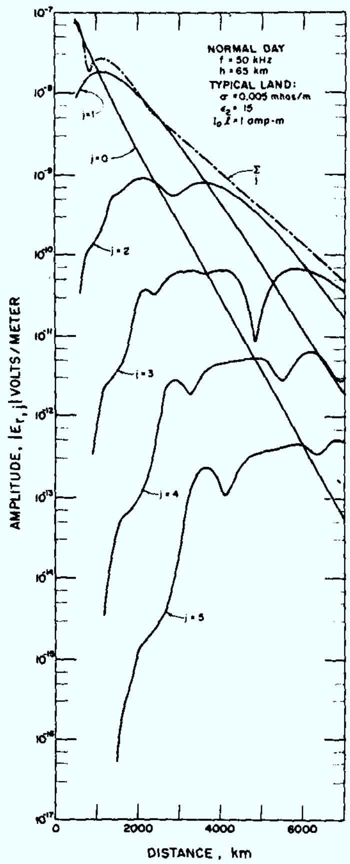

Fig. 7. Illustrating the amplitude of the normal daytime field variation with distance for the complete field, $\sum_j$, and the various geometric series components, $j = 0, 1, 2, 3 \ldots$, at a frequency of 50 kc/s. Magnetic dip $I = 60°$, magnetic azimuth $\phi_a = 270°$, magnetic intensity $|\vec{H}| = 40$ amp./m.

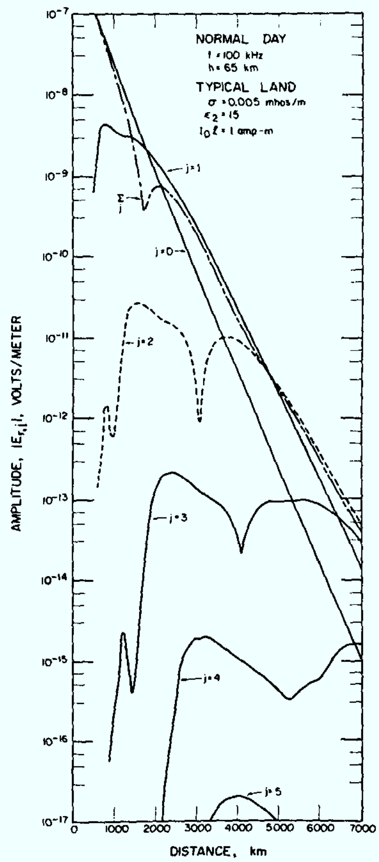

Fig. 8. Illustrating the amplitude of the normal daytime field variation with distance for the complete field, $\sum_j$, and the various geometric series components, $j = 0, 1, 2, 3 \ldots$, at a frequency of 100 kc/s. Magnetic dip, $I = 60°$, magnetic azimuth, $\phi_a = 270°$, magnetic intensity, $|\vec{H}| = 40$ amp./m.

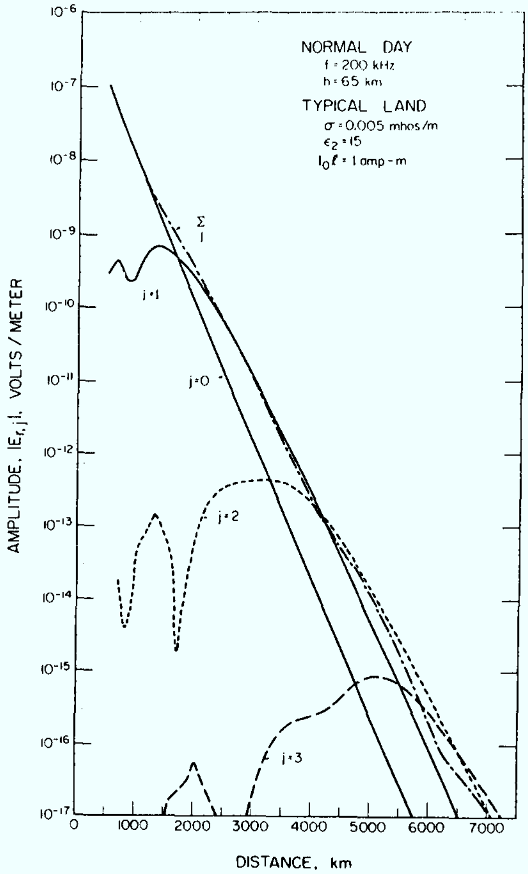

Fig. 9. Illustrating the amplitude of the normal daytime field variation with distance for the complete field, $\sum_j$, and the various geometric series components, j = 0, 1, 2, 3..., at a frequency of 200 kc/s. Magnetic dip I = 60°, magnetic azimuth ϕ_a = 270°, magnetic intensity $|\vec{H}|$ = 40 amp./m.

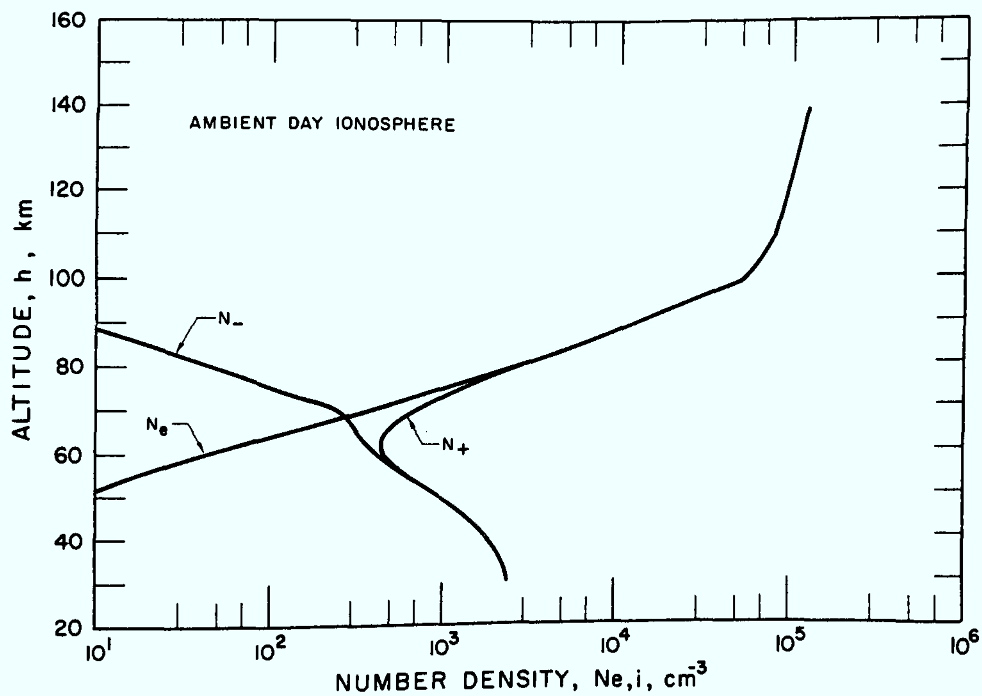

Fig. 10. Normal day ionosphere D-region electrification profile, illustrating electron, positive ion, and negative ion nuclear densities between approximately 40 and 100 km. (after Knapp 1965).

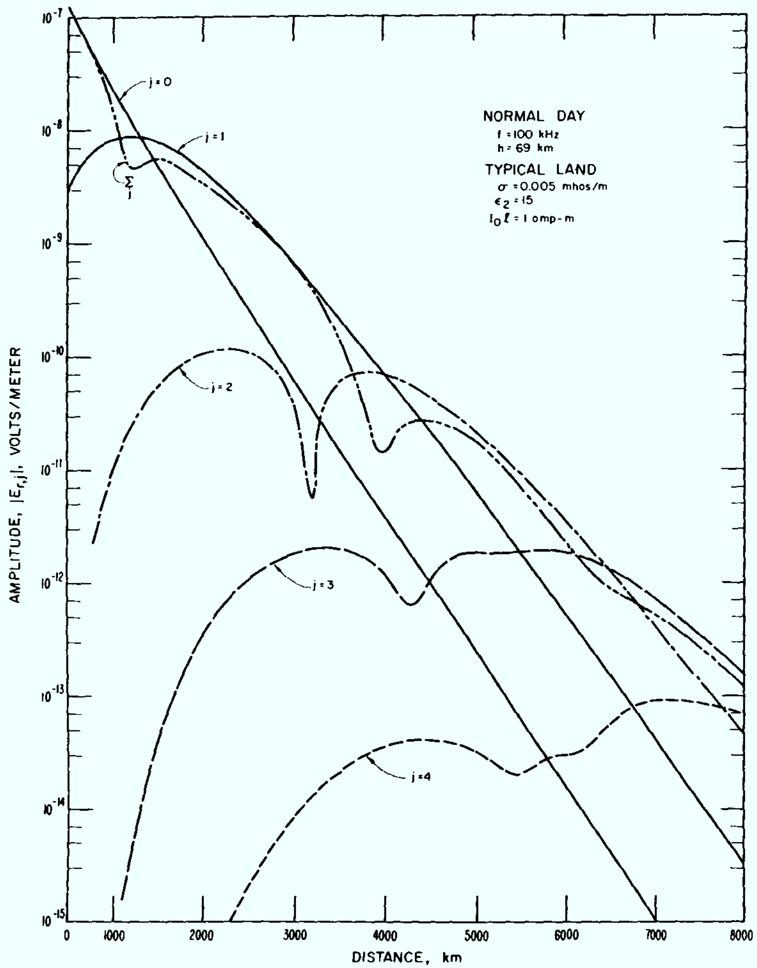

Fig. 11. Theoretical low frequency propagation curve (amplitude of the vertical electric field as a function of distance from an electrical point source) for the terrestrial waveguide, employing normal daytime ionosphere model. $j = 0$ is the ground wave, $j = 1, 2, 3...$ are the ionosphere waves. Magnetic dip $I = 60°$, magnetic azimuth $\phi_a = 270°$, magnetic intensity $|\vec{H}| = 40$ amp./m.

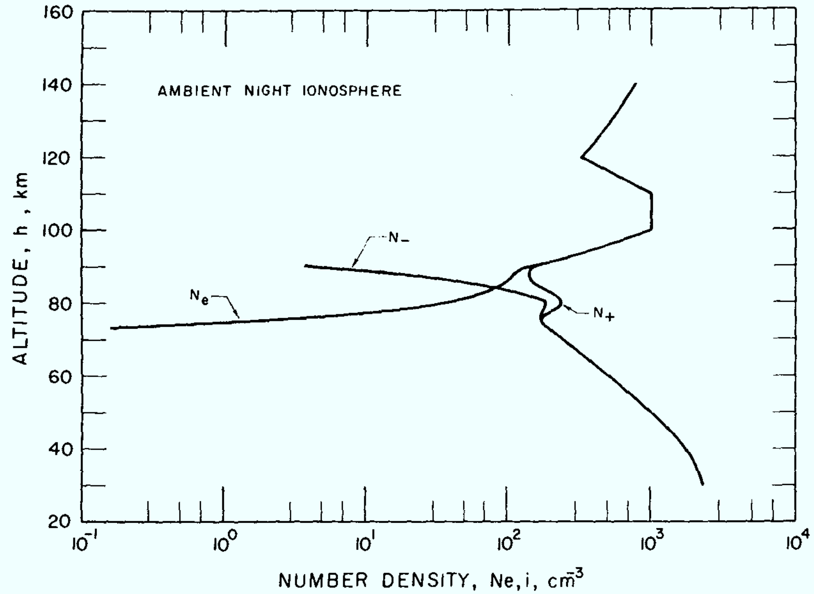

Fig. 12. Normal nighttime ionosphere D-region electrification profile, illustrating electron, positive ion, and negative ion number densities between approximately 40 and 100 km. (after Knapp 1965).

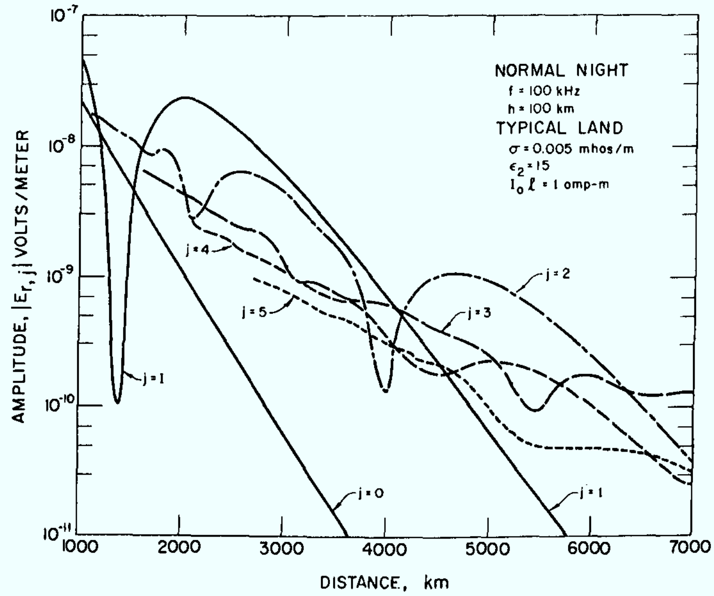

Fig. 13. Theoretical low frequency propagation curves (amplitude of the vertical electric field as a function of distance from an electrical point source) for the terrestrial waveguide, employing normal nighttime ionosphere model. Magnetic dip $I = 60°$, magnetic azimuth $\phi_a = 270°$, magnetic intensity $|\vec{H}| = 40$ amp./m.

Discussion on Paper 4.1.2 presented by J.R. Johler

Volland: Do you use an isotropic ionosphere?

Johler: No, I have used an anisotropic ionosphere; the magnetic azimuth was 270°, the dip angle was 60°, and the magnetic field was 40 amp./m. or one-half a gauss.

Volland: You did not use a dipole field. What sort of magnetic field was used?

Johler: The magnetic field was constant over the path. We can vary it, but for this exercise I kept it constant over the path.

Volland: What is the highest frequency at which you can use your calculations?

Johler: At the present time we stop at around 400 kc.; however, we are exploring the possibility of running it up to a megacycle. At 400 kc. the attenuation with distance becomes steep.

Gossard: How much computer time does it take to run a complete ray trace problem of the sort that you showed here, and on what computer?

Johler: Can Dr. Segal tell us how long the reflection coefficient part of the program takes?

Segal: Depending on the machine, anywhere from 1½ to 5 minutes.

Johler: That is the longest part, the rest is fast. With our IBM 7090 or our CDC 3600 I think we could calculate a hundred distances in about 2 minutes. The main problem at the moment is keeping track of all the calculations.

Gossard: We have essentially the same problem with the program but from a modal standpoint. Instead of solving the ray tracing problem we solve the modal problem, and our times for the first four modes of output are about the same as yours for the ray tracing.

Johler: This is not a ray tracing program.

Gossard: Yes, alright, you do it by hops. It is not a modal solution. You have to get more and more hops. It gives the same answer if you use enough terms.

Johler: What it does is decompose the mode solution into geometrically meaningful components. It gives exactly the same answer under the same conditions.

Belrose: Have you done any calculations at steep incidence?

Johler: We normally do the calculations in to about 400 km. We could run those curves right in; however, we do not have much interest in that.

Belrose: In the program you have developed, it is not possible to tell from the calculated reflection coefficient whether the reflection has been total or partial. In the case of steep incidence, the electron density profile must obviously extend to values greater than the $X = 1 + Y$ reflection condition. How many times greater?

Johler: I think if you get the electron densities too low the program might blow up.

4.1.3 NUMERICAL EXPERIMENTS SIMULATING LOW FREQUENCY AND VLF PROPAGATION IN THE LOWER IONOSPHERE

by

M.L.V. Pitteway

Cripps Computing Centre, University of Nottingham, Nottingham, England

1. Introduction

Recent advances in the speed and availability of digital computers have led to the development of various numerical methods for the solution of the differential wave equations governing the propagation of radio waves in a plane-stratified ionosphere. These computer programs are particularly important in studies of the lower height ranges of the ionosphere, as the reflection properties of low frequency and very low frequency radio waves are sensitive to the small electron densities involved. Experimental studies of these reflection properties are not expensive, but the results cannot be interpreted by conventional ray theory. Some of the numerical techniques available are described briefly in Section 3, but the main purpose of this paper is to consider how modern computing methods could be employed to increase their availability and accelerate their development.

Many radio physicists have been involved at some time in the writing of full wave computer programs. This programming involves a preliminary investigation of ionospheric constitutive relations leading to some kind of differential wave equation, together with the acquisition or development of a suitable numerical technique for their solution by digital computer. Then follows a phase of program development and debugging, with the intended objective of providing a research tool for making theoretical studies of low frequency and very low frequency propagations. The tool consists of a computer program to read in data – prepared in the form of punched paper tape or punched cards – describing electron density and collision frequency models as tabular functions of height, together with specifications of the frequency, gyrofrequency, angle of incidence, azimuth, dip, and other information required before the computation can commence. At the end of a series of calculations, adjustments can be made to the tables of electron density and collision frequency, to study the effect of different height ranges of the ionosphere, or perhaps to obtain a better match between computed and observed results. A large part of the computer programming effort will be directed towards the efficient arrangement of this type of work – for example, the program must be designed to proceed with calculations for a number of different angles of frequencies without the need to specify the electron density and collision frequency tables each time.

Even when great care is taken with the program, however, it remains a laborious business to prepare the tables of electron densities, and the research 'tool' can easily require several full-time key punch operators to act as a buffer between the user and the machine, though the actual computations may run to only a few seconds daily. Modern computing facilities include light-pen display units that can eliminate this human buffering activity, and allow direct communication between the computer and users not interested in the detailed programming or numerical techniques.

2. Summary of Computer Methods

The object of the numerical study is to make calculations determining a quantity such as a reflection coefficient for a plane radio wave of fixed frequency incident onto a plane-stratified ionosphere. The use of a fixed frequency is not a serious limitation. If the computations can be made at one frequency, they can be made at other frequencies, and different frequencies can be synthesized to determine virtual heights and other quantities relating to finite pulse wave forms. Similarly, if calculations can be made with plane waves at different angles of incidence, it is possible – in principle – to synthesize a cylindrical or spherical incident wave. The use of a plane-stratified model ionosphere in which the electron density and collision frequency are supposed to vary in the vertical (height) direction only is a more serious limitation. Correction factors can be applied to allow for earth curvature (e.g. Wait 1962), but little progress has been made in the case when the electron densities or collision frequencies show considerable fluctuations in the horizontal directions.

The differential equations to be solved are determined from Maxwell's equations, together with the constitutive relations for the ionosphere. Most early work uses the Appleton-Hartree constitutive relations based on the equation of motion of an electron with a simple collisional damping term (Banerjea 1947, Clemmow and Heading 1964), but recent developments have led to the adoption of more elaborate forms (Sen and Wyller 1960). Clearly, a rational computer program should allow for the easy interchange of different types of constitutive relations, so that new forms may be tried in a computer environment without the need for extensive reprogramming.

The differential wave equations thus derived involve electric and magnetic wave fields as the dependent variables. When the analysis is applied for a plane incident wave and a plane-stratified ionosphere, time and horizontal space variation factors may be omitted, leaving height as the only independent variable. A convenient form for computer integration uses a set of four linear first-order differential wave equations. For a homogeneous medium, these equations have four solutions corresponding to up-going and down-going ordinary and extraordinary waves. It is convenient to use four wave field components that are continuous at discontinuities of electron density or collision frequency in the vertical direction, as this will allow the computer program to deal with sharp boundary layer problems; in this form, the differential equations will involve no height derivatives of the electron density, collision frequency, or other parameters.

These wave equations contain a great deal of information, some of which is redundant when calculating the conventional reflection coefficients ${}_{\perp}R_{\perp}$, ${}_{\perp}R_{||}$, ${}_{||}R_{\perp}$, and ${}_{||}R_{||}$; with the limited storage capacity of early machines it proved convenient to transform these to work with derived reflection coefficient or admittance variables (Budden 1955, Barron and Budden 1959). The computer integrations take no longer with these equations; using the simple fourth-order numerical techniques available in most computer program libraries, they require twice as many steps, but only involve half as many equations. From a physical standpoint, however, there is one advantage in using the wave field equations to calculate reflection coefficients:

Sometimes the computer integrations yield unexpected answers – for example, a reflection coefficient may prove much smaller than expected. If the wave fields are available, it is easy to examine the detailed wave structure inside the model ionosphere to see where reflection or partial reflection is taking place, where there is coupling, where there is absorption and so on. With the derived reflection coefficient methods, the quantities formed during the integration may be interpreted as the reflection properties of an ionosphere sharply bounded with free space below; such a reflection cannot easily be interpreted in physical terms – for example, a large reflection coefficient of this type will be meaningless if there is a heavy absorption in the lower part of the ionosphere.

The Slough full-wave program developed for Pegasus – an early computer with magnetic drum storage – was based on the wave field equations (Pitteway 1965) partly because if the wave fields are available they may be used as raw material for a simple analytic formulation of scattering by weak horizontal variations of the electron density and collision frequency (Pitteway 1958) and partly because rocket experiments were available actually to measure the wave fields themselves (Hall and Fooks 1965). It has been used to make theoretical studies of the following quantities (Piggott, Pitteway and Thrane 1965, Deeks 1965, May 1965, Pitteway and Jespersen 1965):

1. Conventional reflection coefficients and associated phases.

2. Various measures of the "apparent height of reflection":

    (i) triangulation height (as the angle is varied);
    (ii) virtual height (as the frequency is varied);
    (iii) phase height (which is multi-valued in that it involves an arbitrary number of wave lengths).

3. Hollingworth patterns.

4. Polarizations required for maximum and minimum transmission.

5. Transmission coefficients.

6. Wave fields as functions of height.

7. Transmission coefficients for down-going whistler waves.

8. Internal reflection coefficients for down-going whistlers incident onto the lower ionosphere from above.

9. The "limiting" polarizations with which transmitted down-going whistlers emerge into free space below the ionosphere.

The Slough program used a standard process of numerical analysis to fit fourth-order polynomials to the wave fields. This introduces a serious limitation, in that it proves necessary to take approximately 25 steps for each wave length structure in the vertical direction. Each step takes approximately five seconds on Pegasus, so to integrate through 50 km. for f cos I (frequency × cosine of angle of incidence) equals 350 kc/s. takes about two hours (equivalent to approximately 40 seconds on Atlas). For this reason, the integrations are limited to low frequencies and very low frequencies by the availability of computer time, though a few integrations have been made just over the gyrofrequency (the lower height of reflection shortens the integration somewhat). Some typical integration times are given below:

f cos I	Pegasus integration	Atlas integration
<10 kc/s.	3 minutes	1 second
30 kc/s.	10 minutes	3 seconds
100 kc/s.	30 minutes	10 seconds
300 kc/s.	100 minutes	30 seconds
1 Mc/s.	5 hours	100 seconds

Note that these are the times taken for a single integration. Some problems may require several integrations to give just one result. For example, to compute the propagation characteristics of a mode in the earth-ionosphere wave guide, the boundary conditions are of the 'two-point' type in which the angle of incidence (usually complex) has to be carefully chosen to match the ground characteristics at the bottom of the wave guide (Barron 1959).

Alternative numerical techniques for the solution of differential equations of this type have been developed by dividing the ionosphere into a series of homogeneous slabs (Johler 1963); the technique can be applied to both the reflection coefficient and wave field form of differential equations, and can be extended to take account of slow variations across the slabs (Inoue and Horowitz 1966). Far more work is involved in making the computations for one slab or step, but it leads to the exciting possibility that it should no longer be necessary to work with steps smaller than the wave length. If it proves possible for these methods to match the speed of the conventional techniques at 100 kc/s. or even 300 kc/s., it should be possible to extend the full-wave solutions to high frequencies and very high frequencies to match absorption calculations, true height, and other analyses studied at present using ray tracing techniques, so that the one computer program could be used quite generally in propagation studies of this type.

3. The Importance of Numerical Experiments

Before designing a new computer system of the type described in the next section, it is useful to consider the achievements and limitations of previous programs written with the ultimate objective of providing a research tool to make computer methods available for a number of users, not just the originator of the program. In the case of the Slough long-wave program, the original intention was for users to be able to make calculations for given models, to see whether the models — perhaps obtained from cross modulation or partial reflection experiments — are compatible with experimental observations of long-wave reflection properties. It was also intended to be able to make adjustments to the models to improve the match with experimental results.

With the conventional computing system, the models have to be fed to the computer in the form of punched cards or punched paper tape, as a series of tabular values. This imposes a serious limitation on the work, as each adjustment to the models means the preparation of a new set of tapes — a laborious and error-prone task. Some attempts have been made to reverse the process, so as to deduce profiles from the experimental observations direct (Krasnushkin 1962). However, it may well be that errors in a range of different experimental results may produce incompatibility, in which case a profile must be chosen by an experienced radio physicist who knows which experimental features are reliable and must be matched, and which features are less reliable. It then becomes a matter of finding a model to match a particular pattern of experimental results, rather than all the detailed values; it is not easy to program a computer to recognize the significance of patterns in this way, so the experimentalist becomes an important part of the computational process.

Further, the use of computer programs often has a quite separate impact than that originally intended. Computing with the Slough program, for example, led to the discovery of a new full-wave reciprocity relation (Pitteway and Jespersen 1965). This is the second reciprocity relation of this type discovered through numerical calculation with a computer (Budden 1954, Barron and Budden 1959). In many other cases, analytic results have been established as a result of experiments with a computer — for example, the analytic formulation of weak scattering (Pitteway 1958) was initially discovered through the availability of a computer program.

At first, it might be considered that to find simple analytic answers after investing valuable computer time in a problem might mean that computer resources have been wasted. But like more conventional experiments, it is now becoming recognized that numerical computations often lead to results that were not the original investigation motive. An analogy can be drawn with training the pilot of a new aircraft with a mock-up cockpit, wired through an analog or digital computer, so that he can manipulate the controls and get the feel of the machine. Similarly, a mathematician may be faced with complicated sets of equations, and may make little progress until he is provided with computing facilities. A few numerical results may reveal a pattern — a curve looking like a Bessel function, perhaps — which he will recognize, and then he can approach the original equations with an empirical result to be established.

In the Slough program case, two graphs — transmission coefficients plotted as functions of angles — appeared as mirror images of one another. A comparison of the computer output details revealed correspondence to all eight figures of accuracy, suggesting the full-wave reciprocity relation. A less accurate match would have suggested an approximate relation — ray theory, for example.

Experience suggests that this kind of computer discovery may become increasingly important as numeric work develops, and clearly an efficient system should be designed with this in mind. Progress with punched card or paper tape input is slow and tedious. Many key punch operators and clerks would be required to keep track of the large quantities of input and computer output generated, with the result that originators of programs are often extremely reluctant to organize computer runs for potential customers of a rationalized long-wave computing service. The purpose of this section – indeed the main object of the paper – is to describe how an efficient long-wave computing service for experimental radio physicists could be set up using the facilities available with modern equipment. The programming itself would involve development rather than original research, but could then be used as a test bed for numerical analysts wishing to try new techniques to speed high frequency integrations, and for theoreticians to try new types of constitutive equations in a long-wave computing environment, as well as experimentalists wishing to study the possible significance of a new set of observations.

Certain requirements of the new computing system are almost obvious:

(i) the computer must be fast, i.e. capable of performing arithmetic operations and accessing store at micro-second or even nano-second speeds (Pegasus takes milliseconds);

(ii) it must have a floating point unit (Pegasus is all fixed point, and to use a floating point through software is prohibitively slow);

(iii) it must have adequate core store – i.e. several thousand words. Pegasus has less than 100 words; using a drum for random access is prohibitively slow, and optimizing drum access wastes programming time;

(iv) it should have a high level language with built-in complex arithmetic facilities, e.g. Fortran IV, Atlas Autocode, or PL/1. It is tedious to write out all the complex arithmetic statements in real and imaginary parts, and it is inconvenient to alter the program for special tests;

(v) graphical output is essential. No human can assimilate large quantities of computer output in numeric form, and graph plotting by hand is too slow.

In addition, the computer should have a cathode-ray-tube display unit so that computed curves can be examined without printing, a light-pen display unit so that hand-sketched curves can be input direct, and a keyboard for conversation with the user. The program should be prepared in a versatile form, so that, for example, wave fields can be displayed only when required by the user; and its construction should be modular, so that, for example, a module describing the Appleton-Hartree constitutive relations may be replaced without editing other parts of the program.

The parts of a computer forming such a system are shown in the figure. The computer itself will, of course, be used for many jobs, and will probably be time-shared with other tasks except when making the actual computations required.

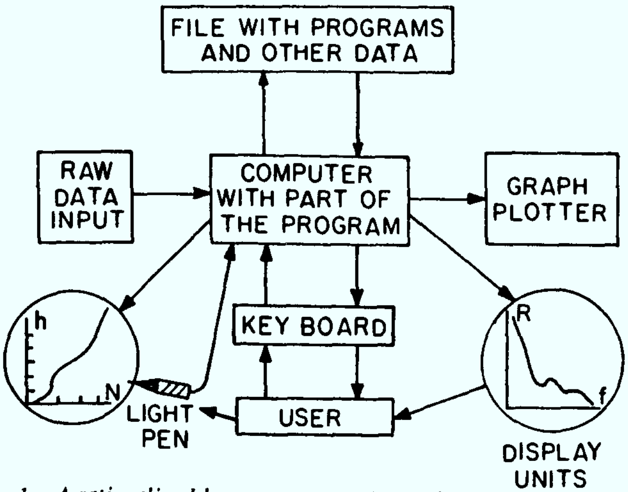

Fig. 1. A rationalized long-wave computer system. The arrows indicate the flow of information.

The user will initiate the program by typing his name and identification at the on-line keyboard, and calling down a long-wave control program from the computer's file. He will then type answers to simple questions describing the calculation he wishes to have performed. A typical conversation might include exchanges like this:

Computer	User
"What do you want?"	"Hollingworth"
"u (h)?"	"Standard atmosphere" (this will be stored in the file with other models)
"N (h)?"	"Pen"

(At this point, the computer would display suitably marked axes, and the user would sketch in a curve using the light pen.)

Computer	User
"Gyro?"	"Ottawa" (since the Ottawa angle of dip would be stored in file along with the gyrofrequency, the system need not ask for this)
"Frequency?"	"16 k/c."
"Azimuth?" etc.	

Then a few seconds pause while the computer calculates and displays a Hollingworth pattern on the cathode display. Perhaps the user has a Hollingworth pattern from an experiment? This will have been processed by the computer at an earlier time, and a record may be kept on file — in which case the user will instruct the machine to display this too — perhaps in a different color. Then, with the light pen, pare away the N(h) curve till satisfied with the match. Perhaps the user will then instruct the machine to display $_{\|}R_{\|}$ as a function of frequency or angle of incidence — this may involve further alterations to the profile. When he is finally satisfied, he will type a directive to the computer to produce graphical output for permanent record or publication.

The file could also be used to maintain a list of users, e.g. for costing purposes. One of the users may have developed a new set of constitutive relations. To avoid unnecessary delays waiting for conventional communication — publication, conferences, and the like — he can ask the computer to print a mailing list of all recent users of the system.

5. Summary

The present rate of progress of radio physicists matching experimental observations could be accelerated by the preparation of an extended computer system. The programming costs would be high, but not as high as each user having to write his own set of computer programs for long wave studies. The value of the system would be greatly enhanced if efficient numerical methods could be developed to handle higher frequencies than the present limit, which is values of f cos I up to not much more than the gyrofrequency.

REFERENCES

Banerjea, B.K. Proc. Roy. Soc. A, 190, 67. 1947.

Barron, D.W. Phil. Mag. 50, 1068. 1959.

Barron, D.W. and K.G. Budden. Proc. Roy. Soc. A, 249, 387. 1959.

Budden, K.G. Proc. Camb. Phil. Soc. 50, 604. 1954.

Budden, K.G. Proc. Roy. Soc. A, 227, 516. 1955.

Clemmow, P.C. and J. Heading. Proc. Camb. Phil. Soc. 50, 319. 1954.

Deeks, D.G. Proc. Roy. Soc. A, 291, 413. 1965.

Hall, J.E. and J. Fooks. Planet. Space Sci. 13, 1013. 1965.

Inoue, Y. and S. Horowitz. (D.R.T.E. Conference Proceedings). 1966.

Johler, J.R. Phys. Soc. Conference (1962) 436. 1963.

Krasnushkin, P.E. Dokl. Akad. Nauk. U.S.S.R. 139, 67; (U.S.A. 6, 576). 1961.

May, B.R. J. Atmos. Terr. Phys. (In Print). 1966.

Piggott, W.R., Pitteway, M.L.V. and E.V. Thrane. Phil. Trans. A, 257, 243. 1965.

Pitteway, M.L.V. Proc. Roy. Soc. A, 246, 556. 1958.

Pitteway, M.L.V. Phil. Trans. A, 257, 219. 1965.

Pitteway, M.L.V. and J.L. Jespersen. J. Atmos. Terr. Phys. 28, 17. 1966.

Sen, H.K. and A.A. Wyller. J. Geophys. Res. 65, 3931. 1960.

Wait, J.R. 'Electromagnetic waves in stratified media' (Pergamon Press, Oxford). 1962.

Discussion on Paper 4.1.3 presented by M.L.V. Pitteway

Wright: If I had offered a paper at this conference on a modern ionospheric sounder I would have gone over much of what Dr. Pitteway has said here, but almost in reverse. It seems to me that for the experimental radio physicist the ultimate, according to today's view, is a system for making measurements on the ionosphere in real time, associated with a computer. One might add an ionospheric sounder or ionospheric radio equipment on line with this system, and we are involved now in a program that is doing what you might say is the reverse of this. We are going to put much of this type of system on line with an ionospheric sounder. The objectives are much the same; the thing I wanted to point out is that having programs that can perform wave solutions, trace rays, calculate electron density profiles, analyze to determine the movements of the ionosphere from some of the radio echo data, or match these various lines of information together in a continuity equation for the electrons that are up there, is an invaluable system for one who wishes to make measurements of the ionospheric medium. I feel that until we have it we won't make a great deal of progress.

4.1.4 NUMERICAL SOLUTION OF FULL WAVE EQUATION

by

Y. Inoue – University of Pittsburgh, Pa.
S. Horowitz – AFCRL, Bedford, Mass.

Presented by S. Horowitz

The equations governing the propagation of electromagnetic waves in a horizontally stratified gyrotropic medium can be written in compact matrix form as:

$$\frac{d\vec{e}}{dz} = i \underline{\underline{T}} \vec{e} \tag{1}$$

where $\underline{\underline{T}}$ is the 4x4 propagation coefficient matrix which is a function of the dielectric tensor and incident direction cosines, $\vec{e}$ is a column vector of horizontal wave field components (E_x, E_y, H_x, H_y), and z is the scaled height.

In a homogeneous layer, $\underline{\underline{T}}$ is constant and has four characteristic roots or eigenvalues, denoted as q_1, q_2, q_3, q_4, (Booker q's) which represent the four magnetoionic modes. Two modes will be upgoing waves and two modes will be downgoing waves, each with its characteristic state of polarization. The characteristic waves are arranged as follows during a downward integration (ground-based signals):

$$I_m[q_1] > I_m[q_2] > I_m[q_3] > I_m[q_4] \tag{2}$$

For upward integration, (satellite or whistler transmissions) the order is reversed. For frequencies below the gyrofrequency the order of (2) represents upgoing fast wave (uf), upgoing slow wave (us), downgoing slow wave (ds) and downgoing fast wave (df) respectively.

The solution to (1) for the homogeneous case can be written as

$$\vec{e}(z) = \text{Exp} \; \{i \underline{\underline{T}} \; (z-z_o)\} \cdot \vec{e} \; (z_o) \tag{3}$$

where $\vec{e}\,(z_o) = \underline{\underline{S}} \cdot \vec{b}$ = sum of linear combination of 4 characteristic waves

$\underline{\underline{S}}$ = eigenvector of $\underline{\underline{T}}$

$\vec{b}$ = boundary conditions

from which it can be directly shown that

$$\vec{e}(z) = \sum_{e=1}^{4} S_{.e} \; \text{E x p} \; \{iq_e(z-z_o)\} \cdot b_e \tag{4}$$

The total wave is therefore represented by the linear superposition of the four characteristic waves.

If $\underline{\underline{T}}$ is not constant, the four modes become coupled and transitions between polarization states and partial reflections occur. The derivation of the total $\vec{e}$ is shown in Fig.1, a and b. Each independent solution will have contributions from all four magnetoionic characteristic waves due to the coupling.

To treat this case the singularities or critical coupling regions are located and removed by a binary search technique based on Clemmow and Headings transformation matrix, the determinant of which is regionally invariant from one singularity to another (Inoue and Horowitz, 1966a).

There are two remaining problems before the integration can be completed (Inoue and Horowitz, 1966b)

1. Degradation of linear independence of solutions.

2. Dividing the inhomogeneous layer into thin homogeneous slabs.

Linear independent solutions have a dissimilarity that manifests itself in different rates of amplitudes and phase variations, wave polarizations, and intrinsic waves impedances. Since T_1 and T_o are not equal in an inhomogeneous medium, the eigenvectors S_z and S_{z_o} are not equal and $S_1^{-1} \cdot S_{z_o}$ is not equal to unity. This will result in degradation of linear independence between solutions unless special care is exercised. The physical reason for this is that in an inhomogeneous medium, partial reflection as well as magnetoionic mode coupling appear everywhere, so that the wave field at a height is the resultant contribution of various waves arriving from the entire region. The starting conditions for the last equation in Fig. 1b must therefore be continuously reset.

This can be shown mathematically as follows: The solutions of the integral matrix is

$$W(z_n) = {}_nS\cdot{}_n\Delta\cdot{}_nS^{-1}\cdot{}_{n-1}S\cdot{}_{n-1}\Delta\cdot{}_{n-1}S^{-1}\cdots \tag{5}$$

$$\cdots\; {}_2S\cdot{}_2\Delta\cdot{}_2S^{-1}\cdot{}_1S\cdot{}_1\Delta\cdot{}_1S\cdot W(z_o)$$

consider 2x2 T matrix so that

$$W(z_1) = {}_1S\cdot{}_1\Delta\cdot{}_1S^{-1}\cdot W(z_o), \tag{6}$$

and let

$${}_1R = {}_1S^{-1}\cdot W(z_o), \tag{7}$$

The two solutions for the 0-th slab are then

1st trial solution
$$W_{\cdot 1}(z_o) = {}_1S_{\cdot 1}\cdot{}_1R_{11} + {}_1S_{\cdot 2}\cdot{}_1R_{21}, \tag{8}$$

2nd trial solution
$$W_{\cdot 2}(z_o) = {}_1S_{\cdot 1}\cdot{}_1R_{12} + {}_1S_{\cdot 2}\cdot{}_1R_{22}, \tag{9}$$

The first column to the right of the equal sign represents the first characteristic wave in the 1st slab, and the second column represents the second characteristic wave. The R matrix elements indicate the magnitudes of the composite characteristic waves included in each special solution. Then:

$$W(z_1) = \begin{pmatrix} {}_1S_{11}, & {}_1S_{12} \\ {}_1S_{21}, & {}_1S_{22} \end{pmatrix}\cdot\begin{pmatrix} {}_1\Delta_{11}, & 0 \\ 0\;, & {}_1\Delta_{22} \end{pmatrix}\cdot\begin{pmatrix} {}_1R_{11}, & {}_1R_{12} \\ {}_1R_{21}, & {}_1R_{22} \end{pmatrix} \tag{10}$$

$$= \begin{pmatrix} {}_1S_{11}\cdot{}_1\Delta_{11}\cdot{}_1R_{11} + {}_1S_{12}\cdot{}_1\Delta_{22}\cdot{}_1R_{21}, & {}_1S_{11}\cdot{}_1\Delta_{11}\cdot{}_1R_{12} + {}_1S_{12}\cdot{}_1\Delta_{22}\cdot{}_1R_{22} \\ {}_1S_{21}\cdot{}_1\Delta_{11}\cdot{}_1R_{11} + {}_1S_{22}\cdot{}_1\Delta_{22}\cdot{}_1R_{21}, & {}_1S_{21}\cdot{}_1\Delta_{11}\cdot{}_1R_{12} + {}_1S_{22}\cdot{}_1\Delta_{22}\cdot{}_1R_{22} \end{pmatrix} \tag{11}$$

$\uparrow$ Increase $\quad\downarrow$ Decrease $\quad\uparrow$ Increase $\quad\downarrow$ Decrease

Always $$|\Delta_{11}|>1, \quad |\Delta_{22}|<1$$

After repeated multiplication of $S\cdot\Delta S^{-1}$, $W(z_n)$ will lose independence. To avoid this degradation, let

$$ {}_1S^{-1}\cdot W(z_o)=\begin{pmatrix} {}_1R_{11}, & 0 \\ {}_1R_{21}, & {}_1R_{22} \end{pmatrix}, \tag{12}$$

then

$$W(z_1)=\begin{pmatrix} \underbrace{{}_1S_{11}\cdot{}_1\Delta_{11}\cdot{}_1R_{11} + {}_1S_{12}\cdot{}_1\Delta_{22}\cdot{}_1R_{21}}, & {}_1S_{12}\cdot{}_1\Delta_{22}\cdot{}_1R_{22} \\ {}_1S_{21}\cdot{}_1\Delta_{11}\cdot{}_1R_{11} + {}_1S_{22}\cdot{}_1\Delta_{22}\cdot{}_1R_{21}, & {}_1S_{22}\cdot{}_1\Delta_{22}\cdot{}_1R_{22} \end{pmatrix} \tag{13}$$

Increase Decrease

This linear independence between two solutions is maintained by making:

$${}_1S^{-1}\cdot W(z_o) = \begin{pmatrix} {}_1R_{11}, & {}_1R_{12} \\ {}_1R_{21}, & {}_1R_{22} \end{pmatrix} \longrightarrow \begin{pmatrix} {}_1R_{11}, & 0 \\ {}_1R_{21}, & {}_1R'_{22} \end{pmatrix} \tag{14}$$

This is accomplished by a linear combination of R·1 and R·2:

$${}_1R_{\cdot 2} - \frac{{}_1R_{12}}{{}_1R_{11}}\cdot {}_1R_{\cdot 1} = {}_1R'_{\cdot 2} = \begin{pmatrix} 0 \\ {}_1R'_{22} \end{pmatrix} \tag{15}$$

The new starting solution is then

$$\begin{aligned} W(z_o)' &= {}_1S\cdot \begin{pmatrix} {}_1R_{11}, & 0 \\ {}_1R_{21}, & {}_1R'_{22} \end{pmatrix} \\ &= \Bigg(W_{\cdot 1}(z_o),\ \underbrace{W_{\cdot 2}(z_o) - \frac{{}_1R_{12}}{{}_1R_{11}}\cdot W_{\cdot 1}(z_o)}_{\text{Linear Combination}} \Bigg) \end{aligned} \tag{16}$$

This is possible since the original differential equations are linear and any linear combination of solutions is also a solution. The integration procedure is outlined in Fig.2. The integration is continued until free space is reached where solutions are combined for polarization matching.

The wave fields are reconstructed by proceeding back through the stored solution values and undoing the linear combinations and applying polarization adjustments.

A pictorial representation of the swamping effects of the intermittent adjustment and backward correction of solutions is shown in Fig. 3.

The inhomogeneous medium is horizontally stratified into homogeneous slabs. $\underline{\underline{T}}$ is assumed to be linearly varying within each slab instead of the traditional assumption of constant $\underline{\underline{T}}$. This results in a series matricant solution (Inoue and Horowitz, 1966b) outlined in Figs. 4a and 4b which converges rapidly.

Fig. 5 illustrates the final solution for the integral matrix and a comparison between the homogeneous and linearly varying slabs. The large step size possible with this method will allow one to extend full wave solutions into the higher frequencies.

The above method has been programmed for computer calculation and one numerical solution will now be illustrated. The model chosen is an exponential electron density profile approaching daytime conditions and shown in Fig. 6. The X, Y, Z are Appleton-Hartree parameters of normalized electron density, gyrofrequency and collision frequency respectively for an operating frequency of 100 kc. Vertical incidence is assumed. The geomagnetic field is 0.569 gauss at a dip angle of -73°

The real and imaginary parts of the Booker q are illustrated in the lower part of Fig. 6. The anisotropy becomes significant above 70 km. The imaginary part of q indicates that before the wave is separated into two modes, the attenuation is considerable and therefore large reflected signals are not anticipated. The large change in the real part of q occurs at $X = 1 + Y$, where the fast wave is reflected.

Fig. 7 illustrates the four major coupling coefficients for this model and incident conditions. When Z becomes greater than Y, the anistropy of the medium disappears. Linearly polarized waves are assumed in the quasi-isotropic region and magnetoionic characteristic waves are used in the anistropic region. The transition occurs at about 63 km. In the quasi-isotropic region there is weak coupling. Its effect on reflections will be small. No peculiar effect occurs at the $X = 1$ level because of the high collision frequency.

In the region above 65 km., the reflection type coupling consistently predominates, that is uf converted to df and us converted to ds. A small peak of the reflection type coupling in the fast mode appears at 79 km., where $X = 1 + Y$. The partial reflections of us waves continues to increase with height. Above 100 km., the electron density has been assumed constant and the small coupling is attributed to the varying collisional frequency.

Coupling echoes from the upper region can not be observed on the ground because of the high attenuation. Main reflections will come from below the strong coupling region. The total reflected energy will be less than −60 db, the reflection height around 78 km.

Fig. 8 shows the equivalent magnetoionic modes at each height plotted on a log scale. Notice the large decrease in the uf wave as it enters into the evanescent region above $X = 1 + Y$ height. The us wave has been reduced by 80 db at 120 km., so we will not expect much of a whistler mode for this daytime model. The incident wave is transverse magnetic. Coupling due to the inhomogeneous medium generates the TEU wave.

The wave polarization of the independent modes is presented in Fig. 9. The phase memory integral has been extracted so that the changes in shape are due to the inhomogeneous medium. The solid line with left-hand polarization represents the uf wave, the broken line represents the us wave and is the whistler mode. Since vertical propagation is assumed, no change in polarization direction is expected.

The computed wave field profiles are illustrated in Fig. 10. The oscillations between 70 and 80 km. are due to the interference between uf and us waves. The remaining structure is somewhat smooth due to collisional damping. Magnetic field rocket measurements, in addition to requiring a low impedance antenna, also have the advantage of smaller dynamic range.

The calculated ground reflection coefficients are:

$$_{||}R_{||} = (-6.138 + j2.712) \times 10^{-4}$$
$$_{||}R_{\perp} = (-1.693 + j7.535) \times 10^{-4}$$

Similar calculations have been made for several other models, to help develop an intuitive feeling of the effects on the wave fields of a changing electron density profile.

REFERENCES

1966a — Inoue and Horowitz. Radio Science, I, No. 4, April 1966.

1966b — Inoue and Horowitz. Radio Science, I, No. 8, August 1966.

Inhomogeneous Layer

T = A Function of Height

Assume : Inhomogeneous Layer $= \Sigma$ Homogeneous Thin Slabs

$$z_0 \quad {}_0T \to {}_0q_\ell,\ {}_0S \qquad \vec{e}(z_0) = {}_0S \cdot {}_0\vec{b}$$

$$z_1 \quad {}_1T \to {}_1q_\ell,\ {}_1S \qquad \vec{e}(z_1) = {}_1S \cdot {}_1\Delta \cdot {}_1S^{-1} \cdot \vec{e}(z_0)$$

$$z_2 \quad {}_2T \to {}_2q_\ell,\ {}_2S \qquad \vec{e}(z_2) = {}_2S \cdot {}_2\Delta \cdot {}_2S^{-1} \cdot \vec{e}(z_1)$$

$$z_3 \quad {}_3T \to {}_3q_\ell,\ {}_3S \qquad \vec{e}(z_3) = {}_3S \cdot {}_3\Delta \cdot {}_3S^{-1} \cdot \vec{e}(z_2)$$

$$\vdots \qquad\qquad \vdots$$

$$\vec{e}(z_3) = {}_3S \cdot {}_3\Delta \cdot {}_3S^{-1} \cdot {}_2S \cdot {}_2\Delta \cdot {}_2S^{-1} \cdot {}_1S \cdot {}_1\Delta \cdot {}_1S^{-1} \cdot {}_0S \cdot {}_0\vec{b}$$

Fig. 1a

$$\vec{e}(z_n) = \underbrace{\prod_{\kappa=1}^{n} \leftarrow {}_\kappa S \cdot {}_\kappa\Delta \cdot {}_\kappa S^{-1} \cdot {}_0S}_{4 \times 4 \text{ Matrix}} \cdot {}_0\vec{b} \quad \text{Constant}$$

$$\vec{e}(z_n) = W(z_n) \cdot {}_0\vec{b} \quad \cdots\cdots \quad \vec{e}(z) = S \cdot \Delta(z) \cdot \vec{b}$$

Inhomogeneous Layer   Homogeneous Layer

Boundary Conditions $\longrightarrow$ 4 Linearly Independent Solutions

Integral Matrix

$$W(z_n) = \prod_{\kappa=1}^{n} \leftarrow {}_\kappa S \cdot {}_\kappa\Delta \cdot {}_\kappa S^{-1} \cdot W(z_0), \quad W(z_0) \overset{?}{=} {}_0S$$

$$\left.\begin{array}{ll} W_{\cdot 1} & \text{1st} \\ W_{\cdot 2} & \text{2nd} \\ W_{\cdot 3} & \text{3rd} \\ W_{\cdot 4} & \text{4th} \end{array}\right\} \text{Linearly Independent Solutions}$$

Column Matrices

Remaining Problems:

I. Degradation of Linear Independence of Solutions
II. Justification of Inhomog. Layer $= \Sigma$ Homog. Slabs

Fig. 1b

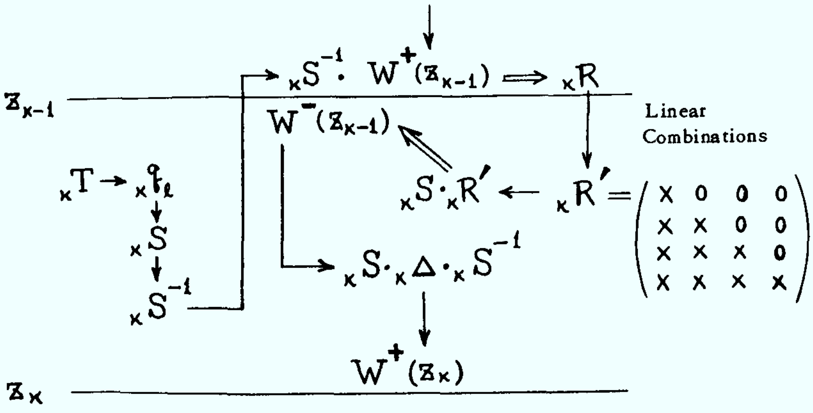

Integration Procedure to Preserve Good Independence

Fig. 2

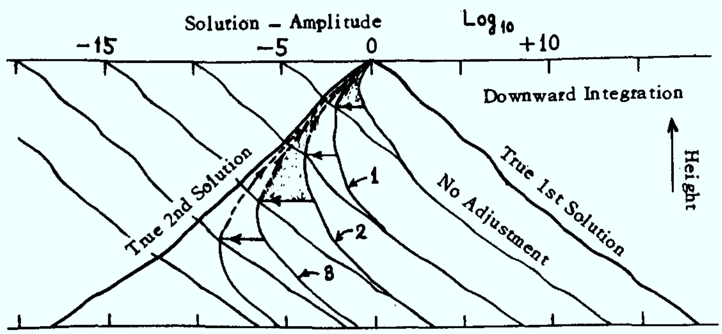

Intermittent Adjustment and Backward Correction of Solutions
in order to preserve Good Linear Independence
between Solutions in an Isotropic Layer

—◄— Adjustment of Solution

– –►– Backward Correction

Fig. 3

Justification of Inhomogeneous Layer $= \sum$ Homogeneous Slabs

Linearly Varying $T(z)$ within a Slab

$$T(z) = T^{-} + \frac{T^{+} - T^{-}}{z_{K+1} - z_{K}} \cdot (z - z_{K})$$

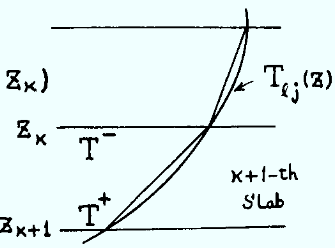

Integral Matrix

$$W(z) = M(z, z_K) \cdot W^{-}(z_K)$$

Assume no Critical Coupling in χ Slabs

(Critical Coupling Height $=$ Subdividing Height)

$$M(z_K, z_K) = I \quad \text{Unity Matrix}$$

Analytic Series Solution

$$M(z, z_K) = I + \sum_{p=1}^{\infty} M_p(z_K) \cdot (z - z_K)^p$$

Constant Matrix

$$\frac{d}{dz} \cdot M(z, z_K) = i \cdot T(z) \cdot M(z, z_K)$$

Fig. 4a

Recursion Formulae :

$$p \cdot M_p = i \cdot T^{-} \cdot M_{p-1} + i \cdot \frac{T^{+} - T^{-}}{z_{K+1} - z_K} \cdot M_{p-2},$$

$$p = 1, 2, 3, \cdots\cdots \infty$$

$$M(z_{K+1}, z_K) = \exp\left\{ i \cdot T^{*} \cdot (z_{K+1} - z_K) \right\}$$

where

$$\begin{aligned} T^{*} = {} & \frac{1}{2}(T^{+} + T^{-}) \\ & + i \cdot \frac{[T^{+}, T^{-}]}{2 \cdot 3!} \cdot (z_{K+1} - z_K) \\ & + i^2 \cdot \frac{[(T^{+} - T^{-}), [T^{+}, T^{-}]]}{2 \cdot 5!} \cdot (z_{K+1} - z_K)^2 \\ & + \cdots\cdots\cdots \end{aligned}$$

$$[A, B] = A \cdot B - B \cdot A \quad \text{non-commutative}$$

Fig. 4b

$$\begin{aligned} W^+(z_{k+1}) &= \exp\{i\cdot T^*\cdot(z_{k+1}-z_k)\}\cdot W^-(z_k) \\ &= {}_{k+1}S^*\cdot {}_{k+1}\Delta^*\cdot\left({}_{k+1}S^*\right)^{-1}\cdot W^-(z_k) \end{aligned}$$

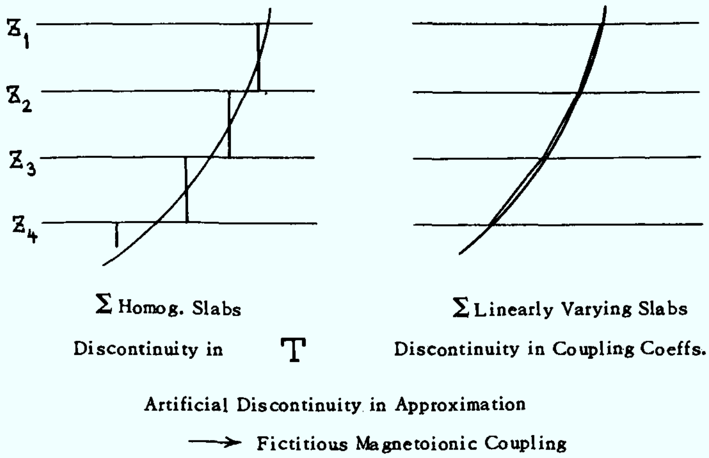

Fig. 5

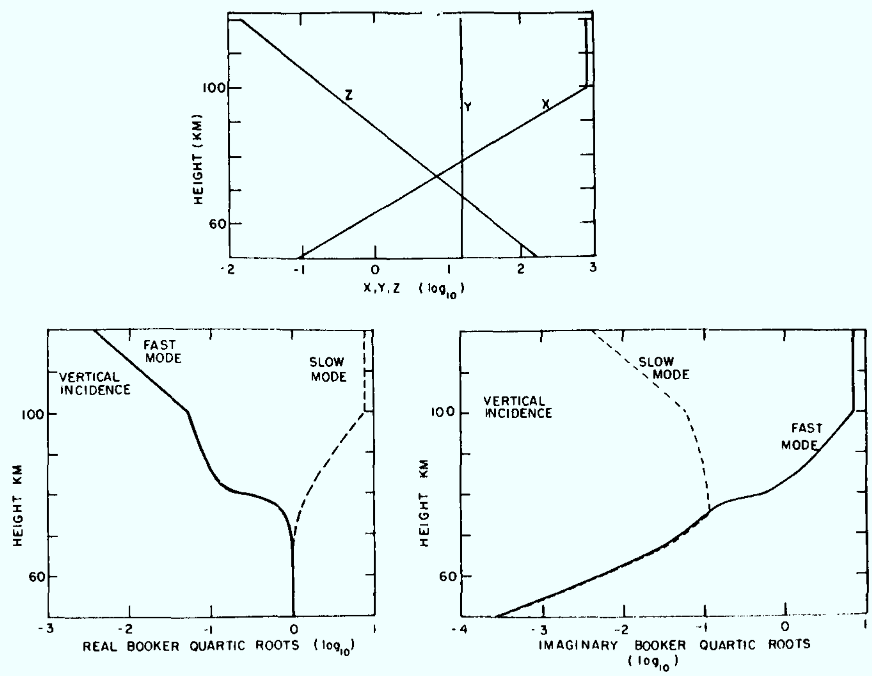

Fig. 6

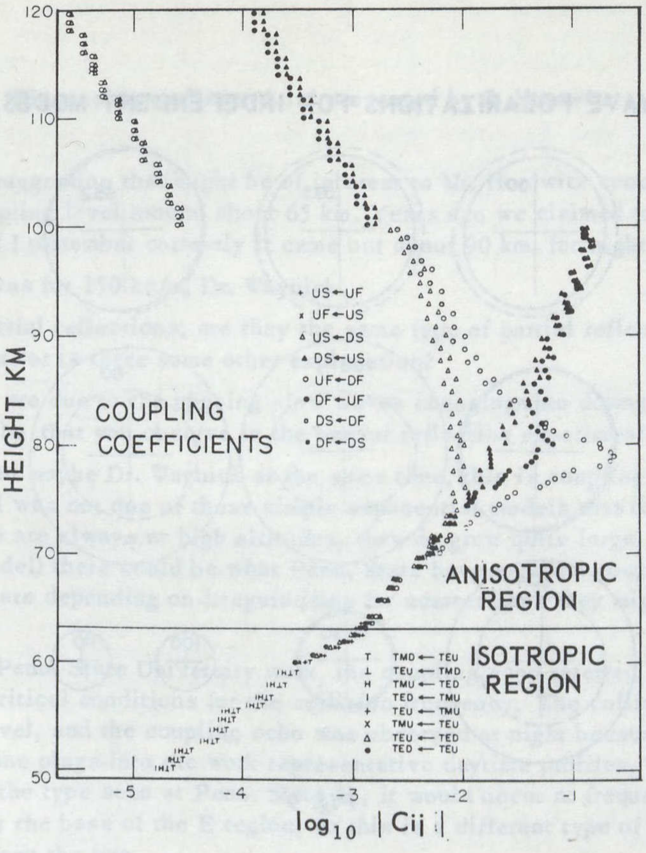
HEIGHT KM
120
110
100
90
80
70
60
50
COUPLING
COEFFICIENTS
US ← UF
UF ← US
US ← DS
DS ← US
UF ← DF
DF ← UF
DS ← DF
DF ← DS
ANISOTROPIC
REGION
ISOTROPIC
REGION
TMD ← TEU
TEU ← TMD
TMU ← TED
TED ← TMU
TEU ← TMU
TMU ← TEU
TEU ← TED
TED ← TEU
-5
-4
-3
-2
$\log_{10}$ Cij

Fig. 7

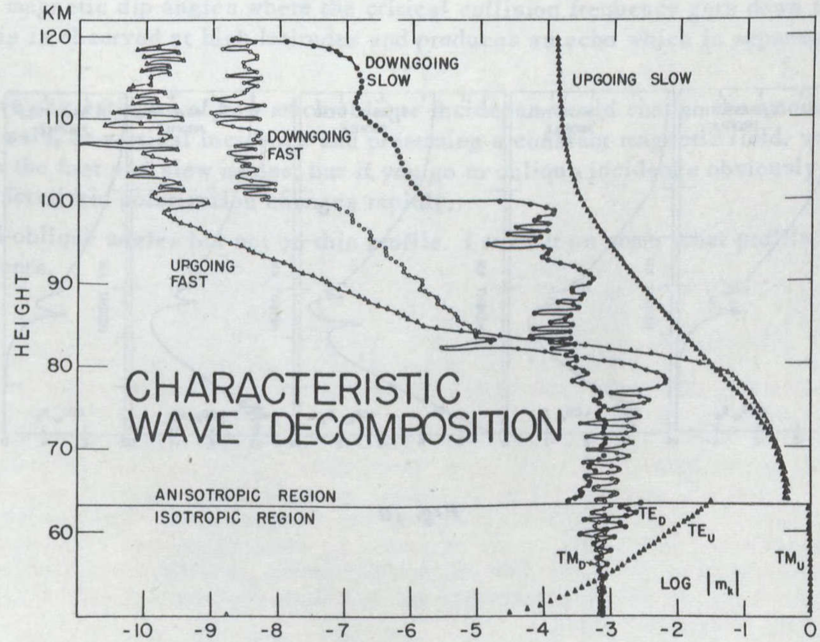
KM
120
110
100
90
80
70
60
HEIGHT
DOWNGOING
SLOW
DOWNGOING
FAST
UPGOING SLOW
UPGOING
FAST
CHARACTERISTIC
WAVE DECOMPOSITION
ANISOTROPIC REGION
ISOTROPIC REGION
TE_D
TE_U
TM_D
TM_U
LOG $|m_k|$
-10
-9
-8
-7
-6
-5
-4
-3
-2
-1
0

Fig. 8

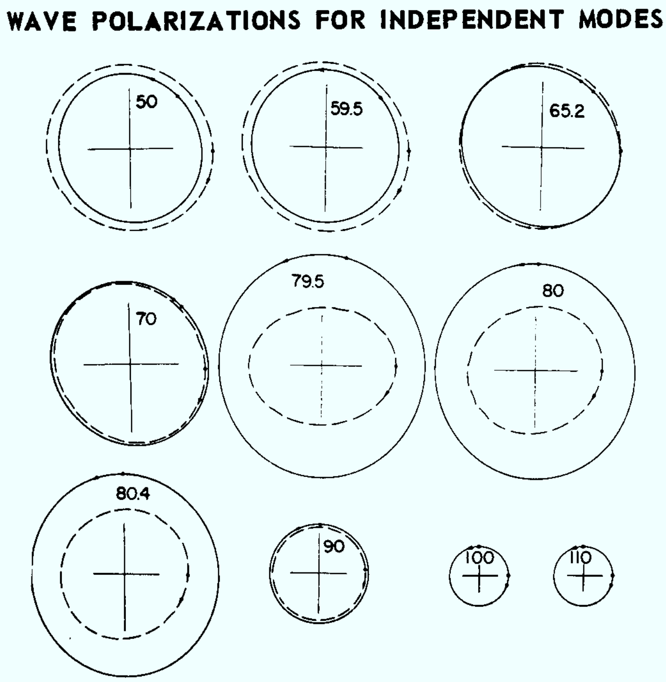
WAVE POLARIZATIONS FOR INDEPENDENT MODES
50
59.5
65.2
70
79.5
80
80.4
90
100
110

Fig. 9

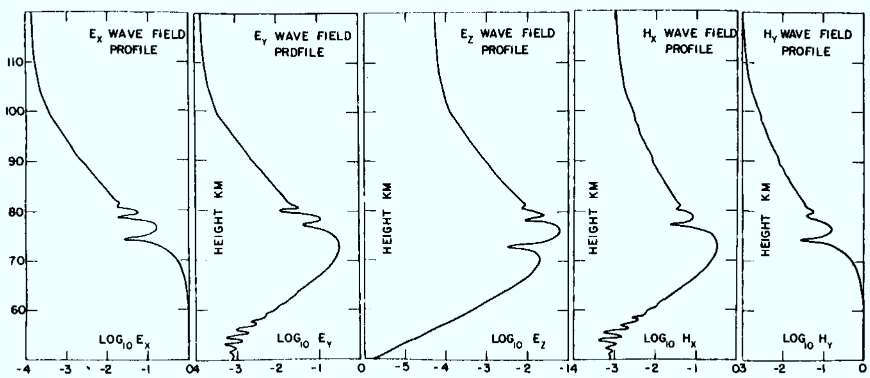
E_x WAVE FIELD PROFILE
E_y WAVE FIELD PROFILE
E_z WAVE FIELD PROFILE
H_x WAVE FIELD PROFILE
H_y WAVE FIELD PROFILE
HEIGHT KM
LOG$_{10}$ E_x
LOG$_{10}$ E_y
LOG$_{10}$ E_z
LOG$_{10}$ H_x
LOG$_{10}$ H_y

Fig. 10

Discussion on Paper 4.1.4 presented by S. Horowitz

Waynick: One possible suggestion that might be of interest to Mr. Horowitz concerns the last slide, in which he showed the coupling level around about 65 km. Years ago we claimed to have observed this separately as an echo. If I remember correctly it came out about 90 km. for nighttime models.

Belrose: I believe that was for 150 kc/s, Dr. Waynick.

Ross: You mentioned partial reflections; are they the same type of partial reflections which we are dealing with in our experiment, or is there some other explanation?

Horowitz: These echoes are due to the upgoing slow waves changing into downgoing waves, so I assume it is the same type of echo that you observe in the partial reflection experiment.

Sales: To answer that and maybe Dr. Waynick at the same time, this is coupling echoes back, and it is possible that if the model was not one of these simple exponential models that this thing could be peaked up at some height. These are always at high altitudes, they do grow quite large, and if the model was right (a more realistic model) there could be what Penn. State have called a coupling echo at higher altitudes. But I think if you are depending on irregularities for scatter back they might not be exactly the same.

Belrose: As I recall the Penn. State University work, the coupling echo referred to occurs at the level where X equals 1 under critical conditions for the collision frequency. The collision frequency has to be a critical value at that level, and the coupling echo was observed at night because it is at night these conditions are found. If one plugs into the work representative daytime profiles, you will find that, if a coupling echo existed of the type seen at Penn. State U., it would occur at frequencies around 500 kcs. and would be well up near the base of the E region, so this is a different type of coupling. I don't know the exact difference between the two.

Wright: I would like to mention that the coupling which occurs under the conditions of critical coupling (critical collision frequency at $X = 1$) that Dr. Belrose described, can be found up inside the E region at sufficiently high magnetic dip angles where the critical collision frequency gets down to 10^4 or perhaps a little less. This is observed at high latitudes and produces an echo which is separated by group delay effects.

Bibl: Do you have any estimate of how much oblique incidence would change the amount of coupling? Because, as you said, at vertical incidence and presuming a constant magnetic field, you minimize the coupling between the fast and slow modes; but if you go to oblique incidence obviously it cannot be true, because the characteristic polarization changes rapidly.

Horowitz: I tried oblique angles but not on this profile. I tried it on some other profile, and I do get larger coupling coefficients.

4.2.1 D-REGION ELECTRON DENSITY DISTRIBUTIONS DEDUCED FROM THE REFLECTION OF LOW AND VLF RADIO WAVES

by

B.R. May

Radio and Space Research Station, Slough, England

Abstract

This paper gives results obtained at the Radio and Space Research Station, Slough, of the determination of the height distribution of electron density in the D region from observations of the reflection of low and very low frequency radio waves. The electron distributions shown were obtained using a "trial and error" process, in which a search was made for distributions of which the calculated reflection properties were in agreement with observations. The reflection properties of the distributions were calculated using the "full-wave integration" technique. The D-region electron density distribution, and the way in which it varies during the day, the year, the sunspot cycle, and during an eclipse and a "sudden ionospheric disturbance", is shown.

1. Introduction

The purpose of this paper is to describe studies made at the Radio and Space Research Station concerning the deduction of D-region electron density distributions from reflected low and very low frequency radio waves. These studies have resulted in a determination of the height variation of electron density in the D region and the way in which it varies during the day, the year, the sunspot cycle, and during a solar eclipse (Deeks 1965a) and a "sudden ionospheric disturbance" (May 1965) — Figs. 2 to 8.

The data used are ground-based observations of the strength and phase of waves reflected by the ionosphere at distances up to about 1000 km. and at frequencies ranging from 16 to 200 kc/s. The observations were mainly made at Cambridge during the years 1948 and 1949 (sunspot maximum) and 1953 and 1954 (sunspot minimum). At 16 kc/s. it was found that there were only slight variations from day to day in the characteristics of the reflected wave, but that there was a considerable variation at 70 kc/s. and higher frequencies. The electron distributions in Figs. 2 to 6 have been deduced from the "average" behavior of the reflected waves, but it is nevertheless believed that the major features in the deduced distributions are necessary to obtain agreement between the observed and calculated reflection properties. Actual records of phase and amplitude were used to deduce the electron density distributions shown in Figs. 7 and 8 during a "sudden ionospheric disturbance" that occurred on 7 October, 1948 (May 1965).

It does not appear to be possible to deduce the electron density distributions directly from the observed data. A "trial and error" process is therefore used in which a search is made for an electron density distribution whose calculated reflection properties are in agreement with observations, these properties being calculated with the aid of a "full-wave" integration technique (Pitteway 1965).

Before the reflection properties of an assumed electron density distribution can be calculated, the height variation distribution of collision frequency of electrons with air molecules must be postulated. The precise way in which the collision frequency in the D region should be taken into account in the "full-wave" theory is complicated, but for the range of radio frequencies under consideration here an "effective" frequency ν_{eff} can be used without excessive error (Deeks 1965b). Independent measurements of the collision frequency by rocket and radio techniques are in good agreement and also indicate that there is negligible day-to-day variation. The height distribution of ν_{eff} used in most of this work is shown in Fig. 1. However, Piggott and Thrane (1965) have shown that during the summer the D-region collision frequency is increased by 60 per cent, and this was taken into account when the appropriate electron density distribution was deduced.

2. The "Full-wave" Integration Technique

This section is devoted to a brief description of the "full-wave" integration technique. It has previously been described in detail by Pitteway (1965).

a) The Integration Procedure

The electric and magnetic wavefields that exist in the D region, with an assumed height distribution of electron density N and collision frequency ν for plane waves, can be found by integrating on a computer a set of 4 first-order linear differential equations. The integration can be carried out for waves at any angle of incidence and azimuth with respect to the magnetic field. Well above the main reflection level at which $X \doteqdot Y$, the upgoing ordinary and extraordinary waves are chosen as initial solutions for the integration, which is then continued downwards to a level where N is effectively zero. The extraordinary or "evanescent" wave increases rapidly in amplitude with decreasing height and is usually the dominant solution, while the ordinary or "travelling" wave increases only slowly in amplitude and gives rise to the "whistler" wave high above the ionosphere. In the literature, the former solution has been called the non-penetrating mode (n) and the latter the penetrating mode (p). At the bottom of the ionosphere each solution is split into up- and downgoing waves, from which can be calculated the reflection coefficients R_n and R_p, their polarizations, and the phase difference between chosen components of the up- and downgoing waves. The two modes can also be combined to give the conventional reflection and conversion coefficients $_{\parallel}R_{\parallel}$ and $_{\parallel}R_{\perp}$ (defined in Section 3 (a)) and the associated phase differences $_{\parallel}\theta_{\parallel}$ and $_{\parallel}\theta_{\perp}$ between the up- and downgoing waves at any chosen height h (see Section 3 (b)).

b) Collision Frequencies

In the D region the energy of the incident wave is dissipated mainly by collisions of the electrons with the air molecules. The simple "full-wave" integration procedure is based on the Appleton-Hartree theory, which assumes that the collision frequency of electrons is independent of their velocity. However, laboratory experiments have shown that the collision frequency for mono-energetic electrons is proportional to the electron velocity. This observation implies that the actual collision frequency to be inserted in the Appleton-Hartree formulae is a complicated function of ν_m and the radio frequency employed. Sen and Wyller (1960) have shown, though, that an effective collision frequency ν_{eff} which is often simply related to ν_m(Fig. 1) can be used for a certain range of radio frequencies, and Deeks (1956b) has demonstrated that the use of an "effective" collision frequency gives calculated values of reflection parameters in acceptable agreement with those obtained using the more vigorous "generalized" treatment.

All of the electron density distributions in this paper have been deduced using the "non-generalized" full-wave theory with the height distribution of ν_{eff} shown in Fig. 1, with the exception of the summer distribution in Fig. 3 for which the collision frequencies were increased by 60 per cent (Piggott and Thrane 1965).

3. The Experimental Data

This section is devoted to an outline of the experimental data from which the electron density distributions in Figs. 2 to 8 were deduced, using full-wave techniques. (Deeks 1965a, May 1965).

a) Reflection Coefficients and Phases of Reflected Waves

An l.f. or v.l.f. radio wave incident upon the ionosphere from a commercial transmitter aerial is usually linearly polarized with the electric vector in the plane of incidence. The resultant downcoming wave is, in general, elliptically polarized, and two parameters (the reflection coefficient ${}_{\parallel}R_{\parallel}$ and the conversion coefficient ${}_{\parallel}R_{\perp}$) are used to measure its strength. These coefficients relate the amplitude of the electric field in the upgoing wave to that in the downgoing wave, and the subscripts $\parallel$ and $\perp$ refer to components parallel and perpendicular to the plane of incidence. Thus ${}_{\parallel}R_{\perp}$ represents the ratio of the perpendicular (sometimes called abnormal) electric field in the reflected wave to the parallel (normal) electric field in the incident wave.

The two components have associated phases, and the phase difference between ${}_{\parallel}R_{\parallel}$ and ${}_{\parallel}R_{\perp}$ along with their magnitudes determine the polarization of the downcoming wave. Experimental determinations of the polarization can be precise, but in general are not; if $0.5 < {}_{\parallel}R_{\parallel} < 2$, and the phase difference between the component is greater than 60°, the wave is considered to be circularly polarized or to be linearly polarized if the phase difference is less than 30°. If ${}_{\parallel}R_{\parallel} / {}_{\parallel}R_{\perp} < 0.5$ or > 2, the wave is considered to be linearly polarized irrespective of the phase difference between the components. At large distances from the transmitter the downcoming wave is nearly linearly polarized with the electric vector in the plane of incidence, so that it is ${}_{\parallel}R_{\parallel}$ that is usually measured. At shorter distances the wave is roughly circularly polarized, and although measurements have been made of both ${}_{\parallel}R_{\parallel}$ and ${}_{\parallel}R_{\perp}$, it is usually ${}_{\parallel}R_{\perp}$ only that is measured.

During the years 1948 and 1949 (sunspot maximum), numerous observations were made of the strength and phase of reflected waves in the frequency range 16 to 127 kc/s. at all times of the day and year, and over distances up to about 600 km. In particular, observations were made at Cambridge and Aberdeen on the 16 kc/s. waves from the G.B.R. Transmitter at Rugby, over distances of 90 and 535 km. respectively. These observations are summarized in a review paper by Bracewell et al.(1951). During the sunspot minimum years 1953 and 1954, Belrose made a further series of measurements at Cambridge at frequencies in the range 16 to 245 kc/s. (Belrose 1956, 1957).

These two groups of observations have been used to deduce the average D-region electron density distribution over southern England and the way in which it varies during the day, the year, the solar cycle, and during an eclipse (Deeks 1965a) and during a "typical" S.I.D. (May 1965). More detailed observations have also been used by May (1965) to determine the change in electron distributions during an S.I.D. on 7 October, 1948.

At this point it is appropriate to mention that the "full-wave" integration technique, used to calculate the reflection properties of a postulated electron density distribution, deals with plane waves. Now the waves emitted by a transmitter are spherical and thus the total field measured at the receiver should be represented by a system of plane waves incident from many directions — an "angular spectrum" of plane waves. However, it is not practicable to use this refinement when deducing electron distributions due to the large amount of computer time involved. This effect can partly be taken into account, though, if a "stationary phase" concept is used to simulate the changes in phase and amplitude that would be observed at a fixed distance — see Section 3 (b). The field strength measurements may also be complicated by the presence of waves that have undergone more than one reflection from the ionosphere. From a consideration of the magnitudes of the reflection and conversion coefficients involved, it appears that in general the contribution to the total field from multiply reflected waves would be small compared with the contribution from the once-reflected wave, and no account of the effect has been taken in this work. Changes in the height distribution of electrons over the distances involved and possible tilting of the ionosphere have also been ignored.

b) Reflection Heights and Change of Phase

In this section, consideration is given to the interpretation of the phase measurements of l.f. and v.l.f. waves and their relation to the results of the "full-wave" calculations.

The wave incident upon the ionosphere is reflected from a range of heights, but nevertheless the phase of a particular field component in the downcoming wave can be regarded as the result of a reflection at a "fictitious" mirror-like surface. The apparent height of reflection and its variations, instead of the phase, are often quoted in the literature, since the parameter can be more easily visualized and often behaves in a regular manner that is related to the variations in the structure of the ionosphere.

The full-wave theory employs infinite plane waves, and Piggott et al. (1965) have shown that the apparent height of reflection of such waves can be expressed in terms of the phase difference θ between the up- and downgoing waves of any particular chosen component. This apparent height of reflection can be expressed in several ways.

1) The upgoing and downgoing waves at an angle of incidence I are assumed to be plane infinite waves reflected by a horizontal surface over a plane earth. If θ_o and θ_h are the phase differences between the up- and downgoing waves at the ground and height h, respectively, then

$$. \; . \; . \; . \; \theta_h = \theta_o + \frac{4 \pi h \cos I}{\lambda} \qquad (1)$$

where λ is the wavelength of the waves.

Piggott et al. have assumed that a π phase change takes place on reflection at a height h, and thus expression (1) can be written

$$. \; . \; . \; . \; \theta_o = 2 \pi (M + ½) - \frac{4 \pi h \cos I}{\lambda} \qquad (2)$$

where M is an integer.

A value of θ_o inserted into (2) leads to a series of "phase heights h_1 separated by a vertical distance $\frac{\lambda}{2}$ sec. I. The most suitable values of h_1 are selected with the help of other criteria.

From equation (2) it can be seen that

$$\frac{\partial \theta_o}{\partial I} = \frac{4 \pi h \sin I}{\lambda} \qquad (3)$$

which can be used to define the "triangulation" height h_2 by examining how θ_o varies with I for a fixed frequency.

Similarly $\frac{\partial \theta_o}{\partial f} = \frac{4 \pi h \cos I}{c}$

is used to define a "virtual" height h_3, which depends on how θ_o varies with the wave frequency for a fixed value of I.

In the work of Piggott et al. (1965) and Deeks (1965a), the calculations were carried out mainly at two fixed angles of incidence of 30^o and 75^o, to represent steep and oblique incidence propagation, and the reflection heights and phases were calculated using the above expressions.

In reality, however, the observations are not made at fixed angles of incidence but at fixed distances, and a direct use of the above equations will not always result in the correct calculated phase at a fixed distance. It is necessary, in more precise determinations of electron distributions, to introduce the relationship between the angle of incidence, the triangulation height of reflection and the distance d over which the wave is propagated. This relationship, which embodies the "stationary phase" concept has been outlined by Piggott et al. (1965) and described in greater detail by Bain (1965).

If the wave were reflected at a mirror-like surface at the triangulation height h_2, then

$$h_2 = \frac{d}{2} \cot I$$

Substituting this value of h_2 into expression (3) gives

$$\frac{\partial \theta_o}{\partial I} = \frac{2\pi d \cos I}{\lambda} \tag{4}$$

A more useful form of this expression can now be obtained. For any height h it follows from expression (1) that

$$\frac{\partial \theta_h}{\partial I} = \frac{\partial \theta_o}{\partial I} - \frac{4\pi h \sin I}{\lambda}, \tag{5}$$

and combining (4) and (5) gives

$$d = \frac{\lambda}{2\pi} \sec. I \cdot \frac{\partial \theta_h}{\partial I} + 2h \tan I, \tag{6}$$

the required relation between d and I.

This latter expression can be applied directly to the results of "full-wave" calculations (see Section 2) to find the angle of incidence appropriate to a given path distance, and hence the correct value of θ_o, though its use involves more computation than the straightforward use of expressions 2 and 3.

In the work by Deeks (1965a), which has resulted in the electron distributions in Figs. 2 to 5, the reflection heights were calculated from components of the non-penetrating mode since, in general, this mode is the dominant one (see Section 2(a)). This is true for steep incidence where, for a particular electron density distribution, calculated heights from the phase of the non-penetrating mode and the phases of $_{\parallel}R_{\perp}$ or $_{\parallel}R_{\parallel}$ are in good agreement, but not so at oblique incidence where the penetrating mode becomes comparable to the non-penetrating mode.

When the electron density distributions for S.I.D. on 7 October, 1948 were deduced (Figs. 7 and 8), the calculated phases of $_{\parallel}R_{\perp}$ and $_{\parallel}R_{\parallel}$ at fixed distances were used for comparison with the observations.

4. Results

This section is devoted to a brief description of the more important features of the average electron density distributions in Figs. 2 to 6.

Fig. 2 – the diurnal variation of D-region electron density at March equinox, sunspot minimum at middle latitudes. It can be seen that during the night the electron density shows a marked "ledge" at about 90 km. with very few electrons below this height. Before ground sunrise, however, the density in the 60 to 70 km. height range increases rapidly, due to the

ease of detachment of electrons from the negative ions which are thought to exist in this region, and thereafter remains almost unchanged during the rest of the day. At greater heights the electron density shows a more gradual dependence on solar-zenith angle, which would be expected from an ionization process.

Fig. 3 — the seasonal variation. In making the calculations appropriate to the summer noon electron distribution, Deeks used the collision frequencies in Fig. 1 increased by 60 per cent (Piggott and Thrane 1965). It can be seen that the electron densities above 70 km. vary in a regular way with the noon solar zenith angle for each season. The variation of the electron densities below 70 km. is unexplained.

Fig. 4 — the solar-cycle variation. Above about 70 km. it is noticeable that the electron density is directly associated with solar activity, which strengthens the belief that this part of the D region is mainly under solar control. However, below 70 km. the density behaves in the opposite manner, which is in agreement with the present-day theory that the ionization in this region is produced by galactic cosmic radiation, whose intensity is observed to be greater at solar minimum than solar maximum.

Fig. 5 — the solar eclipse. The figures on the curve are the percentage obscuration of the sun's disc. Below 70 km. the electron density remains unchanged up to an 80 per cent obscuration of the sun's disc — this again indicates that a detachment process with a low energy threshold is important in this region. Above 70 km. the electron density again shows a more gradual dependence on the strength of the sun's radiation.

Fig. 6 — the S.I.D. Calculations based on these electron distributions show a decrease in reflection height of about 6 km. at 16 kc/s. steep incidence — thus this S.I.D. would be caused by a flare of about class 1 to 2 (Bracewell and Straker 1949). The effect of the S.I.D. is to increase the electron density at a wide range of heights in the D region.

5. The S.I.D. on 7 October, 1948

The final section of this paper is devoted to the electron density distributions deduced for an S.I.D. that occurred on 7 October, 1948 (Figs. 7 and 8). These are discussed in greater detail since they result from a use of actual data rather than the "average" data used to deduce the electron distribution in Figs. 2 to 6 and because they indicate the frequencies and distance at which useful observations can be made, and also the accuracy with which the electron density can be determined from such observations.

The data that were used to deduce these electron distributions are the variation of the apparent reflection height and $_{\parallel}R_{\perp}$ measured on 16 and 70 kc/s. waves propagated over a distance of 90 and 100 km. respectively — these data are shown in Figs. 9 and 10, reproduced from Bracewell et al. (1951). Although not specifically stated in the text of that paper, the plot of change of h_1 actually appears to be h_1 during the S.I.D. relative to h_1 on an undisturbed day, since there is no indication of a diurnal variation of h_1. To avoid confusion this will be referred to as Δh_1.

In the following table are given the times appropriate to the electron distributions in Figs. 7 and 8, deduced from the data in Figs. 9 and 10. The numbers in the table correspond to the numbers on the curves in the figures.

Time U.T.	Electron Distribution number	Comments
15.40	1	Pre-disturbance
15.55	2	
15.57	3	
25.59	4	
		Maximum phase
16.05	5	
16.10	6	
16.16	7	
16.35	8	
17.00	9	Post-disturbance

Figs. 9 and 10 also show the calculated variation of ${}_{\parallel}R_{\perp}$ and on 16 and 70 kc/s., at distances of 90 and 100 km. respectively, using the electron distributions tabulated above and the height distribution of effective collision frequency in Fig. 1. There is good agreement between the observed and calculated values of ${}_{\parallel}R_{\perp}$ and Δh_1, the greatest differences being a factor 2 in ${}_{\parallel}R_{\perp}$ and 2 km. in Δh_1, both at 70 kc/s.

Fig. 11 shows the time-variation of electron density at heights of 65, 70, 75, and 80 km. during this S.I.D. The dashed lines are the estimated variation of electron density that would have occurred in the absence of the S.I.D. It is noticeable that the variation of ${}_{\parallel}R_{\perp}$ during the S.I.D. seem to be related to the variation of electron density at particular height ranges which depend on the frequency. Thus ${}_{\parallel}R_{\perp}$ at 16 kc/s. has a similar time-variation to the electron density at 65 km., while ${}_{\parallel}R_{\perp}$ at 70 kc/s. shows a close relation to the variation of electron density at 75 or 80 km.

A study of Figs. 7, 8, 9, and 10 indicates that a change of more than about 30 per cent in the electron density in the height range from about 60 to 85 km. would make the agreement between observed and calculated values of ${}_{\parallel}R_{\perp}$ and reflection heights unacceptable. This is in good agreement with the value of 20 per cent quoted by Deeks (1965a) from a thorough study of the reflection properties of the noon, equinox, sunspot minimum electron density distribution. These conclusions indicate that simultaneous phase and amplitude measurements at steep incidence on frequencies in the neighbourhood of 16 and 70 kc/s. can be useful in deducing the electron density distributions at heights from about 60 to 85 km. In addition since the behavior of l.f. and v.l.f. waves at oblique incidence is entirely different from that at steep incidence, simultaneous oblique incidence measurements of phase and amplitude at these two frequencies would undoubtedly provide useful supplementary information.

6. Acknowledgement

The work described was carried out at the Radio and Space Research Station of the Science Research Council and is published with the permission of the Director.

REFERENCES

Bain, W.C. Internal Memo., Radio and Space Res. Stn. 251 (The synthesis of a ground interference pattern on 16 kc/s. from full-wave calculations). 1965.

Belrose, J.S. Ph.D. Thesis Cambridge University. Some investigations of the lower ionosphere. 1st copy 1956. Revised copy 1957. 1956, 1957.

Bracewell, R.N. and T.W. Straker. Mon. Not. Roy. Astron. Soc. 109, 28, 1949.

Bracewell, R.N., Budden, K.G., Ratcliffe, J.A., Straker, T.W. and K. Weekes. Proc. Inst. Elect. Engrs. 98, III, 221-236. 1951.

Deeks, D.G. (In publication) Phil. Trans. Roy. Soc. (I.M. 219 — D-region electron distributions in Middle latitudes deduced from the reflection of long radio waves). 1965a.

Deeks, D.G. (In publication) (I.M. 244 — Generalised full-wave theory for energy-dependent collision frequency). 1965b.

May, B.R. (In publication) J.A.T.P. (I.M. 230 — The behaviour of the D-region at mid-latitudes during a sudden ionospheric disturbance). 1965.

Piggott, R.W. and E.V. Thrane. To be published in J.A.T.P. (I.M. 205 — The collision frequency in the E and D regions of the ionosphere). 1965.

Piggott, R.W., Pitteway, M.L.V. and E.V. Thrane. Phil. Trans. Roy. Soc. A, 257, 243. 1965.

Pitteway, M.L.V. Phil. Trans. Roy. Soc. A, 257, 219. 1965.

Sen, H.K. and A.A. Wyller. J. Geophys. Res. 65, 3931. 1960.

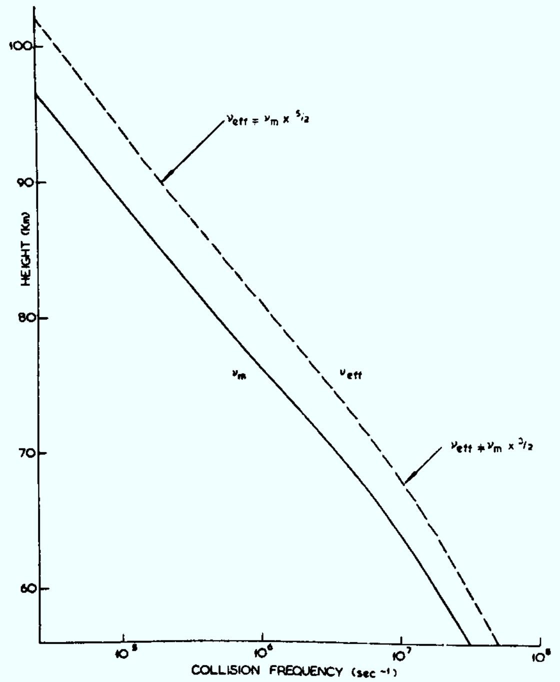

Fig. 1. The height variation of the collision frequency of monoenergetic electrons of energy kT, ν_m, (full curve), and of the effective Appleton-Hartree collision frequency, ν_{eff}, at low frequencies (broken curve). (After Deeks, 1965a).

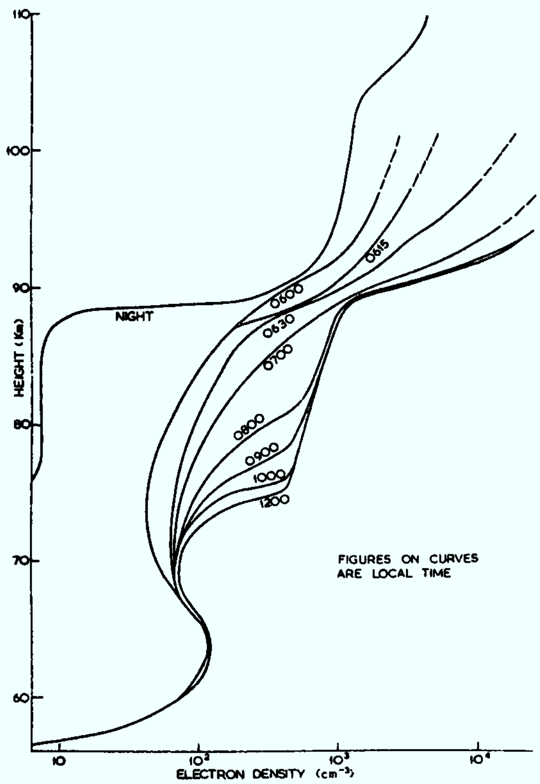

Fig. 2. Diurnal variation of electron densities at March equinox, sunspot minimum. (After Deeks, 1965a).

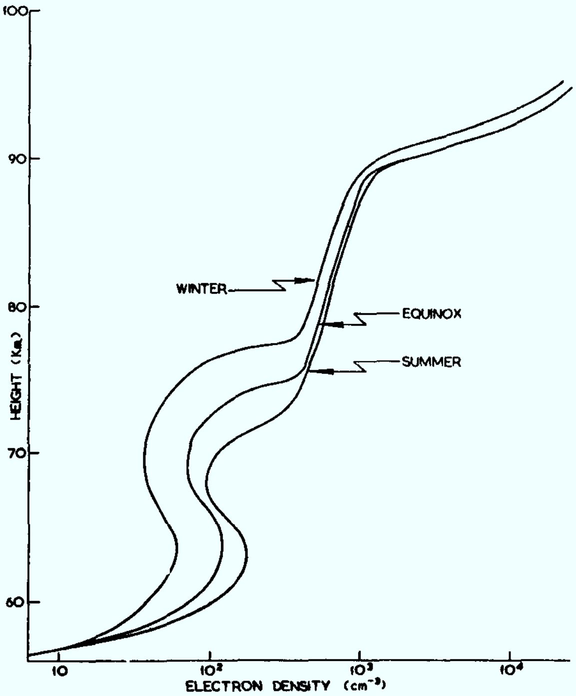

Fig. 3. Seasonal variations of electron densities at noon, sunspot minimum. (After Deeks, 1965a).

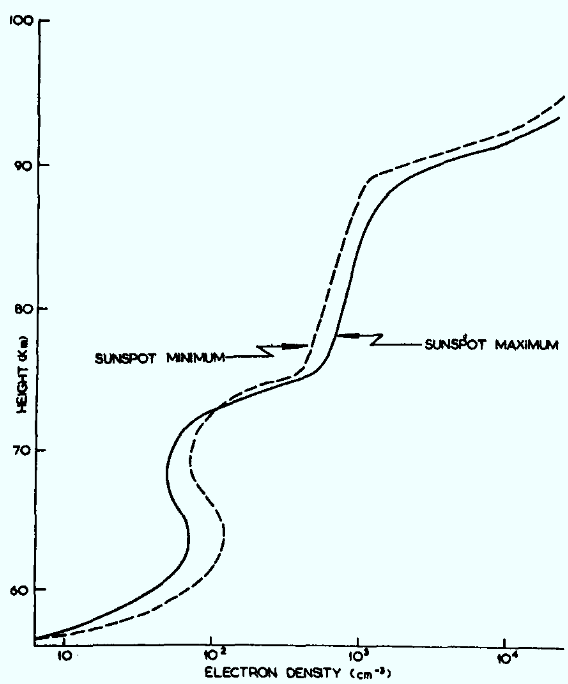

Fig. 4. Sunspot cycle variation of electron density at noon, March equinox. (After Deeks, 1965a).

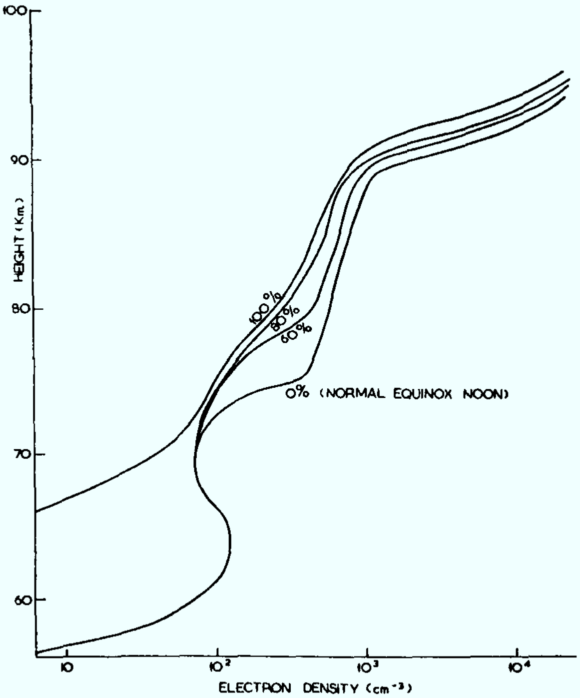

Fig. 5. Electron distributions during a solar eclipse, with percentages of occultation of the sun marked. (After Deeks, 1965a).

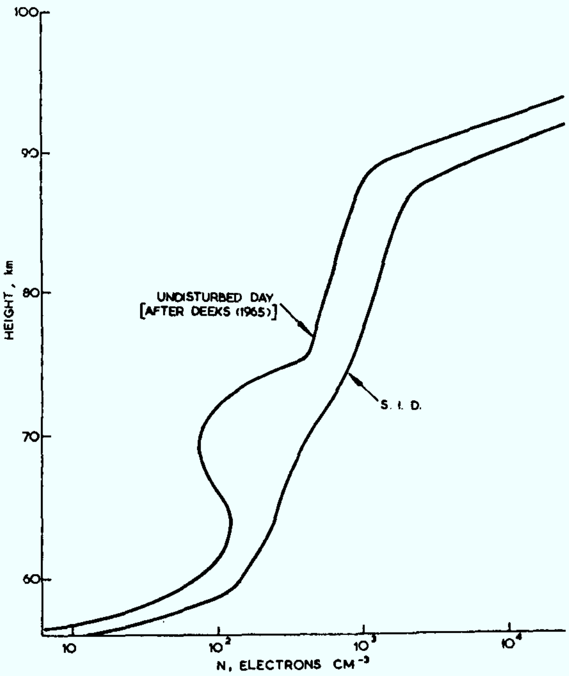

Fig. 6. The change in the height distribution of electron density in the D-region during an "average" sudden ionospheric disturbance.

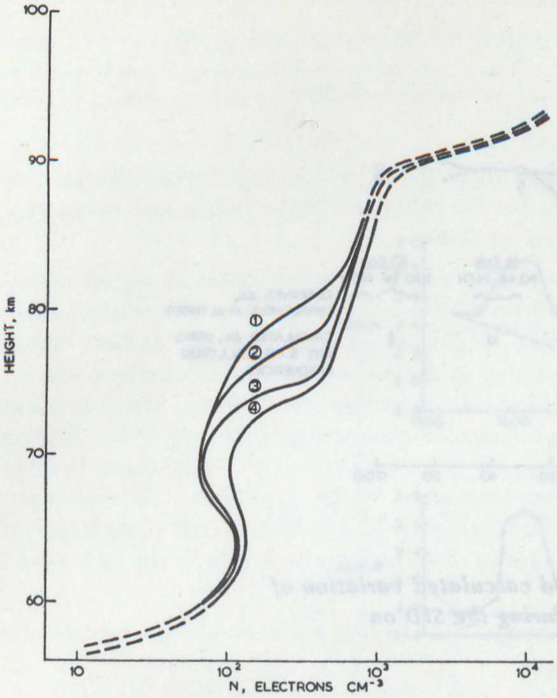

Fig. 7. The variation of height distribution of electron density during the onset stage of the SID on 7 October, 1948.

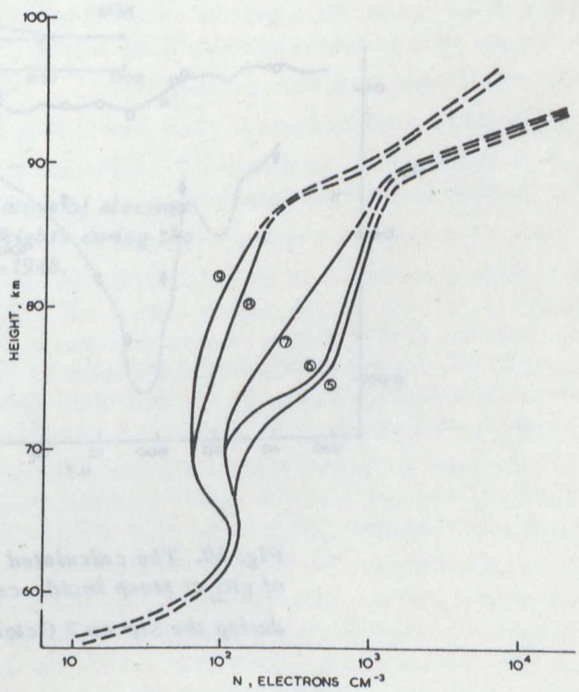

Fig. 8. The variation of height distribution of electron density during the recovery stage of the SID on 7 October, 1948.

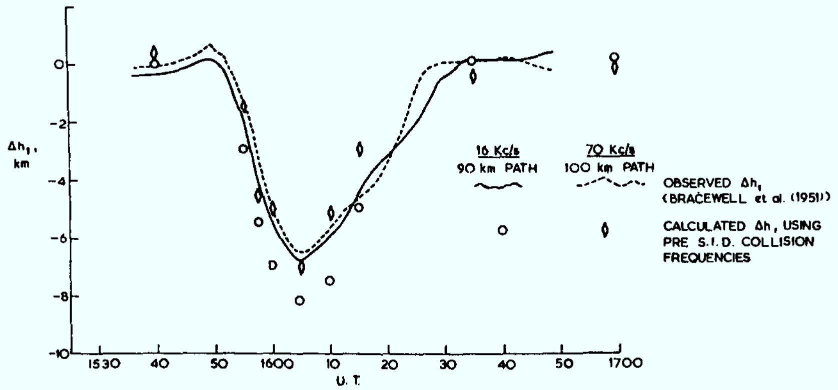

Fig. 9. The observed and calculated variation of Δh_1 at 16 and 70 Kc/s during the SID on 7 October, 1948.

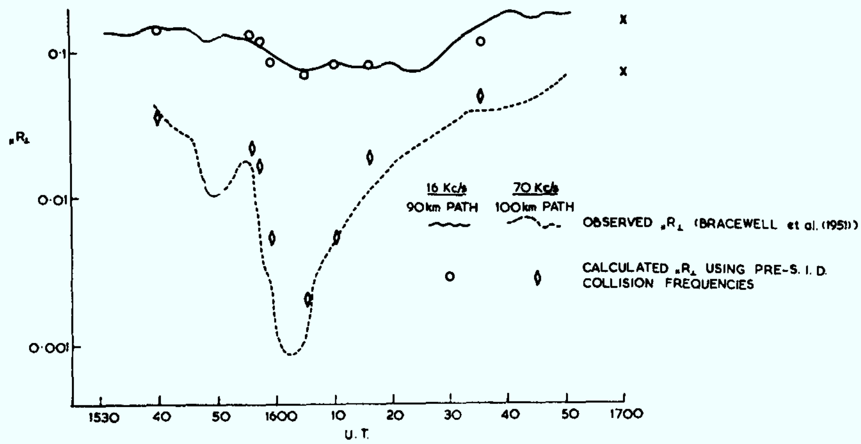

Fig. 10. The calculated and observed variation of $_{\|}R_{\perp}$ at steep incidence, at 16 and 70 Kc/s during the SID on 7 October, 1948.

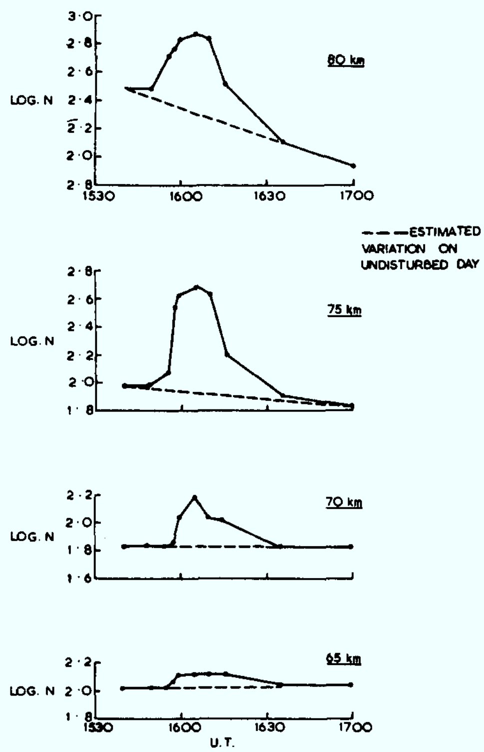

Fig. 11. The variation of electron density at fixed heights during the SID on 7 October, 1948.

Discussion on Paper 4.2.1 presented by B.R. May

Belrose: In your calculations for the normal collision frequency profile and an increased collision frequency profile, you have done detailed calculations only for the change of phase height and not to describe the change of amplitude. Could you comment further on this?

May: This SID had one peculiarity, that at the beginning there was a marked decrease in signal strength at 70 kc/s. and a small decrease in signal strength at 16 kc/s. For an ordinary flare you would associate this with a decrease in phase height; if anything the phase height in this case went up. At first sight it looked as though there was a small sub-flare at the beginning of the main one. It didn't behave like a normal flare, so what I did was to think of the simplest explanation of this phenomenon, which I hasten to add I have never seen in any other SID. I came to the conclusion that at the beginning of the SID the collision frequency had increased by a factor of about 2 to 2½ at all heights, and this increase in collision frequency had died away within a matter of a few minutes; thereafter, for the rest of the SID there was no need to assume that there was an increase in collision frequency. However, this is only a sketchy result and is subject to considerable doubt, since it is not generally observed. In fact, this is the only time I have seen it on a record.

Swider: I wondered about this nighttime profile in the figure. What is this little trickle of electrons below 70 km. due to?

May: I admit that the nighttime profile is suspect. Our knowledge of propagation during the nighttime is sketchy because, as we have seen, at 16 kc. and 70 kc. and higher frequencies the nighttime propagation is irregular – extremely irregular – so I think the concept of average behavior during the nighttime is pushing it a long way, and it would be dangerous to attach great importance to the nighttime profiles. The most you could say is that, from a consideration of the reflection heights of quite a wide range of frequencies from 16 kc/s. upwards, and the fact that during the nighttime there isn't a great change of signal strength with frequency, there must be a marked ledge of ionization somewhere, about 90 km., but what is above that and what is below, I wouldn't like to say.

Belrose: Has Deeks' work been published yet?

May: It should be published now in Phil. Trans. Roy. Soc.

Belrose: I would like to comment that his nighttime profiles seem to be even more suspect if you look at sunspot minimum and sunspot maximum.

May: Yes. They have some rather peculiar features.

Sales: I think also suspect is the height range for daytime models above 80 km. where we know the variability of xray flux would play an important role. I think he also would be relatively incapable of making, from this kind of data, a reasonable guess at the daytime density at those heights. He can make some estimate of those densities at those heights at early times because of sunrise effects when these signals are up there, but during the daytime, when xray flux plays a dominant role in that region, I think the variability would be large and certainly I don't think necessarily represented by these average pictures.

May: Yes, I entirely agree. I think that these profiles are useful as a starting point for having a look at what the D region looks like, but I don't think one would, in all fairness, base too much importance on them. They are important qualitatively rather than quantitatively, because they do indicate the way the D-region ionization must change. The absolute density is obviously suspect.

Belrose: I think Mr. May made the point that these were average profiles. We have also made the point that it is difficult, with variable data, to know how to average the data. This is especially true in winter months. You can have a lump average of the data and you can get an electron density height profile by partial reflections, or by long-wave work, but can you find an individual day which in fact looks like the average? I think this is the problem.

Gossard: I would like to remark that the bulge of approximately 100 electrons per cc. down around 65 km. appears to give too much attenuation on long paths. One has to cut this back to about 30 electrons per cc. before the long path attenuation coefficients begin to agree with those.

May: What latitudes are you talking about? The latitude is a consideration.

Gossard: I was speaking fairly generally for most VLF links. A specific path that we have considered is from NPM in Hawaii to San Diego. I seem to remember that one gets about 5 db attenuation per megameter from Deeks' profile, which is a little high for most VLF paths.

Bibl: I would like to show the striking similarity between the $F_1 - E$ layer development and the $C - D$ layer development in the morning. I have a figure showing the historical development. (Fig. D1).

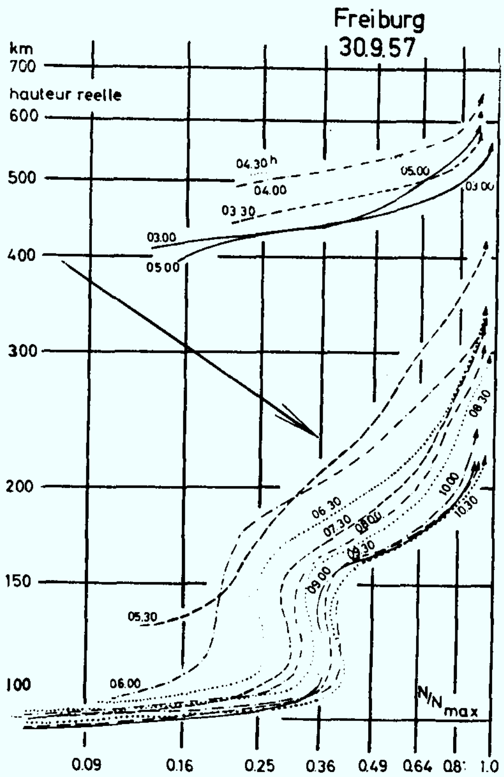

Fig. D1. Morning development in the shape of ionospheric layers using A. Paul's correction in usual true height analysis.

This was on a night that the ionization disappeared almost completely in the upper portion, and we see the development of what I call the F_1 and E layers in the morning. Certainly the electron density is much higher than what you are talking about; however, the change in shape is the point that I want to bring out. We have the nighttime behavior here at 400 km., and in the morning we get this first impact at 0530 which could be a function of the zenith angle of solar ionization, and then we get this building up of the split between what we call the E layer and the F_2 layer. This occurs tremendously fast between 0530 and 0600.

Hayes: Dr. Gossard talked about the Hawaii – San Diego path and I would like to remind us again about Dr. Crain's point concerning the great variability of the cosmic ray production. Between a geomagnetic latitude of 20° and 60° there is about a factor of ten in production and I think that at Hawaii this might cause an appreciable electron density in the C layer.

Gossard: My point was that this value was large for almost any path throughout the whole VLF frequency range at any latitude.

Pfister: I would like to point out that the 100 electron per cc. bulge is the C layer and that its existence depends only on the 16 kc. data.

May: Yes, it strongly depends on that.

Pfister: I wonder whether negative ions might not play a role in the propagation?

May: I do not think there would be any observable effect from ions at frequencies above about 2 kc/s.

4.2.2 THE DETERMINATION OF THE REFLECTION CHARACTERISTICS OF THE LOWER IONOSPHERE USING VLF WAVES

by

H. Volland

Astronomical Institutes, University of Bonn, Germany

Abstract

The first part reviews a method of full wave theory for the calculation of reflection and transmission matrices of plane waves in a horizontally stratified medium, using the scattering matrix and the matrizant solution. Calculations of the reflection coefficients show the influence of the upper part of the ionosphere on the reflection.

The second part deals with methods to determine, by experiment, the propagation characteristics of the ionosphere using VLF waves. The behavior of the ionosphere is approximated by a reflection parameter a and a virtual height h. Plotting amplitude and phase of the propagation function versus a and h allows the determination of a and h from field strength measurements of CW transmitters. Statistical methods for the measurement of atmospherics are described, from which phase and amplitude of the propagation function, depending on frequency and distance, can be derived.

1. Introduction

Two groups of people are interested in the VLF propagation. Engineers dealing with communication systems want to know the influence of the propagation space on the propagation of the waves. They search for a function F (f,ρ,t) which gives the time-dependent magnitude and phase of the electric (or magnetic) field strength of a transmitter of frequency f at a distance ρ from the receiver. The function F is a complicated one, which apart from the variables ρ, f and the time t depends on geographical co-ordinates of the transmitter and the receiver and some other parameters. Such function can be found by experiment. In fact, within the first decades of our century, research work of this kind has been done extensively (Austin 1915).

Ionospheric research workers like to learn something about the D layer of the ionosphere from measurements of VLF propagation. They want to find relations between F and some parameters of the ionosphere like electron density N_e and collision number ν depending on height, time, and local situation. For this reason they have to calculate the behavior of VLF waves within an appropriate model of the atmospheric wave guide, and they must select that model which fits best with the experimental data. Necessarily, such model must be idealized to a great extent, and a number of assumptions have to be made.

2. Results of Model Calculations

The simplest model of an atmospheric wave guide is a plane or curved wave guide with two homogeneous walls, the earth's surface with constant conductivity σ_e and, at the height h, a sharply bounded homogeneous ionosphere of conductivity σ_i. A transmitter aerial will be replaced by a dipole which is situated within the wave guide. The radiation of the dipole within such wave guide can be described either by a ray optic or by a wave optic picture. The ray optic picture is the more customary one. The radiated energy propagates like rays which are considered as independent from each other. The rays are reflected at the walls, and the field strength at the receiver aerial is the sum of the interfering rays which have arrived on different ray paths. A thorough calculation of this problem shows that the reflection of the spherical waves at the sharply bounded ionosphere can be described by Fresnel's reflection coefficients, which is rigorously true only for plane waves.

The next improvement of the model is to replace the homogeneous ionosphere by an inhomogeneous, horizontally stratified ionosphere. We again treat the rays independent from each other. We calculate the reflection behavior of the inhomogeneous ionosphere for plane waves, and then introduce the calculated reflection coefficients into the ray optic sum of the wave guide, which originally hold only for homogeneous walls. Here a new problem arises. The lower boundary of the inhomogeneous ionosphere is indetermined. We have to introduce a virtual height h which can be calculated from the phase ϕ of the reflection coefficient (Budden 1961).

$$h = z_I - \frac{1}{2k} \frac{\partial \Phi}{\partial (\cos \theta)} \Bigg|_{\theta = \theta_o} \tag{1}$$

The reflection coefficient of the ionosphere is related to an arbitrary height z_I. The virtual height h is defined as that height where the ray would be reflected after travelling a straight path at angle of incidence θ_o. The inhomogeneous ionosphere with reflection coefficient.

$$\underline{R} = | R | \exp (j\Phi) \tag{2}$$

behaves like a homogeneous one in the height h and with the reflection coefficient

$$R = - | R | . \tag{3}$$

The earth's magnetic field makes the ionosphere anisotropic. The reflection coefficient R must be replaced by a reflection matrix

$$\underline{R} = \begin{pmatrix} {}_{||}R_{||} & {}_{||}R_{\perp} \\ {}_{\perp}R_{||} & {}_{\perp}R_{\perp} \end{pmatrix} \tag{4}$$

where ${}_{||}R_{||}$ and ${}_{\perp}R_{\perp}$ are the reflection coefficients of TM and TE waves and ${}_{\perp}R_{||}$ and ${}_{||}R_{\perp}$ are conversion coefficents which convert TM waves into TE waves and vice versa. The reflection matrix (4) is a submatrix of the scattering matrix of the ionosphere (Volland 1962).

$$\underline{S} = \begin{pmatrix} \underline{R}_I & \underline{D}_{II} \\ \underline{D}_I & \underline{R}_{II} \end{pmatrix} \tag{5}$$

where $\underline{R}_I$ and $\underline{R}_{II}$ are the reflection matrices below (I) and above (II) the ionospheric layer. $\underline{D}_I$ and $\underline{D}_{II}$ are the transmission matrices below and above.

For the calculation of $\underline{S}$, one starts from the Maxwell equations, which in the specific case of plane waves propagating through a horizontally stratified medium can be written in matrix form

$$\frac{d\underline{e}}{dz} = -\, jk\, \underline{K}(z)\, \underline{e}. \tag{5a}$$

Here the matrix

$$\underline{e} = \begin{pmatrix} E_x \\ H_y \\ H_x \\ -E_y \end{pmatrix}$$

contains the horizontal components of the electric and magnetic field strength. k is the wave number in vacuum. The matrix $\underline{K}$ contains the height-dependent parameters of the ionosphere, like electron density and collision number. It also depends on the earth's magnetic field and on the angle of incidence θ.

The solution of (5a) is the matrizant T_I^{II}. It connects the field strength components in the height z_I with the field strength components in the height z_{II} (Volland 1962):

$$\underline{e}\,(z_I) = \underline{T}_I^{II}\underline{e}(z_{II}).$$

Since T_I^{II} obeys the product rule:

$$T_I^{II} = \prod_{\nu=1}^{n} T_\nu^{\nu+1} \qquad \begin{matrix}(z_I = z_1\ ; \\ z_{II} = z_n)\end{matrix} \tag{5b}$$

the whole layer ($z_I \leqq z \leqq z_{II}$) can be divided into an arbitrary number of sublayers of thickness $\Delta z_\nu = z_{\nu+1} - z_\nu$. These sublayers must not be homogeneous. (5b) therefore does not contain any approximation. But if one takes the sublayers as homogeneous ones, then the matrizant of a sublayer becomes particularly simple:

$$T_\nu^{\nu+1} = \sum_{m=o}^{\infty} \frac{(jk\,\underline{K}_\nu\,\Delta z_\nu)^m}{m!} = \exp\,(jk\underline{K}_\nu\Delta z_\nu)$$

and can be calculated very quickly with help of a large digital computer. Here the knowledge of the eigen values of $\underline{K}_\nu$ is not necessary, and $T_\nu^{\nu+1}$ behaves normally even at points of critical coupling or at reflection points. Since in an actual calculation the whole layer is built up by repeatedly adding one sublayer to the others, one can always print out the intermediate results and therefore obtain the field strength components at any height z_ν compared with the values at z_I (or z_{II}) if one starts the calculations at z_I (or z_{II}).

The transfer from the electric field strength components into the characteristic waves can be arranged in any height z_ν with help of the transformation matrix $\underline{Q}$ which is defined by

$$\underline{e} = \underline{Q}\, \underline{c}.$$

Here

$$\underline{c} = \begin{pmatrix} A_1 \\ A_2 \\ B_1 \\ B_2 \end{pmatrix} = \begin{pmatrix} \underline{a} \\ \underline{b} \end{pmatrix}$$

is composed of the two upgoing waves $A_1\ A_2$ and the two downgoing waves $B_1\ B_2$. The calculation of the elements of $\underline{Q}$ is a well-known algebraic problem. Now $\underline{Q}$ contains the eigen values of the characteristic waves, the solutions of the Booker quartic. The elements of $\underline{Q}$ describe the relations between the single field strength components of the characteristic waves, among these the state of polarization.

The connection between the four characteristic waves below and above the layer is given by

$$\begin{pmatrix} \underline{a}_I \\ \underline{b}_I \end{pmatrix} = \underline{c}_I = \underline{Q}_I^{-1}\, \underline{T}_I^{II}\, \underline{Q}_{II}\, \underline{c}_{II} = \underline{P} \begin{pmatrix} \underline{a}_{II} \\ \underline{b}_{II} \end{pmatrix}$$

where we write for convenience

$$\underline{P} = \begin{pmatrix} P_1 & P_2 \\ P_3 & P_4 \end{pmatrix} = \underline{Q}_I^{-1}\, \underline{T}_I^{II}\, \underline{Q}_{II}.$$

Because of the definition of the scattering matrix (5):

$$\begin{pmatrix} \underline{b}_I \\ \underline{a}_{II} \end{pmatrix} = \underline{S} \begin{pmatrix} \underline{a}_I \\ \underline{b}_{II} \end{pmatrix}$$

a simple algebraic rearrangement gives the relations between $\underline{P}$ and $\underline{S}$:

$$\underline{R}_I = \underline{P}_3 \underline{P}_1^{-1} \quad ; \quad \underline{D}_I = \underline{P}_1^{-1}$$

$$\underline{R}_{II} = -\underline{P}_1^{-1} \underline{P}_2 \quad ; \quad \underline{D}_{II} = \underline{P}_4 - \underline{P}_3 \underline{P}_1^{-1}\, \underline{P}_2.$$

If vacuum exists below the layer, then $\underline{Q}_I$ becomes

$$\underline{Q}_I = \underline{Q}_o = \begin{pmatrix} \cos\theta\, \underline{I} & -\cos\theta\, \underline{I} \\ \underline{I} & \underline{I} \end{pmatrix}.$$

Here $\underline{I}$ is a 2 x 2 unit matrix and θ is the angle of incidence. Now $\underline{a}_I$ and $\underline{b}_I$ are the upgoing and downgoing components of the TM and the TE waves, and $\underline{R}_I$ is identical with (4).

By an appropriate normalizing of the matrix $\underline{Q}$, the values

$$\frac{1}{2} A_i^2 \text{ and } \frac{1}{2} B_i^2$$

give quantitatively the effective energy transported by the single characteristic waves A_i or B_i (Volland 1966). So the matrices $\underline{T}$, $\underline{Q}$, or $\underline{S}$ provide full information about the behavior of plane waves in the layer. They serve as building stones for a composition of several layers, as can be seen in the following paragraphs.

In doing a real calculation of $\underline{S}$ one is always forced to limit the thickness of the ionospheric layer and to make a rather arbitrary assumption about the upper part of the layer. Usually one divides the whole layer into two parts. In the lower part (layer I in Fig. 1) the electron density N_e and the collision number ν are functions of height. The upper part (layer II) consists of a homogeneous layer with constant N_e and ν. Such a model gives correct reflection coefficients if the rather arbitrary upper part (layer II) has only a small influence on the reflection of the waves. This reaction can be described by the formula

$$\underline{R}_{total} = \underline{R}_I + \underline{D}_I \underline{R}_\infty (\underline{I} - \underline{R}_{II} \underline{R}_\infty)^{-1} \underline{D}_{II}. \tag{6}$$

Here $\underline{R}_I$, $\underline{R}_{II}$, $\underline{D}_I$, and $\underline{D}_{II}$ are the submatrices of the scattering matrix $\underline{S}$ of the isolated layer I. $\underline{R}_\infty$ is the reflection matrix from below of the homogeneous layer II. The reaction of layer II on $\underline{R}_{total}$ comes from the second term on the right in (6). If the transmission matrices $\underline{D}_I$ and $\underline{D}_{II}$ of layer I are small enough (the elements of which must be smaller than about 0.1 in magnitude), then the energy of the upgoing waves will be absorbed within the layer I, and layer II has no influence on the wave propagation.

For the results of calculations which now follow, a daytime model with an electron density profile and a collision number profile according to Fig. 1 has been used. The earth's magnetic field is vertical and of magnitude H_o = 0.5 Oersted, which approximates the situation in medium northern latitudes.

Fig. 2 shows the magnitude of the reflection coefficient of TM waves versus cos θ at different frequencies for the daytime model. The full lines have been calculated for layer I only and give the element $_{||}R_{||}$ of $\underline{R}_b$. The circles give values of the element $_{||}R_{||}$ of $\underline{R}_{total}$, layer I and II together. It shows the influence of the upper part of the model, which is rather small apart from steep incidence. In fact, at daytime the ionosphere above 90 km. does not essentially influence the reflection of VLF waves.

Fig. 3 shows the same for TE waves. We see that in the VLF region the magnitude of R can be approximated by a straight line up to about cos θ = 0.5. Since the ordinate of the plot has a logarithmic scale, this straight line is equivalent to the analytic function

$$|R| = \exp(-2 a \cos \theta) \tag{7}$$

where the empirical factor a depends on frequency, time, and earth's magnetic field. Now cos $\theta \leq$ 0.5 means distances of more than 250 km. from the transmitter at daytime. If we take into account only the ionospheric 1. and 2. hop waves, we can use the approximation (7) for distances greater than 500 km.

Fig. 4 gives the conversion coefficients ${}_{\|}R_{\perp}$ of the daytime model. Fig. 4 together with Fig. 2 show that the ratio $|{}_{\|}R_{\perp}/{}_{\|}R_{\|}|$ decreases with cos θ. At large distances from the transmitter we, therefore, can neglect ${}_{\|}R_{\perp}$ as a second order value.

Fig. 5 shows the phase of ${}_{\|}R_{\|}$ related to the lower boundary of the layer I at 60 km. height. On account of (1), a straight line approximating the phase values means a constant virtual reflection height. This again holds up to about cos θ = 0.5 within the VLF region. At steep incidence, however, the virtual height differs considerably from the values at oblique incidence. This is illustrated in Fig. 6, where h is drawn for the two limiting values cos θ = 0 (dashed line) and cos θ = 1 (full line) versus frequency.

The nighttime model differs from the daytime model because the lower values of the collision number ν give rise to rather large transmission coefficients. Now the influence of layer II cannot be neglected. But even here an approximate formula like (7) and a constant virtual height can be chosen for cos θ ≤ 0.5.

3. The Determination of a and h

We now assume that the reflection of VLF waves takes place at height h with the reflection coefficient

$$R = -\exp(-2\ a \cos\theta) \tag{8}$$

We consider TM waves only. Our aim is to find methods of determining a and h experimentally. We start from the well-known formula of the field strength of a vertical dipole within the wave guide between earth and ionosphere, which we write (Volland 1966)

$$\frac{E_z}{E_o} = F\ (a,h,\sigma_e,f_\nu,\rho) = |F|\ \exp\ (j\psi) \tag{9}$$

Here E_z is the vertical component of the electric field strength and E_o is the free space field strength of the dipole. The function F can be calculated for all possible values of a, h, σ_e, and ρ. The result of such calculations is shown in Fig. 7 and is valid for the propagation path Rugby-Berlin (ρ = 1000 km.) and the frequency f = 16 kc/s.

For convenience the magnitude of F is presented by

$$L = -\ 20\ \log\ |F| \qquad [db] \tag{10}$$

In Fig. 7 curves of equal attenuation L (full lines) and curves of equal phase (dashed lines) are plotted in a (a,h)-diagram. This method of plotting is due to Frisius (1965). The dash-dotted line in Fig. 7 gives the daytime course of L and ψ deduced from hourly means of January 1962 measured in Berlin. Fig. 8 shows these values versus time of day. They differ from the values in Fig. 7 by additive constants:

$$\begin{aligned} \Delta L &= L + L_o \\ \Delta\psi &= \psi + \psi_o \end{aligned} \tag{11}$$

If measurements at one station only are available, it is impossible to determine uniquely the parameter a and h from ΔL and Δψ. But looking at Figs. 7 and 8, one sees a deep minimum of field strength along the phase ψ - 155° which separates the nighttime from the daytime conditions. The same valley is seen during sunrise in Fig. 8. Therefore, we know the absolute phase at the time of sunrise. If we do phase comparison with a highly stable frequency normal ($\Delta f/f < 10^{-10}$), we are able to determine ψ_o from this one point for all other times.

From other methods of measurements we know that at daytime the values $h \sim 70$km. and $a \sim 2$ hold. Thus we have a point of reference for the determination of L_o. If the receiver (and the transmitter) show no variation of amplification with time, L_o is fixed for all times. Fig. 9 shows the variation of a and h during sunrise at January and June 1962 deduced from the (a,h)- plot in Fig. 7 and mean values of a and h for the day and night versus seasonal time.

We are aware that during sunrise or sunset the model used here is far away from reality, since neither a constant virtual height nor a constant reflection coefficient exist over the whole propagation path. But for distances between 500 and 1000 km. only, the first hop wave is essential apart from the ground wave. Therefore the values of a and h deduced above are valid for the reflection point of the first hop wave. Certainly, diffraction effects which we wholly neglect may falsify the results; a and h therefore should be considered only as effective values.

L_o and ψ_o can be obtained uniquely by measuring at least at two adjacent stations or at two adjacent frequencies. The latter has been done in Ottawa for the propagation path Cutler-Ottawa at the two frequencies 14.7 and 18.6 kc/s. (data kindly placed at my disposal by Dr. Belrose). Fig. 10 shows the (a,h)- plot of 14.7 kc/s. The dash-dotted line shows the results at sunrise. Since the virtual height at both frequencies must be nearly the same, L_o and ψ_o can be found rather well from the plots in Fig. 10 and from Fig. 11, which holds for 18.6 kc/s. The point $L=\infty$ in both plots should be noted where the sum of the interfering waves is exactly equal to zero. The 14.7 kc/s. field strength goes anticlockwise around this point. The phase and the level increase with time. At 18.6 kc/s. (Fig. 11) this point is circled clockwise. Now the phase decreases with time while the field strength goes through a deep minimum.

Finally Fig. 12 shows a (a,h)-plot for a distance of 580 km. and for 16 kc/s. A normal winter day variation of the expected field strength is plotted as dash-dotted line in Fig. 12 which circles the point $L=\infty$. This means a phase loss of 360^o each day. This phenomenon has consequences for a VLF navigation system using phase comparisons. A station situated at the distance near 600 km. would measure a daily apparent increase of distance of one wave length.

4. The Use of Atmospherics as a Natural Transmitter

A significant handicap of the method described in the last section is the fact that within the VLF region only a small number of transmitters exist, and that furthermore the location of the receiving stations cannot always be freely selected. To overcome this difficulty, one can record the electromagnetic impulses of lightning discharges which are called atmospherics. Each lightning discharge behaves like a broadband transmitter of VLF waves. But here some disadvantages arise. We do not know the location, the pulse series, and the impulse form of the discharges. The first disadvantage, the unknown location, can be overcome by a synchronized bearing of a single atmospheric from several widely spaced stations. Considering the difficulties of such a method, the information received is meager. Furthermore, each discharge is unique, differing considerably from the others. The single atmospheric which can be located by direction finders usually is of great magnitude and cannot be considered as typical.

The way out of these difficulties is to record the bearing of all atmospherics coming into the receiver. This leads to a statistical method. The equipment to realize these ideas consists of a direction finder and a heterodyne receiver for measuring the amplitude spectrum of the atmospherics (see Fig. 13). The aerial of the direction finder consists of two fixed crossed loops and a rod antenna. The impulses produced in the loop aerials by an atmospheric stimulate two identical resonance amplifiers at 11 kc/s. The output voltage of one of the amplifiers becomes phase shifted by 90^o and subtracted from the output voltage of the second amplifier. The amplitude of the difference voltage is independent of the azimuth of the atmospheric. But its phase is proportional to the azimuth compared with the output voltage of the third amplifier, which is connected with the rod antenna. A phase measurement therefore yields a voltage which is proportional to the azimuth of the atmospheric.

For measuring the distribution and the frequency dependence of the magnitude of the spectral amplitudes the impulses coming from the rod antenna are fed to a heterodyne receiver tunable between 5 and 50 kc/s. The output impulses are rectified. Their maximum is proportional to the magnitude of the spectral function of the atmospherics. By a twofold differentiation, a voltage can be derived from the output impulse which controls the brightness of a X-Y oscillograph when the respective impulse has reached its maximum. If the impulse voltage is fed to the X-input, the azimuth voltage to the Y-input, and the brightness control voltage to the Z-input of the oscillograph, each atmospheric produces a point on the screen which is uniquely related to its magnitude and azimuth.

Fig. 14 shows a photograph of the screen exposed for five minutes at 10 kc/s. Five thunderstorms of different size and direction can be separated from the background noise consisting of atmospherics from distant thunderstorms. The azimuth of their centers can be determined to within about 5°. Photographs taken simultaneously at 5 kc/s. and 40 kc/s. show the same thunderstorms but with differences in size on account of the different propagation conditions at the different frequencies.

Now it can be shown that within a narrow-band amplifier of band-width Δf, the rectified output impulse is proportional to the Fourier transform $|\check{E}(f)|$ of the impulse with field strength E(t) at the receiving aerial. The spectral amplitude $\check{E}(f)$ (or Fourier transform) of the field strength of a discharge exceeding a threshold S of the receiver is (Volland 1964).

$$|\check{E}(f)| = \frac{|g(f)\ F(f\cdot\rho)|}{\rho} = \frac{S}{\Delta f} \tag{12}$$

g(f) is the radiation component of the spectral amplitude of the discharge on 1 km. distance from the discharge, F is the propagation function (9) and ρ is the distance. The number of atmospherics exceeding the threshold S is

$$N(S,f,\rho) = n_o \int_{g_o S/\Lambda}^{\infty} W(g,f)\, dg \sim n_o \exp\left\{-\left(\frac{AS}{\Lambda}\right)^m\right\} \tag{13}$$

with

$$\Lambda = g_o\ |F|\ \Delta f/_\rho \quad ,$$

$$A = \frac{(m + \frac{1}{m} - 1)!}{m} \quad ; \quad 0.5 \leq m \leq 1.$$

W(g,f) is the probability distribution of the amplitude g,

$$g_o(f) = \int_o^{\infty} W(g,f)\ dg \tag{14}$$

is the mean of $|g|$ and n_o is the total number of discharges during the recording time. $\ddot{V}$. A detailed analysis shows that the function W can be approximated by

$$W = m \left(\frac{A}{g_o}\right)^m g^{m-1} \exp\left\{ - \left(\frac{Ag}{g_o}\right)^m \right\} . \tag{15}$$

Fig. 15 shows as an example N versus S counted from photographs like Fig. 14 at the three frequencies 5, 10 and 40 kc/s. of a thunderstorm located 1500 km. SSW from the receiving station in Berlin on 4 October, 1963; 1300 UT. The full lines are calculated from (13) using m = 0.5 (A = 2.66) and Λ as parameter.

From Fig. 15 we obtain n_o and the value Λ . If the distance of the thunderstorm is known, for example by measurements at several stations, one can draw Λ versus ρ. This has been done in Fig. 16 for 65 thunderstorms and gives the magnitude of the propagation function F apart from the factor g_o. A theoretical interpretation of F using a, h and σ_e as parameters leads to the dashed curves in Fig. 16. The point of intersection of these curves with ρ = 1 km. gives the value g_o. The parameters of the wave guide which give the best fitting curves in Fig. 16 are

$$\begin{aligned} h &= 70 \text{ km.} \\ \sigma_e &= 3.10^{-3} \text{m hos/m.} \\ a &= 0.34\ f^{-2/3} \quad (\text{f in kc/s.}) \end{aligned} \tag{16}$$

They are valid for daytime conditions in medium latitudes in the frequency range between 5 and 50 kc/s. The range of distance of this method reaches from about 300 to 3000 km. in summer and to 4500 km. in winter.

The measurement of the phase of the spectral amplitude of the atmospheric, in addition to the measurement of the magnitude, gives almost all possible information from the atmospherics.

The phase of the spectral amplitude $\check{E}(f)$ of the atmospheric is

$$\Phi = \Psi + \phi - k(\rho - \rho_o) \qquad (\rho_o = 1 \text{ km.}) \tag{17}$$

ϕ (f) is the phase of g related to 1 km. distance from the discharge.
$\Psi(\rho,f)$ is the phase of F (see 9). k = ω/c is the wave number.
Ψ and ϕ are small values compared with $k\rho$. Ψ gives the departure of the phase velocity v_{ph} of the waves from the velocity of light c:

$$v_{ph} = \frac{c}{1 - \frac{1}{k}\frac{\partial \Psi}{\partial \rho}} \tag{18}$$

The group time delay of the atmospheric is

$$t_{gr} = \frac{\partial \Phi}{\partial \omega} \tag{19}$$

Its derivative

$$\frac{\partial t_{gr}}{\partial\ \omega} = \frac{\partial^2}{\partial \omega^2} (\Psi + \phi) \tag{20}$$

does not more contain the large value $k\rho$. It is a measure of the dispersion of the impulse form during its way through the wave guide.

Fig. 17 shows a circuit diagram of the equipment which measures the difference of group time delay Δt_{gr}. Three resonant circuits are tuned at three adjacent frequencies f_o, $f = f_o - \Delta f$ and $f = f_o + \Delta f$. The frequency f_o is multiplied, the two other frequencies are mixed within converters. The resultant phases are compared giving the phase difference (Heydt 1965)

$$\Delta^2 \Phi = 2\Phi_o - \Phi_1 - \Phi_2 = \Delta t_{gr} \cdot \Delta\omega \sim \frac{\partial^2 \Phi}{\partial \omega^2} \cdot d\omega^2 \tag{21}$$

which is proportional to the group time delay at the frequency f_o. If only one mode chiefly transports the energy of the atmospheric, which is the case for $5 < f < 10$ kc/s. and distances larger than 500 km., it follows from theory

$$\Delta t_{gr} = \frac{c\,\Delta f}{16\,h^2\,f^3}\,\rho + \frac{\partial^2 \phi}{\partial \omega^2} \cdot \Delta\omega \tag{22}$$

Thus Δt_{gr} is proportional to the distance ρ apart from the phase of the spectral amplitude. If the distance is known, $\frac{\partial^2 \phi}{\partial \omega^2}$ can be derived. If otherwise $\frac{\partial^2 \phi}{\partial \omega^2}$ is known, the measurement of Δt_{gr} leads directly to the distance of the source of the atmospherics. Fig. 18 shows the dependence of Δt_{gr} on azimuth in the manner described above. We see certain accumulations of points caused by the discharges of individual thunderstorms. We now are able to separate even thunderstorms which are situated within the radial direction from the receiver.

REFERENCES

Austin, L.W. Quantitative experiments in radio telegraphic transmissions. Bull. Bur. Standards, (USA) 11, 69, 1915.

Budden, K.G. Radio waves in the ionosphere. Cambridge Univ. Press. 1961.

Frisius, J. Über die bestimmung von längstwellen-ausbreitungsparametern aus feldstärken-messungen am erdboden. (On the determination of VLF propagation parameters from field strength measurements on the ground). Diss. Univ. Göttingen, 1965.

Heydt, G. Messung der Verteilung der spektralen amplituden von atmospherics unter berücksichtigung des einfallswinkels. (The measurement of the distribution of the spectral amplitudes of atmospherics taking into account their azimuthal angle of incidence). Internat. Elektron. Rdsch. 18, 680, 1964.

Heydt, G. Messung spektraler gruppenlaufzeitdifferenzen von impulsen. (The measurement of spectral differences of group delay time of impulses). Internat. Elektron. Rdsch. 19, 426, 1965.

Volland, H. The propagation of plane electromagnetic waves in a horizontally stratified ionosphere. J. Atm. Terr. Phys., 24, 853, 1962.

Volland, H. Untersuchungen über das statistische amplituden-spektrum atmosphärischer störungen von einzelnen gewitterherden. (Research on the statistical amplitude spectrum of atmospherics coming from single thunderstorms). Nachr. Techn. Zeitschr., 17, 407, 1964.

Volland, H. Die ausbreitung langer wellen. (The propagation of long waves). Veröffentlichungen des NGG Reihe II, Band 1, Heft 2. 1966.

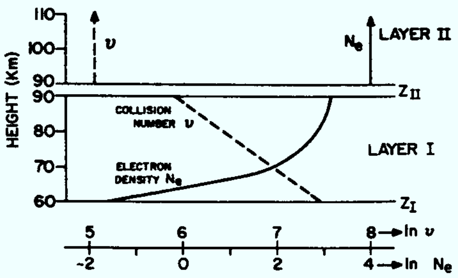

Fig. 1. Daytime model of the ionosphere.

$S = \begin{pmatrix} R_I & D_{II} \\ D_I & R_{II} \end{pmatrix}$ *Scattering matrix of layer I*

R_∞ *Reflection matrix (below) of the homogeneous layer II*

$R_{total} = R_I + D_{II} R_\infty (1 - R_{II} R_\infty)^{-1} D_I$ *Reflection matrix (below) of layers I and II*

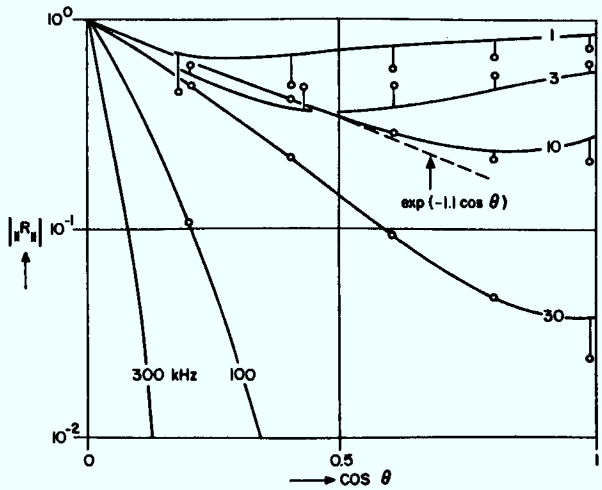

Fig. 2. Magnitude $|_{\parallel}R_{\parallel}|$ of TM waves of the daytime model versus angle of incidence θ. Full lines: layer I only. Circles: Layers I and II.

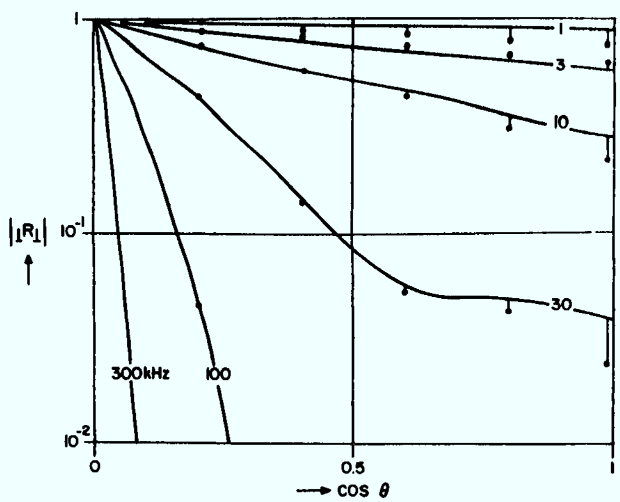

Fig. 3. Magnitude $|_{\perp}R_{\perp}|$ of TE waves of the daytime model. Full lines: layer I only. Circles: layers I and II.

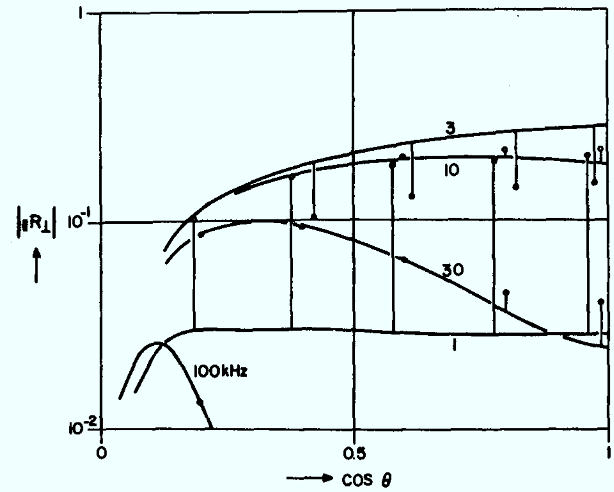

Fig. 4. Magnitude $|{}_{\|}R_{\perp}|$ of the daytime model. Full lines: layer I only. Circles: layers I and II.

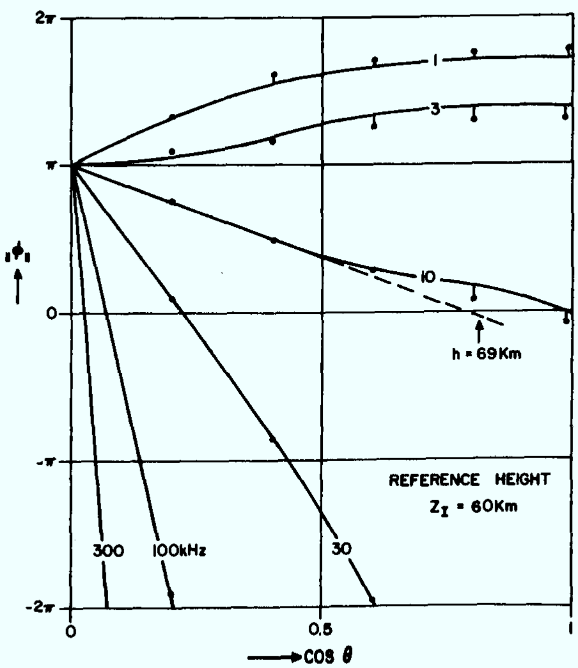

Fig. 5. Phase of $_{\|}R_{\|}$ of the daytime model. Full lines: layer I only. Circles: layers I and II.

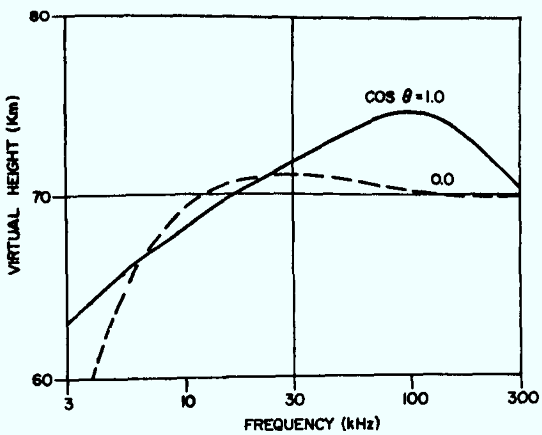

Fig. 6. Virtual height h versus frequency f of TM waves at steep incidence (full line) and at oblique incidence (dashed line).

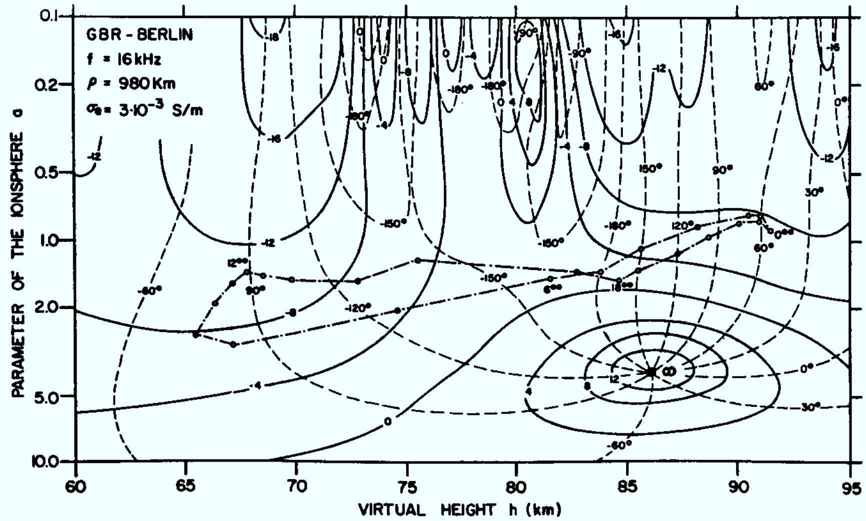

Fig 7. (a,b) – plot of the propagation path Rugby-Berlin for the frequency 16 kc/s. Full curves: lines of equal attenuation L (in db); dashed curves: lines of equal phase (in degrees). Dash-dotted curve: measured hourly means of January 1962.

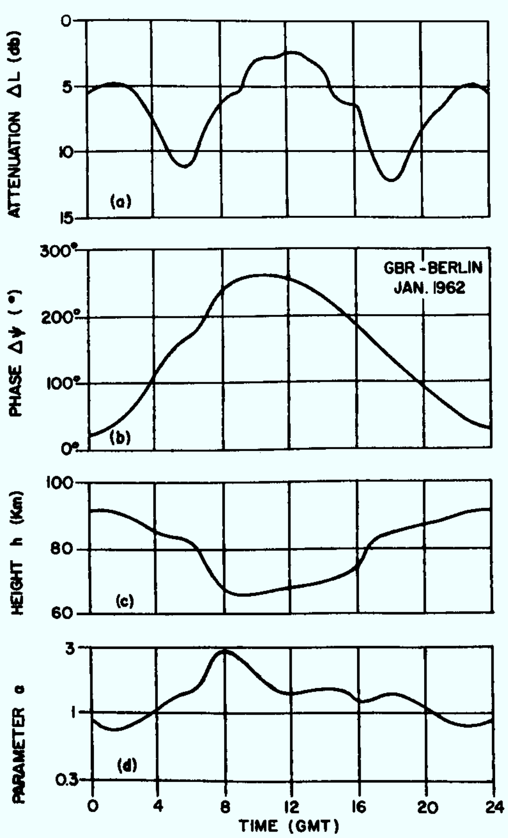

Fig 8. Hourly means of measured field strength of the transmitter GBR measured in Berlin at January 1962. Magnitude ΔL in db (Fig. 8a) phase $\Delta\Psi$ in degrees (Fig. 8b) and the parameters h in km (Fig. 8c) and a (Fig. 8d) deduced from Fig. 7.

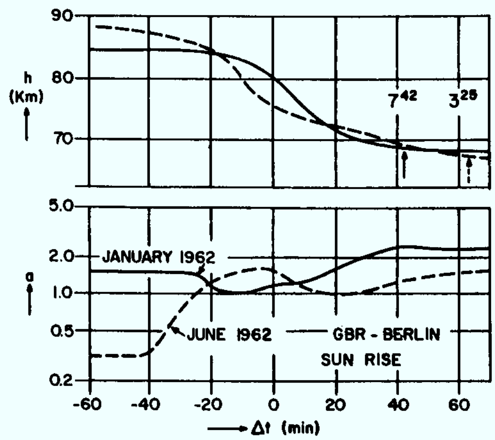

Fig. 9a. Monthly means of h and a during sunrise at the reflection point of the one hop wave of the propagation path GBR-Berlin. The time Δt is related to sunrise in 35 km height. The arrows give time of sunrise at the ground.

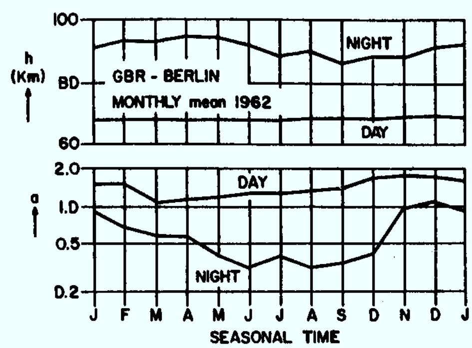

Fig. 9b. Monthly means of h and a during the time 1100 – 1300 GMT (daytime) and 2300 – 0100 GMT (nighttime).

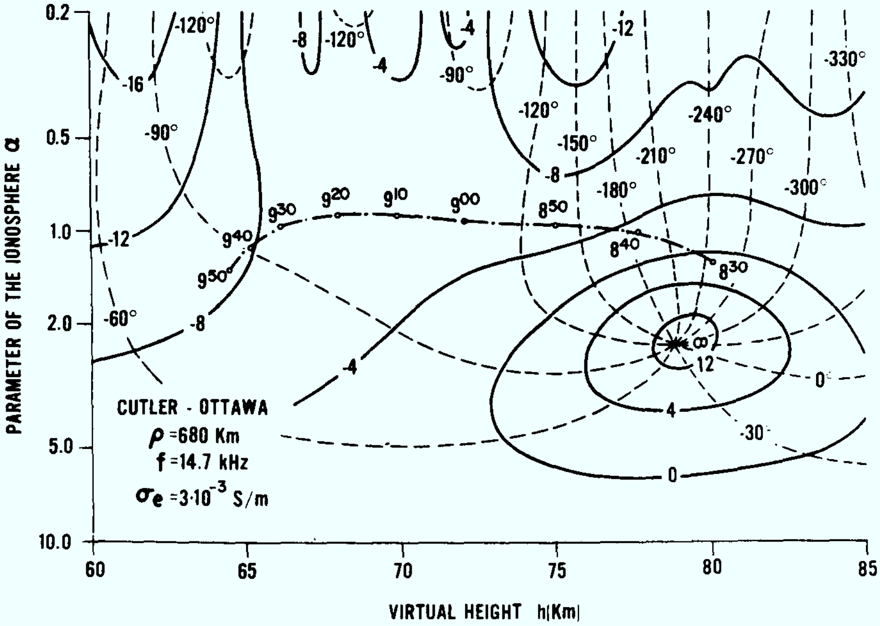

Fig. 10. (a,b) – plot of the propagation path Cutler-Ottawa for the frequency 14.7 kc/s. Full curves: lines of equal attenuation L; dashed curves: lines of equal phase. Dash-dotted curve: measured field strength during sunrise at 23 July, 1963 according to Belrose (time in UT).

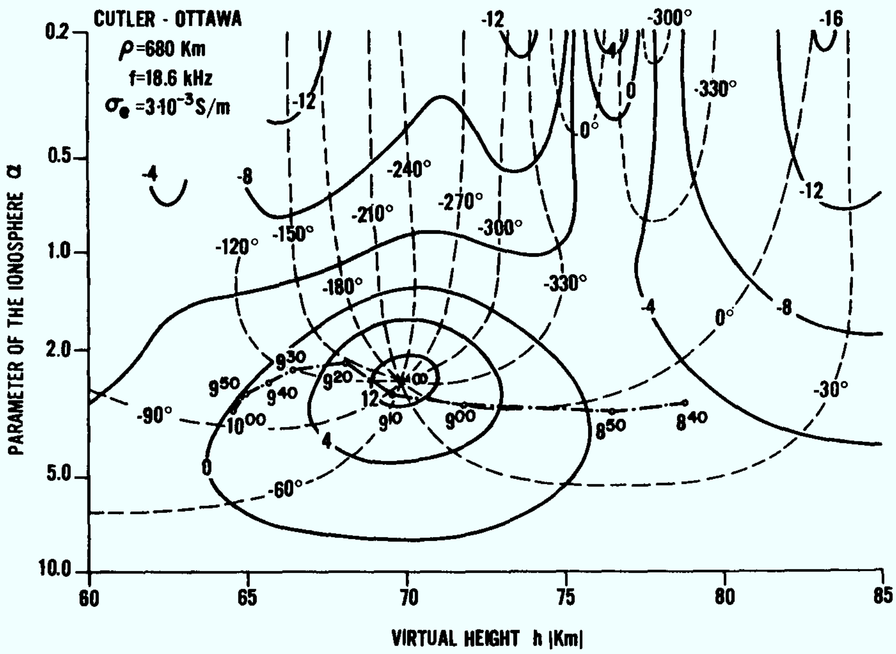

Fig. 11. (a,b) – plot like Fig. 10 but for the frequency 18.6 kc/s. Dash-dotted curve: measured field strength during sunrise at 6 August, 1963 according to Belrose (time in UT).

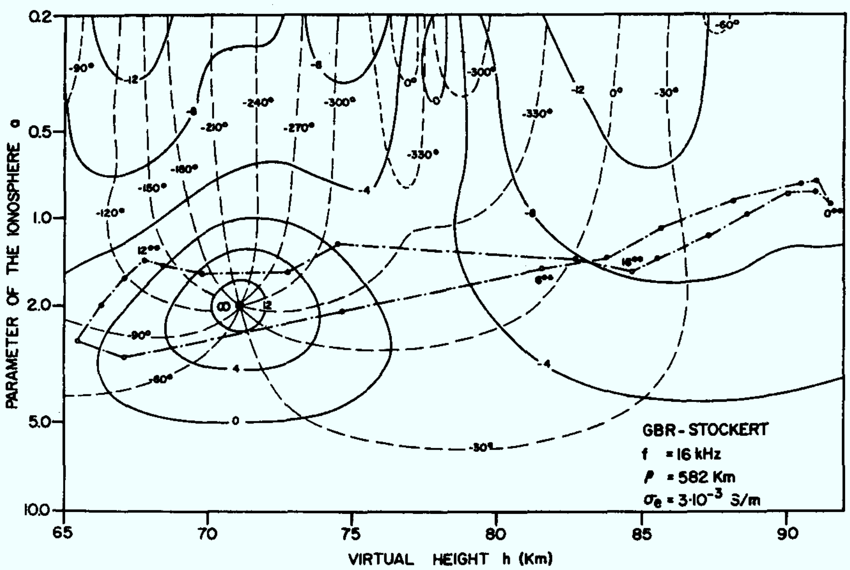

Fig. 12. (a,b) – plot of the propagation path Rugby-Stockert for the frequency 16 kc/s. The dash-dotted curve is taken from Fig. 7 and shows the expected field strength variation.

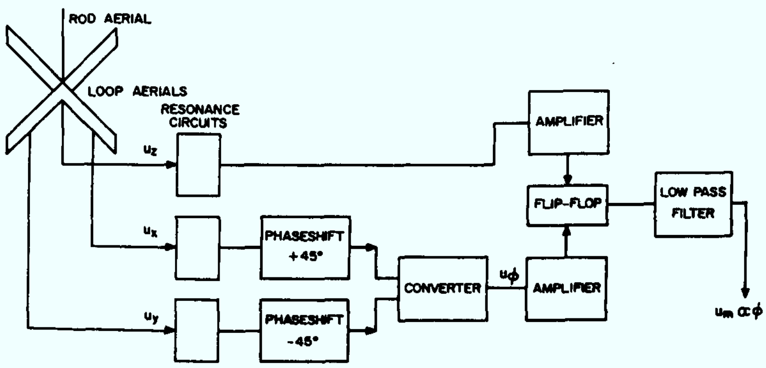

$u_x = C_1 \frac{dH}{dt} \cos\phi = C_1 j e^{j\omega t} \cos\phi$ *voltage at loop I*

$u_y = C_1 \frac{dH}{dt} \sin\phi = C_1 j e^{j\omega t} \sin\phi$ *voltage at loop II*

$u_z = C_2 Z_o H = C_2 Z e^{j\omega t}$ *voltage at the rod aerial*

$u_\phi = C_1 j e^{j(\omega t - \phi)}$ *voltage behind the converter*

$u_m \propto \phi$ *output voltage proportional to the azimuth* ϕ *of the atmospheric*

Fig. 13. Circuit diagram of the receiver for the measurement of the amplitude spectrum of atmospherics.

96414—8½

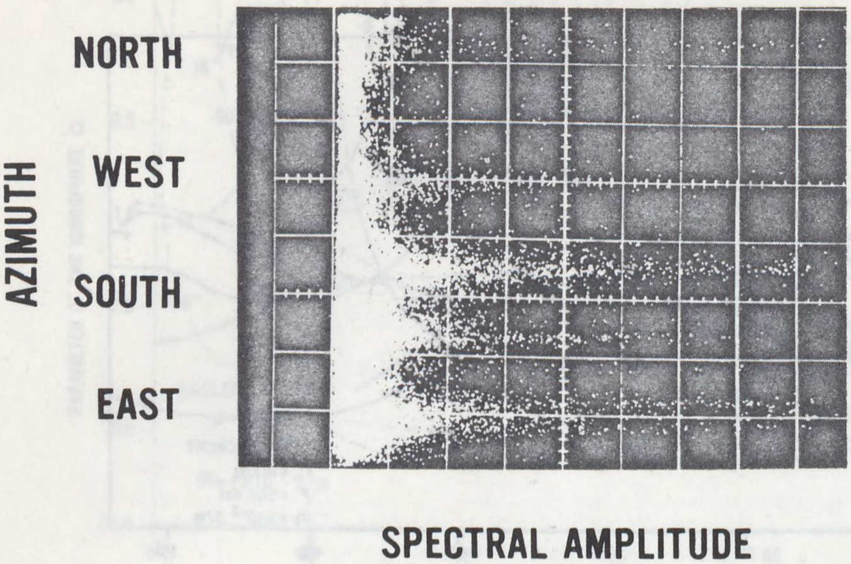

Fig. 14. Photograph of the oscillograph screen showing spectral amplitudes of the atmospherics versus azimuth at 10 kc/s Berlin, 18 September, 1963, 1300 UT. Time of exposure: 5 minutes.

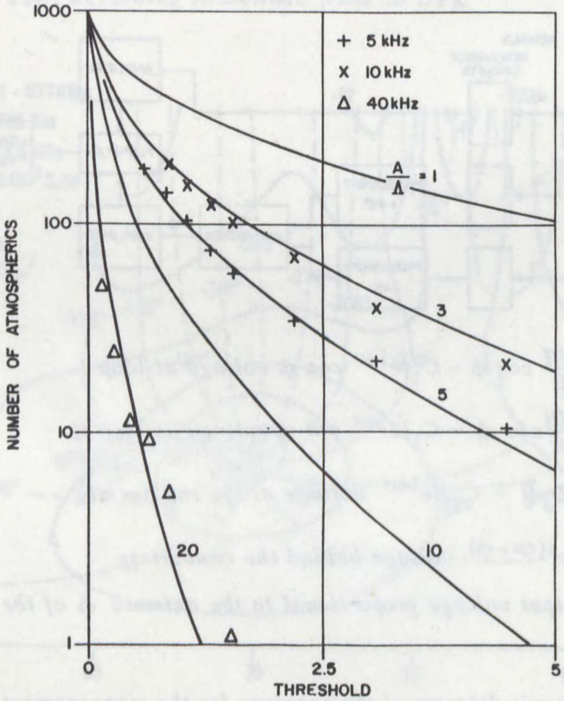

Fig. 15. Number of atmospherics N versus threshold S counted from a photograph like Fig. 14 for the frequencies. 5, 10 and 40 kc/s. Berlin, 10 October, 1963; 1300 UT.

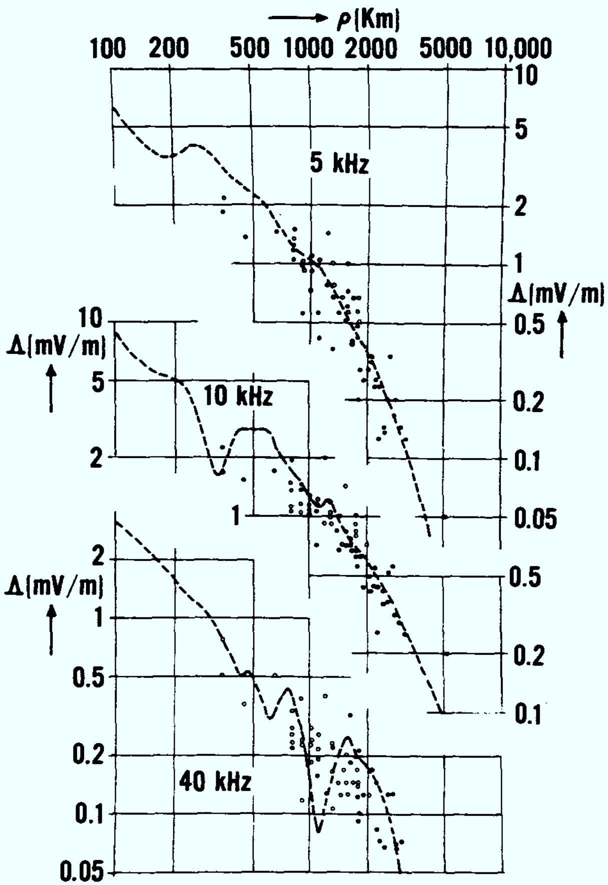

Fig. 16. Λ versus distance ρ derived from different thunderstorms at noon received in Berlin at three frequencies. Circles: winter values; points: summer values. The dashed lines are theoretical curves.

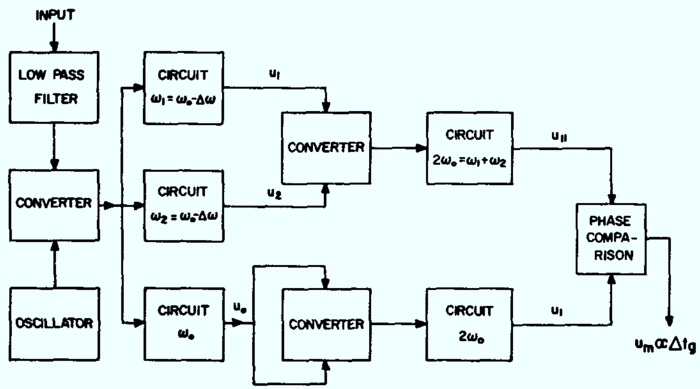

$$u_o = C_o e^{j(\omega_o t + \Phi_o)} \qquad u_I = C_I e^{j(2\omega_o t + 2\Phi_o)}$$

$$u_1 = C_1 e^{j(\omega_1 t + \Phi_1)} \qquad u_{II} = C_{II} e^{j(2\omega_o t + \Phi_1 + \Phi_2)}$$

$$u_2 = C_2 e^{j(\omega_2 t + \Phi_2)}$$

$$u_m \propto 2\Phi_o - \Phi_1 - \Phi_2 = -\Delta t_g \, \Delta\omega - \frac{\partial^2 \Phi}{\partial \omega^2} \, \Delta\omega^2$$

Fig. 17. Circuit diagram of the receiver for the measurement of time delay differences of the atmospherics.

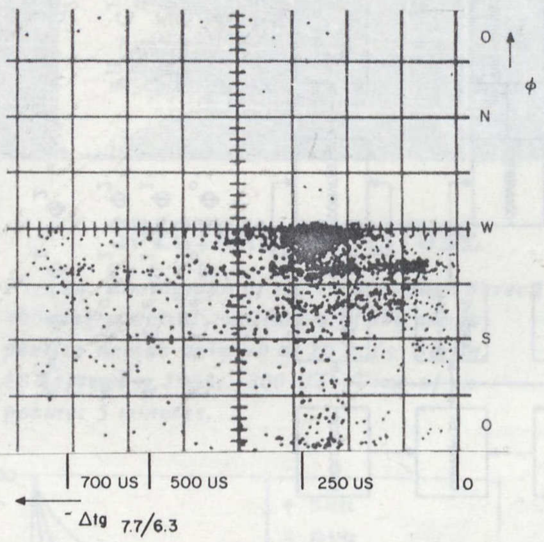

Fig. 18. Photograph of the oscillograph screen showing time delay difference Δt_g of the atmospherics versus azimuth between the two frequencies 6.3 and 7.7 kc/s. Berlin, 20 March, 1966, 1300 UT.

Discussion on Paper 4.2.2 presented by H. Volland

Ross: Can your parameter *a* be used in the low frequency region? You mentioned that it could be used up to 50 kc/s. and I wondered whether you can use either the value which you have derived here or a similar cosine function for the reflection coefficient up to say 100 kc/s.

Volland: Perhaps you remember one of the first slides (Fig. 2) where I plotted the magnitude of *R* versus the cosine up to 300 kc/s., and you saw that it is possible to find a straight line even for say 100 and 300 kc/s. When I confine myself to 50 kc/s., that is only valid for the atmospheric recordings because the magnitude of *F* becomes very small at higher frequencies, and we are no longer able to make such measurements as I showed you.

Elkins: When you made the spectral analysis of the atmospherics, did you find it necessary to include the transfer function of the antenna and, if so, how did you find what it was?

Volland: These values which you saw are valid at a point outside the antenna. You have to make some corrections which come from the amplifier and from the counter.

Elkins: But the antenna has its own transfer function, its own phase and amplitude response, which should also be considered if the power varies with frequency of the wave field of the atmospherics. Is that what you are doing?

Volland: I don't understand the question. We should speak later.

Reinisch: The actual numerical values for *h* and *a*, in which area are they valid? Are they only valid in the area where you made the measurements, or are they average values which you think are valid for a large area?

Volland: They are valid as a mean value for the atmospherics. They were recorded for three months.

Reinisch: This mean value is valid for the area in Europe where you measured it, but *h* and *a* depend on the magnetic field.

Volland: Yes. Really, *a* and *h* depend on geographical latitude, time, and direction against the magnetic field.

4.2.3 SOME REMARKS ON IONIZATION CHANGES IN THE LOWER IONOSPHERE INFERRED FROM THE PROPAGATION OF LONG RADIO WAVES

by

J.S. Belrose and D.B. Ross

Radio Physics Laboratory, Defence Research Telecommunications Establishment

Presented by D.B. Ross

1. Introduction

The Radio Physics Laboratory has undertaken a series of experiments for the purpose of studying the lower ionosphere at high latitudes by the propagation of long radio waves. While much work has been done in recent years on the theory of propagation of these long radio waves, and we can expect this theory to be applied to the propagation data in the near future, with the aim of explaining them in terms of reasonable models of the lower ionosphere (as in the case of propagation data at middle latitudes by Deeks 1966, see Section 4.2.1), this has not yet been done. Meanwhile, the propagation studies have provided valuable information relating to a morphological description of disturbance phenomena (cf. Belrose and Ross 1962, Belrose 1965); as well as some information about regular diurnal changes on undisturbed days (Belrose and Ross 1966). In this paper we present some of the qualitative information, particularly the latitudinal and seasonal variations, that one can infer from the propagation data during undisturbed periods without the use of a sophisticated theory.

2. The Transmission Paths

The experimental observations with which we are concerned are field strength, and in some cases phase recordings, of CW transmissions at frequencies about 80 kHz. propagated to distances of about 2000 km. The various transmission paths that have been monitored regularly for the past few years are shown in Fig. 1, which also shows the location of the maximum of the radio wave auroral absorption zone. The mid-points of the transmission paths are marked by open circles. As we shall see, the transmissions are dominated by a sky-wave reflected once from the ionosphere near path mid-point, and so lend themselves to fairly simple qualitative interpretation. It can be seen that we have recordings for propagation paths that lie south of, through, and north of the auroral absorption zone.

One short-distance propagation path is indicated: Cutler to St. Stephen. In this experiment, a loop antenna oriented perpendicular to the transmission path is used to isolate the ground- and sky-waves, in a manner as described by Straker (1955), and the steep incidence reflection of very low frequency (14.7 and 18.6 kHz.) waves are recorded.

3. Low Frequency Propagation

We shall consider first 80 kHz. propagation over the path Ottawa to Moosonee, about 745 km. distant, and Ottawa to Churchill, about 1911 km. distant, i.e., along approximately the same path. Fig. 2 shows the variation for the same day in July 1963 of both amplitude and phase of the wave field as measured by an in-plane loop antenna (normal component). The times for solar zenith angles at path mid-point of 102°, 98°, 94°, and 86°, as well as ground sunrise (SR) and sunset (SS) at 90° 50', are shown by short vertical bars. Over both of these paths in summer the variations at dusk are essentially the reverse of those at dawn. The changes that occur during the dawn and dusk periods are quite similar for both transmission paths, differing mainly in magnitude. This similarity in form is evidence that both transmissions are essentially by once-reflected sky-wave: that at Moosonee there is little remaining ground-wave and at Churchill little twice-reflected sky-wave. This conclusion is supported by field-strength measurements made during two aircraft flights (see Fig. 1) along the same path (Belrose and others 1965), which gave a very low ground conductivity. The measurements are shown in Fig. 3, the two curves being separated by 20 db for clarity. The field begins to show sky-wave effects at about 450 km., and the ground-wave ceases to have effect at about 800 km., however, it should be borne in mind that these distances refer to the field received in the aircraft, where the ground-wave is more strongly received to a greater range than in the case of ground-based receivers.

Propagation effects that occurred during a solar eclipse are also shown in Fig. 2. The path of totality at 80-km. height for this solar eclipse, which occurred on 20 July, 1963, is shown in Fig. 1. The field strength over the Ottawa - Moosonee path increased, then decreased, and finally increased to a maximum about six minutes after totality. This variation and the accompanying increase of phase are similar to those that occur during a normal dusk up to $\chi \simeq 98°$. The recovery from the eclipse was essentially the reverse of the onset, and so similar to the normal dawn. An auroral zone disturbance of limited extent was in progress at this time (Vogan 1964), which may explain the much poorer correspondence between eclipse and sunset effects over the longer Ottawa - Churchill path. These eclipse effects must be due to ionization changes in the lower ionosphere caused by the gradual disappearance and reappearance of radiation directly from the sun. It is interesting to note the similarity to the normal dusk and dawn variations, since the solar geometry in the two situations is quite different. In the case of the eclipse, all radiations from the sun are uniformly eclipsed; whereas during a normal sunset the solar radiation is changing in wave length as well as weakening, with the short ultraviolet radiations being first attenuated and finally the visible light is cut off by the solid earth shadow at about $\chi \simeq 101°$.

We will consider next the dawn variations of the normal component of the field strength over the other low frequency transmission paths: Comfort Cove to Ottawa, 70.384 kHz., 1637 km.; Goose Bay to Ottawa, 82.05 kHz., 1450 km.; Goose Bay to Churchill, 2157 km. and Thule to Churchill, 77.15 kHz., 2200 km. (see Fig. 1). There is quite a large day-to-day variation, which may be even greater than that shown in Fig. 4, especially in winter or at high latitudes. In spite of this, the average dawn variation may be obtained.

Fig. 5 shows the results for equinox months for the Comfort Cove - Ottawa path, obtained by averaging about 15 days. The vertical lines show the zenith distance of the sun at path mid-point. There is similarity in form between the two equinoxes and also from one year to the next. The curves in Fig. 6 are the results at solstice, which are little different from equinox for this mid-latitude path. The results for this path characteristically show a pronounced peak at a zenith distance of 100°, and smaller peaks at smaller χ values, the principal one being at about 95°. These general conclusions are borne out by a similar analysis of the Goose Bay - Ottawa data, except in winter. This similarity in form is good additional evidence that the dawn features at middle latitudes are not due to interference between once- and twice-reflected sky-waves, or to path length, but are caused by ionization changes closely linked to the zenith distance of the sun affecting the once-reflected sky-wave. The Goose Bay - Churchill path shows similar summer results. In winter the propagation is quite variable and the peaks at equinox occur when the zenith distance is 2° or 3° greater, suggesting perhaps that the reflecting region is higher at equinox in this latitude.

The equinox results shown in Fig. 9 for the Thule - Churchill path, a transmission path that lies well above the auroral absorption zone, are not significantly different from the mid-latitude results. At solstice (Fig. 10) the variations are consistent with the ones we have seen for 1960 through 1963. The lack of variation in summer was expected and is due to the sun always being above the horizon at path mid-point, since the maximum zenith distance is about 88 1/2°. The years 1964 and 1965 are completely different. The propagation appears to have lost the close connection with solar zenith distance. This is made clear by the differences between these illustrations of diurnal variation for 1961 (Fig. 11) and 1965 (Fig. 12), which show that winter dawn occurs earlier and summer dawn later, and also that propagation is much poorer in 1965 than in 1961. There is no obvious reason for the difference between 1963 and 1964, where the June decrease in 2800 MHz. solar flux was 17% and the December decrease 0%. On the other hand, the corresponding changes between 1960 and 1961 were 32% for both months, so that greater differences in propagation might have been expected there. This striking change was not found at the lower latitudes, as may be seen by comparing the typical winter, spring, and summer field strength curves of Comfort Cove - Ottawa for 1961 (Fig. 7) and 1965 (Fig. 8). In fact 1965 shows generally higher field strengths at night, in contrast with the higher latitude results.

Good dawn/dusk symmetry was found on the Ottawa - Churchill and Ottawa - Moosonee paths in mid-summer. We see (Fig. 7) that this is so for Comfort Cove - Ottawa, but it was rather asymmetrical in January and March 1961 and Thule - Churchill was very asymmetrical, particularly in March (Fig. 11) (Belrose and others 1964). There was better symmetry in 1965 (Figs. 8 and 12). This suggests that at dusk the ionization decayed more slowly at high than at medium latitudes, and at equinox than at solstice during the period 1960 - 1963, but that it decayed more rapidly in the period 1964 - 1965.

4. Very Low Frequency Propagation at Steep Incidence

As we have seen, measurements of the normal component of the low frequency field at long distances show small field strength variations and little phase variation during the day. Measurements made with a perpendicular loop antenna of the abnormal component of the very low frequency field at short distances, such as the 60-km. Cutler - St. Stephen path (Fig. 1) where the waves penetrate the ionosphere more deeply, show more pronounced field strength variations, and a slow phase variation that reaches a maximum (minimum apparent reflection height) near midday. Straker (1955) found a small dawn/dusk asymmetry in phase of a 16-kHz. field at 90 km. We have found marked irregularity in the daily variation of both field strength and phase of 14.7 kHz. over this path (Fig. 13), which was thought to be due to residual ground wave in the signal. However, a change of transmitter frequency to 18.6 kHz. (Fig. 14) almost eliminated the phase plateaus seen at 14.7 kHz. and reduced the daytime field strength variations. We now believe that the 14.7 kHz. phase plateaus in the morning and afternoon are a real feature of the daily variation at this frequency, and are the result of diurnal changes in the electron density structure in the lower ionosphere.

5. Discussion

The most noticeable feature in the LF propagation data discussed in this paper is the regular oscillatory changes that occur over dawn (and dusk). These changes have the same form for transmission paths at different distances and frequencies, and although the amplitudes of the variations are variable from day to day, and over the season, they are observed at all epochs of the solar cycle.

At high latitudes, however, marked differences are found. In equinox months the changes are not unlike those observed at lower latitudes; but during solstice months in sunspot minimum years the field strength variations occur at times that are quite unexpected. In the period 1960 to 1963 the variations observed in winter are not unlike those at equinox or those observed at lower latitudes. The variations in summer are small, as might be expected since the D region is always sunlit. In the period 1964-65 the propagation appears to have changed markedly. The amplitude changes that occur at dawn begin earlier in winter, and occur later in summer than expected. While the marked difference in diurnal variation in summer in 1964 and 1965 compared with previous years was not anticipated, it is probably explainable by reasonable changes in D-region structure over the cycle. Certainly marked ionization changes would be expected, especially at high latitudes: i.e., the ionization densities in the C layer should be greater in quiet sun years, since the intensity of cosmic radiation is larger; whereas the ionization densities in the D layer (as well as the electron density gradient) should be larger at the maximum epoch of the solar cycle, since "background" short wave length (2 - 10Å) solar X-rays are larger by up to four orders of magnitude. The winter results for the period 1964-65 are, however, not interpretable in any simple way. The changes that occur before $\chi \simeq 102°$ cannot be linked to solar radiations.

The field strengths are clearly influenced by the epoch of the solar cycle in a most complex way. The Thule - Churchill field strengths are larger in sunspot maximum years during both day and night; whereas the reverse is true in winter for the Comfort Cove - Ottawa path. In summer the Comfort Cove - Ottawa field strengths are small by night and larger by day during sunspot maximum years. The diurnal change of field strength is markedly asymmetrical in equinox at sunspot maximum for the Thule - Churchill transmission.

Low frequency waves (70 - 82 kHz.) obliquely reflected from the ionosphere show little variation in phase or amplitude during the day ($\chi < 86°$). Very low frequency waves (14.7 and 18.6 kHz.) steeply reflected from the ionosphere penetrate the ionosphere more deeply and show pronounced phase and amplitude changes throughout the day. Marked "plateaus" in the phase observable more strongly at the lowest frequency (14.7 kHz.), during the period 1 to 3 hours after ground sunrise (and before ground sunset), are clearly related to structural changes in the D region.

It is anticipated that some of the propagation features discussed in this paper will be quantitatively explained in terms of reasonable models of the lower ionosphere; but it will be some time before all details of the observed changes are quantitatively explained or understood.

REFERENCES

Belrose, J.S. LF propagation changes associated with the absorption of HF radio waves for a transmission path which traverses the auroral zone, paper presented at Spring USNC-URSI Meeting, 20 - 24 April, 1965.

Belrose, J.S. and D.B. Ross. Observations of unusual low frequency propagation made on 12 November, 1960. Canadian Journal of Physics, 39, 609 - 614, 1961.

Belrose, J.S. and D.B. Ross. Long wave propagation changes during the total solar eclipse of 20 July, 1963, to be published in Can. J. of Physics, 1966.

Belrose, J.S., Bode, L.R. and L.W. Hewitt. Physical properties of the polar winter mesosphere obtained from low frequency propagation and partial reflection studies. Radio Science J. of Res. NBS and USNC-URSI, 68D, 1319 - 1323, 1964.

Belrose, J.S., Goodwin, G.L., Hewitt, L.W., Ross, D.B., Segal, B., Berry, L.A. and J.R. Johler. Numerical calculation and experimental measurement of long wave fields over distances of about 2000 km., (presented at Fall USNC-URSI Conference, Hanover, New Hampshire, 4 - 6 October, 1965).

Deeks, D.G. D-region electron distributions in middle latitudes deduced from the reflexion of long radio waves. Proc. Roy. Soc. A, 291, 413 - 437, 1966.

Straker, T.W. The ionospheric propagation of radio waves of frequency 16 kc/s. over short distances, Monograph No. 114R. Institution of Electrical Engineers, 1955.

Vogan, E.L. Absorption measurements during the solar eclipse of July 20, 1963. Canadian Journal of Physics, 42, 1382 - 1386, 1964.

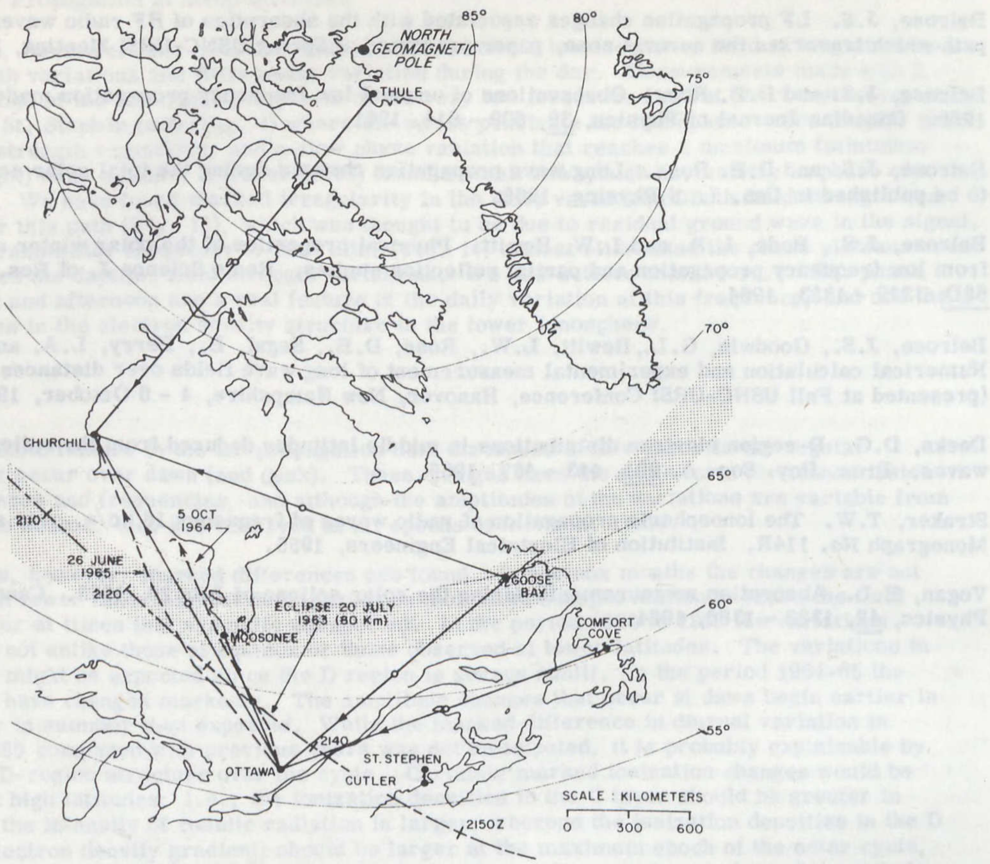

Fig. 1. Map of transmission paths, flight paths, and path of solar eclipse of 20 July, 1963 (solid, dashed, and dot-dashed lines respectively). The location of the maximum of the radio wave auroral absorption zone is also indicated.

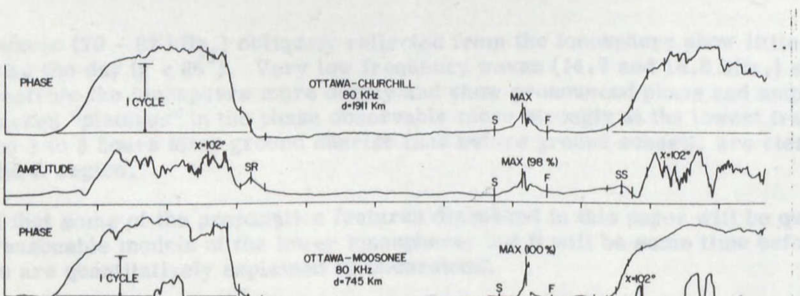

Fig. 2. Diurnal variation in the phase and field strength of 80 kHz. from Ottawa to Moosonee and Churchill in summer, showing the effect of a solar eclipse.

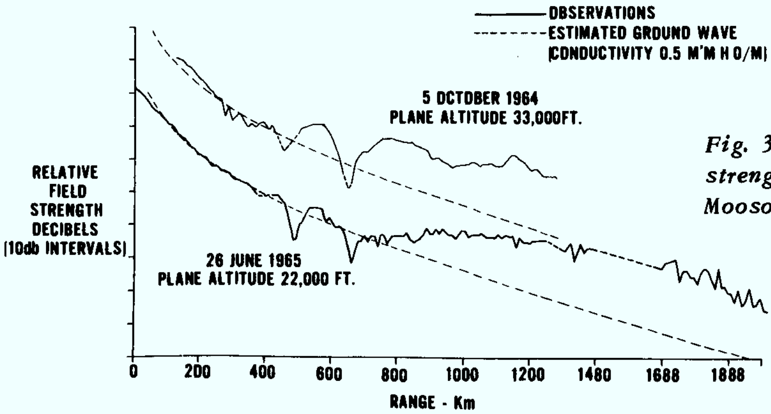

Fig. 3. Aircraft measurements of 80-kHz field strength versus range over the Ottawa – Moosonee – Churchill path.

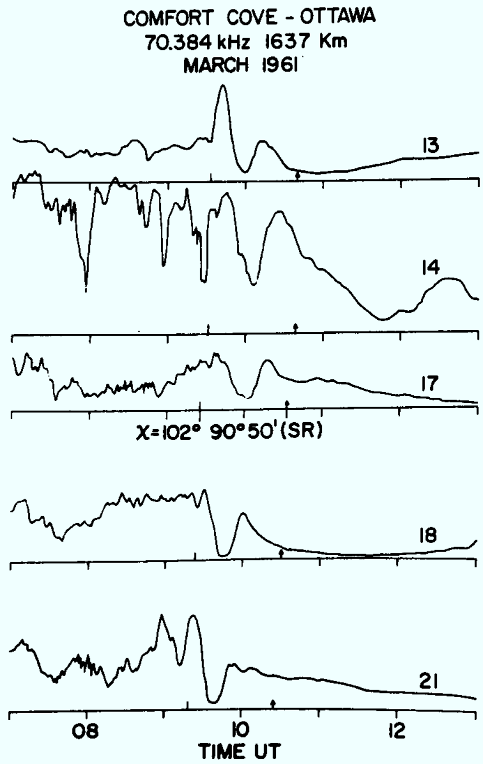

Fig. 4. Daily variability of low frequency field strength changes over dawn.

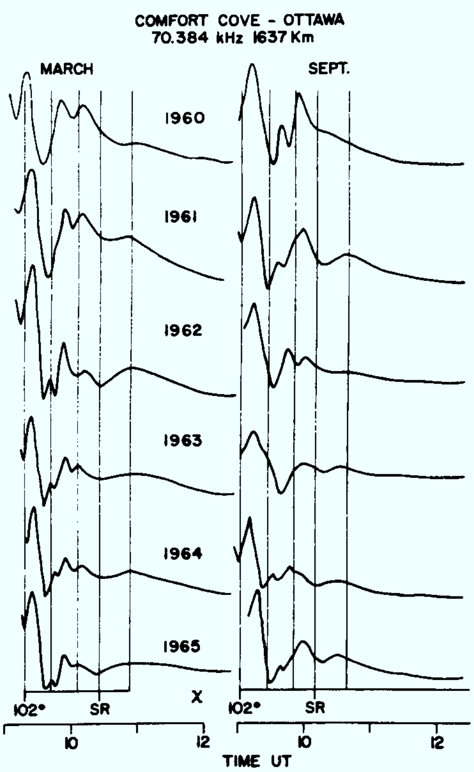

Fig. 5. Variation of Comfort Cove – Ottawa field strength over dawn at equinox.

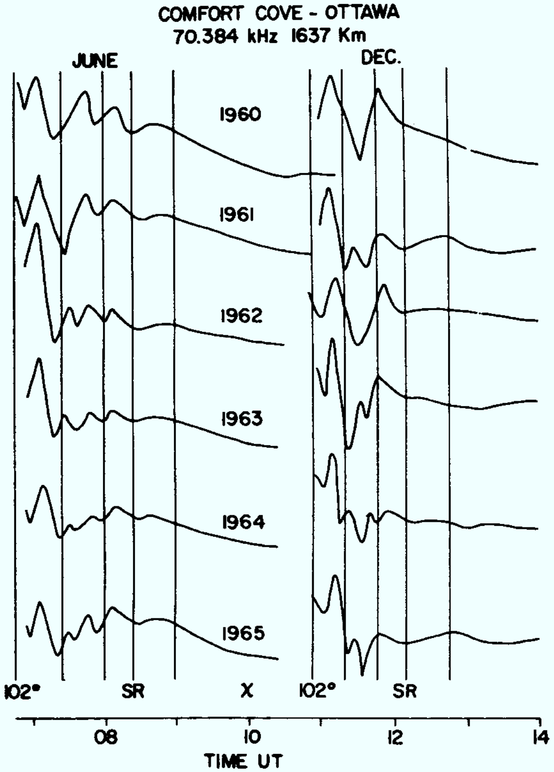

Fig. 6. Variation of Comfort Cove – Ottawa field strength over dawn at solstice.

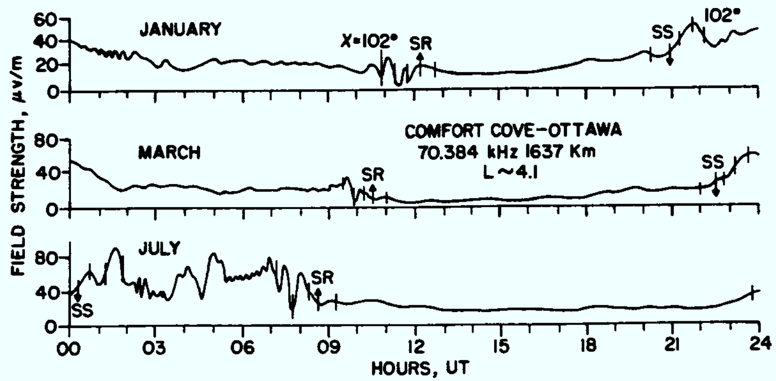

Fig. 7. Diurnal variation of Comfort Cove – Ottawa field strength at three seasons in 1961.

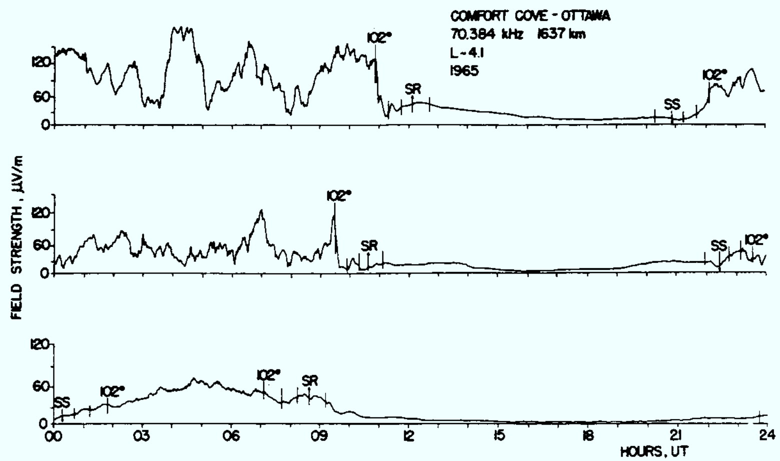

Fig. 8. Diurnal variation of Comfort Cove – Ottawa field strength at three seasons in 1965.

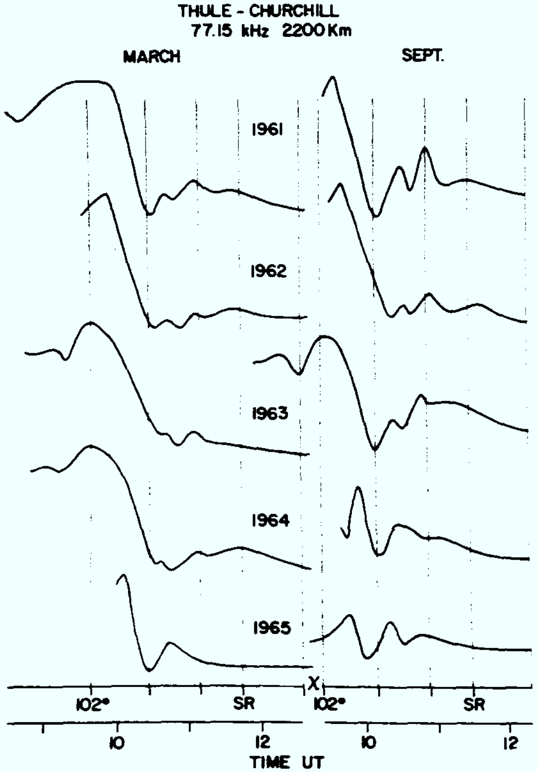

Fig. 9. Variation of Thule – Churchill field strength over dawn at equinox.

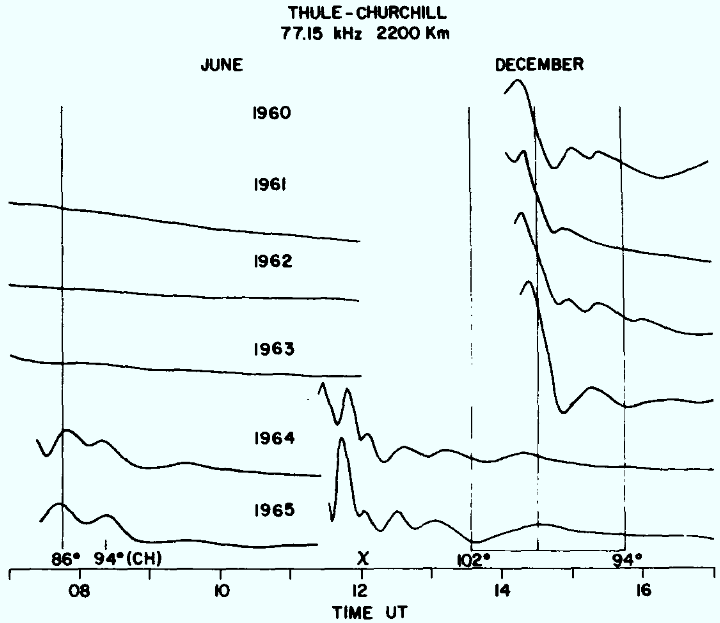

Fig. 10. Variation of Thule – Churchill field strength over dawn at solstice.

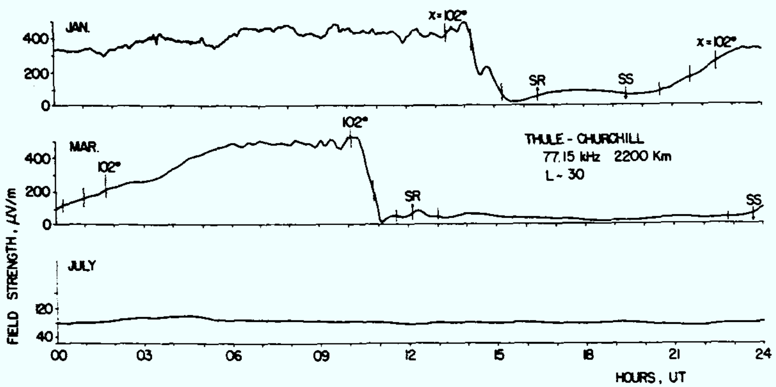

Fig. 11. Diurnal variation of Thule – Churchill field strength at three seasons in 1961.

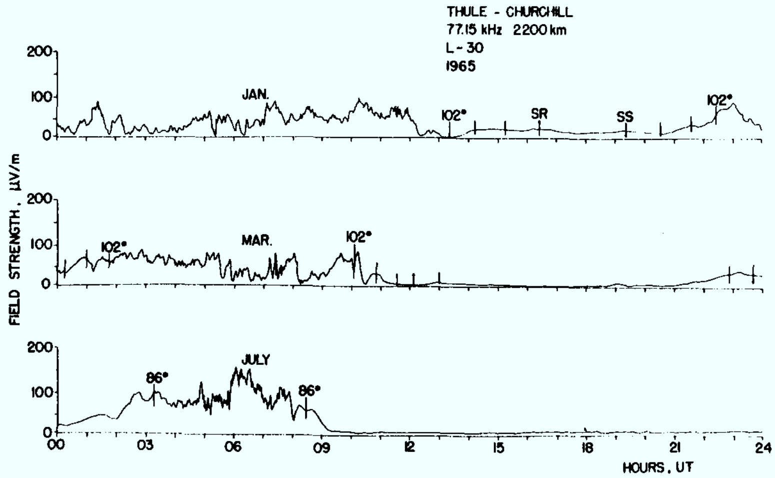

Fig. 12. Diurnal variation of Thule – Churchill field strength at three seasons in 1965.

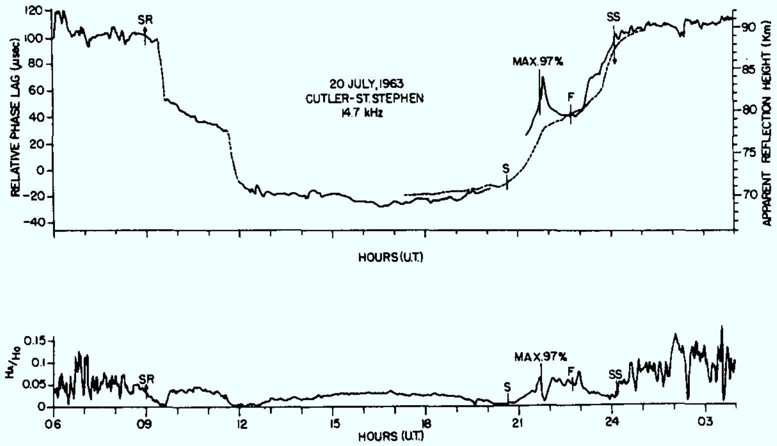

Fig. 13. Diurnal variation in the phase and field strength of 14.7 kHz. over the Cutler – St. Stephen path in summer.

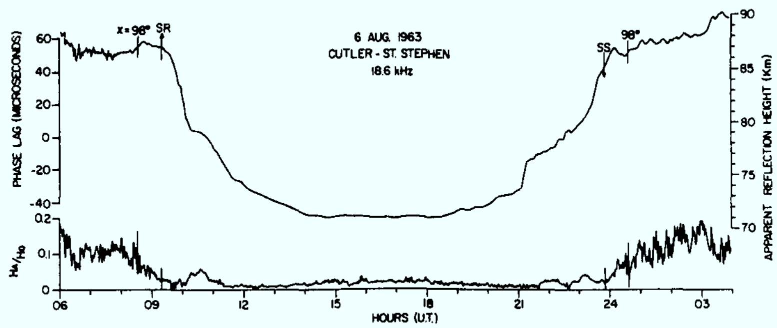

Fig. 14. Diurnal variation in the phase and field strength of 18.6 kHz. over the Cutler – St. Stephen path in summer.

Discussion on Paper 4.2.3 presented by D.B. Ross

Volland: What is the distance between Cutler and St. Stephen?

Ross: It is 60 km.

Belrose: I don't think the point was made clear that this is what is called the abnormal loop experiment in which a loop aerial is rotated to suppress the ground-wave and one is always concerned whether the ground-wave was completely suppressed. The marked phase plateaus, which were observed at 14.7 kHz., could be interpreted as perhaps being a residual ground-wave which was not adequately suppressed. However, without touching the antenna system, the transmitter changed frequency to 18.6 kHz. and the phase plateaus practically disappeared, so we interpreted it as being a real propagation phenomenon.

4.2.4 D-REGION SOLAR ECLIPSE EFFECTS

by

G.S. Sales

Air Force Cambridge Research Laboratory, L.G. Hanscom Field, Bedford, Mass.

1. Introduction

This is a description of the behavior of the lower ionosphere below 100 km. when disturbed by a total eclipse of the sun. Various production sources are considered and for each the effects of solar obscuration are calculated. The production variation is used as input for the rate equations for electrons, negative and positive ions. The time-dependent solutions of the pair of independent rate equations are obtained on a digital computer, resulting in electron density profiles for the passage of the solar eclipse. These profiles are considered in the light of VLF and rocket data obtained during the 20 July, 1963 eclipse, and parameters of the rate equation are varied so as to obtain profiles that are in agreement with radio data.

This paper has two purposes: first, to give a clear picture of D-region behavior in order to understand which processes are important at the various altitude regimes in the lower ionosphere. Second, an attempt is made to deduce values of reaction rates that must exist in order to explain VLF and rocket probe data.

2. Production Sources

Four main production sources are considered over the altitude range 100 to 60 km. (Fig. 1 and Table 1).

TABLE 1

Source	Region of Importance
Ultraviolet	> 95 km.
Xrays	85 to 95 km.
Lyman α	75 to 85 km.
Cosmic rays	< 75 km.

Ultraviolet and Lyman α are considered to be completely obscured at totality, while xrays (2-8Å) are only 85 per cent obscured due to coronal emission. Finally, cosmic rays are unaffected by the solar eclipse. The function applied for obscuration was calculated for two equal discs as one covers the other. The parameter α in Fig. 2 is a function of the separation of the centers and is a linear function of time.

TABLE 2

Time	Separation	α	
00 min.	L = 2R	1	First contact
60 min.	L = 0	0	Second contact
61 min.	L = 0	0	Third contact
121 min.	L = 2R	1	Fourth contact

For the time between second and third contacts, arbitrarily set equal to one minute to simulate the eclipse of 20 July, 1963, the obscuration function is kept at zero (Table 2). At each altitude of the calculation, the production function Q is the sum of the four sources and is composed of a fixed part and a part that varies with time according to the obscuration function.

A Lyman α flux of 3.3 ergs/sq.cm./sec. was measured on 20 July, 1963 by Smith at Churchill, and this value is used in this calculation. Unfortunately, no hard xray flux was measured. In this work two different xray models were used. Cosmic ray flux and ultraviolet production were taken from Pierce.

3. Rate Equations

The equations used for this analysis are a simplified form using only electron, negative and positive ion densities with no reference to species. These equations are to be considered as a guide to which processes are important at various altitudes, and also to reasonable values of the rate coefficients.

$$\frac{dN_e}{dt} = Q(t) - \alpha_D N_e N^+ + \gamma N^- + \rho(t) N^- - \beta N_e$$

$$\frac{dN^-}{dt} = -\alpha_i N^- N^+ - \gamma N^- - \rho(t) N^- + \beta N_e$$

$$\frac{dN^+}{dt} = Q(t) - \alpha_D N_e N^+ - \alpha_i N^- N^+$$

where

Q = production rate/cc./sec.

α_D = dissociative recombination cc./sec.

α_i = ion-ion recombination cc./sec.

γ = detachment coefficient/sec.

ρ = photodetachment coefficient/sec.

β = attachment coefficient/sec.

These equations consider besides production, attachment, photo and other detachment process, dissociative and ion-ion recombination. The three equations are reduced to two by using the constraint

$$N^+ = N_e + N^-$$

All the coefficients are functions of altitude. However, only Q and ρ are also functions of time. Photodetachment follows the obscuration function exactly.

The pair of equations is solved simultaneously on a digital computer with the temporal variation of the electron and ion densities as outputs.

4. VLF Radio Sounding and Rocket Data

During the eclipse of 20 July, 1963, an off-vertical VLF experiment was organized to monitor the CW high-power transmissions of NAA in Cutler, Me. on 14.7 kHz. The receiving station was located in Dorham, N.H., a distance of 315 km. away from the transmitter along a line nearly perpendicular to the path of the eclipse as it crossed Maine from NW to SE. The one-hop reflection was located at the 75 km. totality. The width of totality was some 50 km. horizontally and extended ±25 km. vertically. The abnormal component of the skywave was monitored continuously day and night for approximately one week prior to this eclipse. Figs. 3 and 4 show the signal strength and phase height variations respectively. The solid curve indicates the mean variation with the vertical bars equal to two standard deviations. The eclipse was in the late afternoon in Maine and the mean signal strength is seen to gradually increase as sunset approaches.

On the eclipse day (dotted curve), the signal strength is seen to behave normally through first contact and then show a systematic trend towards greater signal as the eclipse progresses. The signal continues to increase through totality and reaches a peak value some six minutes after totality. From this point on the signal decreases more rapidly than the rise (the gaps in the record are caused by the transmitter being turned off). The two important features are the time lag and the asymmetrical behavior after totality.

The phase change (Fig. 4) shows a similar behavior with a six-minute lag and a total phase change corresponding to 6 km. of vertical motion.

Fig. 5 shows the electron density profiles made at Churchill during the same eclipse by L.G. Smith (1965). Here on a plot of electron density vs. height are the results of four rocket flights launched at 2 min. before and 8 and 35 min. after totality. It must be remembered that these are launch times, to be corrected by approximately 2 min. for the flight time to the D region (all data are for ascent). The important features are gradual but complete decay of the lower D region, the smaller loss at 80 km. and above and the crossover of the −2 min. and +8 min. curves in the region of 80 and 90 km.

Consider first the 90 km. crossover. This implies that at totality and at +10 min. (allowing 2 min. for rocket ascent) the electron density was found to be equal. This leads to a time constant of 5 min. at 90 km. As will be shown shortly, it is not permissible to carry out a similar calculation at 80 km.

Before going on, it is important to consider what is meant by a time constant of the ionosphere. Consider the rate equation further simplified for altitudes 85 km. and above, where only production and dissociative recombination need be considered.

$$\frac{dN_e}{dt} = Q - \alpha N_e^2$$

For a step function Q, the time constant of the solution of this equation is

$$t = \frac{1}{2[\alpha_D Q]^{\frac{1}{2}}}$$

It can be shown empirically that this number represents the time lag observed during an eclipse only for time constants of 10 min. or less. It is important to recognize that this time constant is not just a function of the recombination rate but also of the production at the height of interest, and therefore the time constant observed for any measurement will vary with place and time.

5. Eclipse Calculations

Two production models are considered using first the largest xray production (Fig. 1) with a dissociative recombination rate coefficient of 2×10^{-7} cc./sec., while for the second model the intermediate xray production is used with a recombination rate coefficient of 2×10^{-6} cc./sec. In the first case, called Model Q, two detachment processes are considered. The first is collisional detachment, which decreases with altitude following the neutral density. The second is associative detachment, which increases with increasing altitude following the density of atomic oxygen. As will be shown shortly, one of the detachment mechanisms is to be preferred over the other on the basis of the eclipse data.

First, consider the associative detachment model (solid curve, Fig. 6). Here we have the time variation of the electron density at various altitudes. Totality occurs between T = 60 and T = 61 min. At low altitude, near 60 km., the electron density changes by more than an order of magnitude and follows the obscuration curve closely. The important processes are attachment and photodetachment. The low electron density at totality is caused by the small amount of associative detachment at this altitude, so that when photodetachment is zero at totality, most electrons form negative ions. This same behavior, though to a lesser degree, is found at 70 and 75 km. (not shown). No time lag is observed since the time constants of attachment and detachment processes are extremely short, of the order of seconds or less. Complete symmetry is maintained and recovery is complete by fourth contact.

Now consider the higher altitudes of this model, where the eclipse behavior is controlled by production and dissociative recombination of electrons and positive ions. At 100 km. where the production is highest, the time constant is of the order of 1 min., while at lower altitudes, where the production becomes smaller, the time constant increases. As the time constant becomes larger, the magnitude of the electron density change becomes smaller, decreasing from a factor of five at 100 km. to less than a factor of two at 85 km.

If now the associative detachment is replaced by a collisional detachment model, the dotted curve is obtained. Differences are observed at both low and high altitudes. At low altitudes, where a weak detaching mechanism is replaced by a strong one, the photodetachment becomes less effective, and the eclipse effect is reduced. At higher altitudes, the strong associative detachment has been replaced by a weak collisional detachment and the effects of photodetachment are more apparent at totality. Considering the large loss of electrons at low altitudes as observed by the rocket measurements and the lack of any double humping at high altitudes, as should occur in the VLF data if the collisional detachment model were applicable, it is concluded that an associative detachment mechanism must dominate at high altitudes and that there must be little detachment at low altitudes except for photodetachment.

Now consider the same data in another form. Here four time cuts are made at totality, T + 7, T + 20, and pre-eclipse, and electron density profiles are constructed for the associative detachment model (Fig. 7). The decay of electron density from first contact until second is rather uniform for all altitudes and is not shown. The recovery phase is the more interesting time. After totality the lower D region starts to recover promptly. At high altitudes, considering the short time constants, the recovery also begins quickly and is symmetrical. The interesting region is between 80 and 90 km. Here the electron density continues to decrease after totality and little recovery is apparent even at T + 20 min. Before leaving this model, consider the reflection height of the VLF signal as around 300 electrons/cc. and its variation during the eclipse. Starting near 65 km., the reflection height moves above 70 km. and then recovers symmetrically and with no time lag. Thus from this model both signal phase and amplitude would be expected to change symmetrically and with no time lag. This is not in agreement with the VLF data.

A second model considered, called Model N, has a smaller xray flux, but, more important, a dissociative recombination of 2×10^{-6} cc./sec. For this model only associative detachment was considered. The D-region behavior as seen in Fig. 8 is not significantly different from the previous model and all the comments made for the previous model are applicable. Here the 80-km. curve is included, which was unfortunately omitted from Fig. 6, and the transitional behavior between attachment - detachment processes and production - recombination processes can be seen. Consider these curves, keeping in mind Smith's rocket measurements, where at 90 km. he deduces from the 5-minute lag a recombination rate of approximately 2×10^{-6} cc./sec. However, he attempts to make a similar deduction at 80 km. It is easy to see how this can lead to incorrect results considering the asymmetrical behavior at 80 km. In fact, a rocket launched at +20 min. would probably see little change in electron density at 80 km.

To compare this model with radio sounding data, the same four time cuts are made again (Fig. 9). The general behavior is the same as in Model Q. Following the reflection point for the VLF signal, it can be seen that the reflection height changes by some 6 or 7 km. reaching its peak value some 7 min. after totality. The asymmetrical behavior may be qualitatively seen from the fact that after totality, while the reflection height comes down slowly, the lower D region reforms and produces higher absorption than at the equivalent time prior to totality.

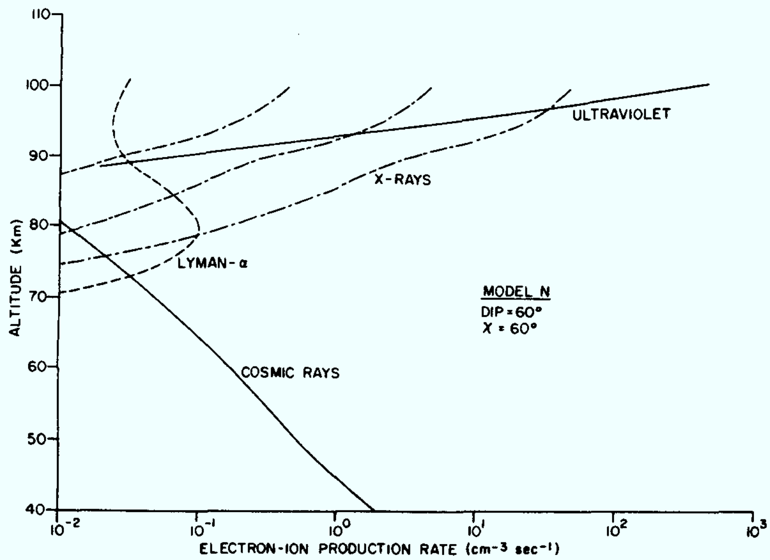
ULTRAVIOLET
X-RAYS
LYMAN-α
MODEL N
DIP = 60°
χ = 60°
COSMIC RAYS
ALTITUDE (Km)
ELECTRON-ION PRODUCTION RATE (cm-3 sec-1)

Fig. 1.

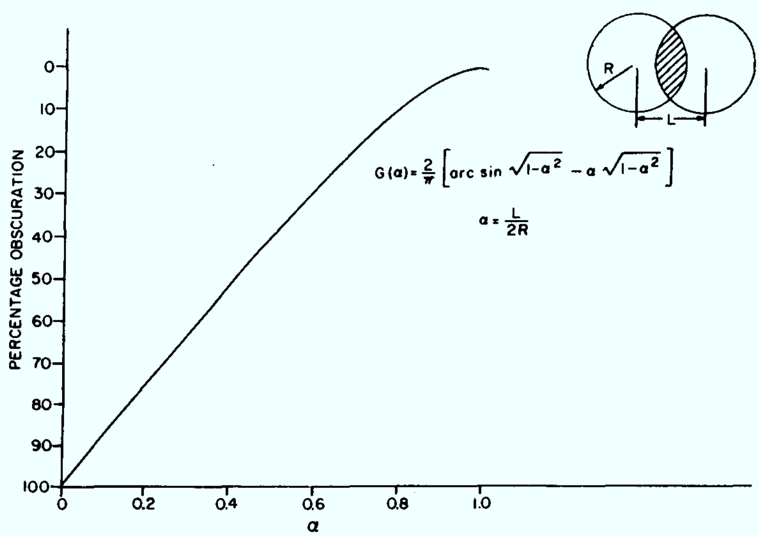
R
L
G(a) = 2/π [arc sin √(1-a²) - a √(1-a²)]
a = L/2R
PERCENTAGE OBSCURATION
a

Fig. 2.

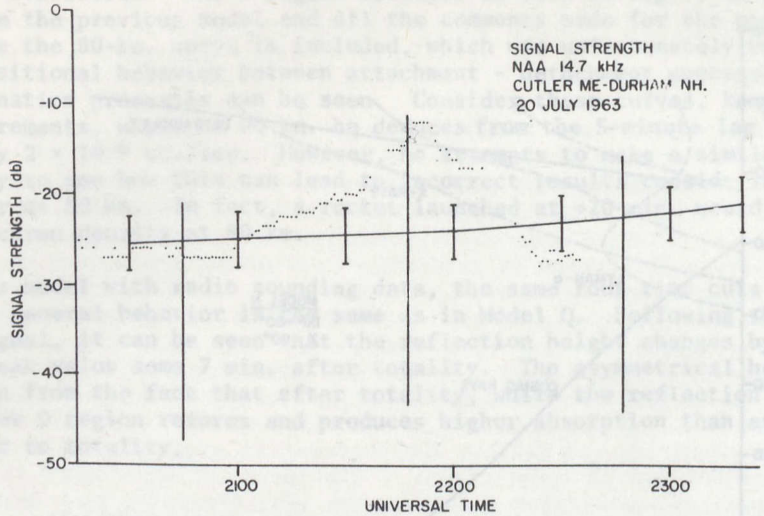
SIGNAL STRENGTH
NAA 14.7 kHz
CUTLER ME-DURHAM NH.
20 JULY 1963
SIGNAL STRENGTH (db)
0
-10
-20
-30
-40
-50
2100
2200
2300
UNIVERSAL TIME

Fig. 3.

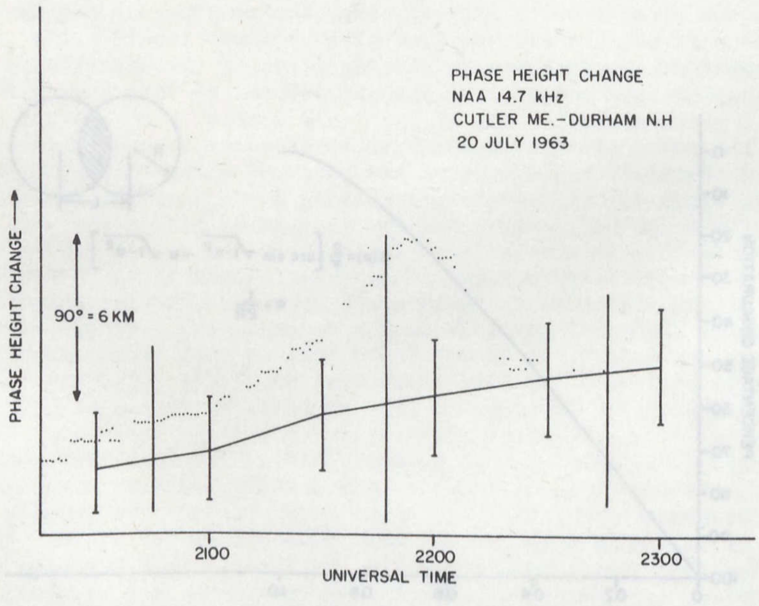
PHASE HEIGHT CHANGE
NAA 14.7 kHz
CUTLER ME.-DURHAM N.H
20 JULY 1963
PHASE HEIGHT CHANGE
90° = 6 KM
2100
2200
2300
UNIVERSAL TIME

Fig. 4.

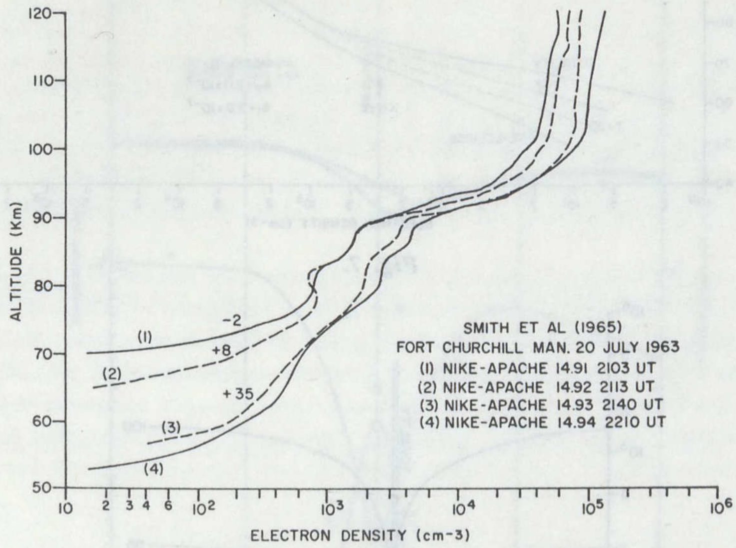

ALTITUDE (Km)
ELECTRON DENSITY (cm-3)
SMITH ET AL (1965)
FORT CHURCHILL MAN. 20 JULY 1963
(1) NIKE-APACHE 14.91 2103 UT
(2) NIKE-APACHE 14.92 2113 UT
(3) NIKE-APACHE 14.93 2140 UT
(4) NIKE-APACHE 14.94 2210 UT
-2
+8
+35

Fig. 5.

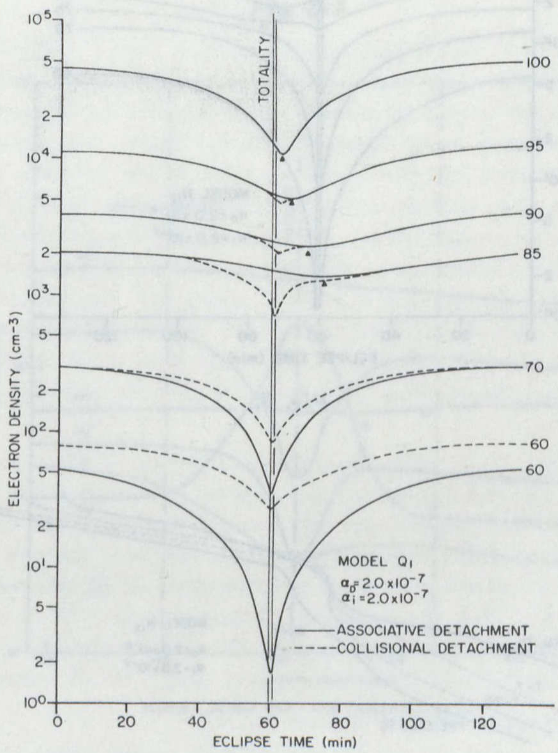

TOTALITY
ELECTRON DENSITY (cm-3)
ECLIPSE TIME (min)
MODEL Q1
$\alpha_D = 2.0 \times 10^{-7}$
$\alpha_i = 2.0 \times 10^{-7}$
ASSOCIATIVE DETACHMENT
COLLISIONAL DETACHMENT
100
95
90
85
70
60
60

Fig. 6.

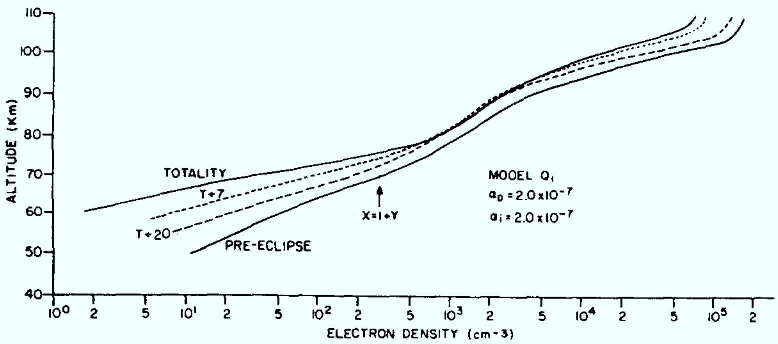

Fig. 7.

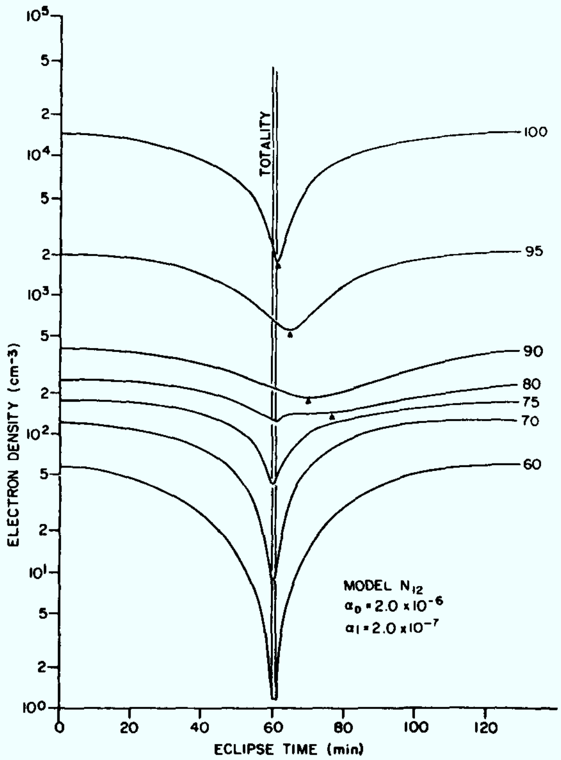

Fig. 8.

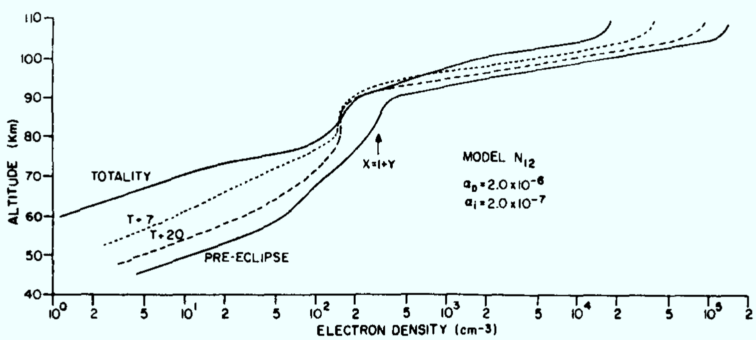

Fig. 9.

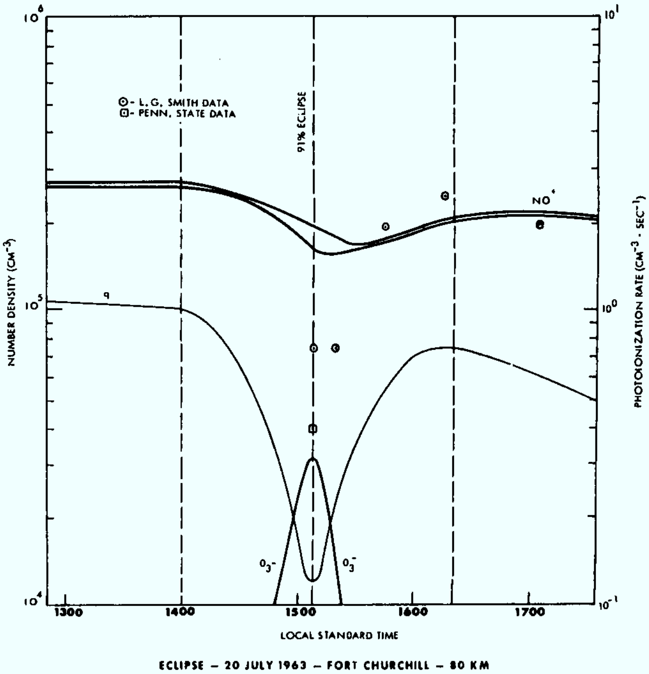

⊙- L.G. SMITH DATA
⊡- PENN. STATE DATA
91% ECLIPSE
NO+
q
O3-
NUMBER DENSITY (CM-3)
PHOTOIONIZATION RATE (CM-3 · SEC-1)
1300
1400
1500
1600
1700
LOCAL STANDARD TIME
ECLIPSE – 20 JULY 1963 – FORT CHURCHILL – 80 KM

Fig. D-1.

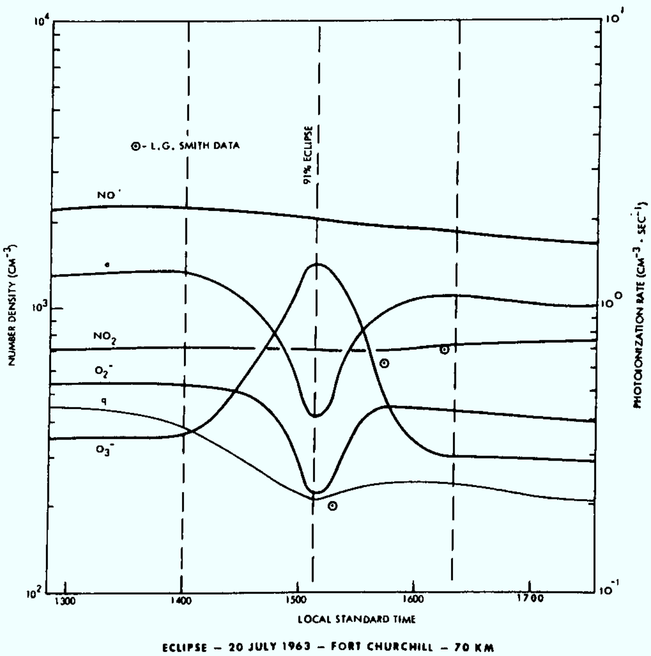

⊙- L.G. SMITH DATA
91% ECLIPSE
NO+
e
NO2
O2-
q
O3-
NUMBER DENSITY (CM-3)
PHOTOIONIZATION RATE (CM-3 · SEC-1)
1300
1400
1500
1600
1700
LOCAL STANDARD TIME
ECLIPSE – 20 JULY 1963 – FORT CHURCHILL – 70 KM

Fig. D-2.

Discussion on Paper 4.2.4 presented by G.S. Sales

Belrose: My first comment concerns the apparent asymmetry in the experimental observations of the abnormal component at 14.7 kc/s. over the 300-km. path. We have not observed an asymmetry of this magnitude in our observations; there was a small asymmetry, because the peak of the effect is not reached for some six minutes after totality. But we cannot discuss the point further here, since our eclipse data are not plotted out on a large enough time scale. We will look at this point later.

The second comment concerns Smith's Langmuir probe data measured at Churchill. We must bear in mind that this is not electron density data, and that it is meaningless to interpret the probe current in terms of electron densities below a height of something like 85 km. It seems that Smith's data is exactly the opposite to what one would expect. At least in my interpretation, the right sort of picture was suggested by Mr. May; that is the C layer stays until the end and major changes are occurring in the D layer. This would be expected with normal diurnal variation. I gather Dr. Sales says that Smith's data suggests the complete disappearance of the C layer, and he seems to end with an interpretation which is at least self-consistent.

Finally, you showed us the data during the eclipse. Can you show us the normal diurnal variation of the phase and amplitude of the 14.7 kc/s. abnormal component over the 300-km. path?

Sales: I can't right now. I do have it, but not with me. It would be a good idea to include these average diurnal variations, for we do have them over a week.

Let me say something about this disappearance of the C layer. I think that May's or Deeks' analysis is totally inconsistent with any physical processes in this lower ionosphere. He says something in his paper about there being a low energy threshold, which implies that almost anything can detach these particles – meaning sunlight can keep these things detached. There is no question that the sunlight is obscured according to the obscuration function and after 20 or 30 min. half the sunlight is gone. If what he says is true then I think that when half the sunlight is gone half the electrons essentially have to be gone, and after 40 min. when three-quarters of the sunlight is gone, three-quarters of the electrons have to be gone. On the other hand if the implication is that it is a collisional process that keeps them detached, then obscuring all the sun doesn't change it and they will never go. You cannot have both. I don't think there is any explanation for that data that is consistent with any processes in this lower ionosphere. I don't think that I have made it just to fit my data. I can either have it all stay and stay all the time, or I can have it disappear according to this fashion, and I am not sure that there is an intermediate case possible.

Pfister: These two figures (Figs. D1 and D2) were presented by Mr. T. Keneshea at the spring URSI meeting in 1965 as an example of his reaction rate program for 15 constituents. In the meantime, Mr. Keneshea has improved his computer program and only recently has rerun the Churchill eclipse with updated values of the reaction rates, which resulted in an improved fit of the new curves with the rocket measurements. The main features of the curves are not changed. At 80 km. the time constant of recombination is responsible for a shift in the minimum electron density. At 70 km. the equilibrium between attachment and photodetachment determines the shape of the electron density curve. Interesting is the rise of O_3^- during the maximum of the eclipse at the expense of O_2^-, which reflects the assumption that photodetachment is the only important removal process for O_3^-.

Megill: This is about the altitude that you would expect excited molecules to start to become important. This is a significant detachment mechanism which is controlled by the ultraviolet light. Its lifetime would be of the order of 30 min. at these altitudes.

LaLonde: Did you say that at 85 km. the electron density profiles didn't change very much?

Sales: Unless you have a very good experiment you might not see any change in electron density for rockets flown from totality to plus 20 min.

Aikin: There is a good deal of evidence in the literature that the positive ion density may exceed the electron density throughout the most of the D region. Did you try different negative ion to electron ratios at different altitudes, to see what this would give you?

Sales: I don't play the game that way. I take the rate equations and put them in, compute an equilibrium value, and then vary the source function.

Aikin: Did you try different rate coefficients?

Sales: No, I did not.

Aikin: Did you take into account any possible variation in neutral constituents, such as atomic oxygen?

Sales: No, I did not. All I can say is I asked Keneshea if he thought atomic oxygen could vary during the eclipse, and he said that he didn't think so and I took it at that. I am sure that at the lower altitudes atomic oxygen will have changed.

Belrose: What we need is better experimental electron density profiles during an eclipse.

4.2.5 DETERMINATION OF A D-REGION NITRIC OXIDE DENSITY PROFILE BY VLF RADIO PROPAGATION

by

D.P. Hayes

Lowell Technological Institute Research Foundation
Lowell, Massachusetts
and
G.S. Sales

Upper Atmosphere Physics Laboratory
Air Force Cambridge Research Laboratories
Bedford, Massachusetts

Presented by D.P. Hayes

1. Introduction

Over the last several years a great deal of speculation has arisen in the literature over the density of nitric oxide in the D region. Fig. 1 shows models postulated by different workers. In each of these models, nitric oxide is considered to be a constant proportion of the atmosphere, i.e., a mixing model is assumed. Of special interest are Curves No. 3 and No. 4, which are taken from Nicolet's latest work (Nicolet 1965). The uncertainty of the nitric oxide profile at these heights is underscored by the fact that Nicolet cites no preference for either one.

This paper will be concerned with a D-region nitric oxide density profile obtained by monitoring the skywave of a 19.8 kHz. CW transmitter at a distance of 190 km. The experiment was conducted during June and early July 1962 at a geomagnetic latitude of 20 degrees. The experimental arrangement consisted of observing the abnormal skywave signal component by means of a loop antenna placed perpendicular to the plane of propagation. Fig. 2 shows nine sunrise and morning variations of the skywave phase lag with respect to ground wave. A small phase height change is initiated somewhat before ground sunrise, and the time and magnitude of this effect exhibit some variability. A repeatable change commences after ground sunrise at a solar zenith angle, χ, of approximately 87 degrees. The apparent height change from ground sunrise to noon is approximately 600 deg., which is equivalent to an 18 km. vertical height change.

An understanding of this VLF skywave phase variation must be based on chemical and ionic production and loss processes in the D region at sunrise. In the D region at least three different ionization processes (Cosmic rays, Lyman-α radiation, and xrays) must be considered.

2. Cosmic Rays

The fact that the experiment was carried out at a relatively low geomagnetic latitude of 20 deg. should be borne in mind, since the latitude dependence of cosmic-ray ionization is quite marked. D-region cosmic-ray ionization at 60 deg. geomagnetic latitude is more than a factor of 10 greater than that produced at 20 deg. This cosmic-ray latitude dependence is of special interest, since almost all previous steep incidence VLF work has been conducted at relatively high geomagnetic latitudes.

A cosmic-ray production model described by Pierce and Arnold (1963) for a geomagnetic latitude of 20 deg. has been utilized in this work.

3. Lyman α

The importance of Lyman-α radiation in ionizing NO in the D region was originally discussed in 1945 by Nicolet and elaborated on in a later paper (Nicolet and Aikin 1960). The ionization rate of NO by Lyman α at a height h is given by

$$Q = n(NO)\ \sigma'_{NO}\ Q_\infty \exp\left(-\int_h^\infty \sigma_{O_2}\ n(O_2)\ dh\right) \tag{1}$$

where σ'_{NO} is the ionization cross section of NO (2×10^{-18} sq. cm.); σ_{O_2} is the O_2 absorption cross section for Lyman α (1.04×10^{-20} sq. cm.) and Q_∞ is the flux of Lyman α incident on the atmosphere. Q_∞ may range anywhere from 3 to 6 ergs/sq. cm./sec. and the former value will be utilized throughout this discussion.

The optical depth is given by

$$\int_h^\infty (\sigma_{O_2})\ n(O_2)\ dh \tag{2}$$

and is set equal to $\left[\sigma_{O_2}\ n(O_2) H\ F\right]$, where H is the scale height and F is the optical depth factor. For solar zenith angles between 0 deg. and 60 deg., F equals sec χ. Ely (1962) computed the optical depth factor as a function of solar zenith angle and height using the ARDC Model Atmosphere and numerically integrating (2). These values have been utilized in this paper.

Fig. 3 exhibits the Lyman-α production rate as a function of altitude and solar zenith angle. Nitric oxide profile No. 1 appearing in Fig. 1 has been used for illustrative purposes. The production for any other NO model may be obtained from these curves by simple multiplication by the appropriate factor.

4. Xrays

The D-region xray ionization rate in the 2 to 10 Å energy range is given by

$$Q = 5 \times 10^7 \int \lambda\ \sigma_\lambda^e\ J_\lambda\ d_\lambda$$
$$J_\lambda = (J_\lambda)_\infty \exp\left(-\int_h^\infty \sigma_\lambda\ n\ dh\right) \tag{3}$$

where J_λ equals the spectral irradiance while σ_λ and σ_λ^e are the absorption and effective total ionization cross sections, respectively. The cross sections utilized are those of Ivanov-Kholodnyy (1965).

This production mechanism is complicated by the fact that the solar flux is highly variable over the solar cycle. Fig. 4 displays three different xray spectra in the 2 to 10 Å range. Spectra No. 2 is representative of fairly quiet periods of solar activity — the conditions that prevailed during the time of our experiment. Spectra No. 1 represents very quiet solar conditions, while Spectra No. 3 would apply for a moderately active sun.

Fig. 5 compares the relative contribution of Lyman α, xrays and cosmic rays near ground sunrise. For illustrative purposes the Lyman-α production curves assume a constant nitric oxide mixing ratio up to an altitude of 90 km. The nitric oxide profiles illustrated are those of Nicolet and Aikin, Clyne and Thrush, and Barth, which are summarized by Aikin, Kane and Troim (1964). The xray curves correspond to the fluxes shown in Fig. 4. Except for the case of the smallest nitric oxide model (QL1), and under conditions of quiet sun, Lyman α dominates xray production at all altitudes below 90 km. at $\chi = 85^{\circ}$.

From this figure we conclude that between 90 and 70 km. under the assumed conditions the production of electrons is first controlled by nitric oxide ionization. Therefore, it is only necessary to consider Lyman α and cosmic rays in order to explain VLF sunrise effects under solar conditions appropriate to our experiment.

Consider now the variation of electron density at a particular altitude as a function of time. The D region can be characterized by a set of rate equations for the electron and ionic components which take the following form:

$$\frac{dN_e}{dt} = Q - \alpha_D N_e N^+ - \beta N_e + \gamma N^- + \rho N^-$$

$$\frac{dN^-}{dt} = -\alpha_i N^- N^+ + \beta N_e - \gamma N^- - \rho N^-$$

$$N^+ = N_e + N^-$$

where

α_D = dissociative recombination coefficient

α_i = ion-ion recombination coefficient

β = attachment coefficient

γ = detachment coefficient (collisional and associative)

ρ = photodetachment

Q = electron-ion pair production rate

At the various altitudes under consideration the Lyman-α ionization rate was calculated for solar zenith angles ranging between 94 deg. and 0 deg. and the preceding pair of simultaneous differential equations were numerically solved.

The rate coefficients utilized in this work appear below in tabular form.

TABLE 1. Reaction Rate Coefficients as a Function of Altitude

Altitude (km.)	α_D cc./sec.	α_i cc./sec.	γ per sec.	β per sec.	ρ per sec.
70	6×10^{-7}	2×10^{-7}	1.4×10^{-2}	3.9×10^{-1}	0.1
75	6×10^{-7}	2×10^{-7}	2.4×10^{-2}	8.8×10^{-2}	0.1
80	6×10^{-7}	2×10^{-7}	4.5×10^{-2}	1.9×10^{-2}	0.1
85	6×10^{-7}	2×10^{-7}	3.9×10^{-1}	4.1×10^{-3}	0.1
90	6×10^{-7}	2×10^{-7}	9.5×10^{-1}	1.9×10^{-3}	0.1

The values used essentially conform with those published recently by Cole and Pierce (1965). Note that a dissociative recombination coefficient of 6×10^{-7} cc./sec. was used throughout the height range investigated.

The time varying solution of the rate equations depends on the nitric oxide profile chosen. The NO profile was adjusted until the time variation of electron density was in satisfactory agreement with the VLF data appearing in Fig. 2. The reflection of the VLF wave is considered to take place from the $X = 1 + Y$ level. At the geomagnetic latitude of the experiment, $X = 1 + Y$ is approximately 250 electrons/cc.

The nitric oxide profile obtained appears in Fig. 6. The most recent mixing models postulated by Nicolet (1965) also appear in the figures for purposes of comparison. It was found that neither of Nicolet's models considered separately could account for electron density variations in satisfactory agreement with VLF data. Nicolet's lower density model satisfactorily describes electron density variations at low altitudes but is unsatisfactory above 80 km.; while the other mixing model gave good agreement at the higher altitude but produced too much ionization near 70 km. By trial and error the starred nitric oxide model was obtained.

Also appearing in the diagram is an ionic reaction model proposed by Nicolet to give satisfactory agreement with Barth's measured value of the total nitric oxide content.

Using this new NO model yields the electron density profiles shown in Fig. 7 as a function of solar zenith angle. At $\chi = 94$ deg. the presence of the cosmic-ray C layer is apparent. As Lyman α penetrates into the D region at later times, the increase in electron density at lower heights is evident. Fig. 7 shows that the $X = 1 + Y$ level is located in the vicinity of 90 km. before layer sunrise. A rapid decrease in phase height takes place until $\chi = 75$ deg.; the downward motion of the reflection level virtually ceases after $\chi = 55$ deg.

Fig. 8 displays the measured phase height variation superimposed on the altitude and time variation of the $X = 1 + Y$ level deduced from the NO profile described in this paper.

5. Conclusions

A nitric oxide density profile has been obtained by solving the ionization density rate equations and utilizing experimental VLF data.

The work described in this paper is still of a preliminary nature. The effect of varying the reaction rate coefficients is being thoroughly investigated. The validity of using the $X = 1 + Y$ condition to describe the main reflection level is currently being examined by numerical analysis of the full wave equations.

6. Acknowledgment

The research of one of the authors was sponsored by the Air Force Cambridge Research Laboratories under Contract No. AF19(628)-4801.

REFERENCES

Aikin A., J. Kane and J. Troim. Some results of rocket experiments in the quiet D region. J. Geophys. Res. 69, (No. 21): 4621-4628, 1964.

Cole, R and E. Pierce. Electrification in the earth's atmosphere for altitudes between 0 and 100 kilometers. J. Geophys. Res. 70 (No. 12): 2735-2749, 1965.

Ely, J. Atmospheric depth and effective solid angle for radiation penetrating the atmosphere. Air Force Cambridge Res. Lab., AFCRL-62-260, Geophys. Res. Paper No. 74. 1962.

Ivanov-Kholodnyy, G.S. Ionization mechanism of the lower ionosphere, I. Geomagnetism and Aeronomy 5, (No. 4): 544-556, 1965.

Nicolet, M. Ionospheric processes and nitric oxides. J. Geophys. Res. 70 (No. 3): 691-702, 1965.

Nicolet, M. and A. Aikin. The formation of the D region of the ionosphere. J. Geophys. Res., 65: 1469-1483. 1960.

Pierce, E. and H. Arnold. The ionosphere below 100 km. (D region). Interim Tech. Report 6, Contract DA-36-039-SC-87197, Stanford Research Institute.

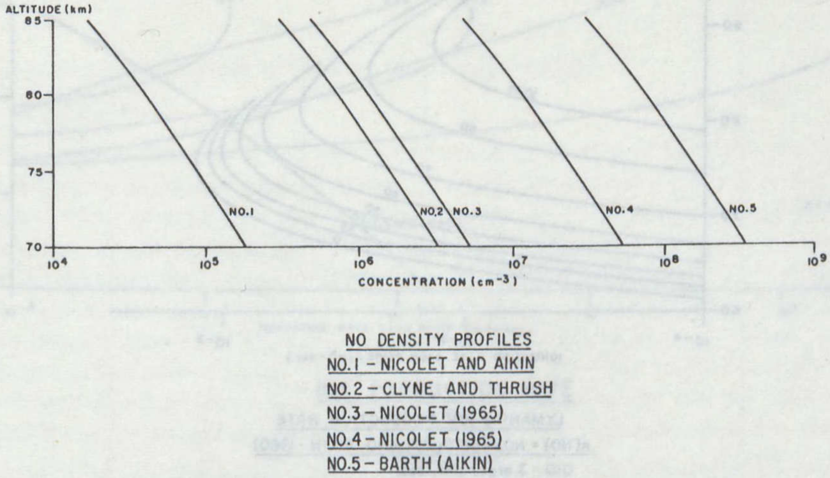

Fig. 1. Comparison of some nitric oxide profiles appearing recently in the literature.

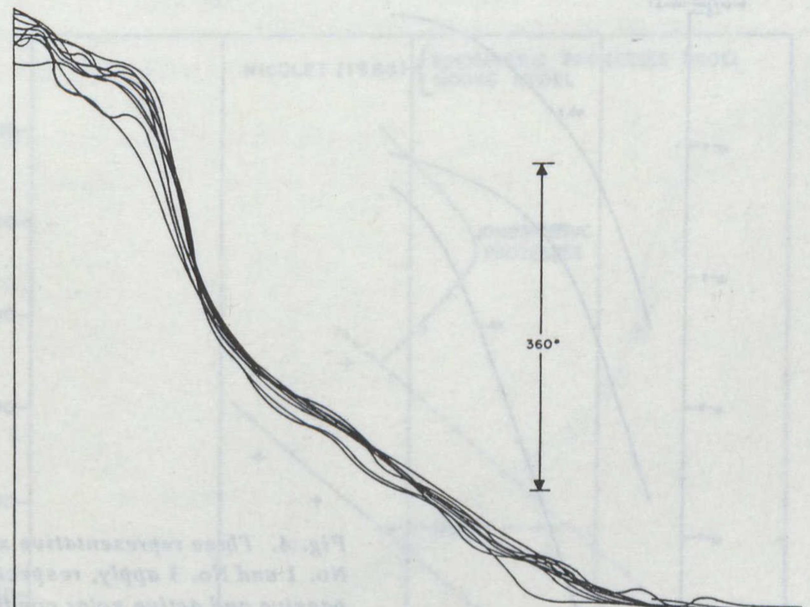

Fig. 2. Nine representative curves displaying the phase of NPM (19.8 kHz.) abnormal skywave component with respect to ground wave. The transmitter-receiver separation was 190 km. and the experiment was conducted during June and early July 1962. Ground sunrise time (GSR) is also shown.

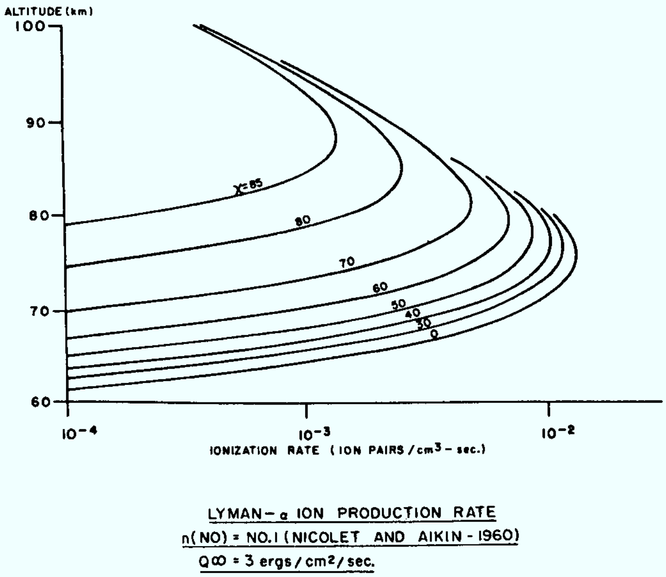

Fig. 3. Ionization rate of nitric oxide by Lyman α as a function of altitude and solar zenith angle (χ). Profile No. 1 appearing in Fig. 1 was used to represent the density of NO.

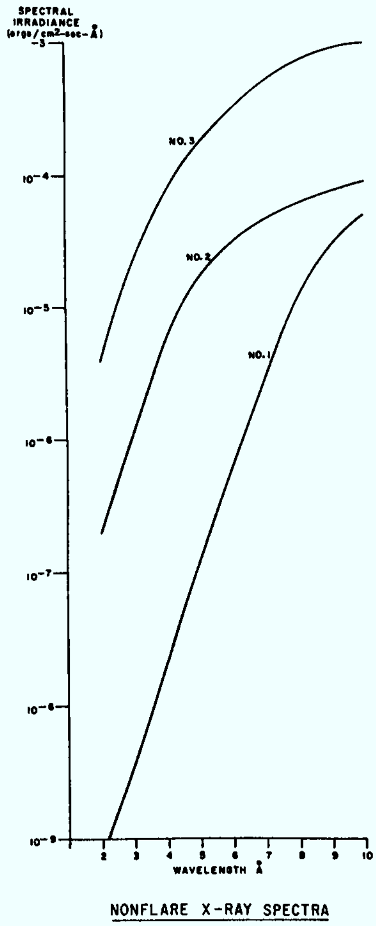

Fig. 4. Three representative xray spectra. No. 1 and No. 3 apply, respectively, for passive and active solar conditions. No. 2 is representative of conditions prevailing during June and early July 1962.

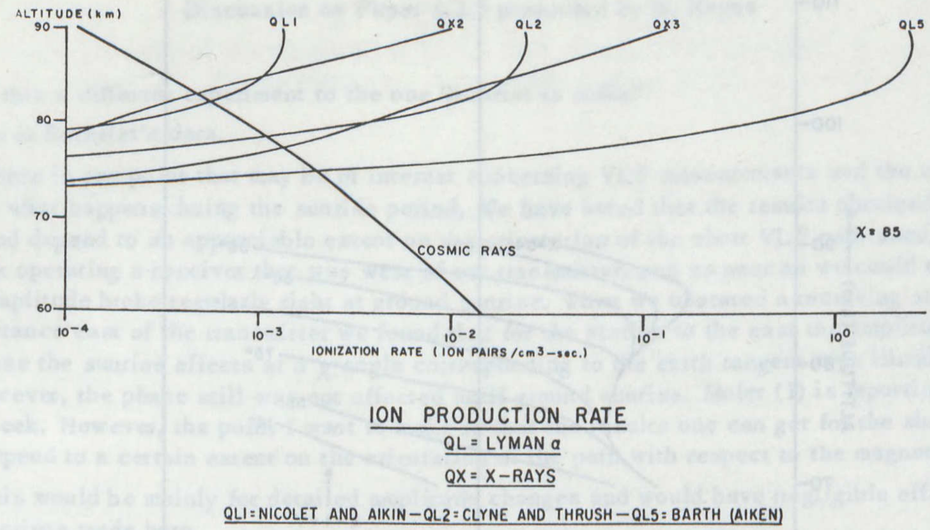

Fig. 5. Comparison of ionization production rate due to Lyman α, xrays, and cosmic rays. Curves QL1, QL2 and QL5 correspond to NO profiles No. 1, No. 2, and No. 5 appearing in Fig. 1. Curves QX2 and QX3 correspond to xray spectra No. 2 and No. 3 appearing in Fig. 4.

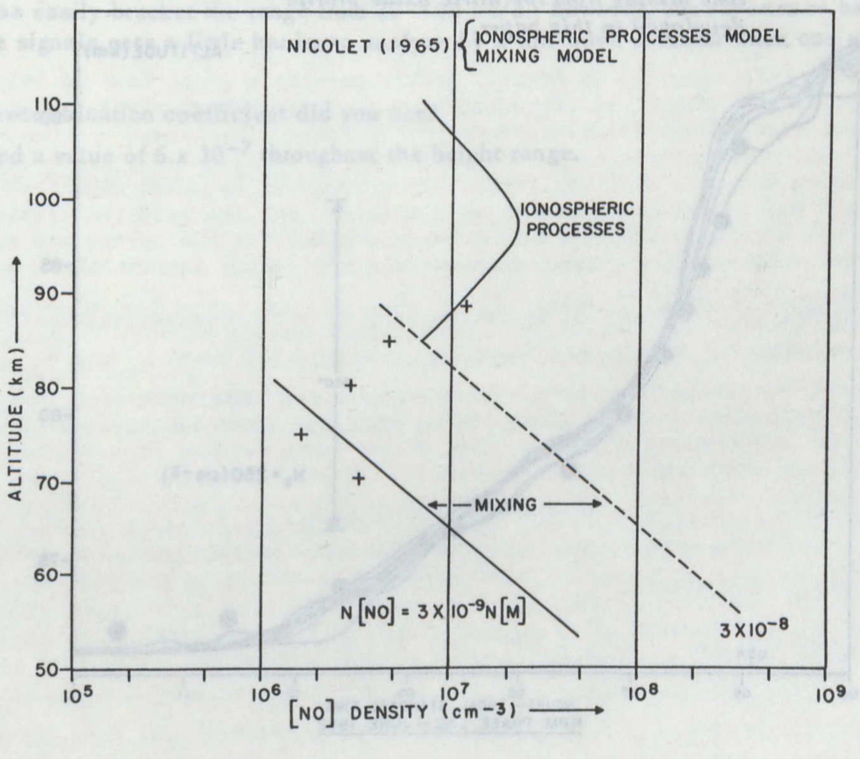

Fig. 6. Nitric oxide density in the D region. The ionospheric processes and two mixing models of Nicolet (1965) are compared with the NO profile developed in this paper (+).

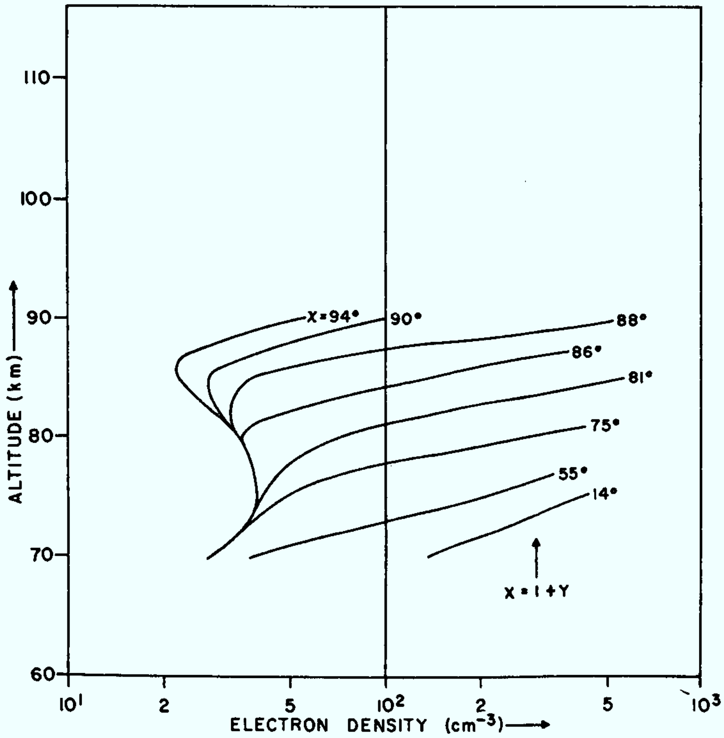

Fig. 7. Electron density profiles as a function of time arising from the nitric oxide profile developed in this paper.

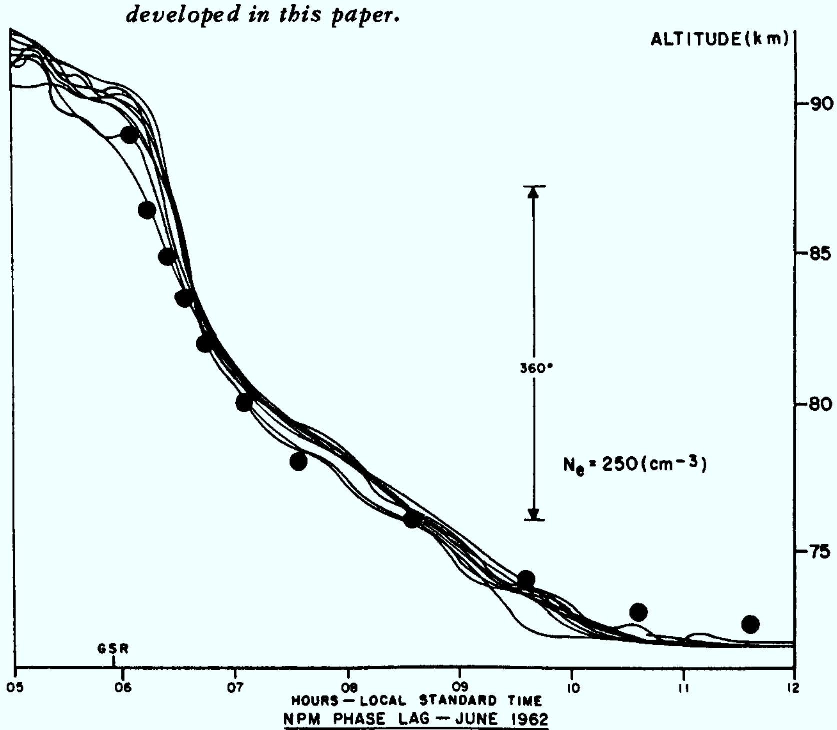

Fig. 8. Phase height change deduced from the NO profile developed in this paper (dots) superimposed on Fig. 2.

Discussion on Paper 4.2.5 presented by D. Hayes

Belrose: Is this a different experiment to the one Sechrist is doing?

Hayes: This is Sechrist's data.

Gossard: There is one point that may be of interest concerning VLF measurements and the use of them to determine what happens during the sunrise period. We have noted that the results obtained over the sunrise period depend to an appreciable extent on the orientation of the short VLF path used. For some time we were operating a receiver that was west of our transmitter, and as near as we could tell both the phase and amplitude broke regularly right at ground sunrise. When we operated a receiving station at the same distance east of the transmitter we found that for the station to the east the amplitude trace began to sense the sunrise effects at a χ angle corresponding to the earth tangent rays illuminating the E layer. However, the phase still was not affected until ground sunrise. Moler (1) is reporting on this at URSI next week. However, the point I want to make is that the results one can get for the short path VLF links may depend to a certain extent on the orientation of the path with respect to the magnetic field.

Belrose: This would be mainly for detailed amplitude changes and would have negligible effect on the sort of comparison made here.

Gossard: I am sure that is right. It permits us to get a tight figure on the number of electrons photodetached by the visible rays.

Belrose: Dr. Gossard has a good installation and I would like him to consider making measurements at higher frequencies – say from 10 to 70 kc/s.

Gossard: We are transmitting simultaneously at three frequencies; 13.2 kc/s., 23.2 kc/s. and 35.2 kc/s. We could just as easily bracket the range from 10 – 70 kc/s.; however, our experience has been that the behavior of the signals gets a little harder to analyze by a full wave solution when one gets up near 70 kc/s.

Swider: What recombination coefficient did you use?

Hayes: We used a value of 6×10^{-7} throughout the height range.

1. Moler, W.F., *Non-reciprocal VLF wave propagation over short paths during sunrise*, presented at the 1966 Spring USNC-URSI Meeting, 18 to 21 April, also appears as a contributed paper in these Proceedings.

4.2.6 THE STRUCTURE OF THE ATMOSPHERE NEAR 90 KM. FROM SHORT PATH VLF MEASUREMENTS

by

E.E. Gossard

U.S. Navy Electronics Laboratory, San Diego, California

1. Introduction

A short transmission path near Sentinel, Arizona has been used to study the nature of the ionization irregularities in the nighttime D region. The angle of incidence is 30° off vertical, and a triangle of receiving stations about 16 km. on a side was used to obtain direction, velocity, and size of irregularities.

2. Correlograms of Phase and Amplitude

An analytical technique due to Bowhill (1961) permits a great deal of information about D region irregularities to be extracted from a comparison of phase and amplitude statistics. Bowhill considers two specific kinds of reflecting screen — a phase screen and an amplitude screen. Irregularities in the phase screen modulate only phase and those in the amplitude screen modulate only amplitude. As a receiver is moved away from either screen, both phase and amplitude fluctuations are noted, but the relative statistics of phase and amplitude depend on the distance in wavelengths from the screen and the size of the irregularities. Thus much information about the reflecting screen can be obtained.

Bowhill assumes the D region to be represented by a two-dimensional Gaussian auto correlogram of the form $\rho_o(\xi,\zeta) = \exp\left[-\{(\xi/2D_1)^2+(\zeta/2D_2)^2\}\right]$ where D_1 and D_2 are the structure sizes of the diffracting screen in the x and y directions respectively. The correlograms for both phase and amplitude of the radio wave are likewise Gaussian far from the screen, but at intermediate distances they depart considerably from Gaussian and another definition of structure size is required. Bowhill suggests d_1, d_2 defined as $d_1, d_2 = -\{\partial^2\rho/(\partial\xi,\zeta)^2\}^{-\frac{1}{2}}$. For a Gaussian correlogram $d_1, d_2 = D_1, D_2$. For a non-Gaussian correlogram, d_1, d_2 is the structure size of the Gaussian correlogram that would fit the actual correlogram at the origin.

Bowhill calculates (d/D) for an amplitude screen and a phase screen, and RMS_{amp}/RMS_{phase} as a function of dimensionless distance ($a = \lambda\, z/\pi\, D^2\cos\theta_o$) from an isotropic screen. θ_o is the oblique angle of incidence. A comparison of the experimental and calculated values is shown in the following table:

		$\bar{a}$	Amplitude Screen d	Amplitude Screen RMS Ø / RMS A	Phase Screen d	Phase Screen RMS Ø / RMS A	Measured d	Measured RMS Ø / RMS A
13 kc	Phase	2.5	10.5	0.85	13.4	1.17	15.5	1.93
	Amp		13.4		10.5		9.0	
23 kc	Phase	3.2	7.4	0.92	8.6	1.08	9.0	1.77
	Amp		8.6		7.4		7.0	

The measured values of d are taken from Fig. 1 and divided by 2 to obtain the corresponding size at the reflector. The distance from the screen z is likewise divided by 2 (e.g. 45 km.) to account for the point source being at the ground rather than infinity. The solid curve is the median temporal auto correlogram fitted to the spatial data.

It is seen that the measured quantities agree much more nearly with a phase screen than with an amplitude screen and that Bowhill's calculations somewhat underestimate the difference between the variance and structure size of the phase fluctuations and the amplitude fluctuations. A possible reason for this discrepancy may be seen when the power spectrum is considered.

3. Power Spectra of Phase and Amplitude

Bowhill's analysis leads to the following relation between phase spectra, W_p, and amplitude spectra, W_a. He finds for a phase screen that

$$W_p = W_o \cos^2 [\pi/\lambda \{(C_2 - C_o)z + (C_1 - C_o)z\}] \text{ and}$$

$$W_a = W_o \sin^2 [\pi/\lambda \{(C_2 - C_o)z + (C_1 - C_o)z\}],$$

where W_o is the angular power spectrum at the screen, and where

$$C_1 = \{1 - (S_o + \nu)^2 - \chi^2\}^{\frac{1}{2}} \text{ and } C_2 = \{1 - (S_o - \nu)^2 - \chi^2\}^{\frac{1}{2}}.$$

S_o is the sine of the oblique angle of incidence and ν and χ are the sines of the perturbed angle of incidence in and normal to the plane of incidence. Bowhill's expressions have here been modified to include oblique propagation. Therefore the spectrum at the screen can be found as $W_o = W_p + W_a$. The median spectra of 15 nights of data are shown in Fig. 2. It is pointed out that these are time spectra rather than spatial spectra and any conclusions to be drawn from them depend on the assumption of similarity between spatial and temporal correlograms.

The spectra show certain interesting features. First, they do not appear to be Gaussian, but are approximately linear on a log-log plot, as might be expected from spectra due to turbulence at the reflector. This may partially explain why Bowhill's calculations underestimate the observed amplitude-phase differences. Secondly, instead of an $f^{-5/3}$ spectrum as would be expected from turbulence in an incompresible fluid, the slope is more nearly that of an $f^{-7/3}$ spectrum as would be expected if the turbulence were dominated by compressibility. Finally, the median spectra show a tendency to "bulge" at a period of 5 to 6 min.

4. Cross Spectrum Analysis and Internal Waves

Many individual power spectra show clear evidence of oscillations of fairly high q. Part of such a record is shown in Fig. 3, and its power spectrum (the average of the three receivers) is shown in the top frame of Fig. 4. Four lines are clearly evident in the power spectrum at periods of 23, 6.25, 3.85 and 2.49 min. Records from the three stations were subjected to cross spectrum analysis.

Cross spectra consist of the spectrum of the "in phase" components in two records, called the co-spectrum, $C(\omega)$, and the spectrum of the out-of-phase components, called the quadrature spectrum, $Q(\omega)$. They are related by $\tan \omega\tau = Q(\omega)/C(\omega)$ where ω is the fading frequency and τ is the time lag of the component of frequency ω. Thus the C_o and quadrature spectra shown in the lower frames of Fig. 4 permit the isolation of the various Fourier components in the records over the triangle., and their speed and direction of movement can be obtained.

Experience has shown that the flow is fairly consistent over a period of about 2 hours and the records are fairly time-stationary statistically. The records analyzed for waves are therefore 2 hours long. The long period flow patterns are extremely variable, and longer samples tend to smear the results.

The spectral line at a period of 23 min. is undoubtedly due to internal gravity waves traveling toward the east-northeast (78.5^o) at a speed of 100 mps. The other lines are not compatible with wave theory and another explanation must be sought.

5. Conclusions

(1) The lower ionosphere causes a phase modulation rather than an amplitude modulation of VLF radio waves.

(2) The scale size of the ionospheric irregularities is about 12 km. at 13 kc. and 8 km. at 23 kc. when referred to the $e^{-\frac{1}{2}}$ point of the correlogram.

(3) A Gaussian assumption for the correlogram of ionospheric irregularities may be significantly in error.

(4) The angular power spectrum is approximately proportional to $f^{-7/3}$ for both 13 kc. and 23 kc., suggesting a basically turbulent regime whose density fluctuations are dominated by adiabatic compressibility.

(5) Evidence of internal waves is frequently observed, indicating typical phase velocities of 50 to 100 mps.

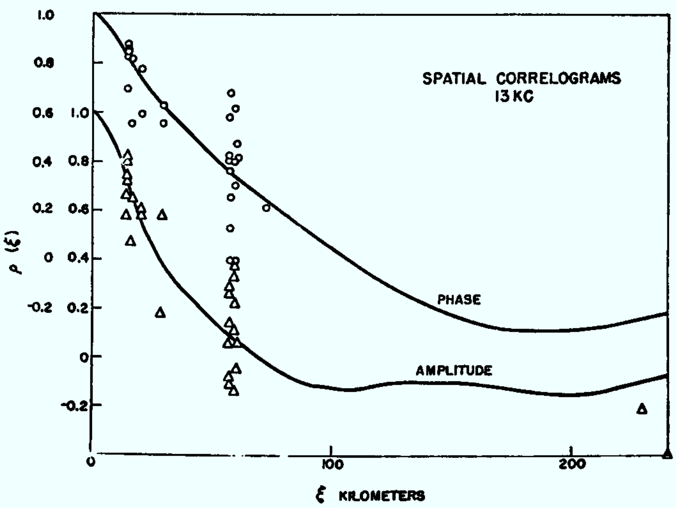

Fig. 1.

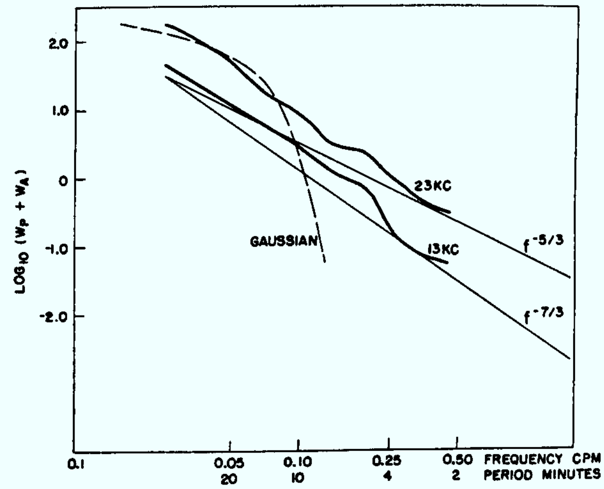

Fig. 2.

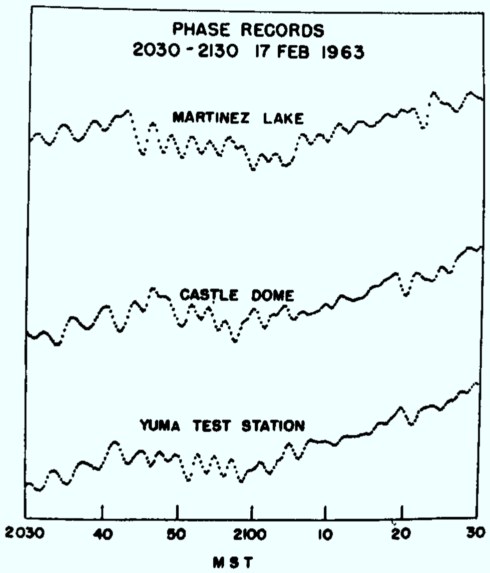

Fig. 3.

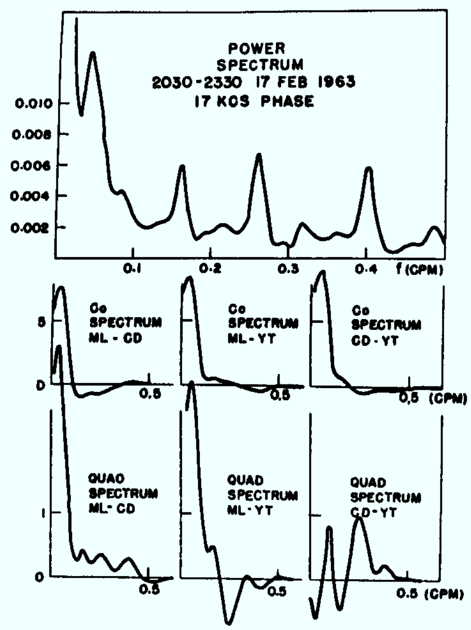

Fig. 4.

Discussion on Paper 4.2.6 presented by E.E. Gossard

Georges: I would like to mention the results of some CW doppler soundings done at vertical incidence at 3.3 and 4 Mc. by Dr. Davis of our laboratory. These were made several hours before sunset on 11 November, 1965, and the interesting feature is that there is a slight phase lag between corresponding features on 4 and 3 Mc., which indicates a vertical propagation of whatever disturbance is causing it – at least the vertical component of that velocity. If true reflection height is calculated for the two frequencies and time lag measured between the two – which is a minute – a vertical component of the velocity is obtained that is remarkably close to the sound velocity at that height. I have no information on any possible horizontal velocity components.

Gossard: That does point up one big difference between his observations and ours. The velocity of propagation across our grid of stations was relatively slow, of the order of 100 mps., whereas if the vertical component of Dr. Georges' phenomenon has acoustic velocities the horizontal velocity would probably be tremendous, depending on how much the tilt of the phase front was. His would almost have to be Lamb waves if one is talking about a vertically propagated acoustic wave across the density gradient. I think that if that could be verified, he would have his tied down.

Georges: It might be worth noting that some unusual infrasonics events were noted at the same time at Boulder.

4.2.7 NON-RECIPROCAL VLF WAVE PROPAGATION OVER SHORT PATHS DURING SUNRISE*

by

W.F. Moler

U.S. Navy Electronics Laboratory, San Diego, California

Abstract

VLF transmissions at 8.2, 13, 17, and at 23 kHz. from the US Navy Electronics Laboratory VLF transmitter at Sentinel, Arizona (32^{o}N. lat.) were received at sites about 100 km. geomagnetically east and west of the transmitter. The data, recorded periodically over several years, show that the observed phase and amplitude changes are not only a function of the radio frequency but the non-reciprocal propagation effects resulting from the anistrophy of the ionosphere are also important. When the wave propagation is from east to west, the phase advance associated with daybreak is delayed until ground sunrise for 13, 17, and 23 kHz. transmissions. At 8.2 kHz. and for propagation from west to east, the phase excursion begins when the solar zenith angle is 98^{o}. For propagation in either direction the diurnal amplitude fade begins when the solar zenith angle is near 98^{o}. The total diurnal phase-height change also shows a dependence on the direction of propagation.

A dynamic model of electron density changes over sunrise must explain the various propagation features summarized in the conclusion of the paper. While a realistic model has not been developed, an artificial model has been assumed and sample full wave numerical calculations are made, which demonstrate that the apparent sunrise phase and amplitude onset times would depend on the polarization and direction of propagation of the received waves.

In the early 1950s a group at the Cavendish Laboratory, Cambridge University, made extensive measurements of GBR 16 kHz. transmissions over short propagation paths. They obtained a wide variety of information about the D region. Since then, many other investigators have been using similar techniques in attempts to solve problems of D-region aeronomy.

---

*Paper presented at the USNC-URSI/IEEE 1966 Spring Meeting 18-21 April. The data contain much information relative to the change of electron density with time over the sunrise period, and demonstrate that VLF phase changes over sunrise should not be interpreted as being entirely due to a change in reflection height, especially at the lowest frequencies. The paper is published in this *Proceedings* by the kind permission of the author.

Much effort has been expended in attempts to identify the dominant negative ion species important for electron attaching and detaching processes at D-region heights. The methods used are indirect and results are obtained by inference only. One technique is to observe the phase and amplitude of once-reflected VLF skywaves during the sunrise period at ionospheric heights. It is assumed that, at the onset of photodetachment at and below the height of the ambient reflection level, the increase in electron density will produce a change of phase and/or amplitude of the received signal. If the time of this onset is obtained precisely, one may (by knowing the available photon energy at the detaching height) deduce the threshold detaching energy and, by inference, the identity of the negative ion involved. In principle the experiment is straightforward, but in practice it is difficult to establish onset times and even more difficult for one researcher to obtain data that are in agreement with those of other researchers.

The difficulty lies, not so much in a day-to-day or location-to-location variation of onset time with respect to solar angle, but in the inability to recognize the onset time from the records. The onset time may be obscured by the random phase and amplitude fluctuations normally observed over short paths before ground sunrise. Until the randomness is removed by averaging over many observations, the onset time appears to be widely varying.

A second difficulty, and one that will be discussed here, arises from the mechanics of wave propagation and reflection in an anisotropic medium. Data will be presented that shows that the behavior of the received signal during the sunrise period is not only frequency dependent, but depends on the wave polarization and the direction of propagation as well.

The data were obtained by the NEL VLF ionospheric sounding system in Arizona. Fig. 1 is a map of southwestern Arizona, which shows the transmitter location at Sentinel and the receiver sites at Castle Dome and Gu Komelik. Castle Dome is 107 km. magnetically west and Gu Komelik is 120 km. magnetically east of the transmitter.

The transmitting system consists of a 30 kw. broadband power amplifier and a half-wave horizontal dipole antenna which is resonant at 14.4 kHz. Switches are opened to shorten the antenna for resonance at higher frequencies and loading coils added for lower frequencies or for fine tuning. Two identical orthogonal antennas are available but, for the data to follow, only the antenna in the local magnetic meridian was used. Such an antenna provides a deep null in the vertically polarized field normal to the antenna axis at its center. A rapidly attenuating horizontally polarized ground wave component exists broadside to the antenna which becomes negligibly small 3 to 4 wavelengths from the transmitter. The bulk of the radiated power is horizontally polarized and is a maximum in the vertical.

Two phase and amplitude recording receivers were located at each site. One tracked the normal (horizontally polarized) component of the once reflected skywave and the other the abnormal (polarized in the plane of propagation) component of the skywave. In the illustrations the curves of phase and amplitude with time are identified by $_{\perp}R_{\perp}$ for the normal component and $_{\perp}R_{\parallel}$ for the abnormal component. Transmissions were monitored on 8.2, 13, 17, and 23 kHz. periodically during 1961-62-63 and 1964. The curves presented in Figs. 2 to 9 are averages of records obtained during this period. The largest data sample was obtained at 13 kHz. and the smallest at 8.2 kHz. Also the bulk of the data were obtained during periods when the solar zenith angle χ was greater than 80^{o}.

Fig. 2 shows the average apparent relative height and amplitude change of the normal component of the 23 kHz. transmissions as a function of χ. Of interest is the slow phase advance beginning near $\chi = 100^{o}$ with an abrupt advance beginning at ground sunrise ($\chi = 90^{o}$). The only evidence of non-reciprocal effects is the striking difference in amplitude for solar angles greater than 90^{o}.

Fig. 3 shows the average diurnal behavior of the abnormal component of the 23 kHz. transmissions. Four significant features appear in the records: (1) a slight phase advance beginning near $\chi = 100^{o}$; (2) a rapid phase advance at $\chi = 90^{o}$; (3) a rapid decrease in signal amplitude beginning at $\chi = 90^{o}$; (4) a difference in the signal level and diurnal change of signal between the two directions of propagation.

Evidence of non-reciprocal propagation in the phase records appears in Fig. 4, the plots of the diurnal behavior of the normal component of the 17 kHz. transmissions. For W-E propagation the rapid phase advance began at $\chi = 90^o$, whereas for E-W propagation a slow variation of phase began at $\chi = 100^o$ and a rapid advance at $\chi = 90^o$. There were not enough good quality data (because of instrument failures) to make a meaningful presentation of the W-E amplitude data. The E-W amplitude shows that the large amplitude fade begins for $\chi = 98^o$.

Fig. 5 shows the diurnal behavior of 17 kHz. abnormal propagation. Of interest is the phase advance beginning at $\chi = 100^o$ for W-E propagation, with a change in slope at $\chi = 99^o$ and $\chi = 90^o$. For E-W propagation the maximum phase change begins at ground sunrise. The amplitude trace shows the non-reciprocal nature of the wave propagation during the sunrise period.

The largest quantity of experimental data is represented in Figs. 6 and 7, which show the diurnal behavior of the normal and abnormal components of the 13 kHz. transmissions. The non-reciprocal propagation characteristics are clearly evident from the normal component records. For W-E propagation the diurnal phase and amplitude change begins abruptly at $\chi = 98^o$, whereas the E-W traces show a slight backing of phase and decrease of amplitude at $\chi = 100^o$, with an abrupt phase advance at $\chi = 90^o$. In addition the magnitude of the phase and amplitude changes is much greater for E-W propagation. For the abnormal component the major diurnal phase advance begins for $\chi = 98^o$, and the major diurnal amplitude change occurs between $\chi = 98^o$ and $\chi = 90^o$. There is slight evidence for non-reciprocal propagation effects from the abnormal polarization records.

Figs. 8 and 9 show the diurnal behavior of the normal and abnormal components of the 8.2 kHz. transmission respectively. Of principal interest is the apparent diurnal onset time at χ slightly greater than 100^o.

There were insufficient data to obtain the normal polarization record for W-E propagation at 8.2 kHz. so that an evaluation of non-reciprocal effects was not obtained to date.

From the rather confusing experimental data it is possible to abstract the propagation characteristics that a dynamic sunrise model of the ionosphere must be able to produce when tested in a computer.

The test consists of calculating by numerical methods a full wave solution for wave propagation through and reflection from an arbitrary continuous anisotropic and lossy ionosphere. Models are tested in the computer until one is found that predicts reflection and conversion coefficients that agree with measurements. A dynamic model would consist of a set of models that vary with solar time. The characteristics that such a set must produce (for the propagation geometry shown in Fig. 1) are as follows:

(1) At χ near 100^o, enough electrons must be placed below the pre-sunrise ambient reflection height to produce a phase advance on both polarizations at 8.2 kHz. and a slight increase in the conversion coefficient at 13 kHz.

(2) At $\chi = 98^o$, a decrease in both the reflection and conversion coefficients must begin for 23, 13, and 17 kHz. waves. The phase must begin an advance for 13 and 17 kHz. for W-E propagation and back for 13 kHz. E-W propagation.

(3) At $\chi = 90^o$, a rapid phase advance begins for E-W propagation at 13 and 17 kHz. and for both polarizations and directions of propagation at 23 kHz. In addition, the conversion coefficient of the 13 kHz. waves must show a minimum in the diurnal curve for both directions of propagation and a minimum of the reflection coefficient for W-E propagation.

Although such a model has not yet been developed, it is of some interest to observe how anisotropy in the ionosphere may produce a strikingly different signal behavior during a sunrise period, depending on the wave polarization and the direction of propagation. The model selected for test (Fig. 10) is highly artificial but helps to illustrate a point.

Reflection and conversion coefficients are calculated for a sharply bounded ionosphere based at 92 km. and then repeatedly as a series of slabs containing 28 electrons per cc. are added sequentially below the main layer until the tenuous layer is at 66 km. Calculations are performed for both E-W and W-E propagation for the transmission link geometry and geomagnetic conditions operative during the Arizona measurements. The reflection coefficients for vertically polarized transmissions are shown in Fig. 11 for comparison. The results of the calculations are shown in Figs. 11, 12, and 13. If it is assumed that the height of the layer is a function of the solar zenith angle, it is clear that the apparent sunrise phase and amplitude onset times would depend on the polarization and direction of propagation of the received waves.

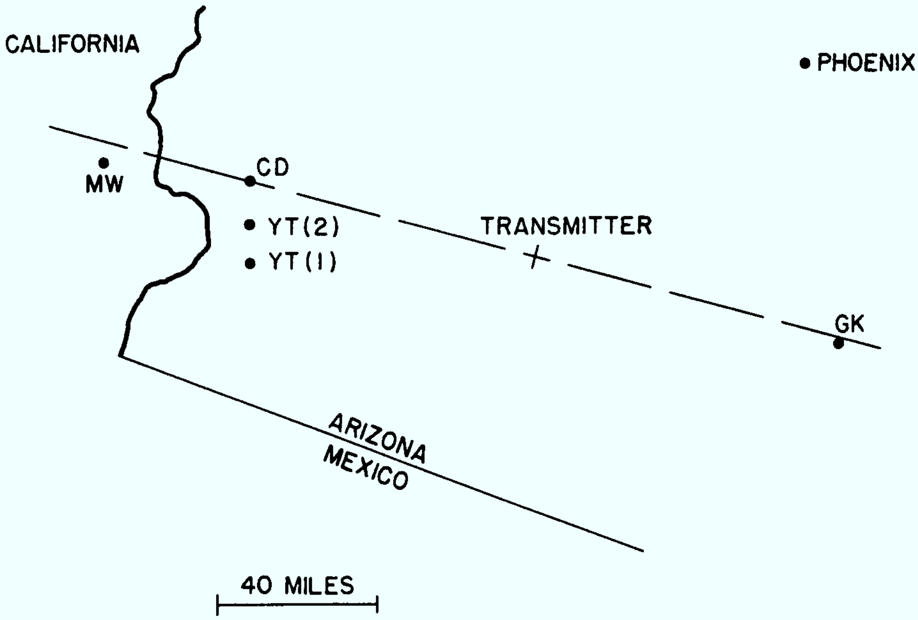

Fig. 1. Map of Arizona showing the transmitter location at Sentinel and receiver locations at Castle Dome and Gu Komelik.

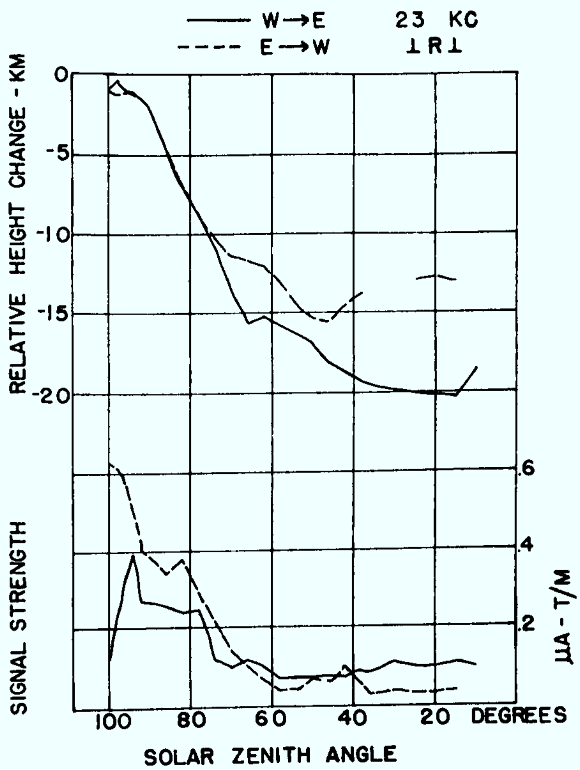

Fig. 2. The apparent relative reflection height and amplitude as a function of solar zenith angle χ for the normal component of 23 kHz. transmissions.

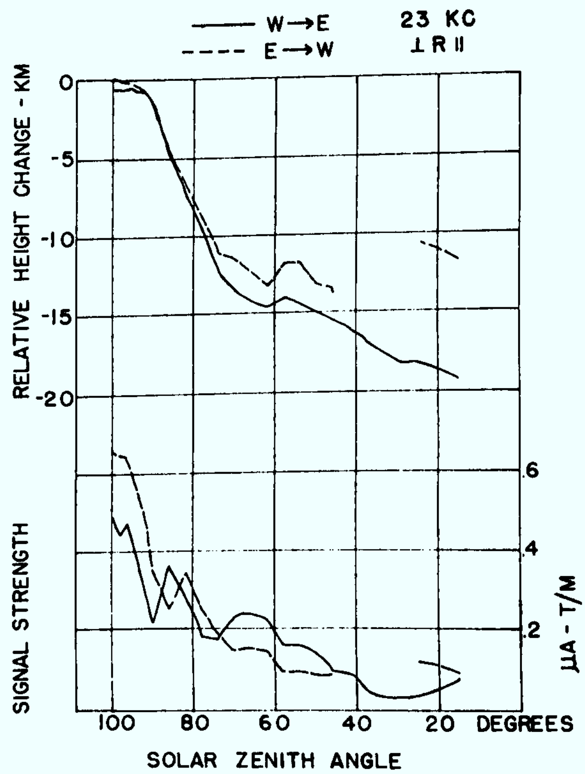

Fig. 3. The apparent relative reflection height and amplitude as a function of solar zenith angle χ for the abnormal component of 23 kHz. transmissions.

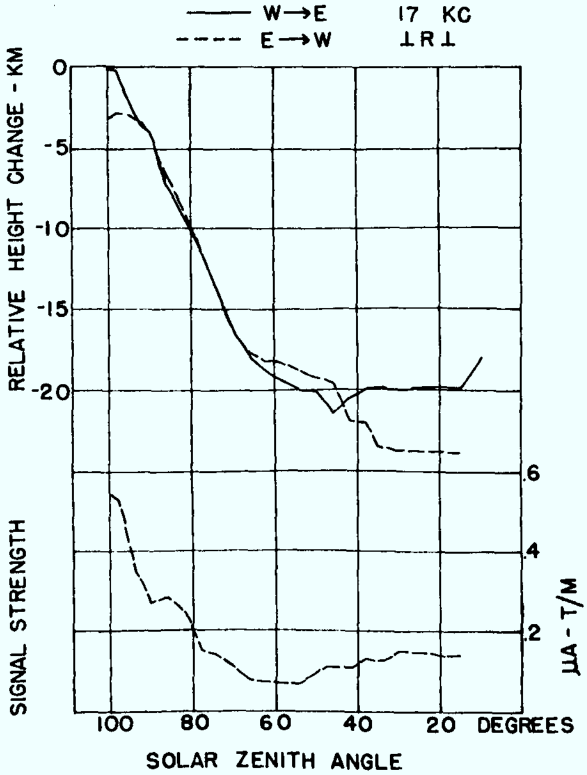

Fig. 4. The apparent relative reflection height and amplitude as a function of solar zenith angle χ for the normal for 17 kHz.

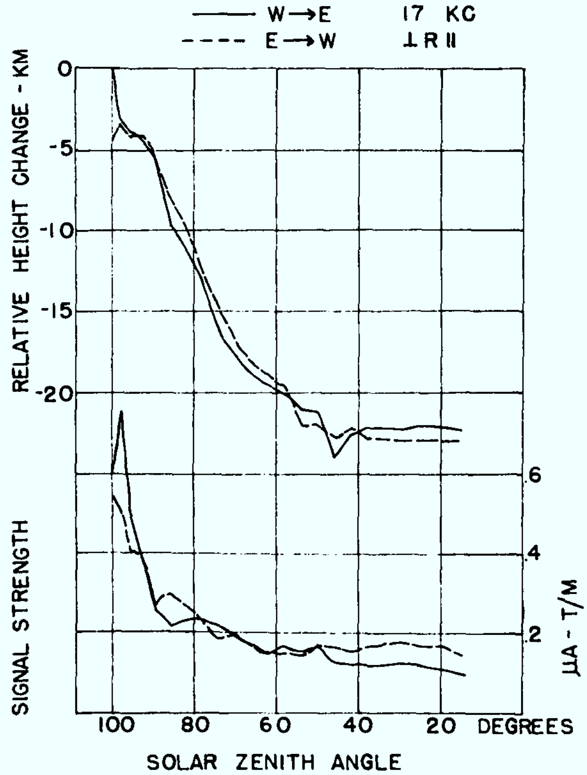

Fig. 5. The apparent relative reflection height and amplitude as a function of solar zenith angle χ for the abnormal 17 kHz.

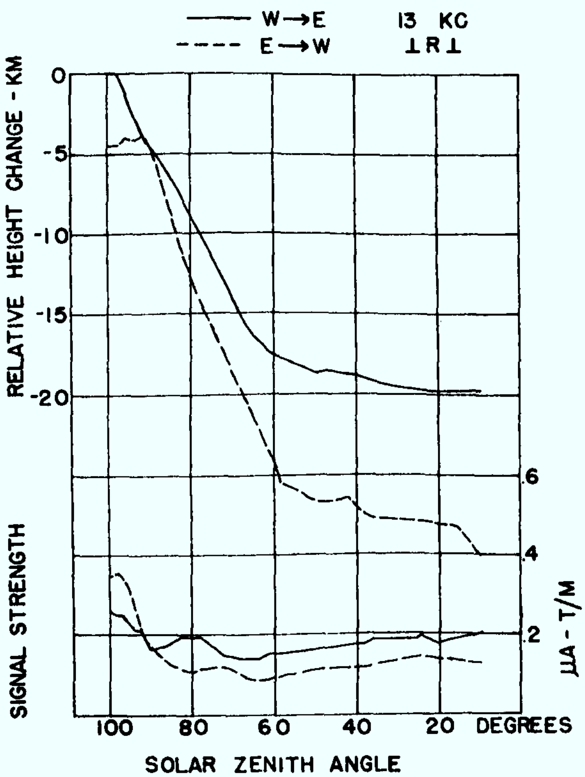

Fig. 6. The apparent relative reflection height and amplitude as a function of solar zenith angle χ for the normal for 13 kHz.

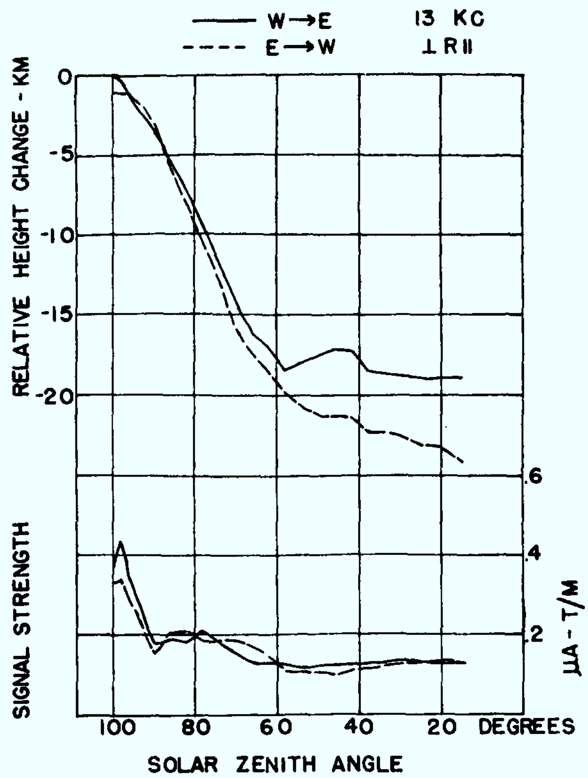

Fig. 7. The apparent relative reflection height and amplitude as a function of solar zenith angle χ for the abnormal for 13 kHz.

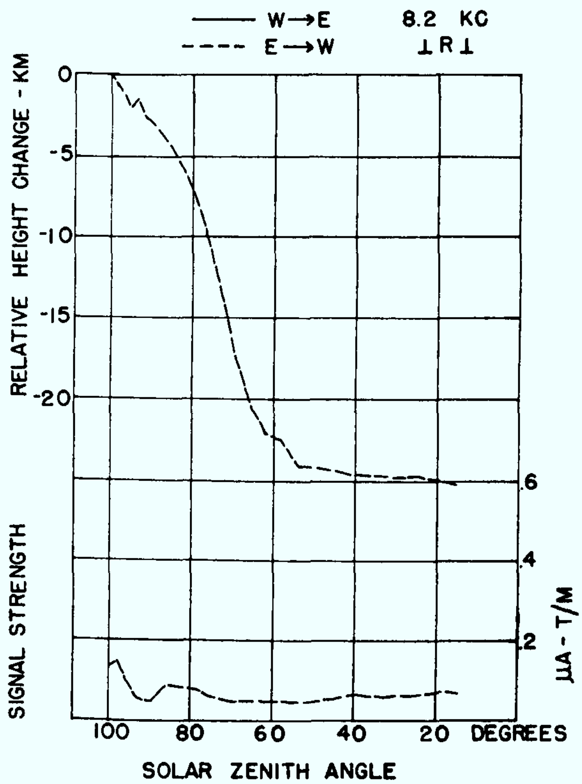

Fig. 8. The apparent relative reflection height and amplitude as a function of solar zenith angle χ for the normal for 8 kHz.

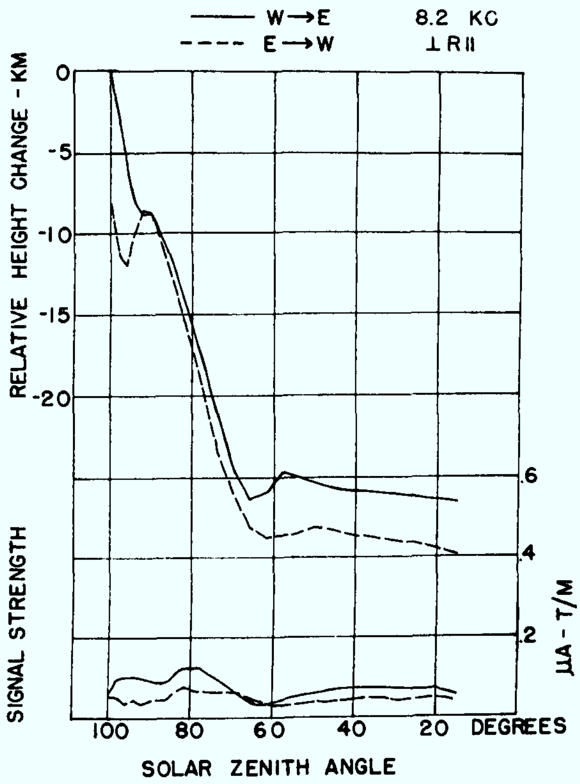

Fig. 9. The apparent relative reflection height and amplitude as a function of solar zenith angle χ for the abnormal for 8 kHz.

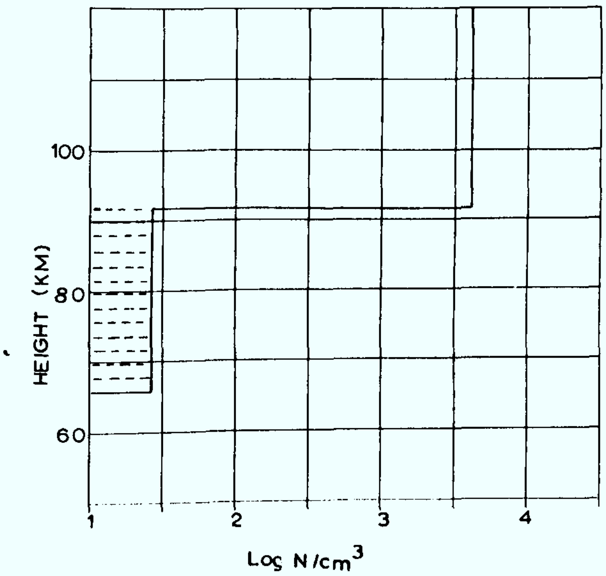

Fig. 10. A simplified model of the ionosphere having a sharply bounded layer of 3600 electrons per cc. at 92 km. and a series of slabs containing 28 electrons per cc. added sequentially.

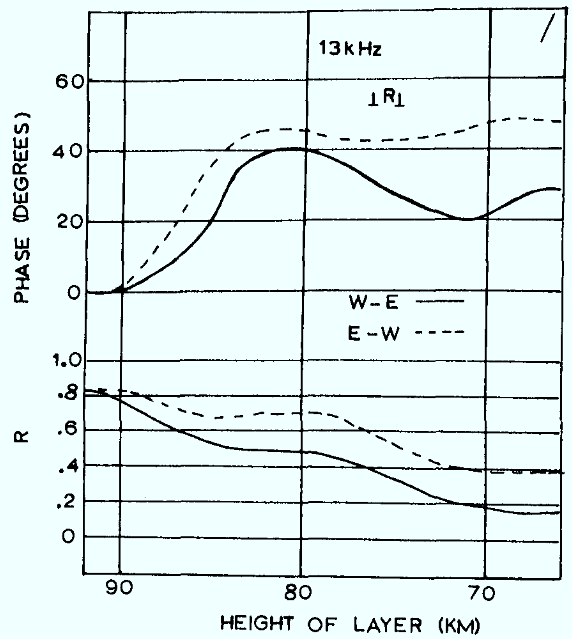

Fig. 11. Calculated reflection coefficients as a function of the model layer height for vertically polarized 13 kHz. transmissions.

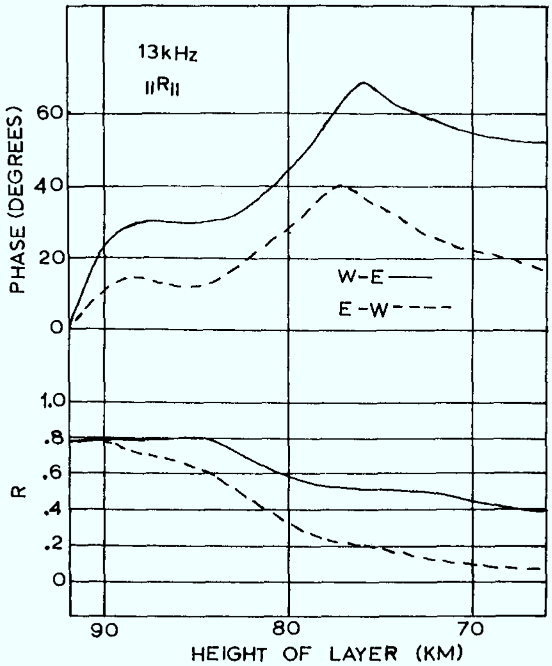

Fig. 12. Calculated reflection coefficients as a function of the model layer height for horizontally polarized 13 kHz. transmissions.

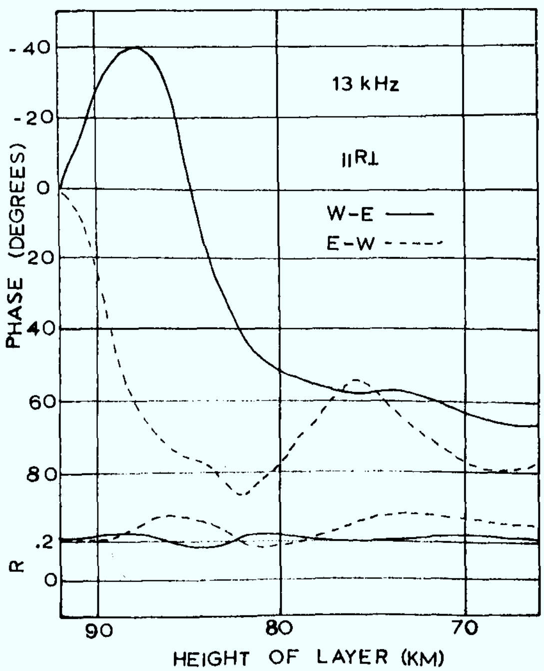

Fig. 13. Calculated conversion coefficients as a function of the model layer height for 13 kHz. transmissions.

SECTION 5

IONOSPHERIC SOUNDING

5.1 IONOSPHERIC SOUNDING OF THE E REGION

by

J.S. Belrose

Radio Physics Laboratory
Defence Research Telecommunications Establishment
Ottawa, Ontario, Canada

The swept frequency ionospheric pulse sounder is the instrument most widely used to probe the ionospheric layers. Accurate h'f soundings contain much information necessary for determining the electron number distribution, and both topside and bottomside ionospheric sounders have provided much information about the distribution of electrons in the F layer. Routine ionosonde data, however, have only limited application to studies of the distribution of electrons in the E region due to observational limitations. The absence of reflection traces below some minimum observed frequency, usually 1.5 to 2 MHz., leads to a "starting" ambiguity in the h'f to N(h) analysis, caused by a lack of knowledge of the group retardation of the E-region echoes; and the imposed requirement that the electron density increase monotonically with height leads to a "valley" ambiguity, which limits the accuracy of determining real heights in the F layer.

In principle these difficulties can be avoided if the extraordinary wave could be observed (Titheridge 1959), but it is normally missing for the E region because of high daytime absorption. To improve the height resolution and to detect reflections at lower frequencies more sophisticated ionosondes have been developed and are now coming into use. A record made by such an ionosonde system installed at Ottawa (described briefly in the Appendix) is shown in Fig. 1. For comparison an ionogram made by the routine ionosonde operated at Ottawa for many years is also shown. Note the additional complexity evident in the ionogram made by the sophisticated ionosonde with a high-gain antenna. E-region reflection traces are observed down to 300 kHz., and at high frequencies both the ordinary (O) and (X) traces are clearly observable. The X trace, however, is complicated near the E-region penetration frequency due to sporadic E traces, and the presence of partial reflections from a scattering region near 100 km. The apparent E-layer penetration frequency is not observed very well for the first reflection trace, but is more clearly evident in the multiple reflection traces from the E region. Besides the normal O and X traces for the F layer, the F-layer Z reflection trace, between the first and second multiple reflection traces from the E-layer, can be observed. Little of this complexity is evident in the ionogram made with the lower-powered ionosonde.

The ionogram presented in Fig. 2 shows that E-region reflections are complicated by cusps on both the O and X traces near the penetration frequency, and by the presence of partial reflections from a scattering region near 100 km.

High-resolution ionosondes indicate in addition that the E-layer echo is seldom a "clean" single return but is more often made up of two or more overlapping signals of comparable amplitude, returned from almost the same height. Such overlapping signals, which limit the accuracy of measurement of group height in the E-layer, are caused by small-scale variations in the otherwise horizontally stratified ionosphere. The main difficulty with E-region reflections, however, is due to sporadic E reflections, which can often obscure the normal E-region reflection trace. An example of Es reflections from a scattering layer below the normal E-layer is shown in Fig. 3. This ionogram was made at Ottawa, at about 0930 LST on 12 May, 1964.

While sporadic E reflections are a frequent limitation to the measurement of the h'(f) curve for the E layer, sporadic D reflections can also be troublesome, especially in winter months, although with high system gain and low operating frequencies the D-region echoes can also be observed in summer. Low echoes observed with ionosondes were first reported by Dieminger (1955) and Gnanalingham and Weekes (1955). On some occasions sporadic D echoes, scattered from 80 to 85 km. heights, are observed together with normal E-layer reflections (see Fig. 4), but on other occasions the low-level echoes only are observed, or they are observed together with E-layer echoes only over a limited frequency range (see Fig. 5). This figure shows the transition from total reflection in the D layer, through partial reflection or scattering in the D layer accompanied by total reflection in the E layer, to the case where there is reflection only from the E layer (c.f. also the discussion by Watts and Brown (1954) who made sweep frequency ionograms with a LF ionosonde). The absence of group retardation is explained by the thinness of the D layer, in much the same way as reflections from the E layer in the presence of sporadic E, but an electron density height profile obtained by an independent experiment has not confirmed this suggestion. When sporadic D echoes are particularly intense the absorption of high-frequency radio waves is markedly greater, to a point where a significant "winter anomaly" is recognized (see Papers 1.7 and 6.5 for a further discussion of winter days of anomalous absorption).

There are difficulties also with E-region ionograms made at night. Fig. 6 is an example of a Boulder ionogram, showing the complexity of the reflection traces. It shows echoes from three distinct strata, with virtual heights of 90 to 100, 120 to 130, and 220 to 230 km. respectively. Each stratum is seen twice by a splitting of the transmitted wave into O and X modes. The 90 km. stratum appears patchy and shows no substantial group retardation. The echo may result more from scattering than from reflection, in which case the interpretation of the penetration frequency is by no means direct. On the occasion illustrated, however, the observed penetration frequencies correspond to reflection at electron concentrations of about 3×10^3 electrons per cc., and this is representative also of direct probe results. More often the stratum at 90 km. is seen at still higher frequencies, and may extend into the normal ionosonde range as sporadic E. The origins of this stratum are not understood, but may include meteoric ionization with an enhancement due to wind shears. Reflections from this stratum are strongly influenced by magnetic activity, and so-called "breaking of the nocturnal E region" has been reported by Watts and Brown (1951) and Linguist (1953), when reflections at frequencies about 150 kHz. are not observed from the 90 to 100 km. heights but from 150 km. heights.

That stratum at 120 to 130 km. has been interpreted (Belrose, 1963) as being the true nocturnal E layer, in that it shows continuity with the daytime layer (Watts and Brown, 1954) and exhibits the same response to the influence of solar activity. Its penetration frequency decreases by about 200 kHz. during the nighttime hours, to a pre-dawn minimum of about 500 kHz., although the latter varies by about 250 kHz. for a sunspot cycle (Hough, 1961). The value of 730 kHz. found on the occasion illustrated here, corresponds to an electron concentration of 6.3×10^3 electrons per cc. Direct observations of the nighttime E layer (called by some workers an intermediate layer) are possible for only a small part of the time, because of blanketing by underlying stratum. It will be noted, however, that the X mode reflected from the F layer exhibits a cusp at foE, due to group retardation within the E layer (Watts, 1958), and this characteristic (marked A in the figure) can be employed to determine foE when blanketing occurs. On some occasions the cusp is missing, and the E layer peak is then believed to have merged with the tail of the overlying F layer. Thus, while E-region ionograms made by high-power high antenna gain ionosondes reveal much complexity not evident in ionograms made with routine ionospheric sounders, and in fact ionograms can be made when the routine ionosonde is "blacked out" due to increased ionospheric absorption, their availability does not necessarily lead to a better determination of the E-region electron density distribution. The main limitation is the difficulty on many occasions of recognizing true magnetoionic reflections from scatter reflections due to thin layers (sporadic E), critical propagation condition, etc., in fact scatter-like reflections can obscure the main reflections from the regular E layer, and in measuring the height of the E-region reflection traces with sufficient accuracy. The dynamic variations in the E region have not been studied in sufficient detail.

Nevertheless, in spite of the various limitations discussed above, the ionosonde is still a principle tool for studying the ionosphere, including the E region. Considerable work is being done to improve the analysis techniques, as well as in improving the instrumentation. At this conference (see the paper by Paul (Paper 5.4)) we learned of the recent progress that is being made on the joint use of O and X reflection traces. While this type of analysis will undoubtedly lead to a better interpretation of the electron density profile between the E and F layers, this analysis will not, in the view of the author, avoid the "starting" ambiguity, since the X reflection trace for the E region cannot be observed to a sufficiently low frequency. It cannot be observed at all on days when ionospheric absorption is too high. Since we at DRTE have gone about as far as is reasonable in improving the system gain for pulse sounders, other techniques must be considered if a significant additional improvement is to be made. A CW and digital sounding system were discussed at this conference (see Fenwick and Barry (Paper 5.2) and Bibl and Olson (Paper 5.3)). Other papers in the session are concerned with the results of a study of LF nighttime ionograms, with the valley between the F layer and thick Es (night E), and with sporadic E and wind structure of the E region. A paper by Elling (Paper 6.2) shows recent results of observation of D-region echoes employing a system of high dynamic range at Tsumeb.

APPENDIX

The DRTE Research Ionosonde at Ottawa

A significant improvement can be realized by employing a better antenna system than that used at routine ionosonde stations. The upwards radiated field strength for the 'standard' delta antenna varies markedly over the band, and falls off rapidly below 2 MHz., where, because of increased ionospheric absorption, good radiation efficiency is particularly desirable. Typically for a frequency range 1.3 to 20 MHz., the field strength 1 km. above the antenna would vary between 37 and 52 db above 1 mV/M (Bailey, 1951). In this frequency band there would be three frequencies at which the upwards radiation would be negligible compared with undesired radiation at other angles. A log periodic antenna (DuHamel and Ore, 1958), of the size and configuration described below, would have a constant beam width and gain for the 1.3 to 20 MHz. band, and the field 1 km. above the antenna would be about 51 db above 1 mV/M. At the low frequency end of the band, the radiated power would be 25 times greater than that for a standard delta antenna.

The ionosonde used at Ottawa is a Model 1005W, manufactured by Magnetic AB, Sweden, which sweeps in frequency from 0.25 to 20 MHz. The sounder pulse output power is 25 kw. minimum. The frequency range is covered in four bands, and the anodes of the rf amplifier and the transmitter mixer are tuned and tracked with the variable frequency oscillator that determines the transmitted and received frequency. A two-plane log periodic antenna is used for the frequency band 1.3 to 20 MHz. mounted on a 360-foot tower. Three folded dipoles having lengths of 1428, 823 and 476 ft., mounted one above the other on 90-foot wooden poles, are used for the frequency band 0.25 to 1.3 MHz. Each folded dipole is made up of two "conductors" spaced 50 ft. horizontally (30 ft. in the case of the shortest dipole); each conductor comprises four parallel wires equally spaced 3 ft. apart horizontally and jumped at least every 1/10 wave length. The receiver employs differentiation (various time constants are available), essentially a high-pass filter ahead of the video amplifier, which, together with AGC, aid echo detection in the high interference of the broadcast band; but this can be switched out if desired. The ionogram shown in Fig. 1 was made with a 100 μsec. time constant in the differentiating circuitry.

Various investigations are in progress or planned, employing the research ionosonde at DRTE, but no results are yet available. Dr. G.L. Nelms has developed a computer program that uses the electron density height profile measured by the partial reflection experiment as the starting point in computing the real height profile in the E region. Dieminger (1955) has shown that with a sensitive ionosonde equipment one can observe, on some days in winter, scatter-like echoes from the D region. The research ionosonde at Ottawa is being operated in conjunction with the partial reflection sounder to identify these days, and the purpose of the study is to investigate what structure differences are discernable in the D-region electron density distribution at these times.

REFERENCES

Bailey, R. Aperiodic aerials use with vertical incidence ionospheric recorders. Wireless Eng., 28, 208, 1951.

Belrose, J.S. The present knowledge of the lowest ionosphere. AGARDOgraph 74: Propagation of radio waves at frequencies below 300 kilocycles, (ed. Blackband), 3 – 23, Pergamon Press, 1963.

Dieminger, W. Short wave echoes from the lower ionosphere, in the physics of the ionosphere. Phys. Soc. (London), 53, 1955.

DuHamel, R.H. and F.R. Ore. Logarithmically periodic antenna designs. IRE National Convention Record, 6, (Pt. 1, 2, 3), 139 – 151, 1958.

Gnanalingham, S. and K. Weekes. D-region echoes observed with radio waves of frequency 1.4 Mc/s, in the Physics of the Ionosphere. Phys. Soc. (London), 63 – 70, 1955.

Hough, W.S. The nocturnal E-layer. Paper presented at the USNC-URSI/IRE Meeting, 4 May, 1961.

Linquist, R. An interpretation of vertical incidence equivalent height versus time recordings at 150 kc/s. J. Atmos. Terr. Phys., 4, 10 – 27, 1953.

Titheridge, J.E. The use of the extraordinary ray in the analysis of ionospheric records. J. Atmos. Terr. Phys., 17, 110, 1959.

Watts, J.M. The interpretation of nighttime low frequency ionograms. J. Geophys. Res., 63, 717, 1958.

Watts, J.M. and J.N. Brown. Effects of ionospheric disturbances on low frequency propagation. J. Geophys. Res., 56, 403, 1951.

Watts, J.M. and J.N. Brown. Some results of sweep frequency investigations of the low frequency band. J. Geophys. Res., 59, 71, 1954.

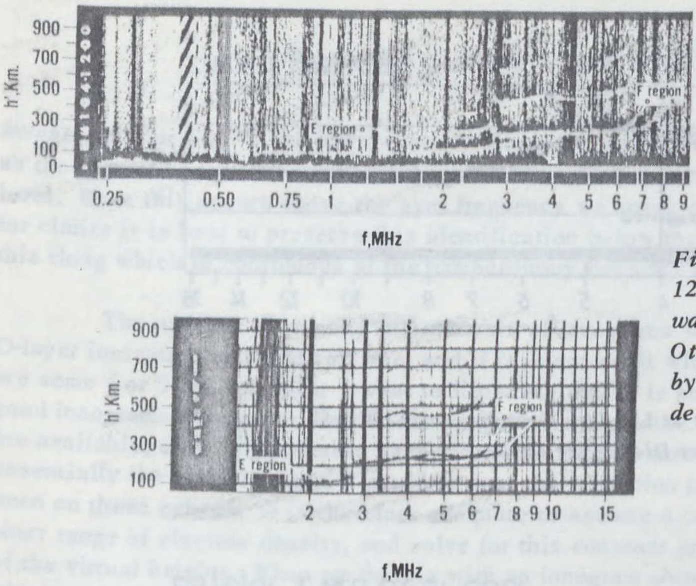

Fig. 1. Ionograms taken at Ottawa, Canada, at 1200 EST 4 January, 1966. The bottom record was made by the routine ionosonde operated at Ottawa for many years; the top record was made by the more sophisticated ionosonde installation described in the paper.

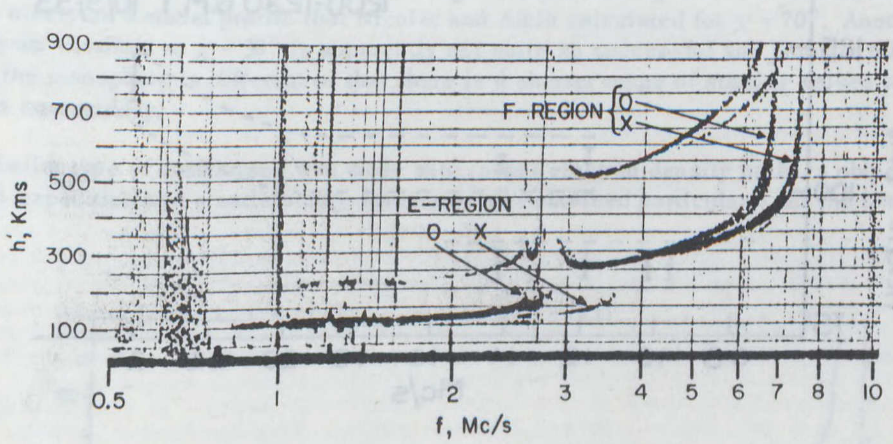

Fig. 2. Ionogram taken at Uppsala, Sweden, at about 1800 LST, in June 1958 (by W. Stoffregen).

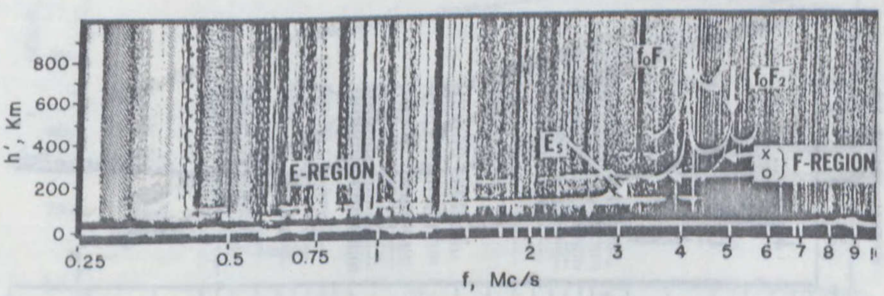

Fig. 3. Ionogram taken at Ottawa, Canada, at about 0930 LST, 12 May, 1964.

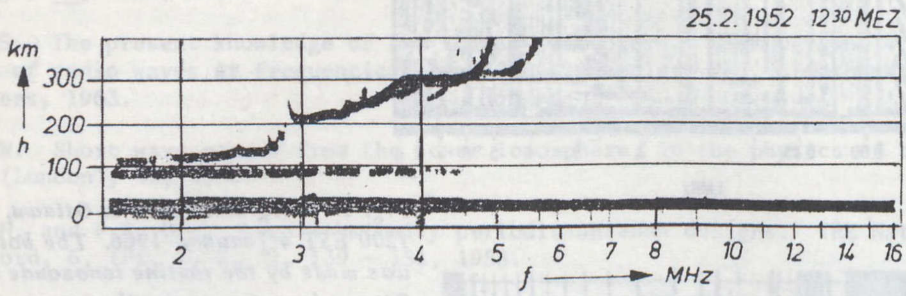

Fig. 4. Ionogram taken at Lindau, Germany, at 1230 LST, 25 February, 1952 (after Dieminger 1955).

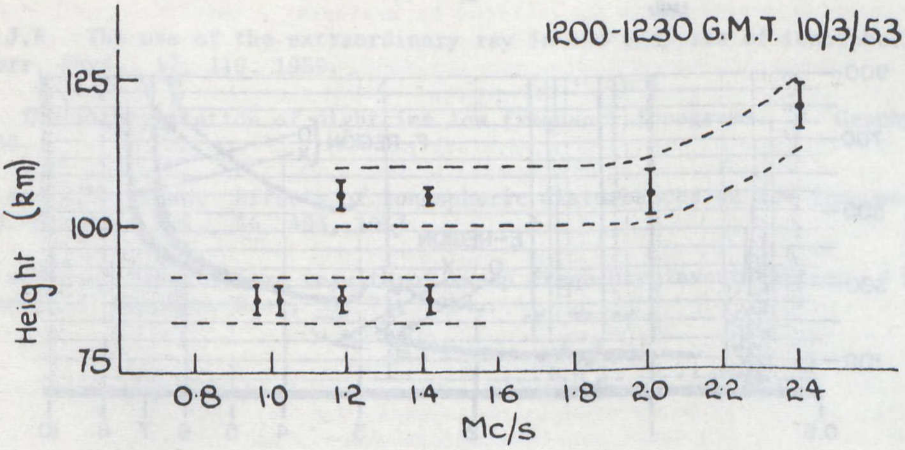

Fig. 5. Ionogram taken at Cambridge, England, employing a series of frequencies, at midday, 10 March, 1952 (after Gnanalingham and Weekes 1955).

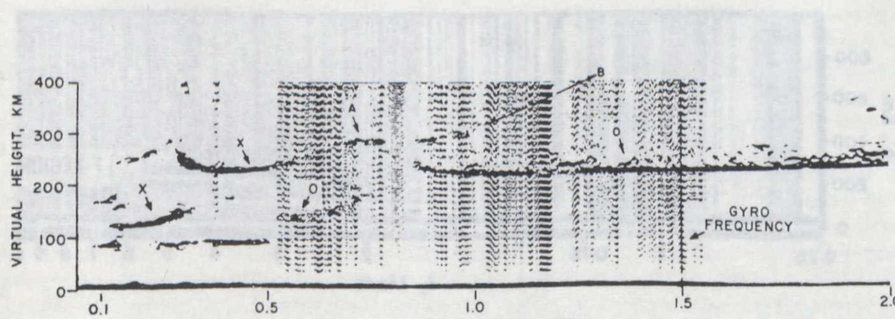

Fig. 6. Low-frequency ionogram recorded at Boulder, Colorado (by J.M. Watts).

Discussion on Paper 5.1 presented by J.S. Belrose

Wright: In your Fig. 6, the low frequency ionogram, you referred to the lowest of the two reflection levels as the extraordinary. It is at least the non-ordinary component, but it is of course the $1 + Y$ reflection level. When this occurs above the gyro frequency we speak of it as the Z trace, so it seems to me that for clarity it is best to preserve this identification below the gyro frequency as well, recognizing that this thing which is continuous at the extraordinary does not exist down there.

The problem of starting the analysis of ionograms with a sufficient correction for the underlying D-layer ionization is a difficult one, and if it is not dealt with then one gets profiles which at the bottom are some 4 or 5 km. too high. I want to illustrate that it is possible to make a correction for this on most good ionograms whether or not the extraordinary is available. When the reflections from only one component are available, they will probably have virtual heights of around 106 km. Our analysis shows that it is essentially the electron density gradient near the reflection point which contributes most of the retardation seen on these echoes. It is therefore adequate to assume a constant gradient, project this back over a short range of electron density, and solve for this constant gradient and the starting height from several of the virtual heights. When we do this with an ionogram obtained at $\chi = 75°$, we obtain a profile (Fig. D-1) which comes nicely on a model profile that Nicolet and Aikin calculated for $\chi = 70°$. Another calculation from an ionogram obtained at $\chi = 30°$ is apparently not quite so successful and perhaps reflects either the fact that the ionosphere is different or that there is a shorter range of starting values available from the ionograms near midday.

A similar type of comparison was made with rocket electron density profiles obtained from NASA's mobile launch expedition and a satisfactory agreement was obtained particularly for the lower part of the E region.

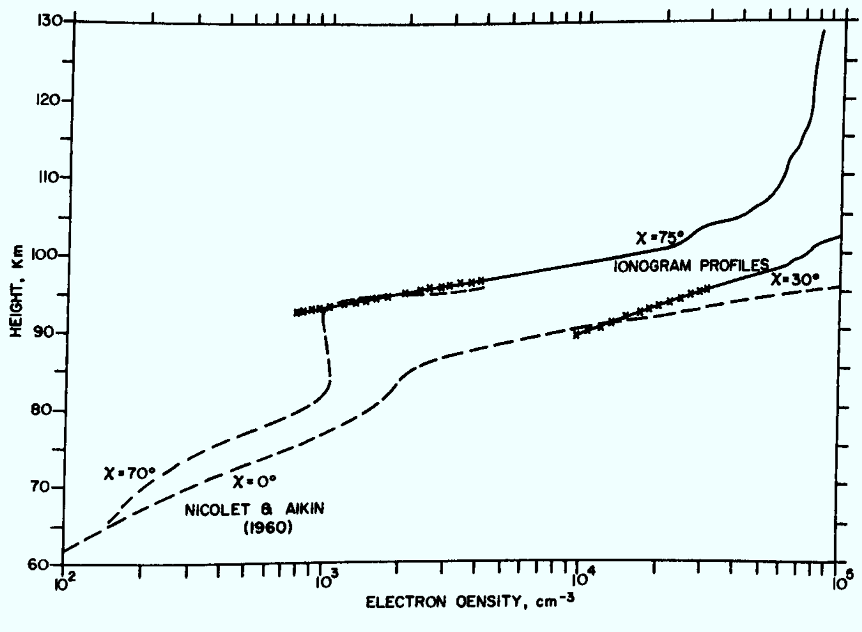

5.2 A HIGH RESOLUTION CW SOUNDER FOR USE AT VERTICAL INCIDENCE

by

R.B. Fenwick and G.H. Barry

Radioscience Laboratory, Stanford University,
Stanford, California

Presented by R.B. Fenwick

Currently used ionosondes, providing sweep frequency measurements of ionospheric virtual height, often do not produce satisfactory results due to either inadequate average power capability or to interference from other spectrum users. While in principal these problems may be overcome by increasing the peak pulse power of the sounder, this solution is unattractive because powers are currently reaching impractical limits (Belrose, 1966). Increasing antenna directivity will improve the situation, but the maximum practical antenna size may be reached before adequate sensitivity is achieved.

Frequency-modulation cw techniques have for some years appeared attractive for sounding (Gnanalingham, 1954), particularly from the viewpoint of decreasing transmitter peak powers while increasing the transmitted energy per unit time. For identical average powers and transmitted bandwidths, assuming white gaussian noise and a stationary medium, pulse and fm sounding systems can provide equal sensitivity and time-delay resolution (Kay, 1959, Hymans and Lait, 1960). However, use of linear-sweep "chirp" (see Klauder et al. 1960) techniques can provide a number of significant advantages over pulse in ionospheric sounding. These include higher average power, virtual immunity to interference from fixed-frequency stations, and flexible trade-offs between time delay resolution and data acquisition rate.

The background noise afflicting a vertical-incidence sounder is usually — as a result of the high occupancy of the 0.1 to 10 MHz. range — neither white nor gaussian. This interference is difficult to reject using a pulse sounder, since receiver bandwidths of from 20 to 200 kHz. are necessary to obtain the desired time delay resolution. With a cw chirp system, however, the receiver bandwidth may be made arbitrarily small by slowing down the sweep rate; the only limit is imposed by doppler shifts or other changes in the ionosphere. Seen through a sufficiently narrow bandwidth, the radio spectrum is nearly unoccupied. Further, the receiver may be gated off when interference is encountered, usually with negligible loss of desired signal. The analogous process may, of course, be performed by inserting multiple notch filters in the frequency passband of any sounder, but the rejection is notably simpler to implement in the time domain.

Fig. 1 shows a frequency/time representation of pulse and chirp signals together with sounding echoes at fixed range. It is clear that Δt can be obtained from Δf to an accuracy dependent on the linearity of the frequency sweep and the transmitted bandwidth. The present availability of direct frequency synthesizers has greatly improved the linearity of conveniently generated frequency sweeps (Barry and Fenwick, 1965), making high resolution chirp ionospheric sounding practical.

Though probably not the slowest practical rate, frequency sweeps of 25 kHz./sec. have been employed at Stanford for vertical-incidence sounding. For this rate a receiver bandwidth of roughly 100 Hz. is appropriate. The upper sketch of Fig. 2 illustrates a typical interference spectrum with a pulse receiver bandwidth of, say, 100 kHz. superimposed. The identical frequency range must, of course, be covered by a chirp signal in order to realize the same (10 μsec.) resolution. The 100 Hz. chirp receiver passband, however, allows the sounder to utilize only the clear spectrum between interfering stations.

The frequency sweep sounding signal must be generated by the use of a frequency synthesizer because the advantages of cw chirp sounding (improved signal-to-noise ratio and interference rejection) are realized most fully at slow sweep rates; and at a sweep rate of 25 kHz./sec., 10 μsec. is equivalent to only 0.25 Hz. Aside from the frequency synthesizer and required spectrum analysis equipment, the chirp sounding equipment is quite simple (Fig. 3). The sweep frequency, cw output from the synthesizer is amplified and radiated directly. The chirp receiver converts the echoes to fixed-frequency tones (whose frequencies are proportional to the echo time delays) by mixing the received signals with a frequency sweep identical to that transmitted (except translated by an amount equal to the receiver IF). The resulting signals are tape-recorded and later spectrum-analyzed to produce records of time delay vs frequency. Since the recorded signals represent a phase-continuous sweep across the entire spectrum, the tape can be analyzed using any desired filter bandwidth to provide the optimum trade-off (consistent with the dispersion of ionospherically reflected signals) between frequency resolution and time-delay resolution. With a pulse system, one is committed to a particular time resolution by the transmitted pulse length; cw frequency sweep recordings may, on the other hand, be processed to best display whatever dispersion is observed. For F-layer sounding, a resolution of 20 μsec. has been generally found to be a good compromise. However, oblique incidence records made in the MF range have shown 10 μsec. structure and this is probably not the ultimate.

The upper record of Fig. 4 is an example of a chirp ionogram made with a radiated power of only 20 mw. (the 1-volt output from the synthesizer applied directly into an antenna). A conventional 2 kw., 50 μsec. pulse sounder record is shown below for comparison. The records were made within 15 min. of each other.

No vertical-incidence sounding has yet been attempted on frequencies lower than 2 MHz.; however, oblique incidence sounding from 600 to 2000 kHz. has been performed over the 1900 km. path from Stanford, California, to Lubbock, Texas.

These experiments have been described by Fenwick and Barry (1966). For these soundings, a sweep rate of 25 kHz./sec. was employed at radiated power levels ranging from 25 to 250 w. The reduced power occurred at lower frequencies due to the poorer efficiency of the vertical transmitting antenna. Two examples of the records taken during this experiment are shown in Fig. 5. The ionograms were taken near local midnight, midpath, on two evenings in June 1965 and exhibit a time-delay resolution of approximately 10 μsec. Despite the fact that the frequency range includes nearly the entire AM broadcast band and a broadcast station a few miles from the receiver, no interference is evident.

The MF oblique-sounding results indicate that the chirp technique should make possible highly satisfactory vertical-incidence sounding at medium wavelengths, while radiating at most a few watts of power. It should be possible to extend the frequency range down to 100 kHz. without requiring transmitter power levels greater than the order of 100 w.

Fig. 6 shows qualitatively the relation between required average power and sweep rate for a chirp sounder. For very slow rates, receiver bandwidths can be very small and interference is all but ignored; the sensitivity of the sounder is determined by atmospheric noise. At very fast rates, necessary receiver bandwidths become large. When the inter-station spacing, Δf, is small compared with the receiver bandwidth, the chirp sounder and pulse sounder interference vulnerabilities are equal. If Δf is, for example, 3 kHz., it is implied that interference-caused desensitizations would become serious at a sweep rate of approximately $(\Delta f)^2 = 9$ MHz./sec.

Chirp sounding does create some equipment problems not inherently so difficult in pulse sounding; these difficulties may render cw sounding unattractive in some applications. Since in cw sounding all echoes are being received simultaneously, a receiver and spectrum analyzer dynamic range problem can exist. Over-all system dynamic range in the results reported here was about 30 to 35 db — limited by the spectrum analyzer. Means exist for improving this figure, of course, but they may not be overly attractive. Doppler shift ambiguities can be difficult to overcome in chirp sounding, and may rule out its use in such applications as incoherent scattering (Shearman, et al. 1963). However, doppler shifts have been successfully compensated when using a chirp system, e.g., in lunar radar studies (Howard et al. 1965). Finally, it is unquestionably more difficult to convert a chirp sounder receiver output to ionograms — especially to ionograms having a logarithmic frequency scale — than it is with a simple pulse sounder. In automated systems of the future, however, this feature will not be objectionable. On balance it is clear that there are applications in ionospheric sounding where the use of chirp cw waveforms will be most advantageous.

REFERENCES

Barry, G.H. and R.B. Fenwick. Extraterrestrial and ionospheric sounding with synthesized frequency sweeps. Hewlett-Packard J., 16, 8-12, July 1965.

Belrose, J.S. Ionospheric sounding of the E region in this conference proceedings, 1966. (Paper 5.1).

Fenwick, R.B. and G.H. Barry. Step by step to a linear frequency sweep. Electronics, 38, 66-70, July 1965.

Fenwick, R.B. and G.H. Barry. Sweep-frequency oblique ionospheric sounding at medium frequencies. IEEE Transactions on Broadcasting, (in press).

Gnanalingham, S. An apparatus for the detection of weak ionospheric echoes. Proc. IEE, 243-248, (Paper No. 1670), March 1954.

Howard, H.T., Eshleman, V.R., Barry, G.H. and R.B. Fenwick. Radar measurements of the total cislunar electron content. J. Geophys. Res., 70, 4357-4364, 1 September, 1965.

Hymans, A.J. and J. Lait. Analysis of a frequency-modulated continuous-wave ranging system. Proc. IEE, 365-372, (Paper No. 3264E), July 1960.

Kay, L. A comparison between pulse and frequency-modulation echo-ranging systems. J. Brit. IRE, 105-113, (Paper No. 489), February 1959.

Klauder, J.R., Price, A.C., Darlington, S. and W.J. Albershein. Theory and design of chirp radars. Bell Sys. Tech. J., 30, 745-808, July 1960.

Shearman, E.D.R., Bain, W.C. and K. Weekes. Analysis of radar systems for the observation of incoherent radio-wave scattering in the ionosphere. Proc. IEE. 110, 887-896, 5 May, 1963.

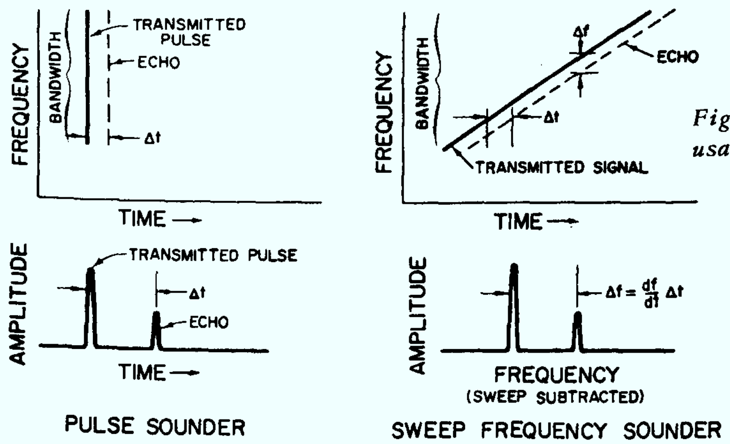

Fig. 1. Comparison of pulse and chirp spectrum usage.

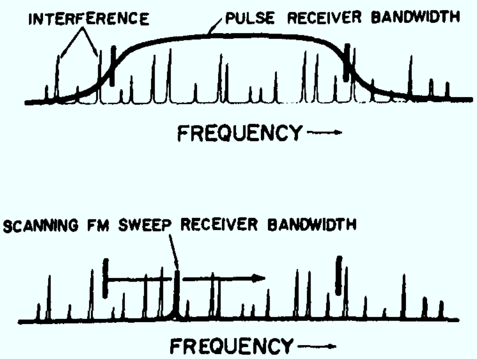

Fig. 2. Comparison of receiver bandwidths required for pulse and from chirp sounding.

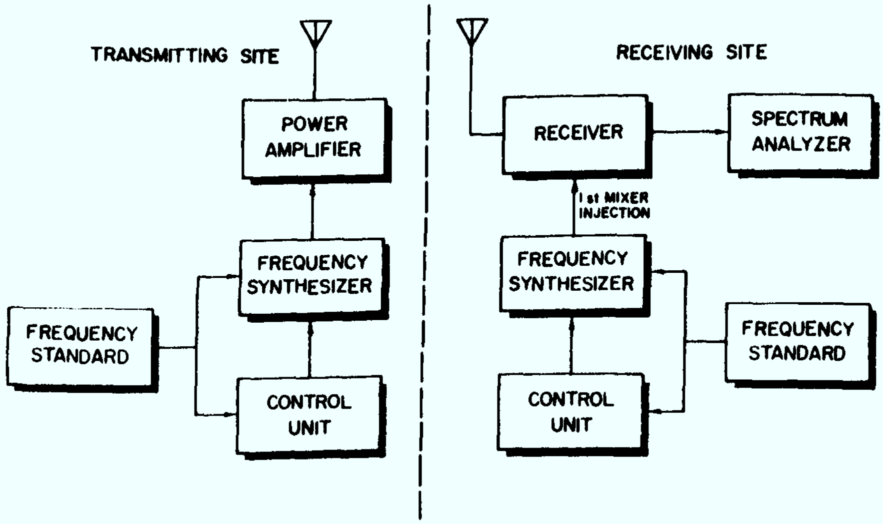

Fig. 3. Block diagram of chirp sounding equipment.

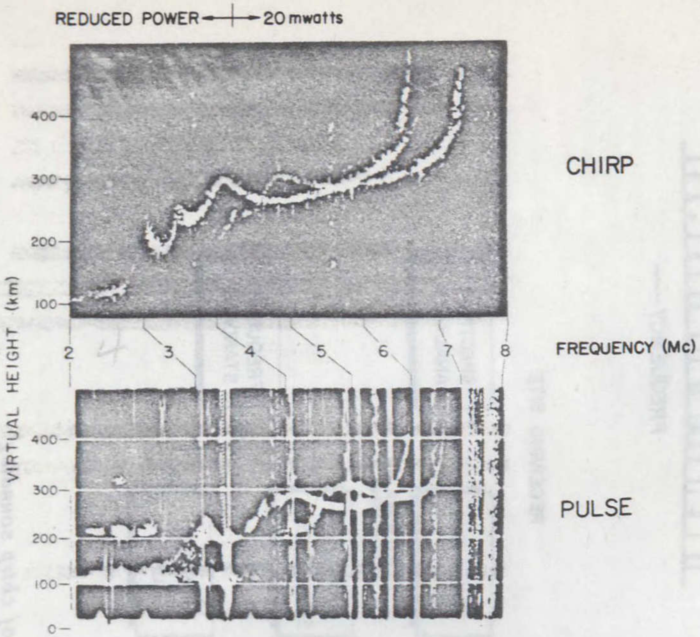

Fig. 4. Comparison of chirp and pulse vertical-incidence ionograms.

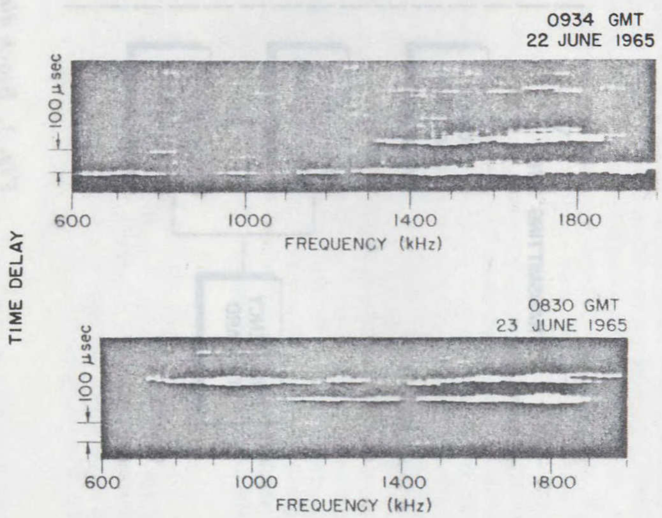

Fig. 5. Oblique-incidence chirp ionograms over 1900 km. path, Stanford, California, to Lubbock, Texas (25 to 250 watts).

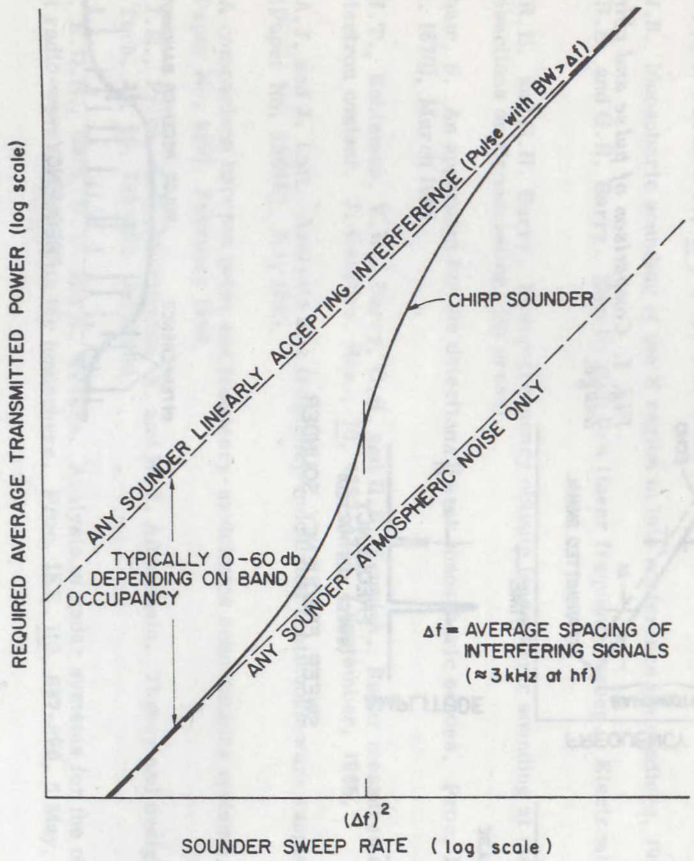

Fig. 6. Qualitative dependence of required power on sweep rate in chirp sounders.

Discussion on Paper 5.2 presented by R.B. Fenwick

Bibl: What is the tape speed when you record at 25 kHz. per second?

Fenwick: It should be 1 7/8 in. per sec.

Bourne: What was the cost of your installation?

Fenwick: It required $50,000 and six man-months to build the two terminals.

Wright: Do you feel the word 'chirp' is best suited to describe your technique or would the cw radar term or FM be better?

Fenwick: It is true that the word chirp does bring to mind pulse chirp as used in normal radar. The analogy here to the chirp radar used in microwaves would be sweeping many times across the spectrum at a fast rate and adding the returns. We could do that, but would not get any of the advantages of interference rejection; in fact it would be like any other sounder. The point is well taken, chirp is easy.

Wright: Are the ambiguities between ordinary and extraordinary or any other echoes which appear relatively close together intermixed in this method of measurement? Are they a problem in data analysis?

Fenwick: As long as one did not have a doppler shift on it or something that the other one did not have, the frequency difference would just be proportional to the group time delay on it.

Belrose: The fact that you have a dynamic range of only 30 to 35 db would limit the possibility of seeing the extraordinary trace, because the F-region echoes would certainly be well above this in amplitude.

Fenwick: The dynamic range of 30 to 35 db is a function only of the particular spectrum analyzer that we own. There are ways in which you can get around this problem; a larger dynamic range is possible.

5.3 A DIGITAL IONOSONDE

by

K. Bibl and K. Olson

Lowell Technological Institute Research Foundation, Lowell, Massachusetts

Presented by K. Olson

1. Introduction

For pulse observations in crowded radio bands, an ionosonde is needed which can see through this interference without creating a remarkable nuisance to other services. Increased resolution is important for a world-wide system, capable of synoptic use. Real-time data are required in a format acceptable for transmission to an evaluation center and for processing by a computer.

Application of the precepts of communication theory, the technology of data processing, and the results of scientific investigations using pulse sounders, have resulted in the design of an improved ionosonde.

2. Pulse Receiver

A solid state receiver, designed for stable reception of pulses, permits nearly instantaneous recovery following transmission. Single-tuned amplifiers having gains of 10 to 20 db per stage with an over-all bandwidth of 40 kHz. are used. Symmetrical overload characteristics are designed into these stages.

Phase decoding is provided by selecting one of two receiver outputs which are displaced by 180°. These outputs are available simultaneously to permit the correct phase to be chosen for any range interval. Thus twice 2.5 msec. are necessary with differently delayed decoding sequences to cover a 750-km. height range.

Most ionosondes mix a variable frequency, f_1, with a gated fixed frequency, f_o, to generate $(f_1 + f_o)$ as a transmitted frequency. Using f_1 as the local oscillator of the receiver, $(f_1 + f_o) - f_1$ is generated in the receiver to produce an IF of f_o. Since f_1 is common to the transmitter and receiver, no phase contribution of f_1 appears at the receiver IF provided that f_1 is stable for an interval equal to the group delay.

The gate that pulses the amplitude of the fixed frequency oscillator, f_o, has a fixed phase with respect to f_o; thus phase-coherent integration becomes possible and phase height can be determined by measuring the phase change with frequency:

1. After decoding, the direct signal at the receiver IF output has the same stationary phase for all frequencies, i.e., each positive zero-crossing of the IF occurs at a point that is fixed with respect to the envelope at every frequency.

2. In case of free space propagation, equal-step changes of frequency result in constant step changes of phase. Thus, in the ionograms the reflections trace a pattern determined by the reflection height.

3. In the presence of the ionosphere, reflection height and phase speed (in the penetrated part of the layer) change simultaneously with increasing frequency. Modifications of the phase pattern by these ionospheric effects can be used for accurate determination of the electron density profile.

3. Data Processing

The intermediate frequency output of the receiver contains much information that is not used. Envelope detection allows recovery of group height, but all other information is modified or destroyed.

Sampling the IF amplitude 3 times in 2 cycles of the last IF (50 kHz.) and integrating corresponding samples of 80 consecutive pulses provides 20 db improvement of signal-to-random noise ratio.

Positive and negative amplitudes are integrated separately. After integration, corresponding positive and negative samples are subtracted to determine the signal amplitude and the sign in that sampling interval. Three adjacent amplitude samples are added disregarding the sign, and the sign of the first sample is associated with the resulting number. This number represents pulse amplitude in one 6-km. height range. More accurate group delay is given by the ratio of the consecutive amplitude samples; phase information of the IF is revealed by the sign.

Separate integration of the positive and negative amplitudes permits improvement of signal-to-coherent noise ratio, even when the coherent noise is larger than the desired signal.

Real-time processing of the information is provided digitally. Advantages of digital processing include:

1. High speed, permitting real-time processing,
2. Precision amplitude information, yielding resolution of 0.5 per cent of the total range,
3. Digital data output, reducing translation and tape requirements.

Although high speed is normally associated with high cost, we have been able to develop a system of memory organization that is fast, accurate, and inexpensive (Fig. 1). Basically, our invention resides in obtaining the average of a signal by comparing the instantaneous value with the average stored in the memory. Initially, the number stored in the memory is one-half of the range. Successive comparisons add or subtract an appropriate amount from the stored number, converging it rapidly to the average value of the desired signal. Since 80 pulses are to be integrated, only one bit is added to or subtracted from the stored average on each comparison. The first 16 comparisons modify the average by ±16; the second 16 by ±8; the third 16 by ±4; the fourth 16 by ±2; and the last 16 by ±1. This technique is fast and permits integration of 80 pulses with 256 level resolution. Since positive and negative amplitudes are stored in separate memory words, almost twice the number of cores are required. The cost can be comparable to storing 8-bit numbers and signs because the digital-to-analog converter needs only a single polarity.

After averaging 80 pulses, before sampling at the next frequency, positive and negative amplitudes are compared to form average amplitude and sign of each 2-km. sample range. Three adjacent averages are added disregarding sign. The sign of each first sample and the resultant amplitude of three adjacent samples will be stored and put on magnetic tape during the next frequency sounding. Integration and readout of all height levels on a single frequency requires only 0.25 sec.

Using 25 kHz. frequency steps and a repetition rate of 400 Hz., a band of 1 MHz. is covered in 10 sec., thus the entire range from 0.5 to 18.5 MHz. requires only 180 sec.

4. Digital Tape

We are now using 4 track recording to put data on magnetic tape in digital form. Each track carries one weighted bit of a BCD number; the IBM code is used which represents decimal zero as 8 + 2. Thus there is always one bit laterally across the tape and no other synchronizing is required. Each data point contains 4 bits along the length of the tape; three are decimal digits, one represents time code information and sign.

Recording in this way simplifies translation to IBM computer tapes but allows data to be recorded on inexpensive ¼" tape. Additional electronics required to generate computer tape directly can be added whenever desired.

5. Printed Ionogram

The digital output of the ionosonde can be printed directly by a multi-pen recorder. Amplitude information for each frequency is presented by printing a number of dots which can be counted to determine the amplitude. A curve, drawn manually through the maximum amplitude of each frequency, presents an ionogram that can be read to 1 km. in height and 10 kHz. in frequency.

When simulated using a typewriter, digital ionograms appear as shown in Fig. 2. Numerical values represent signal amplitudes. Echoes are distinguished by consistently high amplitudes. When phase is printed, using special symbols in additional columns, phase height can be read from these ionograms. Fig. 3, an expanded region of Fig. 2, shows a phase height profile from 2 to 4 MHz. The key for reading phase height from the printed phase code is shown in Fig. 4 and explained in Appendix 1.

6. Other Processing

Subsidiary data processing can provide special characteristics as continuous functions of time. Examples would be fmin ftEs, h'E, h'F, foF2 and MUF3000F. These data can easily be transferred to remote locations by telephone or wireless communication links.

APPENDIX 1

Phase-height and Phase-path Measurements

Phase-height and phase-path measurements are extremely useful in determining reflection heights and electron density profiles with the help of vertical and oblique ionograms. Phase heights follow the true reflection heights much closer than they follow group heights and have less discontinuity. The group height is always above the true height, whereas the phase height lies only a few kilometers below the true height. Thus, quick interpolation or unambiguous determination of the true height is possible if both phase and group height are measured simultaneously.

The phases of consecutive frequencies form a periodic pattern which is dependent on frequency-stepping intervals and reflection height. Because of the ambiguity of phase measurements, the pattern is repeated in certain path-length intervals: for 25 kHz. frequency stepping, the repeatability is 12 km.; and for 10 kHz. the repeatability is 30 km. of path length. In vertical sounding this means an ambiguity in phase height of 6 or 15 km., respectively. At oblique incidence the height ambiguity is reduced. For a 2000-km. oblique path, equal patterns appear only in height intervals of 60 or 150 km. Therefore, the representation of six different phase values becomes necessary. For vertical incidence the representation of three phases is adequate for a phase-height resolution of better than 1 km. The sequence of the three phases and the phase-repetition rate determine the phase height as shown, for frequency-stepping of 10 kHz., in Fig. 4. The indicated period is the number of frequencies necessary to repeat the pattern.

The direction of the phase sequence is cyclic in the height ranges from 90 to 97.5; 105 to 112.5 km. and noncyclic in the height ranges from 97.5 to 105; 112.5 to 115 km., and so on.

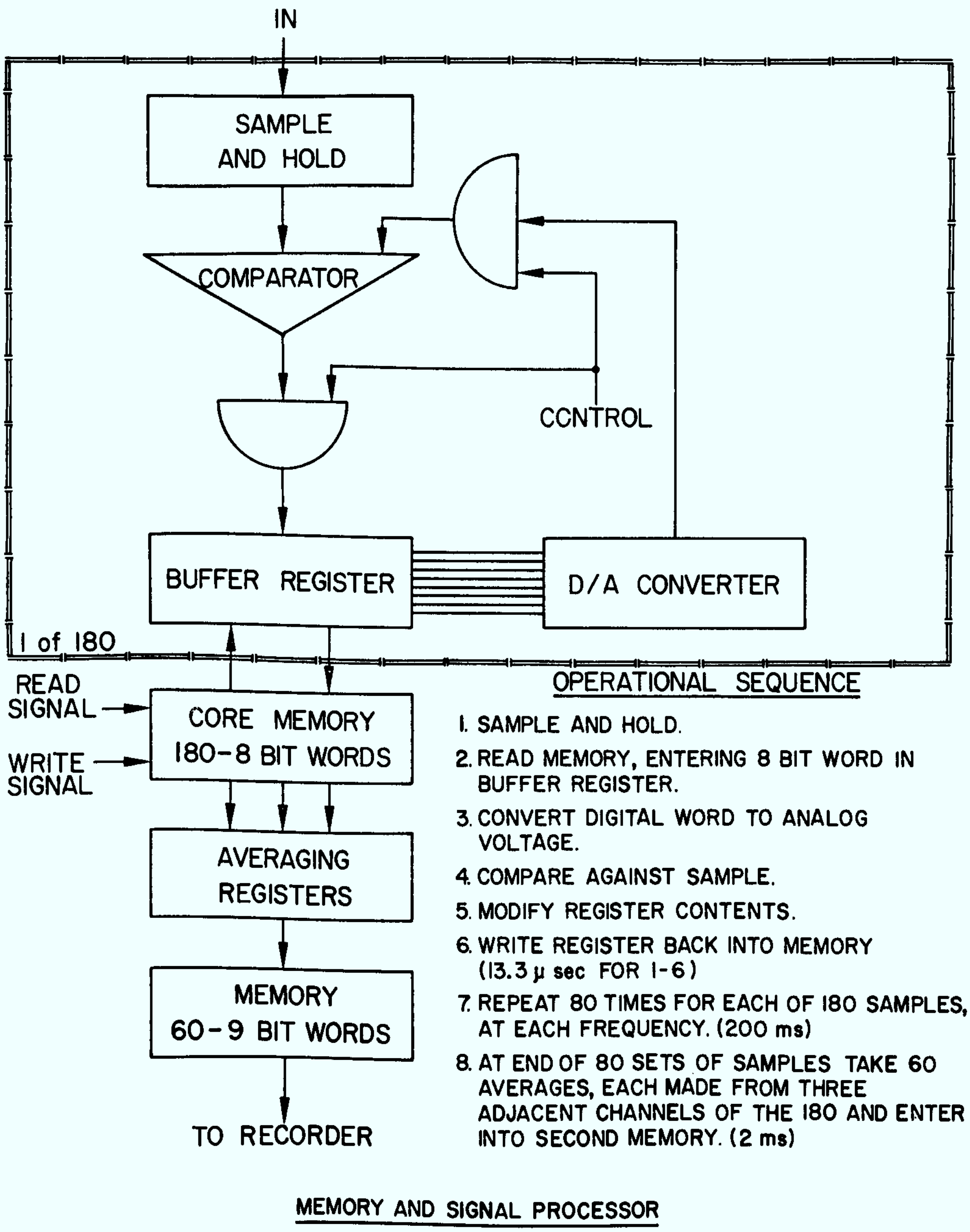
IN
SAMPLE AND HOLD
COMPARATOR
CONTROL
BUFFER REGISTER
D/A CONVERTER
1 of 180
READ SIGNAL
WRITE SIGNAL
CORE MEMORY 180-8 BIT WORDS
AVERAGING REGISTERS
MEMORY 60-9 BIT WORDS
TO RECORDER
OPERATIONAL SEQUENCE
1. SAMPLE AND HOLD.
2. READ MEMORY, ENTERING 8 BIT WORD IN BUFFER REGISTER.
3. CONVERT DIGITAL WORD TO ANALOG VOLTAGE.
4. COMPARE AGAINST SAMPLE.
5. MODIFY REGISTER CONTENTS.
6. WRITE REGISTER BACK INTO MEMORY (13.3 μ sec FOR 1-6)
7. REPEAT 80 TIMES FOR EACH OF 180 SAMPLES, AT EACH FREQUENCY. (200 ms)
8. AT END OF 80 SETS OF SAMPLES TAKE 60 AVERAGES, EACH MADE FROM THREE ADJACENT CHANNELS OF THE 180 AND ENTER INTO SECOND MEMORY. (2 ms)
MEMORY AND SIGNAL PROCESSOR

Fig. 1.

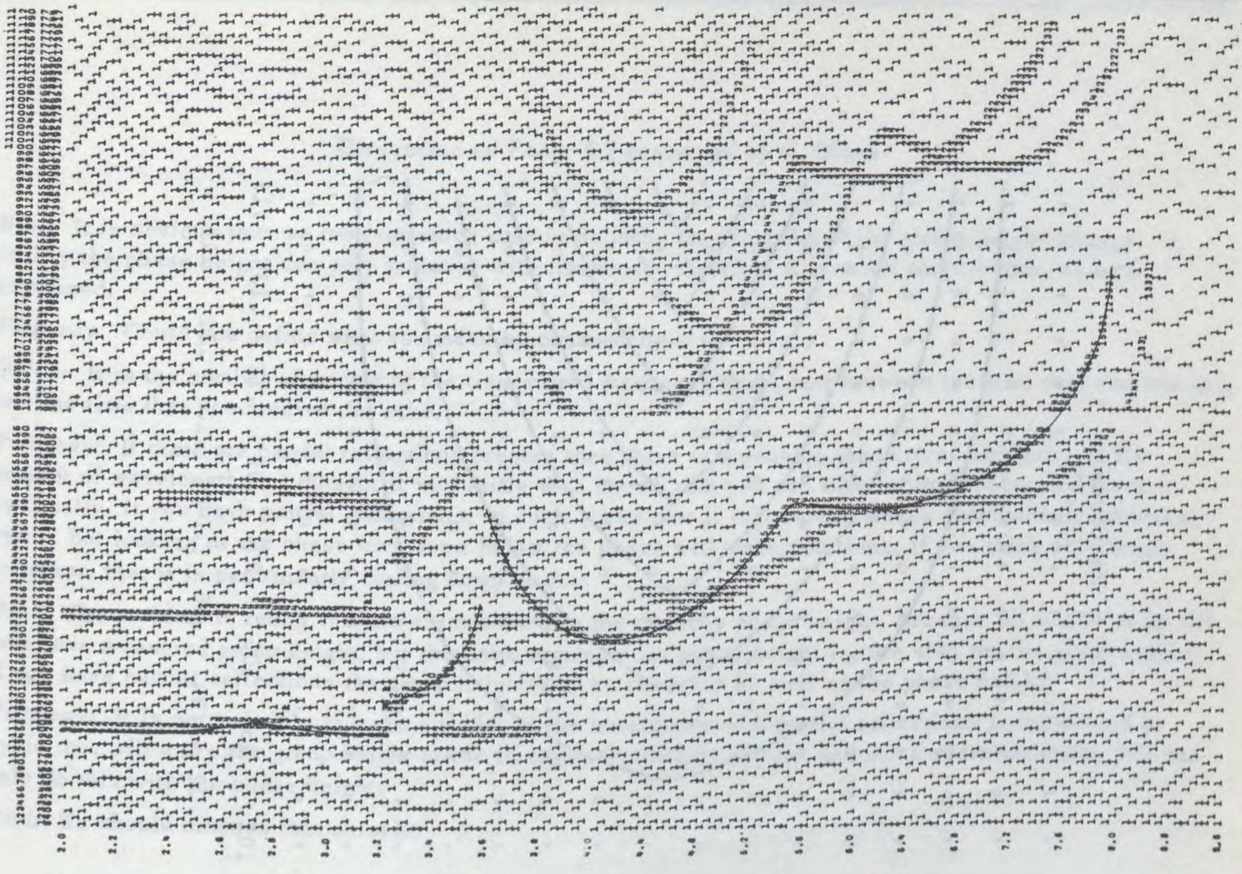

Fig. 2.

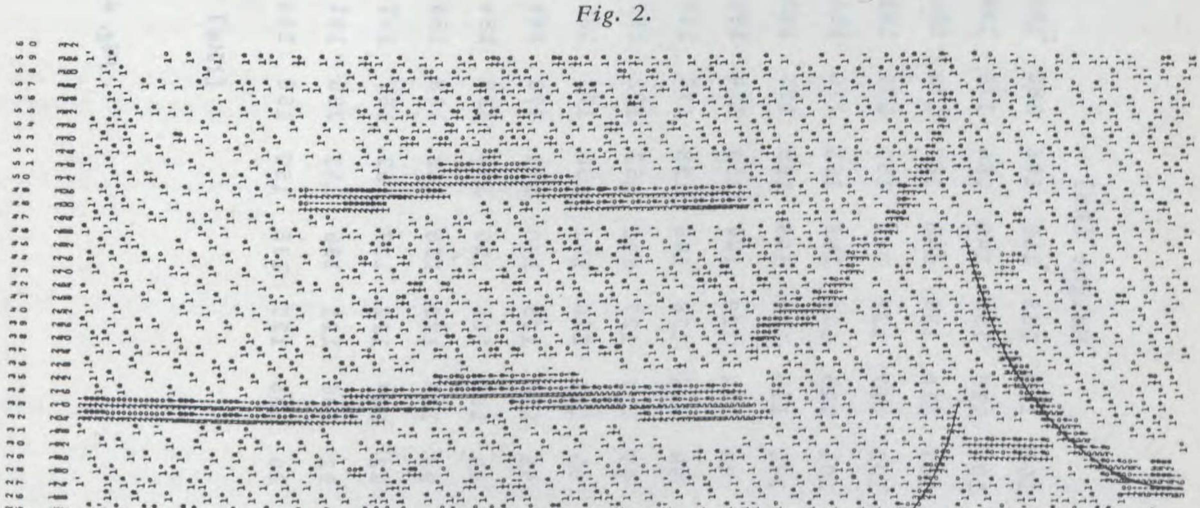

Fig. 3.

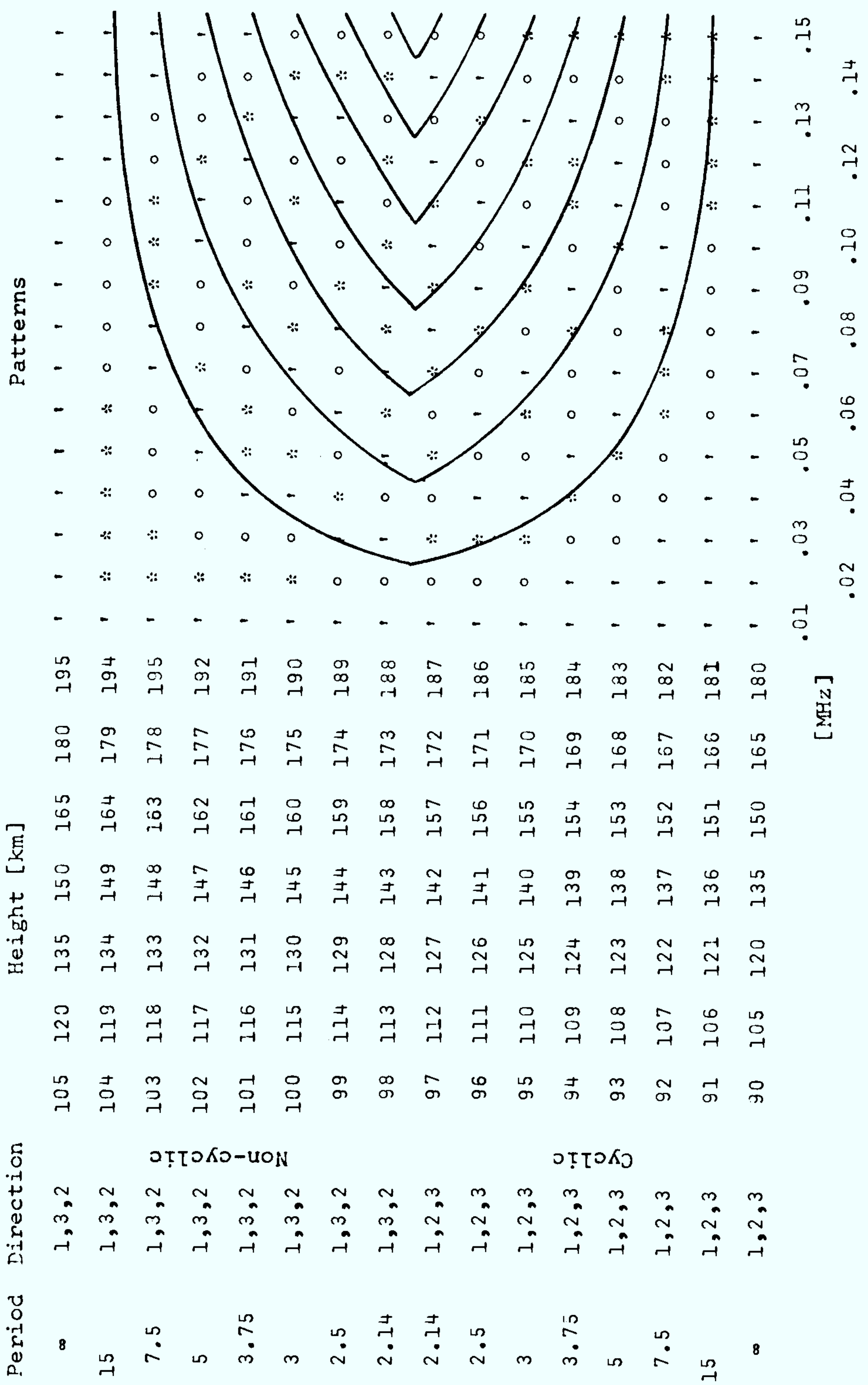
Period Direction Height [km] Patterns
Non-cyclic
Cyclic
∞ 1,3,2 105 120 135 150 165 180 195
15 1,3,2 104 119 134 149 164 179 194
7.5 1,3,2 103 118 133 148 163 178 195
5 1,3,2 102 117 132 147 162 177 192
3.75 1,3,2 101 116 131 146 161 176 191
3 1,3,2 100 115 130 145 160 175 190
2.5 1,3,2 99 114 129 144 159 174 189
2.14 1,3,2 98 113 128 143 158 173 188
2.14 1,2,3 97 112 127 142 157 172 187
2.5 1,2,3 96 111 126 141 156 171 186
3 1,2,3 95 110 125 140 155 170 185
3.75 1,2,3 94 109 124 139 154 169 184
5 1,2,3 93 108 123 138 153 168 183
7.5 1,2,3 92 107 122 137 152 167 182
15 1,2,3 91 106 121 136 151 166 181
∞ 1,2,3 90 105 120 135 150 165 180
[MHz]
.01 .02 .03 .04 .05 .06 .07 .08 .09 .10 .11 .12 .13 .14 .15

Fig. 4.

Discussion on Paper 5.3 presented by K. Olson

Bibl: It is obvious that we took too much care in defining the direction of the phase height change. In reality the phase height can only increase with frequency, therefore it is much simpler than we have explained.

Pitteway: Could you define what you mean by phase height?

Olson: It is the number of cycles of the transmitted frequency that occur between the time that you transmit and the time that you receive the echo.

Pitteway: If there are partial reflections present then there is a genuine theoretical ambiguity of the number of wavelengths. I thought it was fairly well known that you can take an ionosphere and move it cyclically, if you have partial reflections, in such a way that it just sort of moves continuously around a cycle, but looking at the phase from down below the phase will make you think, if you think of a single reflector, that it is permanently coming down at you.

Bibl: The problem is really that we are not used to the quantity phase height, because all sounders up till now have measured group height, but the same argument for phase height is true also for the group height. If you have partial reflections the group height will be changing as well as the phase height.

Pitteway: It is not possible to make a model of the ionosphere with partial reflections going around a cycle that will make the group height or the triangulation height kid you and move systematically, you can only do this with the phase height.

Bibl: We should discuss this outside.

5.4 GENERALIZATION OF ABEL'S SOLUTION FOR BOTH MAGNETOIONIC COMPONENTS IN THE REAL HEIGHT PROBLEM

by

A.K. Paul *

ITSA, ESSA, Boulder, Colorado

* Now at Max-Planck Institut fur Aeronomie, Lindau, Germany

1. Introduction

In recent years several methods have been developed using the virtual heights of reflection of ordinary and extraordinary components to calculate the electron density distribution in the ionosphere. Use of both components is essential in order to reduce uncertainties caused by parts of the profile which cannot be directly observed, such as a valley between E and F regions or the lowest part of the ionosphere. There has been some discussion as to whether a unique electron density profile or only a limited correction can be derived from the joint use of both virtual height curves. In this paper an approach is developed which permits a systematic study of what can be learned by using both components.

For comparison of ordinary and extraordinary components, it is convenient to introduce the symbol ϕ for the plasma frequency at the reflection level of a radio signal of frequency f:

$$\phi = \begin{cases} f , & \text{ordinary component,} \\ \sqrt{f^2 - f\, f_H} , & \text{extraordinary component.} \end{cases} \tag{1}$$

We further define $X = f_N{}^2/\phi^2$. For a given electron density distribution the virtual heights are defined by

$$h'_{o,x}(\phi) = \int_0^{h(\phi)} \mu'_{o,x}\, dz , \tag{2}$$

where the double suffix indicates separate equations for ordinary and extraordinary rays.

For an isotropic medium the integral equation (2) can be solved by Abel's method to give the height at which the plasma frequency f_N is equal to the particular value ϕ_n:

$$h(\phi_n) = \frac{2}{\pi} \int_0^{\phi_n} \frac{1}{\sqrt{\phi_n{}^2 - \phi^2}}\, h'(\phi)\, d\phi. \tag{3}$$

This equation can be applied only if the electron density is a monotonic function of height.

In an anisotropic medium the group refractive index for a fixed dip angle can be considered as a modification of $1/\sqrt{1-X}$. The modification depends on X and Y and for each component may be defined by

$$\mu'_{o,x} = \frac{M_{o,x}(X, Y)}{\sqrt{1-X}} \quad . \tag{4}$$

We therefore expect to find solutions by modification of (3) in the forms

$$h(\phi_n) = \int_0^{\phi_n} \frac{S_{o,x}(\phi, \phi_n)}{\sqrt{\phi_n^2 - \phi^2}} h'_{o,x}(\phi)\, d\phi. \tag{5}$$

The equations (5) are correct only for a monotonic profile. In this case we may also write

$$h'_{o,x}(\phi) = h_0 + \int_0^{\phi^2} \mu'_{o,x} z' df_N^2, \text{ where } z' = \frac{d z}{d f_N^2} . \tag{6}$$

Introducing (6) into (5) and inverting the order of integration yields:

$$I_{o,x} = h_0 \int_0^{\phi_n} \frac{S_{o,x}}{\sqrt{\phi_n^2-\phi^2}} d\phi + \int_0^{\phi_n^2} z' \int_{f_N}^{\phi_n} \mu'_{o,x} \frac{S_{o,x}}{\sqrt{\phi_n^2-\phi^2}} d\phi\, df_N^2. \tag{7}$$

We see that I_o and I_x give the real height $h(\phi_n)$ if and only if

$$\int_{f_N}^{\phi_n} \frac{M_{o,x}}{\sqrt{1-X}} \frac{S_{o,x}}{\sqrt{\phi_n^2-\phi^2}} d\phi = 1 \tag{8}$$

for fixed ϕ_n and all f_N in $o \le f_N \le \phi_n$. Condition (8) can be used to determine S_o and S_x. Examples of S_o and S_x are shown in Fig. 1.

Equations (5) are applicable only to a monotonic profile. However, their formal application in the non-monotonic case, followed by subtraction of the resulting equation for the ordinary ray from that for the extraordinary, gives

$$\int_0^{\phi_n} \frac{S_x h'_x - S_o h'_o}{\sqrt{\phi_n^2 - \phi^2}} d\phi = \int_{\phi^2_{min}}^{\phi_E^2} z'_v \int_{\phi_E}^{\phi_n} \frac{S_x M_x - S_o M_o}{\sqrt{1-X}\sqrt{\phi_n^2-\phi^2}} d\phi\, df_N^2 , \tag{9}$$

where $z'_v = |z'_2| + z'_3$ and is the slope of the equivalent valley distribution for a profile such as that in Fig. 2. Equation (9) provides a direct relation between the observed ordinary and extraordinary virtual heights and the equivalent electron density distribution in that part of the profile from which no reflections can be obtained. The inner integral on the right side, which we shall call K, is a function of ϕ_n and, through μ'_o and μ'_x, also of f_N:

$$K(f_N , \phi_n) = \int_{\phi_E}^{\phi_n} \frac{S_x M_x - S_o M_o}{\sqrt{1-X}\sqrt{\phi_n^2-\phi^2}} d\phi. \tag{10}$$

The question of what can be learned by the joint use of both components in N(h) calculations can now be answered by studying the function $K(f_N, \phi_n)$. Equation (10) can, in principle, be used to obtain the equivalent distribution in a valley between two layers.

To obtain the distribution in the lower part of the ionosphere a similar formulation can be obtained. If ϕ_1 is the lowest density observed in both components, we have

$$\int_{\phi_1}^{\phi_n} \frac{h'_x S_x - h'_o S_o}{\sqrt{\phi_n^2 - \phi^2}} d\phi = h_0 \int_{\phi_1}^{\phi_n} \frac{S_x - S_o}{\sqrt{\phi_n^2 - \phi^2}} d\phi + \int_0^{\phi_1^2} z' \int_{\phi_1}^{\phi_n} \frac{S_x M_x - S_o M_o}{\sqrt{1-X}\ \sqrt{\phi_n^2 - \phi^2}} d\phi\, df_N^2. \quad (11)$$

This equation can be used to study the starting problem.

Examples of $K(f_N, \phi_n)$ for several dip angles and values of f_H are shown in Fig. 3. For fixed ϕ_n there is always some variation of K with f_N, but the variation of K with ϕ_n for fixed f_N is small. For the valley and starting problems it seems possible in principle to obtain z'_v or z'_u, (where the indices v and u indicate equivalent valley distribution and equivalent underlying distribution, respectively) if the left-hand sides of (9) and (11) are precisely known. For practical applications the accuracy of h' is limited and in many cases the presence of horizontal gradients in the ionosphere does not provide ideal conditions for the joint use of ordinary and extraordinary virtual heights. Since the curves for fixed values of ϕ_n are almost linearly related to each other, the same would hold for the corresponding coefficients of an equation system resulting from a lamination method of solution of (9) or (11). The determinant of such a system would be small and therefore errors in h' would have very strong influence on the results. What seems to be possible for all latitudes and all frequencies is to obtain a first order correction for the valley or the underlying ionization. At some latitudes it may be possible to derive also second or higher order corrections, but surely not for dip angles around 39°, as can be seen from Fig. 3. Generally, the additional information which can be obtained by the joint use of the two components depends more on dip angle than on ϕ_E for a fixed dip angle. Nevertheless, the dependence on $Y_E = f_H/\phi_E$ is such that in all cases more may be inferred concerning unobserved ionization for small values of ϕ_E. Thus the nighttime valley problem should have more stable and accurate solutions, for a given measurement accuracy and magnetic dip angle, than the corresponding daytime problem.

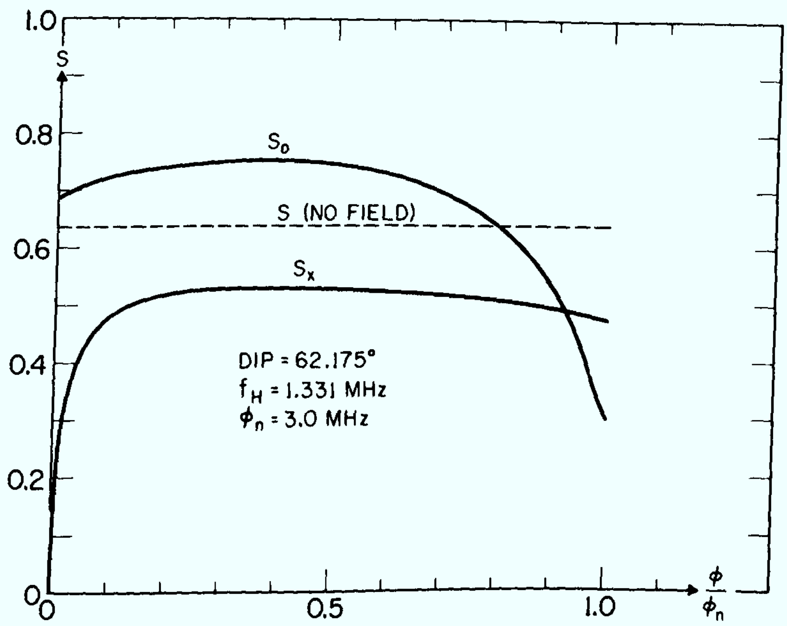

Fig. 1. Functions $S_o(\phi, \phi_n)$ and $S_x(\phi, \phi_n)$, solid lines. The corresponding function without magnetic field equals the constant $\frac{2}{\pi}$, shown as dashed line for comparison.

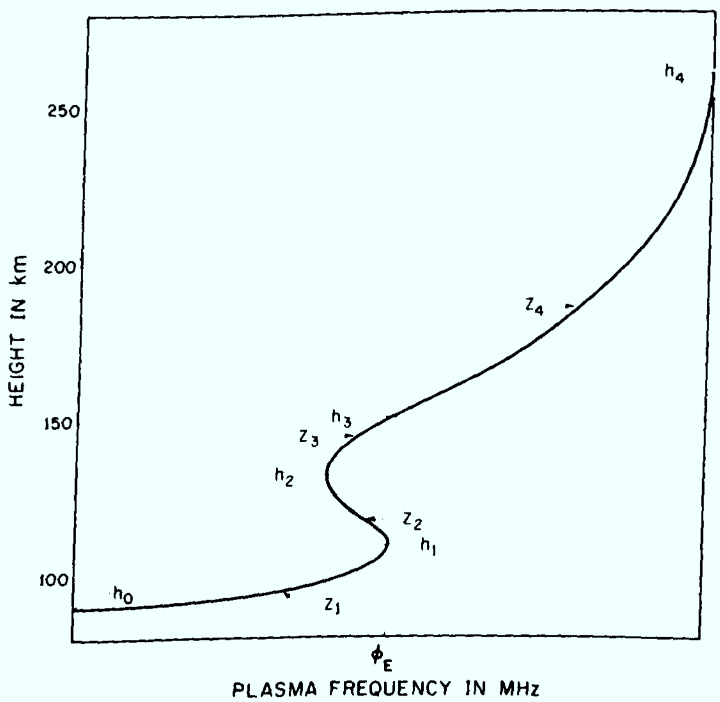

Fig. 2. Model ionosphere with valley.

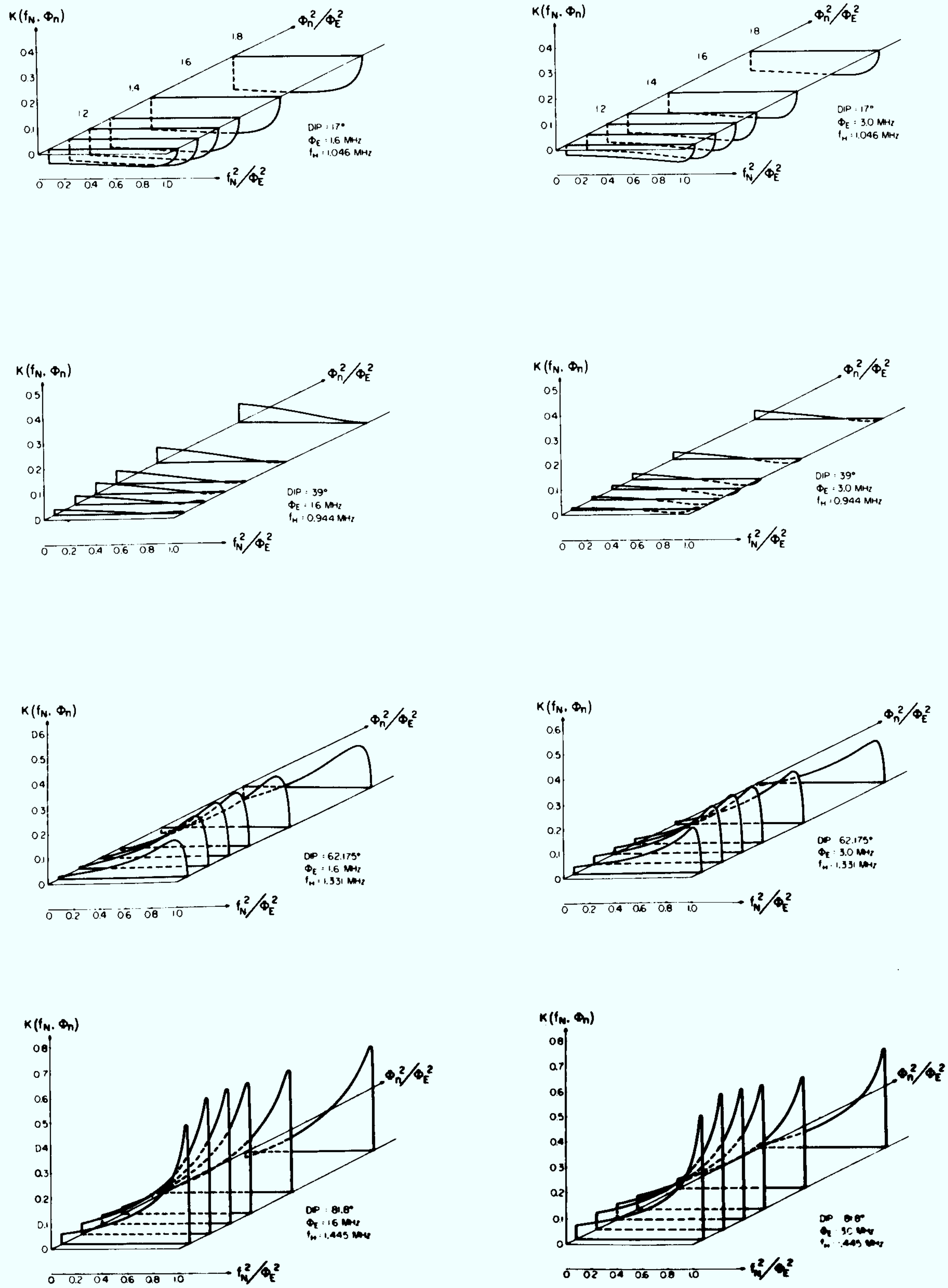

Fig. 3. Kernel function $K(f_N, \phi_n)$ for starting and valley problems at several latitudes.

Discussion on Paper 5.4 presented by A.K. Paul

Bibl: You have shown very nicely the dependence of this type of analysis on the dip angle. I have a short comment for those who are not absolutely sure what this dependence means. At equatorial stations, all virtual heights of the extraordinary component are greater than the virtual heights of the ordinary component. At temperate or northern stations this holds for the minimum virtual height, but at greater heights the extraordinary component is below the ordinary. I think that this different behavior for the virtual height curves is the key for the possible simultaneous use of the ordinary and extraordinary components. Is this correct?

Paul: Yes, that is right.

Bibl: Do you think that phase height measurements would be more useful than virtual height observations?

Paul: I wrote a paper about half a year ago concerning the use of phase height measurements in the determination of electron density distributions, which I think will be published in the April issue of Radio Science. It would be too lengthy to discuss in detail, although I'm sure you will find it answers your question.

Wright: This difficulty near 39° magnetic dip is real. We have been attempting to correct for valley effects in ionograms obtained from all over the world, and we have methods which worked, or seemed to work, pretty well at most latitudes. Their spectacular failure at and near 39° dip angle showed the singularity introduced into the equations by the near proportionality of the ordinary and extraordinary mode retardations.

My other comment is more complicated. Your work shows how much information can be obtained concerning this problem of the valley ambiguity. No assumptions were made here about the detailed shape of the electron distribution. On the other hand, solving the real and practical problem of obtaining profiles from ionograms requires that some assumptions be made about some feature or other of the electron density distribution. For example, one might fit the underlying or the unobserved ionization by segments of constant electron density gradient or curvature or by polynominal expressions and it is difficult to separate the effects of making model assumptions, and the constraints they put on the problem, from the effects that are brought into the matter by these magnetoionic considerations alone. In other words, if you choose the parameters of this assumed model, and happen to be close to the correct solution, the use of ordinary and extraordinary virtual heights may enable you to realize a successful valley correction that contains a great number of parameters, even though in principle there is information for only one or two parameters. This explains why complicated models can be more successful than these considerations have shown. Of course if you make a bad assumption about the shape of the valley you will be even worse off.

Paul: I would say again it depends on latitude, but in principle there is variation on the frequency scale, and if you had an ideal ionosphere (with ideal echoes and no lateral deviations caused by horizontal gradients and so on) there is some hope that we could get more details according to the Kernel function analysis. The reason that we are restricted, on the average, to one or maybe two parameters is that we know that we do not have ideal measurements or an ideal ionosphere.

5.5 MEAN VARIATIONS OF THE NIGHTTIME IONOSPHERIC E LAYER

by

N. Wakai *

Abstract

Low frequency ionograms (50 - 2000 kc/s.) obtained at Boulder are analyzed for July 1957, January 1958, June-July 1960, January-February 1961, and August-September 1961. Comparison of the mean variations of the nighttime E layer with those found by Elling at Tsumeb and Hough at Boulder show generally good agreement except for the first few hours after sunset.

The minimum E-layer critical frequency is reached near midnight in summer and about 0300 to 0400 in winter. At midnight the value of f_oE for h'E below 100 km. shows a clear dependence on solar activity. The peak electron density follows the relation: $N = 1.62 \times 10^3\ (1 + 0.0098\ R)$ where R is the smoothed relative sunspot number. An expression for N as a function of R is also found for sunrise and sunset conditions.

Good agreement is found with individual values of maximum electron density obtained from rocket experiments carried out at mid-latitudes at night. Some examples are given of the variation with latitude of the quiet and disturbed nighttime E layer.

1. Introduction

It is generally accepted that the nighttime ionospheric E layer varies irregularly with time and altitude, in contrast to the regular behavior of the daytime E layer as maintained by the radiation from the sun. However, a full understanding of the variation of the nighttime E layer has not been obtained because of insufficient data in the frequency range below 1 Mc/s.

Mean variations of the nighttime E layer in middle latitudes are described in this paper principally as a function of local time and solar activity, in order to investigate the effect of the nighttime E layer on the absorption of MF and lower HF waves. Low frequency ionograms (50 - 2000 kc/s.) obtained at Sunset Field Station, Boulder, Colorado, are used for the analysis.

*Paper written while a Guest Worker at the Institute for Telecommunication Sciences and Aeronomy, Environmental Science Services Administration, Boulder, Colorado.
Present address: Radio Research Laboratories, Kokubunji P.O. Koganei-shi Tokyo, Japan.

The ground-based observation of the nighttime E layer is limited to that made possible by a specially designed ionosonde having a frequency range extending down below 1 Mc/s. Parkinson and Prior (1939 and 1940) published mean hourly values of f_oE throughout the 24 hours at Watheroo (30^o19'S, 115^o53'E) from July 1938 to July 1939, using an ionosonde with a frequency range extending down to 0.516 Mc/s. In Fig. 1 the nocturnal variation of f_oE at Watheroo is shown for January, April, and July 1939. After a careful examination of those ionograms, however, VanZandt and Knecht (1964) point out that the measurements of penetration frequencies below 1.0 Mc/s. are not reliable, because the cusp which was routinely measured at Watheroo does not correspond to the actual penetration frequency but is apparently due to instrumentation. Elling (1961) reported nocturnal variations of the E region reflection at Tsumeb (19^o14'S, 17^o43'E) for August 1957, using an ionosonde with a frequency range of 0.35 to 5.6 Mc/s. Fig. 2 shows the variation of f_oIL and f_oE at Tsumeb with time after layer sunset. The symbol f_oIL is used to denote the critical frequency of the intermediate layer (Watts and Brown, 1954), which is often observed at around 150 km. virtual height, and the symbol f_oE corresponds to the critical frequency of the normal E layer near 100 km. The effective recombination coefficients for these two layers evaluated from the decay of critical frequencies, are also indicated in the figure. Hough (1966) also examined the nocturnal variation of f_oE with local time at both Sterling, Virginia, (38^o59'N, 77^o20'W), for the sunspot minimum period and at Sunset Field Station (40^o02'N, 105^o28'W) near Boulder, Colorado, for the sunspot maximum period. He analyzed ionograms of the low frequency sounder (Blair et al., 1953) having a frequency range of 50 to 2000 kc/s., and found a clear dependence of f_oE on solar activity as shown in Fig. 3, though no evidence could be obtained of a seasonal variation of f_oE. It should be noted that the f_oE measured by Hough corresponds to the critical frequency of the intermediate layer, which tends to be associated with geomagnetic disturbance.

Several direct rocket measurements of the electron distribution in the lower ionosphere have been made during nighttime including sunrise and sunset hours. These are listed in Table 1 and illustrated in Fig. 4. Since there is usually considerable difference between the N(h) profiles in the up-leg and down-leg of a flight, the averaged electron density between them is shown in Fig. 4. It is to be noted that all peaks of the E layer are seen between 100 and 110 km., while deep valleys in the profiles labelled (1), (2), (3), and (7) are observed around 120 km., with an electron density of about one order less than the lower E-layer peak. The only profile showing a clear appearance of the intermediate layer is profile (7) (Cartwright, 1964) which was obtained by observation of the doppler shift of VLF signals. The increase of electron density above 130 km. in profile (3) may correspond to the base of the intermediate layer.

Using conventional ionograms, many workers have reported frequent occurrences of the intermediate layer associated with large geomagnetic disturbances (Haubert, 1959; Wakai and Sawada, 1964).

2. Determination of f_oE and h'E from Low Frequency Ionograms

Sounding observations of the ionosphere by the low frequency sounder (50 - 2000 kc/s.) were made near Boulder, Colorado, from 1956 to 1961. Periods of data reduced for this analysis are 1 - 31 July, 1957, 1 - 31 January, 1958, 3 - 30 June, 1 - 31 July, 1960, and 11 - 23 January, 8 - 14 February, 5 - 18 August, and 3 - 16 September 1961. Only midnight (0000 - 0100) ionograms were reduced for June - July 1960.

Critical frequencies and minimum virtual heights of all thick stratifications with group retardation observed at a lower height than the F-layer echoes are scaled for both the ordinary and extraordinary components. Interference in the broadcast band and blanketing due to the sporadic E layer often make it difficult to accurately reduce the ionospheric parameters on low frequency ionograms. The extraordinary component, however, is helpful in the interpretation of observed echoes, because even when the ordinary component is not discernible due to the severe interference of MF broadcasts, the cusp of penetration of the extraordinary trace is often observable, since it occurs below 500 kc/s. Furthermore, the additional retardation (Watts, 1958) on the extraordinary trace which is observed at a frequency near the peak plasma frequency of an underlying layer is also taken into account.

It is desirable that the frequency separation between the ordinary and extraordinary components be determined experimentally in order to extrapolate the critical frequency of the ordinary wave, f_o, from the extraordinary-trace critical frequency, f_x. Records in which clear group retardations are observable on both traces from the E region were selected for July 1957, and January 1958. Scaled values for f_o and f_x are plotted in Fig. 5. The value of f_H at the 100 km. level above Boulder is equal to 1.5 Mc/s. as calculated from the magnetic field intensity measured near Boulder, Colorado. The curve in Fig. 5 shows the relation

$$f_o^2 = f_x^2 + f_x f_H,$$

where f_H = 1.5 Mc/s.

It is seen that observed plots closely follow the curve. Thus, f_o is deduced from f_x in this manner when f_x can be scaled but f_o is masked by severe interference.

No parameters of the sporadic E echo are reduced in the present analysis.

Fig. 6 shows two examples of low frequency ionograms. It is seen in Fig. 6 (a) that the group retardation is recorded on both the lower end of the F trace and higher end of the uppermost E trace which is stratified into three parts. In Fig. 6 (b), the sporadic E echo blankets a lower portion of the F trace so completely up to 1.33 Mc/s. that no information can be obtained on the nighttime E layer.

3. Presentation of Results

3.1 Mean Nocturnal Variation of E-region Echoes

Several cusps with various minimum virtual heights are usually observed in the nighttime E-layer echoes on low frequency ionograms, in contrast to the consistency of virtual height of the E-layer echoes observed by conventional ionosondes during the daytime.

First, the occurrence rate of nighttime E-region echoes is examined in virtual height ranges of 10 km. Fig. 7 shows the occurrence rate which is calculated for echoes observed during nighttime. Early morning and late evening echoes are included in each period except June - July 1960. It is seen in the figure that there are no marked differences among the general features of each period, about 50 to 65 per cent of observed echoes having a virtual height equal to or less than 100 km.

Accordingly, the monthly median value of f_oE is found separately for both the predominant lower echoes with h'E (virtual height of the E layer) ≤ 100 km. and the higher ones with h'E ≥ 105 km.

(a) July 1957

Fig. 8 (a) shows a f- and h'-plot for the E reflection during the night of 2 - 3 July, 1957. The critical frequencies of echoes with h'E ≥ 105 km. and h'E ≤ 100 km. are plotted for the whole month in Figs. 8(b) and (c) respectively. Since the sporadic E layer is much more prevalent in summer than in winter, a smaller number of scaled f_oE's is available than for the following January 1958, due to blanketing by the sporadic E layer. Fig. 8 (d) shows monthly median curves for the plots in Figs. 8 (b) and (c), in addition to two curves of lowest critical frequency observed within the month, for echoes at 100 km. and echoes below 90 km., respectively. Discussions on the latter two curves will be given in another paper in connection with the maintenance of ionization in the nighttime E layer.

(b) January 1958

A f- and h'-plot for E reflections on 20 - 21 January, 1958, is shown in Fig. 9 (a). Here the changing virtual height of echoes can be seen as well as a continuous decrease of critical frequency below 100 km. Illustrations in Figs. 9 (b), (c), and (d) correspond to the critical frequencies of E-region echoes above 105 km., below 100 km., and the median and lowest frequency curves, respectively.

(c) January - February 1961

Observations by the low frequency sounder were continued intermittently after the IGY. Since data on only 13 and 7 days in January and February, respectively, are available for analysis, the median values are obtained for the two months taken together. Fig. 10 (a) shows a f- and h'-plot on 14 - 15 January, 1961. A sudden occurrence of the intermediate layer after midnight can be seen from the h'-plot of the figure. In Figs. 10 (b), (c), and (d), are shown the critical frequencies of E-region echoes above 105 km., below 100 km., and the median and lowest frequency curves, respectively.

(d) August - September 1961

Observations by the low frequency sounder were not made during the first half of the night after June 1961. Fig. 11 (a) shows a f- and h'-plot starting at 0020 hours on 8 August, 1961. In Figs. 11 (b), (c), and (d), are shown the critical frequencies of E-region echoes above 105 km., below 100 km., and the median and lowest frequency curves, respectively. The observations ended after 16 September, 1961, due to damage to the antenna, which was a 3300-foot wire installed across a mountain canyon.

Four nocturnal variations of the median critical frequency of E-region echoes below 100 km. are illustrated in Fig. 12.

As seen from the curves for January 1958 and January - February 1961, the electron density variation during the night in winter is characterized by the following:

(1) The electron density initially decreases rapidly until a transition to a more gradual decrease follows. This occurs at 105 to 108^{o} in solar zenith angle, χ, (80 to 100 min. after ground sunset).

(2) The gradual decrease lasts until the minimum is reached a few hours before sunrise, say, 3 to 4 a.m. Then a gradual increase takes place.

(3) A sudden increase of the electron density in the morning occurs at χ = 99 to 100^{o} (50 to 55 min. before ground sunrise).

Although these results are handicapped by the absence of data before midnight in August - September 1961, they indicate the following tendencies in summer.

(1) The electron density decreases more rapidly in summer than in winter until the transition to a gradual decrease occurs at χ = 97 to 99^{o} (40 - 50 min. after ground sunset).

(2) The gradual decrease lasts until around midnight, when it is followed by a gradual increase of electron density.

(3) The sudden increase in the morning takes place at χ = 99^{o} (50 min. before ground sunrise).

(4) The features of the nocturnal variation are symmetrical with respect to midnight.

The solar zenith angle of sudden increase in the morning is consistent between summer and winter, and also agrees well with the value given by Hough (1966). It is to be noted, however, that the transition from the rapid to gradual decrease in the evening takes place later in winter than in summer.

Since the characteristics of E-region echoes having h'E ≥ 105 km. are probably more sensitive to magnetic activity than those below 100 km., further discussion on the nocturnal variation of higher echoes in the E region will be made in another paper concerning the disturbed variation of the nighttime E layer.

A comparison between the mean nocturnal variation obtained in the present analysis and several individual values of the maximum electron density of the E region measured from rockets in mid-latitude nighttime is made in Fig. 12. Details regarding each of the rocket flights are listed in Table 1. Almost all peak plasma frequencies measured by the rockets are within a reasonable allowance of the median curves for the corresponding solar activity, except (1) whose relatively high value is not easily understood. Since only (7) is obtained at midnight, 0030, 12 April, 1963 (RSSN = 29), it can be compared with the lower regression line in Fig. 13, which expresses the relation between the smoothed relative sunspot number and the midnight electron density in the E layer below 100 km. Good agreement is evident.

3.2 Solar Activity Dependence of Midnight f_oE

The value of f_oE at midnight may be examined in order to investigate the dependence of the nighttime E layer on solar activity. This choice of parameter is made in view of the marked difference in nocturnal variation of f_oE between summer and winter, and the occurrence of the electron density minimum at midnight in summer. In addition to the median f_oE for the four periods dealt with in the previous paragraph, f_oE at midnight (0000 - 0100) in June and July 1960, is analyzed.

Median f_oE's at midnight are obtained for the following five categories of virtual height range and are listed in Table 2 with the smoothed relative sunspot number (RSSN):

(1) The first column of median f_oE in the table involves f_oE's with the lowest height ($h'E \leq 100$ km.), which are not only predominant and stable, but also less sensitive to magnetic activity than higher echoes. If a linear relation is assumed between the smoothed relative sunspot number, R, and the peak electron density, N in electrons/cc., the following expression is obtained:

$$\left[N(h'E \leq 100)\right]_{midnight} = 1.62 \times 10^3 \left[1 + 0.0098R\right].$$

This relation is plotted in Fig. 13 by a dotted line with the median f_oE's shown by open triangles.

(2) The second column involves f_oE's with $h'E \leq 135$ km., representing the peak plasma frequency in the nighttime E region, excluding the intermediate layer. If a linear relation between R and N is assumed, the following expression is obtained:

$$\left[N(h'E \leq 135)\right]_{midnight} = 2.21 \times 10^3 \left[1 + 0.0062R\right].$$

The dashed line and open squares in Fig. 13 show the regression line and median f_oE's, respectively.

(3) The third column involves f_oE's with a medium range of virtual height (105 km. $\leq h'E \leq 135$). It is to be noted that both winter f_oE's for January 1958, and January - February 1961, have lower values than summer f_oE's for July 1957, June - July 1960, and August - September 1961.

(4) Lower f_oE's in winter are also seen in the fourth column in which all higher echoes with $h'E \geq 105$ km. are contained. The sporadic E echoes, however, mask upper traces so frequently in summer that fewer observed echoes are available than in winter. Furthermore, it should not be overlooked that there is the possibility of much more inclusion of higher f_oE's in summer, resulting from the blanketing due to the sporadic E ionization.

In these circumstances, there is some danger in concluding that a seasonal dependence of f_oE exists at higher levels in the E region, although the median values show a remarkable difference in f_oE between summer and winter.

(5) The fifth column of median f_oE in Table 2 involves f_oE's with $h'E \geq 140$ km., corresponding to the so-called intermediate layer. Appearance of these echoes is usually accompanied by rather severe geomagnetic disturbances. The dependence on magnetic activity, as well as solar activity, should be taken into account in analyzing the variations of these echoes.

Fitting of an approximate expression is not attempted for the values in the third, fourth, and fifth columns, because of the seasonal differences which reduce the reliability of a fitted relation. Median f_oE's at midnight in the first, third, and fifth columns in Table 2 are converted to peak electron density and plotted in the lower part of Fig. 14 against smoothed relative sunspot number.

3.3. Values of f_oE at Sunrise and Sunset

It has been found experimentally that the maximum electron density of the daytime E layer, $N_{max}E$ in electrons/cc., when the solar zenith angle χ is less than about 75^o, is expressed approximately as follows (VanZandt and Knecht, 1964; Davies, 1965):

$$N_{max}E\ (\chi,\ R) = 1.35 \times 10^5 \left[(1 + 0.008R) \cos \chi\right]^{\frac{1}{2}}.$$

The values of f_oE, however, at sunrise and sunset ($\chi = 90^o$) have never been determined experimentally, because they fall around the lower frequency limit of conventional ionosondes. The values of f_oE at sunrise and sunset throughout the solar cycle are required in order to determine the mean nocturnal variation of the E layer for a given RSSN.

Accordingly, f_oE at $\cos \chi = 0$ was reduced in detail from the low frequency ionograms. It is obtained from interpolation between two observed f_oE's, one for a small positive $\cos \chi$ and the other for a small negative $\cos \chi$, using a value of $\cos \chi$ computed on a day-to-day basis for Boulder.

The data for January - February 1961, are not available for this purpose because no measurements were made during sunrise and sunset hours. Since the same situation was found in a part of June 1960, as well as in almost all of July 1960, all usable data for June, July, and August 1960, are combined as representative values for medium solar activity (RSSN = 112).

The median f_oE which is observed when $\cos \chi = 0$ is summarized in Table 3 for various sunspot numbers. Although the analysis was made separately for sunrise and sunset hours, no significant difference could be found. Therefore, the relation described below is valid for both the sunrise and sunset hours.

When it is assumed a priori that the square of the peak electron density is linearly related to the relative sunspot number, the following relation is obtained from a least squares fit of the median f_oE for $h'E \leq 100$ km. (Table 3):

$$\left[N(h'E \leq 100)\right]_{\cos \chi = 0} = 1.40 \times 10^4 \left[1 + 0.0077R\right]^{\frac{1}{2}}.$$

This assumption, implying the same dependence on the sunspot number as the daytime E layer exhibits, is reasonable because the sun still affects the E layer ionization even though the sunrise and sunset exist at ground level.

In the above equation, the coefficient of R is so close to 0.008 that the second least square fit could be made on the assumption that $[N]_{\cos\chi = 0}$ is proportional to $[1 + 0.008R]^{\frac{1}{2}}$. Thus, the following relation between R and N around 100 km. when $\cos\chi = 0$ is determined experimentally:

$$[N\ (h'E \leq 100)]_{\cos\chi = 0} = 1.38 \times 10^4\ [1 + 0.008R]^{\frac{1}{2}}.$$

This equation is illustrated in a curve in the middle part of Fig. 14, together with the f_oE values at three different height ranges as given in Table 3. Similarly, for the f_oE with 105 km. $\leq$ h'E $\leq$ 135 km., $[N(105 \leq h'E \leq 135)]_{\cos\chi = 0} = 2.00 \times 10^4\ [1 + 0.008R]^{\frac{1}{2}}$.
For the f_oE with h'E $\geq$ 140 km.,

$$[N(h'E \geq 140)]_{\cos\chi = 0} = 2.49 \times 10^4\ [1 + 0.008R]^{\frac{1}{2}}.$$

4. Discussion of Results and Conclusions

4.1 Comparison with Other Studies

It appears likely that the vertical soundings at Watheroo in 1938 and 1939 suffered much less interference from the MF broadcasting band than that encountered in recent years. Nevertheless, these measurements of the nighttime variation of f_oE shown in Fig. 1 are not reliable because of uncertainty in identifying penetration frequencies near the lower frequency end of the sounder (VanZandt and Knecht, 1964). Accordingly, no further discussion of the nocturnal variation of f_oE at Watheroo will be given in this paper.

In Fig. 15 the nocturnal variations of f_oE obtained here are compared with f_oE and f_oIL at Tsumeb on a time scale beginning at ground sunset (Elling, 1961). It is appropriate to compare f_oE (h'E $\geq$ 105 km.) with f_oIL at Tsumeb and to compare f_oE (h'E $\leq$ 100 km.) with f_oE at Tsumeb, as is done here for the sunspot maximum period. There is some risk that f_oE with h'E $\geq$ 105 km. is not identical with f_oIL, which was observed exclusively above 150 km. at Tsumeb. However, the comparisons show remarkably good agreement, with no difference exceeding 10 kc/s. throughout the night. The discrepancies of the f_oIL points within about 2 hours after sunset may be ascribed to the difference in classification just mentioned. The variation of f_oE at Boulder in July 1957 is too different in character to compare directly with values at Tsumeb obtained in local winter.

The definition given in Hough (1966) indicates that values of f_oE shown in Fig. 3 almost correspond to the higher f_oE (h'E $\geq$ 105 km.) in this paper. Contrary to his conclusion that no appreciable difference is found between f_oE in summer and in winter, the midnight f_oE of higher traces is lower in winter than in summer, as is seen in Table 2 or Fig. 14. For comparison with the sunspot maximum curve in Fig. 3, median f_oE for h'E $\geq$ 105 km. was recalculated from present results for hours 2000 to 0500 and for July 1957 and January 1958 combined. The resulting variation is shown as a dash-dot curve in Fig. 16. An estimate of the probable range of f_oE for the sunspot minimum period is also shown in Fig. 16.

Barghausen (1964) reports the variation of f_oE at night at Huancayo (12° 03' S, 75° 20' W) for three months in 1964. The results are derived from extended range ionograms (250 kc/s. to 20 Mc/s.) made with support of the National Bureau of Standards as part of the IQSY program. The average f_oE curve at Huancayo for May to July 1964 is shown as a dotted line in Fig. 16, compared with Sterling observations in the preceding sunspot minimum period. Good agreement is seen between the two variations, in spite of the difference in latitude between the two sounding stations.

From the above considerations it is concluded that no great difference exists in the nighttime E region ionization between middle and low latitudes. Values of f_oE obtained in this analysis are in good agreement with the results of Elling and Hough.

4.2 Latitudinal Variation of the Quiet and Disturbed Nighttime E Layer

The latitudinal variation of the nighttime E layer is a matter of major concern to those studying the maintenance of ionization in the layer. The term "nighttime E layer" is usually applied to a thick layer appearing at night in lower latitudes. The "night-E layer", on the other hand, is defined exclusively as a high latitude layer to be distinguished from the sporadic E layer (Wright, Knecht, and Davies, 1957). In the absence of the F-layer echo, however, it is difficult to determine whether an echo with the retardation cusp is reflected from the night-E or from the r-type sporadic E layer (Wright, Knecht, and Davies, 1957). It is not known whether the high-latitude night-E layer is essentially the same as the low-latitude nighttime E layer with respect to latitudinal continuity in electron density, height, or mechanism of formation.

The nighttime E layer associated with large geomagnetic disturbances in middle latitudes can be detected from conventional ionograms. Even when E-layer echoes are not observed, the group retardation of F-layer echoes, especially that of the extraordinary component, reveals the critical frequency of the underlying layer. Special attention is required to interpret cases of no echo available other than the extraordinary F trace, as the retardation cusp approaches the gyrofrequency.

The three examples presented below may serve as a clue to the understanding of the behavior of the nighttime E layer throughout the whole range of latitudes.

Two events are selected from the disturbances in April 1960. Penetration frequencies of the ordinary and/or extraordinary components of the nighttime E-layer echoes are shown in Figs. 17 and 18, plotted against geomagnetic latitude in either hemisphere. Fig. 17 is for 1 April (Σ Kp = 65+) and Fig. 18 is for 30 April, 1960 (Σ Kp = 57+). Since blackouts were recorded at almost all high latitude stations on 30 April, ionograms for 29 April (Kp = 41_o) were also reduced.

The symbols used in Figs. 17 and 18 are listed in Table 4, which shows geographic and geomagnetic coordinates as well as magnetic dip and gyrofrequency for 100 km. above the ground. Most of the stations used are located between the 75^oW and 105^oW meridians. The figures are intended to show the latitudinal variation at 0100 local time. Nevertheless, when critical frequencies at 0100 cannot be obtained due to blanketing by the sporadic E layer (A), blackout (B), or no observation (C), they are replaced by values recorded at 0100 ± 1 hour.

In both figures, a smooth increase in critical frequency of the nighttime E layer is seen as the geomagnetic latitude increases up to 52^o (Fort Monmouth). After an observational gap of about 5^o in latitude, discontinuously high critical frequencies follow up to about 80^o. Somewhat lower frequencies seem to be observed in the polar cap region above 80^o. On the whole, critical frequencies on 1 April (Σ Kp = 65+) exceed those on 30 April (Σ Kp = 57+).

One example of the latitudinal variation of the quiet nighttime E layer at 0100 local time on 20 April, 1960 (Σ Kp = 4-) is shown in the lower right corner of Fig. 17. No evidence of the nighttime E layer is found on 20 April at latitudes less than that of Fort Monmouth. This would be expected from the tendencies mentioned in the preceding paragraph.

It is seen in Fig. 17 that critical frequencies of the quiet nighttime E layer in high latitudes have a peak around 70°; the critical frequency decreases gradually towards the pole and rather steeply towards lower latitudes.

A complete explanation of the latitudinal variation of the nighttime E layer must await further experimental and theoretical work. However, the following qualitative explanation may be suggested. The latitudinal variation of the disturbed nighttime E layer resembles that of the electric current density of the SD field flowing in the ionosphere (Chapman and Bartels, 1940). If the sudden jump in electron density is taken as the transition from the nighttime E to the night-E layer, it seems to occur within the 52 to 57° range of geomagnetic latitude. The latitude of the transition seems to vary with magnetic activity. Furthermore, the transition may correspond to the main trough in the F layer which was disclosed by the topside sounder Alouette (Muldrew, 1965).

A further study of this subject will be published in the near future.

REFERENCES

Aono, Y., Hirao, K. and S. Miyazaki. Rocket observation of ion density in the ionosphere, J. Rad. Res. Labs., 8, No. 40, 441 - 451, 1961.

Barghausen, A.F. Private communication.

Blair, J.C., Brown, J.N. and J.M. Watts. An ionosphere recorder for low frequencies, J. Geophys. Res., 58, No. 1, 99, March 1953.

Cartwright, D.G. A 10-kilocycle per second doppler observation of the intermediate layer of the nighttime ionosphere, J. Geophys. Res., 69, No. 19, 4031, 1 October, 1964.

Chapman, S. and J. Bartels. Geomagnetism, Oxford, 1940.

Davies, K. Ionospheric Radio Propagation, NBS Monograph 80, 1965.

Elling, W. Scheinbare Reflexionshöhen und Reflexionsvermögen der Ionosphäre über Tsumeb, Südwest-Afrika, ermittelt mit Impulsen im Frequenzband von 350 bis 3500 kHz, Archiv Elektrischen Übertragung, 15, 115, 1961.

Hanson, G.H. Hagg, E.L. and D. Fowle. The interpretation of ionospheric records, Defence Research Telecommunications Establishment Report R-2, 1953.

Haubert, A. L'ionisation nocturne de la région-E et l'activité géomagnétique, J. Atmos. Terr. Phys., 15, 84, 1959.

Hough, W.S. Ionospheric E-layer observations at night, to be published, 1966.

Muldrew, D.B. F-layer ionization troughs deduced from Alouette data, J. Geophys. Res., 70, No. 11, 2635, 1965.

Parkinson, W.C. and L.S. Prior. The ionosphere at Watheroo, Western Australia, May to December, 1938, Terr. Mag. Atmos. Elec., 44, 199, 1938.

Parkinson, W.C. and L.S. Prior. The ionosphere at Watheroo, Western Australia, January, February, and March, 1939, Terr. Mag. Atmos. Elec., 44, 341, 1939.

Parkinson, W.C. and L.S. Prior. The ionosphere at Watheroo, Western Australia, April, May, and June, 1939, Terr. Mag. Atmos. Elec., 44, 401, 1939.

Parkinson, W.C. and L.S. Prior. The ionosphere at Watheroo, Western Australia, July to September, 1939, Terr. Mag. Atmos. Elec., 45, 45, 1939.

Smith, L.G. Rocket measurements of electron density and temperature in the nighttime ionosphere, Geophys. Corp. of America, Tech. Report 62-1-N, 1962.

Smith, L.G. Measurements of electron density profile in the nighttime E region, Geophys. Corp. of America, Tech. Report 63-22-N, 1963.

VanZandt, T.E. and R.W. Knecht. The structure and physics of the upper atmosphere, Ch. 6 in Space Physics edited by LeGalley and Rosen, Wiley, New York, 1964.

Wakai, N. and K. Sawada. Nocturnal variation of the ionospheric E region in a temperate latitude with geomagnetic disturbances, J. Rad. Res. Labs., 11, No. 53, 1 - 17, 1964.

Watts, J.M. and J.N. Brown. Some results of sweep-frequency investigation in the low frequency band, J. Geophys. Res., 59, No. 1, 71 - 86, 1954.

Watts, J.M. The interpretation of nighttime low-frequency ionograms, J. Geophys. Res., 63, No. 4, 717 - 726, 1958.

Wright, J.W., Knecht, R.W. and K. Davies. Ionospheric vertical soundings, Pt. I of Vol. III, Annals of the IGY, Pergamon Press, Oxford, 1957.

Table 1. Nighttime electron density measurements by rockets

No.	Date	Time	Launching Site (Position)	Remarks
1	1960, Sept. 26	2025, 135° EMT	Akita (39°44'N, 140°08'E)	Fig. 4(1), Aono et al., 1961 RSSN = 98
2	1961, Aug. 17	2206, 75° WMT	Wallops Is. (37.9°N, 75.5°W)	Fig. 4(2), Smith, 1962 RSSN = 53
3	1961, Oct. 27	0435, 75° WMT	Wallops Is. (37.9°N, 75.5°W)	Fig. 4(3), Smith, 1962 RSSN = 51
4	1962, Nov. 7	0525, 75° WMT	Wallops Is. (37.9°N, 75.5°W)	Fig. 4(4), Smith, 1963 RSSN = 30
5	1962, Nov. 30	0557, 75° WMT	Wallops Is. (37.9°N, 75.5°W)	Fig. 4(5), Smith, 1963 RSSN = 30
6	1962, Dec. 5	1700, 75° WMT	Wallops Is. (37.9°N, 75.5°W)	Fig. 4(6), Smith, 1963 RSSN = 30
7	1963, Apr. 12	0030, 75° WMT	Wallops Is. (37.9°N, 75.5°W)	Fig. 4(7), Cartwright, 1964 RSSN = 29

RSSN: Smoothed relative sunspot number for the month.

Table 2. Median f_oE at midnight (0000 - 0100) in five virtual height ranges

Sunspot Number	Period of Data Used	Median f_oE at midnight (00^h - 01^h) in kc/s.					Remarks
		h'E≤100	h'E≤135	105≤h'E≤135	h'E≥105	h'E≥140	
191	July 1-31, 1957	600	610	780	830	950	
199	Jan. 1-31, 1958	630	640	660	700	700	
112	June 3-30, 1960 July 1-30, 1960	530	565	800	800	800	No observation: 5~10, 14, 15, 19~21 June 4~16 July
78	Jan. 11-23, 1961 Feb. 8-14, 1961	480	510	550	570	590	
52	Aug. 5-18, 1961 Sept. 3-16, 1961	440	480	670	725	750	

Table 3. Median value of f_oE in various height ranges at cos χ = 0

Sunspot Number	Period of Data Used	Median f_oE in Mc/s. at cos χ = 0			Remarks
		h'E≤100 km.	105≤h'E≤135 km.	h'E≥140 km.	
191	July 1957	1.32	1.58	1.74	
199	Jan. 1958	1.35	1.60	1.84	
112	June July Aug. 1960	1.25	1.52	1.69	
52	Aug. and Sept. 1961	1.16	1.38	1.51	

Table 4. List of stations used for analysis of latitudinal variation of the nighttime E layer

Station	Geographic Lat.	Geographic Long.	Geomagnetic Lat.	Geomagnetic Long.	Dip	f_h in Mc/s. at 100 km. height
TH Thule	76°33'N	68°50'W	+88.1°	01.1°	86°	1.49
RB Resolute Bay	74°41'N	94°55'W	+82.9°	289.3°	89°	1.54
GH Godhavn	69°16'N	53°30'W	+79.9°	32.6°	82°	1.54
NR Narssarssuaq	61°11'N	45°25'W	+71.2°	37.6°	77°	1.42
CH Churchill	58°46'N	94°10'W	+68.7°	322.7°	84°	1.60
FB Fairbanks	64°54'N	147°48'W	+64.0°	256.0°	77°	1.50
WP Winnipeg	49°54'N	97°24'W	+59.6°	322.7°	78°	1.60
SJ St. Johns	47°32'N	52°47'W	+58.4°	21.4°	72°	1.41
OT Ottawa	45°24'N	75°54'W	+56.9°	351.3°	75°	1.53
FM Fort Monmouth	40°15'N	74°01'W	+51.7°	353.9°	71°	1.51
WA Washington	38°44'N	77°08'W	+50.1°	350.1°	71°	1.50
BL Boulder	40°02'N	105°18'W	+48.9°	316.4°	68°	1.50
WS White Sands	32°18'N	106°30'W	+41.0°	316.4°	60°	1.38
CK Cape Kennedy	28°29'N	80°30'W	+39.6°	346.4°	61°	1.35
GB Grand Bahama	26°40'N	78°22'W	+37.9°	349.3°	60°	1.30
SS San Salvador	24°06'N	74°30'W	+35.2°	354.8°	57°	1.28
MX Mexico City	19°20'N	99°11'W	+29.2°	327.2°	46°	1.19
BG Bogota	04°38'N	74°05'W	+15.9°	354.5°	32°	0.95
TL Talara	04°34'S	81°15'W	+06.6°	347.7°	13°	0.85
HU Huancayo	12°03'S	75°20'W	-00.6°	353.8°	2°	0.77
LP La Paz	16°29'S	68°03'W	-05.0°	0.9°	- 5°	0.73
BA Buenos Aires	34°36'S	58°29'W	-23.3°	9.4°	-31°	0.70
CC Concepcion	36°35'S	72°59'W	-25.3°	356.5°	-36°	0.78
BY Byrd	79°59'S	120°01'W	-70.6°	336.1°	-75°	1.57

96414—13½

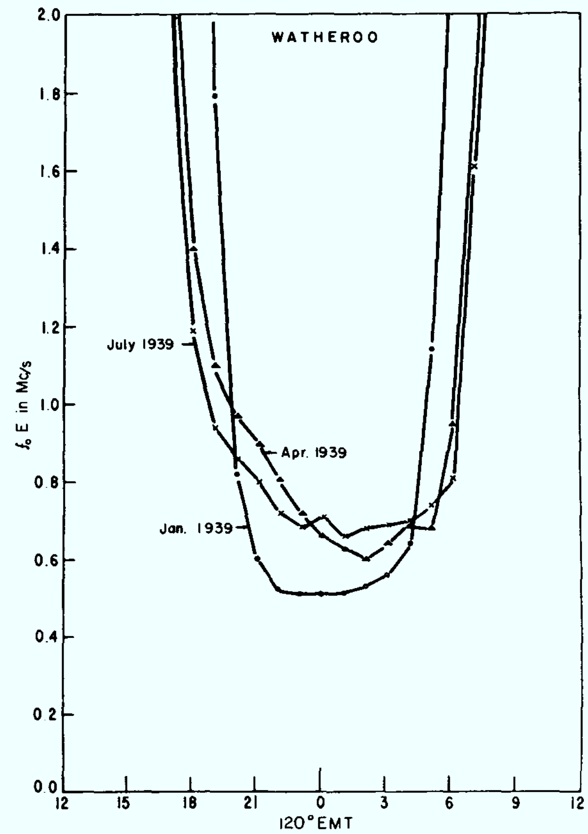

Fig. 1. Monthly median f_oE during the night at Watheroo in January, April, and July 1939.

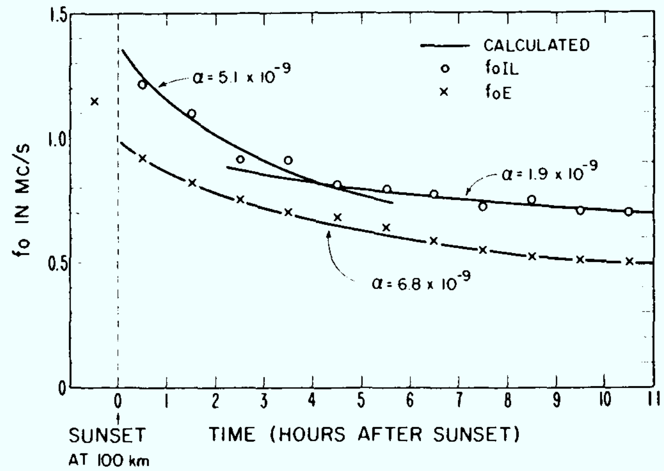

Fig. 2. Variation of f_oE and f_oIL after sunset at Tsumeb, August 1957.

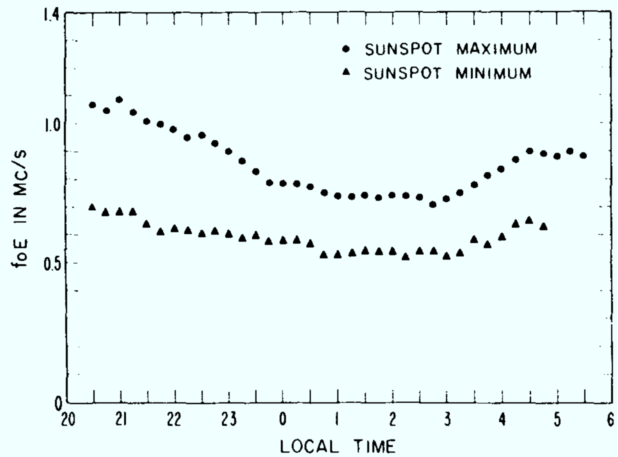

Fig. 3. Twelve-month smoothed median f_oE versus time at Sterling, Virginia (sunspot minimum curve) and Boulder, Colorado (sunspot maximum curve).

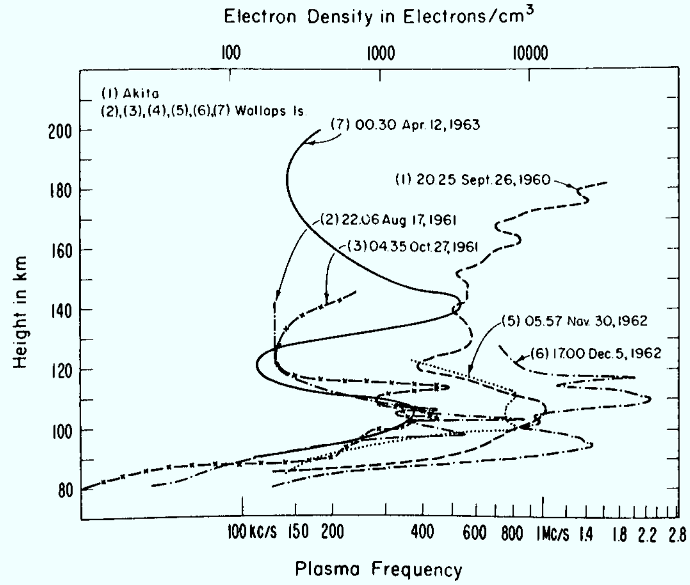

Fig. 4a. Electron density profiles obtained by rocket at night.

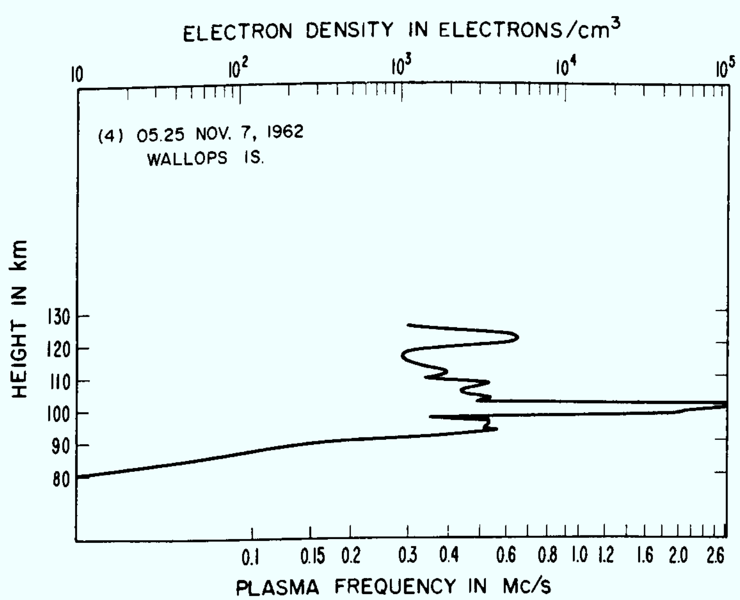

Fig. 4b. Electron density profiles obtained by rocket at night.

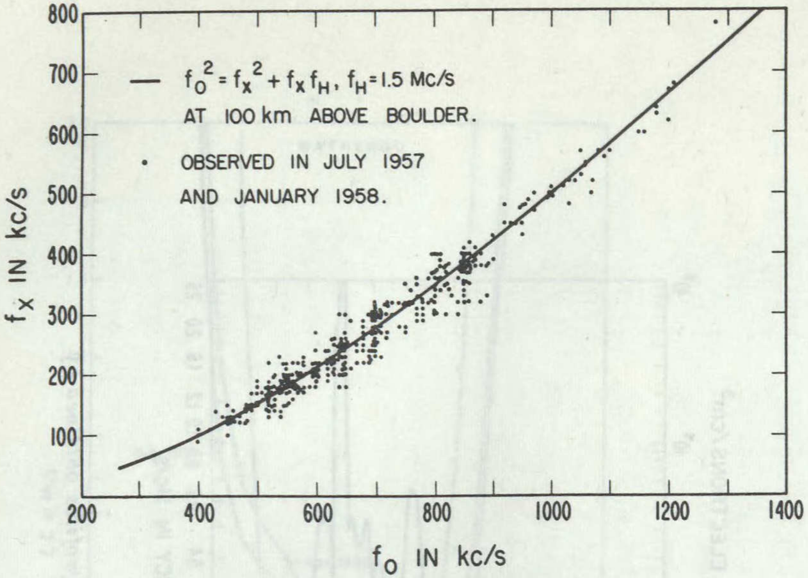

Fig. 5. Observed separation between f_o and f_x in July 1957 and January 1958.

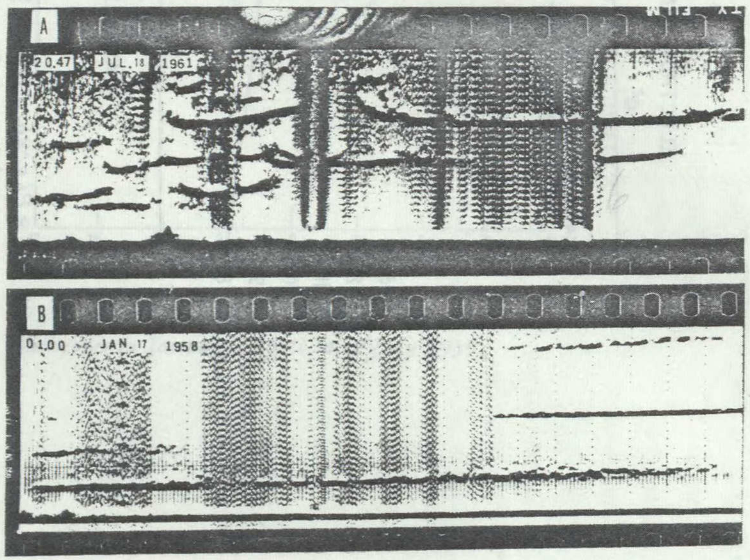

Fig. 6. Two examples of the low frequency ionograms used in the analysis.

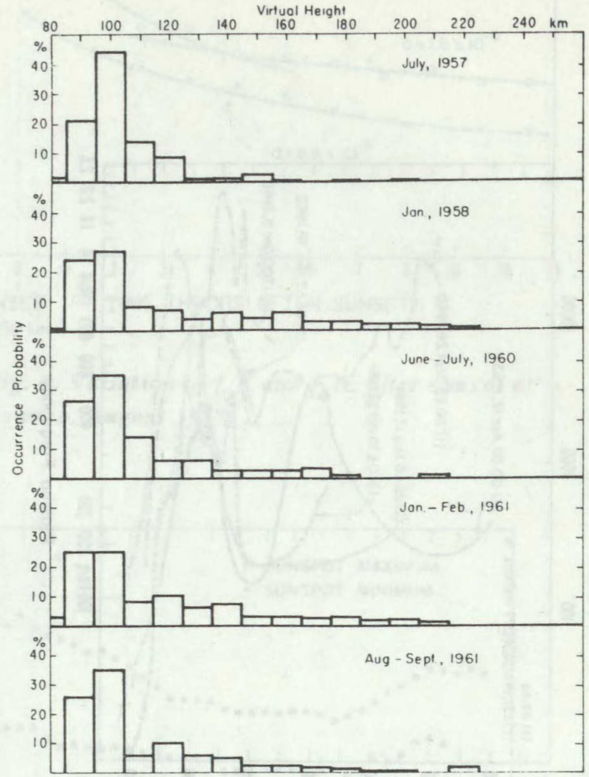

Fig. 7. Occurrence rate of the nighttime E layer echoes in various virtual height ranges.

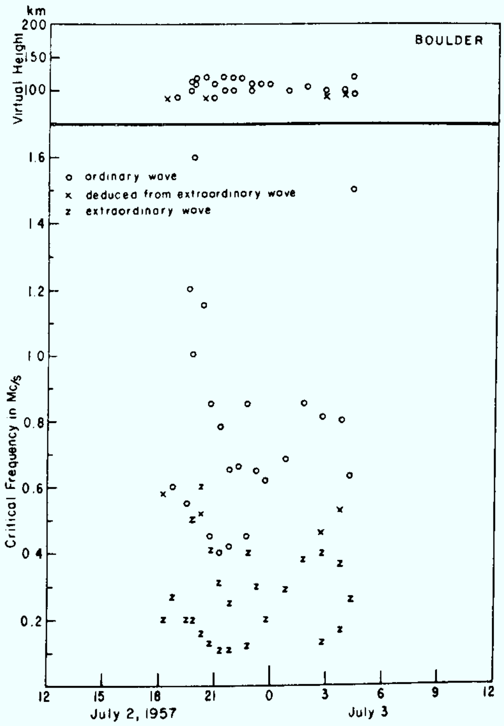

Fig. 8a. f- and h'-plots of E-region echoes on 2 - 3 July, 1957.

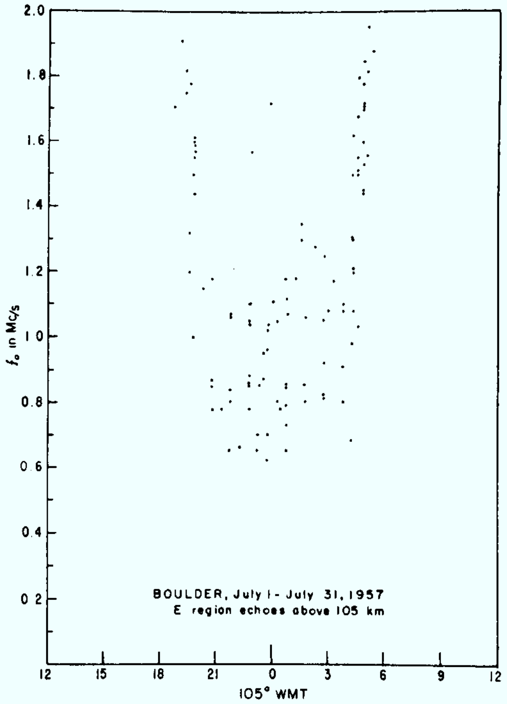

Fig. 8b. Critical frequency of E-region echoes above 105 km. for July 1957.

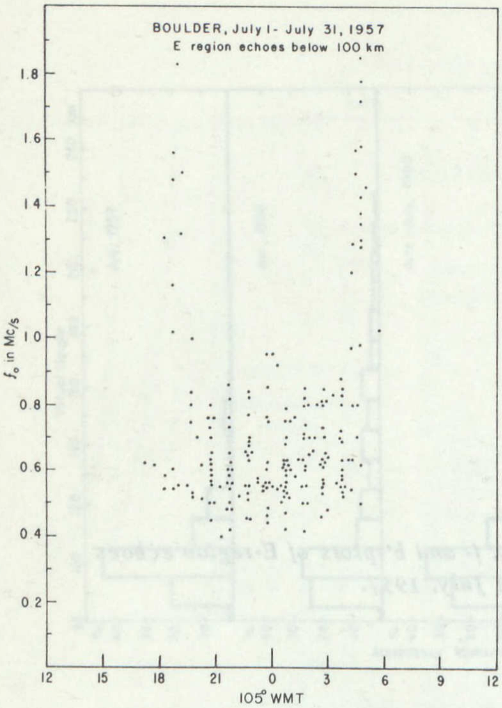

Fig. 8c. Critical frequency of E-region echoes below 100 km. for July 1957.

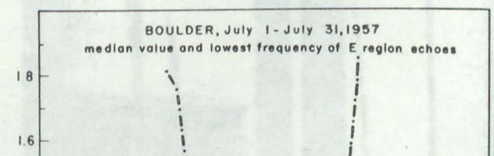

Fig. 8d. Median value and lowest critical frequency of E-region echoes in various height ranges, July 1957.

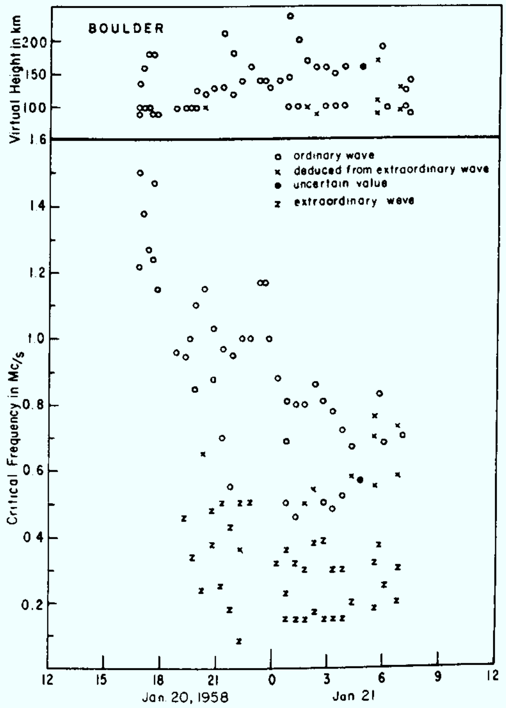

Fig. 9a. f- and h'-plots of E-region echoes on 20 - 21 January, 1958.

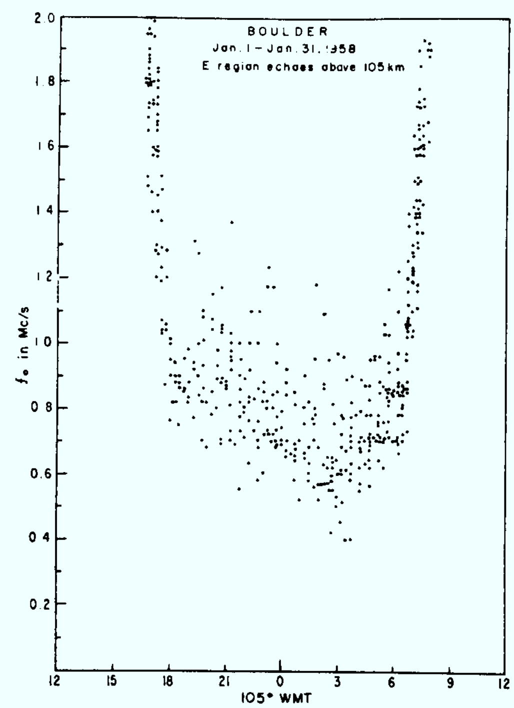

Fig. 9b. Critical frequency of E-region echoes above 105 km. for January 1958.

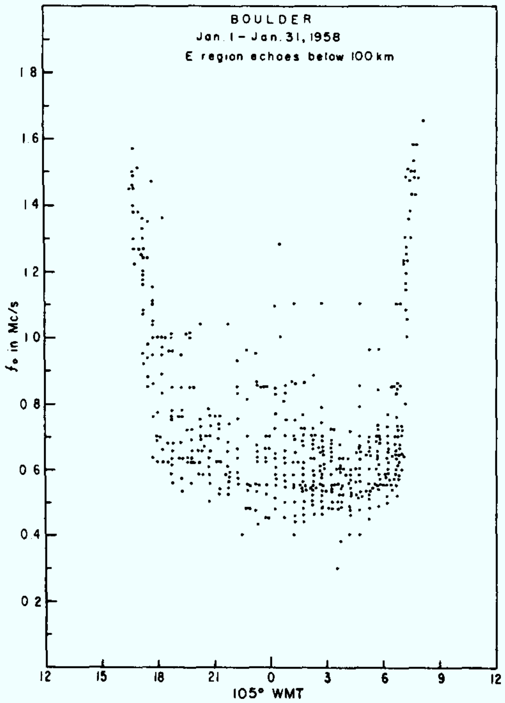

Fig. 9c. Critical frequency of E-region echoes below 100 km. for January 1958.

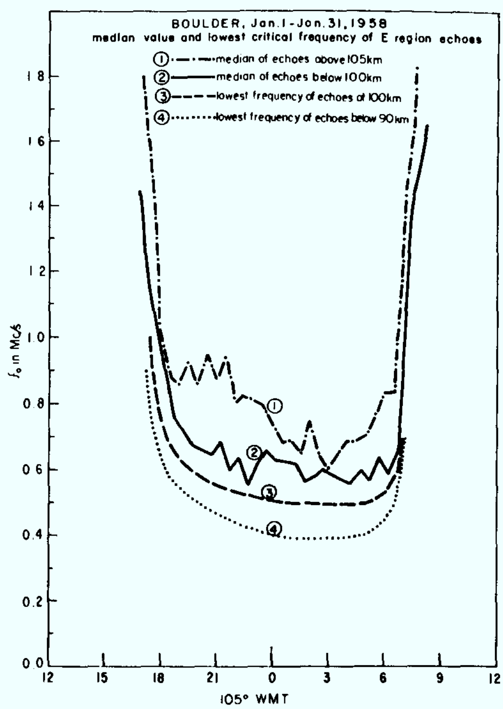

Fig. 9d. Median value and lowest critical frequency of E-region echoes for January 1958.

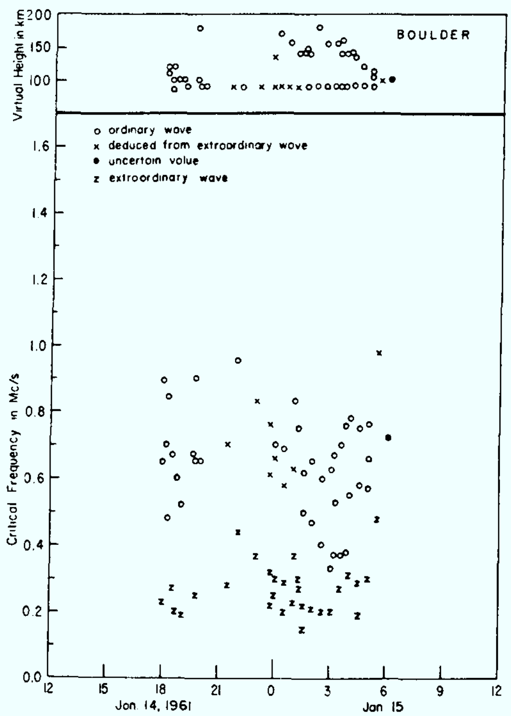

Fig. 10a. f- and h'-plots of E-region echoes on 14 - 15 January, 1961.

Fig. 10b. Critical frequency of E-region echoes above 105 km. for January - February 1961.

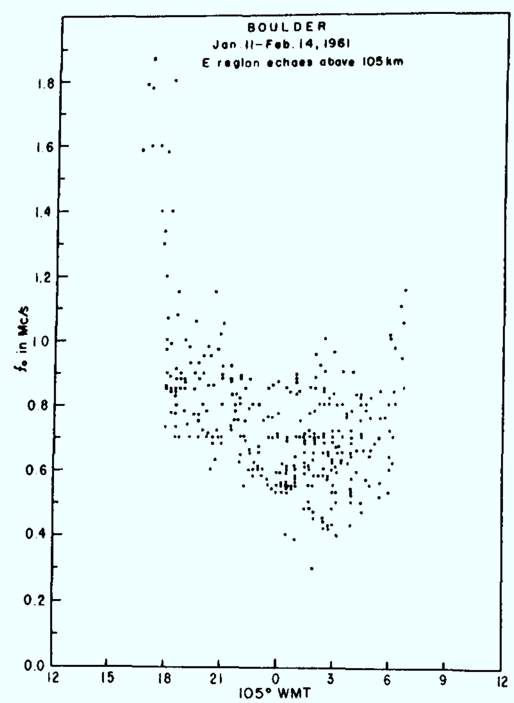

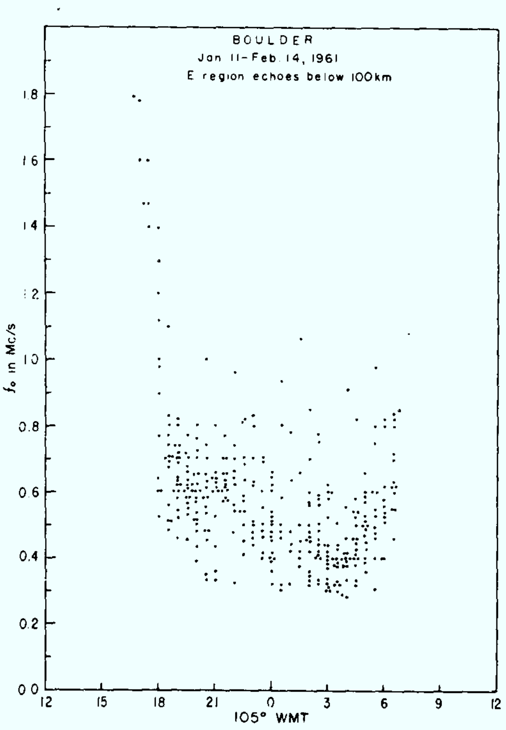

Fig. 10c. Critical frequency of E-region echoes below 100 km. for January - February 1961.

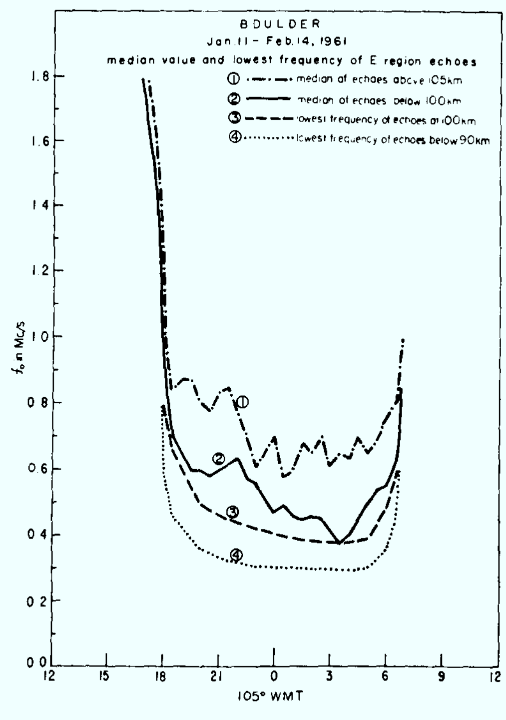

Fig. 10d. Median value and lowest critical frequency of E-region echoes for January - February 1961.

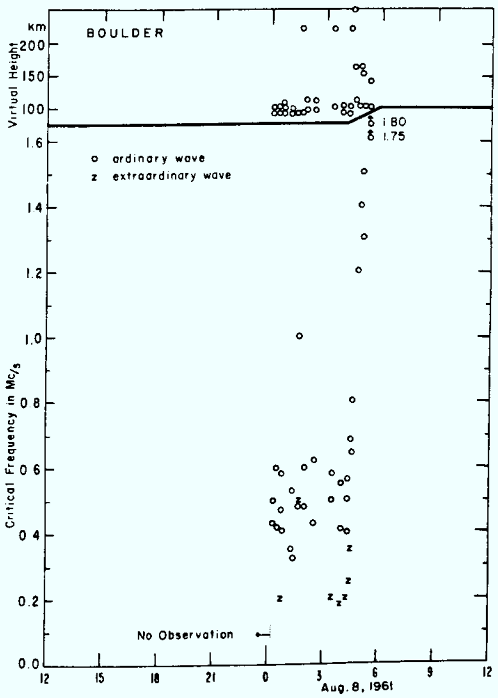

Fig. 11a. f- and h'-plots of E-region echoes on 7 - 8 August, 1961.

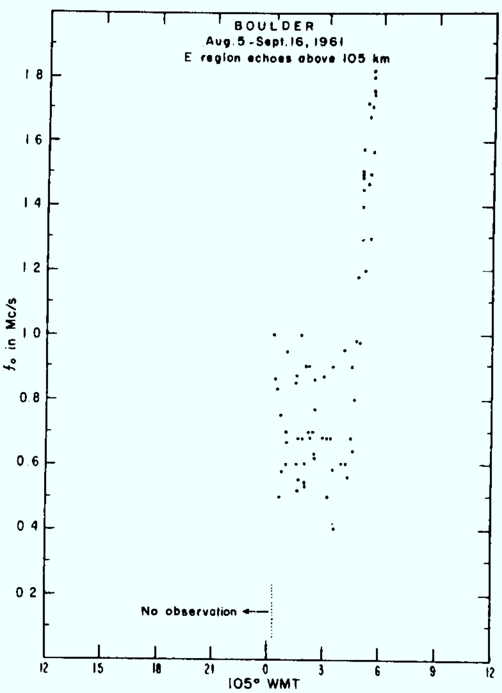

Fig. 11b. Critical frequency of E-region echoes above 105 km. for August - September 1961.

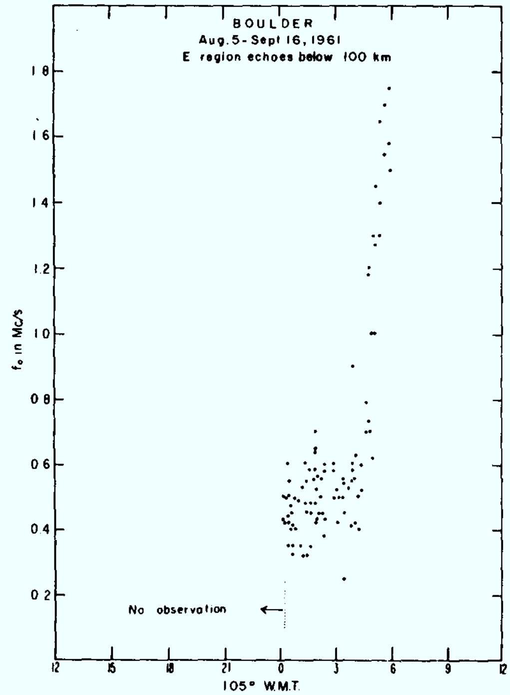

Fig. 11c. Critical frequency of E-region echoes below 100 km. for August - September 1961.

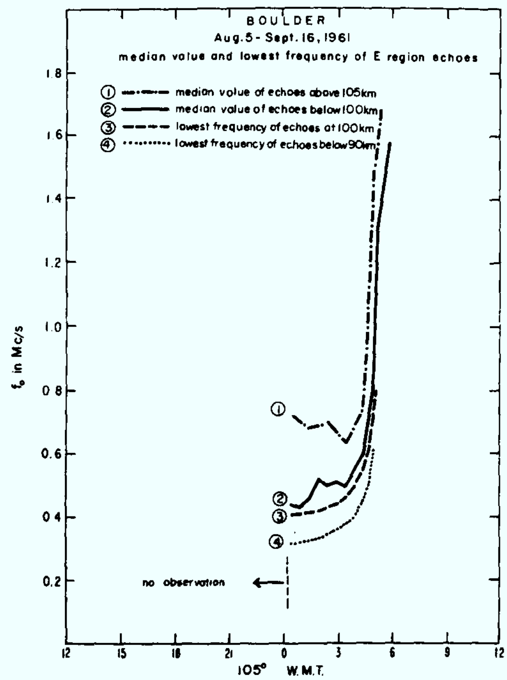

Fig. 11d. Median value and lowest critical frequency of E-region echoes for August - September 1961.

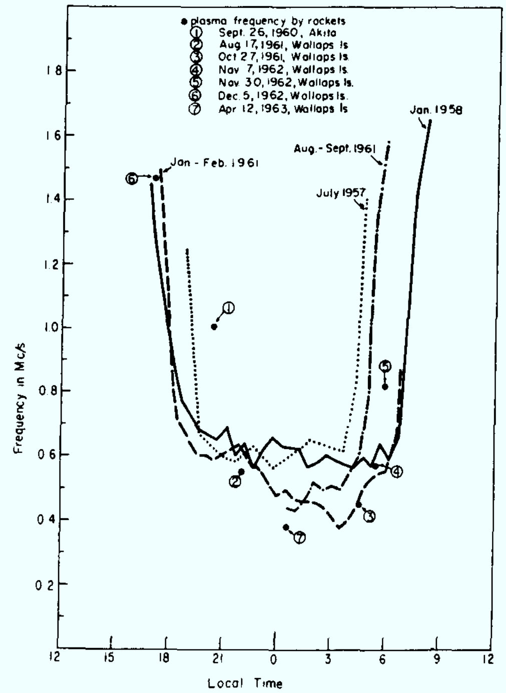

Fig. 12. Critical frequency of E-region echoes below 100 km. compared with the plasma frequencies obtained by rockets.

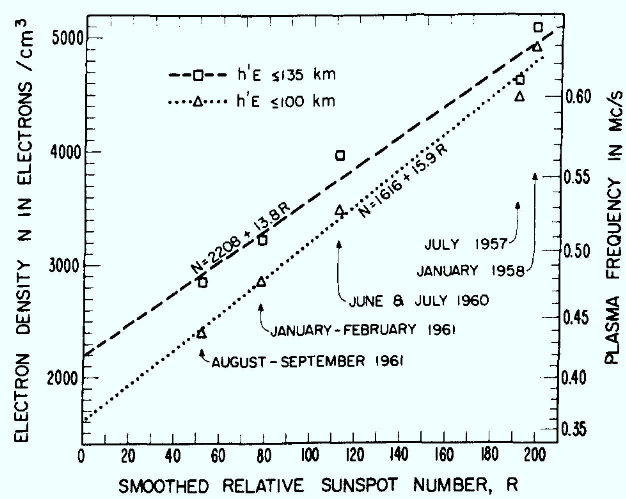

Fig. 13. Median f_oE at midnight in two height ranges versus smoothed relative sunspot number.

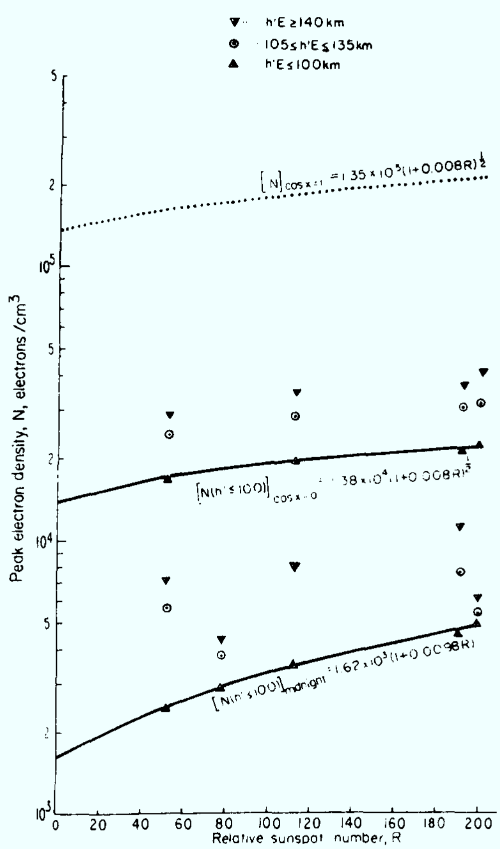

Fig. 14. Solar activity dependence of the peak electron density in the E region.

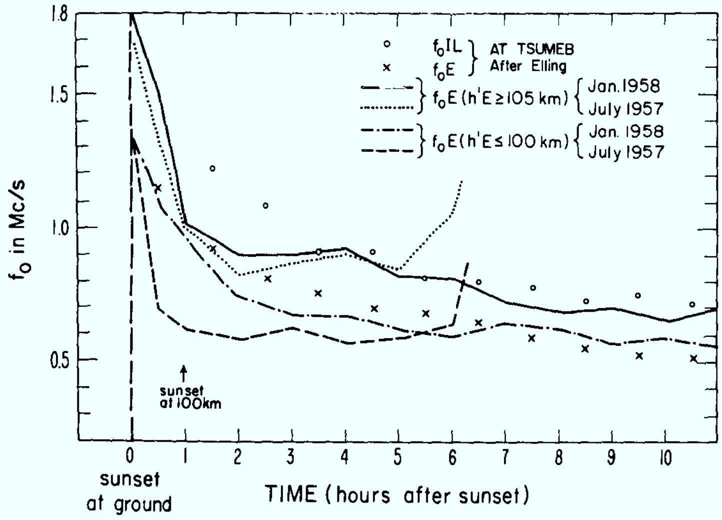

Fig. 15. Comparison of the nocturnal variation of f_oE at Tsumeb and Boulder.

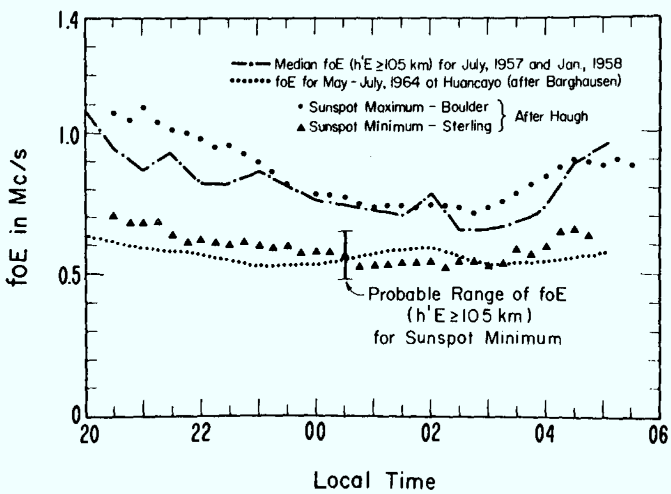

Fig. 16. Comparison of the nocturnal variation of f_oE's at Boulder, Sterling, and Huancayo.

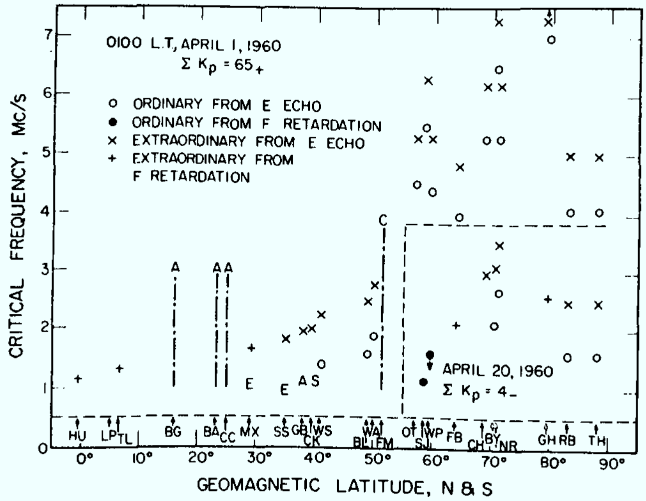

Fig. 17. Latitudinal variation of the disturbed (1 April, 1960) and quiet (20 April, 1960) nighttime E layer.

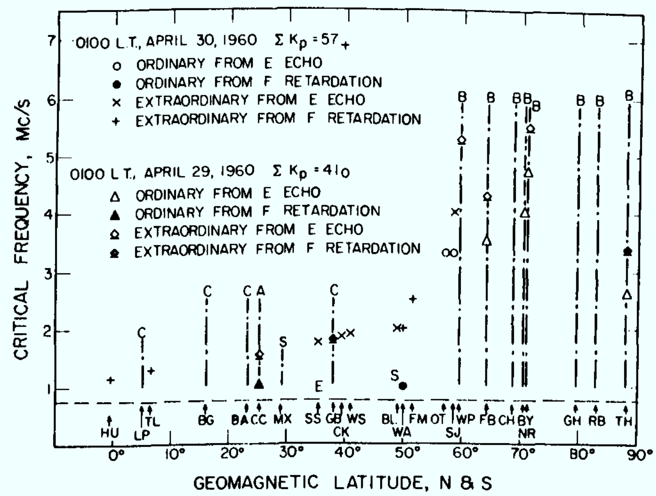

Fig. 18. Latitudinal variation of the disturbed (30 April, 1960) nighttime E layer.

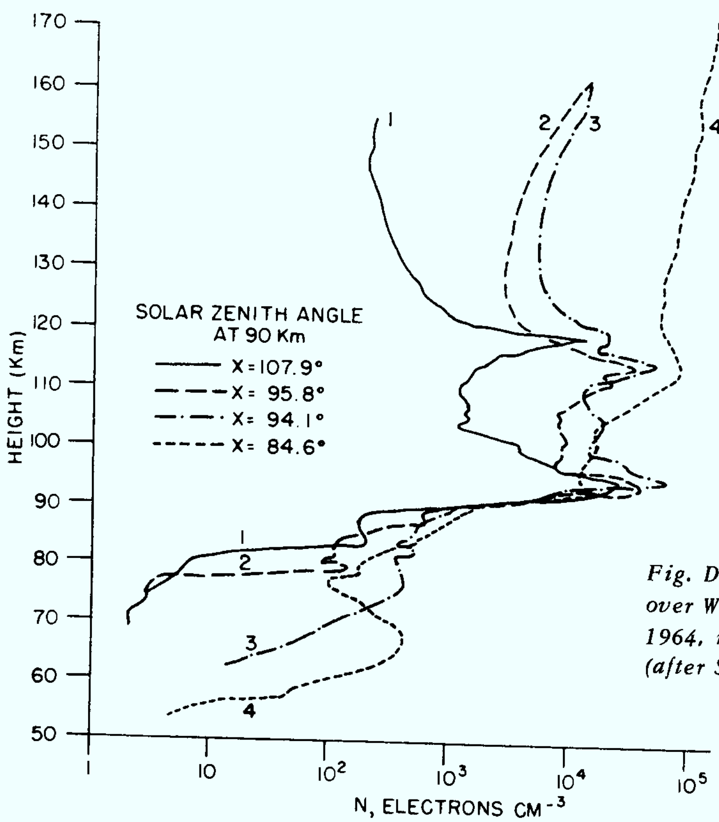

Fig. D-1. Sequence of electron density profiles over Wallops Island on the morning of 15 July, 1964, measured by rocket-borne Langmuir probes (after Smith 1965).

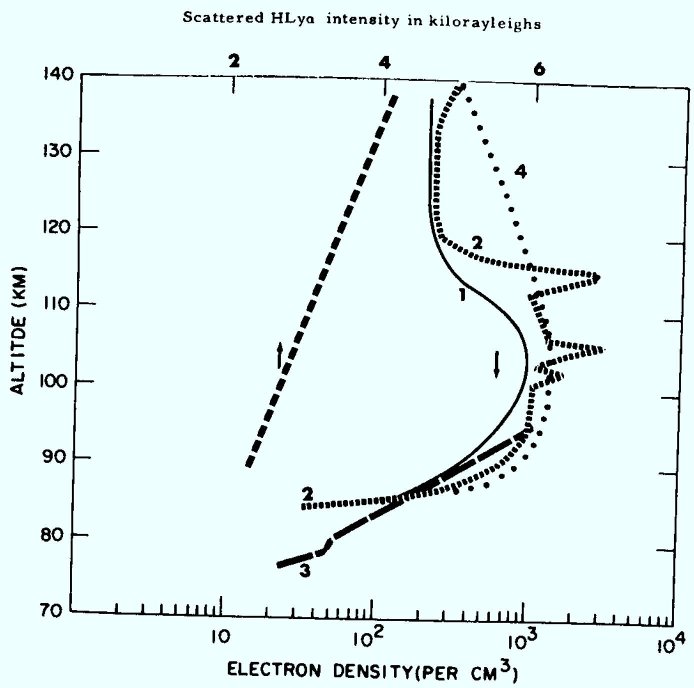

Fig. D-2. Nighttime E-region measurements compared to a simple model (see Paper 1.3).

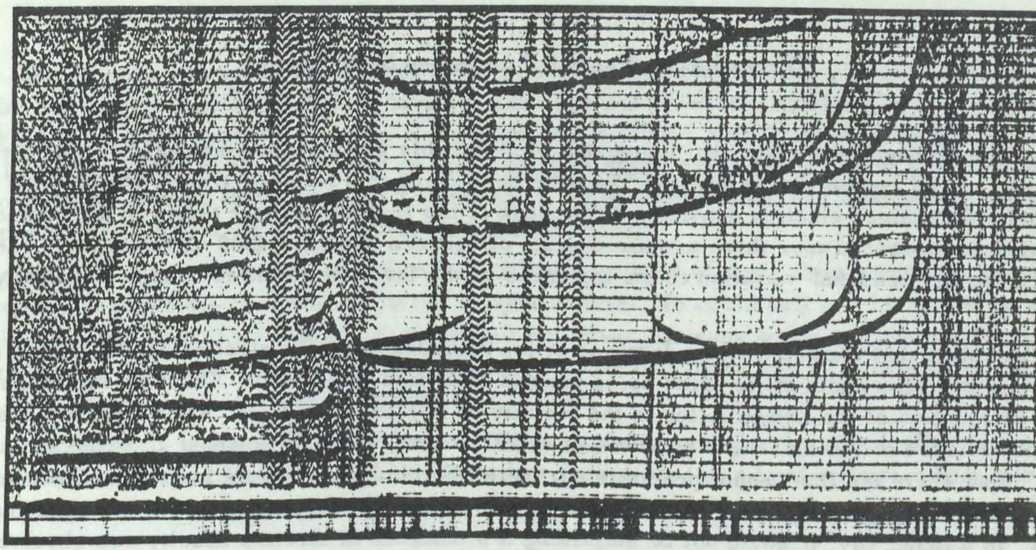

Fig. D-3. Ionogram illustrating intermediate layer return between E (with sporadic E) and F region. Group retardation shows that the intermediate layer is a "thick" layer.

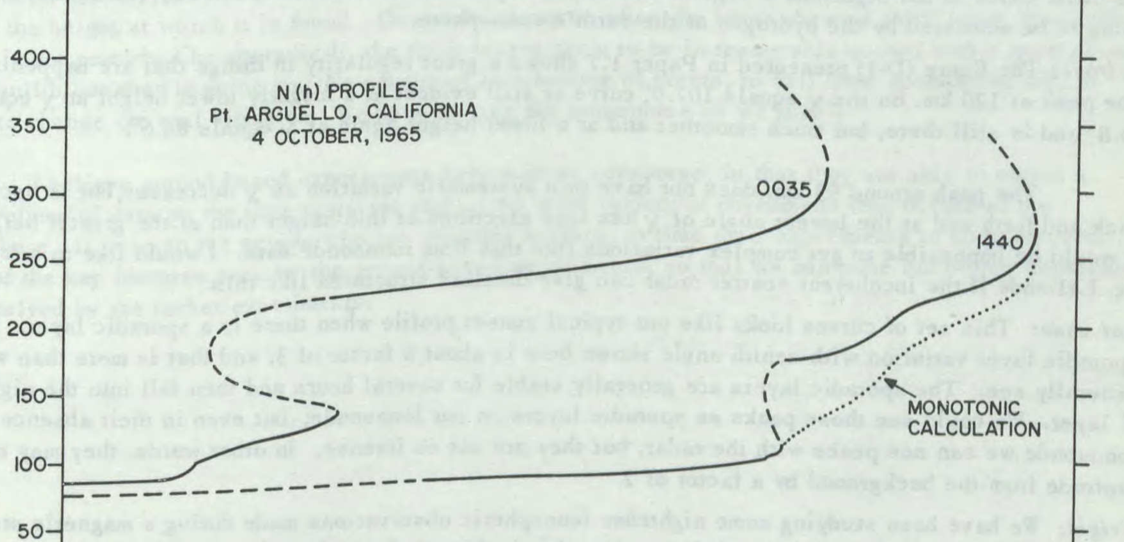

Fig. D-4. Electron density profile calculated at I.T.S.A. Night profile calculated from ionogram shown in Fig. D-3 shows thick intermediate layer at 140 km. Full valley corrections have been applied to the F-region profile (although the valley distribution itself is speculative). The lower height of the intermediate layer is probably too low, since no valley correction was possible just above 100 km.

Discussion on Paper 5.5 presented by N. Wakai

LaLonde: The comment was made that ionograms were the only ground-based measurements of the nighttime E layer, and of course that is not true. We have been doing this for some time at Puerto Rico and have actually determined electron densities at the peak of the E layer, without regard to the sporadic layers which are almost always there to some degree, of between 3000 and 4000 electrons/cc. There does not seem to be any seasonal variation to the thickness of the layer; it seems to change drastically every night.

Swider: The slide that showed a sharp decrease of the nighttime E-region electron density at twilight supports this business about nitric oxide being ionized by Lyman α very well. What this corresponds to is the rapid attenuation of the Lyman α flux in the vicinity of 100 km. at twilight. Remember, the Lyman α flux is unattenuated at 100 km. until χ equals 91 or 92°; then it turns off in about 2° as the sun sinks to about 95° from where the flux cannot penetrate any more. Some nighttime level is then reached, and is sustained by the scattered radiation that comes from the scattering of Lyman α by the hydrogen corona of the earth. In a rough way, it would not be surprising if a minimum in electron density was observed around midnight when the scattered Lyman α flux would probably reach a minimum. The same effect can be seen in your results for the morning. This effect of Lyman α in the daytime E region is completely swamped out by the normal ultraviolet and x-ray radiation, but it seems to be an important effect at twilight. I would say it also explains this nighttime E region. Now, this may not be true, but it is highly compatible with the results shown and would explain some transient solar activity, because we detect some variation of the nitric oxide in the nighttime E region. Also, you expect some variation in the way the Lyman α is going to be scattered by the hydrogen of the earth's atmosphere.

Belrose: The figure (D-1) presented in Paper 1.7 shows a great regularity in things that are happening. The peak at 120 km. on the χ equals 107.9° curve is still evident at a slightly lower height at χ equals 95.8° and is still there, but much smoother and at a lower height again at χ equals 84.6°.

The peak around 93 km. does not have this systematic variation as χ decreases, but is oscillating back and forth and at the lowest angle of χ has less electrons at this height than at the greater heights. It would be impossible to get complex variations like this from ionosonde data. I would like to ask Dr. LaLonde if the incoherent scatter radar can give detailed structures like this.

LaLonde: This set of curves looks like our typical sunset profile when there is a sporadic layer. The sporadic layer variation with zenith angle shown here is about a factor of 3, and that is more than we generally see. The sporadic layers are generally stable for several hours and then fall into the nighttime E layer. We could see those peaks as sporadic layers on our ionosonde; but even in their absence on the ionosonde we can see peaks with the radar, but they are not so intense. In other words, they may not protrude from the background by a factor of 2.

Wright: We have been studying some nighttime ionospheric observations made during a magnetic storm on 18 April, 1965. Over a great part of the northern hemisphere and at a few places where we have sounders that can observe the nighttime E region, the enhancement was remarkable. The hypothesis of nitric oxide ionization by Lyman α is attractive. If that is the case here, and enhancement of the earth's hydrogen corona explains the increased Lyman α, we may find ourselves searching for connections between the lower ionosphere and the magnetosphere at the same time that we are looking for connections between the lower ionosphere and the upper troposphere.

Pfister: The figure (D-2) presented by Dr. Swider in Paper 1.3 shows a curve 1 obtained by Ulwick and myself. This curve is a smooth result, and it does not show any of the fluctuations that are shown on curve 2. We have since reduced the results in more detail and any fluctuations are still much smaller than on curve 2.

Belrose: What sort of structure are you able to resolve with this standing wave impedance probe?

Pfister: We can resolve structures as fine as that shown on curve 2.

The electron density at the peak of curve 1 is approximately 1000 per cc., so this is lower than any of the curves shown by Mr. Wakai. I have assumed that our curve was obtained on a rare occasion when we don't have any sporadic E on top of our nighttime E layer. This assumption is supported by chemical releases, made at the same time on that particular night, which did not show any wind shears. We can reasonably assume that this curve 1 is the nitric oxide contribution, and whatever is on top of this is something else. This is, of course, a sunspot minimum result.

Bibl: I think it is dangerous to attach f_oE to the critical frequency of these thick stratifications with group retardation which are observed below the F-layer echoes. We could call it f_oEs or f_om for meteoric or anything like that; but if we call it f_oE we commit ourselves, because we do not know yet if it is really the background E ionization. Following my definition, I would call those layers, if they appeared in the daytime on the higher frequency scale, abnormal E.

Wright: This figure (D-3) is a typical ionogram for Point Arguello on 4 October, 1965. Notice the presence of two layers, the intermediate one which Mr. Wakai has spoken of, and a faint reflection from a lower layer that is mostly blanketed by sporadic E.

The electron density profile (Figure D-4) for this ionogram, which is labelled 0035, shows the intermediate layer and a deep valley above it. It is obvious from this and the ionogram that this is a thick layer. The lower layer is not given accurately here, but we can get a bit of information that it is thick. When one performs calculations from a number of such instances and looks at the best fitting Chapman layer scale heights for these two layers, one finds them in close accord with the scale heights from a model ionosphere; namely, around 6 km. for the lower one and between 15 and 30 km. for the higher layer, depending on the height at which it is found. On these instances when the layer shows a thick layer character and it is not perturbed by sporadic E, the thick layers seem to be in reasonable accord with a production loss equilibrium that is going on. No amount of re-labelling of layers, to call them sporadic or not, is going to change the real situation. We have to take the ionosphere as we find it.

I believe ground-based experiments have a great advantage, in that they are able to obtain a large volume of data on the time variation and on the wide variety of phenomena that occurs in the ionosphere. It is up to the people who are shooting rockets, to time their experiments to coincide with some of the key features seen by the ground-based experiments, so that we can pose the proper questions to be solved by the rocket experiments.

5.6 SOME REMARKS ON THE VALLEY BETWEEN THE F LAYER AND THICK E_s (NIGHT E) DETERMINED FROM SIMULTANEOUS BOTTOMSIDE AND TOPSIDE IONOGRAMS

by

Doris H. Jelly

Radio Physics Laboratory
Defence Research Telecommunications Establishment
Ottawa, Ontario, Canada

In general, the ambiguities that limit the accuracy of electron density height profiles that are determined from bottomside ionograms, i.e. the "starting" and the "valley" ambiguities, do not affect the analysis of topside ionograms. There is no "starting" ambiguity, since reflection traces and plasma resonance "spikes" are observed at the height of the satellite; there is usually no "valley" ambiguity since normally there are no subsidiary layers above the F-layer maximum.

On occasions, however, reflections from E_s are observed at frequencies above the F-layer penetration frequency. Both transparent and thick types of E_s are seen in topside ionograms. The observation of thick E_s (an auroral zone phenomenon often referred to as "night E" since it occurs during the night) in topside ionograms is interesting, since information can be obtained about whether there is a "valley" between the E_s and the F layer. On these occasions, the F layer is not usually observed by the bottomside sounder since the thick E_s is not transparent, and so reflection traces from the F layer are not obtained. The characteristics of night E have been described by King and by Maehlum who grouped night E with all other retardation-producing E_s.

In this brief communication, two examples are given, one which indicates a possible valley between the F layer and the underlying night E layer, and one which shows a continuous distribution with no distinction between E and F layers. The topside ionograms, taken from Alouette I passes near the auroral zone stations of Anchorage and College, Alaska, were selected on the basis of there being night E observed by the bottomside ionosondes at either of these stations.

Fig. 1 (example 1) shows a topside ionogram and the corresponding ionogram from College. The bottomside ionogram, taken at 2030 local time, 1 1/2 min. prior to the satellite ionogram, shows a thick layer with $f_o E_s = 4.5$ Mc/s. plus irregular E_s reflections at greater frequencies and heights possibly due to oblique reflections. Although the satellite was some 250 km. distant at closest approach, the night E layer lasted for several hours and extended to Anchorage, hence it seems reasonable to interpret the E_s seen by the satellite as night E. From the topside, a well-defined cusp in the X trace at 3.2 Mc/s. marks the maximum of the F layer.

There is no definite E_s critical frequency, but the appearance of ground reflections 100 km. below the reflections at 6.7 Mc/s. indicates that the $f_o E_s$ is less than 6.7 Mc/s., and that the reflection is indeed from a sporadic E layer. By assuming that there was no electron density valley between the E and F layers, and that the $f_x E_s$ was 5.7 Mc/s., the real-height profile shown in Fig. 3 was derived. The real-height reduction program (developed and supervised by G.E.K. Lockwood, RPL) calculates the profile of electron number density as a function of height from the X-wave reflection trace. The profile is plotted in Fig. 3 in terms of plasma frequency so that the profile can be related to the O-wave frequencies on the ionogram.

The presence of a definite cusp at 3.2 Mc/s. indicates that there may have been a valley. Assumption of a valley would not change the profile above 220 km., but would drop the portion of the profile that is below 220 km. by an amount equal to the valley thickness and would change slightly the slope of the profile over the region between 2.4 and 5 Mc/s. Assumption of a valley would not change the fact that the profile is formed of at least two distinct distributions; one above 220 km. and one or more below 220 km.

Fig. 2 (example 2) shows a night E layer at Anchorage. The topside ionogram was recorded 1 1/2 min. after the bottomside and less than 50 km. to the north. Although there is little, if anv, retardation at the highest frequency on the topside ionogram, it is close enough in frequencv to f_x E_s on the bottomside ionogram to suggest that the highest frequency is the critical frequency. The most interesting feature of this ionogram is the almost complete absence of retardation to indicate an F maximum. At 3.7 Mc/s. there is a slight change in slope in the X trace, which is reflected in the real height profile shown in Fig. 3. However, the absence of a cusp indicates that it would be unreasonable to assume that any valley existed in the range over which the X-wave trace is visible.

This interpretation mav be consistently related to the sequence of ionograms which followed. In the first ionogram to the north of the one shown in Fig. 2, there is evidence of a cusp at 3.7 Mc/s. which is probably f_xF. An extension of the trace to 4.2 Mc/s. is probably due to reflections from E_s. In the next ionogram, f_xF is quite definite at 3.8 Mc/s. with little evidence of E_s. The next in the sequence shows that f_xF has dropped to 2.5 Mc/s. and there is transparent E_s at higher frequencies. Thus from the sequence it would appear that the ionosphere changes over four ionograms from low electron density to higher densities, such that the whole region is filled in between the E and the F layer.

A comparison of the two real height profiles shows the same main features as the ionograms; the first profile is formed of at least two distinct distributions, the second appears to be one continuous distribution. Making allowance for a possible valley in the first example would only increase the essential differences between the profiles.

From the foregoing it is concluded that, at least on occasion, the E_s layer becomes thick enough to fill in the valley between the E_s and the F layer, so that one continuous monotonic distribution exists between 1000 km. altitude and the peak of the E_s layer. On other occasions the presence of a well-defined cusp indicates that a valley may be present between the E_s and F layer.

From the foregoing it is concluded that, at least on occasion, the E_s layer becomes thick enough to fill in the valley between the E_s layer becomes thick enough to fill in the valley between the E_s and the F layer, so that one continuous monotonic distribution exists between 1000 km. altitude and the peak of the E_s layer. On other occasions the presence of a well-defined cusp indicates that a vallev mav be present between the E_s and F layer.

The vallev ambiguity poses a serious barrier to the study of E_s from the topside data. The type of E_s can be determined from the topside data if there is no valley (example 2), in which case it can be concluded that thick E_s is present. If there is a valley, the type of E_s can be determined only if ground reflections are visible through the E_s, in which case transparent E_s is present. Unfortunately, the majority of cases fall in neither of these categories.

REFERENCES

King, G.A.M. The night-E layer from ionospheric sporadic-E. Pergamon Press, 1962.

Maehlum, B. The sporadic E auroral zone. Geofysiske Publikasjoner, XXIII, 1, 1962.

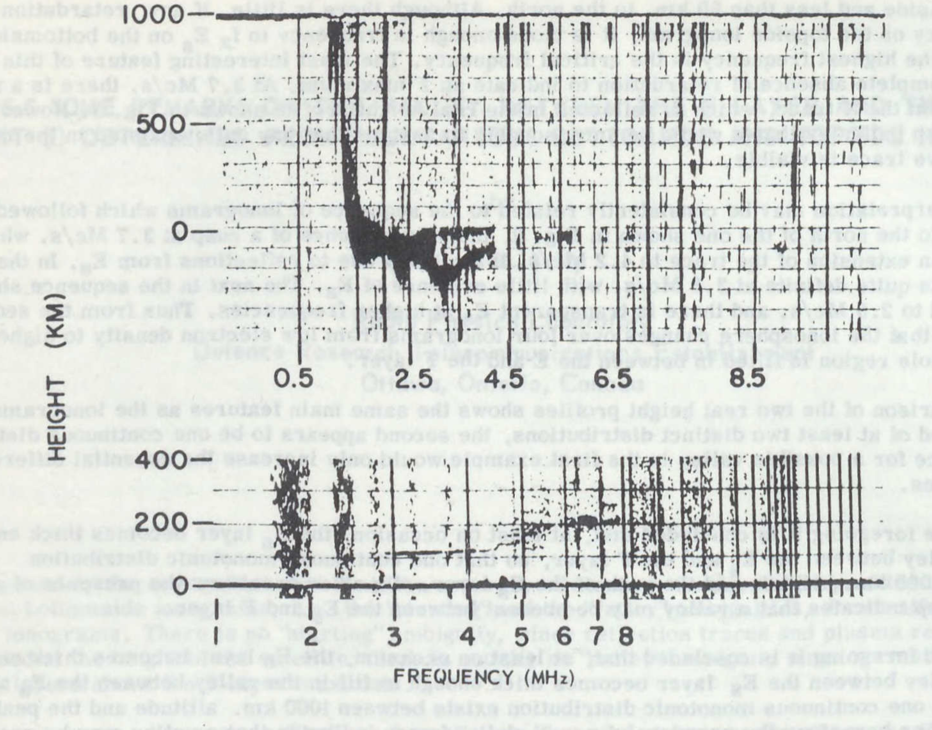

Fig. 1. Night E at College, 30 September, 1962, 0631 UT.

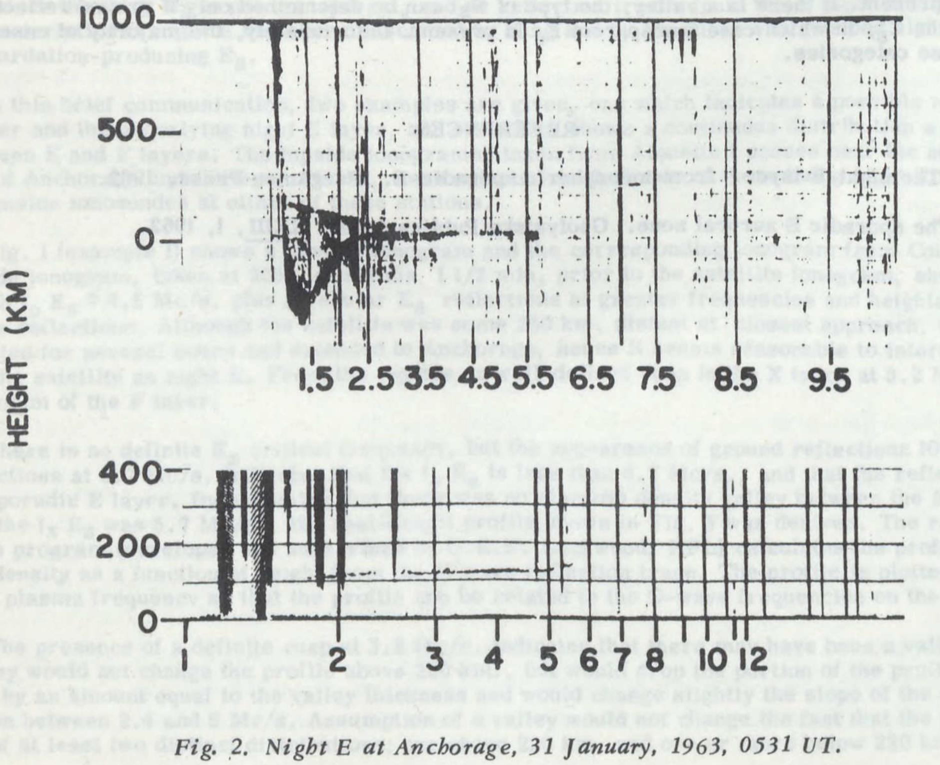

Fig. 2. Night E at Anchorage, 31 January, 1963, 0531 UT.

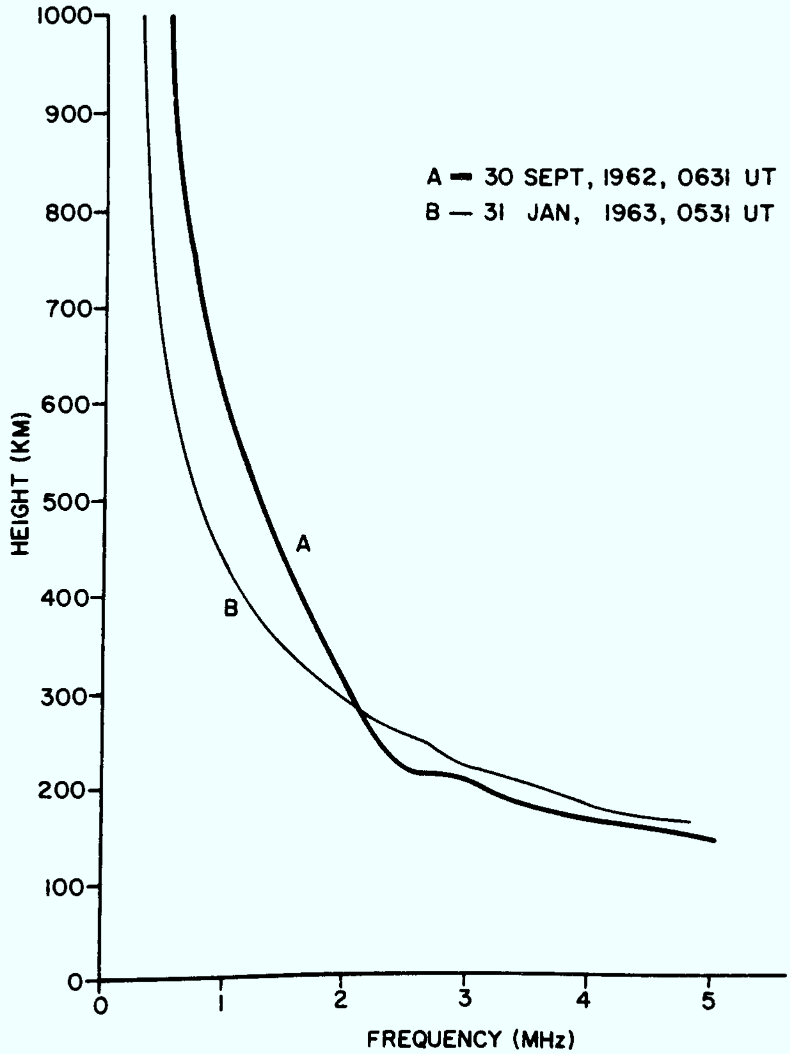

Fig. 3. Real height profiles above night E.

Discussion on Paper 5.6 presented by D.H. Jelly

Wright: I don't fully understand the kind of valley correction that has been made here. It isn't impossible that there could be a continuous distribution of electron density from the satellite down to the sporadic E layer. I have seen electron production curves from particle precipitation that look something like this, although they would imply somewhat thicker layers than what seems to have appeared from the topside. Aside from those two extremes, one might get an electron density distribution that looks like this with no valley correction, or perhaps an inadequate valley correction, and the layer height as flat as seen from the topside as from the bottom but with an improper starting height, namely, at the satellite. This will give a distribution that asymptotically approaches this flat height, which is somewhat the way these curves appear. This can be considered a valley from the sounder all the way to the sporadic E; so it seems that whether this profile actually represents the sporadic E or the improper starting height depends on the sophistication of your attempt to correct for a valley.

Jelly: In the one distribution that showed no valley, no corrections were put in. It is only where there is a cusp – where the traces become vertical-that one would consider introducing a valley correction. At least on occasions there is one continuous distribution through the F layer from a maximum in the E layer.

Wright: That is what I don't want to be convinced of until I know about the valley correction.

Belrose: There is no valley correction. The point of the paper is emphasizing the need for valley corrections, when you can see that you need a valley correction on the basis of looking at the ionogram.

Wright: There was a second thing that disturbed me about the ionogram, and it was that the virtual height curve seems to become asymptotic almost at the ground. Is that correct? What is the meaning of this 'zero' height?

Jelly: It is arbitrary.

Wright: But the satellite is known to be at 1000 km., so this is the real height of the ground.

Nelms: The satellite can be up to 1060 or it can be less than 1000. You have to know about a particular pass.

Petrie: I think there is evidence of a ground return – it's those few dots in the higher frequency end and to the right, of Fig. 2. From a sequence of records you can determine quite accurately the ground returns, and that horizontal portion that you referred to seems to be slightly above the ground returns.

Wright: If one knew that this was the ground return, it would be impressive evidence, but, for example, one knows that some of these dots are not ground returns.

Jelly: I don't have with me the sequence for this, but it does change into obvious sporadic E in the next couple of ionograms.

Nelms: We did show a whole series in which there was clearly sporadic E and ground reflections occurring simultaneously.

Wright: Do I understand that the O and X were not used together to calculate the electron density profile?

Jelly: Just the extraordinary.

Wright: It seems that if there is a relatively low electron distribution from the height of the satellite down to the sporadic E layer, then the joint use of O and X is necessary to resolve that type of thing unless you have a sensitive measure of what this gradient is.

Nelms: The information from the ionogram tells you without ambiguity what the distribution is down to where there is a valley, and this trace that is seen down at the O km. level is the continuous distribution from the higher height. You know with great accuracy what the density is at the satellite, so your starting point is obtained with little ambiguity.

Wright: Dr. Paul and I have argued that even though the electron density at the satellite is well known, presumably the electron density gradient at the satellite is difficult to determine, and effects such as I have talked about here require a knowledge of both the electron density gradient, and the electron density at the satellite. Whether an uncertainty in the gradient leads to as great a difference in the profile, I'm not prepared to say.

Nelms: I feel not, because there is information at the satellite and continuous information below the satellite; consequently, this gradient can be established quite accurately. The major difficulty, of course, is if there is a valley low down.

Wright: On the other side I will re-emphasize that some calculations done by Prof. Kamicama at ITSA, together with work by Rees and several others, have shown that certain portions of the high energy electron spectrum can produce layers which are almost like the outer envelope of the drawings I made; and these are much like the profile Miss Jelly showed. Therefore, there is a great deal to be said on the other side.

Nelms: It does occasionally happen that there is hardly any ionization at the satellite; but you can tell when it occurs.

Paul: The thing that upsets me is that this profile ends at a height of about 180 km., but the topside electron density doesn't show any indication of retardation. On the other hand, the bottomside ionogram virtual heights are at 130 to 140 km., a difference of 40 km. Do you have any explanation?

Jelly: No, I don't. As I pointed out, I have not seen a topside ionogram with a well-defined retardation cusp, and I don't know what the explanation is.

Bibl: As Dr. Paul pointed out yesterday, the use of an extraordinary component is dangerous. He has given some correction of his own computations. I am sure that if he slipped a factor of – I don't know how much – other people would have made similar mistakes if they used extraordinary components for analysis. What is the gyro frequency you obtained? It is important to know because of the gyro frequency effect, which is sometimes forgotten in the true height analysis of the X component, for example; Dr. Paul has pointed out you don't start with zero delay for zero electron content. We don't know exactly how much we have to consider this question.

Nelms: This is taken into account in the reduction of the record.

Wright: Something may be wrong, the gyro frequency at 200 km. at Anchorage is at least 1.6 Mc. Therefore at the satellite, it will be about 30 per cent less, perhaps 1.4 Mc. It seems unlikely that one will see the extraordinary ray so close to the gyro frequency, and if the gyro frequency is actually a little above the place where the virtual height curve joins the 1000 km., there isn't an extraordinary ray there at all.

Nelms: The gyro frequency at the satellite can be determined from the spike that is seen on the records. When the reduction is done, the gyro frequency must be calculated at all heights, and this we have done.

5.7 PROFILES OF WINDS IN THE LOWER THERMOSPHERE BY THE GUN-LAUNCHED PROBE TECHNIQUE AND THEIR RELATION TO IONOSPHERIC SPORADIC E

by

J.W. Wright
Institute for Telecommunication Sciences and Aeronomy

C.H. Murphy
U.S. Army Ballistic Research Laboratories

G.V. Bull
Space Research Institute, McGill University

Presented by J.W. Wright

1. Introduction

Two all-night series of upper atmosphere (90-140 km.) wind profiles have been obtained using gun-launched trimethylaluminum (TMA) payloads from the island of Barbados, September 20/21 and September 22/23, 1965 (Murphy et al. 1966). Concurrent radio soundings of the ionosphere have been performed with a C-4 ionosonde and the spaced receiver ionospheric 'drifts' technique; results from the latter experiment are summarized separately at this conference (Wright and Fedor, 1966). In the present paper we describe the association observed between ionospheric Sporadic E and the neutral wind structure in the light of recent theory (MacLeod, 1966). We trace the development of the Sporadic E layers from a formation process beginning the previous day. We review evidence supporting the view that such thin layers of Sporadic E consist largely of slowly recombining metallic ions that gradually accumulate during the day, are maintained at favorable levels of convergence of the neutral wind profile, and often persist in this manner through the night. Some observed variations of Sporadic E which remain unexplained by these processes are also noted.

2. Observations

Twilight and nighttime wind profiles were obtained for the nights September 20/21 and September 22/23, 1965. No wind data are available for the intervening night of September 21/22. Sporadic E observations are available from radio soundings over the period 1900 20 September through 0600 23 September, except for an interval of equipment failure 0220-1600 21 September. The Sporadic E parameters of principal interest are the layer height and peak electron density, and their time variation. At night, the Sporadic E height may be presumed to be free from retardation effects, and height values accurate to within $\pm$ 0.5 km., have been obtained by a least-squares process from the recorded multiple echo reflections. Electron densities have been deduced from the 'blanketing' frequency.

The wind data from these dates have been discussed by Murphy et al. (1966). Here we are principally concerned with profiles of the vertical ion velocity induced by the wind; this is calculated by the method described by MacLeod (1966, and private communication) and it reduces the wind profile to a form suitable for comparison with the Sporadic E observations.

3. Results

The observations will be discussed in chronological sequence in order to emphasize the manner in which Sporadic E layers evolve and are transported through the E region by the neutral winds. For brevity and to preserve continuity in the discussion, events will be qualified as "probable" (P) if they are not clearly demonstrated by the observations.

September 20/21, 1965

1900 - 0200: Two layers of Sporadic E are observed near 92 and 107 km. The calculated vertical ion velocity profiles are shown in Fig. 1. Positive (upward) velocities are plotted to the right, for each profile, and the times of the corresponding gun-launched trails are shown at the top. Sporadic E layer heights are given by the short horizontal lines with times and electron densities (x 10^{-4}/cc.) indicated nearby. The upper layer is clearly located at a stable level of maximum ion convergence (i.e., where the ion velocity is upward from below and downward from above). The lower layer (which disappears after 2050) is observed to be descending slowly in a stable region of upward ion velocity of small magnitude.

0017 - 0031: (P) Another Sporadic E reflection was observed for a short time at a range of 122 ± 1 km. This is not marked on Fig. 1, as the layer gave no multiple reflections and was therefore probably seen obliquely. However, it is reasonable to associate this layer with the new region of ion convergence, which develops sometime between 2052 and 0024 and is seen at 0024 at 118 km.

0024 - 0220: (P) The ion velocity profiles are consistent in giving a large region of downward velocity above 108 km., except for a narrow interval of upward velocity, which descends from 117 to 110 km. over this period (it remains near 110 km. through 0335). This probably shields the observed Sporadic E from appreciable ion input from above, but the prevalence of transient oblique reflections, at large ranges, from ion clouds throughout this period suggests that in some parts of the sky the narrow shielding region disappears. Only relatively minor shifts of neutral wind direction could cause this locally significant change in the vertical ion velocity profile.

0200 - 1600: (P) The failure of Sporadic E observations (and the absence of daytime wind measurements) preclude any certain identification of the Sporadic E layers discussed above with the sequence to be described later for the period September 22/23. However, a single layer of Sporadic E is observed at 1600 September 21, which slowly descends in the height range 110 to 90 km. through the night September 21/22 and can be identified with the lower layer, which persists throughout the following day and night, as discussed below.

September 22/23, 1965

0802 - 1605: Ionograms and electron density profiles (Paul and Wright, 1964) representative of this period are shown in Figs. 2 and 3a, b, respectively. The most remarkable event of this period is the development of a thin layer of Sporadic E by accretion of ions in the height range above 110 km. The layer begins as a thick stratification above 130 km. (0831); in its systematic evolution, it descends to lower heights, becomes thinner, and increases in peak electron density. By 1605 it is at 112 km., has an underside half-thickness of only 1 km., and exceeds the background electron density by a factor of four, as shown on the N(h) profiles of Fig. 3b.

The lower Sporadic E layer is visible intermittently on these daytime soundings, for example, at 0831, 1031, and 1605. During the middle part of the day the layer is probably submerged in the more densely ionized background E region and reappears in the late afternoon and evening as the E region decays. This is evident from the profile sequence of Fig. 3b, in which the lower layer is visible near 100 km. only at 1605.

1605 - 0600: Several ionograms from the second night of wind profiles are shown in Fig. 4, and the detailed height variation of the Sporadic E layers is given by the irregular lines in Fig. 5. The upper layer is clearly continuous with the profile sequence discussed above, while the continuity of the lower layer is somewhat irregular.

Neutral wind profiles were obtained at times marked along the lower axis of Fig. 5, and the calculated vertical ion velocity profiles are given in Fig. 6. The Sporadic E layers are considerably more complicated in their behavior on this night. We shall attempt to point out some of the more important explainable and unexplainable variations evident by comparison of Figs. 4 and 6.

Little can be said concerning variations of the lower layer; the vertical ion velocities are always small below about 95 km. (this is a consequence of the large ion collision frequency), and while the layer is often 'properly' located on the ion velocity profile (e.g., between 1820 and 1930, and again near 0400) insufficient wind data are available to examine critically all of the height variations observed.

The higher layer undergoes remarkable variations of height during this night, some of which are quite consistent with the available wind data.

1924 - 0150: (P) The higher layer undergoes a large height variation over this period (Fig. 5), which is probably explainable from the ion velocity profiles of Fig. 6. At 1924, the layer is at 112 km. and satisfactorily close to a node of ion convergence. Some time before 0150 the large region of upward velocity above 115 km. reverses and becomes uniformly downward. If we assume that the narrow region of downward velocity at 1924 is removed during this variation, the rise of the Sporadic E layer is thereby accounted for. The ionograms show that the layer becomes patchy and less ionized during the rise. It seems probable that the fall of the layer after 2205 (at which time it has again become strongly ionized) is in response to the major change of neutral wind pattern giving downward drift velocity above 112 km., as seen at 0150. The Sporadic E height variation can be used in this way to interpolate the time variation of some features of the wind profiles. This is the purpose of the smoothed curves in Fig. 5, which are not discussed further in this summary.

Note that the "midnight reversal" of wind implied above 112 km. by the first two profiles of Fig. 6 also occurred between the second and third profiles of the earlier date (Fig. 1); the principal difference between the two cases is the persistence of the region of downward ion velocity above the Sporadic E layer on the earlier night, which stabilizes the position of the layer as noted above.

0150 - 0600: (P) The Sporadic E layer was descending in the manner discussed above when, at 0150, it abruptly rises by 4 km. With the observations available, it is impossible to determine more exactly the nature of this rise, but the occurrence of multiple echoes throughout the sequence confirms that the rise is real. Several possibilities may be considered in future work:

(a) The rise may be in response to a rapid variation in wind, not detected with the TMA trail timing available here. This could occur in such a manner that the Sporadic E layer is effectively replaced by a higher layer descending from above. Since the amplitude of this height variation is less than the echo pulse length, oblique echoes from the edge of the "old" layer might be rapidly lost in the overhead "new" layer.

(b) The rise of the layer might occur in response to electric field or vertical air current variations, both of which are unknown and ignored in the vertical ion velocity calculations in Figs. 1 and 6 (MacLeod, 1966).

In any case, by 0150, the layer is beginning to descend to the equilibrium height of 114 on the ion velocity profile. This is in agreement with the sense of the ion velocity. Confirming evidence that the Sporadic E layer "sees" the effects of the neutral wind at its transient altitude of 117 km. (0150) is found in the spaced receiver drift observations reported separately (Wright and Fedor, 1966).

Parenthetically it may be noted that a sharp descent of the F region also occurs over the period 0157-0226. This is again understandable as a response of the ionization to the neutral wind, if the downward ion velocity at 130 km. (0150) persists to greater heights.

Another large Sporadic E height variation occurs over the period 0300 - 0500. This seems difficult to explain as a response to the neutral wind variations in view of the general similarity of the three ion velocity profiles at 0315, 0407, and 0505. A reversal of wind direction would be required above 110 km. and between 0315 and 0407, passing through a profile similar in shape to that at 1924 in Fig. 6. This cannot be ruled out, but it is hardly demonstrated by the observations. Electric fields and vertical wind currents are other possibilities. Following 0407, the rapid descent of the layer agrees in sense with the calculated ion velocity.

4. Discussion and Conclusions

Enough agreement is found between the positions of Sporadic E layers and calculated features of the vertical ion velocity to confirm that the neutral wind plays a dominant (and probably causative) role in the behavior of Sporadic E. Although no wind observations are available in daytime, a Sporadic E layer which agrees with the evening twilight wind profile is observed to have its origin in a gradual accumulation of ions throughout the preceding daylight period. This evolution is by no means rare: it has long been recognized as a phenomenon of frequent — if varied — occurrence (Wright, Knecht and Davies, 1957, p. 104). It seems probable that these "Sequential Sporadic E" events involve the accumulation of metallic ions in the daytime E region in response to the neutral winds. The long lifetime of monatomic ions in the E region can explain the large electron densities observed (Axford and Cunnold, 1966; Whitehead 1966); they have been detected in thin layers in the E region (Istomin, 1963). Thin layers of metallic ions have recently been observed at the same height as a Sporadic E layer, resembling the present case in behavior and daytime-formation (Narcissi 1966; Wright, unpublished).

The features of wind profiles with which Sporadic E is associated typically descend through the night (Rosenberg et al., 1963; Rosenberg and Justis, 1966; Murphy et al., 1966). This also occurs in the first of our two nights observations, but is absent in the second. Since most cases of daytime Sporadic E development also show descent during the ion accumulation process (cf. Fig. 2), this suggests that the associated daytime wind system possesses inclined wave fronts, which appear to descend with time when observed from a ground-fixed location. Rosenberg and Justis (1966) note that a descent of about one vertical wavelength (10-20 km.) per night is characteristic of the north-south component in their data. This is likely to characterize the daytime period also, and is consistent with the Sporadic E development described here: at heights above 130 km., the north-south component exerts the greater contribution to vertical ion movement (MacLeod, 1966), and the observed descent of daytime Sporadic E layers is therefore mainly in response to the north-south structure of the wind. If future observations confirm that the necessary features of the neutral wind profile do descend by about two vertical cycles per 24 hours, then we may perhaps view the Sporadic E sequence as including the following essential steps:

(a) ablation and thermal ionization of metallic atoms from meteors; photoionization and charge transfer, resulting in a relatively large metallic ion population between 90-140 km. in daytime.

(b) 'scavenging' of metallic ions into nodes of ion convergence of the neutral wind profile.

(c) descent of the ion maxima day and night, ultimately to below 90 km.

(d) ultimate loss of the metallic ions below 90 km., either by charge transfer or by dissociative recombination with negative ions at night.

REFERENCES

Axford, W.I. and D.M. Cunnold. The Wind Shear Theory of Temperate Zone Sporadic E. Radio Sci. 1 (New Series) p. 191, 1966.

MacLeod, M.A. Sporadic E Theory I. Collision-Geomagnetic Equilibrium. J. Atmos. Sci. 23 p. 96, 1966.

Murphy, C.H., Bull, G.V. and H.D. Edwards. Upper Atmosphere Winds Measured by Gun-Launched Projectiles. Proc. COSPAR VII, Space Science Symposium, 1966.

Narcissi, R.S. Ion Composition of the Mesosphere. Proc. COSPAR VII, Space Science Symposium, 1966.

Paul, A.K. and J.W. Wright. Some Results of a New Method for Obtaining Ionospheric N(h) Profiles and Their Bearing on the Structure of the Lower F Region. J. Geophys. Res. 68, 19, p. 5413, 1963.

Rosenberg, N.W., Edwards, H.D. and J.W. Wright. Ionospheric Winds: Motions into Night and Sporadic E Correlations, Space Research 4, p. 171 (North Holland Publ. Co., Amsterdam), 1963.

Rosenberg, N.W. and C.G. Justis. Space and Time Correlations of Ionospheric Winds. Radio Sci. 1 (New Series) p. 149, 1966.

Whitehead, J.D. Mixtures of Ions in the Wind Shear Theory of Sporadic E. Radio Sci. 1 (New Series) p. 198, 1966.

Wright, J.W. and L.S. Fedor. Comparison of Ionospheric Drift Velocities by the Spaced Receiver Technique with Neutral Winds from Luminous Rocket Trails. Proc. COSPAR VII Space Science Symposium, 1966.

Wright, J.W., Knecht, R.W. and K. Davies. Annals of the IGY, Vol. III Pt. 1, Ionospheric Radio Soundings, p. 104, 1957.

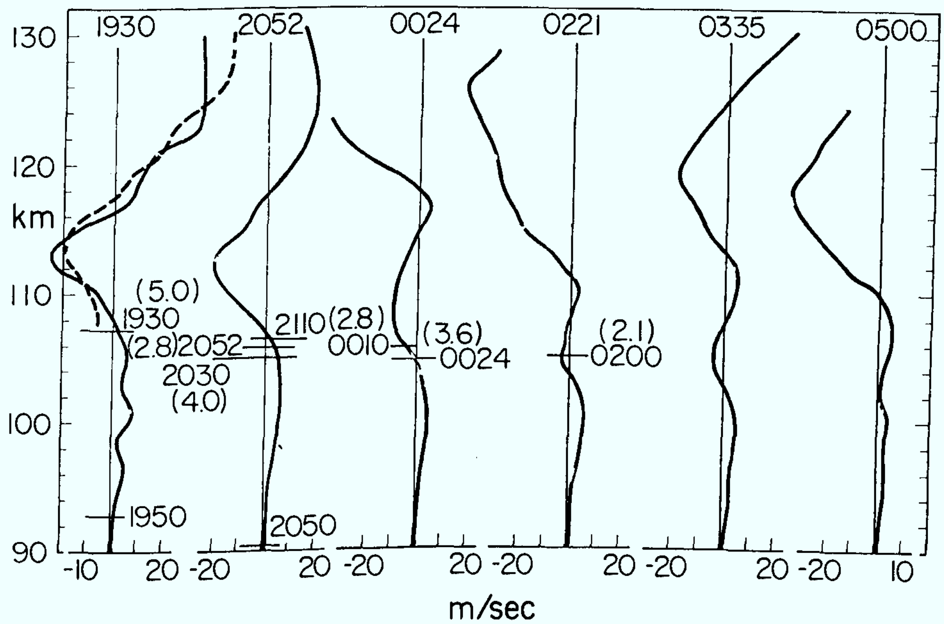

Fig. 1. Vertical ion velocities, versus height, calculated from observed neutral wind profiles, Barbados, September 20/21, 1965. Atlantic Standard Times of wind observation are at the top of each graph. Upward ion drifts are considered positive, plotted to the right. Ionosonde observations of sporadic E are also plotted: heights are given by the horizontal lines and adjacent figures give the time of observation; electron densities (x 10^{-4}/cc.) are deduced from the blanketing frequency and are marked nearby.

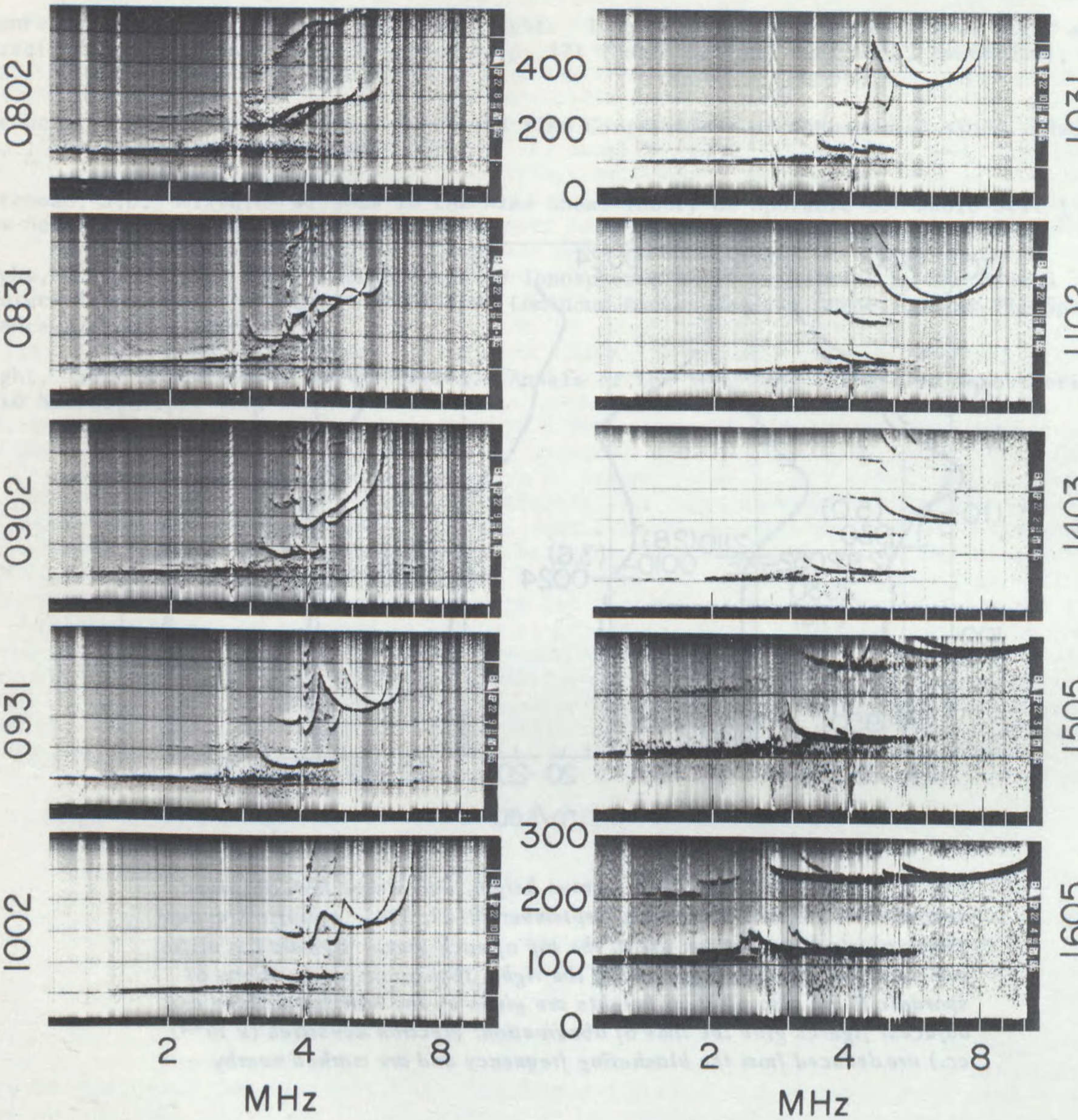

Fig. 2. Barbados ionograms from the day preceding the nighttime wind observations of September 22/23, 1965. These show the progressive development of the sporadic E layer which persists through the night of wind data. The layer begins as a stratification in the lower F region (0831), descends, and becomes thinner through the day.

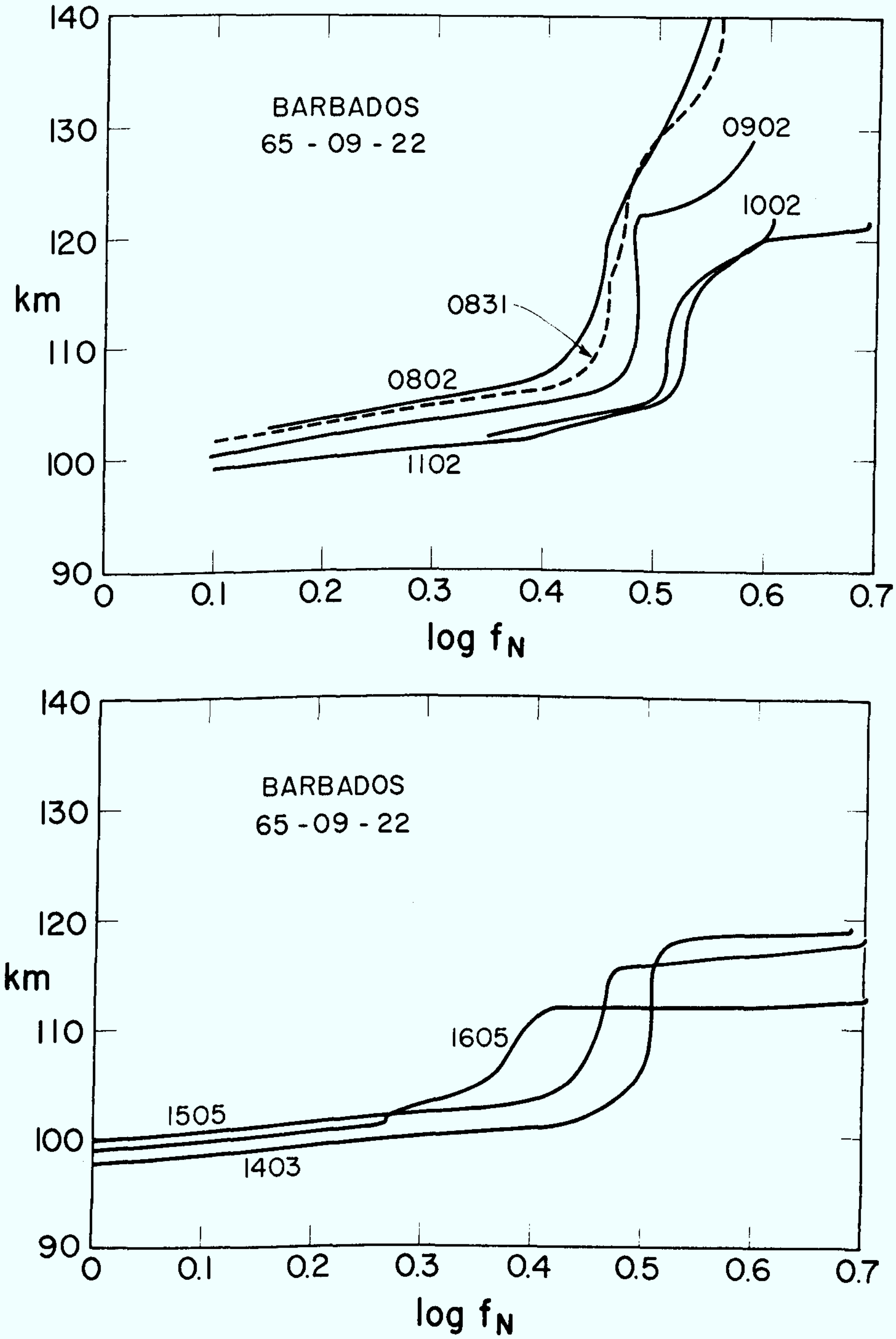

Fig. 3a, b. Electron density profiles calculated from the ionograms of Fig. 2, showing progressive development of the thin sporadic E layer from a stratification in the lower F region. Electron densities are represented by the log f_N scale: 2 log f_N + 4.093 = log N (cc.).

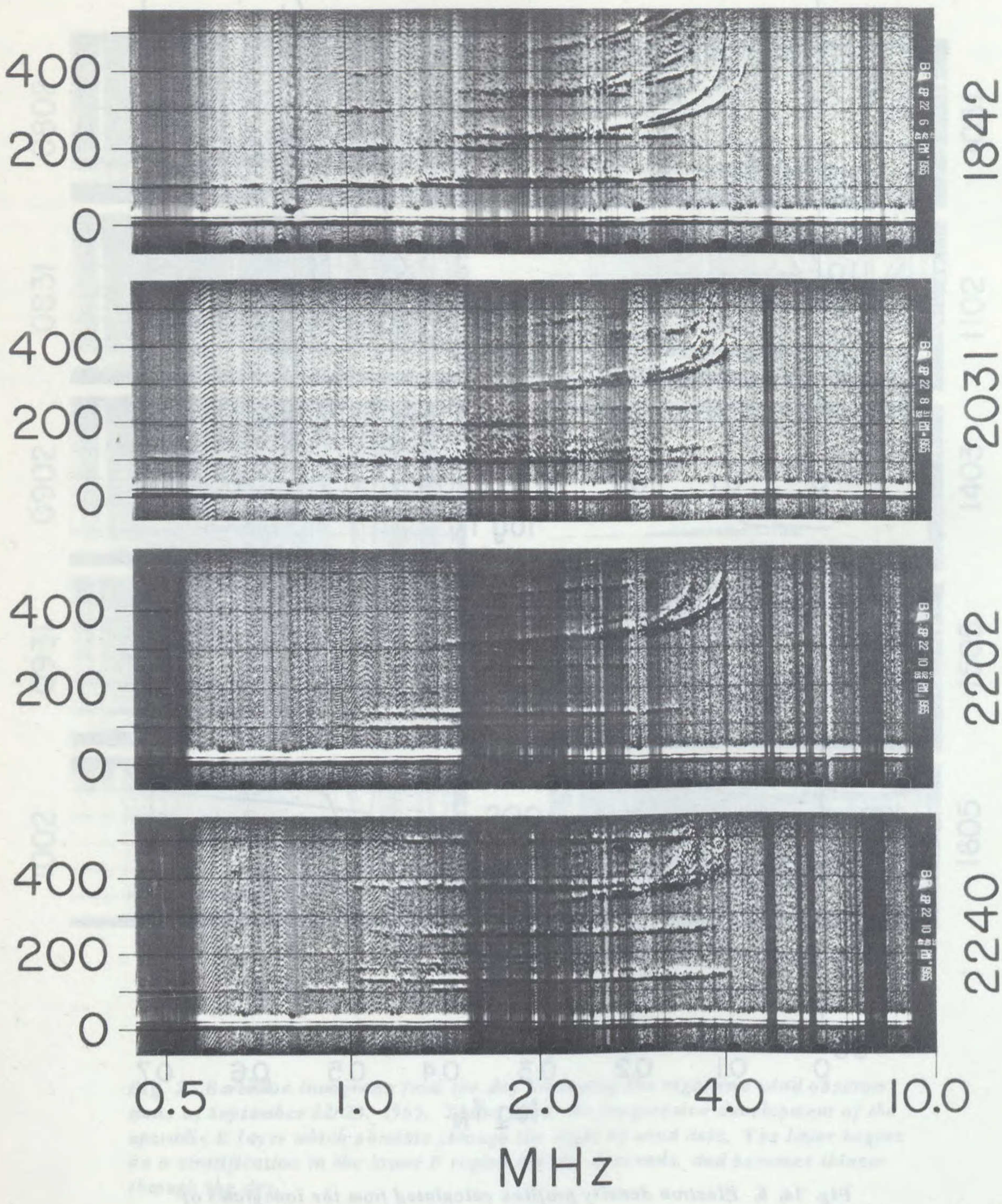

Fig. 4. Barbados ionograms during the night of September 22/23, 1965 showing the two layers of sporadic E discussed in the text. Note the great height attained by the higher layer at 2202.

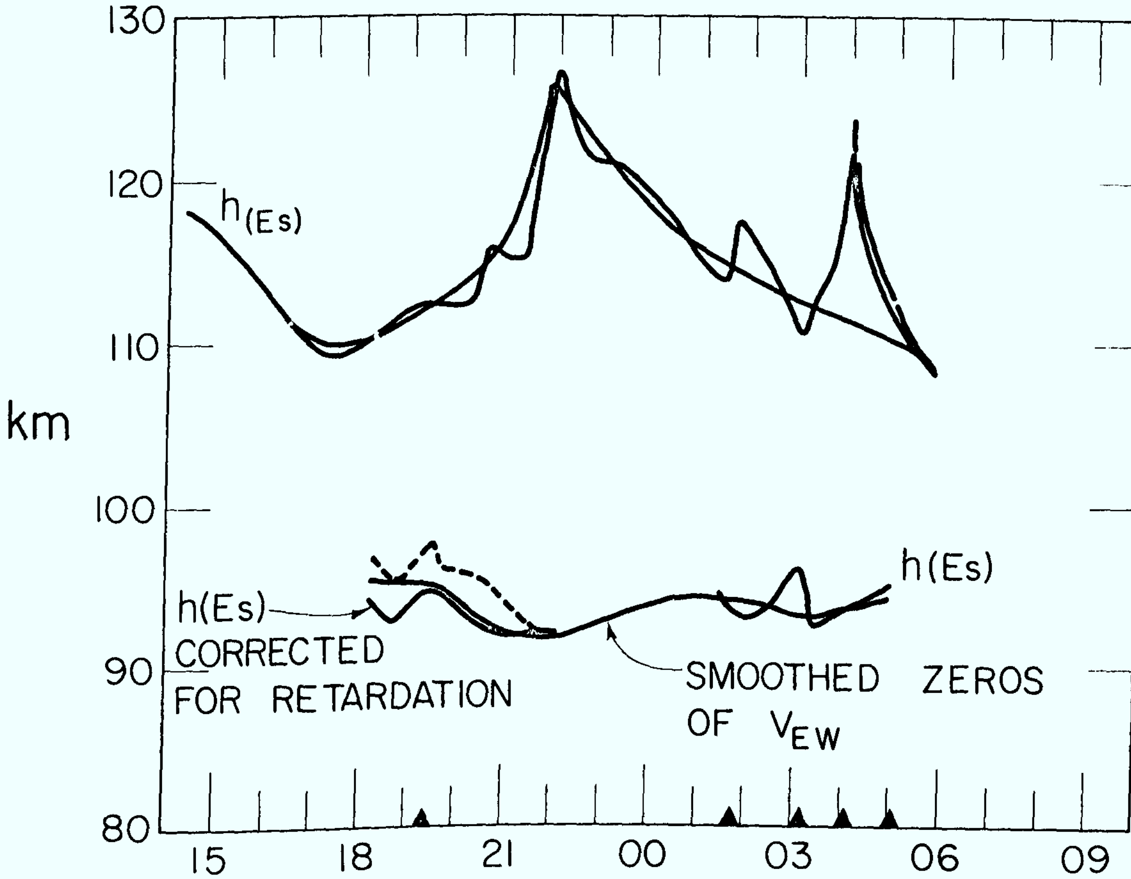

Fig. 5. The variation of sporadic E layer heights during the evening and night of September 22/23, 1965. Observed variations are given in detail by the irregular line, and a smoothed curve is also shown which preserves observed agreement with nodes of the E-W wind profile. The latter curve is not discussed in this paper. Observed heights of the lower layer, which is less densely ionized, are more affected by retardation in underlying ionization near sunset; a corrected variation is also shown.

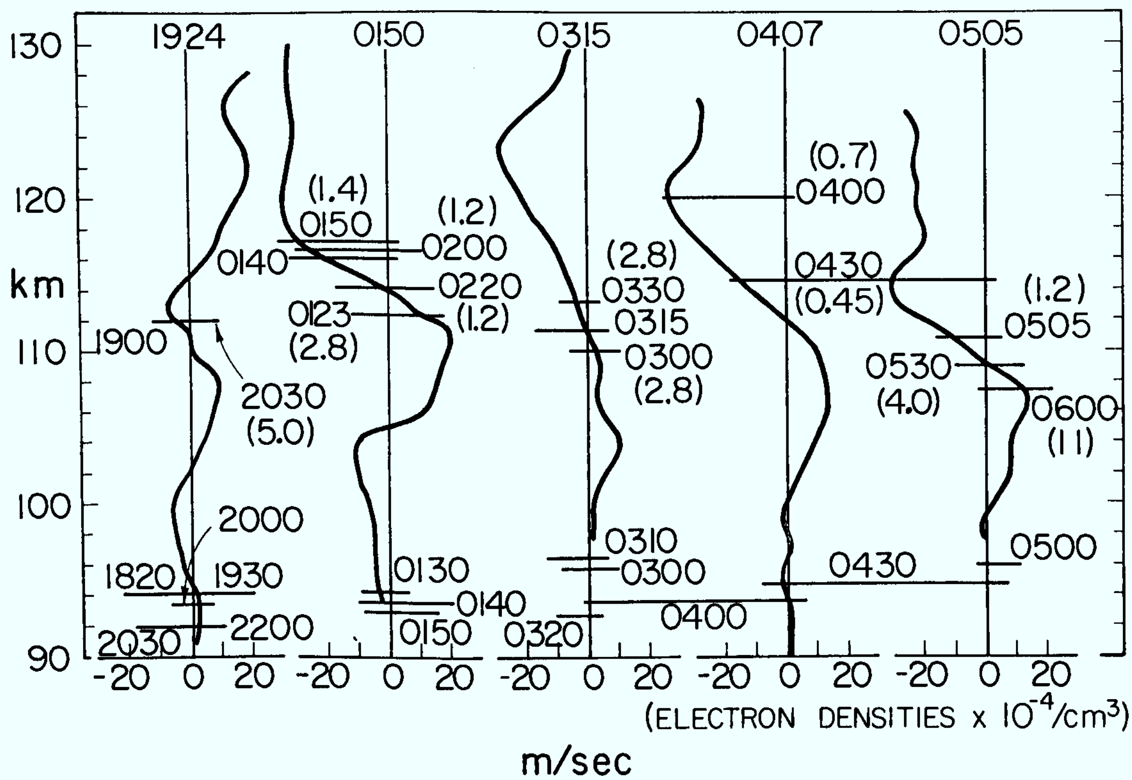

Fig. 6. Vertical ion velocities, versus height, calculated from observed neutral wind profiles, Barbados, September 22/23, 1965. Times of observation are at the top of each graph. Upward ion drifts are considered positive, plotted to the right. Ionosonde observations of sporadic E are also plotted: heights are given by the horizontal lines and adjacent figures give the time of observation; electron densities (x 10^{-4}/cc.) are deduced from the blanketing frequency and are marked nearby.

Discussion on Paper 5.7 presented by J.W. Wright

Georges: The horizontal velocity you calculate using the gravity wave dispersion diagram is the horizontal phase velocity of the gravity wave. No simple relation exists between it and the maximum velocity (amplitude) of the vertical wind profile.

Wright: It was only intended to be a rough estimate. Perhaps it is a wrong inference. No; it seems to me that if such a pattern is a gravity wave of about 120 min., and if there is, as in most wave motion, no net displacement by the wave of the medium that supports the wave, then the air particles, which are rushing this way over one half of the period, and that way over the other half, must have a velocity of something like what was estimated here.

Georges: But the wave velocity is a measure of the amplitude of the wave, not of the phase velocity.

Wright: My estimate wasn't of the phase velocity, it was just an attempt to infer the amplitude of the particle velocities from the period of the wave and its wave length.

Georges: As I understood your interpretation of the gravity wave propagation vector, you were attempting to verify the horizontal phase velocity of the gravity wave.

Wright: No. The horizontal wave length was deduced from that diagram simply by observing that the period of the wave and its vertical wave length were in agreement with the dominant undamped gravity wave component at that altitude. Since those two numbers were in agreement, that diagram was used to infer the horizontal wave length, and that horizontal wave length was divided by the period of the wave to get a rough estimate of the particle velocity that is contained inside the wave.

Fenwick: If your movie was for December 16, I think it would be interesting to note that the oblique ionogram I showed yesterday, which was made on a path which passes near that ionosonde on December 16 shows that the one long trace over a wide frequency range is probably Sporadic E. It certainly shows to a tremendous extent.

Wright: There's no doubt in my mind that that was Sporadic E. The movie was run just to try this new J5 sounder for movies. We had no idea we were going to get this sort of thing. However, having found it, I thought it would make a good illustration of the time development of that type of Sporadic E.

Belrose: What do you mean by the maximum value of the electron density in this Sporadic E layer; and does this invert to the maximum frequency that you saw in this thin layer, or what do you mean by that number?

Wright: The only densities I have permitted myself to quote for Sporadic E are inferred from blanketing frequencies, and I consider them doubtful if those blanketing frequencies are judged from one hop or from one measurement only. What I consider a valid measurement of electron density in Sporadic E is if a well-defined value of this quantity F_{bes} is observed, and if it is in reasonable agreement within a tolerable margin of error in a multiple echo too, or if the extraordinary component gives the same electron density when converted to electron density. The only values of F_{bes} used here satisfied one or another of these conditions.

Belrose: This assumes that you know F_{oE}. If you can't see a cusp for F_{oE} on the trace, then F_{bes} is a meaningless quantity that could be F_{oE} and the other thing is the scatter layer superimposed on E.

Wright: I don't think there is any great danger of that because of the variation of virtual height near this. If there is a thick layer with an electron density nearly equal to this, this is sure to show some variation in retardation because of that, whereas the effect by Sporadic E is typically very small.

5.8 COMPARISON OF IONOSPHERIC DRIFT VELOCITIES BY THE SPACED RECEIVER TECHNIQUE WITH NEUTRAL WINDS FROM LUMINOUS ROCKET TRAILS

by

J.W. Wright and L.S. Fedor

Institute for Telecommunication Sciences and Aeronomy
Environmental Science Services Administration
Boulder, Colorado

Presented by J.W. Wright

1. Introduction

The radio spaced-receiver method permits inference of the speed and direction of movement of an irregular ionospheric echo pattern across the ground. Exactly how this may be related to movements of the medium in which the radio pulses are reflected is not clear theoretically; the movement of irregularities in the ionized medium is implied, but whether they are carried along with the flow of the neutral air or are propagated through it, and whether there are corresponding irregularities in the neutral air, is not known. Finally, whichever of these combinations occur, the relation of the radio echo pattern to the irregular structure of the ionosphere is not clearly understood.

Visible trails of neutral gas released from rockets and gun-launched vehicles reveal the neutral particle flow (wind) over a range of height between 80 and 140 km. In the present work, we compare the neutral wind at the level of radio reflection in the ionosphere with individual determinations of the ionospheric "drift" as deduced from the radio spaced-receiver technique. Since the trails are visible only in darkness, when the general ionization of the lower ionosphere has decayed to low values, the only comparisons of the kind practical to date are those in which the radio reflection returns from a sporadic E layer.

The radio spaced-receiver data have been obtained at various frequencies with the usual three-antenna system at the vertices of a 100-meter equilateral triangle. Analysis of the observations has been performed by the correlation analysis of Keneshea et al., (1965). Most of the measurements reported here were obtained during gun-launched trail experiments conducted at the US Army Ballistic Research Laboratories/McGill University facility at Barbados, West Indies, on the nights of 20/21 and 22/23 September 1965; a few measurements are also available from an AFCRL program at Eglin AFB, Florida, during December 1962.

2. Results

Fig. 1 shows the north-south and east-west components of three neutral wind profiles (in magnetic coordinates) on the night of September 22/23, 1965 at Barbados. The causal relation of the neutral wind profile to occurrence, height, and variation of the sporadic E layer is discussed in a paper appearing elsewhere (Wright et al., 1966). Horizontal lines, marked by adjacent times of night, show the height of the sporadic E layers and hence the height of radio reflection for the spaced receiver measurement. These heights are accurate to within ± 0.5 km. and have been obtained by comparison of sporadic E multiple echoes on ionograms made concurrently.

Wind velocity components of the steady drift of the echo pattern at the ground (usually assumed to be twice the ionospheric velocity) for a number of measurements at times near that of the trail experiments are shown by the points plotted at the sporadic E altitudes. Two layers of sporadic E occurred on this occasion, near 92 and 112 km., and measurements are available from each. Fairly good agreement is found in most cases; it even appears that as the sporadic E layer moves vertically through the wind profile, successive radio measurements tend to trace out the vertical profile of wind velocity in each component.

Fig. 2 compares the wind speeds and wind directions by the two techniques for all of the occasions so far available. The wind directions are generally in good agreement, with the exception of a few extremely bad cases, and there is no evident tendency for agreement or disagreement at particular neutral wind directions. The wind speeds show somewhat greater relative scatter than the directions, although the neutral wind speed tends to agree on the average with that of the steady drift of the radio echo pattern at the ground.

The standard theoretical description of the spaced-receiver experiment (Ratcliffe, 1956) in which the radio echo fading is explained as the effect of diffraction from a random irregular screen, predicts that the ground echo pattern should move at twice the speed of the screen when illuminated from a point source at the ground. To explain the present result we are faced with two alternatives:

(a) The irregularities responsible for the radio echo fading move with half the speed of the neutral wind, or

(b) The 'point source effect' does not apply, which in turn disables diffraction from an extended screen as the explanation of the correlated echo fading from which the drift is inferred.

A partial test of alternative (a) is possible by comparing the radio results with the horizontal ion drift imposed by the neutral wind. The latter have been calculated by MacLeod (1965 and private communication) from the available wind profiles, and the results are shown as the dashed curves in Fig. 3. In most cases, the calculated ion drift at the sporadic E altitude is so nearly equal to the neutral wind that the two media can be said to move together. This of course does not assure that irregularities in the ionized gas are transported with the same velocity, and a more complete treatment of the wind described by Kato (1959) is desirable. For one case, where the sporadic E occurs at the relatively great height of 116 km. (0140 23 September, 1965) the radio results are seen to agree better with the neutral wind components than with the calculated ion drifts; if the radio drift speeds were halved the disagreement would be increased, and this is also true for most of the other cases in Fig. 3.

It seems useful to consider alternative (b), for if the point source effect does not apply, these results would be consistent with the simple view that the irregularities causing the radio-echo fading move with the neutral wind. One way in which alternative (b) might arise is if the ionosphere re-radiates the energy returning from total reflection as if it were a point source itself. This possibility has been considered as a consequence of plasma resonance oscillation from small irregularities at the level of total reflection by Herlofson (1951). Support for this interpretation has been found within the present data by considering separately the cases of total versus partial reflection from the sporadic E layers observed in this work. These cases occur when the observing radio frequency lies respectively below or above the "blanketing" frequency of the sporadic E layer as shown by the concurrent ionogram.

Fig. 4 shows the result of this separation of the data. Each circle represents a polar diagram in which a vector to the dotted end of the plotted line represents the neutral wind while a vector to the other end of the line shows the radio result. The vector disagreement between the two techniques is then shown by the plotted line.

It is obvious that the vector error of the radio technique is much smaller for cases of total reflection than for cases of partial reflection. If the radio drift speeds are divided by two, we find that 9 of the 11 partial reflection cases are improved while 8 of the 12 total reflection cases are made worse. The partial reflection cases disagree badly in direction as well as in speed, however, so that it cannot be concluded that the "point source effect" is not applicable even in this case.

Enough scatter is evident in the results available so far, that a clear need for additional comparison is indicated. In particular, the three-way comparison of calculated ion drifts, neutral winds, and the spaced receiver results (attempted in Fig. 3) is of interest only at heights above 110 km., and only one such case is yet available. The experimental program is continuing, however, and additional results will be published elsewhere.

REFERENCES

Herlofson, N. Plasma resonance in ionospheric irregularities. Ark. f. Fysik, 3, 247-297, 1951.

Kato, S. Ionized irregularities and wind motion in the ionosphere. Rept. Ionos. Res. Japan, 13, 62-78, 1959.

Keneshea, T.J., Gardner, M.E., and W. Pfister. Analysis of ionospheric winds and turbulence over Puerto Rico with a correlation method — I. J. Atmos. Terr. Phys., 27, 7-30, 1965.

MacLeod, M.A. Sporadic E theory, I. Collision-geomagnetic equilibrium. J. Atmos. Sci., 23, 96-109, 1966.

Ratcliffe, J.A. Some aspects of diffraction theory and their application to the ionosphere. Rept. Prog. Phys., 19, 188, 1956.

Wright, J.W., Murphy, C.H., and G.V. Bull. Profiles of E-region neutral winds by the gun-launched probe technique: their relation to ionospheric sporadic E and ionization movements. Proc. VII Intern. Space Science Symposium, COSPAR, 1966.

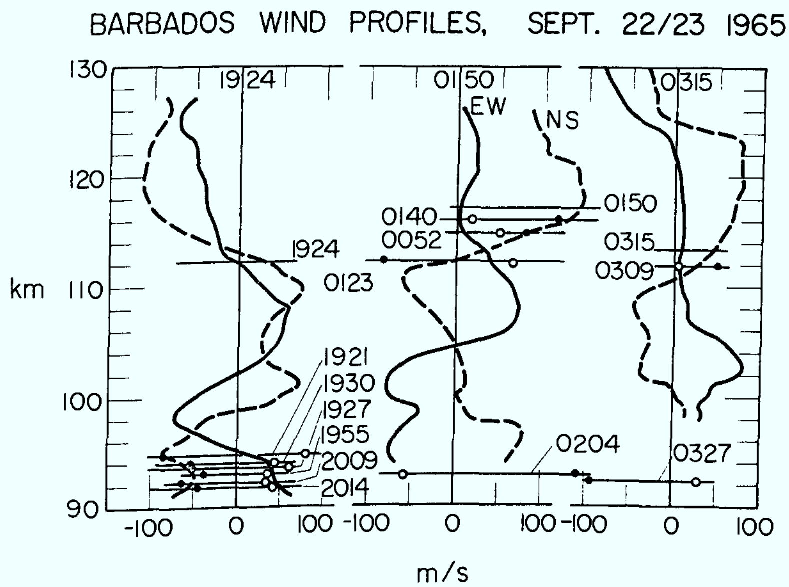

Fig. 1. Profiles of neutral wind speed components along (- - - -) and across (——) the magnetic meridian. Results of spaced receiver radio drift measurements are plotted on lines at measured Sporadic E heights and at times shown. ● = NS, 0 = EW.

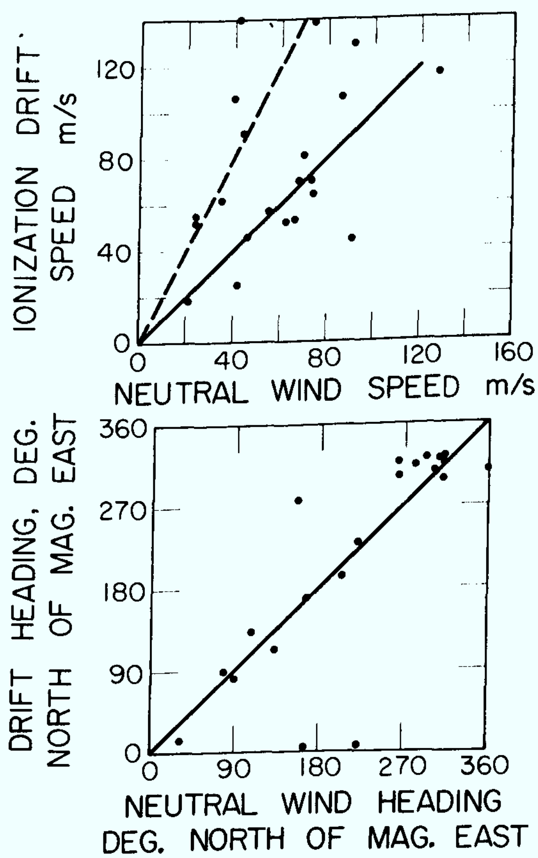

Fig. 2. Comparison of the headings and speeds observed for the neutral wind with the radio spaced receiver results. Dashed line in the upper diagram shows the results of assuming that the ionospheric drift speed is one-half that of the radio echo pattern at the ground.

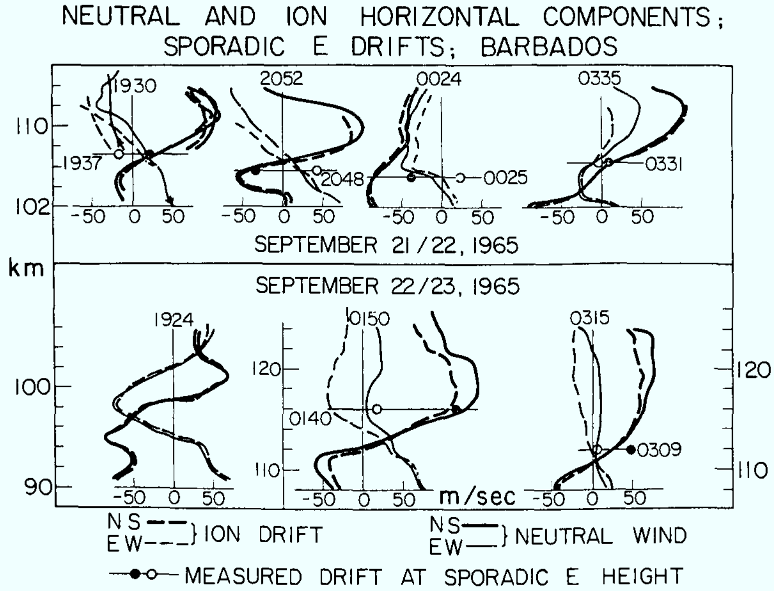

Fig. 3. Horizontal ion drift components (- - - -) calculated from neutral wind speeds (——), together with spaced receiver drift (● = NS, 0 = EW) of ground pattern.

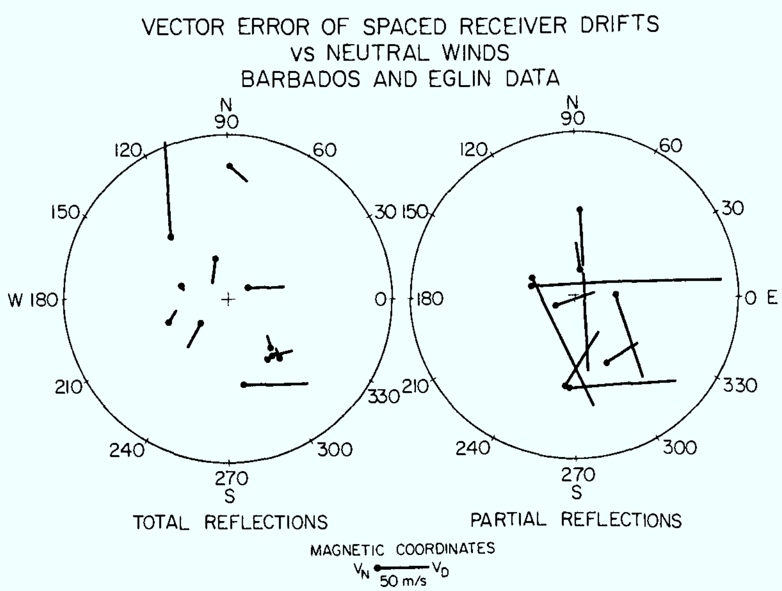

Fig. 4. Vector differences between the neutral wind (vector to the dotted end) and the radio spaced receiver results (vector to the plain end), separated according to radio reflection below or above the Sporadic E blanketing frequency (hence total or partial reflection, respectively).

Discussion on Paper 5.8 presented by J.W. Wright

Bibl: I think there is a simple explanation of the different behavior of the partially reflecting and the blanketing Es events. In the partially reflecting case, it is clearly possible that the reflectors are Es patches which move in those areas where the drift speed is largest; whereas we are pretty sure that blanketing type Es is caused by wind shear, and what is moving then is, in most cases, only the modulation of the wind shear surface, which could have a completely different speed to that of the neutral atmosphere above and below.

Wright: This is hypothetically possible, and might be the case if you consider two distinct Sporadic E layers, one of which was partially reflecting over a wide frequency range, and the other was totally reflecting over its frequency range. In fact, these Sporadic E layers were all totally blanketing up to a certain frequency, which varied with time, and partially reflecting above that point. The observations were made on various frequencies from the same Sporadic E layer, so that the heights of reflection and the types of irregularities present were one and the same thing within this narrow height range. The conclusion seems to be inescapable that the difference between the two sets of data has to do with the reflection mechanism itself, which in one case is total and in the other partial.

Volland: Can you say anything about the characteristics of the movements? Is there a periodicity of, say, 24 hr. or 12 hr. especially in the west-east direction?

Wright: I think the answer must be 'yes' although we have not tried to represent the data in that way. Most of the cases observed here were from the same cases of Sporadic E, as I discussed in Paper 5.7, and I spoke about the time periodicity in the neutral movements. Now the radio measurements agree substantially with the neutral movements, which means they have to show about the same sort of time periodicities as the neutral trails.

Bibl: I have a small survey which I think is important, and I would like to read it. Woodbridge (1962), reported large vertical wind components over Florida and Australia of 25 meters per second for average horizontal speeds of 50 m/s. The results were partially confirmed by Edwards and others (1963), and co-workers, who found vertical components of -6 to $+15$ m/s. Rosenburg's (1964) sequential measurements during two nights show a height decrease of a strong wind shear region over several hours. Vertical wind components and the decrease of wind shear heights favor a strong relation between wind shear and blanketing Es phenomena which showed similar behavior.

Wright: The Rosenburg data quoted is, in fact, data also contained in my sample.

Bibl: But Rosenburg doesn't put emphasis on this thing, and it is obviously clear that the accumulation of electrons has nothing to do with that drift speed because it is a real wind. I'm somewhat curious how you fit it into the wind shear theory, because it has a strong component, the average is not zero, and it is isometric, and this is exactly the picture that fits a development of our Es phenomena; that is, you have a high number of cases that have a negative vertical component, with an average speed of -3, which is sometimes the speed of Es.

Wright: I don't think there is any contradiction in this type of measurement. It is true that in most cases Sporadic E is observed to descend over a period of time. It is misleading to think of this in terms of velocity. What appears to be happening is that some feature of the wind profile is occurring at lower heights at later times, and is carrying the Sporadic E down with it as it goes. This sense of movement for a node on the wind profile is predicted by the gravity wave theory, and so actually, the hard things to explain are the few cases where the Sporadic E appears to be rising.

Bibl: We are talking about real wind measurements, and this means that if you had a shear, it looks as if the shear direction is the same as the direction of the wind component that goes down with it. I think Rosenburg has shown this nicely.

Wright: This is essentially what I was attempting to show in Paper 5.7.

SECTION 6

IONOSPHERIC ABSORPTION

6.1 THE ELECTRON DENSITIES IN THE E AND D REGIONS ABOVE KJELLER*

by

W.R. Piggott

Radio and Space Research Station

and

E.V. Thrane

Norwegian Defence Research Establishment

Presented by E.V. Thrane

The purpose of this paper is to study the height distributions of electron density and collision frequency in the E and D regions above Kjeller (60°N 11°E) at a spring equinox when the sunspot number was 110.

The results are based on data from several different types of ground-based experiments:

a) Measurements of ionospheric cross modulation at Kjeller giving estimates of electron density and collision frequency (Barrington et al. 1963).

b) Measurements of collision frequencies by means of rocket techniques (Kane 1959 and 1962).

c) Measurements of virtual height as a function of frequency made at Kjeller.

d) Measurements of vertical incidence absorption as a function of frequency (1 to 6 MHz.) made at Kjeller.

The results of experiments (a) and (b) are used to suggest the height distribution in the lower part of the D region, and it is assumed that the height distribution of electron concentration in the main E layer is parabolic. Our objective is to find the distribution of electrons between these regions. The height variation of collision frequency is important for calculating the absorption. The chosen variation is shown in Fig. 1. (Thrane and Piggott 1966).

As a first trial the lower D-layer and the E-layer electron density distributions are connected by an arbitrary smooth distribution curve. The absorption and the virtual height of waves of different frequencies reflected vertically are then computed, and are compared with the experimental results. The portion of the postulated height distribution between heights of 80 and 100 km. is then altered until, by trial and error, there is good agreement between all the measured and the calculated quantities.

The diurnal variations of absorption and virtual height have been measured at Kjeller, Norway from October 1954, to October 1958, using ten different frequencies in the range 1.2 to 6 MHz.

* Extended summary of a paper to be published in J. Atmos. Terr. Phys. 28, 1966.

The cross-modulation experiments were made in March and April 1960, and absorption data during six ionospherically quiet days in a closely similar period of the solar cycle, March and April 1956, was chosen for comparison. The average values of the virtual heights for these days have been used to compare with the computations. The absorption of high frequency radio waves was calculated by a phase integral method described by Budden (1961, chapters 16 and 20). The virtual heights were calculated by a simplified phase integral method programmed for the Mercury computer at Kjeller.

The models of electron density distribution adopted as a starting point for the analysis are described below.

a) Below 80 km. the electron density distributions are those deduced by Barrington et al. (1963) from cross-modulation experiments near the spring equinox.

b) The height distribution of the electron concentration in the E layer is assumed to be parabolic with a half thickness, $y_m = 2H = 15$ km. down to a distance H below the peak. This is a good approximation to a Chapman layer.

c) The dependence of the critical frequency on solar zenith distance was assumed to be $f_oE \propto \cos^{0.3} \chi$.

d) The height of the maximum of the E layer varies as predicted for an ideal Chapman layer with scale height 7.5 km. and the height where $\cos \chi = 1$, is 105 km. (Robinson (1959)).

e) The relaxation times are consistent with a recombination coefficient $\alpha \approx 10^{-8}$.

f) The electron density is kept constant between h_mE and 130 km.

g) Above 130 km., the electron density is made to increase rapidly with height so that the absorption during reflection near this level is negligible.

The method of deriving an electron distribution that would explain noon absorption and virtual heights is illustrated in Figs. 2 and 3. The well-established parts of the distribution are shown by the thick lines in Fig. 2, and three ways of joining them smoothly are suggested by the three lines marked a, b, and c. Fig. 3 shows that model a produced far too much absorption for frequencies below f_oE and that model b gives too little absorption. Model c gives the simplest possible height variation of electron density that will give the observed frequency variation of absorption. Fig. 4 shows the agreement between observed and calculated virtual heights.

In a similar way, electron density distributions for different times of days were derived using the additional assumption that the electron density for any particular height must vary smoothly throughout the day and likewise that the height of a level with a particular ionization density must have a smooth diurnal variation. The collision frequency is assumed to be time-independent.

These requirements impose severe limitations on the possible ionization models. Fig. 5 shows the results of the analysis. The absorption in the afternoon is considerably greater than that in the morning hours, and hence the derived distributions are not symmetrical about local noon.

The noon model has been compared with N(h) curves deduced by Belrose and Cetiner (1962) for two quiet days in March 1962 (when the sunspot number $R \approx 55$), using the backscatter technique, which agree well with the rocket results of Hall (1963) for Woomera obtained when $R \approx 50$.

The electron densities between 75 and 85 km. for Kjeller are considerably greater than those given by Belrose and Cetiner and by Hall. This discrepancy may be due to a solar cycle variation in the electron densities in this height region, since the propagation of waves of frequencies near 100 kc/s. and HF absorption show large changes with solar activity.

REFERENCES

Barrington, R.E., Thrane, E.V., and B. Bjelland. Can. J. Phys. 41, 271, 1963.

Belrose, J.S. and E. Cetiner. Nature, Lond. 195, 688, 1962.

Budden, K.G. Radio waves in the ionosphere. Cambridge University Press, 1961.

Hall, J.E. Nature, Lond. 20, 642, 1963.

Kane, J.A. J. Geophys. Res. 64, 138, 1959.

Kane, J.A. J. Atmos. Terr. Phys., 28, 338, 1962.

Pitteway, M.L.V. Phil. Trans. Roy. Soc., A257, 219, 1965.

Thrane, E.V. and W.R. Piggott. J. Atmos. Terr. Phys. (in press)

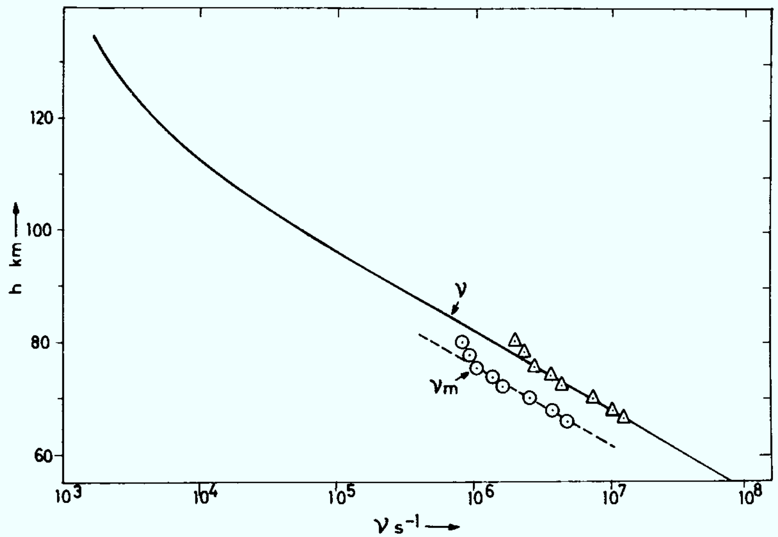

Fig. 1. The height variation of the collision frequency ν. The triangles indicate values of ν measured by Kane (1959) while the circles indicate the corresponding values of ν_m, the collision frequency of electrons with energy KT (Kane 1962).

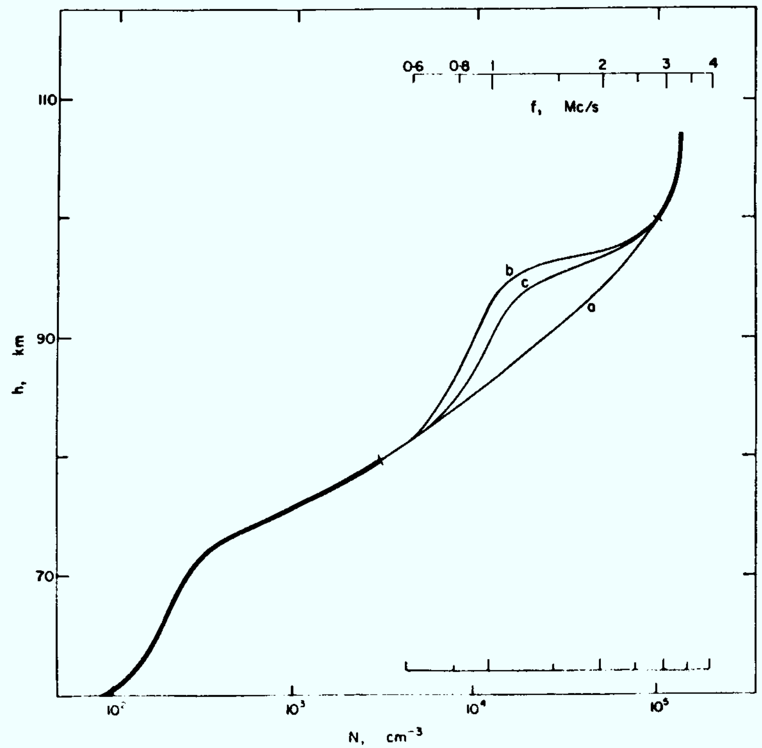

Fig. 2. Noon electron density models. The thick lines show the parts of the models determined by wave interaction and E-layer data. (a) Original smooth interpolation; (b) Model with too little E-layer loss; (c) Adopted model. The plasma frequencies corresponding to the electron densities are shown on the subsidiary scale.

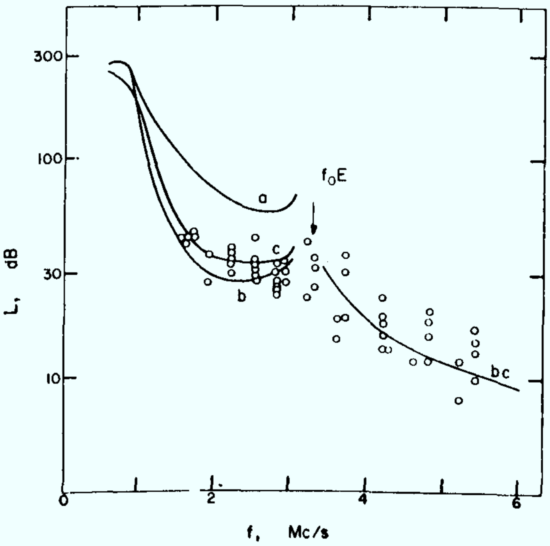

Fig. 3. Comparison between computed and observed values of absorption at noon, spring 1956. Curve (a) Absorption computed for model (a) in Fig. 2. Curve (b) Absorption computed for model (b) of Fig. 2. (c) Absorption computed for model (c) of Fig. 2. For frequencies above f_oE curves (b) and (c) indistinguishable.

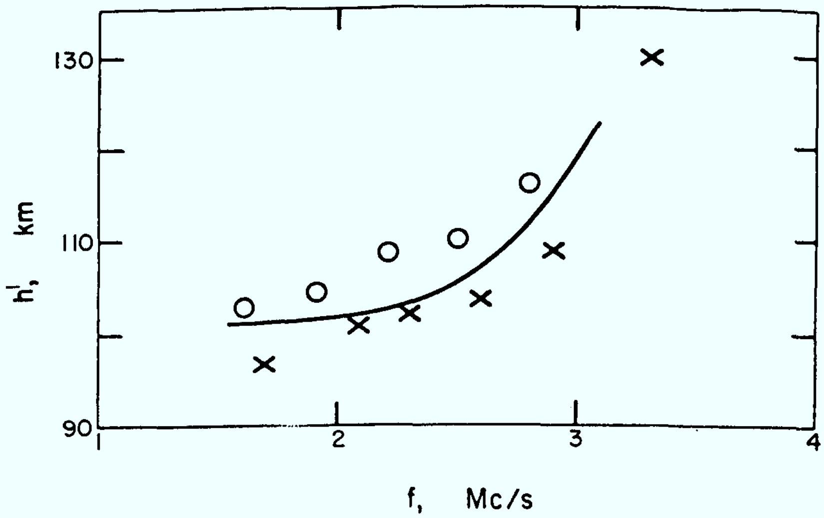

Fig. 4. Comparison of calculated and measured virtual heights for noon model. 0 – Average measured values for March 1956, X – Average measured values for April 1956.

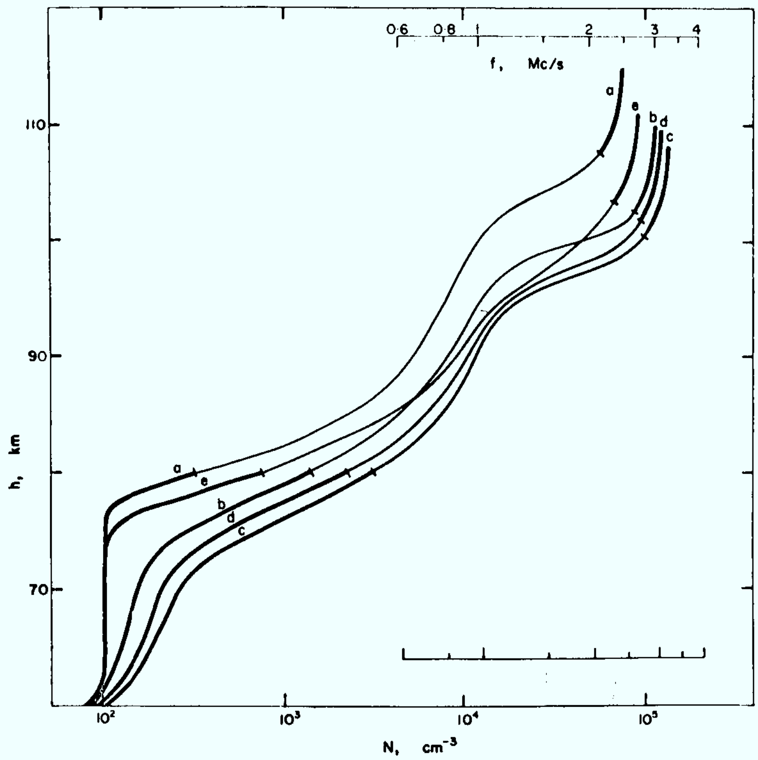

Fig. 5. The diurnal variation of electron density. (a) 0700 – 0800 M.E.T.; (b) 0900 – 1000 M.E.T.; (c) 1200 – 1300 M.E.T.; (d) 1400 – 1500 M.E.T.; (e) 1600 – 1700 M.E.T. The conventions are identical with those of Fig. 2.
Note: The solar zenith angle is smallest at 1215 M.E.T.

Discussion on Paper 6.1 presented by E.V. Thrane

Shirke: Have you taken full account of the deviative attenuation?

Thrane: Yes, this is included in the calculations. Dr. Budden uses the phase integral method, which does take account of what happens near the reflection height.

Belrose: Why did you not use an h'f analysis and fit it into the program? You did not try to reduce true heights from the h'f curve.

Thrane: No, we did not. This is because it is difficult to get accurate D-region profiles with the data we had from Kjeller at that time. I forgot to say that we did calculate the virtual height for reflection from the E region and compared it with the virtual height measured during the absorption measurements. Unfortunately, the virtual heights measured were inaccurate, so this does not give a good test. It is difficult to derive an accurate E-region profile unless you have good h'f recordings.

Belrose: I agree. I would also like to emphasize the point Dr. Thrane has brought out, that we don't really know what the electron densities are at about 75 km. during sunspot maximum years.

Thrane: There is little evidence for sunspot maximum. The only one I found was the one from the Russians.

Nelms: You are lucky to some extent that you don't get overlapping data, which can be embarrassing in some of these operations. As mentioned yesterday, we have an operation going where we try to join up the partial reflection D-region profile with the sounder profile. We have concluded two things: one, as you have just said, is that it is difficult to get sufficiently accurate measurements to derive a good profile from the sounder measurements in this region; the other is that we need more complicated calculation of the retardation given by the D-region profile. On the occasions when we had almost, but not quite, overlapping data, we would have had to put the sort of step that you have in your profile into our data to get a meaningful profile for the total region. We have been reluctant to do so, because it did not look all that real, but this gives us encouragement to think that it may be real.

Bibl: What was the limit of sensitivity in the absorption measurements?

Thrane: The equipment covers a big dynamic range. You can measure high absorption.

Bibl: This leads to the question of identification of E_s and E reflections.

Thrane: We tried to pick out days when the ionosonde did not show marked E_s.

Shirke: You said that the use of generalized theory did not make too much difference.

Thrane: It will make some difference, but it couldn't possibly make a 30 *db* difference.

Belrose: You have to be careful that you use the right collision frequency. I presume you were using the ν Appleton – Hartree and not the ν_m.

Thrane: Yes, you will have to use effective collision frequency.

6.2 MEDIUM WAVE REFLECTION PROPERTIES OF THE IONOSPHERE ABOVE TSUMEB

by

W. Elling

Max-Planck-Institut für Aeronomie, Institut für Ionosphären-Physik
Lindau üb. North./Han., Germany

1. Introduction

Medium wave pulse echo soundings at vertical incidence have been carried out at Tsumeb, South West Africa ($19^{\circ}14'$S, $17^{\circ}43'$E; Dip = -57.1°; Gyrofrequency f_H = 860 kc/s. at 100 km. height). Tsumeb is a suitable place for medium wave propagation experiments, since the interference level is low. The measurements at Tsumeb covered two periods, one during the sunspot maximum from August 1957 to March 1958, and a second during the sunspot minimum from November 1964 to June 1965. From pulse amplitude measurements, applying the constant gain technique, the attenuation of waves, characterized by the loss coefficient values $R = -20 \log \rho$ in decibels (ρ = apparent reflection coefficient) was measured at different fixed frequencies) (1). Nighttime amplitude-height snapshots of ordinary waves were made in 1957/58 for 7 fixed frequencies between 350 and 1100 kc/s.; in 1964/65 the amplitudes of ordinary and extraordinary waves were recorded at 15 fixed test frequencies between 250 and 1400 kc/s. during daytime and nighttime. In addition, sweep frequency ionograms were recorded over a range of 250 to 4000 kc/s. A survey about nighttime medium wave propagation conditions during sunspot maximum was obtained by compiling the results of amplitude and equivalent height measurements as a function of frequency (2). In the next section the principal contents and recent results, concerning the lower E region, will be presented.

2. Results of Nighttime IGY Measurements

When first starting the medium wave measurements and during the time of first experiments, it was difficult to recognize and separate a number of superimposed mechanisms affecting the nighttime propagation. The more regular effects were often masked by irregular reflection characteristics of Es layers predominantly responsible for the reflection of medium waves. The reflection capacity and the propagation paths changed with frequency and time. First, the reflection capacity of Es layers, observed at heights between 90 and 115 km., enters as an essential part of the measured loss; it depends on the ratio of test frequency to Es blanketing frequency f_bEs, on the thickness and on the degree of irregular structure of the Es layer. Secondly, a part of the measured loss may be due to deviative absorption generated by an ionization occurring in heights between 90 km. and the F layer. For a given frequency the deviative absorption is determined, among other things, by the value of the electron number density N, the gradient dN/dh (h = height) and the value of the collision frequency in the region of interest.

2.1 Mean Electron Density Profiles in the Lower E Region (90 to 115 km.)

Some mean electron density distributions for the nighttime lower E region were derived from loss coefficient measurements at different fixed frequencies in the range from 350 to 800 kc/s. According to the principles of measurement applied, the distributions deduced are nighttime mean values for several weeks. By recording measurements for each fixed frequency on a sufficient number of nights, reflections from all Es-layer heights between 90 and 115 km. may be observed. This height range was subdivided into intervals of one kilometer and the mean loss coefficient values belonging to each height section were calculated. Because of the large variations of Es characteristics, causing a great dispersion of single R values, mean values of the loss coefficients were formed for the nighttime data; 13% of all measured R values were selected corresponding to propagation conditions easy to survey. Values connected with oblique echoes or simultaneous echoes from different Es heights were neglected. The operating frequencies were 365, 440, 540, 605, 750, 830 and 1070 kc/s. The curves of mean loss coefficient values versus sporadic E-layer height had considerable positive slopes at frequencies below about 600 kc/s. For instance, the mean loss coefficient value at 365 kc/s. increased from 4 db at 90 km. height to 16 db at 100 km. The increase of loss with increase of Es-layer height is due to an ionization below the Es layers, which causes appreciable deviative absorption at frequencies slightly above the critical frequencies of the ionization. At higher frequencies, the increase is less marked. At 750 kc/s., for instance, the loss amounts to 8 db at 90 km., 13 db at 100 km. and 14 db at a height of 115 km. At frequencies above about 800 kc/s. the deviative absorption is small, and therefore the mean loss coefficient values are nearly independent of Es-layer height, that is, the measured R values represent the mean reflection capacity of Es layers.

The electron density distributions were calculated using the gradients of loss coefficients measured as a function of height, the complete Appleton-Hartree equation and the assumed collision frequency values. The results are plotted in Fig. 1. The results are preliminary because of the uncertainty of the adopted nighttime Appleton-Hartree collision frequency profile, ranging from 5 x 10^5/sec. at 90 km. to 1 x 10^4/sec. at 115 km. height. The accuracy of this method of determining electron density profiles is improved if one has a sufficient number of observations to get smooth curves of loss coefficient values as a function of Es-layer height.

2.2 Mean Electron Density Values In The Upper E Region (110 to 140 km.) and In The Intermediate Layer Region (140 to 170 km.)

The nighttime mean ordinary critical frequencies for these regions were deduced from ionograms for August 1957 and plotted in Fig. 2. The corresponding electron number density values N are marked on a second scale. The deviations of single values from the means are large. At midnight, sometimes the minimum frequency of ordinary F echoes is about 500 to 600 kc/s. and therefore coincides with the critical frequency in the upper E region plotted in Fig. 2. Also the ionization below the F layer is smaller than about 4000 el/cc., corresponding to a critical frequency of 570 kc/s. Sometimes the minimum frequency of ordinary F echoes amounts to about 1000 kc/s. and may be equal to the ordinary critical frequency of an intermediate layer. In this case the electron density of about 12000 el/cc. in the intermediate layer region is larger than the values plotted.

2.3 Frequency Dependence of Nighttime Propagation

The frequency dependence of nighttime ionospheric medium wave propagation properties at Tsumeb results from the existing Es-layer characteristics and the electron density distributions, described above. Waves with frequencies up to approximately 600 kc/s., which are reflected from Es layers, are penetrating a plasma in the lower E region with critical frequencies of about 200 to 350 kc/s. and will be more or less absorbed. Waves in this range of frequencies, which pass through the Es layers ($f > f_b$Es) will be reflected by the ionization in the upper E region and will suffer large deviative absorption as a result of the existing values of electron density and collision frequency and because of small dN/dh-values (20 to 100 el/cc./km.). No echo traces from above the Es-layer heights have been observed on the ionograms. Depending on the sensitivity of equipment, the loss coefficient values of reflections from above the Es-layers are greater than approximately 80 db at frequencies below about 600 kc/s. Starting from about 600 kc/s., F echoes have been noticed occasionally. The percentage of F observations increases with increasing operating frequency provided that $f > f_b$Es. The deviative absorption of waves, penetrating through the upper E region and the intermediate layer region, decreases with increasing frequency. At Tsumeb the deviative absorption occurring in the region below the F layer is small for frequencies higher than 800 to 1000 kc/s. The resulting reflection capacity for a given frequency depends on the Es-layer data and on the present N(h) distribution, and consequently will be variable. Results especially useful for propagation predictions and planning of medium wave broadcasting networks are published in some reports, (3, 4, 5).

It is concluded from visual inspections that the ionograms from 1964/65 essentially have the same characteristics as those of 1957/58. As a result of a 30 db-improvement of sensitivity, even weak echoes, and therefore more detail, can be seen. Some illustrative material is given in Fig. 3 to Fig. 6. Apart from Es-layer data, the ionograms give no information about the ionosphere at frequencies below about 500 kc/s. Marked intermediate layers with large retardations near the critical frequencies, sometimes noticed on the ionograms of 1957/58 during periods of high magnetic activity, were rarely observed in 1964/65.

3. Preliminary Results of Daytime IQSY Measurements

To continue the IGY measurements, extensive medium wave measurements were carried out at Tsumeb from November 1964 to June 1965. An appreciably improved antenna system, consisting of $\lambda/2$ folded dipoles at a height of 120 m. (1957/58 : 30 m.), was used together with an elaborated recording technique. The high sensitivity of equipment, permitting the measurement of loss coefficient values up to 80 db (1957/58 : 50 db), yields loss values not only for the night period but in many cases for the daytime also. The evaluation of the data from the experimental campaign during the IQSY and the interpretation of values, included in the following discussion, have just been started. Possibly these results are not characteristic of all of the collected data.

On daytime ionograms, D echoes can be seen from 250 to 1000 kc/s. and higher frequencies. The equivalent heights of main D reflections vary from 70 to 80 km. Starting from about 500 kc/s. at noontime, signals from the lower E region appear in addition to the D echoes. The lowest observed equivalent E-layer heights are approximately 85 km. Some examples of noontime ionograms presented in Fig. 7 illustrate this fact.

Results of measured loss coefficient values and equivalent reflection heights as a function of frequency, deduced from pulse amplitude measurements, recorded on 5 February, 1965 and 24 December, 1964 are plotted in Fig. 8. On 5 February, 1965 (Fig. 8a and Fig. 8b) ordinary (o) and extraordinary (x) waves were separated using crossed dipoles (2 x 80 m. in length ; 30 m. high) and a polarimeter device (suppression ratio : 25 to 30 db). The nighttime values (Fig. 8b) for extraordinary Es propagation show a positive slope for the loss coefficient-frequency curve and an insignificant negative slope for the ordinary waves; the curves cross at about 570 kc/s. This frequency dependence can be observed from time to time and is probably due to the characteristics of thin reflecting Es layers (6). The daytime values of 24 December, 1964 (Fig. 8c) refer to the total field strength, i.e. the dipoles are used for transmitting and receiving simultaneously. The graph shows a flat maximum of loss at 400 to 500 kc/s. Probably the maximum can be explained as follows: starting with 250 kc/s., the reflection capacity of the D ledge is decreasing with increasing frequency (Fig. 8a). At about 500 kc/s., lower E-region echoes appear, the reflection capacity is small at $f_{min}E$, and the loss decreases at the higher test frequencies (Fig. 8a). The absorption maximum seems to be associated with the transition from D- to E-layer reflections. Other reasons for this maximum may become evident as more data is examined. The change of reflection levels in Fig. 8c is not particularly marked because the mean values were derived from data taken between 0600 and 1030 hours.

REFERENCES

1. The measurement of ionospheric absorption. Annals of the International Geophysical Year, III, Part II, 1957.

2. Elling W. Scheinbare reflexionshöhen und reflexionsvermögen der ionosphäre über Tsumeb, Südwest-Afrika, ermittelt mit impulsen im frequenzband von 350 bis 5600 kHz. Arch. Elektr. Übertragung, 15, 115-124, 1961.

3. CCIR-Beiträge. Bundesrepublik Deutschland. Dok.VI/83, 1958, Dok.44, 1959, Dok.VI/6, 1961.

4. Niederschrift 21. Sitzung d. Expertengruppe ARD/DBP, 2./3. Dez. 1965.

5. UER/EBU Conference, Com.T.(B) 85-E, 9.März, 1966.

6. Ferraro, A.J. and C.P. Tou. Studies of the echo polarization from high gradient profiles. AGARDograph 74, Propagation of radio waves at frequencies below 300 kc/s., 83-99, 1964.

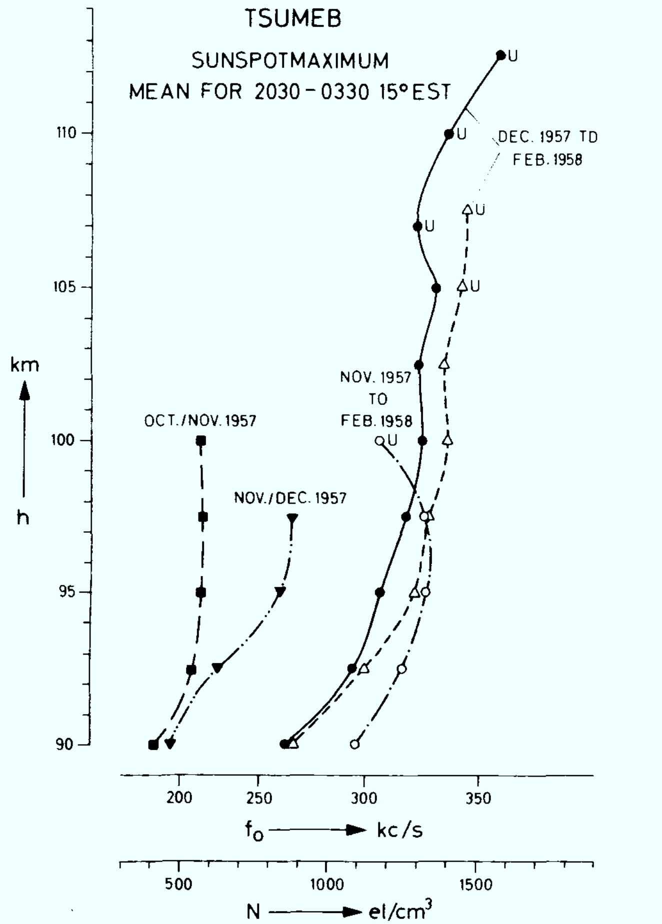

Fig. 1. Mean nighttime electron number density N in el/ cm^3 (or ordinary critical frequency f_o in kc/s.) for October 1957 to February 1958 as a function of height h in km. in the lower E-region, deduced from loss coefficient measurements.

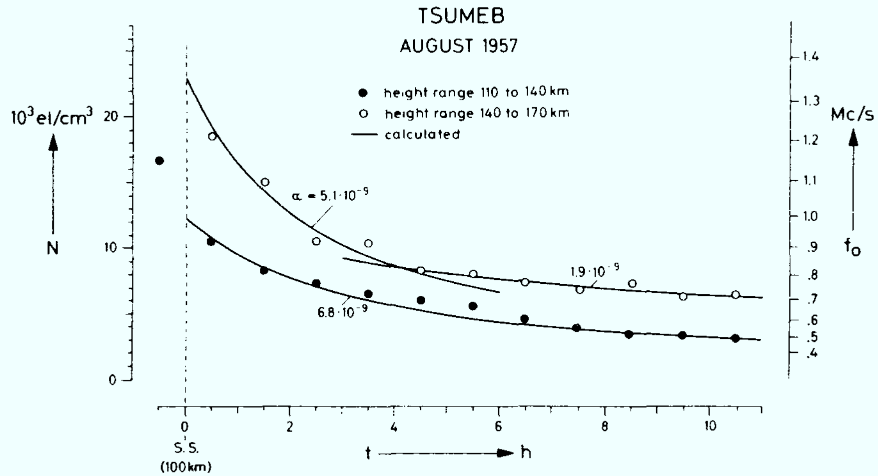

Fig. 2. (After Ref. 2) Observed mean nighttime electron number density N in 10^3 el/ cm^3 (or ordinary critical frequency f_o in Mc/s.) for August 1957 as a function of time t in hours after layer sunset S.S. at a height of 100 km. for the upper E and the intermediate layer region. α = calculated apparent recombination coefficient in cm^3/sec. ($dN/dt = -\alpha \cdot N^2$; t = time).

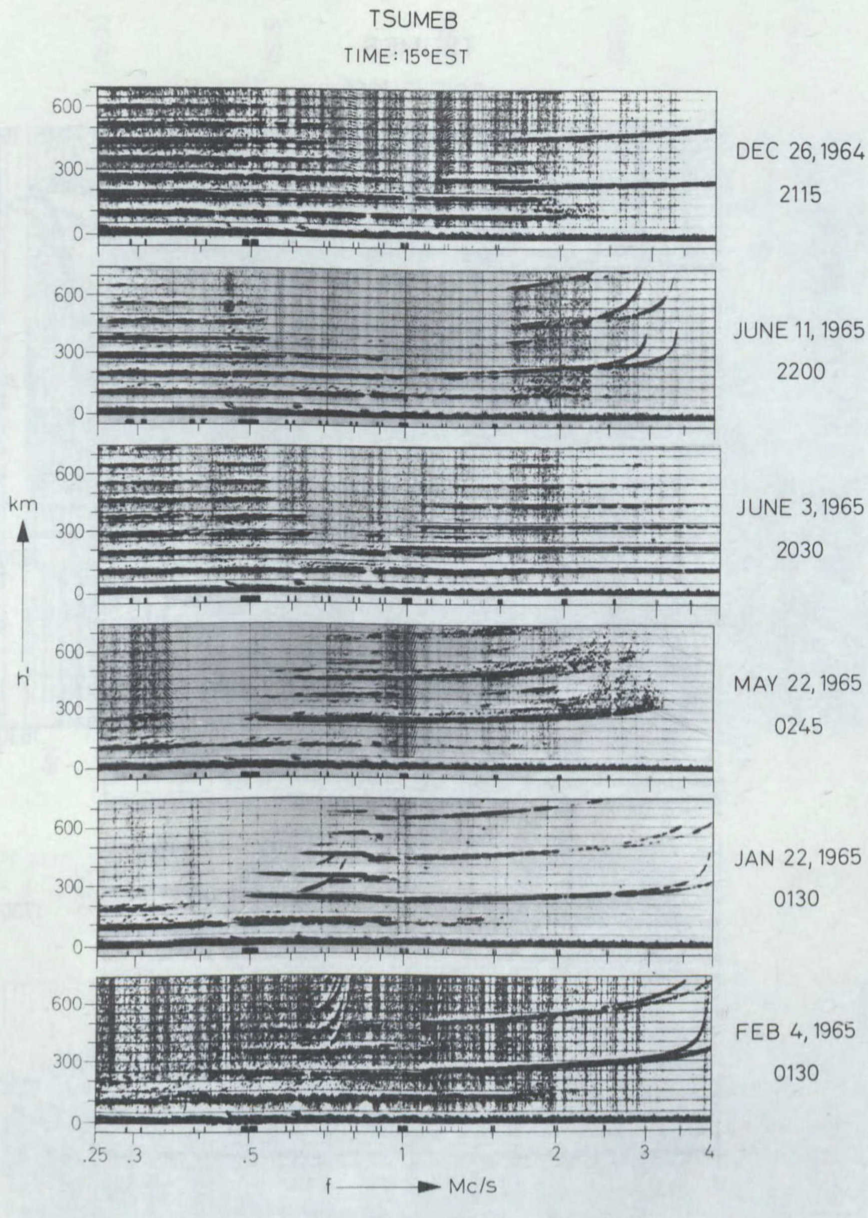

Fig. 3. Typical low frequency nighttime ionograms. (f = frequency, h' = equivalent reflection height).

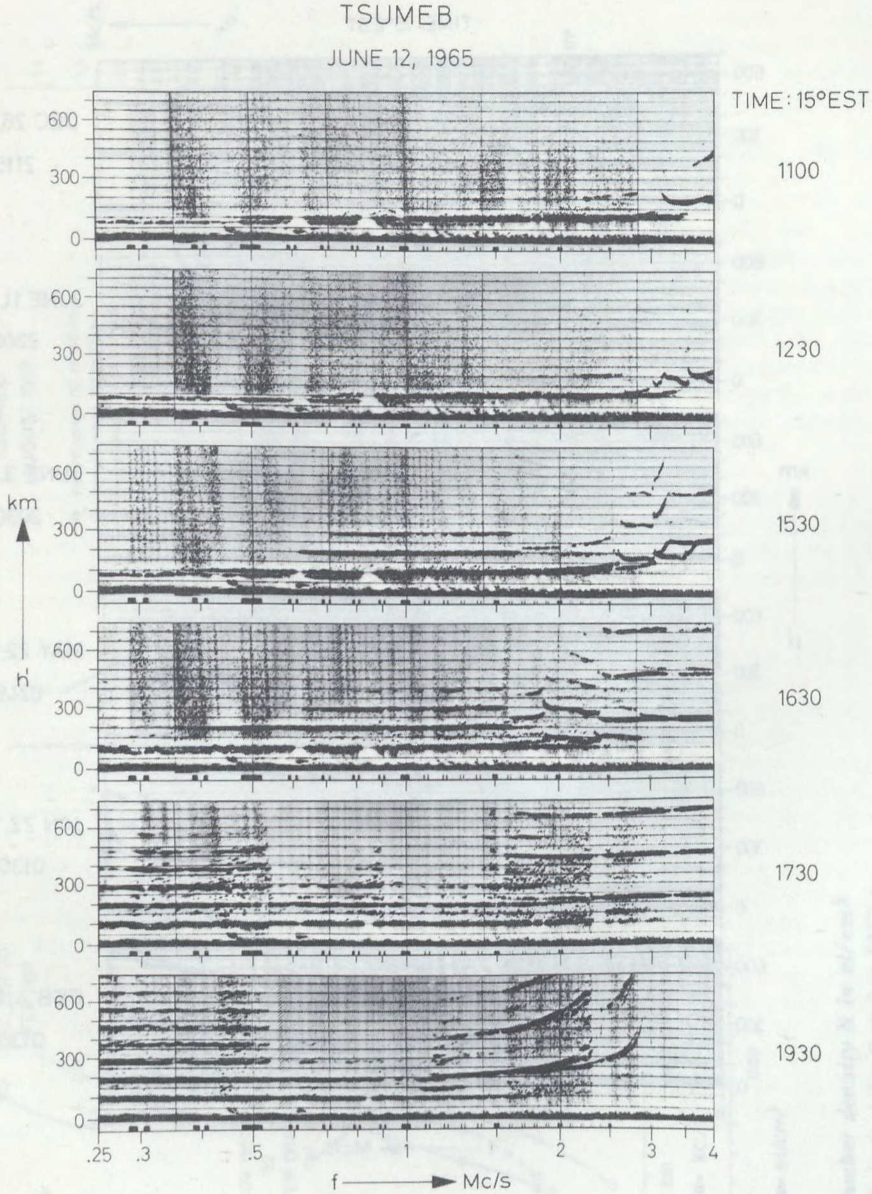

Fig. 4. Typical local winter daytime and sunset low frequency ionograms. Sunset at 100 km. height: 1807 hours. (f = frequency, h' = equivalent reflection height).

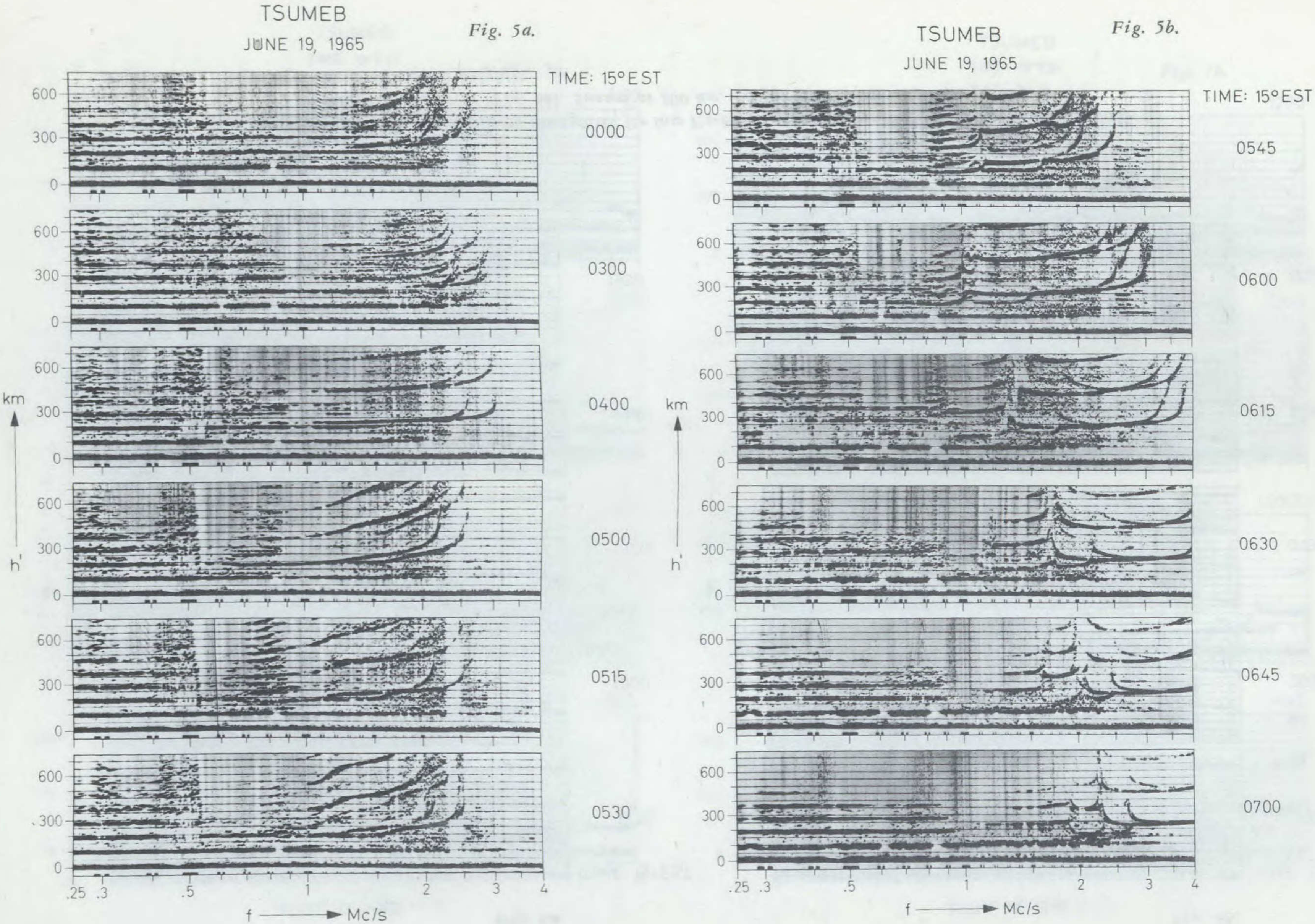

Fig. 5. Typical nighttime (Fig. 5a) and sunrise (Fig. 5b) low frequency ionograms. Sunrise at 100 km. height: 0540 hours. (f = frequency, h' = equivalent reflection height).

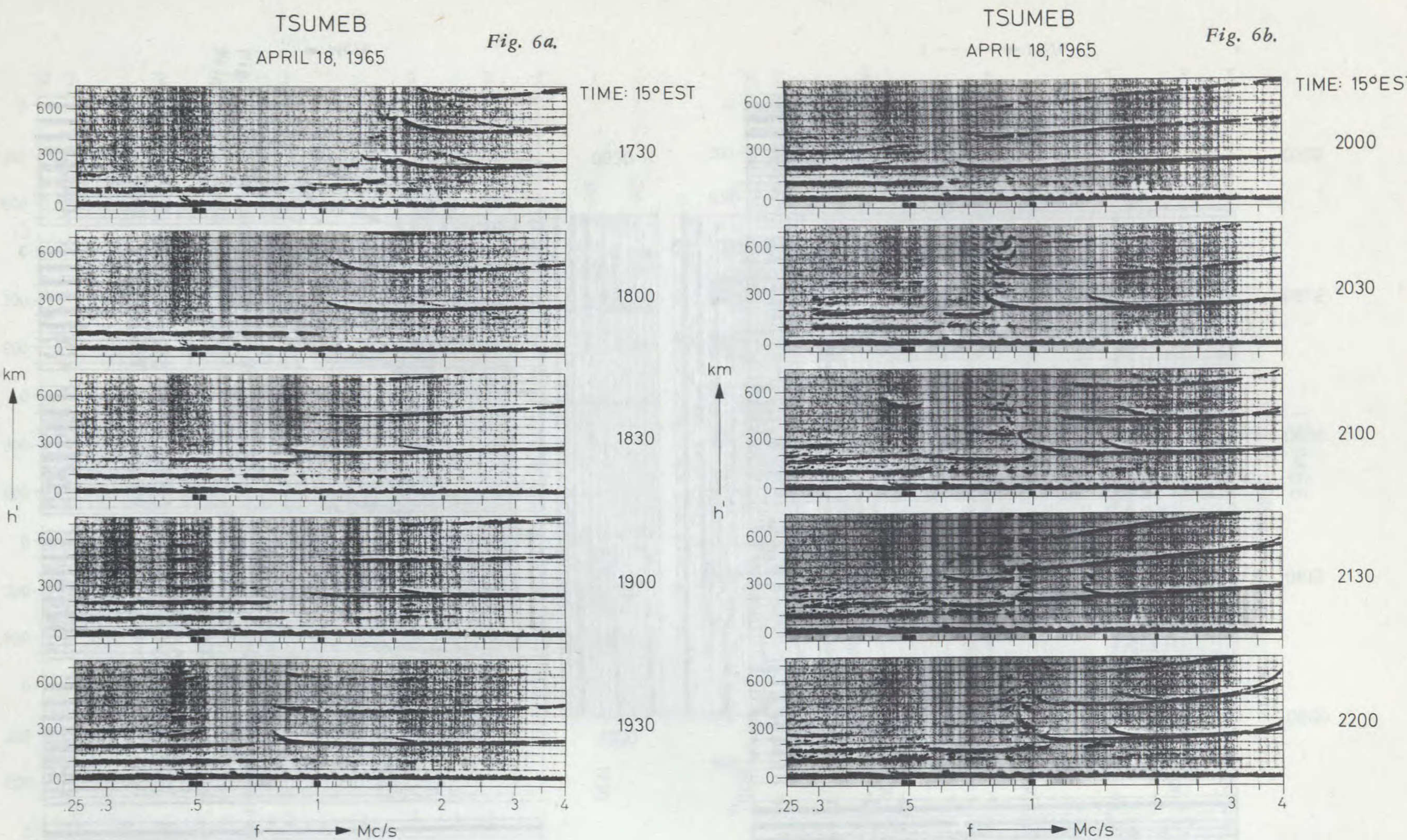

Fig. 6. Sunset low frequency ionograms for low Es-blanketing frequencies (Fig. 6a) and formation of an intermediate layer (Fig. 6b). Sunset at 100 km. height: 1825 hours. (f = frequency, h' = equivalent reflection height).

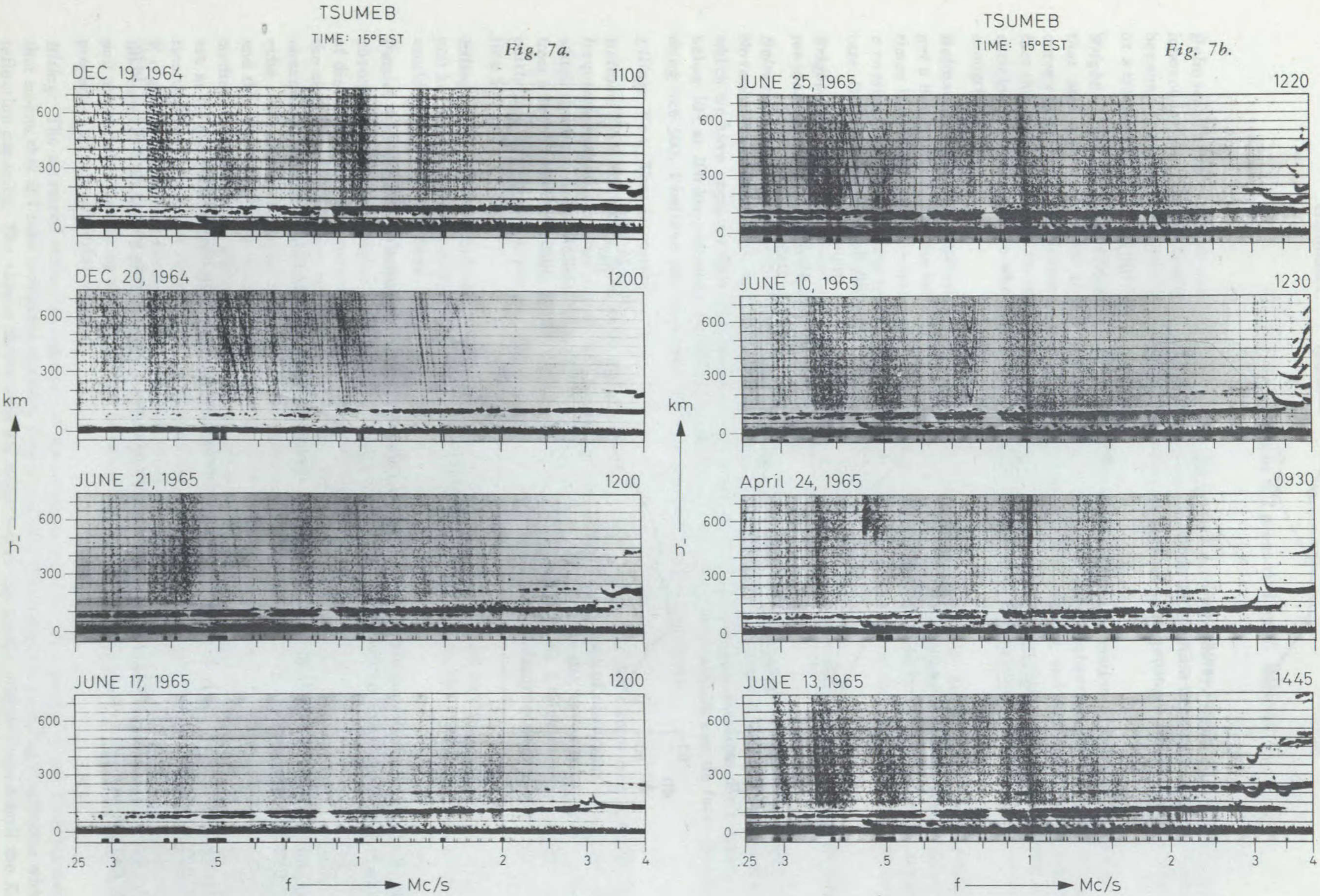

Fig. 7. Typical noontime low frequency ionograms for local summer and local winter. (f = frequency, h' = equivalent reflection height).

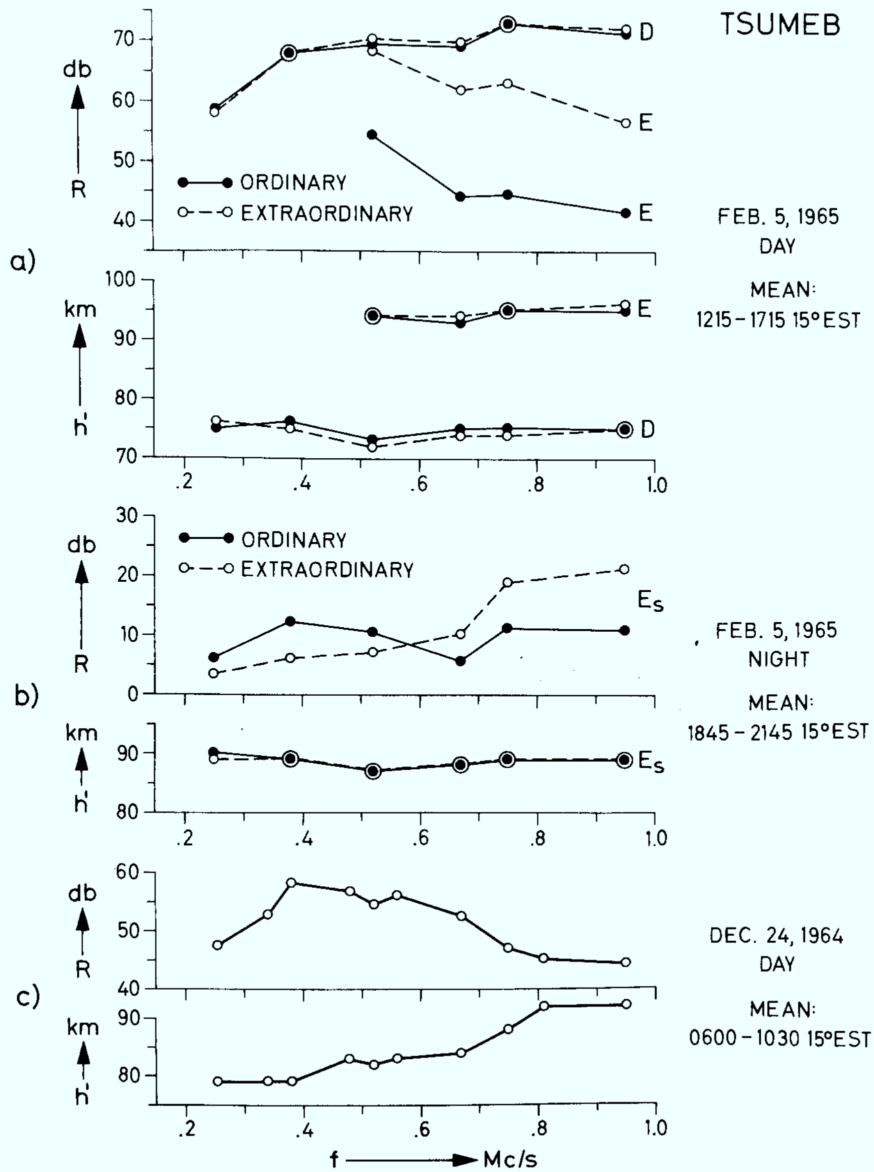

Fig. 8. (After Ref. 5) Measured loss coefficient values R in db and equivalent heights h' in kilometers as a function of frequency f in Mc/s.

Fig. 8a. 5 February, 1965, R-values for o and x waves, mean values for 1215 to 1715 15°EST (daytime values).

Fig. 8b. 5 February, 1965, R-values for o and x waves, mean values for 1845 to 2145 15°EST (nighttime values).

Fig. 8c. 24 December, 1964, R-values for the sum of o and x waves, mean values for 0600 to 1030 15°EST (daytime values).

Discussion on Paper 6.2 presented by W. Elling

Belrose: These excellent ionograms illustrate the point I made yesterday. By lowering the limit of ionosondes you don't necessarily improve ability to calculate an electron density profile from an ionogram, because you have to be careful in knowing whether, in fact, you are getting a scatter type of reflection or a true magnetoionic reflection.

Wright: I don't believe anyone would try to use the group delay information to calculate a profile. All that one does is use the O and X if they're both available and the observed slopes of the virtual height curves to provide a sufficient correction for the underlying ionization, and then continue the profile. The fact that reflections can be seen at all at such low frequencies is interesting, and I don't think it was anticipated by the people who dreamed up the quantity F min. for absorption. What is F min. on such an ionogram?

Belrose: I wanted to emphasize that lowering the limit of an ionosonde does not necessarily allow you to get a better answer for the base of the E layer, and this becomes apparent with high sensitivities. Sometimes it does, if you don't have any scattering types of things. Sometimes on our ionograms at Ottawa, a continually varying group retardation begins at 250 kc. and goes up to the E region, but this is extremely rare. One doesn't generally see this change of group retardation.

Wright: We should remember that these comments concern the daytime and there are many significant reasons for low frequency observations at night.

Belrose: I would also like to comment on the low electron densities seen in October-November, 1957, and November-December 1957, which you showed in Fig. 1. From other nighttime electron density profiles which we have seen, we find that on the basis of rocket data the electron densities don't appear to drop below 10^3 at 100 km., whereas Dr. Elling suggested that the electron density can, in fact, drop to something like 500. I believe you have used Appleton-Hartree in your analysis.

Elling: Yes. That is correct.

Belrose: You are likely to be in great error using Appleton-Hartree. I don't know how low you can go in frequency and still manage to use Appleton-Hartree, but the long series of observations and calculations which the Penn State workers did at 150 kc. illustrated that at 150 kc. the waves at night are reflected from a level somewhere near $X = 1 + Y$ and not near where $X = 1$ at all. I think that you are liable to be partly in danger because you should be doing a full wave calculation for frequencies below something like 500 kc.

Elling: Yes. The critical collision frequency at Tsumeb is at about 80 km. The gyrofrequency is low: 900 kc/s. at the ground and around 800 kc/s. at 200 km.; consequently, the problem is not as bad as it would be at other locations.

Petrie: I would like to comment generally on the calculation of the apparent reflection coefficient due to absorption at slightly higher frequencies (frequencies above 2 Mc/s.). There is no doubt that a number of discrepancies have existed in the two methods of measuring the apparent reflection coefficient. One of the methods is to measure the amplitude of the echo at these higher frequencies at night, assume negligible absorption, and calculate the absorption during the daytime by measuring the amplitude of the first hop echo. The other method is to measure the amplitude of a first hop and second hop echo, take the difference, and this should give the losses that the radio wave suffers. Piggott has found discrepancies between these methods of about 6 db. Pillet, in France, suggested that the discrepancies may be as high as 15 db; these are at frequencies in the range 2 Mc/s. to about 5 Mc/s. In an article in September JGR, there is indication that they are about 10 to 15 db. It appears that the amount of energy you get back, at least from the F region at night, is a function of the degree of spread on the ionogram or a function of the roughness of the surface. I wonder if at these frequencies this may be entering into some of the calculations. Perhaps you are not only measuring the absorption (deviative or non-deviative), but you may also be measuring the properties of the reflecting surface.

Elling: The measured reflection capacity of the ordinary wave is independent of the Es-layer height, and that means that if I take sufficient numbers then I can take this reflector as being a reflector with mean reflection capacity. The values shown here are mean values for weeks, I have waited until the Es layers have occurred with sufficient frequency at all heights.

6.3 NEW RESULTS IN D-REGION CHEMISTRY

by

G.W. Adams and A.J. Masley

Space Sciences Department
Douglas Missile and Space Systems Division
Santa Monica, California

Presented by

G.W. Adams

Paper withdrawn from These Proceedings at the request of the authors.

6.4 CONTRIBUTION OF THE D AND E REGION TO ABSORPTION AT 2.35 MHz.

by

K. Bibl and B.W. Reinisch
Lowell Technological Institute Research Foundation
Lowell, Massachusetts

Presented by B.W. Reinisch

Abstract

In the course of a 2.35 MHz. fixed-frequency drift experiment, routine pulse absorption measurements were made on a daily eight-hour basis. Precise phase height records, as well as ionograms, determine the type of the reflecting layer. The contributions of the non-deviative absorption in the D region and the deviative absorption in the E region are investigated. High turbulence in the E region may explain the winter anomaly of absorption. The fading rate of the amplitude shows no correlation with time of day, but depends on the occurrence of Es and on turbulence in the E region.

1. Introduction

Total attenuation of radio waves transmitted vertically and reflected in the E region is determined by three phenomena:

a. Non-deviative absorption in the D region,
b. Deviative absorption in the E region,
c. Reflectivity of the E layer.

Absorption decrement of the D region is described by

$$L_D = B/(f + f_H)^2$$

where

$$B = B_o \cos^n \chi$$

(χ = solar zenith angle, n = value between 0.7 and 1.0).

In quasi-transversal approximation, the integral

$$L_E = N \int \frac{\nu}{\mu} X \, ds$$

describes the deviative absorption decrement of the E region (ν = collision frequency, μ = real part of the refraction index, $X = (fo/f)^2$).

This expression of L_E shows its dependence upon the ray path in the E region; the path length as well as the values of μ and ν along the path are significant parameters. For a smooth normal-E layer, the integral can be evaluated along the vertical z-axis adopting a reasonable model of the E-layer electron density and collision frequency distribution (Bibl and Rawer, 1951). The integration path in the region of small μ becomes shorter when the reflection occurs at a sporadic-E layer, embedded in normal-E. Height decrease of the Es layer results in diminished deviative absorption (Bibl, Paul, and Rawer, 1962). For absorption measurements, the conclusion is to treat cases with Es reflections separately. Obviously, L_E is practically zero when the wave is reflected at a blanketing low-Es layer. Greater deviative absorption results if the Es layer is closer to the height where the plasma-frequency, fo, of the normal-E layer equals the operational frequency, f. During daytime the Es-layer height is determined accurately by the ratio, $\frac{foE}{fr}$, where the cusp frequency, fr, is the frequency above which the wave is reflected at Es.

As long as there is specular reflection, the integration can be taken along the vertical z-axis. The situation changes when the E region becomes structured or turbulent. First, the reflection coefficient, R, may differ from one. When the bottom of the E region is undulated, R may be greater than one, because of oblique scatter. Even in the case of a cloudy E region, a value of R greater than one is possible when the scatter depth is small. When part of the energy penetrates the E region (partial reflection) or is scattered away, R is smaller than one (Reinisch, 1965). For the study of the absorption processes, cases with R not equal to one should be disregarded.

Even when R equals one, the contribution of the cloudy E region to the total attenuation is appreciably higher than in the case of specular reflection, because multiple scattering causes an increased path length in the deviative medium. Of course, integration can no longer be taken along the z-axis and the integral becomes a complicated function of the structure in the E region.

2. Observation and Analysis

In the following analysis, the considerations given in the Introduction were taken into account. A fixed-frequency drift experiment at 2.35 MHz. was used for routine absorption measurements. Pulse amplitudes were recorded daily during eight daytime hours for the seven months from July 1965 to January 1966. This period covered the summer, fall, and winter seasons. Every 15 min. a sample was taken for 2 2/3 min., an average amplitude for the sample determined, and the numbers of fadings larger than 3 db and larger than 10 db were counted. For each sample, the type of the reflecting E layer, determined from an ionogram taken 2 min. after the amplitude sample, permitted distribution of the data into four classes:

1. Specular reflection at a normal-E layer (Fig. 1),
2. Specular reflection at a blanketing low-Es (Fig. 2),
3. Specular reflection at a cusp- or high-Es (Fig. 3),
4. Non-specular reflection (Fig. 4).

This classification is not made in normal absorption analysis. Monthly medians of the amplitude are plotted in Fig. 5, which demonstrates the importance of differentiating between types of reflection. The solid curve represents the amplitude without regard to the type of reflecting layer; the dashed line represents Class 1 of the preceding four classes. In July, August, September, October, and December, the two curves follow each other closely. This indicates that the generally higher absorption for cases of diffuse reflection are approximately compensated by the cases of specular Es reflections where the deviative absorption is small.

November and January show exceptional behavior. In November, normal E-layer reflection (Class 1) amplitudes are approximately 7 db smaller than the amplitudes averaged over all measured values (Fig. 6). As indicated in Fig. 5, the number of Es reflections, especially low-Es, is extremely high in November. Therefore, the average amplitude level is high. For comparison, the medians for reflection at blanketing low Es (Class 2) are plotted for November. The difference in echo amplitude for low-Es and normal-E reflection is 13 db, which gives the deviative absorption in a normal E-layer.

For January the situation is opposite to that in November. Amplitudes for normal-E are 6 db higher than the average values. A non-selective absorption analysis would only find relatively high absorption for that winter month, confirming the winter anomaly of absorption. Here, the applied selective data analysis shows the origin of this anomaly to lie in a turbulent E region. The number of Es reflections in January is not smaller than the number for most of the other months. A high turbulence in the E region on many January days results in high deviative absorption because of deep scatter and/or a reflection coefficient R smaller than one. The question which remains to be answered is whether the D region is also affected during these turbulent periods. Riometer observations in which the E region absorption is less pronounced than here will give the answer.

Results of the fading-rate analysis are plotted in Figs. 7 and 8. In the course of the analysis, it became obvious that the difference between normal-E reflection and the averaging case is not significant for the monthly medians of the fading rate. Therefore, we have plotted, in Fig. 7, the fading rate for all samples disregarding the type of reflection. It is evident from this figure that the monthly medians do not show a correlation with the time of dav. The rate of fadings with an amplitude larger than 3 db varies rather irregularlv between 2 and 6 per minute; fadings with a depth of more than 10 db have a rate between 0 and 3 per minute. In Fig. 8, the seasonal variation for local noon is plotted. It is interesting to notice that the shallow fadings have a high maximum for the disturbed month of January, as expected. The deep fadings, however, do not show a maximum for January, but thev do show a maximum for November. As noted in Fig. 5, November has a high occurrence of sporadic E. We conclude that sporadic-E layers cause deep fadings, whereas the rate of shallow fadings is correlated with E-region turbulence.

3. Summary

Selective data analysis has been applied to determine the contribution of D and E regions to the total attenuation. We showed that averaging over different types of reflection destroys all information about the physical properties of the layers. High occurrence of low-Es decreases the average attenuation. Separate treatment of low-Es and normal-E reflection permitted determination of the deviative absorption for reflection at a normal-E layer in November. The origin of the winter anomaly of absorption was found to lie in a high turbulence in the E region.

The rate of shallow fadings (> 3 db) seems to correlate with this turbulence, the rate of deeper fadings (> 10 db) with the occurrence of Es.

Acknowledgments

This work was carried out under Air Force Cambridge Research Laboratories Contract No. AF19(628)-4784 and No. AF19(625)-412. We are greatly indebted to Dr. K. Toman for encouragement of this absorption analysis. Thanks are due to Dr. W. Pfister and Mr. T. Keneshea for permission to use their data and for help in discussing the problems of this subject.

REFERENCES

Bibl, K. and K. Rawer. Les contributions des région D et E dans les mesures de e' absorption ionospherique. J. Atmos. Terr. Phys., 2, 51, 1951.

Bibl, K., Paul, A., and K. Rawer. Absorption in the D and E regions and its time variations. AGARDograph 53. Radio wave absorption in the ionosphere (Pergamon Press). 1962.

Reinisch, B.W. Die bedeutung von echos an der sporadischen E-schicht, AEÜ, 19, 361, 1965.

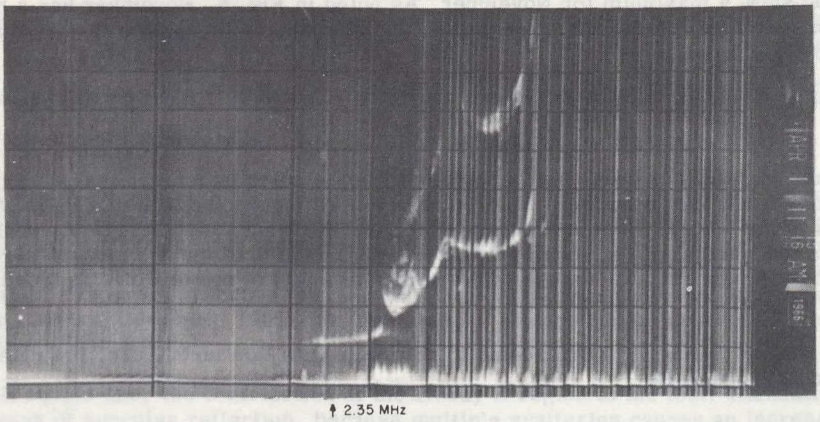

Fig. 1. Ionogram with normal-E layer.

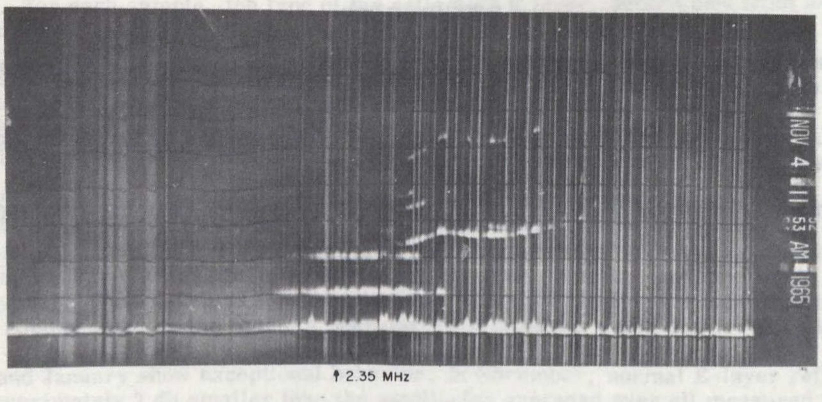

Fig. 2. Ionogram with blanketing low-Es

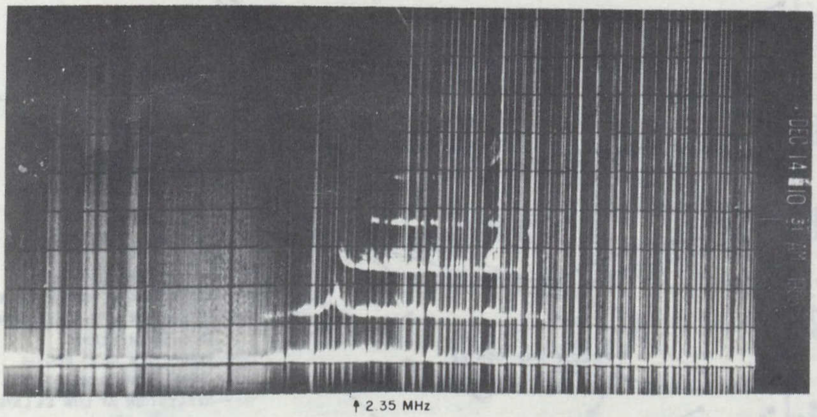

Fig. 3. Ionogram with cusp-Es

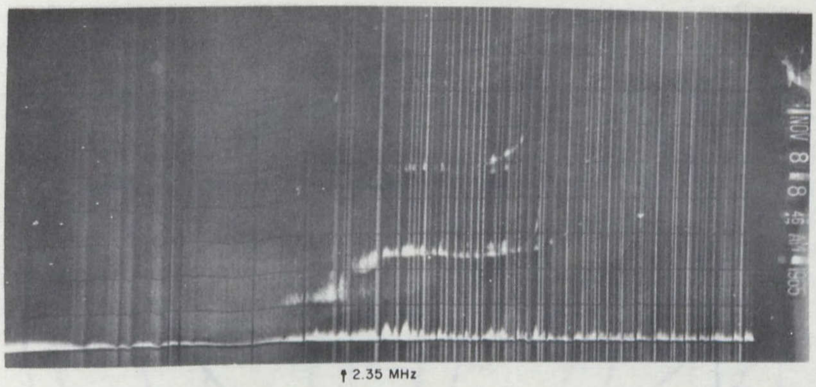

Fig. 4. Ionogram with turbulent E region.

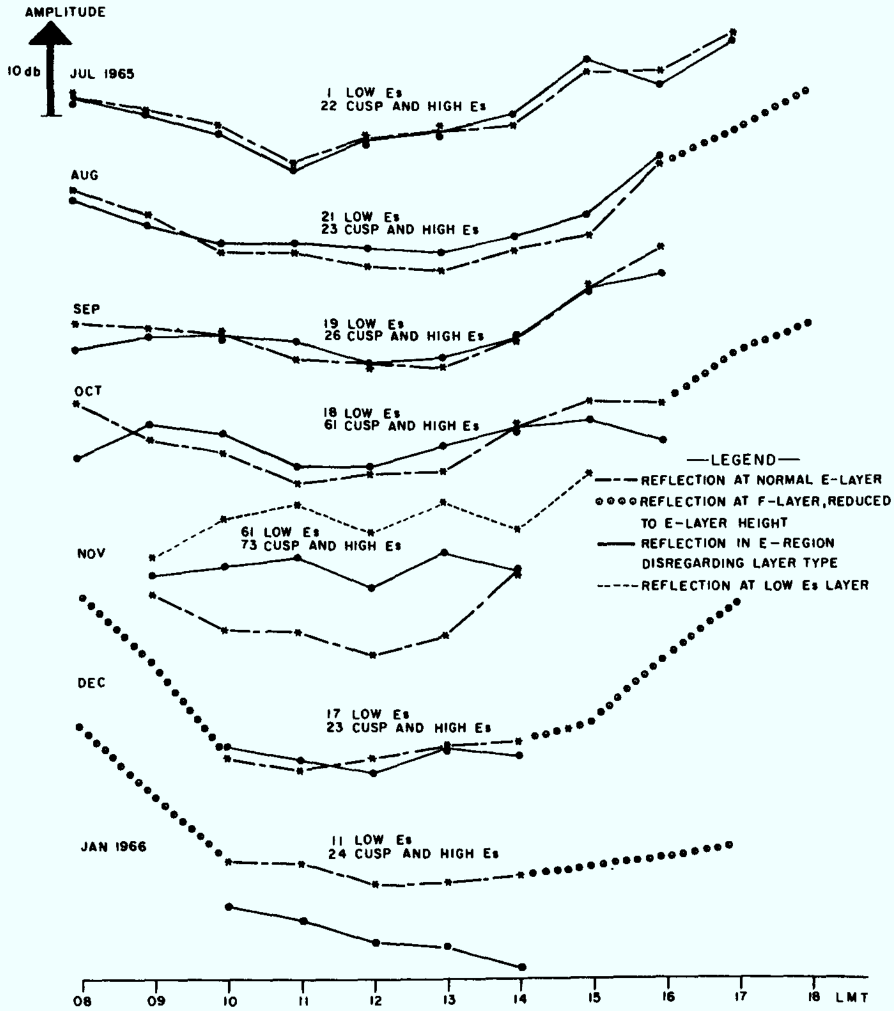

Fig. 5. Diurnal variation of amplitude, monthly medians.

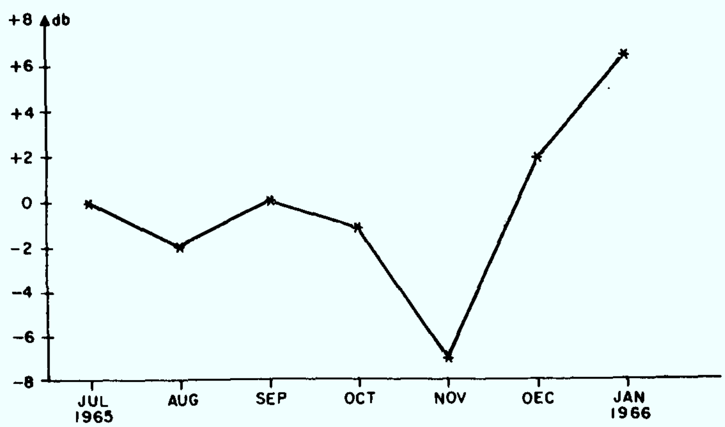

Fig. 6. Deviation of absorption from normal-E reflection, measured at local noon.

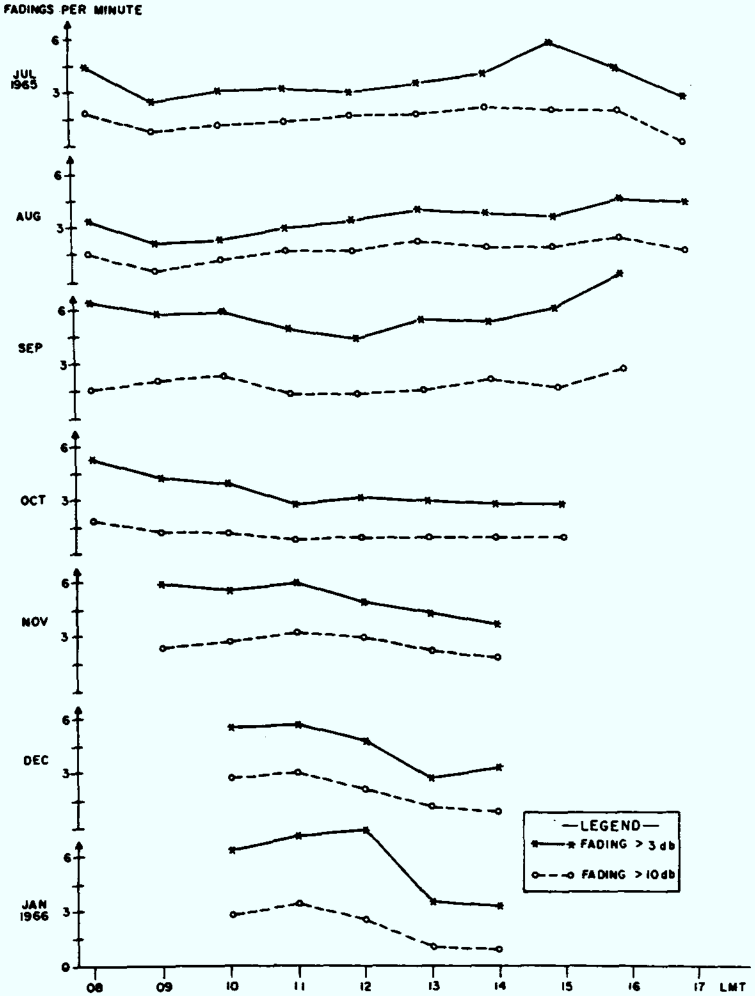

Fig. 7. Diurnal variation of the fading rate, monthly medians.

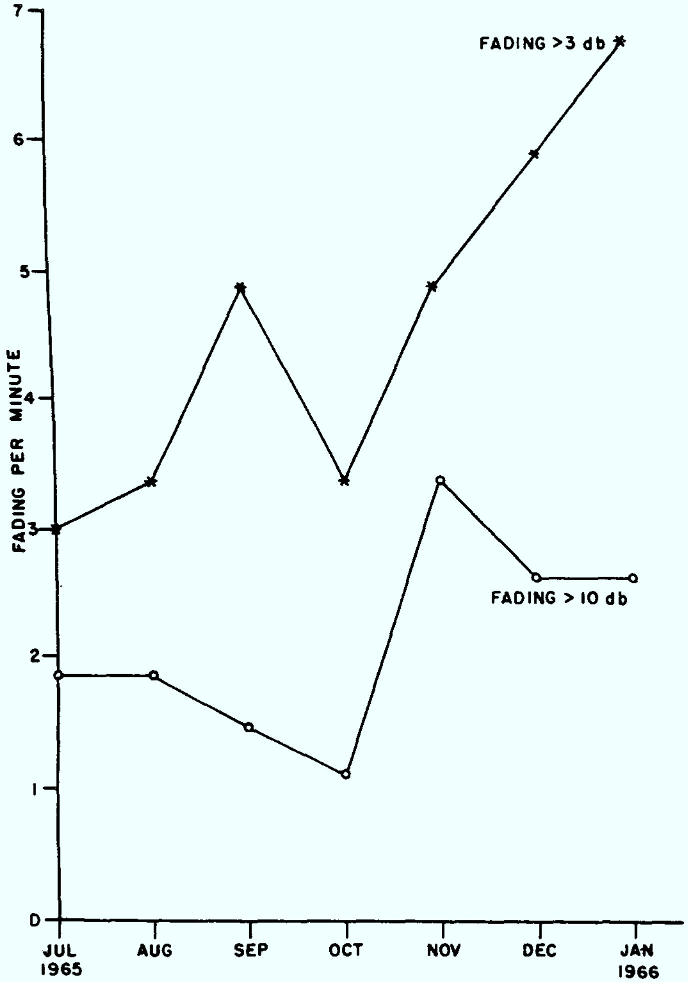

Fig. 8. Seasonal variations of the fading rate at local noon.

Discussion on Paper 6.4 presented by B. Reinisch

Shirke: I agree with some of the classifications you have made of the different types of reflections that were features of the observations at that time, but your conclusions seem to differ from those one would normally draw. Assuming that the D region was enhanced, as we have some evidence now from rocket measurements, I do not see how you can conclude from your results that the effect is purely E region.

Reinisch: We have two points which speak against that. One point is that Dr. Volland has found that the height of the reflection level did not show any correlation with days of abnormal winter absorption; this is indicative that the E region does not show correlation with days of winter anomaly.

Shirke: I'm suggesting that the densities in the D region get enhanced during the winter anomaly. Would you not see excess absorption if the E region also enhances?

Reinisch: It should be seen in the riometer observations which are also made. We obtained some data from AFCRL which show that in this last winter at least (I didn't look at the other years), the riometer observations did not show any increase in absorption in those months. At the high riometer frequencies, the deviative contributions of the E region should be negligible, so the riometer observation should just be influenced by the D region and not the E region.

Belrose: It is a question of sensitivity. Unless you do a riometer experiment very carefully, you will not see any absorption whatsoever. I am sorry that Dr. Gallet is not here as I know he was going to describe some high-quality riometer absorption data which he has. I am sure he could have thrown a lot of light on this.

Shirke: The other aspect concerns these diurnal variations that you show. The winter anomaly, as far as we know, shows a considerable diurnal variation. Do you agree that it does not show a maximum around noon, but goes on increasing to 1400 hours? I would guess the absorption gradually increases before noon and then falls off.

Reinisch: You shouldn't take the actual slope too seriously because some cases of sporadic E which I didn't show separately are included.

Shirke: Yes. So the emphasis is, I would suggest, in the D region instead of the E region.

Bibl: I think I should make some general statements. Mr. Reinisch underestimated the knowledge of people of our work conducted in Freiburg of the frequency dependence of absorption. It is tremendously important for everyone to know that the total absorption in the range between 2 and 5 Mc/s. is controlled by 2 parts of absorption, one in the D layer, and one in the E layer, and the relative contribution to the total depends strongly on frequency if you have real E-layer reflections. You have seen in many of those figures in our paper, that, if you throw all the data together and get something out, you get the same effect as if you don't make any separation. In November, we have many *Es* cases which showed that for the frequency we purposely chose the effective absorption is predominately governed by E-layer absorption; by means of deviative absorption, which gives that flattening of the daily diurnal variation because we are coming closer and closer to the critical frequency. If you have carefully observed our diagram, you will see that we have shown F-layer reflections which is an indication that we are really above the E critical frequency. At noon we are operating somewhat away from the critical frequency, but in the morning and evening we are operating close to the critical frequency. We had only one frequency that we could choose. We used it for a certain study mainly, but we chose that frequency to get into the E region and to get different heights of the E region. It is certainly clear that if we had several frequencies we would be better off. We didn't have enough money for several frequencies, and if we get more we will solve the problem independently of the riometer data. In the next two or three months, we will have riometer data from Air Force Cambridge Laboratories, and we will try to get this question rechecked and see if the riometer data show any correlation with days of higher or lower absorption. That should be significant although it is medium-quality riometer data, because we have seen that there is on the average 8 *db* of absorption, which means that on some days there may be up to 20 *db* which should be detectable on 30 Mc/s. riometer data. On the other hand, people cannot neglect in riometer data the significance of the E layer. Because you are nearer ground one must be lower by a factor of either infinity or 2 depending on the absorption in the E layer. Even if you were wrong by a factor of 2 in your estimate of the E layer for riometer data, you should reconsider it. I think we made a valid contribution and that in the range between 2 and 4 Mc/s. as an average, half of the absorption takes place in the D layer and half in the E layer.

Jones: Does it not seem that average absorption in December was anomalously high or was it what one should expect on the basis of the smoothed seasonal variations?

Reinisch: It was high, but I must say I don't want to give the comparison between months.

Jones: The two curves for December with and without the Es or rough days are similar, whereas November and January were widely different. Shouldn't the December curves be widely different when December had anomalously high absorption?

Reinisch: In December, that was just not the case. In December, there was not this high increase in absorption. It was a bit higher than normal and it should have been separated a bit more. We should have separated out the sporadic *E* cases completely. However, the fact is that if you have a limited set of data, and if you divide it into ten classes, you cannot make any more statistics.

96414—18½

6.5 IONOSPHERIC RADIO WAVE ABSORPTION STUDIES AT MID-LATITUDES

by

W.J.G. Beynon and E.S. Owen Jones*

Department of Physics, University College of Wales
Aberystwyth, England

Presented by E.S. Owen Jones

* Now at Bedford College, London

1. Introduction

The ionospheric absorption of radio waves is often classified into two types: the so-called 'deviative absorption', which arises during the process of refraction, and 'non-deviative absorption', which occurs in those parts of the trajectory where there is little refraction of the wave. The basic physical process involved is, of course, essentially the same at all levels and throughout the trajectory, and in this sense the division into two types is somewhat arbitrary. However, in practice one or other type often dominates, and the division is then quite valid and useful. The present work is mainly concerned with a study of the deviative component and has involved measurements of the absorption of waves reflected from the E, Es, and lower F regions. Although the total absorption of a radio wave which is reflected in the ionosphere has been extensively studied, comparatively little work has hitherto been published on the separation of the two components. Both deviative and non-deviative absorption are primarily dependent on the height distribution of the collision frequency and the electron density, and a full study of the variation of absorption with frequency requires that some knowledge of the associated electron density distribution be available. In the past, most workers have assumed some model for the height distribution of the electrons and, since much more information exists on the nature of the E region than on the D region, it is the deviative absorption occurring in the E region which is generally calculated. The non-deviative component is then assumed to be the absorption remaining after subtraction of the calculated deviative absorption from the measured total absorption. In most cases the theory used to calculate the deviative component has also neglected the effect of the earth's magnetic field.

In the present work we have not used any model N(h) profiles, but calculated the appropriate E layer profile from ionograms taken at the time of the absorption measurements. We have then computed the deviative absorption in this E layer, using numerical integration of the absorption coefficient, and compared this with that observed. The effect of the magnetic field has been included throughout the analysis. Some model for the collisional frequency profile is, of course, still required in this analysis.

2. The Absorption Measurements

An extensive series of ionospheric absorption measurements was carried out at Aberystwyth between 1100 and 1300 LMT on a large number of days in the period March 1961 to September 1962 and the analysis that follows is based on a large sample of these data.

A critical study of the relative magnitudes of the non-deviative and deviative components of the ionospheric absorption calls for careful selection of the frequencies on which measurements are to be made. In this work it was desirable to make observations first on the lowest frequency at which a reflected signal of good amplitude could be regularly observed over the noon period. With the transmitter available, this lower frequency was near 1.9 Mc/s. It was also desirable to make as accurate absorption measurements as possible on frequencies at which the deviative type absorption would be large. Consequently, measurements were made each day on two frequencies just below and on two frequencies just above foE. An essential requirement for accurate absolute measurement of ionospheric absorption is a reliable nighttime calibration of the equipment at the precise frequencies used to measure the absorption, and in this work careful calibrations were carried out on many nights. The ionograms used to calculate the N(h) profiles were such that equivalent heights could be read to an accuracy of about 1 or 2 km. and the critical frequency to ±0.05 Mc/s.

3. Theory

An expression for the deviative absorption coefficient that includes the effect of the earth's magnetic field may be written in the form

$$k = \frac{\nu}{2c} \cdot A, \tag{1}$$

where

$$A = \frac{X(1 + 2Q_2 \cot^2\theta)}{(1 + Q_1 Y_L)^2} \left\{ 1 - \frac{X}{1 + Q_1 Y_L} \right\}^{-1/2} .$$

Here we use the normal magnetic-ionic nomenclature with $X = \frac{4\pi Ne^2}{mf^2}$, $Y = p_H/p$ and θ as the angle between the magnetic field and the direction of propagation. Q_1 and Q_2 are functions of X, Y_L and Y_T viz. $Q_1 = [(1 + m^2)^{1/2} - m]$ and $Q_2 = m^2[(1 + m^2)^{1/2} - m]/(1 + m^2)^{1/2}$ where $m = \frac{Y_T{}^2}{2Y_L} \cdot \frac{1}{1-X}$. The only major assumption required in the derivation of these expressions is that $1 - X >> Z(= \frac{\nu}{p})$ and for frequencies of the order of 3 Mc/s. this inequality will be valid to within a short distance of the reflection level.

4. The Collision Frequency Profile

One of the main points that emerges from this work concerns the variation of the collision frequency ν with height. Many workers have made direct experimental estimates of ν these being usually based on measurements of the ionospheric absorption of radio waves. However, there has always been a measure of uncertainty and inaccuracy in the various published data, and often considerable divergence between values deduced from direct radio wave sounding experiments and values predicted from laboratory measurements. From time to time various theoretical ν(h) profiles have also been published, but again there has always been uncertainty because such profiles have lacked reliable data on the essential atmospheric parameters.

The theoretical analysis of absorption just outlined is based on the usual formulation of the Appleton-Hartree magnetoionic theory, in which the electron collision frequency is assumed to be independent of the electron energy. The collision frequencies estimated on the basis of this theory are thus to be regarded as 'effective' values, which may differ significantly from the true collision frequencies. In recent years, various authors have attempted to generalize the Appleton-Hartree analysis so as to allow for the effects of the electron velocity distribution. A comprehensive analysis has recently been given by Shkarofsky (1961), which is applicable for any variation of the collision frequency with electron velocity and for any degree of ionization of the medium. Shkarofsky has shown that provided $p \gg \nu$, then the averaged collision frequency between electrons and neutral gas molecules is given by

$$\bar{\nu}_m = 1.99 \times 10^{-11}\, n_m\, T, \qquad (2)$$

where n_m is the number density of the gas molecules and T the absolute temperature.

To derive the $\nu(h)$ profile from equation (2), we have inserted mean values of n_m and T given in the report of the COSPAR Working Group on the International Reference Atmosphere. The profile is shown in Fig. 1, marked S.

A theoretical $\nu(h)$ profile was published by Nicolet in 1959. This is also shown in Fig. 1, marked N. This profile is based on the assumption of mono-energetic electrons and, as might be anticipated, lies everywhere above the Shkarofsky profile in which allowance is made for the distribution of electron energies.

Some radio wave experimental values of ν for the height range 100 to 130 km. published by Schlapp (1959), Whitehead (1959), and Ataev (1959) are also included in this figure.

The profile shown in Fig. 1 is based on the assumption that the electrons are in thermal equilibrium with the neutral gas. This is probably valid in the D and lower E region, but at higher levels in the ionosphere it seems likely that the electron temperature during the daytime may be significantly in excess of the ambient gas temperature; and some recent rocket results suggest that the difference may possibly be quite appreciable even at a height of 110 km. If the electron temperature at 110 km. is as much as twice the gas temperature, then the electron collision frequencies at this level will also be increased by a factor of about two. This would also bring the Shkarofsky profile into agreement with the experimental values deduced from radio wave studies. In the lower ionosphere, up to about 80 km., the $\nu(h)$ profile seems reasonably well established, but above this level the consequences of factors such as the dissociation of molecular oxygen and the possible effects of higher electron temperature have yet to be resolved. For the work described here the present uncertainties about ν are of no great consequence, and it can readily be shown that the conclusions do not depend critically on which profile (S or N) is adopted. The present work suggests something that may be much more important, viz., that there may well be day-to-day variations in ν comparable with, or even in excess of, the differences between these two profiles.

5. Analysis of Experimental Results

It will be convenient to denote the total ionospheric absorption by A_T and the non-deviative (D region) absorption by A_D. As we are principally concerned with frequencies below and up to the normal E region critical frequency, the deviative absorption thus occurs in the E region and will be denoted by A_E. The procedure adopted is to calculate A_E, using the accurate ionograms taken at the time of the absorption measurements. We then deduce the N(h) profile and with an assumed $\nu(h)$ profile, we calculate A_E. The effect of the magnetic field is included throughout these calculations.

A_D is then given by the difference between A_T and A_E and can be expressed as

$$A_D = \frac{K}{(f + f_L)^2}, \qquad (3)$$

where

$$K = \frac{e^2}{2\pi mc} \int N\nu \, dh.$$

For a given set of measurements, K should be constant and independent of frequency but will vary with time. In practice, in attempting calculations of this sort, we have almost invariably found that the calculated value of the parameter K varies greatly from one frequency to another. These variations in K were far in excess of anything that would be expected from inaccuracies in the measurements or in the analysis and it was only found possible to keep K reasonably constant with frequency by adjusting the assumed $\nu(h)$ profile and by varying the profile with time.

TABLE 1. Analysis of noon absorption measurements (absorption given in nepers, frequency in Mc/s.)

Date 20.2.61	fE = 2.93 Mc/s.				
	Frequency Mc/s.				
	1.92	2.64	2.88	3.0	3.24
A_T	3.33	3.40	3.82	3.54	2.76
A_E	0.26	1.32	2.03	1.80	1.31
A_D	3.07	2.08	1.79	1.74	1.45
K	29.0	45.0	51.1	47.5	41.1
K'	29.8	30.7	29.8	30.7	28.6

Date 23.2.62	fE = 3.04 Mc/s.				
	Frequency Mc/s.				
	1.92	2.81	2.98	3.22	3.43
A_T	3.35	2.90	3.67	2.91	2.09
A_E	0.28	1.16	2.03	1.47	0.69
A_D	3.07	1.74	1.64	1.44	1.40
K	30.4	37.2	43.7	23.1	21.7
K'	29.8	28.0	28.6	28.2	30.0

Date 30.6.61	fE = 3.40 Mc/s.				
	Frequency Mc/s.				
	1.97	3.09	3.32	3.52	3.65
A_T	4.55	4.60	5.06	4.58	3.15
A_E	0.14	2.10	2.74	2.49	1.36
A_D	4.41	2.50	2.32	2.09	1.79
K	44.3	49.7	45.2	66.0	49.4
K'	44.4	46.0	47.4	46.6	42.0

Date 11.7.61	fE = 3.3 Mc/s.				
	Frequency Mc/s.				
	1.97	3.00	3.22	3.42	3.62
A_T	4.46	4.78	5.45	3.62	3.06
A_E	0.16	2.23	3.36	1.64	1.13
A_D	4.30	2.55	2.09	1.98	1.93
K	44.0	63.5	62.5	53.5	58.2
K'	43.2	44.9	40.8	42.5	44.7

In Table 1, K^1 denotes the value of K after adjustment of the $\nu(h)$ profile, and it will be seen that whereas K varies by about ±30 to 40 per cent around a mean value, the values of K^1 are constant to within about ±4 per cent. The latter fluctuations are no larger than might be expected from the accuracy of the measurements and the analysis.

Data for 48 days on which the absorption measurements were considered to be reliable have been analyzed; in each case it was found that reasonably constant values of the parameter K could be obtained only by appropriate day-to-day adjustment of the collision frequency profile. A sample of $\nu(h)$ profiles derived from the daily absorption measurements is shown in Fig. 2.

The day-to-day values of the derived collision frequency showed a clear dependence on the day-to-day flux of solar activity, as shown in Fig. 3. Two points given by Schlapp some years ago are included.

Fig. 4 shows a set of 14 monthly values of the collision frequency at 59.5 km. published recently by Belrose and Hewitt (1964) on the basis of measurements made with a partial reflection technique.

These completely independent sets of experimental data, referring to levels of 60 and 110 km., suggest a closely similar dependence of ν on solar activity.

6. The Significance of the Solar Dependence of ν

If the observed variation of collision frequency arises from some direct solar influence, then the most probable parameter that might give rise to the observed variations in collision frequency is the electron temperature. Up to the present, only a limited number of E-region measurements of electron temperatures have been made, but such data as have been published suggest a considerable day-to-day variation in the electron energies.

Rocket measurements of the electron temperature at E-region altitudes are relatively few, because for most techniques the electron mean free path at this level is comparable with the probe dimensions, and reliable interpretation of the data is difficult. However, some recent rocket measurements suggest that at E-region altitudes the electron temperature Te may be greater than the gas kinetic temperature, Tg, by a factor of two or more. Spencer in 1962 described a group of four rocket flights designed to measure electron temperature. On one flight, under quiet ionospheric conditions, a value of $T_e = 400^o$ K at 110 km. was obtained, this corresponding (equation 2) to $\nu = 1.65.10^4$/sec., a value which is in reasonable agreement with our results. On the remaining three flights, under more disturbed solar or ionospheric conditions, much greater values of T_e at 110 km. were recorded. A number of other rocket measurements also suggest high electron temperatures.

Hence, despite the existing inaccuracies in the determinations of T_e for the E-region, it would appear that the observed values of collision frequency might well be explained by a significant elevation of the electron temperature with respect to the gas kinetic temperature.

7. Absorption Measurements on Sporadic E Reflections

We have applied the analysis outlined in section 5 to measurements made during the presence of sporadic E ionization. In these cases, accurate absorption data were available for a number of frequencies up to the normal E critical frequency fE, and also for a few higher frequencies which, at the time of the measurements, were being reflected from blanketing type sporadic E ionization.

Blanketing type E_s ionization is usually formed at or near the peak of the normal E layer, and the gradient of electron density on the lower side of blanketing E_s ionization is always exceptionally large, so much so that little or no detectable change in the reflection level can be measured over the whole range of frequencies concerned. As a consequence, it can be safely assumed that the deviative absorption in the E_s layer itself is negligibly small, and that such variation of absorption with frequency as is observed for these E_s reflections arises almost entirely from deviative absorption in the thicker normal E layer underneath. In applying our analysis to these data, it was found that satisfactory agreement between calculated and observed absorption for all the E and E_s frequencies required that the height of the E_s layer be known within narrow height limits. This can be illustrated by reference to the analysis for one set of experimental data. At noon on 30 June, 1961 at Aberystwyth, fE = 3.36 Mc/s. and in addition the ionogram showed blanketing E_s reflections to 4.6 Mc/s. The calculated N(h) profile for the normal E layer from 99 km. to the height of the layer peak at 107 km. was as shown in Fig. 5. Measurements of the equivalent height of the E_s ionization indicated that it was located at or near 107 km., the peak of the normal E layer.

Clearly, the absorption to be expected on frequencies greater than fE will depend on the height of the reflecting E_s layer and Fig. 6 shows the variation in absorption with height of the E_s layer for two frequencies that just penetrate the underlying E layer. It is clear from Fig. 6 that accurate measurements of the absorption on frequencies reflected from the E_s layer should enable the height of that layer to be fixed with some precision. Thus in the present example, on the frequency 3.45 Mc/s. a change of only 1 km. in the height of the E_s layer results in a change of about 1 neper in the absorption. We have found that a satisfactory fit to the measured absorption on all of a number of frequencies reflected from a blanketing-type E_s layer enables the precise height of the layer relative to the peak of the normal E layer to be fixed to within a fraction of a kilometer. For the example just discussed, the height of the E_s layer has been calculated to be about 0.25 km. above the peak of the normal E layer.

REFERENCES

Ataev, O.M. Rad. Eng. and Elect. (U.S.S.R.) 4, 37, 1959.

Belrose, J.S. and L.W. Hewitt. Nature 202, 1964.

Nicolet, M. Physics of Fluids 2, 46, 1959.

Schlapp, D.M. J.A.T.P. 16, 340, 1959.

Shkarofsky, I.P. P.I.R.E. 49, 1857, 1961.

Spencer, N.W. et al. J.G.R. 67, 157, 1962.

Whitehead, J.D. J.A.T.P. 16, 99, 1959.

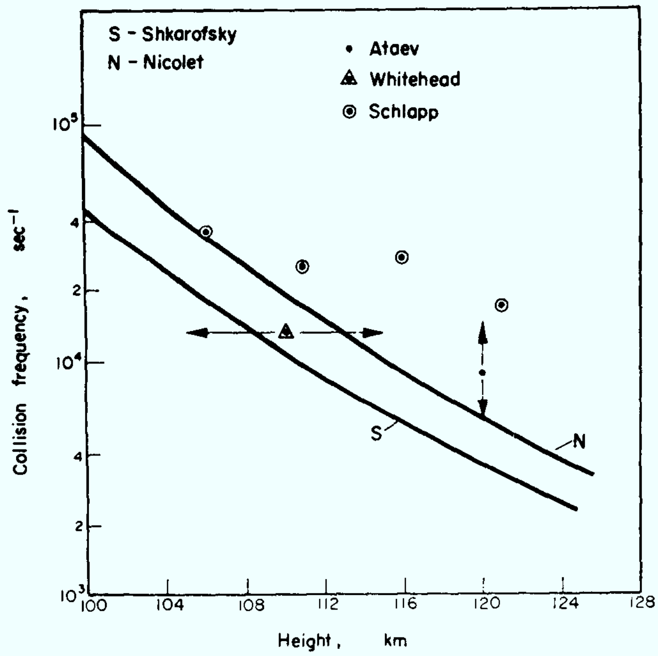

Fig. 1. Theoretical and experimental values of collision frequency.

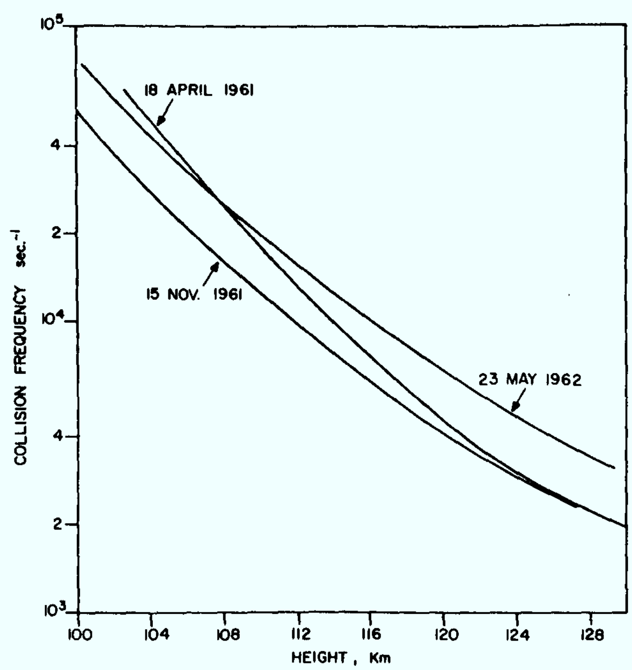

Fig. 2. Typical collision frequency profiles derived from present work.

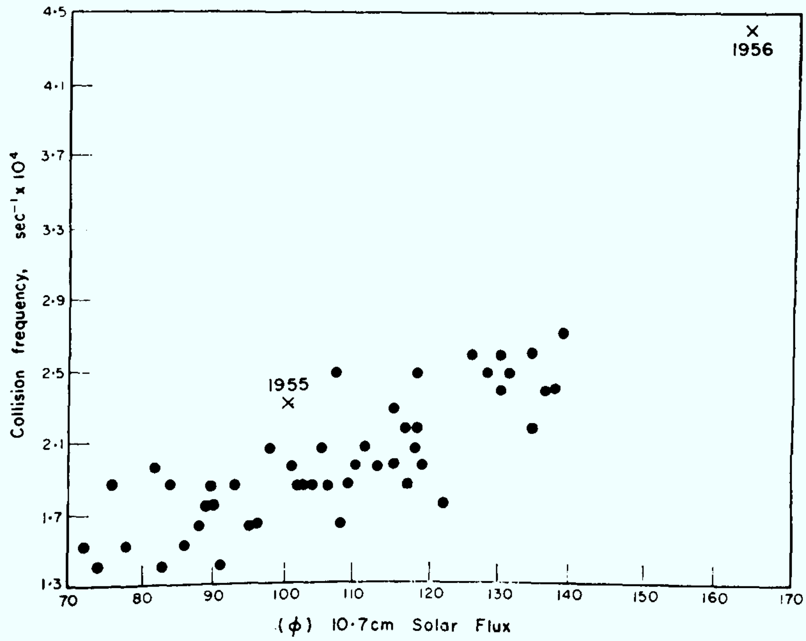

Fig. 3. Variation of collision frequency at 110 km. with 10.7 cm. solar flux (ϕ) . X-values obtained by Schlapp.

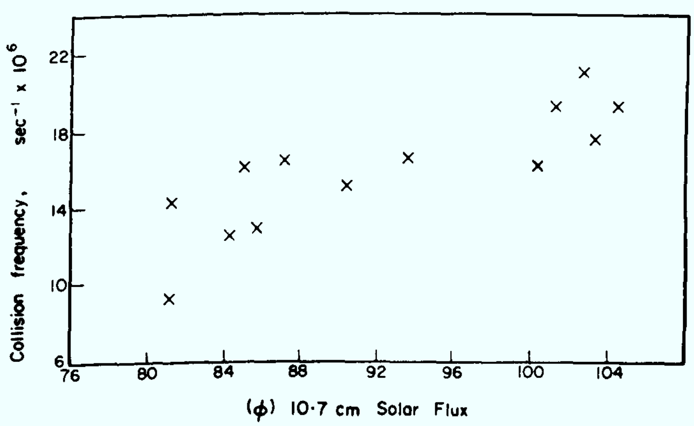

Fig. 4. Variation of collision frequency at 59.5 km. with 10.7 cm. solar flux (ϕ) (deduced from Belrose and Hewitt).

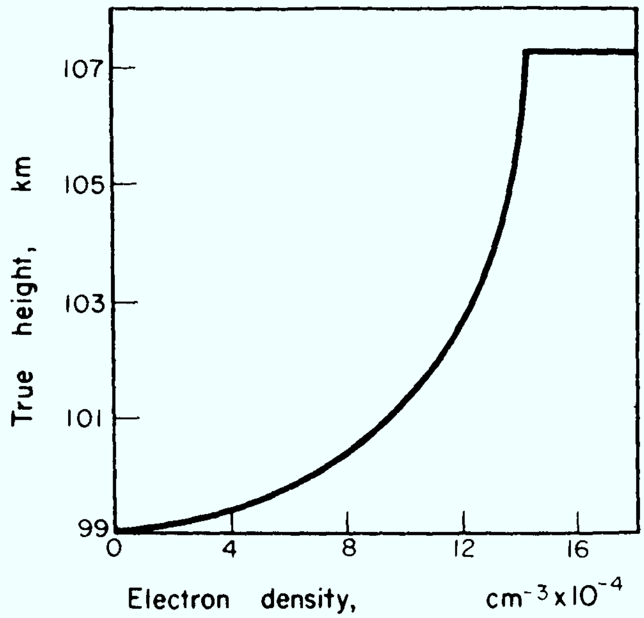

Fig. 5. Electron density profile for 30 June, 1961.

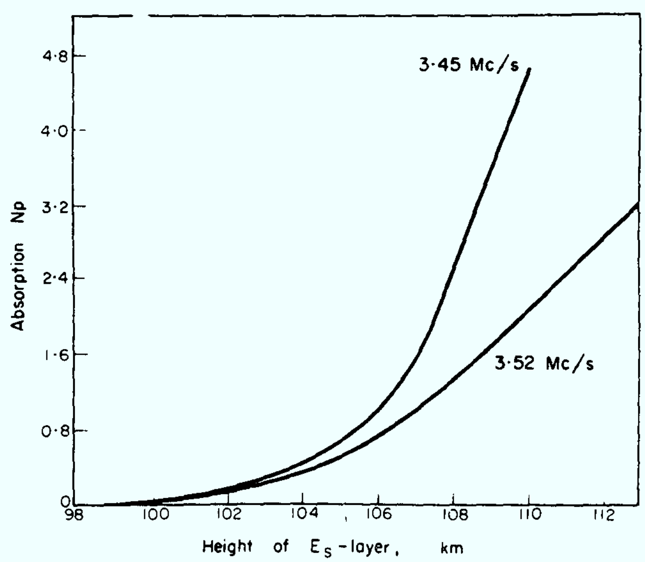

Fig. 6. Variation of deviative absorption with height of E_s layer for N(h) profile of Fig. 5.

Discussion on Paper 6.5 presented by E.S. Owen Jones

Thrane: On what assumption did you base your derivation of the collision frequency? Do you, in fact, assume that $\int N\nu dh$ is constant with frequency?

Jones: Yes.

Thrane: You assume then that the greatest contribution to this integral occurs in the D region?

Jones: A low frequency wave will be reflected near the base of the E region, where dn/dh is a maximum and there is a minimum amount of deviative absorption. There will be a small amount, granted, but you can calculate that and make allowance for it; this is an iterative process, so you can minimize its effect.

Thrane: There must be a considerable contribution to that integral in the E region itself.

Jones: It is taken into account by the deviative component found by integration within the E region.

Shirke: Are you saying that the collision frequency is a function of temperature, and that the winter anomaly is explained by changes of collision frequency?

Jones: When this work was done, we thought that the pressure or density in the D region was constant, and that it exhibited no seasonal variation. It would now seem that there are seasonal variations in pressure, and these would affect the collision frequency, but we do not know what the seasonal variation is. I know of two flights in November and two in February. They show a 30 per cent difference in pressure. Consequently, if the temperature had remained the same, the collision frequency would have changed by 30 per cent. Until we know what the seasonal variation is, we cannot make any correction for pressure changes.

Shirke: Are you suggesting that the winter anomaly is purely due to a change in collision frequency?

Jones: I'm not suggesting that at all. I'm merely pointing out certain similarities between meteorological phenomena at 30 km. and ionospheric phenomena at 70, 80, or 90 km. There are features in temperature which are not reflected in absorption.

6.6 SOME ASPECTS OF METEOROLOGICAL AND IONOSPHERIC VARIATIONS*

by

E.S. Owen Jones† and W.J.G. Beynon

Department of Physics,
University College of Wales,
Aberystwyth, England

† Now at Bedford College, England

Information about the lower part of the ionosphere (up to 80 km. or so) from radio studies comes mainlv from measurements on the attenuation of short wave signals that are transmitted through the lower ionosphere or from studies of the intensity of reflection of long wave signals. As part of a wider study of radio wave absorption in the lower ionosphere (region D and the lower part of region E), we have recently had occasion to examine the seasonal variation in absorption at noon at a number of stations distributed over a wide range of latitude.

Theoretically, we should expect the ionospheric absorption to be some function of the cosine of the solar zenith angle (χ) and a logarithmic plot of the absorption against cos χ should yield a straight line. We generally find that over a day the absorption values do on the average follow some power of cos χ. However, the same logarithmic plots with monthly mean noon values over a season appear to show some significant departures from the simple straight line relation. If ionospheric absorption varied symmetrically over the season, with maxima in local midsummer and minima in local midwinter, then on the logarithmic plot of absorption and cos χ all the 12 monthly points should fall on one straight line. If there is any time lag of absorption on zenith angle, then the two halves of the year will differ and the straight line becomes a 'loop'.

Fig. 1 shows monthly mean noon values of ionospheric absorption for two stations in the northern hemisphere and one in the southern hemisphere. The data for Slough (51 1/2° N) are for a frequency of 2 Mc/s., those for Freiburg (48° N) are for 1.7 Mc/s., and those for Port Stanley (51 1/2° S) are for 2.6 Mc/s. The levels of reflection for such frequencies will be between about 95 and 100 km. The values shown in this figure are based on measurements made over 7 to 10 years and have been reduced to a common sunspot number R = 100. It will be seen that in no case do the values lie on a straight line, but they all lie on a distorted 'figure of eight' pattern. Furthermore, the month-to-month variation in absorption follows the same sequence at all three stations. In the spring and earlv summer months the absorption is consistently lower than in the corresponding months later in the year, and the curves show similar 'loops' again over the local winter months. In all cases the winter values are too high and are particularlv so during the late winter months (December to Februarv in the northern hemisphere, May to August in the southern hemisphere). This latter feature is of course the well-known local winter anomalv in ionospheric absorption.

Fig. 2 shows a further sample of 2 Mc/s. data taken at Swansea (51 1/2° N) during the I.G.Y. (average sunspot number R = 200) and current measurements at Abervstwvth (52° N) during the IQSY (average R = 10). The same pattern of seasonal variation and the same progression from month to month is clearlv discernible.

---

* As this was not designated as a separate paper at the time of the conference, discussion relating to it appears under Paper 6.5.

In Fig. 3 we show absorption data for a frequency of 245 kc/s. and phase height data for 16 kc/s. The 245 kc/s. data were obtained at Kuhlungsborn (lat. 54° N) over a propagation path of 180 km. The 16 kc/s. data refer to measurements over 200 km. at latitude 52° N. The latter refer to a height of about 70 to 75 km. The precise height of the absorption on the 245 kc/s. data is not known, but is probably in the height range 75 to 85 km. For comparison purposes we have also included in Fig. 3 another sample of 2 Mc/s. absorption data (in this case for De Bilt 52° N). All three curves in Fig. 3 show an anomaly in winter. With 2 Mc/s., the effect is pronounced, in that the peak winter value actually exceeds that for the summer. For 245 kc/s. the anomaly is seen in the high values for the months of December, January, and February. The 16 kc/s. phase reflection height data suggest that in the winter months November to February, the mean phase height is from 1 to 3 km. below that to be expected from an extrapolation of the values for the other 8 months of the year.

Seasonal variations in radio wave absorption in the D and lower E regions of the form shown in Figs. 1 to 3 could arise from similar variations in N or ν or in both parameters. The collisional frequency ν may be expected to depend on gas density (p) and on temperature (T). Some data on the seasonal variation in these two parameters at high levels in the atmosphere are now available from balloon and rocket flights. Spencer, Boggess and Taeusch (1964) have published density values for various heights based on rocket flights at Churchill (59° N). These data cover only 23 rocket flights spread over a 2-year period, and perhaps too much reliance cannot be placed on mean curves based on these measurements. However, the data, as published, give the seasonal variations in density at 70 km. shown in Fig. 4(a). The marked similarity between this curve and those in Figs. 1 to 3 is clear. The seasonal variation in temperature at 70 km. for 65° N has been given by Groves (1963) and is shown in Fig. 4(b). In this case there would appear to be little or no variation in T from month to month, but there is some small asymmetry over the year with spring values slightly larger than those for the autumn season. The seasonal variation in collisional frequency at 70 km. will be mainly determined by the variation in the product (pT). This is shown in Fig. 4(c). The similarity between the month-to-month variation in (pT) at 70 km. and that in ionospheric absorption strongly suggests that the latter is produced partly at least by a corresponding variation in collisional frequency at these levels. The fact that the phase height of 16 kc/s. signals exhibits a similar type of variation, and shows abnormally low heights during the late winter months, indicates that these variations in electron density also contribute to the observed seasonal variation in absorption.

We have also studied data on atmospheric temperature now available from high-level balloon soundings, and find that the same type of seasonal variation occurs in atmospheric temperature at levels of the order of 30 km. Fig. 4(d) shows monthly mean values of the temperature at the 20 mb. level (approximately 26 km.) based on measurements over nine years by Scherhag and Clauss (1960) at Berlin (lat. 53° N). An examination of data for many other stations in temperate latitudes shows that this type of seasonal variation in temperature occurs at levels well above the tropopause. From other work (Shapley and Beynon), it is clear that the winter anomaly in absorption observed at temperate latitude stations is correlated with the sudden stratospheric warmings that are a feature of the late winter months. However, the above-mentioned work indicates that the seasonal variation throughout the year at the 30 km. level (probably at greater heights too) appears to be reflected in the seasonal variation of gas density and ionospheric absorption at D and lower E layer heights.

Further evidence of similarities in the behavior of temperature and absorption can be drawn from a comparison of the seasonal variation of temperature at 15 mb. at different latitudes. In Fig. 5 the mean seasonal variation over three years is shown for two stations, New York (40° N) and Shreveport (32 1/2° N), from which it will be noticed that the large winter loop characteristic of the winter anomaly in absorption disappears with decreasing latitude.

As a measure of the variability of this temperature in winter, we have plotted the difference between the mean January and December temperatures against latitude for a number of stations, as shown in Fig. 6. The most striking feature of this graph is the relatively sharp disappearance of the temperature variability at about 32° N. Despite the fact that the latitude variation of winter anomaly is far from being well-established, we would draw attention to an observation reported in this conference which we feel is pertinent to the above feature.

From D-region N(h) profiles (partial reflection method) obtained at Ottawa (45° N), Belrose finds the winter daytime profiles to be highly variable from day to day, whereas Smith finds at Armidale (30° S) that the day-to-day changes are remarkably small, these profiles being obtained by wave-interaction techniques.

Although Smith's results are based on a fairly small sample of data, the proximity of the latter latitude to that at which the above temperature difference disappears is, we feel, far more than coincidental, due allowance being made for some asymmetry in meteorological features in the northern and southern hemispheres. It will be of interest, therefore, to see to what extent seasonal changes in temperature and ionospheric absorption may be related at these and other latitudes.

REFERENCES

Belrose, J.S., Bourne, I.A. and L.W. Hewitt. Paper 2.3.2. These Proceedings, 1966.

Groves, G.V. Report to COSPAR, Warsaw. 1963.

Scherhag, R. and J. Claus. Met. Abb. 11, Pt. II. 1960.

Shapley, A.H. and W.J.G. Beynon. Nature 206, 1242. 1965.

Spencer, N.W., Boggess, R.L. and D.R. Taeusch. J.G.R., 69, 1367. 1964.

Smith, R.A., Bourne, I.A., Lock, R.G. and T.N.R. Coyne. Paper 3.2.4. These Proceedings, 1966.

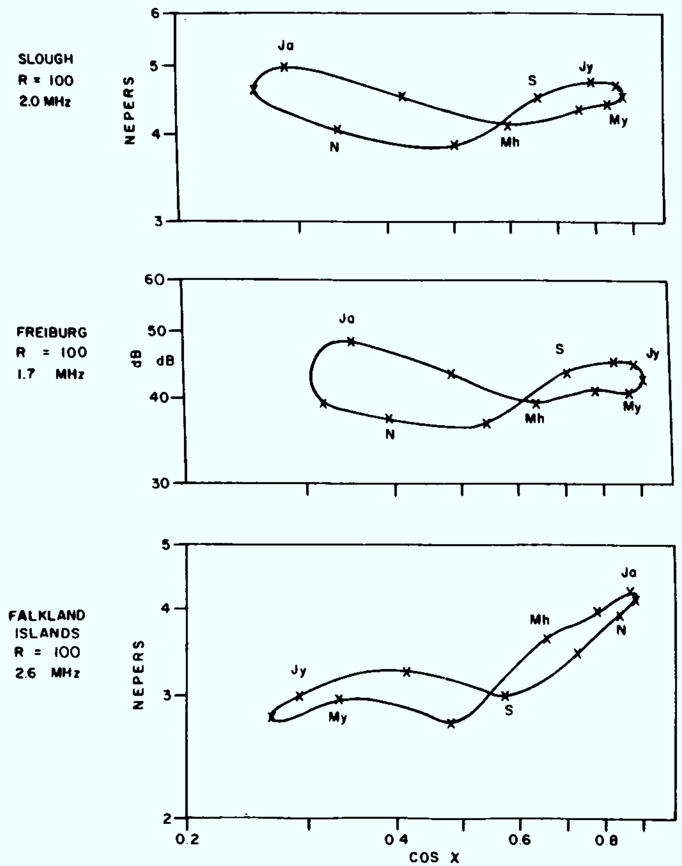

Fig. 1. Seasonal variation of monthly mean noon absorption.

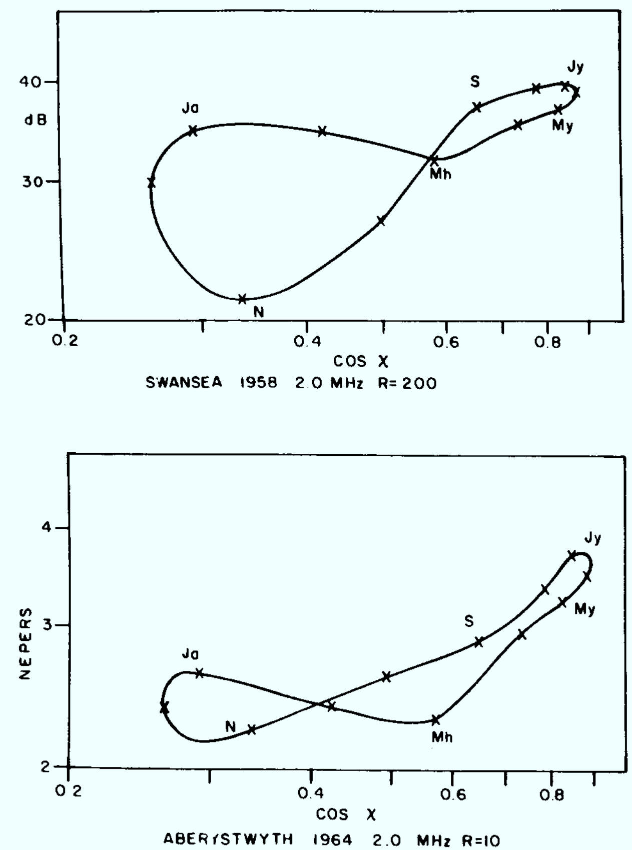

Fig. 2. Seasonal variation of monthly mean noon absorption.

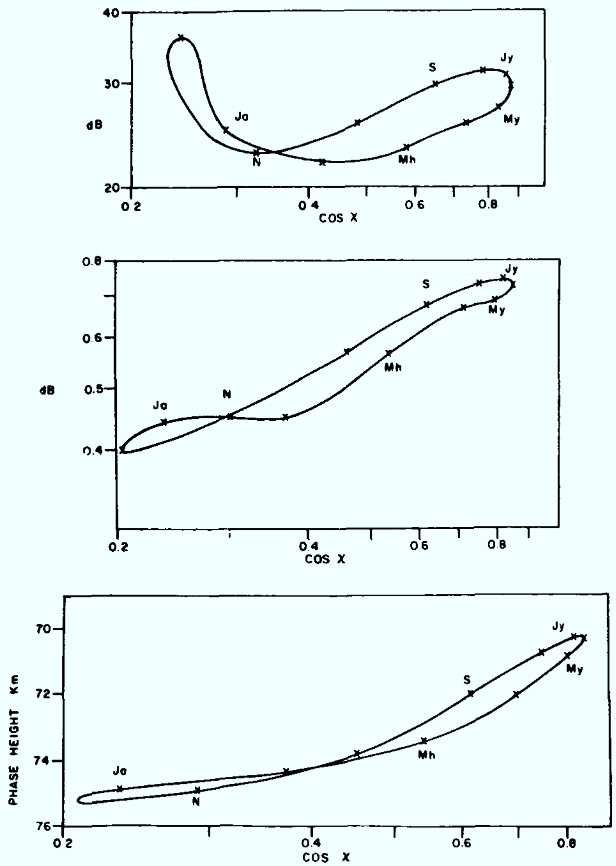

Fig. 3. (Top) Monthly mean noon absorption at De Bilt, 2.0 MHz., 1962.
(Middle) Monthly mean noon absorption at Kuhlungsborn, 245 kHz., 1959.
(Bottom) Monthly mean phase height of reflection on 16 kHz.

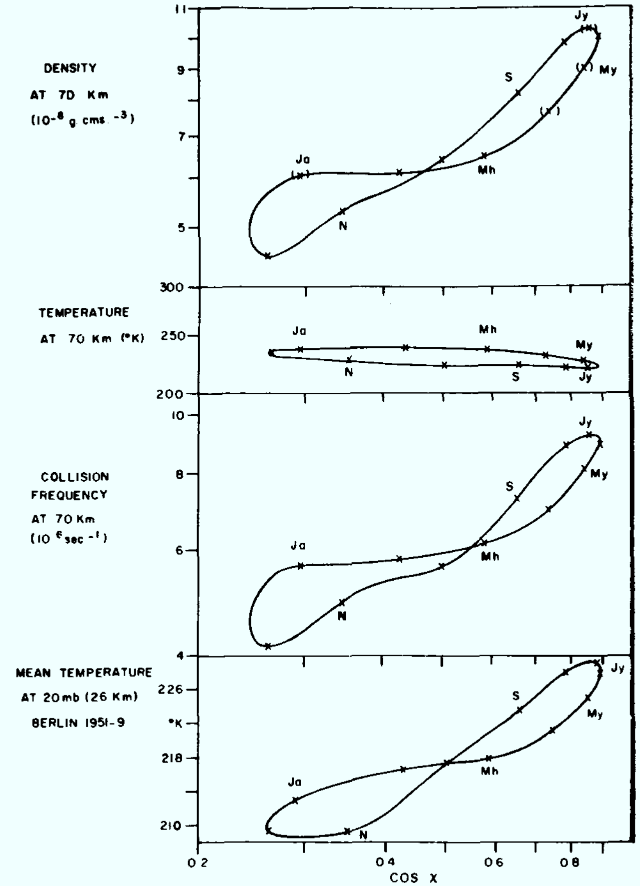

Fig. 4. Monthly mean seasonal variation of (a) density at 70 km., (b) temperature at 70 km., (c) collision frequency at 70 km., (d) mean temperature at 20 mb.

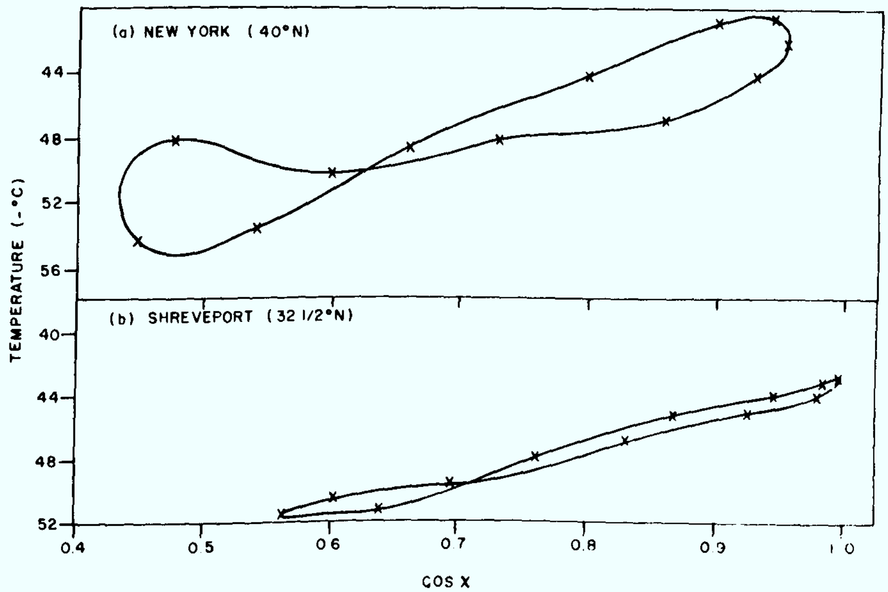

Fig. 5. Three-year mean seasonal variation of temperature at 15 mb.

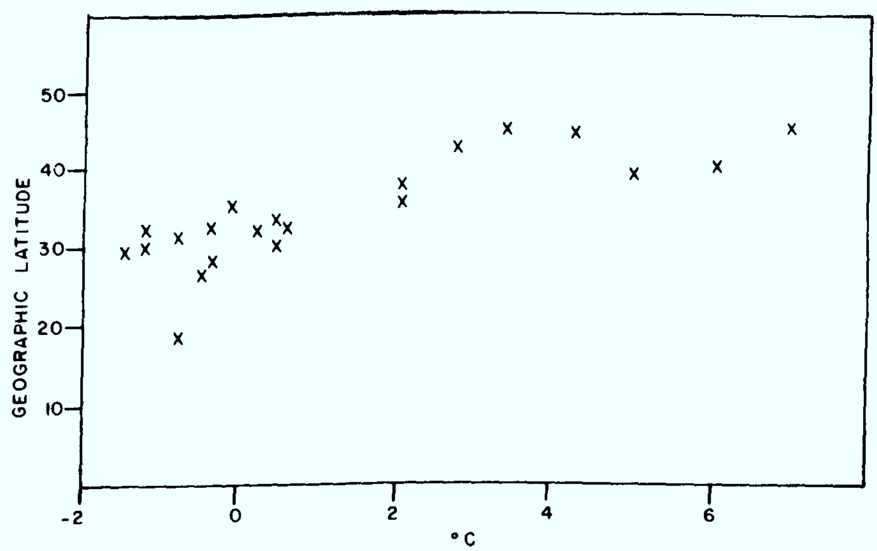

Fig. 6. Difference between January and December temperatures at 15 mb. as a function of latitude.

SECTION 7

DISCUSSION

In the discussion session, key speakers from various disciplines presented summaries of the important points raised at this conference, so that all conference participants would have food for thought before the discussions reached the floor level. (The conference hosts provided the other staple for thought).

Key speakers named by the Conference Chairman in various experimental fields were Dr. I.A. Bourne (partial reflection), Prof. R.A. Smith (radiowave interaction), and Mr. B.R. May (VLF). Dr. E.V. Thrane and Dr. W. Swider spoke on behalf of workers in the ionospheric absorption and theoretical fields respectively.

Although some of the authors of the opening theoretical papers presented at the conference were not able to be present for the Friday discussions, they have submitted summary briefs, which are included in this portion of the Proceedings.

Briefs submitted in absentia and discussions presented at the conference by various key speakers do not appear in the original order; the topics in the discussion session have been rearranged to follow the same order of presentation as the Sessions of the Conference.

Theoretical Models of the Lower Ionosphere

Crain: The various papers showed clearly that understanding of the lower E region and D region of the ionosphere is in a primitive state. Although lumped parameter models of the deionization relations for these regions have been highly developed, and for a wide range of conditions appear to give reasonable agreement with many observations, there is strong evidence that such models do not properly account for all the physical processes involved. Not only do we not know the more important charged and neutral species involved in all cases of interest, but also we do not know how such factors as atmospheric circulation with its diurnal, seasonal, geographical, etc., dependence affect the situation. Papers by Gregory dealing with the effects of the overhead passage of a pressure ridge, and by Belrose et al. showing unexpected D-region profiles at Resolute Bay, are excellent examples of this problem.

While the papers did not, in my view, bring about any immediate improvement in D-region ionization theory, they did bring out many of the factors that bear on such theory and for which we must have better understanding if we are to make much-needed improvements in the theory. The current and potential role of ground-based radio measurements was well presented by the various authors. It is clear that the various types of ground-based measurements have many capabilities that are not provided by other means, and which can be expected to play an important role in our slowly improving understanding of the D and E regions.

Aikin: This conference has been unique in that data on the D region from several sources have been assembled for the first time. While most of the information concerns the variation of the electron density distribution as measured by ground-based techniques, rocket measurements of electron and positive ion density as well as composition have been introduced. It is still too early to assess the impact these measurements will have on the theory, but there must be considerable changes if the ion composition of the D region as measured by Narcisi is to be explained. The excellent data of Smith on the sunrise effect will also require modification of theory, if the profiles are to be explained quantitatively. The wide variability of data has necessitated in many instances averaging several electron density profiles to obtain a profile typical of a quiet or disturbed day. To interpret electron density profiles in terms of ionization and loss processes and meteorological factors, it is necessary to examine closely the criteria used in averaging profiles.

A first step in any averaging process is to choose locations where and times when the ionization sources producing each profile are the same. For this, a knowledge of the solar xray flux at 2-8A is essential as well as the flux and energy spectrum of energetic particles at such locations where particle precipitation is a frequent occurrence. With the advent of satellite measurements, it is feasible to obtain this information directly without having to rely on such imprecise indicators as the sunspot number, 2800 Mc/s. solar emission, and the A_p and K_p indices of magnetic activity. I would suggest that wherever possible the experimenter try to obtain such satellite measurements and incorporate them into any data-averaging process. Only then will it be possible to distinguish other phenomena, such as the effect of sudden stratospheric warmings.

Swider: We may well be close to a good general understanding of the normal daytime D region, as exemplified by the paper by Aikin, Kane and Troim (1964).

A major uncertainty is the nitric oxide distribution. However, the above-mentioned paper plus the work of Nicolet (1965) appear quite reasonable. This latter study is important in its reinterpretation of Barth's (1964) experimental NO profile which has large NO densities in the D region. However, Donahue (1966) argues that these large densities are fully acceptable. The ion composition results of Narcisi and Bailey (1965) below 80 km. apparently oppose any NO model of the D region. This aspect was discussed in my paper, so I shall not dwell on it here. It should be mentioned that the subject of the conventional (with NO) daytime D region was properly developed by Nicolet and Aikin (1960) and that their electron density profiles can be "brought-up-to-date" (with little change incidentally) by using the new nitric oxide distribution of Nicolet (1965) and a dissociative recombination rate of about 3×10^{-7} cc./sec. regardless of ion.

Negative ion formation remains a major problem. The ions O^- and O_2^- are undoubtedly initially formed, but as for the positive ion composition, this does not imply that important ambient quantities of either ion exist. The concentration of O^- ions is highly limited by even slow detachment processes, as mentioned in my paper. The O_2^- ion probably undergoes certain ion-atom or charge exchange processes. Thus, almost certainly, we should expect NO_2^- ions because of the high electron affinity of NO_2. Whether this ion is important in the upper D region or whether O_2^-, perhaps O_3^-, is dominant, remains a matter of conjecture. I would guess that in the daytime O_2^- is the major negative ion from 75 to 80 km. down to say 50 to 60 km., below which height NO_2^- is predominant. Both of these levels probably rise somewhat at night and the ambient NO_2^- concentration becomes more favored, since $NO \rightarrow NO_2$ at night below about 65 km. (Nicolet, (1965)). Thus, direct conversion, $O_2^- + NO_2 \rightarrow NO_2^- + O_2$ becomes more likely. The NO_2^- ion is also formed via $O_2^- + NO \rightarrow NO_2^- + O$ (Nicolet, 1965). A major related problem is the changeover from day to night, and vice versa, of the neutral constituents O, NO, NO_2, O_3, etc. Twilight studies of PCA events (Reid, 1962) are inexplicable at present and the negative ion problem is deeply involved, as well as in the normal twilight case. At night and twilight an ion other than O_2^- may be important. Detachment is the principal loss of this ion by day, but at night more opportunity for reactions of O_2^- with neutrals exist, on a relative basis.

Experimental difficulties hamper our attempts to solve these problems. Dissimilarities exist between electron density profiles deduced by various workers, as seen from these Proceedings. Analysis of ground-based measurements can suffer from incomplete information and thus result in deduced electron density profiles which are compatible with the measurements performed, but incompatible with the results of other experimenters. Rocket-based measurements in the D region also have produced errant ambient profiles in some cases due to shock-induced ionization and other effects. My paper stressed a minimum D-region profile as probably accurate because various techniques arrived at a similar result. It is imperative to the theorist to be cognizant of important inaccuracies in the profile, and it behooves the experimenter to specify the errors involved or areas in which certain assumptions may have serious shortcomings.

In summary, the following points may be emphasized:

(1) Accurate electron density profiles of the day, night and twilight D region are needed. A good knowledge of the lower edges of these profiles would be helpful in making deductions regarding negative ions.

(2) Further studies of the nitric oxide distribution in the D region would be invaluable.

(3) Laboratory experiments regarding reaction rates of O^-, O_2^-, O_3^- and NO_2^- ions* and perhaps others in ion-atom and charge exchange processes with the major and some minor atmospheric gases would be welcome.

Many other problems such as anomalous winter absorption, collision frequency relations, meteorological effects, etc., are also of interest and importance. Naturally, I have concentrated here on those aspects more closely related to my work.

References: All papers are in J. Geophys. Res. for the year indicated.

Partial Reflections

Bourne: I cannot hope to summarize everything that has been said concerning the partial reflection experiment; however, these are my general conclusions at this stage:

(1) The scatter in the partial reflection data at low heights is particularly worrying. We could explain this scatter if we introduced perturbations in the collision frequency. We have no good reason for doing so. If a $\Delta\nu$ process is important to the scattering, the data so far obtained cannot be interpreted. At high heights it is certain that a ΔN type process is applicable.

(2) The variability in the type of echoes received, which must describe the reflection conditions, is also a problem. From the reports we have heard throughout the conference this variability appears to be a function of latitude or location, although any particular location does not have an unique echo structure.

(3) The general consensus has been that high-gain antennas should help to reduce some of the scatter. However, Dr. von Biel suggests that this might result in marked changes in the polarization of the wave within the beamwidth.**

(4) The desirability of using narrow pulse widths is recognized by everyone, but with the present amount of man-made noise in the medium frequency bands this doesn't look hopeful unless you are at a quiet location.

(5) The problem of whether the ΔN or $\Delta\nu$ reflection process is responsible for the partial reflections has received little attention at this meeting. More work must be done to remove this doubt from the results so that their reliability can be assessed.

(6) Little mention has been made of the use of the partial reflection experiment to study winds. This is a future use that should be considered for new installations. Perhaps Dr. Manson or Dr. Gregory will tell us more.

(7) Concerning the chirp radar techniques mentioned, advancement of this type of technique for recording D-region echoes should be encouraged.

We appear to have made good progress during this conference. To me, the important feature has been the frank and open discussion between the various groups concerning reliability of the data. While some discussion was held during the formal conference, a great deal was conducted outside it. It is probably good that the more heated debates will not be printed in the formal Proceedings.

I think it fair to say that the partial reflection experiment has undergone critical examination and been found wanting in some respects; this notwithstanding, it is a valuable tool for synoptic studies of the D region, and, under favorable circumstances, the deduced profiles have an accuracy comparable with (or exceeding) the profiles deduced by other ground-based techniques.

---

* Editorial Comment: laboratory experiments are being made (c.f. Fehsenfeld, *et al.*, 1966, as discussed briefly in Section 8 of the Proceedings.

** Recent computations by Dr. von Biel indicate that for a symmetrical 5 by 5 element array the undesired mode would be more than 30 *db* below the desired mode for all portions of the antenna pattern within a 72° beamwidth.

Pulse Radio Wave Interaction

Smith: Dr. Belrose has put me in a spot where I would have refused to go a few days ago; that is, to assess the reliability of my profiles. (Prof. Smith spent a few minutes discussing the accuracy and reliability of various features of the profiles shown in his paper. These remarks are included as part of paper 3.2.4.)

Electron Density-Height Profiles Deduced from the Reflection of Long Waves

May: VLF work has appeared on the scene only recently and some people have doubted its actual value. It may be of some interest at the outset if I show how Deeks arrived at his profile. This is all in terms of partial reflections at two heights (which Piggott showed might be significant when X is approximately equal to Y and X is equal to Z. What I have done here (see Fig. 1) is to draw a typical value of the Y is equal to Z line. I have also drawn lines for X equal to Y at 70 kc., X equal to Y at 16 kc., X equal to Z at 70 kc., X equal to Z at 16 kc. Now we observe that at 70 kc. the phase and amplitude of the waves are markedly irregular; the simplest way to view this irregularity is to think of it in terms of interfering partial reflections. If we look at the spread of heights that various workers think the waves are reflected from, and also the X equal to Z line, and X equal to Y line for 70 kc., we can then draw a box in which we think the electron densities are going to be. We then transfer our attentions to the 16 kc. observations, which are quite unanimous in that the reflection height under the condition that Deeks considered was about 73 or 74 km. It is interesting to note that, if we draw a box here at a height of about 73 or 74 km., it contains both the levels X equals Y, and X equals Z for 16 kc. We should expect to get strong reflections from this height; but this may be a property of the ionosphere over England only. So I draw here a box to encompass what one would consider reasonable electron densities. Now we go on downwards; we can't have a line too far to the left because we wouldn't get enough absorption on any frequency. We can't have a profile which comes too far to the right because we wouldn't get 16 kc. waves to go up to 73 or 74 km. heights. So we have to keep well to the left-hand side of the line $X = Y$ at 16 kc.

The polarization of steep-incidence 16 kc. waves is usually observed to be fairly circular. This indicates that there are certain limiting slopes of electron density that can exist. The gradient cannot be too great or the down-coming wave would be linearly polarized. So what I have put here is a line that I can move up and down. I have another one that is also going to determine the absorption of the waves. You can now see that a profile that I have deduced from this simple approach has a certain correspondence to the Deeks profile. We can therefore see that there is a fairly simple justification for them, although we cannot easily justify the existence of the C layer and the gradient above from just the simple approach like this. I wanted to show this to give some idea of what we were trying to do.

Our experimental measurements (at RSRS) are going to be made with 16 and 70 kc/s. waves. We are going to run into trouble with the interpretation of the phase at these frequencies, because the phase measured is rather arbitrary, and really you only measure phase changes between various epochs. We have to do some experiments that will tie down the profile at some particular reference epoch, similar to the way Deeks did. To do this, we propose to do some simple Hollingworth pattern experiments, which look as though they are going to give some interesting results. In the Hollingworth pattern experiment you measure the vertical electric field as you go away from the transmitter. You get interference between the sky wave and the ground wave. It appears that on 16 kc., the Hollingworth pattern is dependent, as you would expect, on this region within the small box. This ledge is important for determining the spacing between the maximum and minima of the Hollingworth pattern. You should be able to measure this spacing, as you go away from your transmitter, to within 5 or 10 km. or better. The depth of the amplitude pattern is controlled by the size of the C layer bulge. I have estimated that you should, from a Hollingworth pattern experiment and full wave deductions, be able to find the height of that slope, that little ledge there, to within about 2 km., and you should be able to find the electron densities in the C layer bulge, certainly to an order of magnitude or better. I have calculations based on some of the slides I showed yesterday. If we make a simple approach, and assume that the reflection all takes place at $X = Y$, (this is probably true at 70 kc., not so true at 16 kc.) and also take into account the accuracies of the phases that one can measure, then I come to the conclusion that one can estimate the electron density at the heights of reflection of 16 and 70 kc. waves to within ± 30 per cent. I have also come to the conclusion that an accuracy of about ± 50 per cent is obtainable from the measurement of the conversion coefficients. I think about 40 or 50 per cent is a reasonably conservative figure for the accuracy of N in the height range 90 to 65 km., using 16 and 70 kc. measurements of signal strength and phase of the abnormal components as we intend to do. We also have to measure regularly the Hollingworth patterns to give a good check on the lower part of the profile.

There is an encouraging similarity between the Smith profiles and the Deeks profiles, particularly in the way the D layer develops at about dawn and through the day.

As for the future of the VLF experiments and what I would like to see them do: with the experimental setup we shall have we should be able to find out something useful about the D region during the sunset and sunrise periods and the daytime. This is rather dependent on whether you can still get the sky wave during the day, for 70 kc. as well as 16 kc. The Hollingworth pattern is a useful experiment to do at 16 kc.; we have looked into the Hollingworth pattern at 70 kc. and decided that it is technically difficult, although it has been done.

I would like to see more theoretical work done on determining what are the best frequencies to use. I have chosen 16 and 70 kc. because 16 kc. is a powerful transmitter in England, and 70 kc. is sufficiently different from 16 kc. to enable us to look at different parts of the ionosphere. These may well not be the best combinations of frequencies*. We also want to know whether there are any critical distances in which observations should be made, and whether certain parameters are especially useful. The generalization of the full wave theory certainly warrants looking into; it is a bit worrying, and there is not unanimity on how it should be generalized, or whether it has been generalized correctly by Deeks.

Another value of these VLF measurements is that they give a synoptic view of the D region. This is valuable, although with the frequencies we envisage using, we won't be able to get much more detail into our profiles than the detail we've seen in the profiles here.

Ionospheric Absorption

Thrane: In several papers this morning (Beynon and Jones, Bibl and Reinisch) the importance of distinguishing between deviative and non-deviative absorption of HF radio waves reflected from the E region has been emphasized.

Fig. 2 illustrates this point. It shows the frequency variation of the total absorption of waves reflected vertically from the noon model ionosphere discussed by Piggott and Thrane (these Proceedings). It also shows the contributions to the total absorption from different height levels in this ionosphere. The computations have been made using a phase integral method due to Budden (1961).

The numbers on the curves refer to height intervals in kilometers. Fig. 2a shows the non-deviative absorption. At the lowest heights the non-deviative absorption is nearly independent of frequency, while at the higher levels the absorption is proportional to $1/f^2$.

In Fig. 2b the curve labelled "Top 5 km." shows the absorption integrated along the top 5 km. of the ray path, while the curve marked "reflection point loss" shows the contribution to the absorption which is neglected when the simple ray theory approximation is used. The two curves together represent the deviative losses.

It is worth pointing out that the deviative absorption is an important contribution to the total loss, not only near the critical frequency, but for all frequencies below foE. Furthermore, it should be noted that

---

* Editorial Comment: The work of Bracewell, Harwood and Straker (Proc. IEE, **101**, (Pt. IV), 154-162, 1954) indicates that frequencies near 30 to 35 kc. are much more attenuated in summer than frequencies outside this band, and therefore any planned new experiments should include measurements at such frequencies.

the deviative absorption and its frequency variation is sensitive to the shape of the electron density profile. This is because the absorption near the point of reflection is proportional to $\nu_{AH}/(dN/dh)$ (Ratcliffe 1959).

On the whole, as has been pointed out by many workers in the past, the measured frequency variation of absorption contains a lot of information on the structure of the lower ionosphere. With the use of modern computers, it is not too difficult to use this information for studies of the D region.

References: Budden, K.G. *Radio waves in the ionosphere.* Cambridge University Press, 1961.

Ratcliffe, J.A. *Magnetoionic theory.* Cambridge University Press, 1959.

Editorial Comment: Also see the paper by Piggott, W.R. and E.V. Thrane. *The electron densities in the E- and D-regions above Kjeller.* J. Atmos. Terr. Phys., **28**, 467, 1966, which describes the work discussed here.

General Discussion

Gregory: I wish to comment on the height resolution of partial reflection experiments. I feel satisfied, from discussion and otherwise, that the height resolution to be expected from a partial reflection experiment is not more than about 5 km. At shorter intervals than that we are apt to be making ambiguous measurements, as we are dealing with a vertically stratified medium and are not able to sample it completely normal to the stratifications. I feel that the DRTE experiment should be giving only half a dozen points in the height range where its results can be reasonably well interpreted.

Also, there appears to be a definite lack of lower ionosphere data for latitudes closer than ± 25° to the equator.

Bourne: If the experimental data shows little scatter, it is not necessary to take a three-point running average of the measured $\frac{Ax}{Ao}$ values, and it is then theoretically possible to resolve infinitely thin layers separated by only 2 km. In fact, the system used to average the data will not permit the resolution of two infinitely thin layers unless they are at least 6 km. apart*. Consequently, the scatter in the points plotted at 2 km. intervals should not be interpreted as being the fine structure of the profile.

I would like to comment on the combined use of the partial reflection experiment and the wave interaction experiment; these are to some extent complementary, and operated together would make a valuable contribution to our knowledge of the D region. More attention should also be given to the experiment mentioned by Dr. Smith, in which the modulation on waves partially reflected from the D region is measured, as this looks to be a promising method for deducing D-region parameters.

---

* Editorial Comment: To demonstrate the height resolution of the partial reflection experiment, Dr. Bourne assumed that the ionosphere consisted of a number of slabs of 2 km. thickness, with marked valleys between them. The profiles shown in Fig. 3 have been calculated with allowances for the smoothing of the experimental Ax/Ao values and the uncertainty of the height measurements associated with the DRTE experiment.

It is evident that if the slab separation is less than 6 km., (c), the presence of the valleys is obscured. A slab separation of 8 km. shows the presence of the valleys but does not indicate their true depth.

The height resolution is relatively poor, but compares with the resolution of the wave interaction experiment of Prof. Smith, who showed that his experimental data could be closely synthesized with an ionosphere consisting of slabs spaced at 5 km. intervals.

Smith: I forgot to mention the other day that the plots of electron density as a function of time given by Barrington, Thrane *et al.* and shown by Dr. Thrane in his talk, give general information which is a valid deduction from the observations. There is a marked diurnal change with χ near the bottom which is consistent with what I have shown.

Shirke: I would like to see some provision made in the scaling of ionosonde records to indicate that there was a layer observed in the 70 to 90 km. region.

Wright: Some *F* plots do record the presence of a so-called E_{sb} layer, which is scatter from the 70 to 80 km. region. Its highest frequency of reflection and its occurrence have both been shown to vary with f_{min}. Also, while it is virtually impossible to use f_{min} as a quantitative indicator of absorption or D-region structure, it is often valuable as a qualitative indicator of what is happening.

Radio wave experimenters might well be advised to make more use of the frequency dimension that they have available. Many people are doing this, but if there is the slightest hope that a dependence on frequency would give a different view of the things under study, then it should be investigated.

Manson: I would like to encourage the use of the partial reflection experiment for the detection of winds. Dr. Frazer* in New Zealand has measured winds from 60 to 100 km.and they compare well with meteor winds that have been observed in Australia.

Belrose: My colleague, Dr. Burke, who was with us at the beginning of our experimental program here, was enthusiastic about this type of experiment. He kept pointing out that the people who measure winds with the spaced receiver technique are doing it at a single frequency and in order to get winds at different heights they have to change frequency and this then means they are looking at a different size of irregularity. The partial reflection experiment has the potential of measuring winds over a range of heights at a single frequency, however, I have always been concerned about whether one can actually deduce winds from this experiment because of the rapid fading of the echoes.

Gregory: It has not yet been possible to make a direct comparison between the partial reflection wind observations and those observed by other techniques; however, an indirect comparison with what is known of the major circulation changes (and these are rather crude from a meteorological point of view) suggests that the partial reflection wind measurements are acceptable.

Smith: Wave interaction will give a lot of other information besides the *N(h)* profile. It will give information on gas temperatures, pressures, etc., in different parts of the world. If groups going into the wave interaction field take the trouble to construct a disturbing aerial of known gain, and if we come up with some device that can go from one group to another to make calibration tests on the various equipments, then we would have some synoptic observations which could be compared for one part of the world with another.

Bibl: How fast are the amplitude and phase changes for the partial reflection experiment?

Belrose: I cannot say how fast the phase changes, but amplitude does not change in the 1/15-second that occurs between our *O* and *X* pulses. It can change in the 1-second interval between our pictures, and we have evidence that the rate of fading is a function of latitude. At Resolute Bay for example, there is a small amplitude change in the 1/15-second between our *O* and *X* pulses.

Bourne: Sometimes the phase of a certain echo is stable, not changing by more than 180° in 20 min., while at other times the phase of what we call a turbulent echo can change by 180° in 1 or 2 sec.

Bibl: I asked this question because of the possibility of being able to obtain partial reflection results by using more sophisticated data processing and consequently smaller and cheaper station installations.

Belrose: You must keep in mind that large antennas are not only required to enable one to observe partial reflections, but they are also needed to reduce off-vertical echoes.

Wright: High frequency pulse reflection experiments and partial reflection experiments are not really in competition with each other, because they actually have their best application in different height ranges that only slightly overlap, so there is much to be said for using both experiments.

We are installing a multifrequency high frequency drift experiment at Yuma, Arizona, where there is a 16-inch gun, which can be used to make neutral trail wind measurements; we will also be making spaced receiver measurements and sweep frequency soundings. There is room there for anyone who wants to set up and measure winds with the partial reflection experiment. This area happens to be right in the path of Dr. Gossard's experiment, so VLF wind results will also be available.

---

* Editorial Comment: See G.H. Fraser, An investigation of mesospheric circulation in the South Pacific, Rept. of the Physics Dept., U. of Canterbury, Christchurch, N.Z., February 1966.

96414—19½

Belrose: There remains a real problem in trying to tie the D layer to the base of the E layer. The partial reflection experiment, the cross modulation experiment, and the low frequency long wave propagation experiments that have been done to date, all run into difficulty in the 80 to 85 km. region. The partial reflection experiment is bothered by off-vertical echoes at these higher heights.

Pfister: I would appreciate a statement about the height resolution of the VLF results.

May: The height of the underside of the C layer ledge can be obtained to about 2 km. from the Hollingworth pattern experiment. This is at 16 kc., but I don't see how we can do it at high frequencies. At 70 kc. you can determine the phase height to a couple of kilometers but this does not mean that you can determine the profile height to this accuracy.

Volland: At 16 kc. the wavelength is 20 km. and you can find an infinite number of profiles that all give the correct reflection coefficient.

Pfister: Then your height resolution is 20 km.

Belrose: Not necessarily. You can measure phase to any degree of accuracy you want. The number of wavelengths is the uncertainty, but you are measuring some fraction within these multiples of uncertainty.

Hildebrand: If you do the type of calculation that Johler talks about, and ray trace and find what is happening as the wave goes through the ionosphere, and truly establish a relation between electron density and reflection points, then I am convinced that you can measure heights to within 2 km. It is necessary to use several VLF frequencies and all the information that is available, such as polarization conversion. We are working on a technique where we make reflection measurements through the VLF band at frequency intervals of 2 kc. We can then get an unique reflection height with adequate signal-to-noise ratios, because the slope of phase versus frequency will be unique for any given ionosphere profile. It may not be a straight line, but in many cases it is. With a sharp electron density gradient so that reflections come from essentially the same height with frequency, then you get a linear line and its slope will get steeper as reflection height increases. If the reflection height increases with frequency, this line will have an upward curve to it. With enough data points to determine the characteristics of this line, then I would think that the estimates of 2 km. are good.

Belrose: Is this at steep incidence?

Hildebrand: The transmitter and receiver are separated by 4 km.

Pfister: If you have a monotonically increasing function can you resolve valleys in the profile?

Hildebrand: From an example I had during a sunrise transition period, I would have to say yes. I was comparing the phase changes at 10 kc. and 13.45 kc. and after ground sunrise, in the receiving channel in which we were receiving a signal which was parallel to the plane of propagation, there was a marked decrease in signal strength at 10 kc. on one day and not at 13 kc. The following day it was at 13 kc. and not at 10 kc., so I think we're going to get a lot of information on the characteristics of the so-called C layer, but we're going to have to be careful how we interpret it.

Belrose: Dr. Gregory introduced this problem by saying that the partial reflection experiment had a height resolution of about 5 km., and to conclude this discussion on height uncertainties I wish to make the following comments: Some of the discussion has been about height accuracy, some about height resolution. We don't seem to be distinguishing between the two.

Dr. Bourne has commented on the "height resolution" of the partial reflection experiment. Let me comment on its "height accuracy". We measure the height of our echo peaks to within ± 1 km., and as proof that we're talking about accuracies of this order at low heights I will mention our 1 March, 1962 results during a class 2+ solar flare. We were operating at two frequencies, 6.275 Mc/s. and 2.66 Mc/s., and we obtained data at both frequencies from which we could reduce profiles which overlapped in height. When we first reduced our data there was no comparison between the two profiles. After much work we finally went back to the equipment and found that we had not accurately measured the group delays through our receivers. When we corrected this we got overlapping profiles (over a height range of 5 km.) from the results at the two frequencies. I do not claim that we can see minimums which are a couple of kilometers thick, because these would be smoothed out in the partial reflection experiment. What I am saying is that our profile has a height uncertainty of ± 2 km.

Manson: I would like to show some partial reflection profiles which we obtained at Canterbury, New Zealand, 43° S. With the limited amount of data which we have processed, the interesting point was that the summer profile tended to show lower values than the winter profile at the heights where one would expect the mesopause to form. There are probably 15 or 16 profiles used to compute each average shown here. Our summer and winter profiles are compared with the appropriate DRTE profiles in these two slides (Figs. 4 and 5). The agreement is quite good.

Adams: With regard to the polar cap observations, the data do show changes starting at $\chi = 90°$ going down and at 100° coming up. The problem is that you have to calculate the photodetachment, and then you wind up with no changes before 90° or 95°.

Belrose: The point I tried to make in the discussion following your paper this morning is that we need more work done on these polar cap events before we derive too many theories. We have found that the low frequency propagation data shows a marked diurnal asymmetry at high latitudes. We need more information about the diurnal asymmetry seen in the observational data (latitudinal and seasonal variations) before we spend too much time arguing about a specific event.

Bibl: I am pleased that we saw evidence of work which is trying to separate out the contributions of absorption that occurs in the D and E layers. Absorption measurements do not define the profile in the C and D regions, although there are certainly connections between the absorption measurements and the lower ionosphere profile during a big event like a PCA.

I feel that data processing will become an important subject, and my belief is that we must do all possible pre-processing of the data before recording it, and use automatic means to process it after recording.

Smith: Something that has occupied me for the last few months is the pre-twilight period in the D region ($\chi \sim 100°$). G.G. Bowman published (Australian J. Physics, 17) some results of work he had been doing on high-multiple reflections (10 hops or more) from the F_2 layer. When he plotted the occurrence of high-multiple reflections as a function of sunrise time, he found that a marked increase in the number of high-multiple reflections occurred about an hour or so before ground sunrise (before $\chi = 100°$). This could be explained either by focusing or by a reduction in non-deviative absorption. He came to the conclusion that the explanation was not focusing, and might be reduced absorption.

In our work we have been going back to $\chi = 110°$ or 115° to measure the electron density at the base of the nighttime E region. We have obtained about 10 observations which suggest that the whole bottom of the nighttime E region moves up by about 1 km. This effect occurs in the nighttime lower E region, and I believe that something tied to the sun causes the E region to move or change in the twilight period. The story of the D region is still a long way from being told.

Belrose: I shall now terminate this discussion, and describe what I think the main results of the conference were.

First – sunrise changes and diurnal changes. During the conference we saw some of the best sunrise profiles yet seen; these were profiles in the sunrise transition between $\chi = 98°$ and 90°. Although Dr. Smith pointed out that it is difficult to make observations at these times, I think these data determined by the cross modulation experiment are the best yet obtained.

Measurements of diurnal changes have not been obtained by any of the partial reflection workers for middle or low latitudes for solar zenith angles greater than 70° or 75°. This is not so at high latitudes. At Resolute Bay and at Churchill we can make observations during the day or night. As yet we have examined ionization changes only over sunrise at Resolute Bay. The reason for doing it at Resolute Bay was because the zenith angle of the sun is changing slowly, and observations can be averaged over something like 15 min. and provide data that is appropriate to a 1° change in χ.

We spent two or three months analyzing partial reflection data for 5 quiet days over sunrise, and, while we have good evidence of changes over dawn, unfortunately Resolute Bay is not like low latitude stations. We have twilight changes but the changes are not like those for lower latitudes (particularly at low heights, the C layer). Theoreticians might like to concentrate on low latitudes before considering the interpretation of high latitude results.

At Resolute Bay there are few electrons below something like 70 km. and electron densities at these heights are strongly seasonally dependent (compare March and July profiles at similar solar zenith angles). The midday March electron density profiles at $\chi = 80°$ show many electrons at low heights at Churchill, but not at Resolute. There is something wrong at Resolute Bay: we can't see the development of the C layer in March, because there is no marked C layer. Since we have measurable electron densities at C-layer heights in summer, we might be able to observe a twilight change then (but there is no twilight $\chi > 83°$).

The second point concerns the seasonal variation in more detail. From what Prof. Smith says, it appears that at a latitude of 31° south the electron density profiles seem to be an unique function of the solar zenith angle. We do not find this in our results, which are for latitudes of 45° and greater. We infer from Fig. 6 that there is good agreement between data at Ottawa and at Churchill at the same solar zenith angle in the same season. However, average Ottawa data for March and September, which have similar χ values, are significantly different (Fig. 7) and Resolute Bay data (Fig. 8) indicates that March noon and July midnight profiles are considerably different, even though the solar zenith angles are approximately the same. Consequently, at middle and high latitudes, the electron density profile is not a function of the solar zenith angle alone. We argued that we didn't know how to average data in winter because of the large variability, and concluded that the best way was to average the results themselves. We grouped the data into groups with similar amplitude ratios between the two magnetoionic components at 75 km. The results of this grouping of data (Fig. 9) show that below the 75 km. level the electron density in winter can be greater than the average summer profile representative of magnetically quiet days; a "winter anomaly", which is probably related to the winter anomaly in MF absorption.

Now I shall make certain indirect inferences based on low frequency propagation, the position of which must be made clear. Before you make inferences about when things start and stop at sunrise and sunset, and about the so-called "variability of the onset of sunrise", you must have a general picture of low frequency propagation as a whole. Apparently this picture is not held by some of the people doing experiments in the field. In Prof. Smith's profiles (Fig. 10) there is a marked transition in going from $\chi = 97°$, where the base of the ionosphere is at 80 km., to $\chi = 95.4°$, where the base of the ionosphere has apparently come down to 65 km. Now look at some low frequency propagation records and emphasize what is happening between $\chi = 98°$ and $\chi = 95°$: on this circuit (Fig. 11) between Comfort Cove, Newfoundland, and Ottawa, we see that something begins near $\chi = 102°$; i.e., the signal amplitude starts to increase rapidly. The point is that on some days you can see things beginning back at $\chi = 102°$ and sometimes not. The nighttime signal is variable, and whether you see something beginning at 102° or at 100° depends on what the amplitude was prior to sunrise. The emphasis that seems to have been made about polar cap absorption events, and inferences based on these data about the chemistry of the ionosphere, is that things don't begin until $\chi = 94°$ or 95°. This is a question of sensitivity. If you use low frequencies you can see things beginning at $\chi = 102°$ or 100°.

The variability of the onset of the sunrise effect can be a real problem if you concern yourself with signal amplitude only. For example, on measurements made at VLF at steep incidence, the nighttime amplitude is highly variable. The phase, however, is not so variable at either steep incidence or oblique incidence, unless you have problems of modal interference at night, where 1 or 2 hop sky waves can interfere. If you restrict yourselves to circuits or conditions in which the predominant signal is a 1-hop sky wave, i.e., you are not having sky wave mode interference problems at night, the nighttime phases are fairly steady. If you are talking about the onset of things at dawn, you should be concerned with phase more than with amplitude. Unfortunately, in the VLF steep incidence experiment you don't see things beginning in phase away back at $\chi = 100°$ or 101° (Fig. 12) except at the lowest frequencies (<10 kc.); you see things in phase beginning around sunrise $\chi = 90°\ 50'$. In other words, some sort of oblique incidence experiment is needed to examine precisely when things begin, so that phase changes beginning early in the twilight period can be seen, but it must not be too oblique because of problems due to the 2-hop sky wave coming in. The VLF steep incidence experiment does not give much detail about what is happening over sunrise, but it does give interesting results about what is happening after sunrise, because there are small amplitude changes and regular phase changes after sunrise. On this 60 km. path, Cutler to St. Stephen, the daytime amplitude variations are small at 18.6 kc. However, it appears that if you go down to 14.7 kc. these features can become marked indeed and result in big "phase plateaus". The suggestion is that these features become marked as you go down to lower and lower frequencies (the effect is probably latitude sensitive).

The final point concerns high latitude ionosphere, where we recognize something peculiar. We have not operated the Resolute Bay partial reflection experiment over the epoch of the solar cycle, so we are forced to look at low frequency propagation data where we have data over a whole solar cycle. On the Thule to Churchill path (Fig. 13) we observe fairly regular onsets of the beginning of the dawn transition in March and September. In summer, (Fig. 14), we don't see much variation during sunspot maximum years. This might be expected, since the zenith angle of the sun at path midpoint is always greater than χ equal to 86°. In low sunspot years, however, we are apparently getting diurnal changes, so there is this difference between sunspot minimum and sunspot maximum. The astonishing feature, to me almost unbelievable, is that in December we apparently have changes occurring at large values of χ. In the period from 1960 to 1963 we can see that the main amplitude decrease occurs back around χ 101° or 100°. In 1964 and 1965 something is happening much earlier.

The high latitude ionosphere is a long way from being understood. Our partial reflection data has so far not revealed a C layer, and the low frequency data indicate that there is something complicated going on throughout the epoch of the solar cycle.

Before we depart, I would like to thank everyone for coming to the conference. I hope that we have not been pushing you too hard in keeping to this rather rugged schedule.

Falcon: We all owe a vote of thanks to our hosts at DRTE for a valuable and well-organized conference. I think that we ought to give them a round of applause.

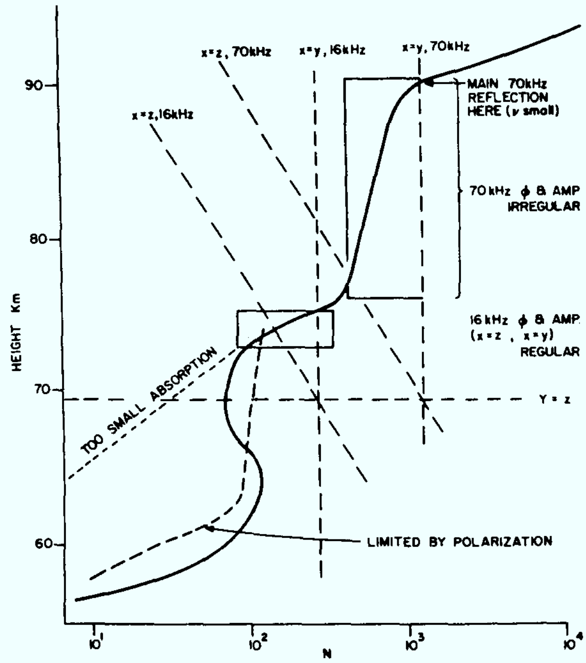

Fig. 1. An electron density-height profile deduced from the reflection of long waves.

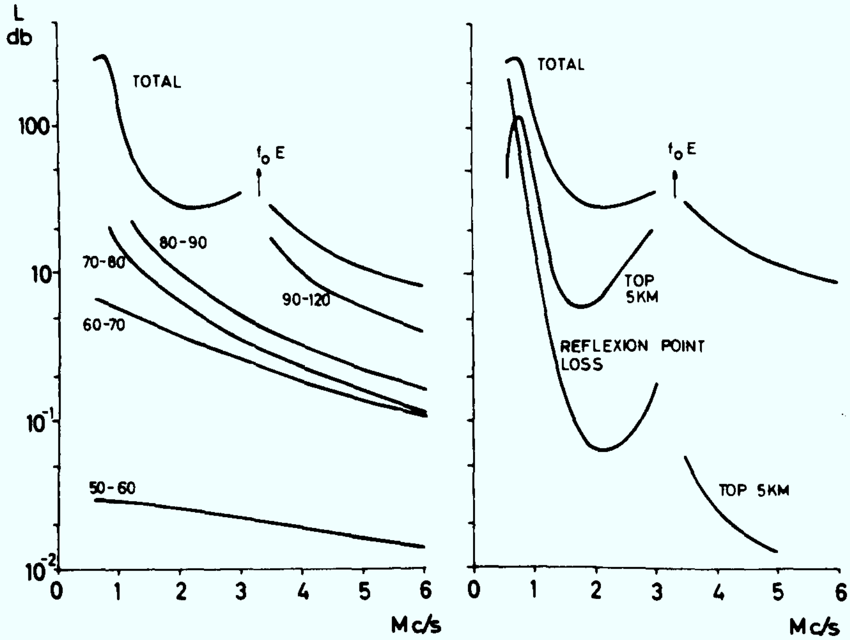

Fig. 2. Frequency variation of absorption of radio waves reflected vertically from the noon model ionosphere discussed by Piggott and Thrane in paper 6.1. (Left – 2a; right – 2b.)

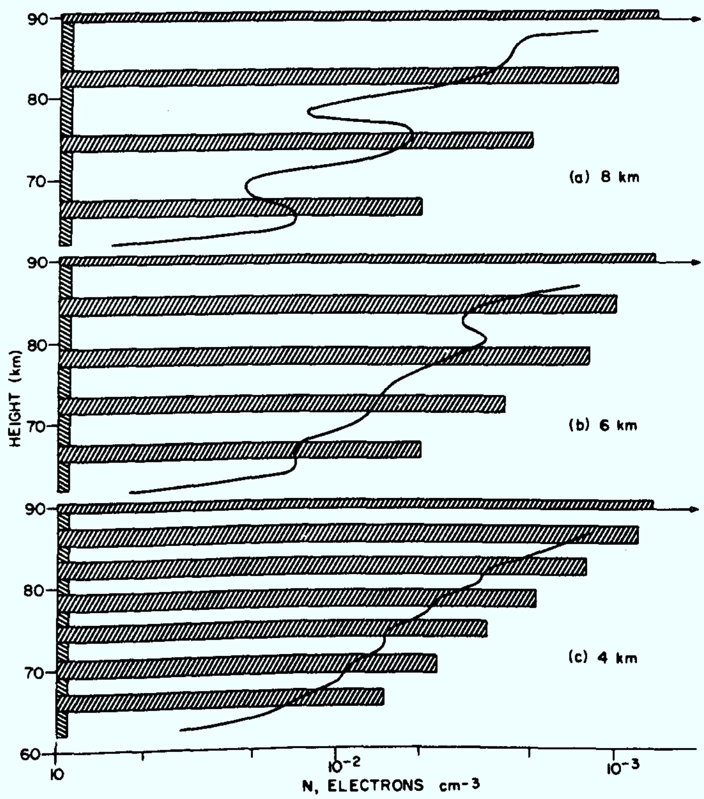

Fig. 3. Height resolution of the partial reflection experiment.

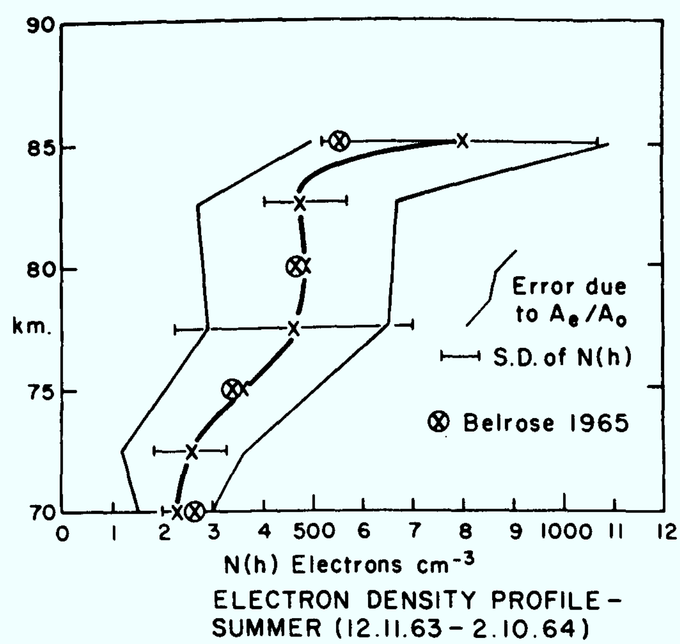

Fig. 4. Average summer electron number density against height as determined by the method of partial reflection at Christchurch, N.Z.

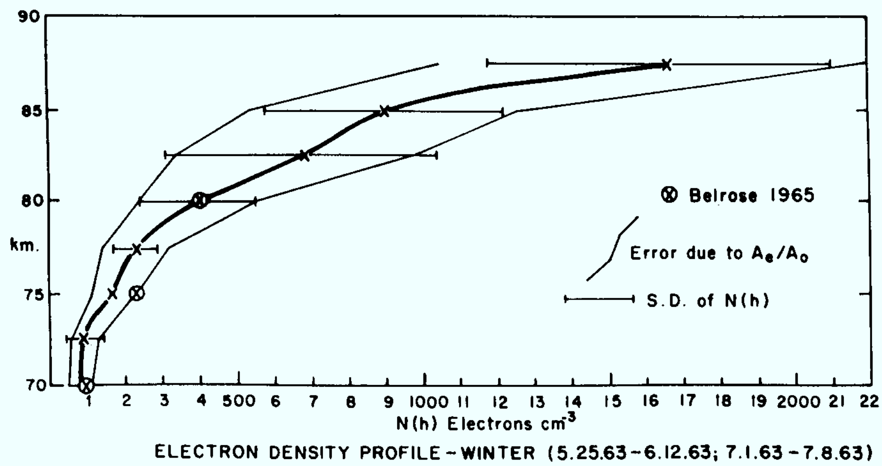

Fig. 5. Average winter electron number density against height as determined by the method of partial reflection at Christchurch, N.Z. (Results attributed to Belrose were taken from Physics of the Earth's Upper Atmosphere, p. 56).

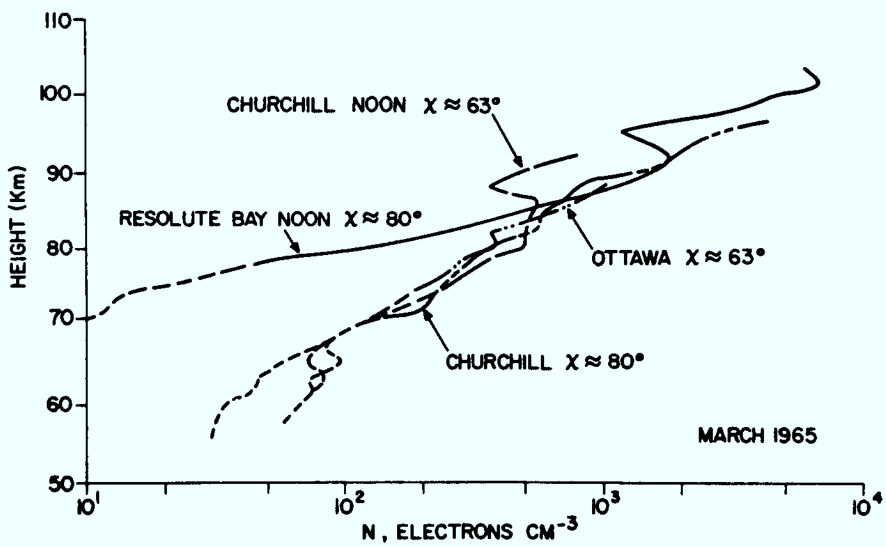

Fig. 6. Average electron number density against height in March 1965, for Resolute Bay noon (χ = 80°) compared with Churchill in the morning at the same solar zenith angle, and Churchill noon (χ = 63°) compared with Ottawa in the morning at the same solar zenith angle.

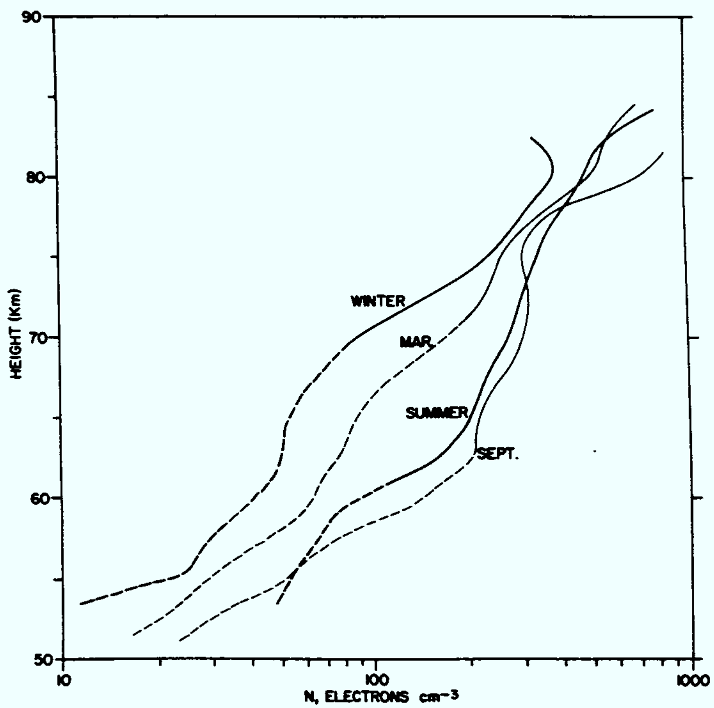

Fig. 7. Average electron number density against height for midday Ottawa data on 15 magnetically quiet days in summer (June, July, August 1962), 15 magnetically quiet days in winter (November 1961, December 1961, January 1962), 5 magnetically quiet days in March 1962 and 5 magnetically quiet days in September 1962.

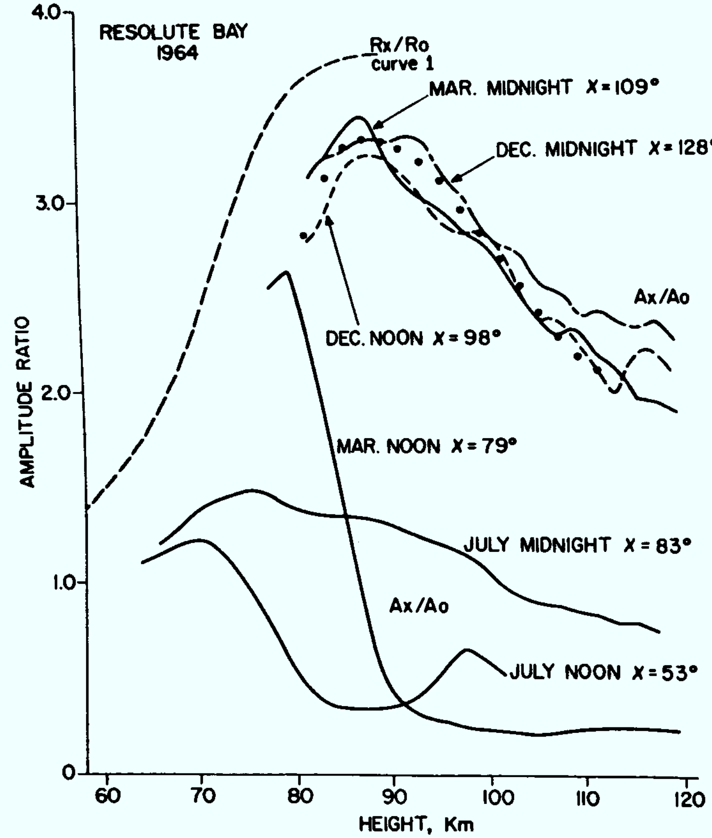

Fig. 8. Seasonal variation in average amplitude ratio, Ax/Ao, against height for midnight and noon at Resolute Bay.

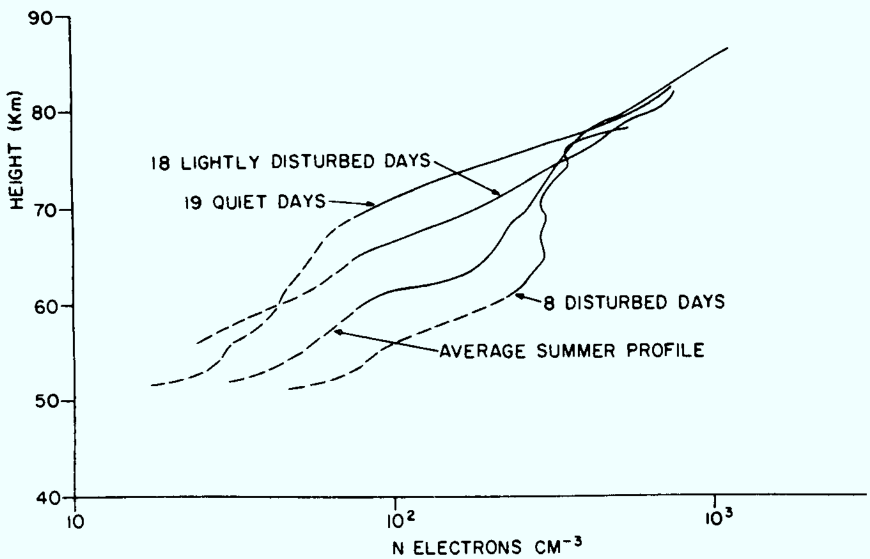

Fig. 9. Electron number density against height for average mid-day Ottawa data for various magnitudes of 'disturbance'. The degree of disturbance is judged from the partial reflection data and is discussed in paper 2.3.2.

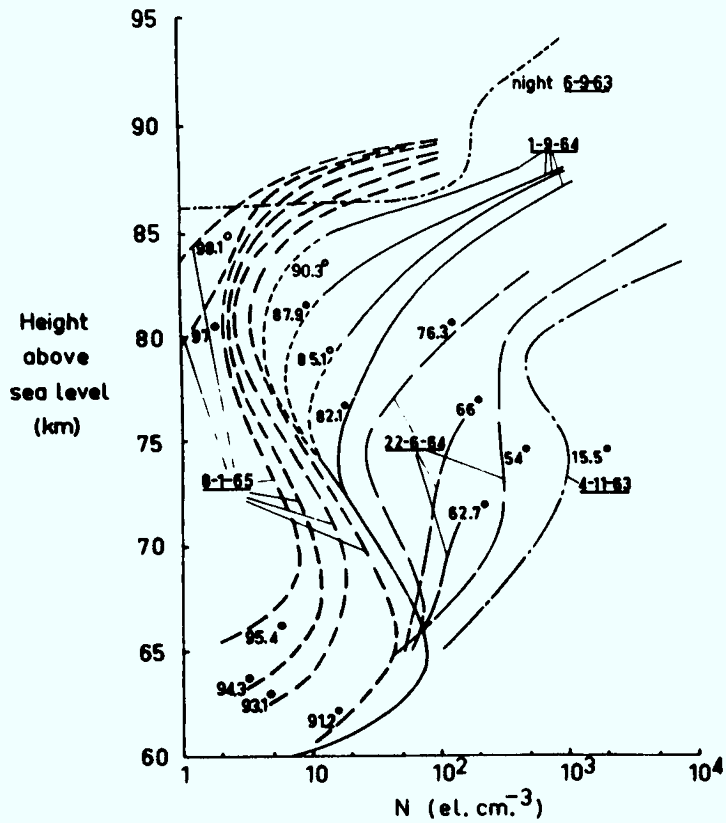

Fig. 10. Electron density-height profiles as a function of solar zenith angle, χ, for various dates (after Smith et al., paper 3.2.4).

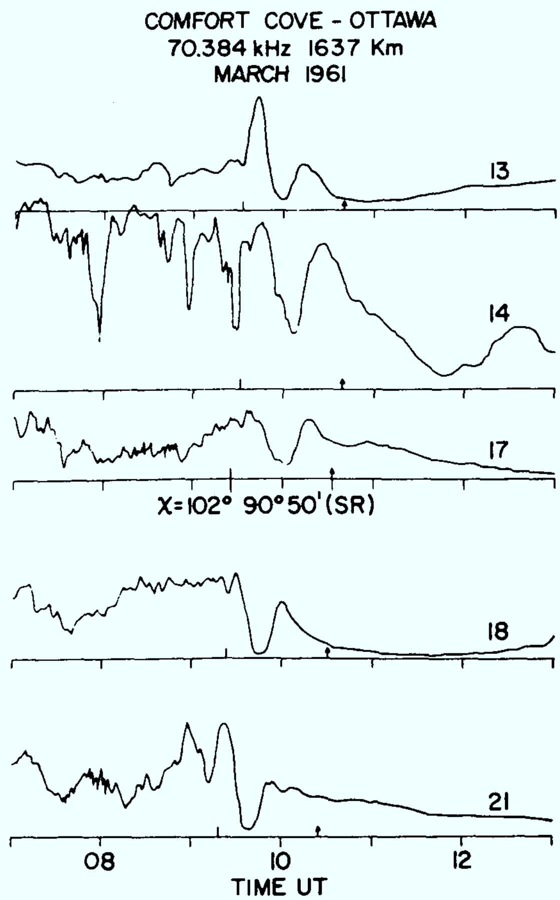

Fig. 11. Variation of low frequency field strength over dawn at summer and winter solstice for six years.

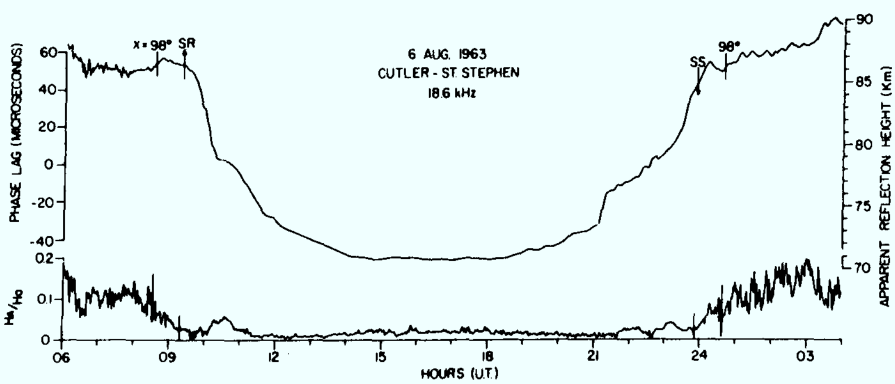

Fig. 12. Diurnal variation in the phase and amplitude of the downcoming wave over a short path in summer at 18.6 kHz.

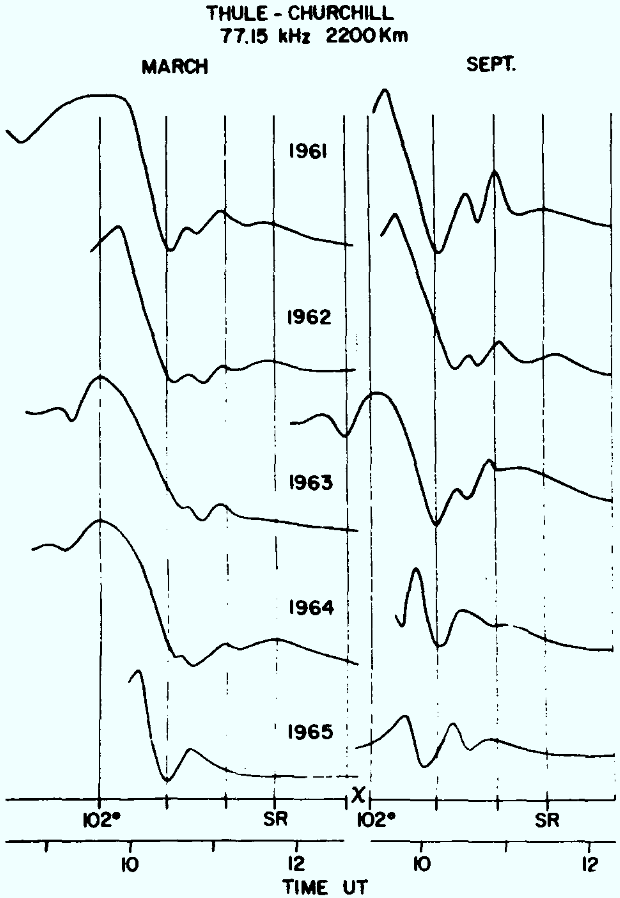

Fig. 13. Variation of Thule – Churchill field strength over dawn at equinox.

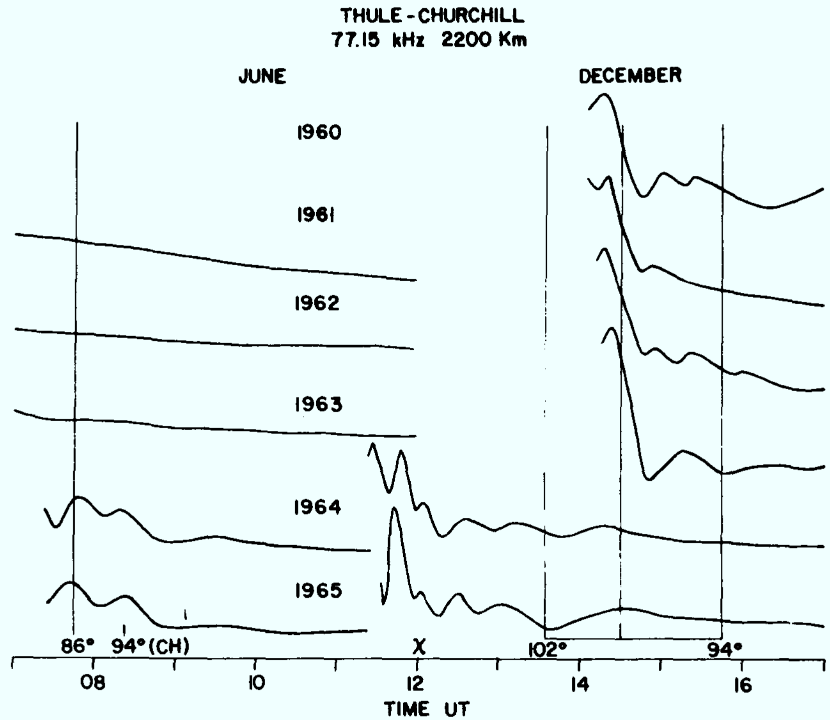

Fig. 14. Variation of Thule – Churchill field strength over dawn at solstice.

SECTION 8

EPILOGUE

In the preceding parts of this publication we have tried by the choice of program, by the arrangement of the various papers into sections, and, to some extent, by the order in which the various papers appear, to present a balanced summary of: (1) existing knowledge of the physics of the lower ionosphere, (2) the various techniques available for studying the lower ionosphere by ground-based radio wave propagation methods (their advantages and disadvantages), and (3) the new results being obtained by these methods. The discussions (in Session 7 of the conference) were intended to compare the various techniques, to assess the reliability of the data, and to update the present knowledge summaries in the light of the observational results presented at the conference, as well as to define the areas where new observational data or new interpretations are needed. To some extent these aims were achieved, but like all conferences there was insufficient time for detailed discussion. Also, during the intervening months while the material of the conference was being prepared for publication, there has been more time to reflect on the new results presented at the conference, and also there have been several important meetings at which other findings relating to the D region and to the subject matter of this conference have been reported. In this concluding part of the Proceedings, the Conference Chairman attempts to review briefly important facts that have emerged from this conference, and to discuss them in the light of new knowledge and ideas being developed about the formation of D-region ionization. While our understanding of the physical processes involved, particularly in regard to the electron loss processes, is still incomplete, the current reasoning is probably on the right track.

Structure and Formation : Day

The papers presented at the conference showed clearly that understanding of the lower E and D regions is uncertain. Although lumped parameter models of the deionization relations for these regions have been highly developed, and for a wide range of conditions appear to give reasonable agreement with many observations (Crain, Section 1.1), there is strong evidence that such models do not account for all the physical processes involved. Not only do we not know the more important charged and neutral species involved in all cases (Aikin, Section 1.2 and Swider, Section 1.3), but also we do not know how such factors as atmospheric circulation with its diurnal, seasonal, geographical, etc. dependence affect the situation. While a paper by Smith and his colleagues (Section 3.2.4) provided beautiful results showing the development of D region over dawn, and the change of D-region structure throughout the day until noon at Armidale (Fig. 1); which is at least qualitatively like those changes expected according to usual speculation about ionization and loss processes responsible for the formation of D-region ionization; papers by Gregory (Section 2.3.5) dealing with the effects associated with the overhead passage of pressure ridges, and by Belrose and his colleagues (Section 2.3.2) showing unexpected electron density profiles over Resolute Bay, are excellent examples of the problems mentioned above.

The latitudinal dependence of D-region ionization is worth discussing in somewhat more detail. Results of measurements at Ottawa and Churchill (Fig. 2) show that the electron density profiles are similar when compared under similar solar conditions, and that these profiles are not very different when compared with results measured at still lower latitudes (e.g. Armidale, See Fig. 1). The data for Churchill indicate that solar control, for solar zenith angles less than 80^o, may be less than at lower latitudes (Armidale). The diurnal change at the various latitudes needs to be studied in more detail.

When, however, a comparison is made between these data and results for Resolute Bay, it is clear that there are important differences (Fig. 2): the bank of ionization at heights below 70 km., designated by some workers the C layer, is apparently not observed over Resolute Bay in March. In winter and spring equinox the electron density profiles over Resolute Bay are steep, the electron density increases rapidly with height, and there are undetectably few electrons below 85 km. in winter and 70 km. in March. The fact that the electron number densities are small at low heights, and the electron density gradient steep in winter (when $\chi > 98^o$) was not considered surprising, since rocket measurements of the effective nocturnal electron recombination loss rates have shown that the loss rate is height dependent; the rate of loss increases sharply for heights below about 90 km. (McDiarmid and Budzinski, 1964). The electron number densities at the base of the ionosphere over Resolute Bay in the polar winter can be reasonably accounted for using accepted values of electron production rates by galactic cosmic rays and effective electron loss rates like those obtained by the rocket experiments (Belrose et al. 1964). The rapid increase in electron loss rate for heights below 90 km. was interpreted to be due to the formation of negative ions.

During the day, however, the negative ions which persisted at low heights throughout the night, would be expected to be photo-detached by visible sunlight. While a clear diurnal change in the electron number densities over Resolute Bay is evident in March, it is surprising that there are few electrons below about 70 km. at local noon ($\chi \simeq 80^o$), whereas under similar solar conditions at lower latitudes, measurable electron densities are observed to much lower heights (~55 km.). If galactic cosmic radiation is the source of electron production at these heights, then the rate of production of electrons at Resolute Bay should be greater than at lower latitudes (due to the smaller magnetic cut-off at this latitude). The explanation must be that the electron loss rates must be different over Resolute Bay than at lower latitudes.

The results for Resolute Bay show in addition that there is a marked seasonal change in the loss (or electron production) rate, since the electron density profile at midnight in July (χ~83^o) differs from the profile measured at midday in March (χ~80^o), even though the altitude of the sun is similar in the two instances (Belrose et al. Section 2.3.2). Electron densities are measurable to lower heights in summer (~65 km.).

It is clear that the latitudinal and seasonal behavior of the ionization at low heights in the D region is not explicable in terms of a single negative ion, 0_2^-, in the D region, and the photodetachment of this negative ion during the daytime. Recent laboratory experiments may shed a new light on electron detachment processes. Rees (1965) and others have found that a three body attachment process occurs in an oxygen atmosphere resulting in the formation of three types of negative ions, viz: 0^-, 0_2^- and 0_3^-. Burch and Geballe (1957) suggest that the 0_3^- ion is formed by the reactions.

$$e + 0_2 \rightarrow (0_2^-) \text{ unstable} \rightarrow 0 + 0^- + \text{kinetic energy}$$

$$0^- + 20_2 \rightarrow 0_3^- + 0_2$$

The experiments of Fehsenfeld et al.(1966) (reported by G.C. Reid at the XVth General Assembly of URSI, Munich, 5-15 September 1966) show that the associative detachment process

$$O_2^- + O \rightarrow O_3 + e$$

is apparently a fast reaction; and it is currently postulated (as a result of this work) that photodetachment of O_2^- (and O_3^- as suggested above) at sunrise, which has long been thought to be the explanation of the development of the C-layer over dawn, plays only a minor part in the dynamics of the D region. The sunrise change of electron densities at low heights in the D region is, according to this reasoning, due to the associative detachment of O_2^-, with O varying over sunrise since it is produced by the photo-dissociation of O_2. The various reactions involved in the negative ion chemistry of the D region suggested by Fehsenfeld and his co-workers is indicated in the block diagram and further discussed below.

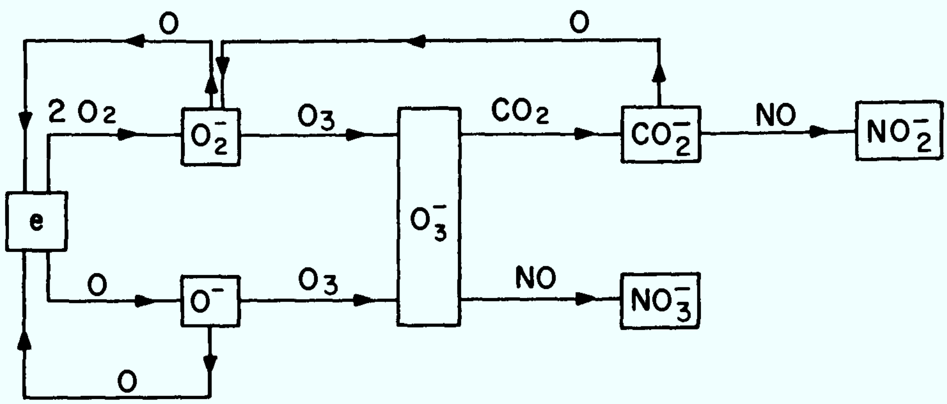

If this negative ion chemistry is in fact important in the D region, although care must be taken in relating the data of laboratory experiments to attachment processes in the undisturbed D region, then the electron density changes that occur over dawn need to be reinterpreted. More important to the present discussion, however, are the charge exchange reactions involving O_3, since these reactions could result in electron density loss through reactions resulting in the creation of CO_3^- or some other stable, tightly bonded negative ion. Certainly O_3 concentrations are large at high latitudes in winter and early spring, at least at stratospheric heights, and O_3 is variable from day to day and seasonally. There is limited evidence for heights > 30 km., but available data show a diurnal change in the concentration of O_3 (at low latitudes) for heights > 50 km. (c.f. Carver et al. 1966).

The variability of O and O_3 may in fact be a part of the explanation of the winter variability in electron density and the winter anomaly in MF absorption; and a part of the explanation of ionization changes associated with and following geomagnetic storms since Maeda and Aikin (1965) have suggested that ozone and atomic oxygen distributions in the mesosphere can be modified by charged particle bombardment during auroral disturbances.

Structure and Formation : Night

Radio propagation data, as well as available electron densities, measured primarily by rocket experiments, show that the electron distribution in the E and upper D-regions is very irregular at night (particularly above a height of 95-100 km., see Fig. 3). The electron density profiles give some evidence for an additional ledge of ionization below about 85 - 90 km. The diurnal change of the phase height of reflection of 16 kHz. waves steeply reflected from the ionosphere (Rugby-Cambridge) in sunspot minimum years reveals (see Fig. 4) that these are regular seasonal and nocturnal variations of the ionization at low heights; winter electron densities being greater at low heights than those in summer. Since the phase heights begin to decrease from about one hour after local midnight, there must be a source of electron production at night which is associated with the position of the sun, scattered Lyman Alpha for example. The fact that the minimum ionization (maximum phase height) is reached one hour after local midnight is explained by a recombination time lag, where $\alpha \sim 5 \times 10^{-7}$ cm^{-3} sec^{-1}. (Belrose and Bourne, Sect. 1.7).

Electron density profiles at high latitudes, particularly in the auroral zone, reveal that at these latitudes there is probably an additional source of electron production at night, viz: the precipitation of weak fluxes of energetic electrons (Haug, Sect. 2.3.1 and Belrose et al., Sect. 2.3.2).

Thus, together with ionization by galactic cosmic radiation, there are at three sources of ionization at night : scattered Lyman Alpha, cosmic radiation, and at least at auroral latitudes weak rather continuous but variable (from night-to-night or during the night) fluxes of energetic electrons.

Collision Frequencies

There has been an increasing realization in recent years that meteorological effects influence the propagation of radio waves in the D region, in part because pressure changes are directly reflected in changes in collision frequency of electrons (which affects the attenuation of radio waves), and in part because properties of the neutral atmosphere have a significant influence on the ionization. That pressure changes in the mesosphere do occur is well established; and collision frequencies calculated from meteorological rocket data, and obtained independently from radio wave propagation data, are in substantial agreement (Belrose and Bourne, Sect. 1.7, and Thrane and Piggott, 1966), at least in the D region. These data reveal that collision frequency changes with season, latitude, possibly time of day, and in the upper part of the E region with solar activity.

Meteorological rocket pressure data for White Sands, Wallops Island, and Churchill provide clear evidence for seasonal changes, which range from negligible at low latitudes (White Sands, 32^{o}N) to a factor of two at high latitudes (Churchill, 59^{o}N). The rocket pressures, and hence collision frequencies, are smaller in winter than in summer. The variability in collision frequency is greatest at high latitudes in winter, where day-to-day changes by up to a factor of two can occur. The high latitude (59^{o}N) data obtained by rocket-borne radio wave propagation experiments are in good agreement with a seasonal change by a factor of 1.5 to 2 in collision frequency. At Ottawa (45^{o}N), a seasonal change in collision frequency has not been found, even though much more data is available than for radio propagation experiments at other places.* Meteorological rocket pressure data would suggest that there should be a seasonal change by about a factor of 1.5. Not only is this not found, as noted above, but the more data one looks at the more curious the situation becomes. It does not seem possible to deduce an average collision frequency during one winter which is necessarily like the preceding or following winter. This fact is illustrated in Fig. 5, which shows the variation of the monthly averaged weighted value for the amplitude ratio, Ax/Ao, (measured by the partial reflection experiment at 57.5 and 59.5 km.). The amplitude ratio, Ax/Ao, at these heights is inversely proportional to collision frequency (Belrose and Burke 1964) and the scale on the right of the figure represents the height variation of a fixed value of collision frequency. This observation might be peculiar to the geographic location of Ottawa (~ 45°N) and the height where collision frequency was measured (~ 60 km.), since atmospheric density data (Whitehead et al. 1965) show (see Figs. 6 and 7) that the greatest change of atmospheric density with latitude occurs at this height and latitude in winter.

Atmospheric Circulation : Association with Mesopheric Electron Density Changes in Winter

The interactions between the upper and lower layers of the atmosphere and the influence of atmospheric circulation on electron densities are attracting an increasing amount of attention. A measure of the current interest in this subject, which brings together the fields of meteorology, the ionosphere, and aeronomy is the number of conferences and symposia that have discussed explicitly or in part this subject. In the past 18 months there have been at least seven : at Mar del Plata, Brussels, Illinois, Ottawa, Vienna, Munich, and Lindau. Two conferences were concerned specifically with this field of research : a symposium at Vienna, 3-7 May, 1966, on the interaction between upper and lower layers of the atmosphere; and an Advanced Study Institute at Lindau, 19 Sept.-1 Oct., 1966, sponsored by NATO, on movements and turbulence of the atmosphere between 30 and 120 km.

Jones and Beynon (Sect. 6.6), Lauter and Nitzsche (1966), Belrose et al. (1966), and others describe radio wave propagation results that demonstrate a well-defined seasonal behavior of ionospheric absorption on the reflection height of long waves, which are undoubtedly related to real seasonal changes in the plasma of the mesosphere. Although the association between these D-region ionization changes and meteorological phenomena is far from being established, there are common features in the two types of data that warrant examination. Lauter and Nitzsche (1966) have shown that LF and MF absorption (for constant solar zenith angle) is minimum in spring (April) and autumn (Sept./Oct.), which has to be interpreted by aeronomical and dynamical processes in the mesosphere structure. These minima coincide with reversals of mean zonal winds in the mesosphere (Appleman 1963) from strong and variable westerlies in the winter to weaker relatively constant easterlies in the summer. The April minimum in absorption, the more pronounced of the two seasonal minima, also coincides with a maximum in the total amount of ozone at middle latitudes (cf. Murgatroyd et al. 1965, Belrose et al. 1966).

Superimposed on these mean seasonal variations is the day-to-day variability, which is a pronounced minimum in summer and maximum in winter. The general patterns of the stratosphere and mesosphere circulation are fairly well established, although much detail is yet to be discovered and the interpretation is still in the development stage. The winter variability of the atmosphere is attributed to a breakdown of the polar-night vortex that is a characteristic feature of the circulation in the northern hemisphere (Murgatroyd et al. 1965). It consists of a strong westerly wind system in the mesosphere and upper stratosphere, extending down to low heights (the 100 mb. level or 15 km.) at high latitudes, which is centered

*Doubt has been cast (Piggott and Thrane, 1966) on the interpretation of the partial reflection data, particularly at low heights where the values of collision frequency are inferred. The evidence to date, however, supports the original interpretation of the partial reflection data (Belrose et al. Sect. 2.1), and provides some confidence in the validity of the collision frequency results inferred from the experimental data, particularly in the case of Ottawa data where, because of the high system gain, partial reflections are obtained from heights well below those at which measurable differential absorption occurs.

on the Eurasian side of the pole (over the Aleutians). A similar system that is less eccentric exists over the south pole, although there are great differences between the two hemispheres in the details of the polar circulation.

The breakdown of the polar night westerlies takes the form of sudden or explosive warmings (of 30 to 60°C) which begin in the upper stratosphere, and spread laterally both upwards and downwards, until the entire stratosphere and a portion of the mesosphere are raised to levels that on occasion can exceed those in summer. The extension of these warmings up into the mesosphere is less well understood, but the extensive meteorological sounding program is expected to bridge, in part, this gap in our knowledge. There is an increasing amount of evidence (Toweles, 1965) that 45 km. (~2 mb.) is the source level of the circulation breakdown and the sudden heating that has been observed at and below the 10 mb. level (31 km.) in several winters since 1952. Simultaneous with the warmings, the direction of the wind is reversed. Marked changeovers to strong easterlies were revealed by the network stations in late January or early February of 1961, 1962, and 1963 (as well as subsequent winters), but with increasing intensity leading to the huge maximum in 1963. The associated ionospheric effects of this event have been studied by several workers, (cf. Lauter and Entzian, 1966, Shapley, 1966). Thus, while the 1961 wind reversals observed at Wallops Island scarcely affected the 30 mb. circulation, the great 1963 reversal dominated the hemisphere and extended downwards to upset the circulation of the lower layers of the stratosphere. This year-to-year variability in the amount of cellular activity indicates that the degree of horizontal (and vertical) mixing and thus the resulting meridional exchange of such mesospheric tracers as ozone, atomic oxygen, and nitrogen oxides, may vary markedly from one winter to the next (or during the course of the winter). This would have a profound influence on the ionization densities in the mesosphere. After a few days the atmosphere cools to its original state. This behavior may be repeated several times until the final warming takes place in spring (March), when the polar-night vortex is replaced by irregular anti-cyclones, which gradually settle into the symmetrical easterlies of the summer. The final warming is often dramatically abrupt, sometimes accompanied by a temperature overshoot.

Only a few systematic investigations that give indications of ionization changes that are undoubtedly associated with the major meteorological phenomena have been made; these are not necessarily made at the same height, and the associations with meteorological data have not always been conclusive. The so-called winter anomaly in MF (2 MHz.) absorption (Appleton and Piggott, 1954), which has been studied in recent years by Bossolasco and Elena (1963), Shapley and Beynon (1965), Shapley (1966) and Dieminger (1966), is probably associated with ionization changes that occur predominantly above a height of 75 to 80 km. (indirect arguments for this are given by Lauter and Nitzsche, 1966). One rocket experiment by Bowhill et al. (1966) gives direct evidence in this regard; see also the discussion below. The winter variability of electron density (Belrose et al. Sect. 2.3.2) is for heights below 80 km. (Fig. 8 upper part and Fig. 9); in fact, the electron density at 80 km. appears to be rather constant. The meteorological data with which associated variations are sought is usually measured at much lower heights, 10 to 30 mb. (25 to 30 km.), since it was measured by radiosonde balloons.

The features of the radio data and their association with stratospheric warmings cannot be so well described as can the meteorological events in themselves. Gregory (1965), (see also Sect. 2.3.5) has presented results that showed rather spectacular association, on one occasion, between electron density isopleths and 20 to 30 mb. temperatures associated with the overhead passage of a pressure ridge in the southern hemisphere (Christchurch)* as well as other examples not so well defined employing f min data. Such clear associations have not been found in the northern latitude. Shapley and Beynon (1965), for example, had to resort to superposed epochs to eliminate statistically extraneous events or "noise"; and partial reflection data at Ottawa (at a comparable geographic but higher magnetic latitude to Christchurch) has not so far shown a clear correlation with 30 mb. temperatures, but a definite correlation with magnetic activity has been found (Belrose et al. Sect. 2.3.2).

* This event (in June 1963) was also associated with an increase in magnetic activity, not reported in the papers by Gregory.

There also seems to be uncertainty about the height region in which the ionization enhancements occur. The MF absorption is thought to be associated, in general, with ionization changes that occur above a height of 75 to 80 km., although one event in February 1961 believed to be a winter day of anomalous absorption (Belrose and Bourne, Sect. 1.7) was associated with large increases in electron density at much lower heights (~60 km.). Gregory's observations also showed that the effect was detected at all heights in the D region. Fig. 8, in which electron density profiles over Ottawa and absorption values obtained simultaneously at Lindau (Dieminger et al. 1966) are compared, shows a rather remarkable correlation between electron densities obtained by partial reflections in Canada and absorption measured in Germany on individual days in winter. While it is not known whether such apparent correlations happen in general (earlier statistical studies have reported that the "winter anomaly" in ionospheric absorption is rather localized in space to areas of the order of 1000 km. or so); nevertheless, the winter variability in electron density is typical of that usually observed at Ottawa, and the absorption changes are typical of those that occur in winter in Europe. The magnitude of the electron density changes are clearly insufficient to explain the magnitude of the absorption changes, and therefore the latter must be associated with ionization change that occur (as well) at heights above 80 km.

The effects on long wave "phase heights" are inconclusive. Data for VLF waves (16 kHz.) steeply reflected from the ionosphere have shown (Belrose, 1956, 1957 and Mawdsley, 1956) that on winter days of anomalous absorption the "phase heights" are lower than normal (by up to 5 km. or so). More recently, observational data for LF waves obliquely reflected from the ionosphere have been interpreted to give higher reflection heights (Lauter and Entzian, 1966) associated with the January 1963, stratospheric warming. Since changes of atmospheric composition as well as atmospheric pressure are probably involved, presumably the electron density profile could move up or down; more experimental data is needed before the winter anomaly can be satisfactorily described.

Many more co-ordinated measurements are necessary to establish a world-wide picture, since the measurements to date can be regarded as pinpricks into the vast volume that needs to be investigated. The ionospheric data are too few, for example, to map the global pattern, as is done by the workers at the Free University of Berlin for 10 mb. pressures. Studies of these pressure maps have revealed many interesting features of the disturbance patterns. For example, polar maps from a paper by Labitzke (1965),(Fig. 10), show the regular movement of 10 mb. (pressure) highs during strong mid-winter warmings in the course of several winters from 1957 to 1964. Note that in 1960, a disturbance can be traced which passed over middle Europe and four to five days later over Eastern Canada. Such disturbances should be looked for in radio data.

Beside the limitation in geographical extent of the observational data compared to that required for a detailed study, there are other problems that complicate the association between atmospheric circulation and mesospheric electron densities. The abnormal increases in electron density that result in anomalous absorption of MF radio waves is a daytime phenomenon, whereas the greatest temperature changes in the upper stratosphere occur at high latitudes in winter when the sun never rises. Also, in middle Europe (at 55° geographic latitude) where the winter anomaly has been extensively studied, it is fairly easy to identify solar disturbances and so eliminate them from the analysis, since the observations are made at places some 10° or so south of the auroral absorption zone; but in North America (Canada) comparable geographic latitudes are right inside the auroral absorption zone.

The difficulties of effective synoptic analysis, of relating data taken at different levels, and in eliminating extraneous events, readily explains the somewhat inconclusive results so far obtained. Nevertheless, certain progress has been made, and the question must be no longer "is there a relation" between stratosphere and ionosphere or mesosphere, but what are the relations and how do they come about? Only speculative guesses as to the causes of the increased electron densities have so far been made; e.g. the absorption changes might be attributed to changes in the minor ionizable constituents in the lower ionosphere (NO is a likely candidate), and in this regard also the negative ion reactions suggested by Fehsenfeld and his colleagues, discussed briefly in this paper, look exciting; but ionospheric composition measurements by rockets are required before firm conclusions can be drawn. It has been suggested that the high values of nitric oxide concentrations measured by Barth (1966) might have been made in an anomalous winter day (Sechrist, 1966, Thomas, 1966), but there is insufficient radio or meteorological data to substantiate this suggestion.

The cause of the meteorological warmings themselves is not understood. For example:

1. What accounts for the great differences between the two hemispheres in winter circumpolar circulation?
2. Why does the stratosphere warm up even during darkness, and what maintains polar mesosphere at temperatures above those in summer?
3. What triggers the sudden explosive stratosphere warmings? Is the source level at 45 km. and if so, why? Interestingly, this height coincides with the portion of the ozone layer most strongly heated by solar radiation (and a subsidiary peak in the nocturnal distribution of ozone is found at this height (Randhawa, 1966); but sudden warmings begin at high latitudes in winter when the polar atmosphere is in darkness.

There has been considerable speculation regarding question 1 (cf. Godson, 1963, Palmer and Taylor, 1960, Labitzke, 1962). There are meteorological phenomena which could account for the mesospheric warming, e.g. chemical heating by recombination of atomic oxygen, (Kellogg, 1961, Young and Epstein, 1962, Maeda, 1963), or dynamic heating by atmospheric acoustic waves from the polar night jet stream (Maeda, 1964), and by turbulence or internal gravity waves (Hines, 1963). According to Toweles (1965), "mounting evidence points to close similarity between the vertical motions and horizontal transports, associated with the respective jet streams of tropopause and stratopause levels. Extension of this similarity suggests that a similar counter-gradient heat flux to that found in the layers just above the tropopause-level jet will be found just above its counterpart at the stratopause. The existence of such a counter-gradient heat flux in the mesosphere might explain the warm wintertime pole in the layers above 55 km., partially or entirely without recourse to heating by subsidence or recombination in the layers of atomic oxygen". We are less able to answer question 3.

Conclusions

This epilogue has attempted to summarize briefly present knowledge of the physics of the lower ionosphere, and particular notice is taken of recent work. The available facts will illustrate the importance of obtaining observational data at different latitudes, the importance of observing diurnal changes (pre-sunrise and post-sunset ionization changes are of particular interest), the importance of obtaining synoptic data for a wide range of geographical locations, and the importance of obtaining rocket observations, at the different latitudes, of composition (of particular value is the composition during abnormal winter days). It is imperative that the technique of composition measurements by meteorological rockets be improved, and reliable measurements of ozone, atomic oxygen, and the nitrogen oxides be made throughout the mesosphere; and the nature of the dominations be determined (especially also negative ions). The lack of adequate data is a serious handicap in the construction of atmospheric models, and while several models of the D region have been suggested, none are fully consistent with all experimentally derived parameters.

The meteorological rocket network program can be expected to lead to important new discoveries. No such synoptic program is underway or planned by ionospheric physists. Progress in this field of research can result only from co-operative synoptic research, jointly conducted by meteorologists and ionospheric physists. The meteorologists are extending their interests to higher heights (>60 km., the ceiling of the present meteorological rockets), and so-called "phase two" of the meteorological sounding rocket program should be planned to include rocket-borne experiments that measure ionization and composition as well as wind, temperature, and pressure. The rocket-borne ionospheric experiments need to be backed by reliable radio experiments capable of synoptic application; the meteorological experiments have a reliable lower atmosphere experimental backup - the radiosonde balloon.

J.S. Belrose, Conference Chairman
October 1966

REFERENCES

Appleman, H.S. The climatological wind and wind variability between 45 and 60 kilometers. J.Geophys. Res., 68, 3611-3617, 1963.

Appleton, E.V. and W.R. Piggott. Ionospheric absorption measurements during a sunspot cycle. J. Atmos. Terr.Phys., 5, 141-172, 1954.

Barth, C.A. Rocket measurement of nitric oxide in the upper atmosphere. Planet. Space Sci., 14, 623-630, 1966.

Belrose, J.S. Some investigations of the lower ionosphere. Ph.D. Thesis, Cambridge University, 1st copy 1956. Revised copy 1957.

Belrose, J.S. and M.J. Burke. Study of the lower ionosphere using partial reflection. 1. Experimental Technique and Method of Analysis. J. Geophys. Res., 69, 2799-2818, 1964.

Belrose, J.S. Bode, L.R. and L.W. Hewitt. Physical properties of the polar winter mesosphere obtained from low-frequency propagation and partial reflection studies. Radio Science J. Res. NBS/USNC-URSI, 68D, 1319-1323, 1964.

Belrose, J.S. Bourne, I.A. and L.W. Hewitt. The winter variability of electron number density in the lower ionosphere over Ottawa. A discussion of results and possible cause, Electron Density Profiles in the Ionosphere and Exosphere (ed. Frihagen), North Holland Pub. Co., 48-60, 1966.

Bossolasco, M. and A. Elena. Absorption de la couche D et temperature de la mesosphere. C.R. Acad. Sci., 256, 4491-4493, 1963.

Bowhill, S.A.,Mechtley, E.A. and C.F. Sechrist. Rocket ionization measurements on a winter day of high absorption. Space Research VII (in press).

Burch, D.S. and R. Geballe. Ionic drift velocities and electron attachment coefficients in oxygen. Phy. Rev., 106, 183, 1957.

Carver, J.H., Horton, B.H. and F.G. Burger. Nocturnal ozone distribution in the upper atmosphere. J. Geophys. Res., 71, 4180-4191, 1966.

Dieminger, W. D-region phenomena associated with meteorological influences, NATO Advanced Study Institute Conference on Movements and Turbulence of the Atmosphere Between 30 and 120 km., Lindau, 19 Sept.-1 Oct., 1966.

Dieminger, W., Rose, G. and H.U. Widdel. The morphology of winter anomaly of absorption. Space Research VII, in press, 1966.

Fehsenfeld, F.C. Schmeltekroph, A.L., Schiff and E.E. Ferguson. Laboratory measurements of negative ion reactions of atmospheric interest. Planet. Space Sci., in press, 1966.

Godson, W.L. A comparison of middle-stratospheric behaviour in the Arctic and Antarctic, with special reference to final warmings. Met. Abhandlungen, Inst. fur Meteor. und Geophysik, Berlin, Bd 36, 161-206, 1963.

Gregory, J.B. The influence of atmospheric circulation on mesospheric electron densities in winter. J. Atmosph. Sci., 22, 18-23, 1965.

Hines, C.O. The upper atmosphere in motion. Quart. J. Roy. Meteorol. Soc., 89, 1, 1963.

Kellogg, W.W. Chemical heating above the polar mesopause in winter. J. Meteorol., 18, 373-381, 1961.

Labitzke, K. Beitrage zur Synoptik der Hochstratosphare. Met. Abhandlungen, Inst. fur Meteor. und Geophysik, Berlin, 28, No. 1, 93 pp., 1962.

Labitzke, K. On the mutual relation between stratosphere and troposphere during periods of stratospheric warmings in winter. J. App. Met., 4, 91-99, 1965.

Lauter, E.A. and G. Entzian. Uberwachung der tiefen Ionosphare mit Hilfe der Quasi-Phasenmessung im Langwellen-bereich (100 ... 200 kHz.), II. Ergebnisse, Veroffentlichungen des NKGG der DDR, Reihe 11, Heft 1, 77-97, 1966.

Lauter, E.A. and P. Nitzsche. Seasonal variations of ionospheric absorption deduced from A3-measurements in the frequency range 100-2000 kc/s. J. Atmos. Terr. Phys., in press, 1966.

Maeda, K. Auroral dissociation of molecular oxygen in the polar mesosphere. J. Geophys. Res., 68, 185, 1963.

Maeda, K. On acoustic heating of the polar night mesosphere. J. Geophys. Res., 69, 1381, 1964.

Maeda, K. and A.C. Aikin. Paper presented at the AGU Meeting, Washington D.C., 19-22 April, 1965.

Madsley, J. Private communication, 1956.

McDiarmid, I.B. and E.E. Budzinski. Angular distributions and energy spectra of electrons associated with auroral events, Can. J. Phys., 42, 2048-2062, 1964.

Murgatroyd, R.J., Hare, F.K., Boville, B.W., Toweles, S. and A. Kochanski. The circulation in the stratosphere mesosphere and lower thermosphere. W.M.O. Tech. Note No. 70, Geneva, 1965.

Palmer, C.A. and R.C. Taylor. The vernal breakdown of the stratospheric cyclone over the South Pole. J. Geophys. Res. 65, 3319-3329, 1960.

Piggott, W.R. and E.V. Thrane. The effect of irregularities in collision frequency on the amplitude of weak partial reflections. J. Atmos. Terr. Phys., 28, 311, 1966.

Randhawa, J.S. Ozone measurements with rocket-borne ozonesondes. J. Geophys. Res., 71 4057-4059, 1966.

Rees, J.A. The behaviour of free and attached electrons in oxygen. Austral. J. Phys., 18, 41, 1965.

Shapley, A.H. Relations between stratosphere and mesophere. NATO Advanced Study Institute Conf. on Movements and Turbulence of the Atmosphere between 30 and 120 km., Lindau, 19 Sept.-1 Oct., 1966.

Shapley, A.H. and W.J.G. Beynon. "Winteranomaly" in ionospheric absorption and stratospheric warmings. Nature, 206, 1242-1243, 1965.

Sechrist, C.F. A theory of winter absorption anomaly at middle latitudes. J. Atmos. Terr. Phys., in press, 1966.

Smith, L.G. Investigation of the D- and E-regions of the ionosphere during the international quiet sun years. NASA Report No. CR-391, 1966.

Thomas, L. The Nitric Oxide concentration in the D region. Internal Memorandum I.M. 292 (privately circulated), Radio and Space Research Station, Ditton Park, Slough, 1966.

Thrane, E.V. and W.R. Piggott. The collision frequency in the E- and D-regions of the ionosphere. J. Atmos. Terr. Phys., 28, 721-737, 1966.

Toweles, S. Application of meteorological rocket network data, in Murgatroyd et al. pp. 79-104, 1965.

Whitehead, V.S. Lancer, A.M., Harper, D.R. and W.J. Saucier. Atmospheric structure and circulation to 200 km. in terms of density, University of Oklahoma Research Institute, AFCRL Report No. 65-242, 1965.

Young, C. and E.S. Epstein. Atomic oxygen in the polar winter mesosphere. J. Atmospheric Sci., 19, 435-443, 1962.

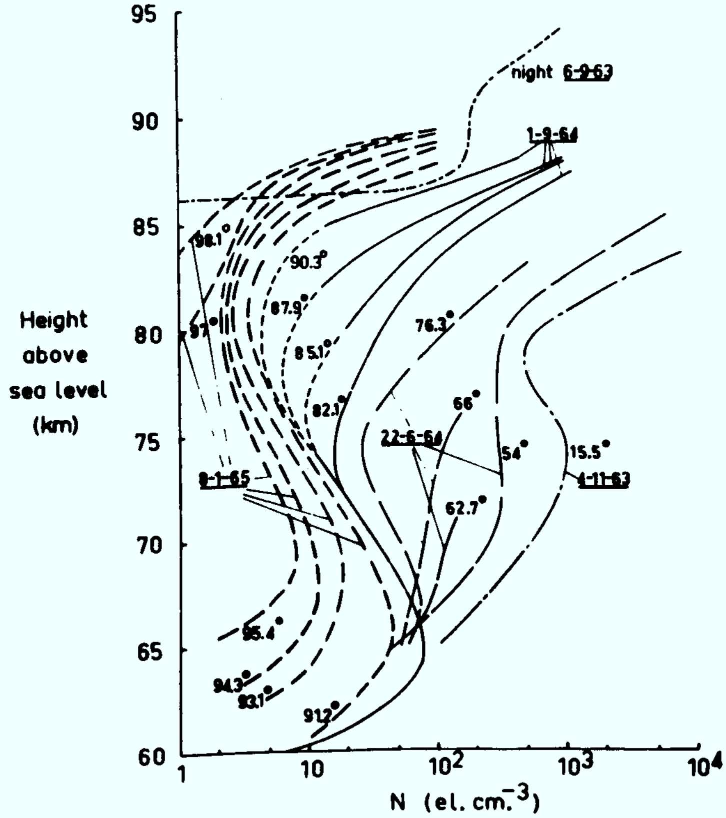

Fig. 1. Electron density height profiles by the method of wave interaction at Armidale (after Smith et al., Sect. 3.2.4).

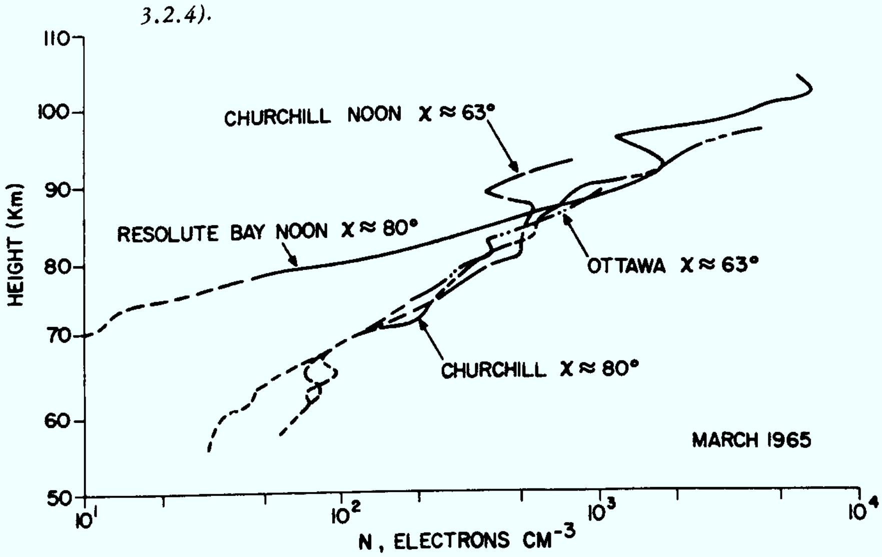

Fig. 2. Average electron density height profiles in March, 1965, by the method of partial reflections, for Resolute Bay noon ($\chi \sim 80°$) compared with Churchill in the morning at the same solar zenith angle, and Churchill noon ($\chi \sim 63°$) compared with Ottawa in the morning at the same solar zenith angle (after Belrose et al., Sect. 2.3.2).

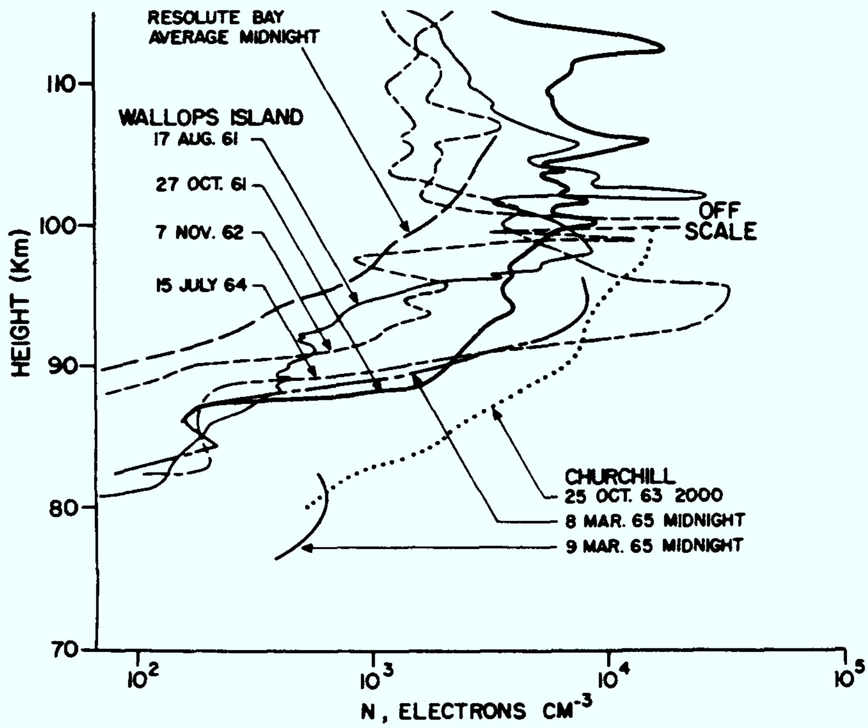

Fig. 3. Electron density height profiles for the E region at night over Wallops Island measured by rocket-borne Langmiur probes (Smith, 1966) and over Resolute Bay and Churchill determined by the method of partial reflections (Belrose et al., Sect. 2.3.2).

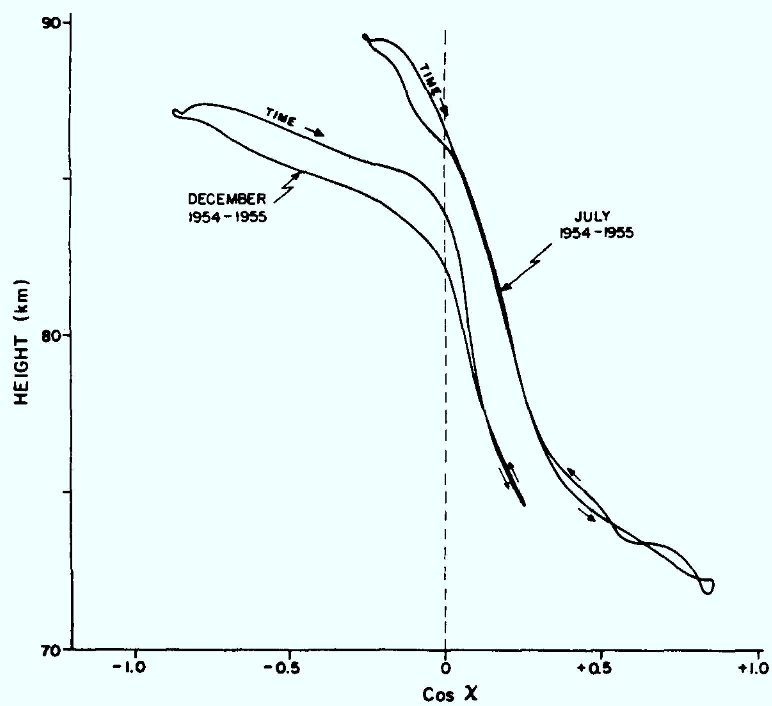

Fig. 4. Monthly mean diurnal change of the phase height of reflection for 16 kHz. waves (Rugby-Cambridge) during quiet sun years (after Belrose and Bourne Sect. 1.7).

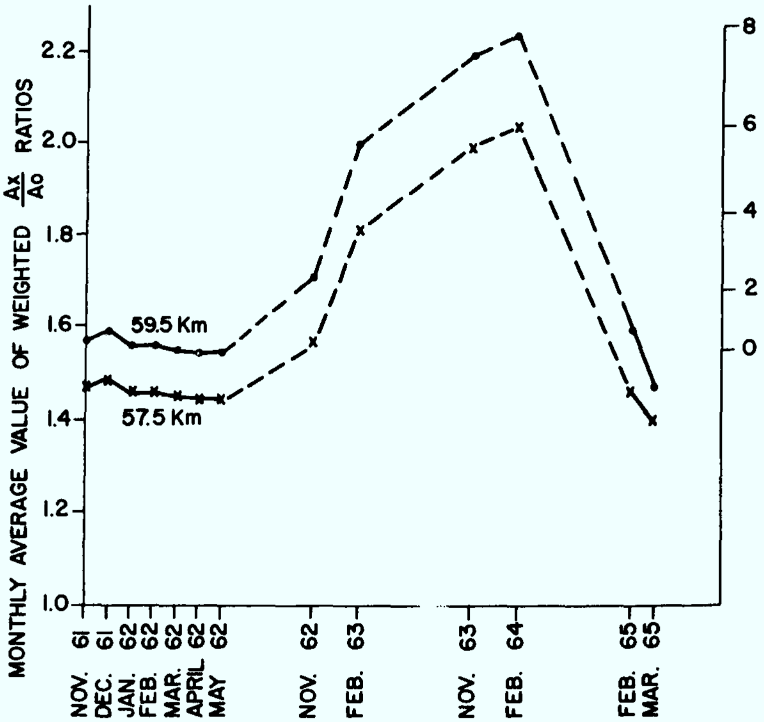

Fig. 5. The variation of the monthly average weighted value for the amplitude ratio Ax/Ao at 57.5 and 59.5 km. for the months on which data at Ottawa have been analyzed. The scale on the right of the figure represents the height variation of a fixed value of νm. (after Belrose et al., Sect. 2.3.2).

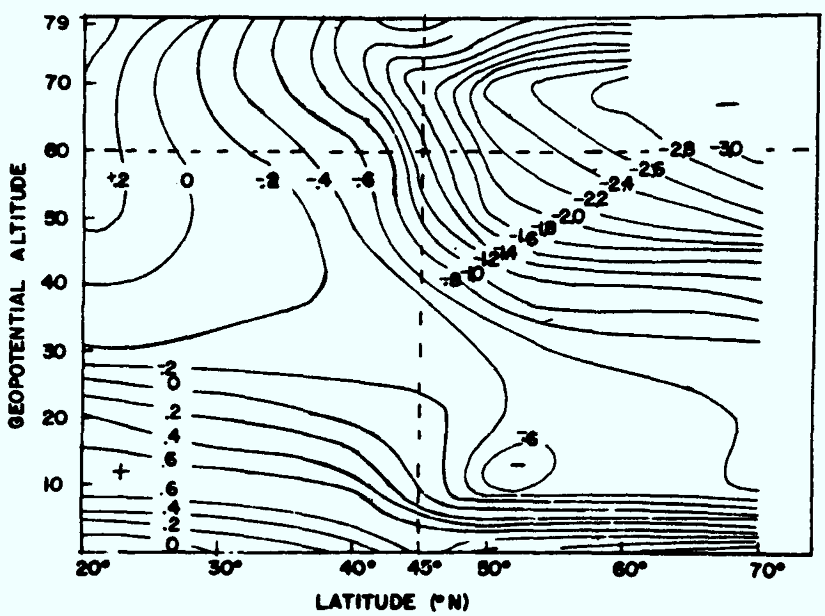

Fig. 6. Departure in height from the US standard atmosphere, 1962, for density surfaces (January), contour interval 0.2 km. (after Whitehead, et al., 1965).

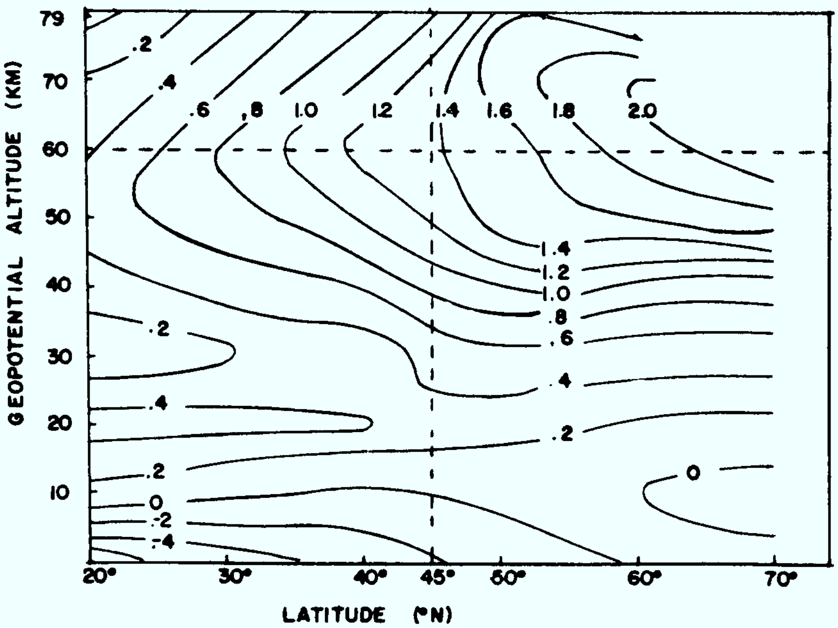

Fig. 7. Departure in height from the US standard atmosphere, 1962, for density surfaces (June), contour interval 0.2 km. (after Whitehead et al., 1965).

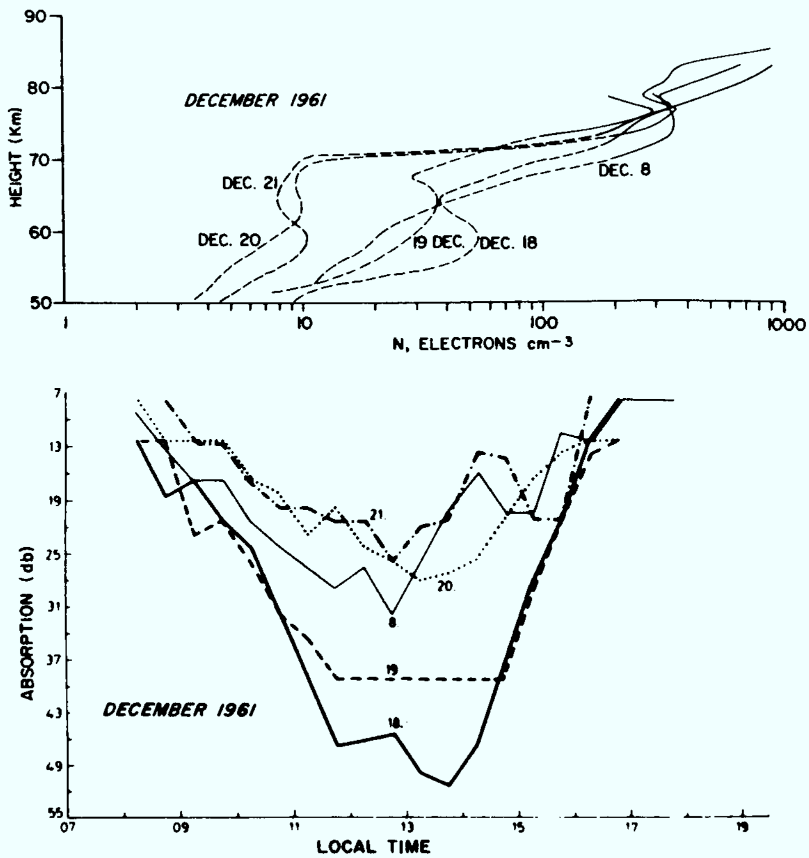

Fig. 8. Electron density profiles over Ottawa, Canada, and absorption values obtained on the same day at Lindau, Germany (after Dieminger et al. 1966).

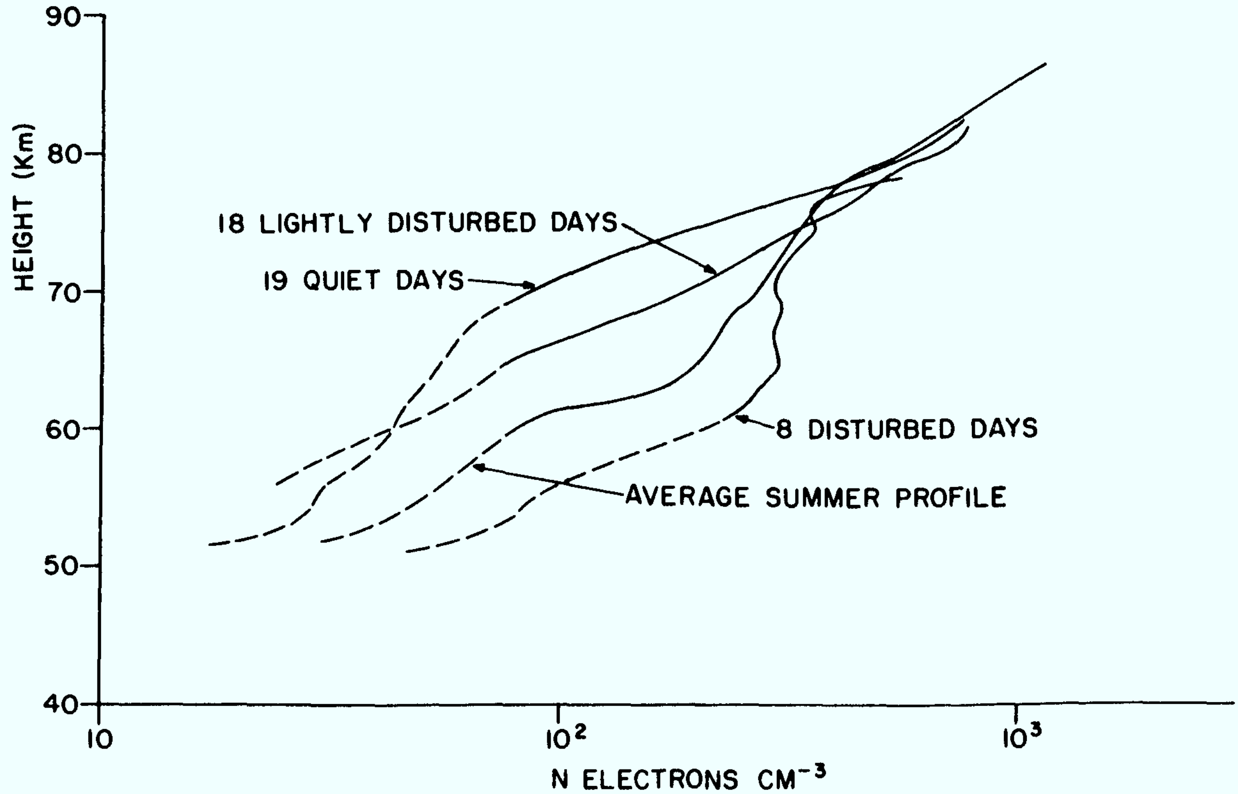

Fig. 9. Electron density height profiles for average midday Ottawa data in winter. The data are averaged in various catagories which are selected according to the amount of absorption below 75 km. (after Belrose, et al., Sect. 2.3.2).

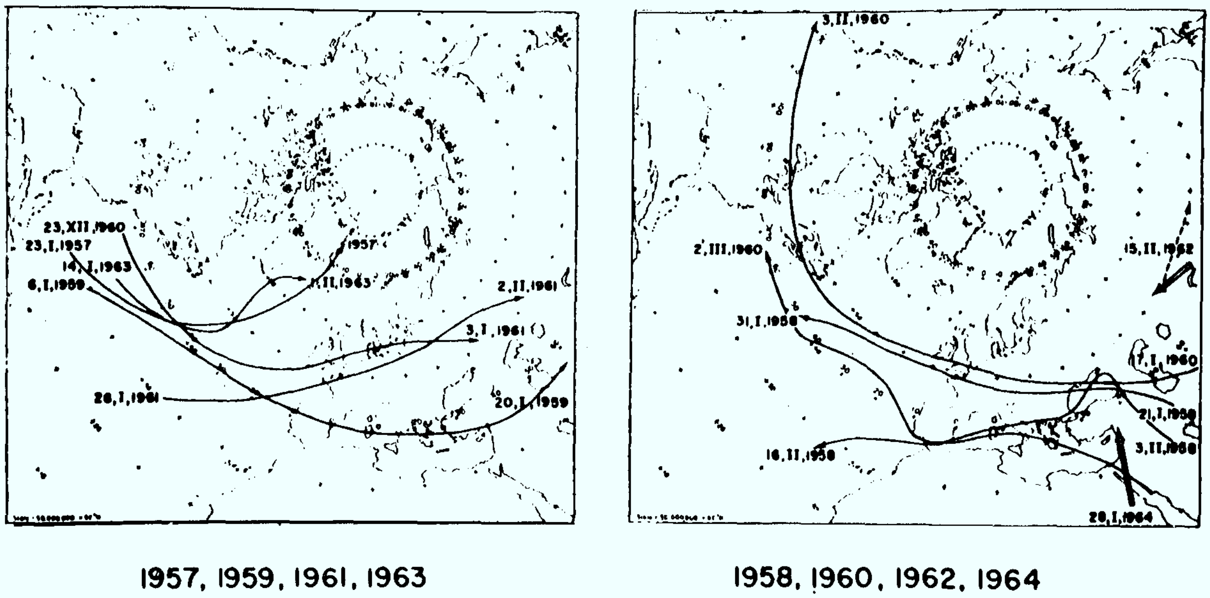

Fig. 10. The movement of (pressure) highs at the 10 mb. level during strong midwinter warmings, (after Labitzke, 1965).

DATE DUE
DATE DE RETOUR

©

Roger Duhamel, f.r.s.c.
Queen's Printer and Controller of Stationery
Ottawa, 1968

Cat. No. DR 51-266/2